GEOLOGIC AND MINERAL AND WATER RESOURCES INVESTIGATIONS IN WESTERN COLORADO, USING SKYLAB EREP DATA

- FINAL REPORT

by

Keenan Lee
Gary L. Prost
Daniel H. Knepper
Don L. Sawatzky
David Huntley
Robert J. Weimer

Remote Sensing Report 75-7

EREP Investigations 380

Contract NAS 9-13394

National Aeronautics and Space Administration

(E76-10383) GEOLOGIC AND MINERAL AND WATER RESOURCES INVESTIGATIONS IN WESTERN COLORADO, USING SKYLAB EREP DATA Final Report (Colorado School of Mines) 638 p HC CSCL 08F

N76-28593

Unclas
G3/43 00383

December 1975

REMOTE SENSING PROJECTS

GEOLOGIC AND MINERAL AND WATER RESOURCES INVESTIGATIONS IN WESTERN COLORADO, USING SKYLAB EREP DATA

FINAL REPORT

by

Keenan Lee
Gary L. Prost
Daniel H. Knepper
Don L. Sawatzky
David Huntley
Robert J. Weimer

Remote Sensing Report 75-7

Remote Sensing Projects
Department of Geology
Colorado School of Mines
Golden, Colorado

National Aeronautics and Space Administration

NASA Contract NAS9-13394

December 1975

SIGNIFICANT RESULTS

Skylab photographs are superior to ERTS images for photogeologic interpretation, primarily because of improved resolution. Similarly, S190B photos provide more geologic information than do S190A photos. Multiband photography shows no apparent advantage over good color photography; S190B stereo color photos, where available, provide maximum geologic information.

Lithologic contacts can be detected consistently better on Skylab S190A photos than on ERTS images. Color photos are best; red and green band photos are somewhat better than color-infrared photos; infrared band photos are worst. With S190B color photos, all stratigraphic units at or above formation-rank can be mapped in this area, and many formations can be effectively subdivided into members. Conjunctive use of topo maps permits estimation of section thicknesses and lateral thickness changes. Stratigraphic pinch-outs, intertonguing sedimentation, and lateral facies changes have been accurately mapped with S190B photos.

All major geologic structures can be recognized on Skylab photographs. Large folds, even those with very gentle flexures, can be mapped accurately and with confidence. Bedding attitudes of only a few degrees are recognized; vertical exaggeration factor is about 2.5X. Faulting is

recognized more easily, but with less reliability, than folds. Fractures as short as 1 km are seen on S190B photos, as are joint spacings of less than 200 m. Anomalous megalineaments are recognized that transect regional tectonic elements. By recognizing and tracing stratigraphic units in detailed mapping, major uplifts can be demonstrated to have recurrent structural movement.

Mineral deposits in Central Colorado may be indicated on Skylab photos by lineaments and color anomalies, but positive identification of these features is not possible. High densities of lineaments may indicate complex fractures that exert controls on mineralization, but they may represent many other types of structures as well. Color anomalies may indicate gossans or hydrothermal bleaching associated with mineralization, but they may also represent sedimentary redbeds and pink, microcline-rich granitic rocks. Orbital photography alone is inadequate to fulfill mineral exploration needs. It is useful in reducing the size of an exploration area to potentially favorable targets, but it is a powerful tool only when used in conjunction with detailed field work.

Water resource studies can use Skylab photography for interpretation of drainage, hydrogeology and ground water flow. S190A stereo color photography is adequate for defining drainage divides that in turn define the boundaries and distribution of ground water recharge and discharge areas

within a basin. Skylab S190B stereo photography has sufficient resolution to map hydrogeologic units and structures that may be sufficient for regional studies. Aircraft photography and field work are still necessary to produce an accurate hydrogeologic map. Both vegetation and soil salinity are surface phenomena capable of being interpreted on Skylab photos that are indicators of shallow ground water.

Regional geologic mapping using Skylab photography is best done by photointerpretation, a deductive process best carried out by a geologist-interpreter. Using S190B photographs, photogeologic mapping at a scale of 1:24,000 is not feasible, and 1:250,000 is, in some cases, too small a scale. Optimum scale for photogeologic mapping is in the range of 1:62,500 to 1:250,000.

Skylab photography will add little new geologic information in areas where 1:250,000 scale geologic maps are available. In such areas, however, the photography should prove useful for re-examining the geology in the light of new concepts or hypotheses. Photogeologic mapping from Skylab S190B color photography can provide invaluable geologic information in areas that are geologically unknown or poorly known.

CONTENTS

INTRODUCTION

This report summarizes the research conducted by the Colorado School of Mines under NASA Contract NAS 9-13394 for the purpose of evaluating Skylab remote sensing data for geologic and mineral and water resources in western Colorado. The primary objectives of the investigation were to:

assist NASA/JSC in mission planning activities,

screen all EREP data obtained over Colorado and select frames for detailed study,

prepare photogeologic maps using selected S190 photographs and analyze them to determine what geologic information may be contained in them,

compare the geological interpretations to interpretations obtained from S-192 imagery and to interpretations made from ERTS-1 imagery,

verify the geological interpretations by means of interpretation of aerial photographs, published geological reports, and field observations, and

prepare recommendations for the optimum imagery to be used for studies of regional geology and exploration for mineral deposits and water resources.

Because EREP is an experimental program, research efforts were directed largely toward evaluations rather than applications.

Research on the Skylab Project was conducted by faculty and graduate students of the Colorado School of Mines. Over the duration of the project, the following geologists contributed to the research: Rebecca Dodge, David Huntley,

Robert Hutchinson, Harry Kent, Daniel Knepper, Keenan Lee, Gary Prost, Don Sawatzky, Robert Spoelhof, John Thigpen, David Trexler and Robert Weimer.

The authors of this report thank Rebecca Dodge, Rosemary Lee and Jean Mbok for their help in preparing the report. Kitty Huntley's assistance was not only valuable - it was critical to the completion of the Project.

The format of this final report is stratified, with three strata being (1) Significant Results, (2) the text of this report, Chapters 2 through 7, and (3) the appendices. This format was designed such that Significant Results is a listing of results; the text of the report is a short, narrative discussion of our results, without any supporting material; and the appendices contain the full arguments, details and evidence. Recommendations are a reflection of the Principal Investigator's opinions and prejudices.

<u>SKYLAB DATA</u>

Five of the six Skylab ground tracks across Colorado were designated EREP passes (App. [illegible] 3). Four of these tracks (16, 30, 34, and 48) traversed what was originally defined as the primary test site, and each of these tracks was photographed at least once, although only one was photographed under very good conditions.

Maps have been compiled that show the total Skylab data coverage of Colorado (App. C, p. 4), total coverage by each sensor (App. C, p. 7), and individual frame index maps (App. C., p. 8 ff.). The maps are used for location reference only; the photography must be examined to determine clouds, snow, etc., over any given location. In general, good clear continuous stereo coverage is available only in the southern part of Colorado and southeastern Utah.

Skylab S190A original-scale transparencies are 57 mm square and have a scale of about 1:2,850,000. These frames are easiest to work with when they are enlarged four times, to a scale of about 1:700,000, with limits of resolution at about twelve magnifications of the original. The S190A photographs can discriminate objects such as clusters of buildings, two-lane roads, and airport runways, and objects as small as Golden Reservoir (300 m diameter) and Interstate 70 (about 70 m wide) can be identified.

The S190B original-scale transparencies are 115 mm square frames and have a scale of about 1:950,000. Two-time enlargements are easiest to work with, at a scale of about 1:475,000, with optical magnification limits similar to the S190A photos. The S190B photography can discriminate clusters of buildings, large isolated buildings (Carleton gold mill at Cripple Creek, with an aluminum roof approximately 100 by 200 meters), and unimproved roads about ten meters wide.

The major data problems involve non-repetitive coverage and the lack of stereo coverage. Limited coverage is largely responsible for extensive snow or cloud cover on available film, and for limited solar illumination angles and spotty ground coverage. The frequent lack of stereo coverage and occasional complete gaps in ground coverage decrease confidence in photointerpretation.

Processing problems encountered include occasional variable color rendition, especially in CIR film, red specks on S190A CIR film (caused by abrasion and emulsion lifting), scratches, emulsion on the underside of the duping film (causing scratches when unrolling film), and reversal of stereo-sequence (in a continuous sequence each frame has been rotated 180 degrees, making stereo viewing of adjacent frames difficult). In general, the data processing quality is excellent.

EVALUATION OF SKYLAB PHOTOGRAPHY
FOR
LITHOLOGY

The utility of Skylab photography for lithologic discrimination was evaluated in two ways. One appraoch was a semi-quantitative study of the detectability of a group of specific formation contacts on different types of photographs (and ERTS images). Detectability was rated, and information content was estimated. The results of this study provide a fairly objective measure of the capabilities and limitations of the different bands of photography. The second approach is qualitative, and consists of the observations made by several geologists who interpreted the photography and correlated these interpretations with ground observations.

Semi-Quantitative Study

The purpose of the semi-quantitative study was to determine if there are optimum bands of photography for discriminating lithologies, and what the bands are. Twelve lithologic contacts in the Canon City area of central Colorado were selected for study on Skylab photographs and ERTS images (App. D). Each contact was defined and located on small-scale (1:100,000) aerial color photographs,

and the detectability (how easily seen) of each of the contacts on the photos was given a value of 1.0.

The defined contacts were then studied on each band of 4 sets of ERTS imagery and 3 sets of Skylab S190A photos acquired at different times of year and the detectability of each contact was evaluated relative to the reference color photos. Neither the ERTS images nor the Skylab S190A photos were studied in stereo, since lack of stereo is the general case for much of the areal coverage of these data. Where stereo is available, the detectability values would be significantly higher than without stereo.

After all the detectability evaluations were completed for the lithologic contacts, statistical tests were run on various subsets of the resulting data matrices. Inspection of the completed Skylab detectability data matrix and the mean values of detectability for the six bands of photography showed that the two black and white photo-infrared bands are so inferior that further statistical testing was unnecessary, and they are excluded from the discussion below.

The band of photography does influence the detectability of lithologic contacts. Results of the statistical analyses show three separable groups:

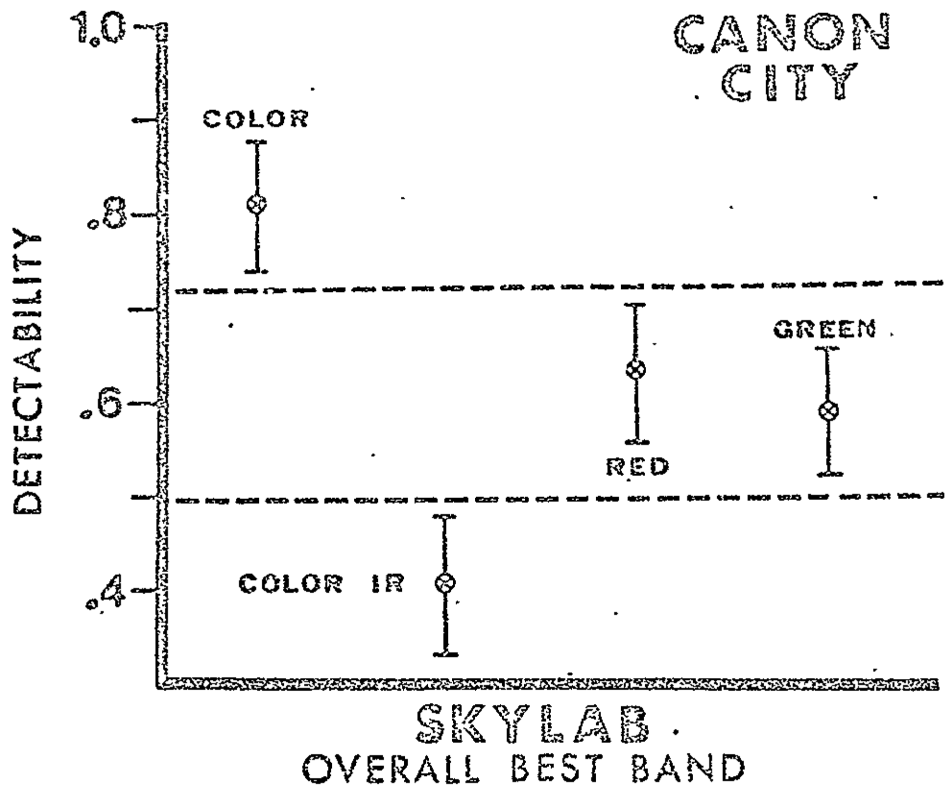

Confidence intervals of mean band detectability of Skylab S190-A photos studied. Dashed lines indicate statistically separable bands at $\alpha = 0.05$.

Confidence intervals of the mean detectability of the lithologic contacts were constructed to compare Skylab and ERTS. Detectabilities on the Skylab photography are consistently higher than on the ERTS imagery. The variations of mean contact detectabilities and the confidence intervals for those contacts studied on both ERTS and Skylab data are:

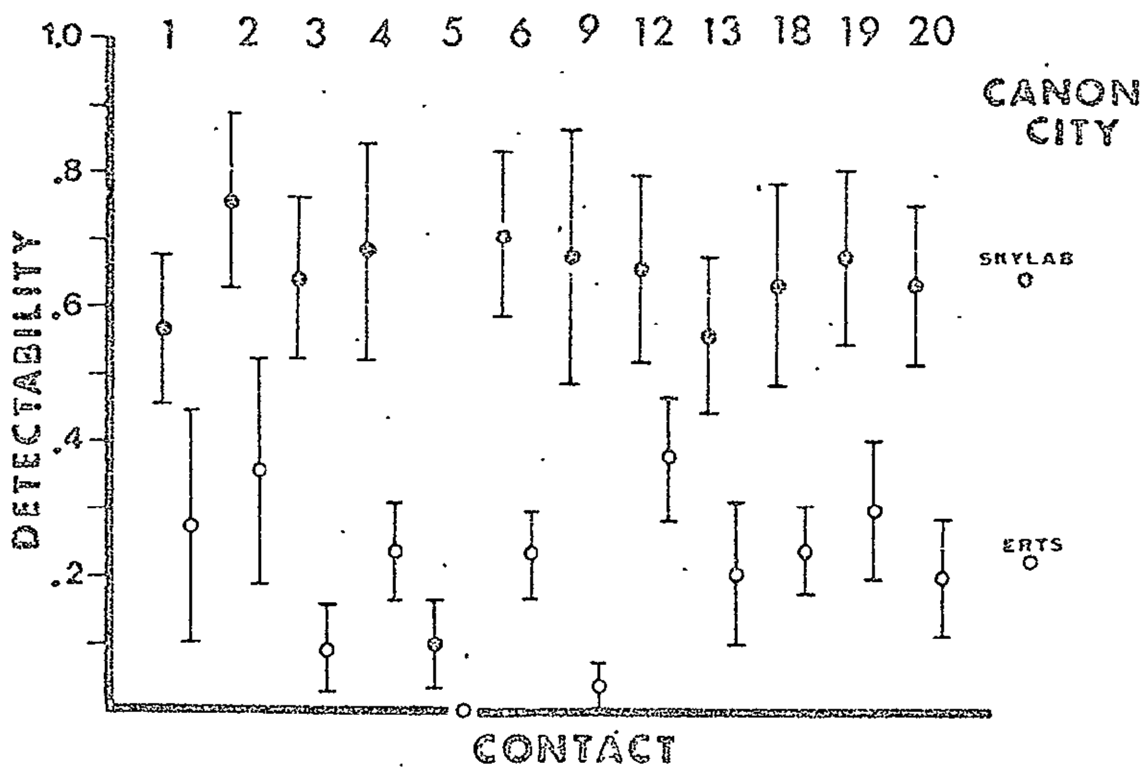

Confidence intervals of mean detectability of the 12 common lithologic contacts studied on both ERTS and Skylab imagery. $\alpha = 0.05$.

Detectabilities of individual contacts on ERTS images are strongly influenced by the time of year the images were recorded, but on Skylab S190A photos there is no significant difference between the June, August and January photos. An explanation for the dependence of ERTS and the independence of Skylab S190A on time of year may be contained in the spacial resolution differences between the two systems. The higher spacial resolution of Skylab S190A photos may allow the subtle surface expression of contacts to be detected even at less than optimum times; the low resolution ERTS system may not be able to show these subdued contacts adequately.

Analysis of the detectabilities of the lithologic contacts does not measure the information content of the images or photo sets. Therefore, the information content of the images and photos must be considered if the optimum imagery is to be determined.

Obviously, the maximum amount of available lithologic information will be gained if each band of each image set is analyzed. But can this same information be found if only one or two specific images or photos are studied? To check this, matrices showing the information content of each ERTS image and Skylab S190A photo were prepared, and the percentage of the contacts that can be seen on each is as follows:

	ERTS				Skylab S190A			
	Band 4	Band 5	Band 6	Band 7	Green	Red	Color	Color IR
January	50	58	58	58	92	100	100	100
June	83	83	83	67	100	92	100	100
August	83	83	83	83	100	92	100	83

A single ERTS image selected for photogeologic interpretation might provide as much as 83% of the available information (number of lithologic contacts mapped) or it might provide as little as 50%. A single Skylab color photo would yield 100%.

CONCLUSIONS

Lithologic contacts can be detected consistently better on Skylab S190A photos than on ERTS images.

Color photos are best; red and green band photos are somewhat better than color-infrared photos; infrared band photos are worst.

Detection of contacts on ERTS images is sensitive to time of year, whereas Skylab photos are able to detect contacts under poor conditions, probably because of higher resolution.

Satisfactory lithologic mapping might be realized using a single Skylab S190A photo, but less than satisfactory results should be expected if only a single ERTS image is used.

It might prove risky to extrapolate the results from this study, conducted in Colorado, to all areas of the world for all lithologic contacts.

Qualitative Study

A difficulty arises in attempting to communicate to others the "lithologic information content" of a Skylab photograph. To state that the stratigraphy can be interpreted "in great detail" is insufficient, and good objective criteria are unknown. For this reason, it is important to study critically some of the S190B color photos (App. F,

Pls. 8-10), in stereo, and to compare these with published geologic maps (App. F, Pls. 3, 6 and 7). Alternatively, photogeologic maps derived from S190B photos (App. F, Pls. 2, 4 and 5) should be examined.

The lithologic discrimination capability of S190B color photography is dramatically superior to S190A black-and-white photography and ERTS imagery. The addition of color, combined with the increased ground resolution, markedly increases the ability to subdivide lithologic units. Most of the formations broken out on 1:250,000 scale geologic maps can be discriminated and mapped where scale permits. Whereas the S190A black-and-white photography (red band) permitted the subdivision of one area into five formations, with S190B color photography it was possible to break out (at least in some places) eleven mappable units.

The general ability to map stratigraphic units is significantly increased on 1:125,000 scale (8X) transparencies as compared with 1:500,000 scale (2X) transparencies. A brief comparison of Plates 2 and 5 (App. F) indicates the amount of stratigraphic subdivision possible.

Photogeologic mapping studies were conducted in southwestern Colorado and southeastern Utah to evaluate S190A and S190B photographs. This region is ideal for the study of Skylab photography because of the large percentage of exposed bedrock in the area. Difficulty in recognizing and tracing stratigraphic units was encountered only in the higher terrain covered by vegetation. Maximum stratigraphic

information derived from the S190B photos was obtained in the Canyonlands National Park area south of Moab, Utah.

Results of the stratigraphic subdivision in this area are shown in the figure on the following page. Inspection of this figure forcibly brings out one salient feature of the photointerpretation: not only can formations and members be interpreted from the EREP photographs, but stratigraphic lateral variations can be determined as well.

Using the base of the Wingate Sandstone as a datum, the figure clearly shows stratigraphic thickening toward the southwest. Almost all of this thickening can be accounted for by changes within the Permian Cutler Formation, but this relationship persists into the Triassic, as evidenced by the pinch-out/facies change of the White Rim Sandstone and Keybed 2 in a northeasterly direction.

The ability to determine stratigraphic thicknesses is quite good. Obviously this capability stems from, and is dependent upon, the conjunctive use of accurate topographic base maps. As an illustration of thickness determination, the stratigraphic section below the Wingate Sandstone and above the Hermosa Formation was estimated to be about 500 m thick in the northeast and about 670 m in the southwest. Interpolation of measured stratigraphic sections by McKnight (1940) gives corresponding thicknesses of about 525 m and 730 m, suggesting the photointerpretive studies are in error by about 4 percent and 8 percent respectively.

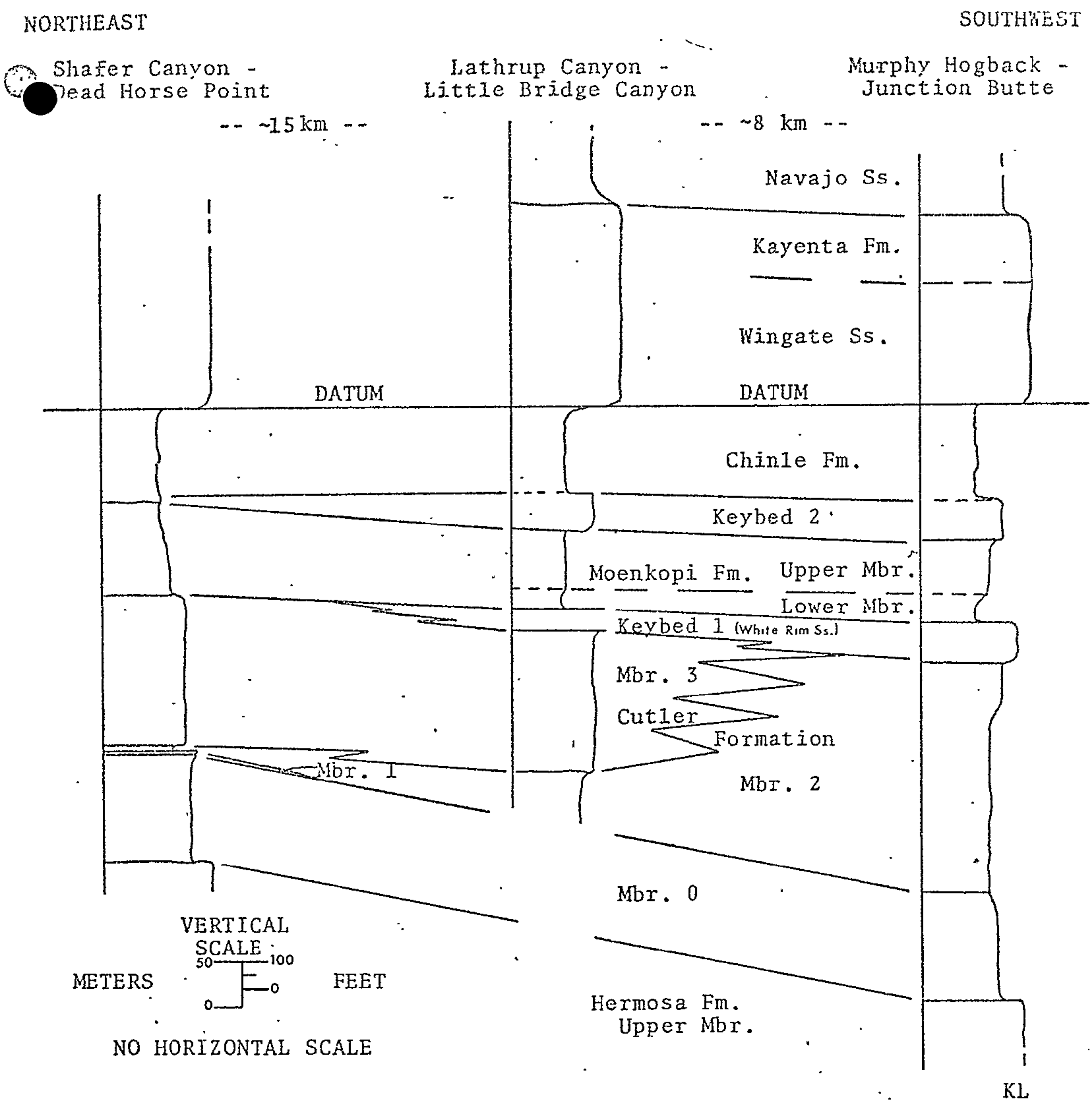

Generalized stratigraphic sections and correlations based on photointerpretation of Skylab S190-B photographs, Moab South area, Utah.

To illustrate the detail of stratigraphic information available in the S190B photos, the following section describes one of the lithologic formations mapped in this area and compares photo observations of the formation with published descriptions.

The Cutler Formation in this area is quite complex. Initial photointerpretation of the Cutler subdivided the formation into three members, called simply Member 1, Member 2 and Member 3. Later photointerpretation broke out a lower unit, which was then called Member 0, and the prominent keybed (kl) at the top of the Cutler Formation was subsequently identified as the White Rim Sandstone and included in the Cutler Formation. Thus, the Cutler Formation, as used here, consists of five members, Members 0 through 3, plus Keybed 1.

Member 0 is differentiated from the underlying Hermosa and from the overlying Member 1 by its red color and lower resistance. Thickness of Member 0 is estimated at about 120 m, compared with an estimate of 177 m by McKnight (1940), but McKnight's section also included what is here designated as Member 1 and part of what is here designated as Member 2.

Member 1 is a very resistant, grey, carbonate unit among the Cutler redbeds. Although the unit is only about 3 m thick, because of its resistance it forms benches and ledges such that it is exposed over fairly wide areas. Field examination shows this unit to be a somewhat rubbly,

brachiopodal crinoidal lime wackestone (Elephant Canyon Formation of Baars, 1975).

Member 2 is very thin in the north part of the area (12 m) and thickens to about 260 m in the south, although it cannot be shown conclusively that this is one continuous unit. Member 2 is characterized by a pink to red to red-brown color and relative non-resistance to erosion.

Member 3 is differentiated from Member 2 by a darker red to a maroon color and by being relatively more resistant.

The relationship between Member 3 and Member 2 is not entirely clear; this photointerpretation suggests that the two members are at least in part facies equivalents. Member 2 appears to correspond to the Cedar Mesa Sandstone Member of Williams (1964) and Baars (1975) and to a transition zone where the Cedar Mesa Sandstone Member interfingers with an unnamed arkose and arkose conglomerate. Member 3 appears to correspond well with Williams' unnamed arkose and arkosic conglomerate and Baars' "Cutler arkosic red beds from the east". Both authors consider the arkose and the Cedar Mesa Sandstone Member to be facies equivalents.

Keybed 1 is an excellent marker bed throughout its area of outcrop. It forms a prominent and conspicuous white ledge that stands out sharply against the red-brown units beneath and above it. This member is relatively thin, yet forms extensive areas of outcrop because of its high resistance to erosion. Keybed 1 is the White Rim Sandstone, considered

by most authors to be the uppermost member of the Cutler Formation.

The White Rim Sandstone was estimated to be about 45 m thick in the southwest part of the map area, which does not compare well with McKnight's (1940) measurement of about 17 m, but agrees well with Baars' (1975) isopach thickness of 30-45 m. The sandstone thins continuously toward the northeast, where it pinches out. It is significant that the point of pinchout of this member could not be more accurately mapped from observations in the field than it was determined from interpretation of the S190B photographs.

CONCLUSIONS

All of the stratigraphic units at formation rank and above that appear on the published geologic map (1:250,000) are recognized on the Skylab photography. In some cases, individual formations were mapped together, but this was done because their contacts were not resolvable at the map scales because of their exposure on cliff faces.

In many cases, stratigraphic units of ranks below formation level could be established. As a result, the study area was mapped to a large extent at member level; seventeen members were mapped.

Not only can vertical variations in the lithology be interpreted, as evidenced by subdividing rock units into formations and members, but some lateral variations can be interpreted as well. The Navajo Sandstone, present throughout

most of the map area, is shown to pinch out to the northeast. Several members of the Cutler Formation are shown to have limited areal distribution; the uppermost member pinches out entirely to the northeast, and Member 2 and Member 3 appear to be lateral facies equivalents.

Intertonguing of gray marine shales with sandstones is recognized and mapped. From this mapping, the direction of more continuous marine sedimentation can be determined.

By recognizing and tracing stratigraphic units in detailed mapping, major uplifts can be demonstrated to have recurrent structural movement. Pennsylvanian and Permian strata are absent on some uplifts, indicating late Paleozoic or early Mesozoic uplifts, with the present structural relief due to Cenozoic structural movement.

References

Baars, D.L., 1975, The Permian System of Canyonlands Country, in Fassett, J.E., ed., Canyonlands Country: Four Corners Geol. Soc. 8th Field Conf. Guidebook, p. 123-127.

McKnight, E.T., 1940, Geology of area between Green and Colorado rivers, Grand and San Juan counties, Utah: U.S. Geol. Survey Bull. 908, 147 p.

Williams, P.L., 1964, Geology, structure, and uranium deposits of the Moab Quadrangle, Colorado and Utah: U.S. Geol. Survey, Misc. Geol. Investigations Map I-360 (1:250,000).

EVALUATION OF SKYLAB PHOTOGRAPHY FOR GEOLOGIC STRUCTURES

Evaluation of EREP data as a source of structural geologic information was carried out by simultaneous evaluation of interpretive techniques, sensors, and information extracted. Interpretation used widely-known photo-interpretation techniques and simple instruments such as magnifiers, stereoscopes, light tables, and devices such as tracing overlays. Sensor evaluation was done for S190A and S190B, considering band stereoscopic availability, resolution and the upper and lower limits of detectability within frames. Information evaluation was concerned with the ability to recognize known geologic structures and to map contiguous or related structures.

The best sensors are those that enhance the linear and curvilinear qualities of most geologic structures in images. This enhancement is due primarily to sharp color or tonal contrasts on the film, so the best characteristics are color and stereoscopic viewing. Secondarily, sensors in red bands and infrared bands bring about enhancement of many linear features by increasing shadow contrast. Color is superior to color IR in the interpretation of folds along the Southern Front Range because of high spectral contrasts of three sedimentary formations involved in the folds. On color IR the spectral contrasts are low and not useful.

Spatial resolution of the elements of structures is important in mapping contiguous structures. The resolution of S190B, as expected, is better than S190A. S190A photographs (red band) revealed a fault about 2 kilometers long; on S190B color photography a fracture 1 kilometer long was observed, as well as joint spacings of less than 200 meters (App. B, p. 17, Fig. 14). Spatial resolution, if high, permits continuation of what could otherwise be unrelated linear segments. Linear features greater than 50 kilometers are frequently observed in satellite photos, though their relationship to geologic structures is often uncertain. However, in the southern Front Range, linear features 35 and 125 kilometers long are related to geologic structures (App. E, p. 17,18).

Few folds are instantly recognized on photos. Most are relatively subtle in expression and must be carefully worked out by determination of opposing dips, with the dip interpretations based largely on the recognition of topographic features. Dip slopes may be directly recognized where stereo viewing is possible. Without stereo, indirect expressions helpful in slope interpretations are shadow relationships and variations of vegetation that are topographically-controlled. Drainage patterns are indicators of slopes, and the rule of V's is the most consistently useful criterion for determination of dips (App. B, Fig. 4,A).

Because the vertical exaggeration factor for the S190B photography has not been reported, a training area southeast

of Moab, Utah, was used to determine empirically the vertical exaggeration factor using a mirror stereoscope (with no magnification). The estimated factor is about 2.5X. A trial area in the vicinity of Moab was used to test this factor. Twenty-two attitudes were interpreted, with apparent dips of 2-20°. Estimated true dips using the 2.5X vertical exaggeration factor were compared with field measured attitudes and agree within 2°.

Maximum enhancement of topography and structural features occurs for about 60 days before and after the winter solstice. Lower sun elevations bring increased areas of shadows and low reflected irradiance. In addition, during this time there is prevalent uniform snow cover, which further adds to the enhancement increase and uniform image contrasts.

NASA Mission 261 was an underflight in support of Skylab designed for low sun-angle photography. Black-and-white infrared film, Type 2424, was used with a Wratten 25 filter to photograph snow-covered areas from 50,000 ft a.m.t. with a 10 degree sun angle. The conclusion of the study was that steep topographic slopes of azimuth of 20 to 30 degrees deviation from the sun azimuth are selectively enhanced because only steeper slopes are shaded. This effect can be used to quantitatively select the azimuth range of linear features to be studied, and the date and time of day to maximize their enhancement by sun and shadow (App. I).

The effect of sun attitude on Skylab photos is shown where three new north-trending lineaments in the Rampart Range

were discovered on SL-2 photography and not seen on SL-3 photography (App. E). This is attributed to the favorable sun attitude of SL-2, when the sun azimuth was 92° and sun elevation was 40°, whereas for SL-3 the sun azimuth was 132° and the sun elevation was 57°. The reverse was true for lineaments in the Royal Gorge arch, which trend N 80 E. Lineaments with greater relief are visible on both SL-2 and SL-3.

One Skylab and ERTS investigation was concerned with those anomalous megalineaments and their associated structures that transect major tectonic features in central Colorado. These anomalous features have not been studied extensively before now because a synoptic view has not been available.

Lineaments are here defined as any unidimensional straight or continuously curved combination of picture elements that appear on photographs or images and that are thought to have geological significance. Lineaments may be the pictorial representation of faults, folds, shear zones, etc. Groups of lineaments that show elongate parallel trends, either end-to-end, overlapping or en echelon, are here defined as megalineaments ("megalinears" of App. E).

Transecting megalineaments are nearly as detectible in a space photo or image as the more structurally-consistent lineaments. Their associated geologic structures are composites of anticlines, synclines, drag folds, monoclines; faults, crush zones, shear zones, and joint sets. Structure

type along the trend of a megalineament is very dependent upon the lithologic terrain in which it is developed. It is this variability, as well as the transecting nature of the megalineaments, that presents a somewhat confusing structural picture and that has delayed the recognition of these major structural features.

In Skylab and LANDSAT images of central Colorado, the normal tectonic elements and their marginal structures are recognizable, as well as transecting megalineaments. The major structural elements of the central Colorado test site (App. E, Fig. 16) are the southern Front Range, a block mountain uplift bounded by typical mountain-flank structures; the Denver Basin on the east; South Park on the west; Canon City Embayment on the south; the Wet Mountains, a block mountain uplift; and Wet Mountain Valley. The basins are downfolded Cenozoic and older sedimentary rocks. The block mountains are Precambrian metamorphic and plutonic igneous rocks, which also underlie the basins. The trend of all of these major tectonic elements is northwest. Two sets of megalineaments occur in the southern Front Range - a north-trending set of three megalineaments in the Rampart Range area (App. E, Fig. 26) and a northeast-trending set of three megalineaments south of Pikes Peak (App. 3, Fig. 27).

In the Rampart Range (App. E, Fig. 26), the Manitou Park megalineament is associated with the Ute Pass fault on the south, which passes into the Ute Pass thrust and

northward in Pikes Peak granite into the Bear Creek shear zone. The one singular feature of this megalineament is that the fault zones all have been intruded with sandstone dikes throughout the length of 125 kilometers.

The Jackson Creek megalineament transects the Rampart Range and offsets the flank structures on the east. The eastern megalineament is associated with a long prominent escarpment that also trends into the flank structure on the east.

The three megalineaments of the Rampart Range are continuations of, or are involved with, long-known structural features. On the west, they are continuations of a major thrust fault and monocline. On the eastern side of the block uplift, the Rampart Range thrust is offset where two of the megalineaments cross. A new interpretation of this block uplift is that it consists of three giant imbricated plates with two thrust faults at the outer margins and two normal faults between the plates.

South of Pikes Peak (App. E, Fig. 27), the Milsap Creek megalineament trends southwest from the Pikes Peak intrusive center 35 kilometers. The associated structures consist of mafic-intruded crushed zones, a major offset of the mountain flank structure on the western margin, a gentle drape fold, and a fault. Two other megalineaments are the Adelaide and Peck's Camp features.

The structural evidence associated with the transecting megalineaments of the Front Range uplift points to a more complex involvement of the crystalline basement in the regional tectonic deformations. These deformations consist not only of the familiar ones of uplifts decoupled from basins along flank thrusts and monoclines, but also independent, or subsequent, continuous cross-cutting deformations that have the spatial unity of a single geologic structure, yet are manifest in different kinds of structural features along that megalineament. Further study of megalineaments may add considerably to our knowledge of tectonic history and kinematics of regions.

CONCLUSIONS

Resolution, color photography, and stereoscopic endlap coverage are the most important sensor characteristics for structure interpretation.

Fractures as short as one kilometer can be recognized on S190B photos, and joint spacings less than 200 m are resolvable.

Geologic folds can be interpreted with confidence.

Bedding attitudes can be estimated, using a 2.5X vertical exaggeration factor, with accuracies of a few degrees obtained in an area of low dips. Dips of only a few degrees are recognized.

Linear structures are selectively enhanced as a function of solar attitude; three new lineaments were detected this way.

Anomalous megalineaments are seen on space images that transect normal structural trends in the Colorado Front Range. These represent geologic structures that may reflect more complex involvement of the crystalline basement.

The amount and detail of structural information contained in the Skylab photos is difficult to quantify. The best evaluation of this information content is gained by examining S190B stereo color photographs (App. F, Pls. 8, 9, 10) and comparing the photos with published geologic maps (App. F, Pls. 3, 6 and 7). Alternatively, photogeologic maps compiled from the Skylab photos (App. F, Pls. 1, 2, 4 and 5) should be examined.

EVALUATION OF SKYLAB PHOTOGRAPHY
FOR
REGIONAL MAPPING

Two photogeologic mapping studies were conducted along Track 34 (southwestern Colorado and southeastern Utah) using SL-2 and SL-3 color photography. One study used S190A color photos and evaluated their use in reconnaissance structural mapping. The second study mapped mostly from S190B color photos, with the objective of more accurately evaluating the scale limitations and level of geologic detail available from these photos.

S190A

Approximately 40 hours were spent analyzing Skylab 3 S190A color photographs from western Colorado and eastern Utah. The objectives of the study were 1) to prepare a photogeologic map to determine the geologic information content of the S190A photographs, 2) to compare the results of this work with a map of the general area prepared from ERTS imagery, and 3) to determine how accurately and rapidly a large area could be mapped by an experienced geologist with a working knowledge of the geology.

A photogeologic map was prepared for approximately 25,000 square kilometers covering the region of the Uncompahgre Uplift and the northern portion of the Paradox Basin (App. F, Pl. 1).

Four frames of S190A color transparencies (~4X, 1:710,000) with stereoscopic coverage were used to study the geology of the region. The images were observed with a mirror stereoscope and interpretations transferred to a transparent overlay on color prints (~8X, 1:360,000).

The investigator was generally familiar with both the geology and geography of the region from detailed mapping that had been conducted in small areas scattered through the region. The observer was continually amazed at the excellent quality of the color photography, the ease of recognizing stratigraphic units and structural elements, and the accuracy of locating oneself relative to geographic points.

Eight stratigraphic units with widely varying lithologies were selected for mapping purposes based on ease of recognizing mappable contacts throughout the area and sufficient detail to define the structural features. Additional stratigraphic units could have been mapped, but, for the purposes of this project, the time required for mapping greater stratigraphic detail was judged to be inappropriate in achieving the stated objectives.

The largest and most significant structure is the Uncompahgre Uplift. The uplift is a large block approximately 160 km long and 60 km wide that is tilted to the northeast and trends N50W. A thin sedimentary sequence covers the uplift, forming long northeast dip slopes. Precambrian rocks are exposed in deeply eroded canyons and on the north side

of the major fault zone separating the uplift from the Paradox Basin. The major faults are believed to be high angle and are obviously basement-controlled systems.

The northern Paradox Basin contains numerous anticlines formed in Pennsylvanian through Cretaceous strata. Five major anticlinal trends have been delineated by both outcrop patterns and dip of strata. Some of the fold axes can be traced for more than 150 km; the flanks of the folds vary in width from 5 to 10 km.

Many more faults have been mapped on the photos than appear on published maps of similar scale (App. F, Pl. 3). Ground checking may eliminate some of the lineaments, but it is believed that the Skylab S190A photographs show fault trends not heretofore known from published geologic maps of the area.

By tracing stratigraphic units on the Skylab photographs, the history of major structural elements can be reconstructed. The Paradox Basin contains Pennsylvanian and Permian stratigraphic units that are not present on the Uncompahgre Uplift. This indicates the uplift was a high area during the late Paleozoic or that rocks of these ages were deposited and subsequently removed by erosion prior to deposition of the Triassic. Under either interpretation, and because the area is an uplift today, the mapping indicates renewed tectonic movement of the uplift through geologic time.

Photogeologic mapping in this area was conducted by use of both ERTS-1 and Skylab 3 images. Band 6 was used in mapping on an ERTS image, whereas color photography was used on Skylab. The major folds, the general distribution of stratigraphic units, and major fault patterns were similar on both types of images. However, much more detailed and accurate information was available from the Skylab photos. The ERTS imagery does not have continuous stereoscopic coverage, and its use must definitely be classed as a reconnaissance mapping technique. By contrast, the quality of the Skylab S190A photographs permits accurate, detailed mapping in a manner equal or superior to any other system of photogeology where an investigator wishes to map a large area in a short period of time.

S190B

The approach followed in this study was to use a designated training area, in which area each type of satellite image was interpreted in a conjunctive way with published geologic maps. Experience derived from this training area was then used to photointerpret the geology of an unknown area.

Initial photogeologic mapping used 1:500,000 scale photos for annotation and 1:250,000 scale topo base maps for geologic compilation (App. F, Pl. 2). It soon became apparent, however, that the amount of geologic information

was greater than could be compiled effectively at this scale. Most detailed photogeologic mapping, therefore, was done at larger scales.

Photointerpretation was conducted using 4X and 8X enlargement positive transparencies of the S190B photographs. Stereo interpretation used a mirror stereoscope with an effective magnification range of 1-2X, so these positive transparencies were examined at about 1:250,000 to 1:60,000 scale. Where geologic information was apparent on the enlargements, the information was directly annotated; areas of structural complexity or subtle detail were studied concurrently on contact transparencies at high optical magnification.

Geologic information was annotated onto clear acetate overlays on top of the positive transparencies. The interpretations were then transferred from the overlays onto topographic maps (1:62,500) using a zoom transfer scope, and using the topographic information as a secondary control. It was often necessary to go back to the original duplicate positive on the zoom stereoscope for resolving detail and resolving complex structures.

The accuracy and validity of the photointerpretation maps were checked in the field. Field observations consisted of examining areas characteristic of the geology of each map area, as well as investigation of areas where geologic interpretations were complex or where no geologic interpretation could be made from the photographs. Four days were spent field-checking the 1:62,500 photogeologic maps.

This research was conducted so that the photogeologic maps produced represent data products that would be obtained from an application of photointerpretation, using Skylab S190B photography, to areas that are geologically unknown or geologically poorly known. The geologic maps (App. F, Pls. 2, 4 and 5) represent geologic mapping by photointerpretation on Skylab S190B photographs, supplemented by minimal field checking. In general, the correlation between the photogeologic maps and the published geologic maps is excellent, but this can be evaluated only by carefully comparing the maps (App. F, Pl. 2 with Pl. 3; Pl. 4 with Pl. 3; and Pl. 5 with Pls. 3, 6, and 7).

CONCLUSIONS

By viewing large structural features of the earth's crust in one or two images, fault and fold patterns can be interpreted in a perspective not previously possible.

Skylab S190A photos permit rapid and accurate photogeologic mapping in areas of complex folding and faulting, if outcrops are good. Approximately 25,000 square kilometers were mapped at a scale of 1:360,000 in about 40 hours.

In areas of heavy vegetation, mapping accuracy is significantly reduced to a reconnaissance level.

The Skylab photos are superior to ERTS imagery. Skylab maps may be equal to or greater in accuracy than some published geologic maps.

An increase in geologic information is associated with increase in scale when comparing the S190A and S190B photography. System resolution is approximately the same for each camera, but ground resolution of the S190B is superior because of its longer focal length and correspondingly greater scale. There is little doubt that an increase in resolution can be directly translated into an increase in geologic information.

Using S190B photographs, photogeologic mapping at a scale of 1:24,000 is not feasible, and 1:250,000 is, in some cases, too small a scale. Optimum scale for photogeologic mapping is about 1:62,500. This conclusion, however, may be valid only for this area.

Photogeologic mapping from Skylab S190B color photography will add little new geologic information in areas where 1:250,000 scale geologic maps are available. In such areas, however, the photography should prove useful for re-examining the geology in the light of new concepts or hypotheses.

Photogeologic mapping from Skylab S190B color photography would provide invaluable geologic information in areas that are geologically unknown or poorly known, provided only that exposures are good and photo quality is high.

EVALUATION OF SKYLAB PHOTOGRAPHY

FOR

MINERAL DEPOSITS

It is economically more desirable to survey large areas for potential ore deposits by remote sensing than by conventional ground surveys. Advantages of satellite imagery, both photography and scanned imagery, include a synoptic view, repetitive coverage, accessibility to remote areas, and relatively low cost. The objective of this research was to evaluate Skylab EREP photographs and, to a lesser extent, ERTS (LANDSAT) and aircraft images, for their utility in locating indicators of mineralization in central Colorado.

The Leadville and Cripple Creek mining districts are typical of mineralized areas in central Colorado. Skylab photos covering these areas were studied, and geology was correlated between maps and photographs. Each area was field-checked to identify exactly what was seen on the photography, and the two control districts were analyzed to determine the geologic features characteristic of mineralized areas that are visible on orbital photography.

Ore deposits of the Leadville district occur chiefly in fissure zones, karst collapse breccias, or as replacement mantos in dolomites intruded by Upper Cretaceous or lower Tertiary felsic to intermediate porphyries. Major faults

contain ore in few places, while auxiliary faults and fissures have served as feeder channels and often are mineralized. Alteration includes local hydrothermal bleaching of porphyries and weathering of disseminated pyrite to hydrous iron oxides. Indicators of mineralization for this district are faulting, intrusion of sedimentary strata by light-colored porphyries, and weathered pyrite. Field checks verified the ability to see some faulting on all orbital photography, and alteration colors were visible on S190B photos.

At the Cripple Creek district, ore deposits lie within or near the margins of a steep, fault-caused basin (caldera?, breccia pipe?) filled with Miocene breccia and phonolite and surrounded by Precambrian granite, gneiss, and schist. The basin, approximately three by six kilometers (two by four miles), is filled with non-volcanic as well as volcanic debris, and is crosscut by dikes of phonolite and lamprophyre. Gold mineralization followed intermittent fissuring and is most commonly found as veins associated with quartz and pyrite gangue. Indicators of mineralization that are visible on satellite images are faulting and alteration of pyrite. Weathered pyrite is seen only on mine dumps.

Results of the study at the Leadville and Cripple Creek mining districts led to the preliminary conclusion that indicators of mineralization visible on Skylab photography over central Colorado are faults and alteration. Breccia-filled basins could not be recognized on Skylab photos

because of a lack of color contrast or unique topographic or vegetation features. Karst horizons and mantos likewise were not visible because of limited stratigraphic extent and frequent soil and vegetation cover.

Faults and alteration are seen on satellite photography as lineaments and anomalous colors. A "lineament" is any line or alignment of features of probable geologic origin; extensive faulting appears as a high density of lineaments and numerous intersections of lineaments. Alteration produces anomalous colors, or a local color that deviates from regional uniformity. Primary color anomalies associated with alteration are red-ocher colors produced by weathering of pyrite, and light-color areas due to hydrothermally-bleached intrusives.

Skylab photos of the central Colorado survey area were studied to find other areas that show indicators of mineralization. Limited cloud-free Skylab photography somewhat narrowed the study area; the primary site was the area covered by Skylab 2, S190A, Track 48, Frame 17, acquired 11 June 1973 (App. G, Fig. 1). Skylab 2 and Skylab 3 photos were used (Skylab 4 photos were received too late to be included), as well as ERTS images (e.g. - E 1154-17143) and aircraft data (NASA Mxs 184, 211 and 235). The entire study area includes 47,000 square kilometers.

In this study to locate other areas of mineralization, structure targets were chosen in areas of high lineament density or at complex lineament intersections, by mapping lineaments as guides to faults, joints, and shear zones.

It has been demonstrated that multiple intrusions and cauldron subsidence are associated with high density radial faulting, while volcanic piles, anticlinal uplifts, and erosion have considerably less radial faulting, and therefore less complex fault intersections. Areas of complex structural intersection have long been considered favorable to ore deposition. It is expected that linear features seen on satellite photography are fractures (faults, joints, shear zones).

A common surface indicator of ore at depth is the gossan, an outcrop of leached and oxidized iron sulfides. Where unobscured, the characteristic red-ocher color can be seen on color photography. In addition, intrusive rhyolite porphyries should appear as light-colored anomalies where intruded into darker sediments. Surprisingly, the color rendition of the S190B film (SO-242) allowed detection of color anomalies that were not obvious on aircraft photography.

An overlay map of the study area was constructed showing all of the mapped lineaments. From this map, favorable structural targets were picked (App. G, Fig. 16). In a similar way, the color Skylab photos were interpreted for color anomalies, and areas of favorable color were picked (App. G, Fig. 17). From the conjunctive use of these two maps, mineral target areas were defined on the basis of concurrence of structural and color anomaly targets, and these target areas were ranked according to priority. The highest

priority target area occurred at Weston Pass, and this area was subsequently field checked.

Evaluation of the primary target at Weston Pass consisted of mapping from satellite and aerial photography (1:500,000 and 1:20,000, respectively) and in the field (1:12,000) to determine the origin of lineaments and color anomalies, and to discern the relationship of these features to ore deposits.

Twenty-two lineaments were mapped from Skylab photography within the Weston Pass study area (App. G, Fig. 24). Detailed field mapping shows that seven of these lineaments, of 32%, are in fact faults (App. G., Fig. 25). One lineament was correlated to a cultural feature (powerline), and the remainder are vegetation and drainage alignments thought to be strongly influenced by structure. A comparison of 53 linear drainage azimuths with 239 joint measurements suggests that one drainage trend is directly controlled by jointing, and that another trend is a consequence of drainages formed on dip slopes normal to fracturing.

Field mapping revealed that red-ocher color anomalies are caused not only by a gossan, but also by red sedimentary rocks and microcline-rich crystalline rocks and grus. The most obvious color anomaly, on the west slope of Weston Peak (App. G, Fig. 17), contains both microcline and hematite/limonite-rich granite talus. Another less visible anomaly consists of microcline-rich outcrop and grus; another comprises

limonite-stained dolomite talus overlying a white quartzite. Most color anomalies at Weston Pass (App. G, Fig. 21) correspond well with the percentage distribution of microcline in Precambrian basement rocks (App. G, Fig. 22).

Indicators of mineralization did lead to an old mining district at Weston Pass, where lead and zinc sulfides formed manto deposits in the Leadville Formation. The ore is thought to have originated either in nearby porphyry sills or in a batholith at depth, and to have migrated along fissures adjacent to large, regional, gouge-filled fractures such as the Weston fault. The (former) presence of these ores, however, was not directly indicated by the Skylab photographs; the extensively limonitized ore horizons at Weston Pass were not visible on orbital photography because of limited outcrops and extensive vegetation and soil cover.

Results of this study suggest the preliminary conclusions were incomplete. Red-ocher colors in central Colorado may result from sedimentary red-beds, microcline-rich crystalline rock, iron-oxide alteration, or combinations of these. Linear features have been identified as aligned streams and cultural features, as well as geologic features such as faults, joints, shear zones, dikes, contacts, folds, and paleovalleys. Intersections and high densities of regional lineaments, where they in fact represent structures, are not the only structural controls on mineralization.

CONCLUSIONS

Skylab photography can cover large areas quickly and inexpensively, and there are some surface features in any given region that are indicators of mineralization. Photo-lineaments and color anomalies are important indicators of mineralization in central Colorado, but positive identification of these features is not possible. Areas where orbital photography may be most useful in the search for mineral deposits include the snow-free alpine portion of mountain ranges and in arid regions.

Orbital photography alone is inadequate to fulfill exploration needs. It is useful in reducing the size of an exploration area to potentially favorable targets, but like other remote sensing techniques, it is a powerful tool only when used in conjunction with detailed field work.

EVALUATION OF SKYLAB PHOTOGRAPHY FOR WATER RESOURCES

Skylab S190-A and S190-B photography, covering the northern closed basin of San Luis Valley, Colorado, was evaluated for its use in regional water resource studies. Specifically, the study evaluated the ability of a photo-interpreter, using only Skylab products, to map surface water divides and drainages, zones of ground water recharge and discharge, distribution of hydrogeologically-significant rock and alluvial units and significant structures, and ground water depth and quality. All interpretations were checked by either field work or comparison with published data.

Some of the most obvious features on Skylab photographs are the major surface water divides and drainages. A drainage map of the northeastern part of the study area interpreted from Skylab 2 S190A photography (App. H, Fig. 2) is much more detailed than the existing 1:1,000,000 scale topo map of the area, but inferior to existing 1:250,000 scale maps. Accuracy of the surface water divide from the photos is comparable to that of the existing 1:250,000 scale topographic map. Mapping of drainage is best using color-infrared photography, because streams within the alluvial

portion of the basin are best defined by the presence of deciduous vegetation along their course.

Knowledge of the positions of the surface water divide and the drainages is significant not only in the evaluation of surface water flow directions and boundaries, but, in most cases, it helps define the boundaries of ground water movement. In most terrains, where the water table forms a subdued replica of the topography, ground water recharge often occurs at topographic highs, and discharge is found at topographic lows. In a homogeneous medium, or in an inhomogeneous medium of horizontal units, the surface water divides and major drainages will act as impermeable boundaries, and there will be no flow across them.

Resolution of the film/camera system is the most important factor determining the amount of hydrogeologic information that can be interpreted. The S190A system does not have sufficient resolution for more than a cursory examination of the distribution of rock and alluvial units. Although no stereo coverage was available for the S190B system, it is obvious that much more information results from the greater resolution. Interpretation of stereo S190B photographs would probably produce a map comparable to that of an interpretation of high-altitude aircraft photography, sufficient for a reconnaissance-level, regional ground water study.

Geologic structures, particularly faults, exert a strong influence on ground water movement in the San Luis

Basin. Fractures provide the most significant permeability in the marginal bedrock units, and faults within the alluvial sequence of San Luis Valley often are ground water barriers. Faults within the mountains can be interpreted only by the presence of linear topographic depressions, or the linear alignment of discontinuous topographic depressions; the capability of mapping stratigraphic units in sufficient detail to delineate fault separations is simply not present using S190A system photography. S190B photography has adequate resolution to map the hydrogeology in some cases, but aircraft photography is a necessity for most studies and field work is a necessity for all studies, even at the regional level.

Ground water depth and ground water quality can be estimated from Skylab photographs. Narrowleaf cottonwood trees (Populus angustifolia) and willow (Salix spp.) are found where saturated sediments are within five meters of the ground surface, and both are capable of being seen on the color infrared photography because of their high photo-IR reflectance compared with surrounding xerophytes. Cottonwoods thrive only in areas of good water quality, whereas the willows are more tolerant. Vegetation maps derived from Skylab 3 S190A color infrared photography (App. H, Fig. 7) correlate well with maps of ground water depth (App. H, Fig. 8).

Possible relations between saline soil and ground water depth were first observed on LANDSAT imagery and studied in

more detail on Skylab 3 S190A photography. The distribution of saline soils was mapped from S190A photography and was studied to determine its relation to ground water depth, quality, and direction of flow.

Comparison of the interpreted soil salinity (App. H, Fig. 9) with ground water depth (App. H, Fig. 8) shows that saline soils develop only where the ground water is relatively shallow, but that saline soils are not present everywhere the water table is near the surface. The presence of shallow ground water associated with non-saline soils indicates that at least one additional parameter limits the distribution of saline soils, and this appears to be position within the ground water flow regime. All areas of high soil salinity can be represented as areas of shallow ground water that are within the zone of potential discharge - that is, in areas where ground water potential (head) increases with depth.

Because the use of soil salinity in the interpretation of ground water depth appears to be potentially more dependable than vegetation, examination of the spectral reflectance of the saline soils was undertaken to attempt to better delineate these soils. Reflectances of dry saline soils, and moist and dry non-saline soils were measured to determine the best method for isolating the saline soils on photography.

Saline soil reflectances were measured in the field, and dry and moist non-saline soil reflectances were measured in

both the laboratory and field, using a filter-wheel photometer. The dry and moist non-saline soils show a wide range of absolute reflectances, but a relatively uniform normalized reflectance curve (App. H, Fig. 16), so normalization should be used as a preprocessing step. Saline soils with a high average reflectance do show a reduced slope of increased reflectance towards the infrared region, suggesting that ratioing may help increase the contrast between saline soils and non-saline soils having the usual range of intermediate reflectances. This has not been tested in application.

A plot of absolute band reflectances for non-saline and saline soils (App. H, Fig. 18) shows separation of the ranges in the photo-infrared bands, the deep-red bands, the minus-blue band, and the no-filter band. These observations in part contradict the subjective evaluation of S190A photography, where the infrared bands show the least contrast. One explanation for this is that the photography is not contrasting non-saline with saline soils, but is contrasting vegetation with saline soils. Vegetation typically exhibits a high photo-infrared reflectance, which would show a low contrast with saline soils, but has a much lower visible relfectance than the saline soils. This may well affect the conclusions reached above concerning band ratioing.

CONCLUSIONS

Both vegetation and soil salinity are useful indicators of shallow ground water, but both must be interpreted carefully.

Resolution is the single most important factor in the application of Skylab photography to hydrogeologic investigations.

Skylab S190A stereo photography is sufficient for defining drainage divides that in turn define the boundaries and distribution of ground water recharge and discharge areas within the basin.

Skylab S190B stereo photography has sufficient resolution to map hydrogeologic units and structures that may be sufficient for regional studies. Aircraft photography and field work are still necessary to produce an accurate hydrogeologic map.

ORIGINAL PAGE IS
OF POOR QUALITY

RECOMMENDATIONS

The Earth Resources Experiment Package was a successful experiment. The photographic part of the package should now be applied.

Photographic sensors should be used to provide reliable, accurate, detailed geologic maps that in turn can be applied to specific programs such as hydrogeology, mineral deposits exploration, petroleum exploration, etc.

This geologic mapping application should be directed toward areas that are poorly-known in a geologic sense - specifically, to areas where geologic maps do not exist at scales as large as 1:250,000 and where exposures are good. Normally, this would direct the application to underdeveloped countries; photogeologic mapping of Colorado from S190 photos is not cost-effective, but for Iran the return should be enormous.

Mineral resource industries should become more involved in the application of Skylab data. Few publications are available to bring Skylab photos to the attention of industry, and at the two main industry-oriented geologic remote sensing meetings of 1975 (U. Kansas, February; EROS Data Center, October), Skylab was little mentioned. It seems that Skylab to date has existed largely in the research lab and university environment, appropriately. But to be applied, industry must begin to use the data. Educate the users rather than use educators.

Geologic applications should emphasize photography and photointerpretation. Computer processing techniques will have specialized uses when they become commonly available, and will require sophisticated equipment. Photointerpretation of space photos requires only minimal re-education of a geologist and builds upon his prior experience.

Future satellite programs should attempt a marriage between ERTS and Skylab. For all geologic uses where we have compared good ERTS data with good Skylab data, there is no doubt that the Skylab photographic data are superior. But the photographs just aren't available for many areas, or they are cloudy. The biggest single advantage of ERTS imagery is that it is there.

Specifically, the global, repetitive coverage of ERTS should be combined with the resolution, stereoscopic capability and color of quality photography. Perhaps an unmanned Skylab, with its huge payload and film storage capability, could use film eject systems, combined with data takes regulated by real-time MSS feedback, to obtain global, cloud-free, stereo, high resolution, color photography.

Sensor improvements in photography should require little effort. Multiband photographs should be de-emphasized; if camera systems have multiple magazine capability, color infrared and panchromatic films would be available for designated uses, and the multiband photography concept has not proved effective. It would be much more desirable to have

multi-focal length (zoom?) cameras, each with 9-inch film format. Consideration should be given to 150 mm, 450 mm and 1500 mm focal lengths that would provide (from 435 km) respectively, ~1:3,000,000 scale photos covering 660 km, ~1:1,000,000 scale photos covering 220 km, and ~1:300,000 scale photos covering 66 km. Parallel MSS systems, especially with sweep detector arrays, could still provide computer-compatible data tapes.

APPENDICES

APPENDIX A

GEOLOGIC AND MINERAL AND WATER RESOURCES INVESTIGATIONS IN WESTERN COLORADO, USING SKYLAB EREP DATA

Monthly Progress Reports

April, May, June 1974

EREP Investigations 380

Contract NAS-13394

Dr. Keenan Lee
Geology Department
Colorado School of Mines
Golden, Colorado 80401

Remote Sensing Report 74-6

Submitted to:

Mr. Martin Miller, Technical Monitor
Principal Investigations Management Office
Code TF6
Johnson Space Center
Houston, Texas 77058

1 July 1974

GEOLOGIC AND MINERAL AND WATER RESOURCES INVESTIGATIONS IN WESTERN COLORADO, USING SKYLAB EREP DATA

Compiled and Edited

by

Keenan Lee

Contributors

R.M. Hutchinson
K. Lee
G.L. Prost
D.L. Sawatzky
R.W. Spoelhof
J.B. Thigpen

Remote Sensing Report 74-6

1 July 1974

CONTENTS

SIGNIFICANT RESULTS

Discovery of three major north-trending, throughgoing faults in the Front Range, previously mapped only as isolated segments, demonstrates the utility of space photography and may lead to reinterpretation of the Front Range tectonic style.

Faulting and alteration appear to be the most useful indicators of mineralization in central Colorado. These phenomena appear on Skylab photography as tonal lineaments and color anomalies.

Twenty - three lineaments have been mapped in the San Juan Mountains, the longest of which is 156 km long. Twelve lineaments intersect or are tangent to calderas. Intrusive domes are aligned along lineaments, but calderas appear to occur at the intersections of major lineaments.

Lineaments can be recognized on some EREP passes but not on other passes over the same area. The difference is attributed to solar elevation effects.

Bedding attitudes can be photogeologically estimated down to surprizingly low dips, on the order of 1-2°, and attitudes can be subdivided easily into quantitative groups.

The primary application of Skylab photography to geologic mapping in montane areas is clearly limited to regional mapping at scales smaller than 1:24,000.

DATA QUALITY

S190-A

There are six bands of S190-A photography: the green band covers 490-600 nm, the red band covers 600-700 nm, and two photo-infrared bands cover from 700-830 nm and >790 nm. There is also a color band and a color infrared (CIR) band.

Duplicate 70 mm positive transparencies were studied in stereo using the Bausch and Lomb zoom stereoscope at magnifications from three to fourteen power. At 3X magnification, all the photos are sharp and properly exposed. Reproduction quality is generally very good. This is also true at 14X except that the two photo-infrared bands are grainy and lack good spatial resolution.

The photo-infrared bands are best for outlining bodies of water or large streams. They also separate forest/consolidated rock areas from grassland/alluvium areas, and snow-covered from snow-free areas. CIR gives excellent detail in distinguishing verdant from water-stressed fields, fields from grasslands, grasslands and fields from forested areas, vegetation-covered from non-vegetated rock, rock from soil/alluvium, and rock of different colors. It does not, however, separate snow from cloud from light-colored barren rock. Bodies of water are

easily distinguished as black when relatively deep (e.g. - Dillon Reservoir), or blue when relatively shallow (e.g. - Cherry Creek Reservoir), and mottled when there is suspended sediment (e.g. - Elevenmile Reservoir).

The color band discriminates the same types of features as the CIR, but it is very difficult to distinguish types of growing vegetation. The color photos are best for distinguishing unvegetated rock of different colors and they are the only photos that show the subtle color changes between cloud/snow-covered and light-colored rocks.

The red band distinguishes snow/cloud from snow-free/cloud-free areas, field patterns, cultivated from non-cultivated areas, and forests/consolidated rock from grassland/alluvial material, although detail is lacking in vegetation-covered areas. The green band is good for discriminating snow and clouds from background. It poorly discriminates field patterns, vegetated from non-vegetated areas, and rock types, possibly due to poor processing, but more probably, to the extensive vegetative cover. (The green band was also studied outside of the primary interest area, with different results. In the Moab Quadrangle, southeast Utah (SL 2, S190-A, Track 34, 5 June 1973), the green band has good tonal contrast, making it superior to the two photo-IR bands for lithologic discrimination. This may be due to a general lack of vegetation in the area.)

Structure is most easily seen on CIR, color, and red bands.

On S190-A photographs at fourteen power buildings in towns (by a speckled appearance), two-lane roads (e.g. - West 44th Ave. in Wheat Ridge, Interstate 24 through South Park), and airport runways (e.g. - at Leadville, 4800 feet long, 175 feet wide) can be discriminated and objects as small as Golden Reservoir (approximately 800 feet diameter) and Interstate 70 (approximately 200 feet wide) can be identified.

S190-B

Positive transparencies 4 1/2-inch square were studied both in the monoscopic and stereoscopic modes (depending upon endlap), using the Bausch and Lomb zoom stereoscope at magnifications from three to fourteen power. Over the central Colorado survey area only color photography without endlap is available. The S190-B photos are easily viewed at three to fourteen magnifications, have sharp contrast, and are properly exposed. Reproduction quality is excellent.

The high-resolution color photography gives excellent discrimination of fields from grasslands, grasslands and fields from forested areas, vegetation-covered from non-vegetated rock, rock from soil/alluvium, rocks of different colors, bedded from non-bedded rocks, fractured from non-fractured rock, snow/cloud cover from light-colored rock, and bodies of water. Large throughgoing (regional or "geotectonic") structures are best observed at three power

magnification, while fairly small structures (e.g. - fracture systems in granite) are easily seen at fourteen power.

On S190-B photography at fourteen power, clusters of buildings in towns, large isolated buildings (e.g. - Carlton Gold Mill at Cripple Creek has an aluminum roof and is approximately 300x600 feet), and unimproved roads (e.g. - power plant road east of Leadville, approximately 30 feet wide including shoulders) can be discriminated and tailings piles and color anomalies approximately one mile in diameter (tailings at Alma or Cripple Creek; weathered pyrite at the Sweet Home Mine, Buckskin Gulch near Alma), islands as small as 300 feet diameter in lakes (e.g. - Electra Lake north of Durango and Elevenmile Reservoir), and linear features such as the paved portion of the runway at the Leadville airport (72 feet wide, 4800 feet long) or improved roads (e.g. - Interstate 285 between South Park and Morrison, approximately 50 feet wide including shoulders) can be identified.

S192

Positive transparency "screening film" (1-inch-wide strips) of Channels 2 (460-510 nm), 7 (780-880 nm), and 11 (1.55-1.75 μm) was studied in the monoscopic mode using the Bausch and Lomb stereoscope from three to fourteen power. When properly exposed and viewed at small magnifications, the film has very good contrast. The film

becomes grainy - that is, the spatial resolution is degraded - at approximately five to six magnifications. Channel 11 appears to have better contrast than Channel 7, and both appear better than Channel 2.

Channel 11 distinguishes clouds (white) from old snow (black), it separates rivers and bodies of water (black) from the background, and is very good for distinguishing structures and lithologies in lightly vegetated areas (area around La Sal Mountains). Channels 7 and 2 show the same features in correspondingly poorer contrast, except that old snow appears white, and water appears gray.

At 3X magnification lithologic contacts between the Jurassic, Triassic, and Upper Permian units in eastern Utah can be discriminated and features such as the goose-necks where the Green River joins the Colorado (as small as one to three miles across) can be identified.

Evaluation of Data Received

a. Skylab 2 S190-A photography taken June, 1973, generally has minor cloud cover (less than 20%), but has snow at all high elevations (over 11,000 feet). In most cases the snow degrades the quality of the photography, although some structural features that are expressed topographically are enhanced by the snow cover (e.g. - Mosquito-London-Weston Fault complex).

b. Skylab 2 S192 multispectral imagery, taken in June 1973, has almost no clouds, and snow only at high elevations (over 11,000 feet). The snow degrades the quality of the imagery.

c. Skylab 3 S190-A photogrpahy taken in August 1973 has very little snow, but cloud cover (generally greater than 60%) degrades the information content.

d. Skylab 3 S190-B photography taken in August 1973, has the same characteristics as the Skylab 3 S190-A photography.

DATA HANDLING

Non-enhanced Photography and Imagery

Photographic and imagery products received from NASA are generally interpreted as received, without further data processing other than magnification and stereoscopic viewing.

Because Skylab images contain more geologic information than can be interpreted at the original film scales, direct interpretation is not efficient, and magnification is necessary. The most effective method of interpretation is through high quality optical systems, rather than photographically enlarging the originals and using enlarged prints or transparencies; this avoids another generation or two of film degradation. Skylab S190A photographs have an original scale of about 1:2,850,000; 12X seems to be about the maximum magnification, to a scale of about 1:240,000. Skylab S190B photos will take similar magnification, from an original scale of 1:950,000 to about 1:80,000. The Richards MIM light tables, with a Bausch & Lomb 240R zoom stereoscope, are ideally suited to magnified stereoscopic and monoscopic photointerpretation.

As Skylab films contain more geologic information than can be interpreted at original scales, they likewise

contain more information than can be graphically represented at original scales. Therefore, photographic enlargements are also required to map the interpreted information, either directly onto the enlargements or onto clear overlays. A good method entails interpretation of low-generation contact positive transparencies under stereo (where available) magnification, with interpretive results transferred to clear overlays on enlarged transparencies or prints. The annotated images can then be transferred to topographic maps with the Bausch & Lomb zoom transfer scope.

At whatever enlargement, or under whatever magnification, the quality of film transparencies is superior to that of paper prints. However, in the ultimate interpretation step - field checking - transparencies are difficult to use, and prints are far handier (and cheaper). A good compromise is to annotate onto clear overlays, which can then be put onto prints for field use.

Data Enhancement

When developing prints of the S190-A and S190-B that will be used for structural analysis or slip masking, high contrast copies are easiest to work with. High contrast is obtained by using a high contrast film or by increasing the developing time. High contrast enhances linear features, which are usually expressed (due to topography) as dark vs. light areas.

Slip Masking

Positive-negative slip masking (Lee, 1972, 1973) can enhance linear features. Features are enhanced that trend from approximately 20-90° from the slip direction. Comparison of photolinears from a slip positive-negative mask with an original positive shows that some significant linears may be found in this manner, but that some are overlooked because of the blurring that accompanies slipping.

Direct Overlay Masking

Direct overlay positive-negative masking was undertaken using 9x9 inch positive and negative transparencies of Frame 17, Track 48, Skylab 2 S190-A taken in June, 1973. Transparencies were available from Bands 15 (700-830 nm), 08 (>790 nm), 06 (600-700 nm), and 10 (490-600 nm). Each positive was masked with the negatives from the three other bands, and each negative was masked with positives of the other bands, eight combinations in all. These were observed, and notes were taken as to which combinations were best for isolating certain features. Features most likely to be isolated are clouds, snow-covered terrain, bodies of water, verdent vegetation (ie. growing fields, streambed vegetation), grassland/alluvium, and forests/consolidated rock. Subdivision of lithologies depends mainly on structure and vegetation, and vegetation is variable from one locality to another (other factors, such as moisture, slope,

elevation, etc., affect vegetation more than rock type). Structure is seen as a textural, rather than tonal variation, and direct overlay masking damps textural features. Therefore lithologic discrimination is difficult.

Good contrast of features other than lithology is seen by masking the positive of Band 08 with the negative of Band 15. Topography is eliminated, snow and clouds are light gray, grasslands and alluvium are medium gray, forests and consolidated rock are dark gray, and water bodies are black.

Good contrast of features is also seen when masking the positive of Band 08 with the negative of Band 06. Snow, clouds, and water bodies are black, verdent vegetation is nearly white, grasslands/alluvium are medium gray, while forests/consolidated rock are dark gray (the negative of the red band gives the same information, except water bodies are white).

It appears that direct overlay positive-negative masking provides little unique geologic information.

Color-additive Viewing

Color-additive viewing (CAV) was carried out using the International Imaging System (I^2S) Mini Addcol and Frames 106 and 107 from Track 48, Skylab 3 S190-A taken August, 1973. Film chips used were the 70 mm positive and negative transparencies of the two photo-infrared bands, the red and green bands, and the positives of the color and CIR bands.

Three combinations were investigated for enhancing color anomalies. To enhance red rock, possibly associated with mineralization, set the color positive on clear light at an intensity of 9 (on scale of 0 to 9, with 9 maximum), the positive of the CIR band on blue at 7, and the negative of the red band on clear at 9. The second combination uses the positive of the color band on clear at 9, the negative of the red band on green at 6, the negative of the photo-infrared on blue at 9, and the positive of the red band on red at 5. This makes all rock/soil varying shades of red. The third alternative is true color.

Another type of color anomaly is the light-colored rock in an area of darker rocks (e.g. - Tertiary intrusions into Permian-Pennsylvanian sediments along the crest of the Mosquito Range in the southern Leadville mining district). The first and third techniques mentioned above do a fair job of isolating light-colored rocks.

The third type of color anomaly is the dark-colored rock in a generally light-rock area (e.g. - Miocene breccia and phonolites surrounded by pink Precambrian granites in the Cripple Creek area). It is very difficult is isolate this type of anomaly because most vegetation cover, as well as shadows, are also dark on the photography. Preliminary work shows the color band is best for finding these anomalies.

Density Slicing

Density slicing of positive or negative transparencies from any band may be used effectively to isolate light or dark color anomalies (anomalous red areas are usually a medium gray on a black/white density slice, and are not anomalous. Slices may be made using high contrast film and varying the f-stop, exposure, or developing time during copying.

Diazo color-additive density slicing was tried on Skylab 3 S190-B photos. The process involves color coding of gray levels on the original. Negatives were made from the positive of the red band. Density slices were made using high contrast film and varying the f-stops on the enlarger, with exposure and developing time constant. f/5.6 gave the darkest and f/22 gave the lightest negative density slice. The diazo film produces color only in the dense (dark) areas of the transparency (in this case, the negative). Using only negatives, a four-colored image may be produced (Fig. 1a).

Black and white negatives were made from frames 38 and 39 (color transparencies), and then contact positives were made (on normal contrast film) from the darkest negative. The density slice color code scheme may be seen in Figure 1b. Using both positives and negatives, a six-colored density image may be produced. Additional densities may be sliced by varying the exposure and developing times.

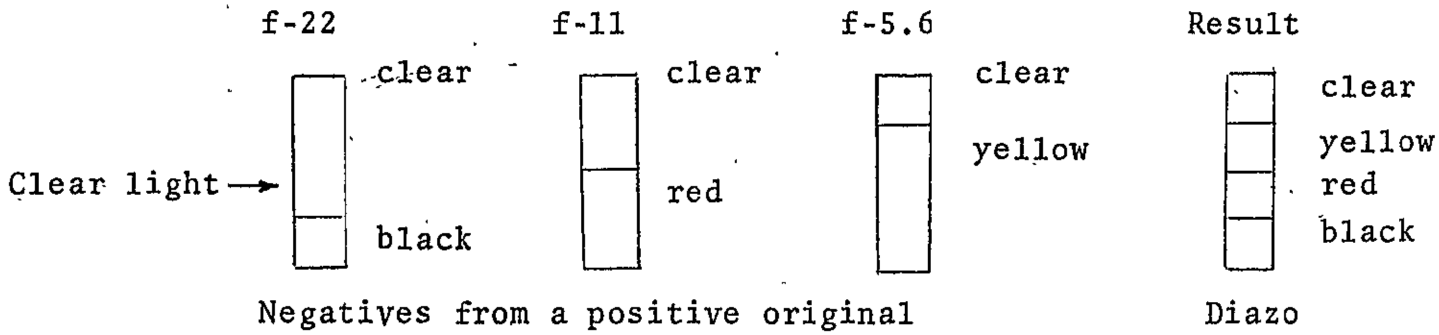

Figure 1a. Schematic of a diazo four-color density slice image produced from negative transparencies.

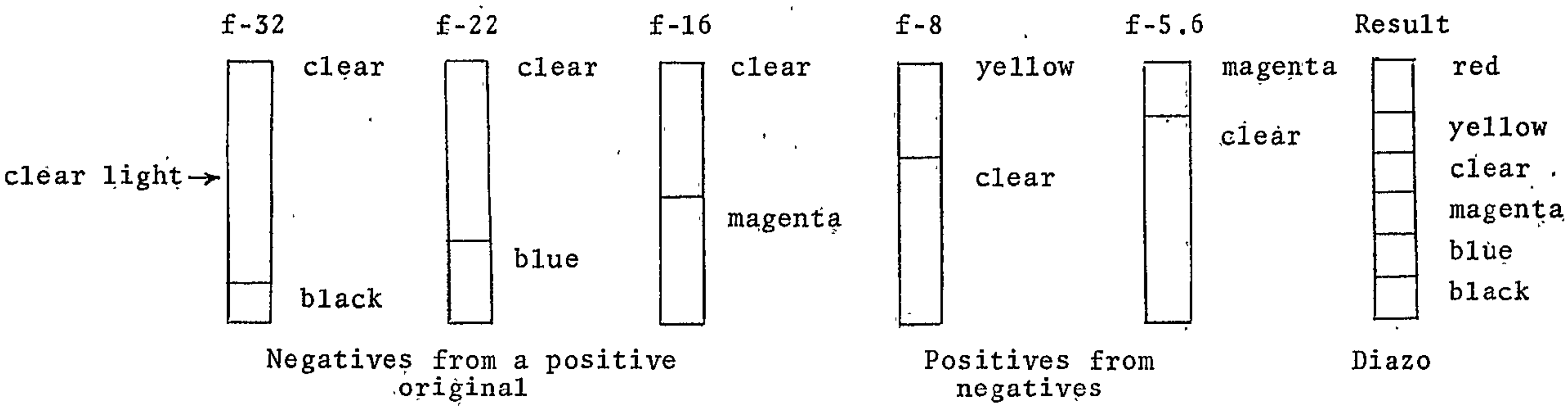

Figure 1b. Schematic of a diazo six-color density slice image produced from negative and positive transparencies.

Color coding of density slices gives inconsistent results due to the change in radiance of an object corresponding to changes in the geometric relationship (aspect angle) between the camera, object, and source of illumination. For example, a lake (smooth surface) will appear light when between the camera and the sun, and dark when the camera is between the sun and the lake (Figure 2). Because of this relationship,

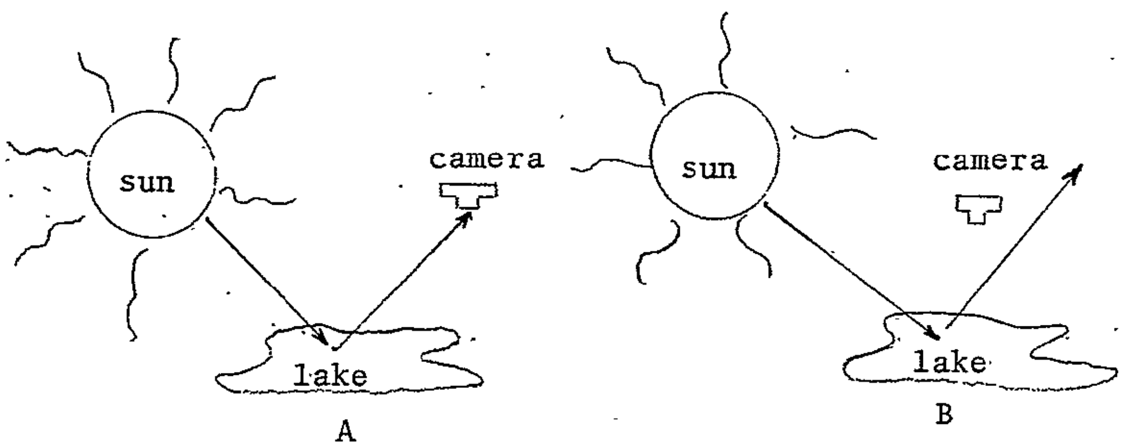

Figure 2. Change in reflectance of a lake corresponding to a change in the geometric relationship between camera, object, and illumination source. In A the lake appears bright, while in B the lake appears dark.

bodies of water were sliced at three densities. The same principle, although opposite in sense, can be extrapolated to rocks, soils, and vegetation (rough surfaces). Red sandstones of the Maroon Formation near Antero Reservoir were on one slice, while outcrops of the same red sandstone were on another slice near Ruedi Reservoir. It is also probable that one density slice contains many different objects of interest. For example, the Maroon Formation near Antero

Reservoir was in the same slice as the water in Elevenmile Reservoir and most of the grassland in South Park.

There is, however, a tendency for vegetation to be the same density from one region to another, and the diazo process may be good for lithologic discrimination in a fairly uniform geologic area. For example, all the outcrops of volcanics in southern South Park are on the same slice (this may be a result of uniform vegetation cover). The diazo process is capable of enhancing the contrast between light and dark areas on a photo or image, and thus may make topographically expressed linears easier to see.

GEOLOGIC STRUCTURES

This study covers (1) the ability to recognize geologic faults and folds, (2) the relationship of long linears to the regional fracture system, and (3) the relationship of the trends in the set of all linears to the rock joint systems.

Central Colorado Test Site

The Central Colorado Test Site lies at the intersection of Skylab Tracks 34 and 48. Specific areas covered are the Rampart Range, southern Front Range, Canon City Embayment, Royal Gorge arch, and eastern South Park. The geologic provinces consist of the Pikes Peak batholith, metamorphic rocks south of the batholith, and the folded and faulted Paleozoic and Mesozoic sedimentary rocks around the margin of the southern Front Range and Canon City Embayment. Royal Gorge arch is a metamorphic terrain, including the Blue Ridge area, flanked by folded Paleozoic and Mesozoic strata. Eastern South Park consists of folded Mesozoic and Tertiary strata and a metamorphic terrain.

Data

Photography of Skylab 2 (June 1973) and Skylab 3 (August 1973) was available for Track 48 only. Photos from S190A black-and-white bands, color, and color infrared were evaluated.

Several published geologic maps are available for ground truth acquisition. In addition, there are many dissertations and theses of the area. These sources are supplemented with abundant private field notes.

Aircraft photography flown in support of Skylab, ERTS, and the Bonanza Project was also used. Mission 261 is low-sun angle, black-and-white IR, RC-8 photography, flown as an underflight to Skylab 4. Missions 205 and 211 are color (RC-8) and color IR (RC-8 and Zeiss). On the 9 in. by 9 in. format, this photography is at a scale of 1:100,000.

Relief models of the area (1:250,000) were painted white and photographed at various sun azimuths at low sun elevation in order to enhance dominant topographic trends. This information is low resolution, but because only topographic relief is conveyed, the information is distinct and free of other confusing elements.

It is clear from these studies that the multi-scale approach yields the most geologic information. Each scale of photography has its distinct features and provides unique information for the whole, whether for evaluation of small geologic features or for interpretation of large features.

Data Recommendations

Because of the extreme variability of cloud cover, seasonal changes in vegetation, the sun's declination, Skylab data are degraded because of the few overflights of

this area. In future missions of the Skylab-type, photographic overflights should be scheduled to take the best advantage of these variations.

In this area, cloudiness over mountainous areas is often a function of the prevailing westerlies and high elevations. In our experience, such local instabilities are decreased or non-existent after the passage of a cold front in all seasons. Local and regional cloudiness can be selectively avoided by observing the regional weather patterns.

For maximum shadow enhancement of structural features, times of optimum sun elevation and azimuth should be used (Sawatzky and Lee, 1974). The effectiveness of sun attitude is demonstrated in this study. Three new north-trending linear features in the Rampart Range were discovered on SL-2 photography and not seen on SL-3 photography. This is attributed to the favorable sun attitude of SL-2, when the sun azimuth was 92° and sun elevation was 40°, whereas for SL-3 the sun azimuth was 132° and the sun elevation was 57°. The reverse was true for linears in the Royal Gorge arch, which trend N 80 E. Linears with greater relief (such as in the Dome Rock area, N 10 E) are visible on both SL-2 and SL-3 on all bands. Linears oriented 45° to the sun azimuth are recognizable on the best imagery of both missions, such as in the Blue Ridge area.

Best Photography Characteristics

The features of Skylab photography that make it preferable to ERTS imagery are its full stereoscopic capability, higher resolution, and better color rendition. These features increase structural information that is very dependent on topographic effects, vegetation differences, soil and/or rock color contrasts. To this is added the synoptic view of orbital photography.

Of all bands, color and color infrared are best for different reasons. The enhancement of linear features depends very much on shadows. Where dark green vegetation masks the effect of shadows on color photography, shadows and vegetation are distinguishable on color IR. This is well shown on the SL-2 photography. Thus, while the unfamiliar color rendition of color IR will not supplant the more familiar true color photography, it will be useful in the interpretation of fractures.

Color is superior to color IR in the interpretation of the folds along the Southern Front Range in the Canon City Embayment. This is demonstrated on SL-3 photography. The reason lies in high spectral contrasts of three sedimentary formations involved in the folds. The Fountain Formation has a reddish-orange soil with little grass and few trees. The Dakota Group is heavily covered with dark-green Utah juniper, some pinyon pine, and Gambel oak brush. The Niobrara Formation has a light-gray to cream soil with

sparse grass and few trees. On color images the boundaries between these formations are sharp, and mapping of the folds is easiest. On color IR the spectral contrasts are low and not useful. In addition, Band 10 shows no contrast between Fountain and Dakota, but Niobrara recognition is good. Band 6 shows some distinction between Fountain and Dakota in the medium gray range, and Niobrara is light gray. Bands 8 and 15 are not useable because of very low contrasts and severe graininess. Table 1 gives an evaluation of the recognition of certain features on SL-2 and SL-3 photography.

New Geologic Information

The unification of one aspect of regional geology by orbital imagery is reflected in some discoveries in the Rampart Range. One strong, north-trending linear was first recognized on ERTS image 1172-17141 (January 1973). This linear was again recognized on SL-2 photography, with the addition of two less prominent linears subparallel to the first. On high-altitude photography, these linears are unmapped extensions of the Ute Pass fault and two other major faults bounding the Manitou Park outlier west of the Rampart Range as described by Harms (1959). The easternmost linear transects the Rampart Range from Manitou Park northward and passes into the Perry Park faults on the east side of the range (Harms, 1959, Plate 1). The central fault

TABLE 1 - Recognition values of lineaments in several areas of the Central Colorado Test Site as a function of Skylab mission and band for magnified stereoscopically-viewed 2 in. by 2 in. positive films. G - good, F - fair, P - poor, N - none, c - cloudy.

A. SL-3 S190A, frame nos. 106-108

Band	Area: Rampart Range	Royal Gorge	Dome Rock	S. Front Range	Blue Ridge	E. South Park	Red Creek Folds	Comments
CIR	GC	G	G	GC	G	NC	P	better than color
color	PC	G	G	GC	G	NC	G	dense positive
10	GC	G	G	GC	G	NC	F	
6	P	G	G	GC	G	NC	F	
8	P	P	G	P	P	NC	N	low contrast
15	F	P	G	P	P	NC	N	low contrast

B. SL-2 S190A, frame nos. 17-19

CIR	G	P	G	NC	G	FC	NC	very blue, crisper in detail than color
color	G	P	G	NC	G	FC	NC	
10	G	P	G	NC	G	FC	NC	
6	G	P	G	NC	G	FC	NC	
8	G	P	G	NC	P	NC	NC	
15	G	P	G	NC	P	NC	NC	

(in part, the Devil's Head fault of Boos and Boos, 1957, Figure 9) trends northward from the monoclinal axis along the east margin of Manitou Park (Harms, 1959, Plate 1) across the range into faults in the Jarre Canyon area (Hutchinson, 1960; Johnson, 1961). The westernmost fault is paralleled by many sandstone dikes and extends northward (Hutchinson, 1960, Figure 1) into the Kassler Quadrangle where it is known as the Bear Creek shear zone (Scott, 1963). These three major faults have been mapped only in isolated parts. Orbital imagery has provided a unifying synoptic view which may bring about reevaluation of the tectonic style of the Front Range.

Four parallel linears trending N 45 E in the Southern Front Range transect the Precambrian rocks and cut folded Paleozoic and Mesozoic sedimentary rocks on both flanks of the range. That these linears extend into known faults and cross the block uplift is a new discovery that will modify the future studies of the tectonic style of the area.

The Skagway linear extends from the offset between Sheep Mountain and the Milsap Canyon thrusts on the west side of the range northeastward some 15 miles into the Pikes Peak intrusive center. The Adelaide fault (Boos and Boos, 1957, Figure 11) extends from the transverse fault at Felch Creek on the west side of the range for about 15 miles into faults offsetting lower Paleozoic strata in the lower Beaver Creek area on the east side. Two shorter

linears lie in between these, one of which extends about 10 miles into the Pecks Camp mineralized area on East Beaver Creek.

The Precambrian core of the Royal Gorge arch has been mapped only with respect to lithology, and the existing map (Heinrich, 1948) shows only ENE trending metamorphic layering. Three prominent topographic linears are visible on SL-3 photography. As found in other areas, these linears extend into and transect upturned strata on both flanks of the uplift. The relationship of these linears to faults can be clearly demonstrated.

In eastern South Park is an example of the discovery of linears extending into known faults. Two major faults cut obliquely across folded Tertiary strata in the San Isabel syncline (Sawatzky, 1967). They are parallel and trend N 30 E. Two linears extend NE from the known faults and cut across the Elkhorn thrust and into the Precambrian rocks of the thrust. One interpretation is that the oblique faulting is post-thrusting.

Linears and Joints

Most prominent linears are related to faults, as discussed above. The origin of the ubiquitous short linears on orbital imagery has been investigated with the search for a relationship with the regional joint systems. Since the area for which there are available ground

measurements, the southern Front Range, is cloud-covered on SL-2 and SL-3 photography, ERTS imagery has been examined in anticipation of clear SL-4 photography.

The first approach was to measure the azimuths of all linears in an image, usually 350 to 400 in numbers. Trend analysis reveals several closely spaced but significant trends, which are difficult to correlate with joint trends for the region. The difficulty appears to lie in strongly localized trends probably resulting from quite variable erosional enhancement. Ground truth is available for analysis for four small areas. The analysis of the southern Front Range area has been done.

Three joint trends were determined from approximately 500 field measurements in the Phantom Canyon: a weakly-displayed N 52-62 W (WNW) trend, and two prominent trends at N 17 W - N 12 E (N-S) and N 66-76 E (ENE). Mission 261 low sun-angle photography (sun elevation = 10°, sun azimuth = 135°, scale = 1:100,000) displays three trends of ubiquitous short linears. The N 53-75 E trend contains few short linears, but includes the Skagway and Adelaide faults, and corresponds to the strong ENE joint set. Another set of linears trends approximately N 14-20 E, includes the Mountaindale fault, and falls within the strong N-S joint trend. This is a very prominent set of linears on the relief map under southwest illumination. A third linear set trends from N 16-31 W and most likely also

corresponds to the broad N-S joint trend. The major fold axes east of the range parallel this trend. This trend is prominent on the relief map under south illumination. Joint analysis has not distinguished these NNW and NNE trends that are so prominently displayed as linears on photography. A fourth linear set is weakly displayed in the range of N 68-81 W and probably corresponds to the WNW joint trend.

The short ubiquitous linears on the relief model of the southern Front Range were measured and combined for four illumination directions 45 degrees apart. The resulting trends are, N 62-63 W, N 14-22 W and N 30-50 E, which correspond well with the joint sets. The linear trends determined for the area from the ERTS image (sun elevation = 23°, sun azimuth = 150°, scale 1:1,000,000) were greater in number and less distinctive. In general, the main trends are WNW, NNE, and ENE. The broad N-S linear trend was not recognized, and the other trends were not strong. The high sun angle (23 degrees) greatly diminishes the effect of shadow enhancement of topographic linears, as few topographic slopes are greater than 23 degrees. This does not completely explain the inability of the orbital imagery to strongly reflect the regional joint systems, as the relative importance is not fully known.

APPLICATION OF EREP DATA TO REGIONAL GEOLOGIC MAPPING

Preliminary regional geologic studies using Skylab photography have been done in some detail in the Moab, Utah area, and in lesser detail in central Colorado, especially from South Park southeast to the Wet Mountains. In general, the Colorado investigations are hindered by vegetation, local snow, and variable, but often widespread, cloud cover.

Data Evaluation

Data evaluation has been mostly confined to the 190B color photography, where available, and the 190A color and CIR photography, with some comparisons with other 190A bands. Brief comparisons with ERTS-1 imagery have been made and will be continued in more detail. The 190B photography is superior, in those areas investigated, to any other Skylab or ERTS-1 data for general photogeologic interpretation, although much of the same information is also present in the 190A color and CIR photography. This superiority is due to the higher resolution, detectability, and recognizability aspects of the 190B photography, which allow smaller geologic elements to be better interpreted. The best 190A band for general photogeologic interpretation, in the areas investigated, is the color band, followed in

utility by the CIR. No significant geologic features were uniquely interpretable, in this preliminary investigation, from the other 190A bands to indicate greater utility than the color or CIR. The black and white infrared 190A photography is excessively grainy; the 190A CIR photography is somewhat more grainy than the color.

Interpretation Techniques

The main interpretation technique used was stereoscopic examination, both with a Bausch and Lomb 240 zoom stereoscope-light table and with a simple mirror stereoscope on a light table. The mirror stereoscope interpretations are easier and to some extent better than those with the zoom stereoscope, especially for regional investigations where the synoptic aspect of the photography can best be utilized. The limited field of view of the zoom stereoscope hinders full utility of the synoptic aspect, although the zoom capability is good for point interpretations.

Annotations have been made on acetate overlays of 190B 2X positive transparency enlargements (scale about 1:472,000) and 190A 4X positive transparency enlargements (scale about 1:711,000). Even with the enlargements, there is insufficient room to annotate all data that can be interpreted. Other techniques being tried include rapid preliminary interpretation annotated on an overlay, followed by a more detailed interpretation and simultaneous visual transfer to an acetate

overlay of an enlarged photographic print at a scale of about 1:250,000. This is a very time-consuming process but best preserves the precise spatial arrangement of interpreted data. Transfer of data from an annotated overlay of the positive transparencies to an enlarged photographic print as above has been attempted with a Bausch and Lomb zoom transferscope but considerable detail is lost in the process. The annotation and posting process is one of the biggest problems with Skylab interpretations.

Study Results

In the Moab area, excellent exposures allow tracing of stratigraphic contacts in considerable detail. Photogeologic unit contacts were selected without previous reference to the established stratigraphic terminology, as if the area were completely unknown. The synoptic aspect of the photography greatly assisted in this interpretation by allowing rapid visual comparisons with contacts mapped in other parts of the area; with conventional aerial photography this process often requires going from one photograph to another or several others. Most contacts could be interpreted from 190A color photography (positive transparencies) in greater detail than could readily be annotated; even more detail is present in the 190B photography, allowing more subdivisions and continuity. Subsequent comparison with a published geologic map

(Williams, 1964) indicated that many of the contacts of the geologic map had been interpreted from the Skylab photography and that others could have been, particularly with 190B photography. Comparisons were less favorable in highly complex areas, especially with small features, and in densely vegetated areas such as the upper slopes of the La Sal Mountains.

Much of the structure of the area around Moab could be readily interpreted from 190A color photography; again, more detail is present in the 190B photography, allowing easier and, to some extent, more accurate interpretations. Bedding attitudes were estimated from the 190A color photography by standard photogeologic techniques, but, in this case, without any previous reference to published attitudes or concern with estimation of the relief exaggeration present in the stereo model. The estimated dips were arbitrarily divided into three dip groups, ranging from the most gentle to the steeper dips of the area. Subsequent comparisons with dips on the geologic map (Williams, 1964) indicated that the category of most gentle estimated dips corresponds to mapped dips of 1-6°, with an intermediate category of about 3-15°, and a steeper category of about 10-30°. Comparison of strike directions was generally quite favorable. It is anticipated that greater experience with the stereo model of the Skylab photography could lead to refinement of this technique. The 190B photography would

probably give better results, with less indecision about problem attitudes. Lee and others(1974) were able to recognize bedding attitudes as gentle as 2° dip on 190B photos. The ability to differentiate these low dips, especially on the 190A photography, was somewhat surprising and should have great significance in regional mapping and structural interpretation. These estimations were made with a simple mirror stereoscope, without additional magnification. The possible advantages or disadvantages of the Bausch and Lomb zoom stereoscope for dip estimation have not yet been investigated in detail. The initial impression was that the relief exaggeration of the Skylab photography stereo model would be too low to allow much differentiation of estimated dips. In practice, the advantageous factors of near-orthographic photography and the synoptic view greatly assist in estimation of dips by presenting a uniform view of a large area, with uniform tip or tilt distortions, if any, and by allowing rapid visual comparison of estimated dips in other parts of the area. In contrast, with conventional aerial photography, similar comparisons often require going through perhaps several individual photographs, each of which could have varying tip and tilt distortions. Of course, greater relief exaggeration can be acquired with conventional aerial camera systems, but this greater relief exaggeration can be a problem, especially in areas with considerable topographic relief. It is likely that without

good exposures of bedding surfaces of considerable areal extent, dip estimations would become more difficult and less accurate as exposures become poorer and bedding surfaces smaller.

Many faults could be interpreted on the 190A color photography as visual traces with stratigraphic or topographic offset. Other probable faults could be interpreted with more study of the photography and better familiarity with the local stratigraphy, but some complex, small, or partly concealed faults mapped in the field probably could not be interpreted from Skylab photography. For a fuller discussion of the expression of faults on Skylab photography, as well as a treatment of geologic folds see Lee and others (1974).

Thick, relatively uniform vegetation tends to obscure geologic features. This was especially noted on the higher slopes of the La Sal Mountains, where little geologic information could be interpreted from the relatively dark photographic tones, except for the general outline of an intrusive.

In central Colorado, only scattered observations have been made, mostly on 190A positive transparencies. Interpretation of Skylab photography is relatively difficult here, mainly because of obscuring effects of dense vegetation, but also because of variable snow cover and often widespread scattered cloud cover. In areas of minor vegetation cover,

as in northwest and southeast Colorado, favorable geobotanical associations may facilitate photogeologic interpretation. In the mountainous, mostly densely vegetated area of central Colorado, only very general contacts, such as contacts between sedimentary/igneous-metamorphic, volcanic/igneous-metamorphic, or, in some cases, volcanic/sedimentary rocks, can be readily interpreted. The igneous-metamorphic Precambrian complex can be discriminated, where sufficient areal exposures exist, by its distinctive fracture pattern and by its resistance to erosion. Good exposures are required for differentiation within sedimentary rock units. Little such differentiation is possible in the more densely vegetated areas, except where units have pronounced and variable topographic expression. In sparsely vegetated areas with good exposures, as in the Canon City embayment, several sedimentary rock units can be differentiated, mostly by topographic expression and, to a lesser degree, by contrasting color tones. Some inferences as to probable composition of the rocks can be made by use of these same criteria.

Several major faults can be interpreted from Skylab photography in central Colorado, but in the densely vegetated areas, only major faults with significant topographic expression can be readily interpreted as distinct from a general category of lineaments. Further investigation and familiarity with the photography and the area may

allow interpretation of less well expressed faults. Numerous, often well-expressed lineaments are present on much of the Skylab photography and ERTS-1 imagery. Many of the better-expressed folds are obvious on the Skylab photography. Estimates of bedding attitudes have not yet been done in any detail here, but in general, such estimates are more difficult in the densely vegetated terrain.

Numerous geomorphic landforms can be recognized on the Skylab photography, including such obvious features as hogbacks, cuestas, mesas, alluvial fans, etc., and less obvious features such as lateral and terminal moraines, cirques, pediment remnants, suggestions of erosion surfaces, igneous dikes, etc.

New Information

New information is, so far, restricted to the demonstrated feasibility of estimating bedding attitudes, with subdivision into different, although presently overlapping, categories, and carrying this photogeologic dip estimation down to dips of 1-5°, including detection of 1° dip reversals on a regional dip slope of 3-5°. This was done with a simple mirror stereoscope in an area of very good exposures on 4X positive transparency enlargements of the 190A photography. Further investigation is planned.

Further Study

The main thrust of planned future work will involve an investigation of the tectonic significance of lineaments interpreted from Skylab and ERTS-1 images. The planned primary study area includes central and western Colorado and eastern Utah. The study will begin with interpretation and annotation of lineaments on Skylab and ERTS-1 images, and transfer to base maps at scales of 1:500,000 and 1:250,000. Comparisons will then be made with lineaments interpreted from shaded plastic relief maps, as well as available geological, geophysical, and previous lineament studies. Representative lineaments and individual study areas will be selected for further study with other remote sensing and field techniques. Remote sensing methods will involve mainly photogeologic interpretation of conventional aerial photography, both now at CSM and some to be acquired in the future. Other remote sensing methods such as LSAP, SLAR, and thermal infrared imagery will be utilized where available. Some aerial reconnaissance with a light plane is planned for selected lineaments, to be followed by field studies, mainly large-scale geologic mapping, but possibly including geophysical surveys and local joint studies. The entire investigation will focus on the expression, origin, and tectonic significance of regional lineaments, in sufficient detail to help explain,

and possibly use, lineaments in regional geologic investigations.

An attempt will be made to relate regional lineaments to tectonic elements, as well as with economic factors such as metallic mineral, hydrocarbon, and geothermal resources.

Several secondary study areas will be selected for a less detailed evaluation of lineaments in differing geologic terranes.

EVALUATION OF SKYLAB PHOTOGRAPHY FOR DETAILED GEOLOGIC MAPPING

This is an evaluation of the use of photography in detailed geologic mapping in an area of high relief. The area under consideration is about 40 square miles in the San Juan Mountains of southwestern Colorado (geology of this area is described in Spoelhof, 1974). Low- and high-altitude color and color infrared aerial photography, black-and-white ERTS imagery, and Skylab color photography were examined to determine the accuracy of geologic mapping with each type of image. In particular, the questions asked during examination of the photos were: 1. Can significant details of the geology in the area be seen? 2. Can more details be seen than are recognizable on standard black-and-white aerial photographs? 3. Does use of the remote sensing data add to the speed with which mapping can be accomplished?

The examination of the images and the answers to the above questions are from the point of view of a field geologist who lacks training in remote sensing. Thus, this report is a subjective evaluation of the usefulness of images as tools for field mapping. This report should be of value to other geologists who wish to increase the accuracy and efficiency of their field work.

Low-altitude Black-and-White Aerial Photography

It was desired to construct a geologic map of the study area at a scale of 1:24,000. The mapping was originally accomplished by plotting observations on 1:20,000 U.S. Forest Service aerial photographs. The photographs were primarily used to pinpoint station locations and to map geologic structures and lithologic contacts between station points.

The main difficulties encountered in using the black-and-white photographs were: 1. Inability to discriminate aspen trees from surrounding grass-covered areas, 2. Inability to discriminate between limestone and sandstone outcrops, and 3. Inability to map any geology in areas of extensive tree cover. This latter difficulty was partially alleviated by using larger scale (1:10,000) black-and-white enlargements.

Low-altitude Color Photography

Near the end of the project, NASA Mission 213 color prints were used in the field as an aid to mapping on black-and-white photos. Initially, the color photography was used only to discriminate yellow aspen trees from surrounding grey-green grass areas, and so allow for more accurate station locations. It was noted, however, that

it was possible to discriminate large areas of grey limestone units that are interbedded with tan-weathering sandstone. It was thus possible to perform rapid studies of the distribution of gross rock types. In addition, since the limestone units are considered to be time-stratigraphic units, the mapping of limestone units means that it was possible to map time lines on the color photographs.

Since the black-and-white and color photography are nearly the same scale (1:24,000), no lineaments were recognized on the color photos that had not already been noted on the conventional photographs.

High-altitude Color Photography

Color photography from NASA Mission 248 proved very useful for rapid mapping of sedimentary rocks and geologic structures. Significant details that could be seen on the low-altitude photographs could also be seen at the scale of the high-altitude photography (1:100,000). Additionally, several lineaments were recognized on the smaller scale photography than had been previously noted. The lineaments may reflect faults that were not recognized in the field, but should have been checked.

It is recommended that the high-altitude photography be examined and interpreted before beginning any detailed

field mapping. The scale of the photography allows for rapid examination of a rather large area on a single photograph, photogeologic interpretation can delineate areas were ground work is needed, and lineaments that should be checked during the field work are expressed on the photos.

ERTS Imagery

ERTS imagery does not appear to offer advantages for detailed field mapping in mountainous areas. Because relief is very high in the study area, drainages are controlled more by topography than by lithologic changes. The scale of the ERTS imagery (1:1,000,000) is small, and the imagery cannot be used to delineate small topographic changes that reflect changes in the bedrock geology.

Examination of ERTS imagery of an area south and west of the San Juan Mountains, however, showed that the imagery can be useful for geologic mapping in areas of low topographic relief. Nearly all the lithologic contacts on the state geologic map (1:500,000) could be recognized on the ERTS imagery. No contacts could, however, be traced from areas of low relief into mountainous areas.

ERTS imagery is not recommended for geologic mapping at scales of 1:24,000.

Skylab Photography

Double enlargements of Skylab color transparencies of the study area were examined briefly. The area with which the investigator is most familiar was, unfortunately, completely snow covered at the time the photographs were taken. Only a topographic change at the top of pre-Pennsylvanian sediments could be seen.

In areas south of the study area, where there was no snow cover, the Skylab data showed many significant details of the geology. In particular, the photos clearly distinguish upper Paleozoic redbeds from underlying light-colored rocks. The light-colored rocks can also be distinguished from Precambrian metamorphic and igneous rocks by the presence of joint patterns in the Precambrian rocks. All areas of outcrop can be easily distinguished from vegetated areas.

The primary limitation of the Skylab imagery is the small scale of the original photos. At that scale (~1:1,000,000), only major geologic features can be mapped, and then with not very great accuracy. Skylab photography is, however, useful for the field geologist who is working on a detailed mapping problem, in that the photos allow for rapid extension of major geologic structures outside a small study area. It should not be anticipated that Skylab data will yield any additional information about small areas.

Summary

The most efficient way to carry out a detailed field-mapping problem in a previously unknown area would be to: 1. examine and interpret NASA high-altitude color aerial photography to obtain gross structural and lithologic patterns; 2. perform detailed photogeologic interpretation of NASA low-altitude color aerial photography to verify and expand the detail of the geology observed on the high-altitude photos, and establish working time-stratigraphic units; 3. use the low-altitude photography as an aid to field work; 4. use orthophotos or greatly enlarged Skylab photos to aid in compiling the field data and photo interpretations onto topographic maps, 5. extend local geology into a regional summary by using Skylab data. Such a procedure would produce the most complete coverage of a small study area, and all significant details will have been examined. Less time would be required in the field since prior photo interpretation would have delineated areas that need to be checked in the field.

The primary utility of Skylab photography for geologic mapping in montane areas is clearly limited to regional mapping at scales smaller than 1:24,000.

APPLICATION OF EREP DATA TO MINERAL EXPLORATION

Objective and Rationale

The objective of this research is to utilize and evaluate Skylab EREP data, and to a lesser extent, ERTS and aircraft data, to locate indicators of mineralization in central and southwest Colorado. The reason for such a study is that it is economically more desirable to survey large areas for potential mineralization by remote sensing than by conventional ground surveys. The advantages of satellite photography and imagery are the synoptic view, repetitive coverage, accessibility to remote areas, and relatively low cost. Despite the desirability of locating potentially economic targets quickly and inexpensively, it must be stressed that field work is always required for verification; it is merely hoped that needless field work may be eliminated.

Indicators of mineralization that can be seen on satellite images are structural features and anomalous colors. "Anomalous", as used here, means a local feature that deviates from a regional uniformity; a feature considered capable of being associated with commercially valuable mineral deposits. Vegetation patterns may be indicators of mineralization, although preliminary study

shows they are probably not significant. This research is based on the assumption that indicators of mineralization can be seen on multiband, color, and color-infrared satellite photography, and on multispectral satellite imagery. During the course of the study this premise will be either proved or disproved.

Study Areas

The area being studied for potential targets is outlined by Frame 17, Skylab 2 S190-A (multiband) photography from Track 48, 11 June 1973, and by Frames 106 and 107, Skylab 3 S190-A from Track 48, 4 August 1973. The area is also covered by Frames 38 and 39, Skylab 3 S190-B (high resolution) photography from Track 48, 4 August 1973; by Frame 172-17141, ERTS-1 imagery from 11 January 1973; by Frame 154-17143, ERTS-1 imagery from 24 December 1972; and by several aircraft underflights, most notably NASA missions 205, 211, 213, and 235. The entire survey area covers approximately 18,000 square miles (46,800 km^2) of central Colorado (Fig. 3).

The S192 is an integral part of the Skylab experimental package, yet there is no S192 coverage of the central Colorado survey area. Therefore it is felt that an area with a wide variety of landscapes, lithologies, and vegetation types that has S192 coverage should also be evaluated. In addition to the survey and target areas mentioned above, a

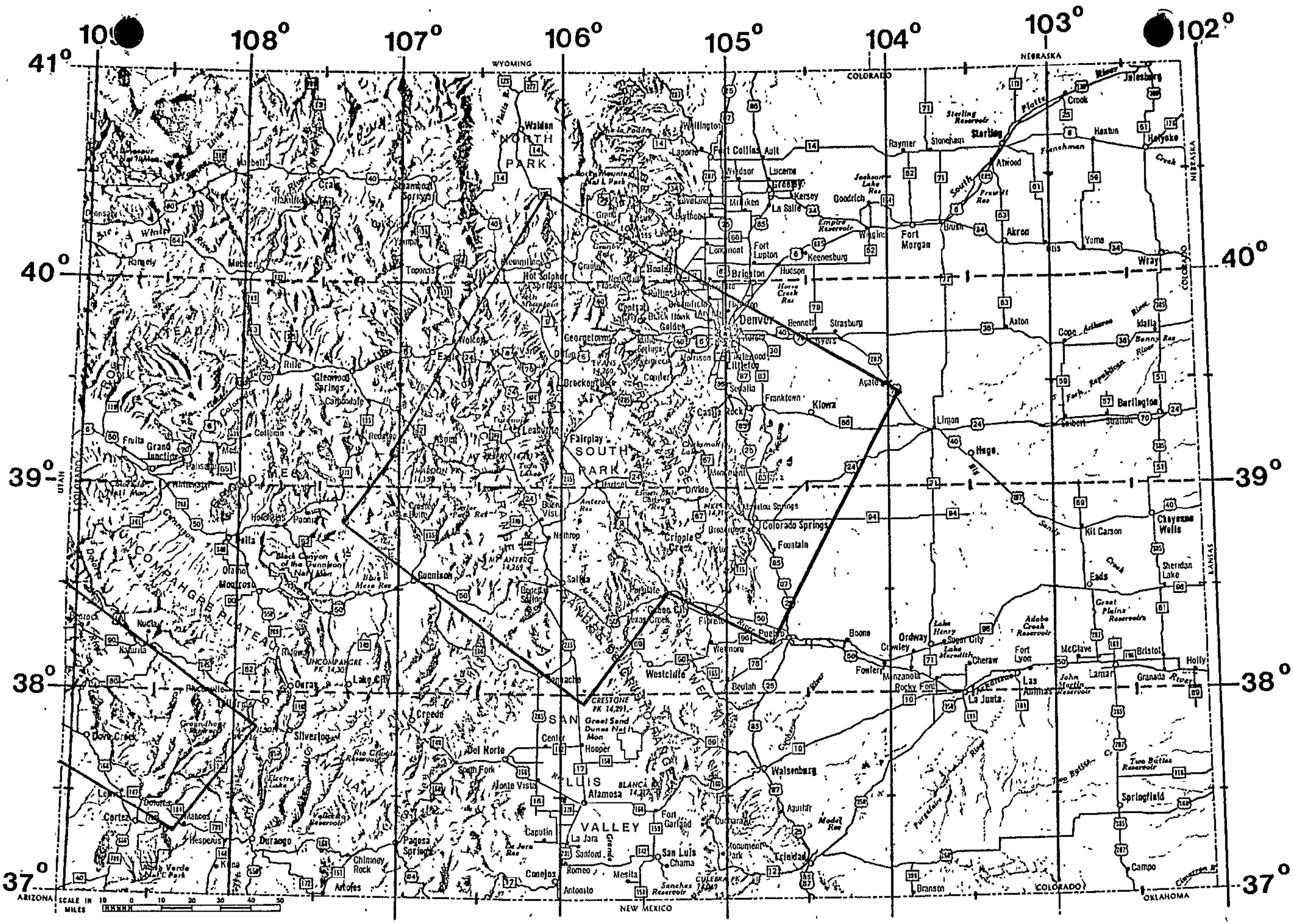

Figure 3. Central Colorado Survey Area; Southwest Colorado Test Site

southwestern Colorado test site has been designated for the evaluation of the S192 multispectral scanner (Fig. 3). The area in Colorado Covered by the S192 is approximately 2800 square miles (7,280 km^2).

Results to Date

The geology of the Leadville and Cripple Creek mining districts was studied as typical of the kinds of mineralization that can occur in central Colorado. At the same time, the Skylab photos covering these areas were observed in an attempt to correlate geology from maps to the photographs. Each area was checked on the ground to identify exactly what was interpreted from the photography. The two control districts were analyzed to determine which geologic features are characteristic of the mineralized areas, and which of these features in turn are visible on the satellite photography. Various enhancement techniques were tried in an attempt to make all of the indicators of mineralization obvious.

Study of the Leadville district reveals that ore deposits are chiefly in shattered rock within fissure zones or in beds of Ordovician limestone that have been intruded by Upper Cretaceous or Lower Tertiary felsic to intermediate porphyries. Faults themselves contain ore in only a few places, while auxiliary faults and fissures along them are

mineralized and have served as feeders to replacement orebodies (mineralization has also been related to karst solution features in the Leadville dolomite paleotopography). Alteration includes local hydrothermal bleaching of porphyries and weathering of disseminated pyrite. Indicators of mineralization for this district are faulting, intrusion of sedimentary strata and thrusting aside of sedimentary blocks by light-colored porphyries, bleached intrusions, and weathered pyrite. Field checking verified the ability to see alteration colors on Skylab photography.

Study of the Cripple Creek district shows that ore deposits are within or at the margins of a steep-sided basin (caldera, breccia pipe?) filled with Miocene breccia and surrounded by Precambrian granite, gneiss, and schist. The basin, approximately two miles by four miles, is filled with volcanic as well as non-volcanic debris, and is cross-cut by dikes of phonolite and lamprophyre. It has been determined that the basin is fault-caused, not volcanic, although it did serve as the locus for intense igneous activity. Mineralization followed recurrent fissuring and consists of veins and fissure fillings, with pyrite a common mineral. Indicators of mineralization for this district are faulting, basins of breccia cut by dikes, and alteration of pyrite. Field checking revealed, however, that photo-color anomalies, in this area at least, are more likely a result of pink microcline in the Precambrian granite.

Weathered pyrite is seen only on the mine dumps, which also are very visible on the photography.

Indicators of mineralization that can be seen on satellite photography over the Leadville and Cripple Creek mining districts are faulting, intrusion of light-colored porphyries into bedded sediments, weathering of pyrite, and hydrothermally bleached intrusives. It is almost impossible to see local thrusting of sedimentary blocks and breccia-filled basins cut by dikes.

The central Colorado survey area was studied in an attempt to locate all indicators of mineralization. These locations (targets) were plotted on a master map of the area, and these were ranked from most to least likely mineralized (Fig. 4). Targets were located by mapping lineaments as guides to faults, and color anomalies as guides to intrusions and alteration. Four lineament overlays were made, one for each of the following:

1) 9x9" pos. color-infrared (CIR) transparency of Frame 17, Track 48, Skylab 2, S190-A,
2) 7x7" neg. CIR print of fr. 106, tr. 48, S.L. 3 S190-A, and 7x7" neg red band print of fr. 107, tr. 48, S.L. 3 S190-A,
3) 9x9" color prints of fr. 38 and 39, tr. 48, S.L. 3 S190-B,
4) 7x7" red band print of pos.-neg. slip masks made from fr. 17, tr. 48, S.L. 2 S190-A, and fr. 106 and 107, tr. 48, S.L. 3 S190-A.

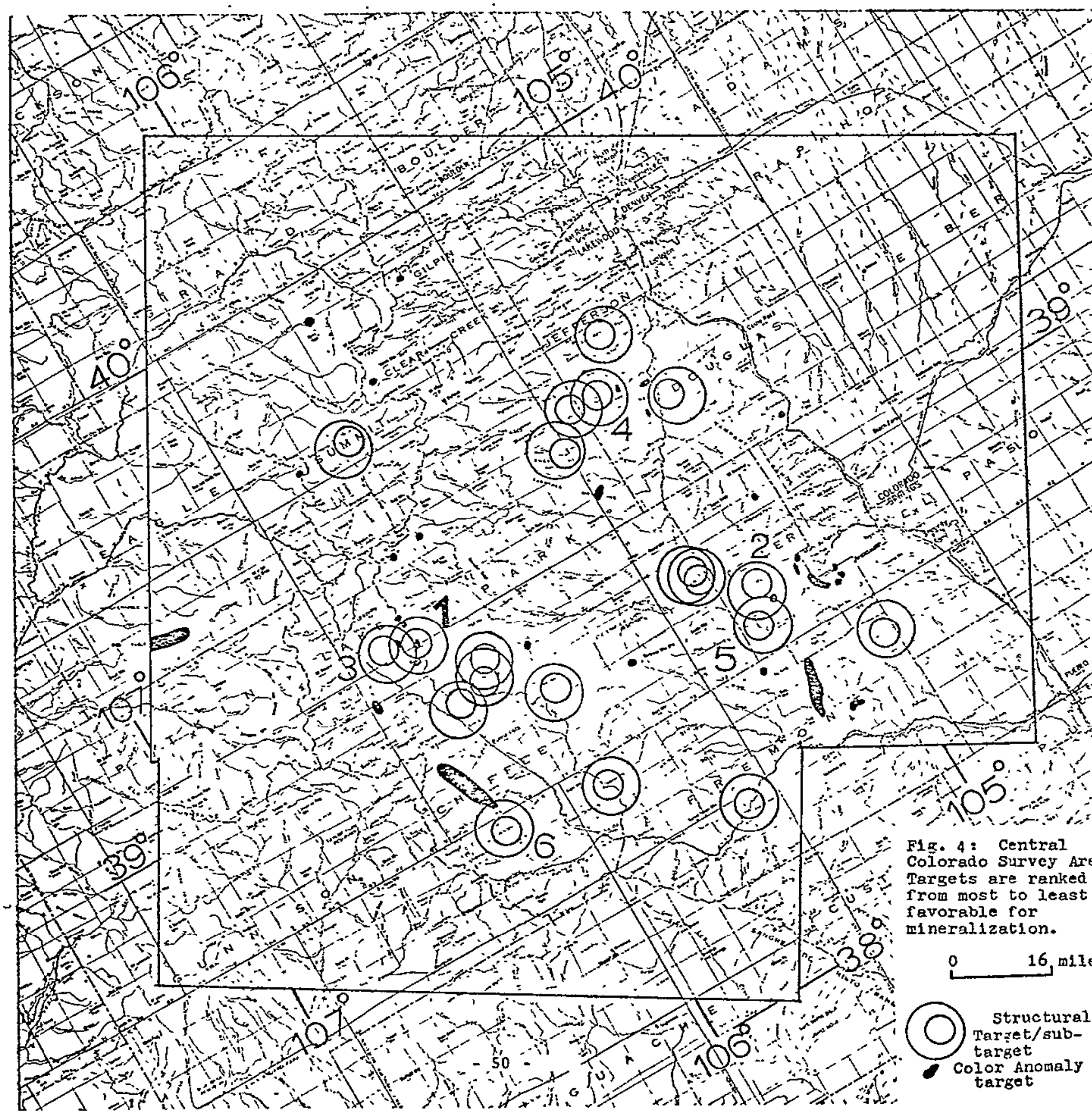

Fig. 4: Central Colorado Survey Are Targets are ranked from most to least favorable for mineralization.

0 16 mile

Structural Target/sub-target

Color Anomaly target

Everything that appeared unquestionably linear was marked as a solid line, while questionable linears were dotted. Care was taken to not include man-made or cloud-caused linears. Targets are those areas with a high density of lineaments and lineament intersections.

Color anomalies were observed by color-additive viewing of Frames 106 and 107, Track 48, Skylab 3 S190-A, and by viewing Frames 38 and 39, Track 48, Skylab 3 S190-B. No color anomalies were seen on unenhanced S190-A photos, nor were any noticed on the diazo color-coded density slices. The possible color anomalies were divided into types A (red to orange), B (light rock surrounded by darker rock), and type C (dark rock surrounded by lighter rock). No type C anomalies were found. The color anomalies were plotted on 1:250,000 topographic maps. Each was considered a target.

Targets were then transferred from the photolineament and color anomaly maps to a master map. Areas considered most likely mineralized (second generation targets) contain both color anomalies and a high density of lineaments. These second generation target areas were ranked from best to worst according to these criteria. The targets arbitrarily are circular areas with a radius of four miles ($6.4\ km^2$), enclosing an area of approximately 50 square miles ($130\ km^2$), and within each is an alternate subtarget, a circular area with a radius of two miles ($3.2\ km^2$), enclosing an area of about 12.5 square miles $32.5\ km^2$). The highest priority targets will be mapped at a scale of 1:24,000, and their subtargets, at a scale of 1:12,000.

The most favorable target/subtarget will become the prime experimental area for this study. It would be significant to learn whether two areas some distance apart, characterized by the same indicators of mineralization, do indeed contain such desired features. Therefore, targets other than the primary may be briefly evaluated as to their indicators of mineralization.

If the interpretations so far are correct, that is, if faulting, intrusion, and alteration have been accurately mapped on satellite photography, then ground mapping and sampling will prove that indicators of mineralization can be quickly and economically found.

Plans For Continued Study

Future research will include a comparison of Skylab photography and imagery to ERTS imagery with respect to finding indicators of mineralization; an evaluation of unenhanced and enhanced S192 imagery with respect to finding indicators of mineralization; mapping of geologic features from medium and/or low altitude aircraft photography and an evaluation and comparison of this information with that from Skylab data, and checking target areas by field mapping and sampling.

APPLICATION OF EREP DATA TO
VOLCANO-TECTONIC-METALLOGENIC STUDIES
SAN JUAN MOUNTAINS

Skylab-2 color and color infrared photography of the San Juan Mts., Colorado, has disclosed several systems of linear fractures both subparallel and intersecting. Caldera development seems to have occurred at several intersections of the larger, longer linears. Several, dome-like, considerably smaller structures, possibly laccolithic, occur along and tangent to linears but not at the intersection of linears.

Base metal and precious metal vein deposits are not apparently structurally controlled by these major linear systems, but have a time-span, time-space relation to structural positioning and volcano-tectonic development of calderas located at intersections of some of the larger linear systems.

Regional studies using low-altitude aerial photography, color, and black and white are complicated by the large numbers of photos requiring examination and by the fact that large regional features may be masked by, or may form the background for, finer detailed features. Skylab-2 provided accurate, small-scale photographs of a large segment of the San Juan Mtn. region on which many of the finer

detailed features are not well defined, and the regional characteristics thus are emphasized or are easier to detect. Both EREP photos and ERTS images are being interpreted and used in this study, along with supporting aircraft underflight data.

Lineaments

Linear features include aligned streams or segments of streams, aligned offsets along several adjacent streams, aligned tributaries over rather long distances, and erosion cuts across summit and divide areas. Those photographic linears thought to indicate possible fracture, joint, or fault systems are termed "lineaments". Breaks in bedding in sedimentary rocks occurred only on one lineament; all other lineaments seem to occur in crystalline plutonic igneous, metamorphic and volcanic units.

Although the criteria used to define the lineaments are those commonly used to define fractures, joints, or faults from photographs, the geologic reason for most of the lineaments observed on the Skylab-2 and ERTS-1 imagery is not as yet specifically known. These linear features are thought to be geologically controlled, but a geologic explanation for them should be investigated in the field.

Lineament Systems

The lineament patterns may be divided into several lineament systems, defined on the basis of their surface

trends and their relation to adjacent systems. Some of the systems are parallel with the topographic grain of the area. Other systems cut across the topographic grain or are oblique to it.

Throughout the 8000 square mile area of the San Juan Mts. studied on Skylab-2 and ERTS-1 images, twenty-three (23) lineaments have been mapped. Names for these lineaments have been assigned using topographic and cultural features such as streams, rivers and towns located along or adjacent to the lineaments.

The Rico-Silverton-Cebolla Creek-Los Pinos-Cochetopa Park Lineament is the longest and strongest lineament dominating the San Juan Mtn. region. It is 97 miles long and trends an average of N 65 E, with near-vertical dips. Another lineament is 72 miles in length, trends N 45 E, with near-vertical dips, and intersects San Luis Peak Caldera. Subordinate yet moderately strong lineaments occur in the southeast portion of the San Juan Mtn. area, trending N 40-45 E and ranging in length from 22 to 57 miles.

Lineament - Caldera Associations

Twelve of the seventeen lineaments in the central and west central part of the 8000 square mile study area intersect, or are tangent to, caldera structures visible of the surface. Dominating this structural scene is the

Rico-Silverton-Cebolla Creek-Los Pinos-Cochetopa Park 97-mile-long lineament. Aligned along and intersected by this lineament are the following calderas: Cochetopa Park, San Luis Peak, Lake City and Silverton. Razor Creek and Tomichi domes, probably laccoliths, lie at the extreme northeast end of the lineament and Rico Dome is at the extreme southwest end. All domes are on the northwest side of the lineament.

Regionally, the smaller dome-like intrusions, probably laccoliths, are situated along lineaments only, but the five mapped caldera structures are located at <u>intersections</u> of the stronger, more dominant lineaments.

Volcano-Tectonic Chronology

Attempts at placing a geochronological parameter (time-space and time-span dependency) on lineaments associated with domes and calderas must be based on "existing ground truth" of lineaments, either as actual zones of movement or as linear fold axial trends, or as both. Some field evidence exists in several areas for actual movement along lineaments.

Field evidence and absolute age determinations show all five calderas and all (except one) of the domes are post-Telluride Conglomerate in age - i.e., post-late Eocene to early Oligocene. If the intersecting lineaments and fold axes served to control the development of calderas

and domes, not only must these structures by pre-late Eocene in age, but the thought is, of course, that prior-existant, primitive, possibly Precambrian age structural flaws were inherited to be rejuvenated prior to and during the Cenozoic volcanism. Field evidence confirming this time-space and time-span chronology needs to be obtained to support the validity of the volcano-tectonic sequence so far indicated by Skylab-2 and ERTS-1 image analysis.

Volcano-Tectonic-Metallogenetic Model

Inherent in this study has been the hope that centers of base metal-precious metal vein deposits and the more recently-discovered replacement deposits may be metallogenetically related to development of the calderas. For this reason, low level, relatively large-scale black-white and color photography have been used to define greater geological detail in selected areas. So selected was the Telluride-Ouray-Silverton Caldera area in which there is an extremely strong development of base metal-precious metal vein deposits and replacement ore deposits.

Surficial and underground mapping within the Telluride-Ouray-Silverton Caldera triangle indicates the presence of three separate, distinct fracture sets formed during rise, emplacement, collapse, resurgence and collapse of Silverton Caldera. In order of formation, these are (1) radial-concentric compressional-dilational fractures, (2) concentric,

inward dipping cone-sheet like fractures related to caldera collapse, and (3) epicycloidal tangential shears also related to caldera collapse.

Field and laboratory studies of fracture development, vein-trends, alteration patterns with associated mineral paragenesis within the Telluride-Ouray-Silverton Caldera area are being reported on separately.

One of the greatest values of Skylab photography, to date, is that it serves as a medium of structural definition superior to field inspection techniques for observing relatively large segments of the earth's surface. The structural domains so defined, especially in the instance of the San Juan Mountains, with their intimate relationship of metalliferous ore deposits to large volcano-tectonic structural domains, enables the geologist to very rapidly define a volcano-tectonic model and to also evaluate it practically in relation to existing structural-tectonic-metallogenetic parameters.

References

Boos, C.M., and Boos, M.F., 1957, Tectonics of the eastern flank and foothills of Front Range, Colorado: Am. Assoc. Petroleum Geologists Bull., v. 41, no. 12, p. 2603-2676.

Harms, J.C., 1959, Structural geology of the eastern flank of the southern Front Range, Colorado: University of Colorado, Ph.D., 50 p.

Heinrich, E.W., 1948, Pegmatites of the Eight Mile Park area, Colorado: American Mineralogist, v. 33, nos. 7-8, p. 420-448.

Hutchinson, R.M., 1960, Structure and petrology of north end of Pikes Peak batholith, Colorado in Weimer, R.J. and Haun, J.D., eds., Guide to the Geology of Colorado: Rocky Mountain Assoc. Geologists, Denver, p. 170-180.

Johnson, D.H., 1961, The geology of the Devil's Head Quadrangle, Douglas County, Colorado: Colorado School of Mines, D.Sc., 138 p.

Lee, Keenan, ed., 1972, Application of remote sensor data to geologic analysis of the Bonanza Test Site, Colorado; Semi-annual progress report: Colorado School of Mines, Remote Sensing Report 72-7, 34 p.

__________, 1973, Application of remote sensor data to geologic analysis of the Bonanza Test Site, Colorado; Semi-annual progress report: Colorado School of Mines, Remote Sensing Report 73-2, 51 p.

Lee, Keenan, Knepper, D.H., and Sawatzky, D.L., 1974, Geologic information from satellite images: 3rd. Ann. Remote Sensing of Earth Resources Conf., Univ. Tenn. Space Inst., reprinted as Colorado School of Mines Remote Sensing Report 74-3, 37 p.

Sawatzky, D.L., 1967, Tectonic style along the Elkhorn thrust, eastern South Park and western Front Range, Park County, Colorado: Colorado School of Mines, D.Sc. 206 p.

Sawatzky, D.L., and Lee, Keenan, 1974, New uses of shadow enhancement: 3rd Ann. Remote Sensing of Earth Resources Conf., Univ. Tenn. Space Inst., reprinted as Colorado School of Mines Remote Sensing Report 74-5, 18 p.

Spoelhof, R.W., 1974, Pennsylvanian stratigraphy and tectonics in the Lime Creek - Molas Lake area, San Juan County, Colorado: Colorado School of Mines, unpubl. Ph.D. dissertation, 193 p.

Scott, G.L., 1963, Bedrock geology of the Kassler Quadrangle, Colorado: U.S. Geological Survey Prof. Paper 421-B, 125 p.

Williams, P.L., 1964, Geology structure, and uranium deposits of the Moab quadrangle, Colorado and Utah: U.S. Geol. Survey Misc. Geol. Inv. Map I-360 [1:250,000].

APPENDIX B

GEOLOGIC INFORMATION FROM SATELLITE IMAGES

Keenan Lee
Daniel H. Knepper
Don L. Sawatzky

Remote Sensing Report 74-3

NASA Grant NGL-06-001-015
NASA Contract NAS9-13394
NASA Contract NAS5-21778

National Aeronautics and Space Administration

27 March 1974

REMOTE SENSING PROJECTS

DEPARTMENT OF GEOLOGY

COLORADO SCHOOL OF MINES ◇ GOLDEN, COLORADO

GEOLOGIC INFORMATION FROM SATELLITE IMAGES

Keenan Lee
Daniel H. Knepper
Don L. Sawatzky

Remote Sensing Report 74-3

NASA Grant NGL-06-001-015
NASA Contract NAS9-13394
NASA Contract NAS5-21778
National Aeronautics and Space Administration

Paper Presented at the 3rd Annual
Remote Sensing of Earth Resources Conference
University of Tennessee Space Institute
26 March 1974

27 March 1974

GEOLOGIC INFORMATION FROM SATELLITE IMAGES

Keenan Lee
Daniel H. Knepper
Don L. Sawatzky

Department of Geology
Colorado School of Mines
Golden, Colorado

ABSTRACT

Extracting geologic information from ERTS and Skylab/EREP images is best done by a geologist trained in photo-interpretation. The information is at a regional scale, and three basic types are available: rock and soil, geologic structures, and landforms. Discrimination between alluvium and sedimentary or crystalline bedrock, and between units in thick sedimentary sequences is best, primarily because of topographic expression and vegetation differences. Discrimination between crystalline rock types is poor. Folds and fractures are the best displayed geologic features. They are recognizable by topographic expression, drainage patterns, and rock or vegetation tonal patterns. Landforms are easily discriminated by their familiar shapes and patterns. Their regional presentation enhances physiographic studies. It is possible to optimize the scale, format, spectral bands, conditions of acquisition, and sensor systems for best geologic interpretation. Several examples demonstrate the applicability of satellite images to tectonic analysis and petroleum and mineral exploration.

INTRODUCTION

Most geologic information will eventually be extracted from space data by geologists without specialized training and without sophisticated data processing equipment. The extraction of geologic information from ERTS and Skylab/EREP images is still a deductive process, involving the geologist-interpreter. The validity of interpretations will therefore depend upon the experience of the geologist in deducing pertinent geology from surface features, and it is imperative that the interpreter understand how those surface features appear on space images and how best to use the images ("space images" are taken to include both scanner imagery and photographs, acquired from space by satellites in earth orbit).

The type of geologic information that can be extracted consists of rock discrimination, geologic structures and landforms - the same as with conventional aerial photography - but the geologic features will, of course, be on a regional scale.

The authors are geologists with experience in geologic remote sensing from aircraft and from spacecraft, mostly in the Colorado Rocky Mountains, and the discussions that follow are based on experience in that area. All illustrative examples are from the Rockies, and consequently do not represent the spectrum of geologic terrains over which ERTS and Skylab images have been acquired. However, the statements and conclusions probably apply to images from much of the world, and the principles, at least, can be transferred easily to other geologic settings.

The following sections of this paper will discuss (1) basic geologic information contained in satellite images, the surface expressions of geologic features and how they appear on satellite images, (2) recommended approaches to the use of satellite images, and (3) some preliminary examples of the application of space data to geology.

GEOLOGIC INFORMATION FROM SATELLITE IMAGES

BASIC GEOLOGIC INFORMATION

Geologic analysis of ERTS and Skylab/EREP images involves the extraction of specific types of information basic to all geologic investigations. This basic geologic information consists of determining the location and distribution of:

1. rocks and soils (lithology)
2. geologic structures (folds and fractures)
3. landforms.

Basic geologic information must be interpreted from ERTS and Skylab images by reading the tones, textures, and geometrical relationships between tones and textures in terms of physical parameters of the earth's surface. The ability to extract basic geologic information from space images depends, in large part, on two primary considerations:

1. How well the information is expressed at the surface, and
2. How well the surface expression is translated to the imagery.

Lithologic contacts, geologic structures and landforms are represented at the earth's surface by changes in 1) color, 2) topography, and 3) vegetation. It is difficult to place exact figures on the changes in color, topography, and vegetation that are necessary in order to be interpreted on ERTS and Skylab images, since all three parameters almost always change together with a change in geologic conditions. In addition, it must be understood that changes in color, topography, and vegetation _all_ serve to change the tone (color) and texture on space images, and it is difficult or impossible in most cases to attribute a change in tone or texture uniquely to _one_ of the parameters alone without extensive ground data. Suffice it to say the minimum "changes" in color, topography, and vegetation that can be mapped on ERTS and Skylab images are quite variable.

The minimum size of geologic features that can be mapped on space images is equally difficult to quantify because mappability depends both on size and contrast. For a given tonal/textural contrast, however, narrow, linear features such as steeply-dipping sedimentary beds, fractures, and dikes are more easily mapped than small, equidimensional features.

In all respects, the tools and skills of the photointerpreter are absolutely prerequisite for analyzing space images, because the interpretation of basic geologic information from small-scale images involves an understanding of many types of indirect information (e.g. - drainage pattern, type, and texture, vegetation distribution and density, land use patterns, etc.). The necessity of interpreting many kinds of indirect features for geologic information on space images severely limits the utility of automated geologic mapping of the imagery by machines--at the present state of the art it is not possible to train a computer to make all the decisions that a photo-geologist must routinely make during the course of geologic interpretation. Hence, the extraction of geologic information from space images remains in the realm of the human interpreter, and we shall discuss the various aspects of basic geologic information in terms that hopefully will be useful to the practicing geoscientist.

LITHOLOGY

A primary objective of all forms of geologic mapping is the determination of the distribution of rock types and soils (including alluvial material). On relatively large-scale photos (1:10,000-1:50,000), lithologic units can be discriminated (and commonly can be identified to some degree) by considering tone or color and texture, among other factors. The relatively large resolution elements of ERTS and Skylab images commonly preclude lithologic identification except in those instances where lithology can be derived by considering the

shape and form of the unit (e.g. - volcanic cones and flows, glacial deposits, alluvial fans, pediments, etc.). However, there are many instances where at least a gross identification can be made (e.g. - resistent sedimentary rocks, fractured crystalline rocks, etc.), and the photo-interpreter is obligated to make these tentative identifications where possible.

The easiest and most consistent lithologic discrimination that can be made on space images is between alluvium covering valley floors and bedrock exposed in bordering uplands. These two types of lithologic terrain differ greatly in topography (micro-relief at the scale of space images) and type and amount of vegetative cover. Areas underlain by bedrock have moderate to high local relief and are commonly covered by coniferous forests. Alluviated areas, on the other hand, are relatively flat and are most commonly covered by grass and small shrubs. These topographic and vegetative differences are easily identified on space images because of the distinctive tonal and textural patterns they produce (Fig. 1).

Lithologic discrimination between bedrock units is more difficult and depends greatly upon the type of bedrock involved. Discrimination is generally best between lithologic units within thick sequences of sedimentary rocks. Where the sedimentary rocks are moderately- to steeply-dipping, lithologic contacts are enhanced by the effects of differential erosion, producing long, linear outcrop bands. Tonal (color) and textural contrast between outcrop bands on the space imagery is enhanced if the spectral reflectance of adjacent units is highly contrasting, or if the units are selectively different in their support of vegetative growth.

Areas underlain by crystalline rocks (extrusive and intrusive igneous rocks and metamorphic rocks) can generally be discriminated from areas underlain by sedimentary rocks or covered by alluvium, but discrimination within crystalline

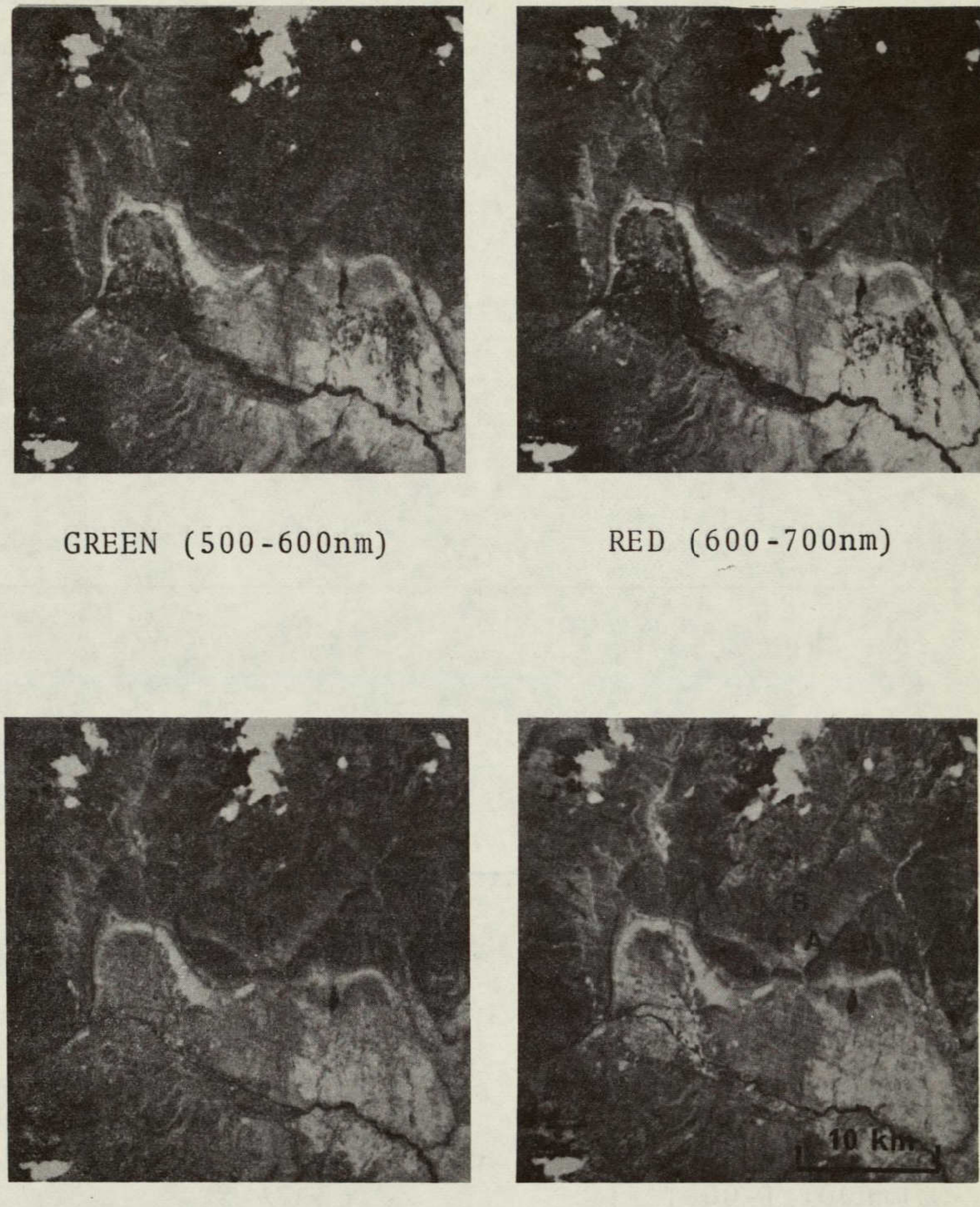

Figure 1: ERTS MSS imagery of the Canon City, Colorado, area. A, alluvium; B, bedrock.

terrain is very poor and identification virtually impossible on space images. The general inability to discriminate between crystalline lithologic units probably stems from two factors:

(1) Crystalline rocks are relatively homogeneous in terms of resistence to erosion, at least at the scale of space images.
(2) Although crystalline rocks in Colorado vary greatly in composition, which should be reflected in selective vegetation growth, the crystalline rocks are exposed only in the mountainous regions of the state where vegetation is more sensitive to elevation changes.

The spectral pass band of the images used for lithologic mapping is an important factor in lithologic discrimination in central Colorado, and probably other areas as well. Where color photographs are available, especially from the S190B, they provide the best medium for mapping lithologies. Recent experiments on ERTS (MSS) and Skylab (S190A) images indicate that among black and white images, the red band generally is best for lithologic mapping, particularly when the image depicts a high sun-angle, snow-free scene (Fig. 1). However, the red band alone is commonly not sufficient for all lithologic mapping, and all available bands should be consulted to insure that the maximum amount of available lithologic information is obtained. No obvious advantage accrues to using two or more bands in register, since spectral reflectance differences of rock units do not appear to favor any one band over others (Raines and Lee, this publ.).

ERTS imagery from June, August, December, and January were studied to determine the mappability of lithologic contacts in central Colorado. Imagery acquired in June (spring) is far superior to the other imagery for lithologic mapping (Fig. 2). Each of the contacts studied is expressed topographically and shows a change in vegetation at the contact, and many of the contacts are

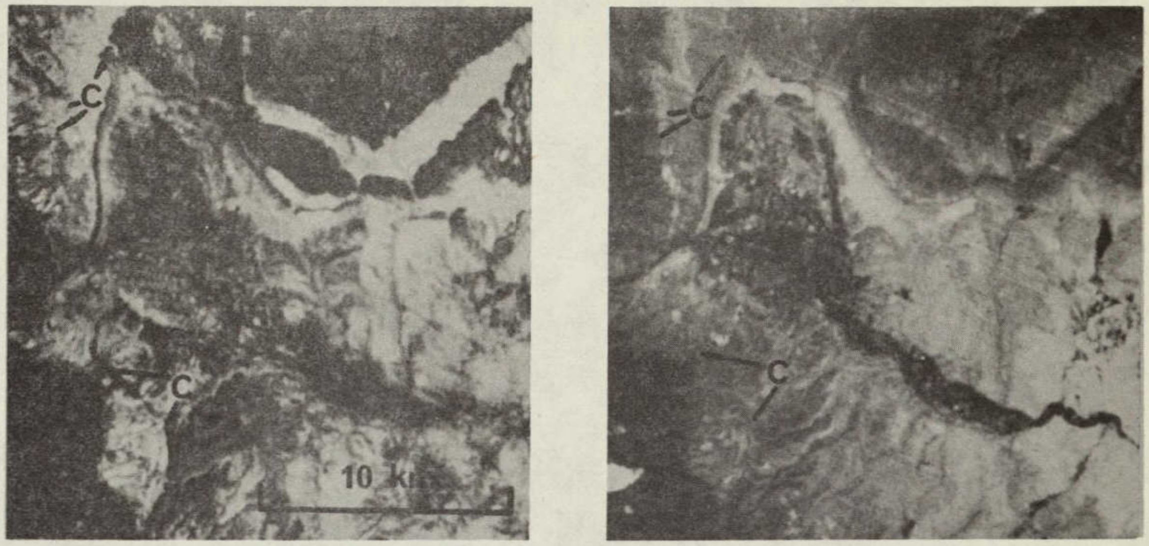

JANUARY JUNE

Figure 2: Winter and spring ERTS MSS imagery of the Canon City, Colorado, area. C's are lithologic contacts located for comparison.

between units that are highly contrasting in spectral reflectance. The fact that the June imagery is superior suggests that vegetation expression overshadows topography and spectral reflectance in defining the contacts on ERTS imagery. In addition, it appears that the red band better displays these vegetative differences than do the green and photo-IR bands.

Some of the contacts not expressed well on the June imagery were very apparent on the winter scenes (Fig. 2). Therefore, although the spring imagery is generally the best, winter imagery must also be used if the maximum amount of lithologic information is to be extracted from ERTS imagery. There is little difference between the lithologic mapping capability of the red and IR bands of winter (snow-covered) scenes.

FOLDS

Space images are capable of yielding good information on geologic folds. Although expression

of folds is not as obvious or dramatic as that of lineaments due to fractures, their interpretation can generally be made with more confidence. This suggests that in well mapped areas, space images will provide minimal new fold information, but in poorly known areas they will yield reliable information on new fold structures. Interpretation of folds is not limited only to regional structures, and structures need not be strongly folded.

Few folds are instantly recognized on images; most are relatively subtle in expression and must be carefully worked out. The surface expression most useful in fold interpretations is topography (and related phenomena). The majority of mappable folds are worked out by determination of opposing dips (Fig. 3), with the dip interpretations based

Figure 3: Subtle expression of syncline, determined by interpretation of opposing dips. ERTS Band 5.

largely on the recognition of topographic features. Dip slopes may be directly recognized where stereo viewing is possible. Without stereo, indirect expressions helpful in slope interpretations are shadow relationships and variations of vegetation that are topographically-controlled. Drainage patterns are indicators of slopes, and the drainage/strata geometry (rule of V's) is the most consistently useful criterion for determination of dips (Fig. 4,A).

Some folds - generally plunging folds - are expressed as tonal (or color) patterns (Fig. 5). Of

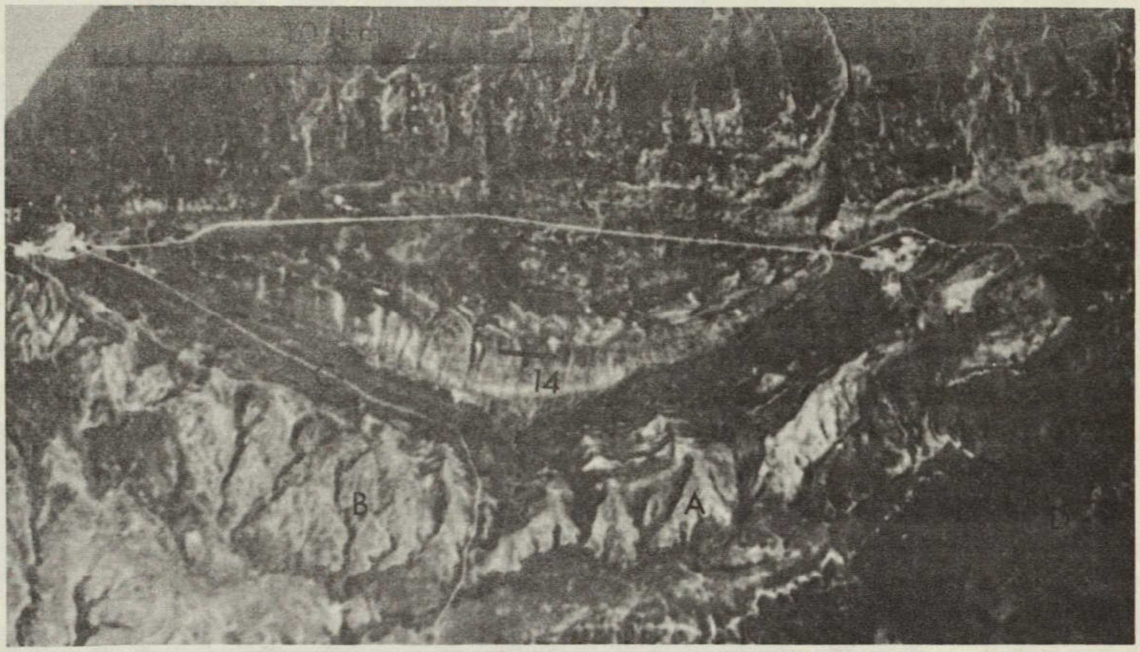

Figure 4: Folded and faulted Permian-Triassic sedimentary rocks. Skylab S190B color photograph.

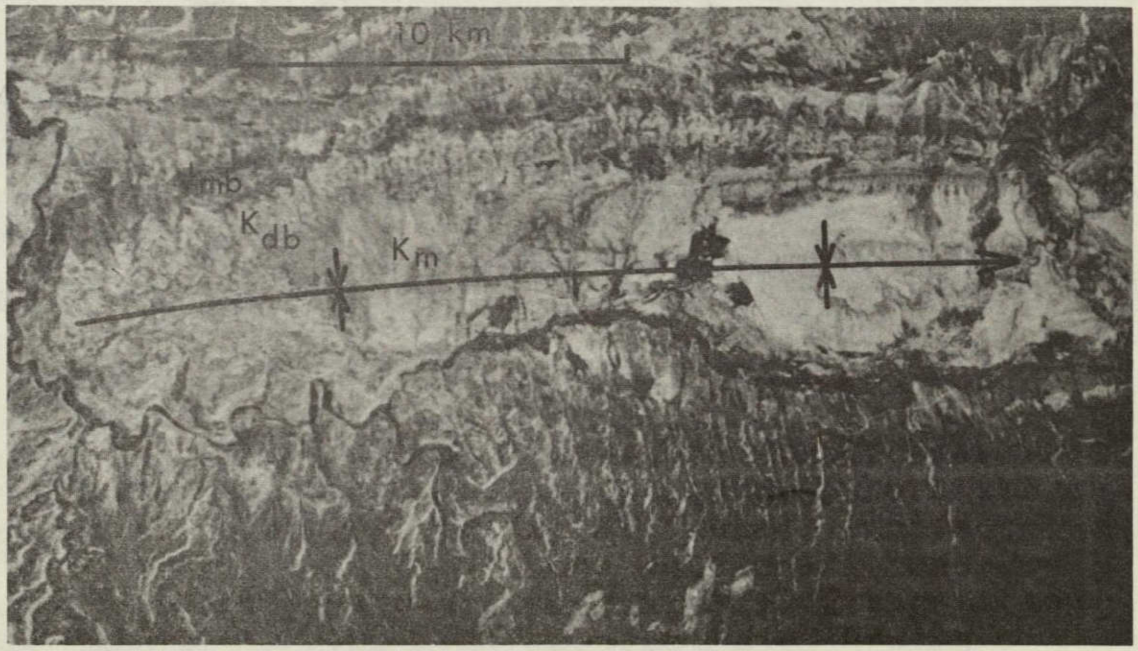

Figure 5: Plunging syncline expressed by tonal pattern. Jmb-Brushy Basin Shale, Kdb-Dakota and Burro Canyon sandstones, Km-Mancos Shale. Skylab S190B color photos.

these tonal patterns, some can be attributed to differences of spectral reflectance between contiguous strata, but this surface expression is probably subordinate to tonal differences related to topography. Topography can produce tonal differences in several ways. (1) Aspect angle (sun-target-camera) differences caused by topography are ubiquitous, and resulting tonal differences are common (Fig. 4,B). (2) Topographically low areas are generally sites of alluvial deposition, and alluvium-bedrock contrasts are often relatively great. (3) Elevation and slope direction control vegetation, often producing sharp boundaries between vegetated and nonvegetated areas and between different types of vegetation. Resulting large image tonal contrasts may then occur between vegetation-bedrock, vegetation-soil, vegetation-alluvium, vegetation-snow, trees-grass and conifer-hardwoods.

Relatively subtle folds can be mapped with confidence. Interpretation of ERTS red band imagery has yielded dip information (dip slopes) in the range of 3°-10° (Fig. 3); dips as gentle as 2°-6° have been observed on Skylab S190B photos (Fig. 4).

Interpretation techniques for using space images are the same as for conventional photogeology using aircraft photos. An obvious difference is in the realization that small fold structures may not be mapped, but a compensatory difference exists in that broad folds may be seen (at least interpreted) in their entirety on one scene.

FRACTURES

Early interpretations and evaluations of space images have stressed the recognition of linear elements in the data. That an abundance of linears occurs on space data is apparent to any observer with geologic interests. Many of these linears are related to geologic phenomena, and many of the

geologically-controlled linears are related to fractures.

Although fractures often are expressed on space images as linear elements, which are more obvious than most fold structures, their interpretation is subject to greater uncertainty. Many linears on space images cannot be interpreted, much less identified as to geologic cause, and many faults and joints cannot be found on space images, even though they are of sufficient scale to be easily resolved.

The corollary to these observations is that, in areas that have already been mapped, fracture information is likely to be the most significant new information gained from photogeologic interpretation of space images, but the information must be extracted with difficulty and with uncertainty.

To avoid possible confusion in terminology, the following terms are defined: a linear is any line or alignment of features, straight or slightly curved, and a lineament is a linear of probable geologic control (the term denotes a degree of interpretation). Linear elements known to be geologically-controlled are designated by their specific descriptive names - contacts, faults, etc.

Space images provide a synoptic view of large areas that permits the recognition of large regional lineaments that in detail may be too subtly expressed to be recognized on aircraft images or in the field. A second advantage that accrues to the use of space images is the ability to recognize and analyze the "fabric" of a region - that is, the dominant trends of lineaments - that relates to the tectonic framework.

The interpretation of fractures (taken to include faults, fault zones, shear zones and joints) is based mainly upon the interpretation of topography and topographically-controlled phenomena such as vegetation. Less common surface expressions

include the distribution and relationship of rock units (note that this is the primary field criterion), and vegetation directly controlled by fractures - generally by controlling availability of ground water.

Faults affect topography in several ways. Late Cenozoic faulting may produce primary landforms (fault scarps). Faults that juxtapose rock units of differing erosional resistance will ultimately produce relief by differential erosion (fault-line scarps, Fig. 6). Faults within homogenous bedrock, as well as joints, commonly are mechanically weak zones that are more susceptible to erosion and consequently tend to form linear topographic lows.

The dominant image expressions of these topographic features are linear tonal contrasts induced by aspect angle changes. The commonest examples, perhaps, are the tonal contrasts associated with linear valleys where one valley slope is fully illuminated and the opposing slope is only slightly illuminated, or even fully shadowed (Fig. 7). Maximum contrast results from

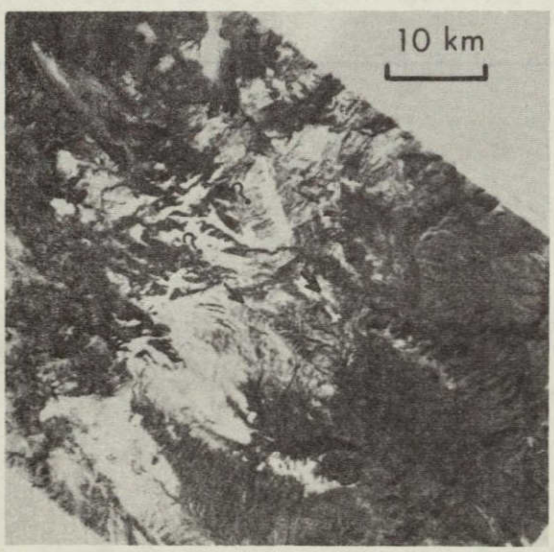

Figure 6: Fault-line scarps. Arrows indicate mapped faults, "?" are possible extensions. ERTS Band 5.

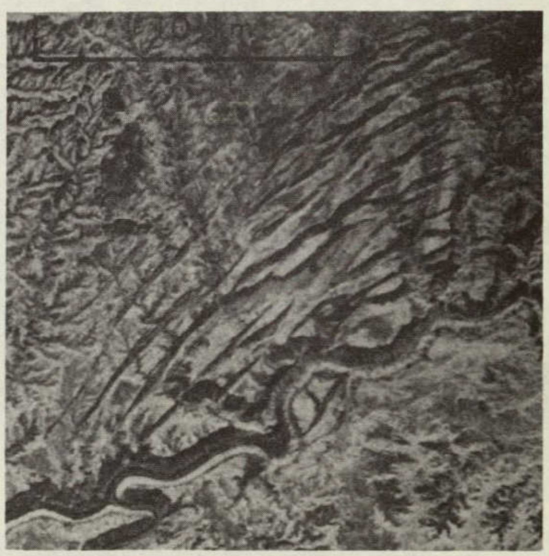

Figure 7: Zone of normal faults in Paleozoic sedimentary rocks. Skylab S190B color photo.

the latter condition, which obtains when the sun's rays are at grazing incidence on one of the slopes - that is, when the solar elevation angle is equal to the slope angle (Wise, 1969; Sawatzky and Lee, this publ.). This relationship is sometimes exploited in low sun-angle photography (LSAP) from airccraft. One significant difference between aircraft and spacecraft LSAP that is not commonly recognized, however, is that the optimum elevation angle is different. Basically, the optimum low sun angle is determined by the slope angles that one wishes to enhance. Relatively large-scale aircraft photography is concerned with small, local structural detail, and in areas of moderate to high relief, such as the Rocky Mountains, these structures are commonly expressed as small, fairly steep slopes. Optimum illumination angle in such a case may be 20°-30°; lower sun angles would tend to obscure large portions of the photography. In space photography, however, small, steep slopes are rarely recognized because they are rarely maintained for any considerable distance, and the slopes amenable to interpretation are usually more extensive. These larger topographic landforms have correspondingly lower average slope angles. For comparative examples, see Fig. 8, which shows

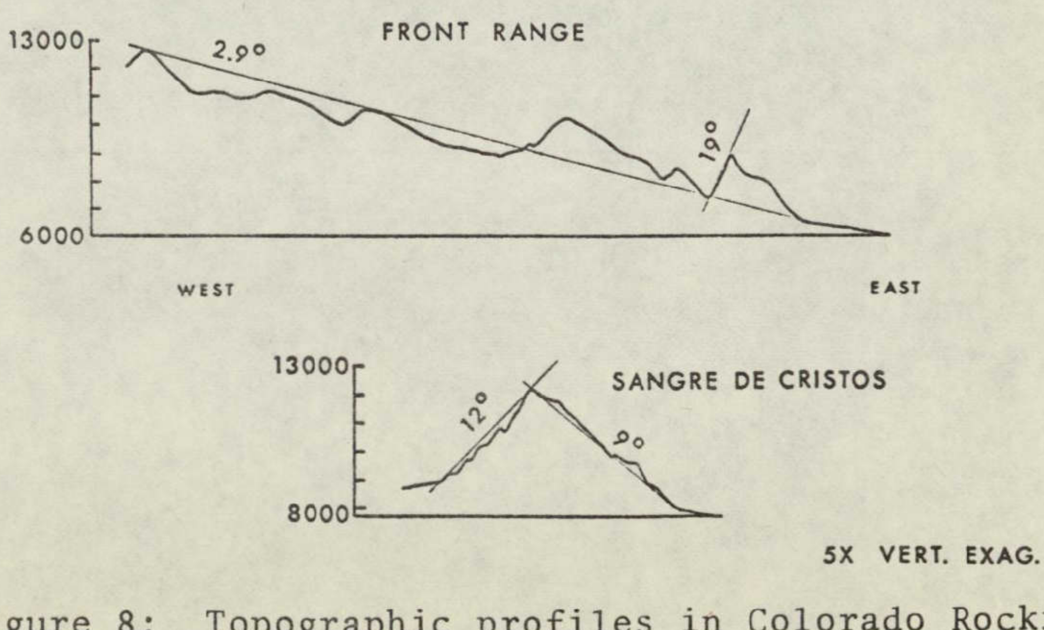

Figure 8: Topographic profiles in Colorado Rockies, with average slope angles. Elevations in feet.

profiles along the Colorado Front Range. The average slope of the range (east slope), from the Continental Divide to the edge of the plains, is 2.9°, whereas individual valleys cut into the range have slope angles commonly 15°-20°. Even the Sangre de Cristo Range, which is an anomalously steep, narrow, faulted mountain range, has average slope angles of 8.8° (east) and 11.8° (west). Thus, optimum sun angle illumination for space images may be on the order of 5°-15°. The space image with the lowest angle illumination available in Colorado is ERTS imagery with a 20° sun angle, and whereas this imagery is far superior to high sun-angle imagery (compare Figs. 9 and 10) for structural

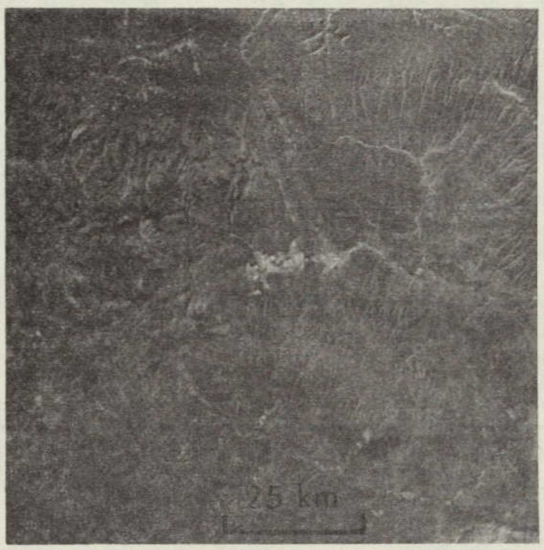

Figure 9: ERTS image with 49 degree sun angle, 4 Sept 1973.

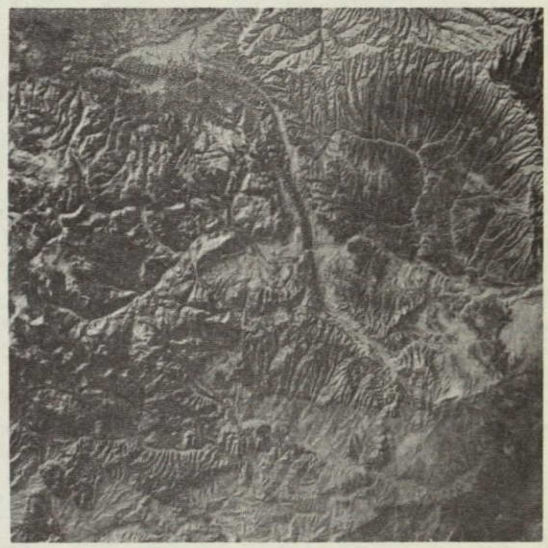

Figure 10: ERTS image (same as Fig. 9) with 21 degree sun angle, 26 Dec 1972.

studies, it may not be optimum. To this end, further studies are warranted with, for example, ERTS imagery taken near the solstices at higher latitudes.

Snow cover further enhances imagery with low-angle illumination (Fig. 11). The contrast between sunlit and shaded slopes is increased by snow, especially when the images are acquired with minus-

blue filtration. Under these conditions the shaded slope is still essentially black (shadow), whereas the sunlit slope is brighter due to the increased reflectance of the snow (reflectance of snow in the photographic region is about four times that of most rocks and as much as 15 times as great as coniferous forests). In some cases, snow will enhance fractures by collecting (or remaining, during snowmelt) against, along or within topographic expressions of the fractures. This enhancement is ephemeral, and acquisition of images while these conditions prevail is largely fortuitous.

Linear topographic lows due to fractures may also appear on space images as narrow tonal lineaments. Light tonal lineaments on snow-free imagery may be caused by alluvium in the valley bottoms, which generally has a greater reflectance than bedrock or vegetation on valley walls. On snow-covered images, light tonal lineaments may be caused by vegetation-free, snow covered alluvial flats, as contrasted with forested valley slopes (Fig. 12,A,B). In arid areas, vegetation

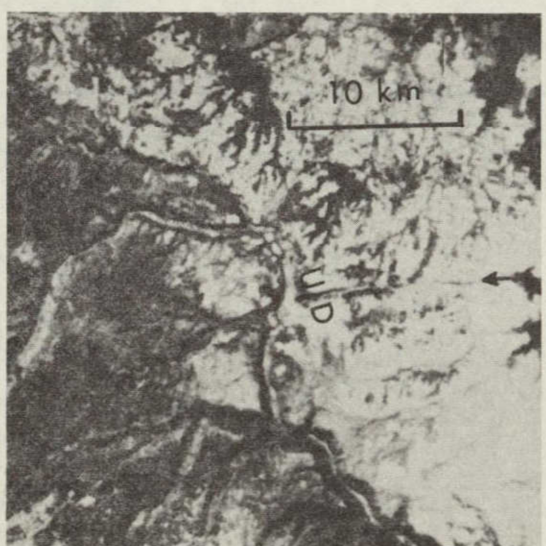

Figure 11: Shadow-snow enhancement of fault-line scarp. ERTS Band 5.

Figure 12: Snow-covered alluvial flats, A,B, contrasted with conifers on bedrock. ERTS Band 5.

preferentially growing along valley bottoms, where there is more available ground water, may show as dark tonal lineaments (or light lineaments in IR bands).

Tonal lineaments associated with contrasting reflectances of rock units juxtaposed along a fault are rare on space images. The observance of such faults is usually based on other criteria, such as topography or vegetation.

Lineaments are most abundant in crystalline rocks. In large part this may be due to the relatively homogeneous appearance of large masses of crystalline rocks, against which tonal linears tend to stand out, but in part it may reflect the higher natural incidence of fracturing in competent rocks.

In sedimentary rocks, fractures are best seen where their trend is at an angle to the strike of bedding (Fig. 13). Fractures parallel to bedding are often masked by contacts and strike valleys; where they do occur parallel to bedding strike, they are best seen where they occur on dip slopes.

Relatively short, sharply-defined lineaments can be seen on space images. ERTS imagery (red band) studied in one area in southwestern Colorado showed most of the faults longer than 10 km and many of the shorter faults; the shortest fault observed was 3 km long. Skylab S190A photographs (red band) in the same area showed more of the faults than did the ERTS imagery, with the smallest observed fault being 2 km long. Skylab S190B color photographs contain still more fault information; most of the faults in the area were observed except those that occur in closely-spaced sets of parallel faults (that is, individual faults in some fault zones were not observed). The smallest fracture seen was about 1 km long, but probably more significant was that joint spacings of about 200 m were clearly seen (Fig. 14).

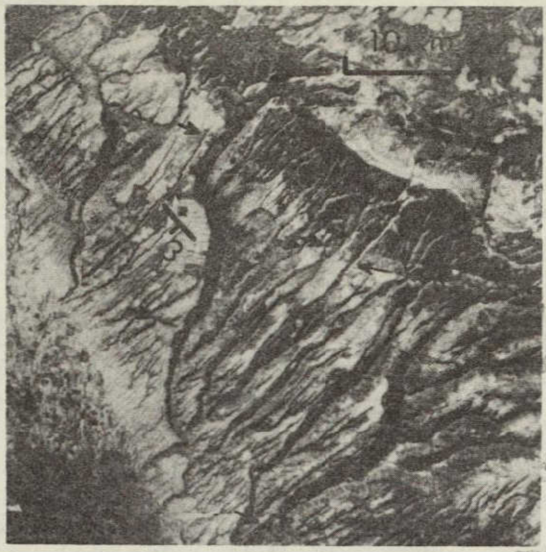

Figure 13: Normal faults on Dakota sandstone dip slope. Arrows show mapped faults, "?", possible extensions. ERTS Band 5.

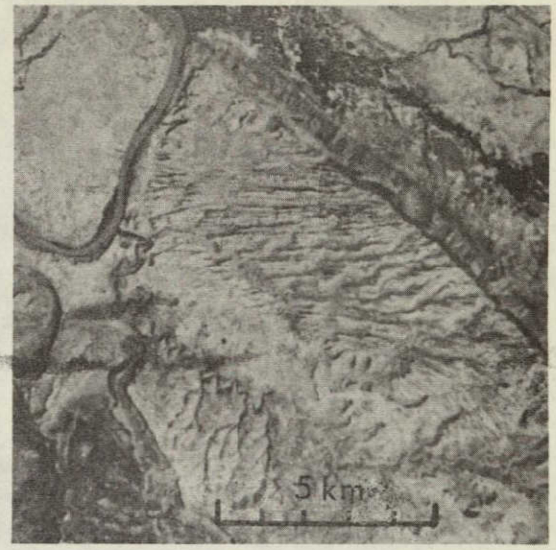

Figure 14: Joints and normal faults in Navajo Sandstone. Skylab S190B color photo.

High-angle faults are more easily seen than low-angle faults, because in areas of moderate to high relief they are expressed as relatively straight lines, whereas low-angle faults have irregular fault traces and correspondingly irregular topographic expression. Long lineaments due to large faults or shear zones can be traced for more than 50 km, but many, if not most, of the long linears that are fairly common on space images cannot be correlated with known fractures (Fig. 15). By the same token, most of these long linears cannot be identified as cultural features either, such as jet contrails (Fig. 16), railroad, roads, field patterns (Fig. 4,C,D), etc., so they remain in the realm of speculation. In many cases, we believe these long linears must be expressions of geologic structure (perhaps basement faults that are manifest at the surface only as lines of weakness) even though they defy identification. Continued research on the origin of these lineaments may provide some of the most exciting geologic results to come from space data.

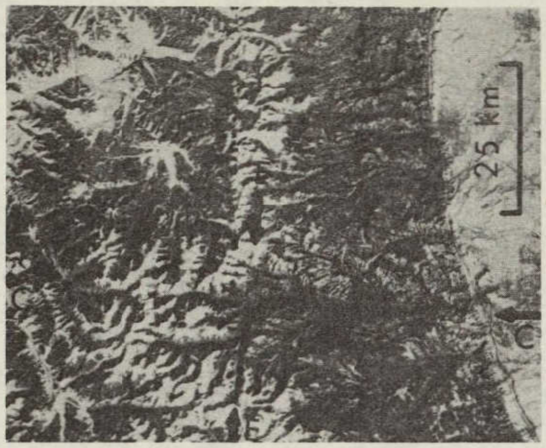

Figure 15: Two major lineaments in Colorado Front Range. C, Clear Ck. lineament; E, Empire-Georgetown lineament. ERTS Band 5.

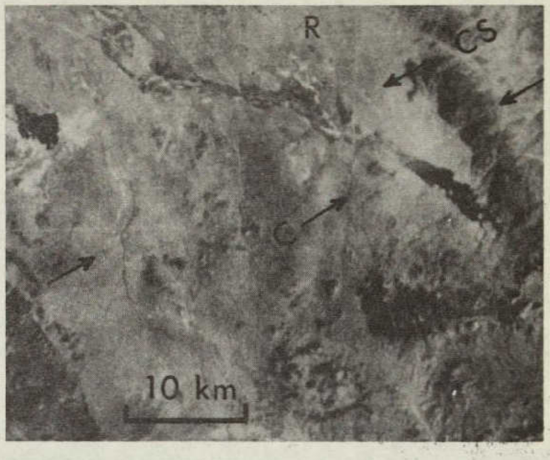

Figure 16: Linears of non-geologic origin. C, contrail of jet aircraft; CS, shadow of contrail; R, road grid. Skylab S190A photo (red band).

LANDFORMS

Landforms can be recognized on ERTS and Skylab images by the shape or form of the tonal and textural patterns caused by topography and vegetation. Color differences associated with landforms, other than those related to topography and vegetation, are relatively rare, although they do exist.

The capability of detecting and mapping landforms on ERTS and Skylab images is highly variable and depends, in large part, on the imagery contrast between adjacent landforms.

Landforms recognizable on space images fall into three major catagories:

1. Those associated with relatively recent tectonic activity (faults, folds)
2. Those associated with recent deposition (alluvium, terraces, talus, glacial deposits, volcanic deposits, etc.)
3. Those formed by differential erosion of a

heterogeneous geologic framework (hog-backs, fault-line scarps, badlands)

In the geologic interpretation of space images it is extremely important that landforms be placed in the proper catagory, since each catagory denotes a different aspect of the geologic history of an area.

Physiographers rely on large-scale topographic maps and airphotos for detailed analysis of land-forms. With ERTS and Skylab images, it is now possible to study the regional spacial relation-ships between widely separated landforms and groups of landforms. In addition, factors affecting the evolution of landforms, such as geologic structure and lithology, may be simultaneously evaluated from the same imagery. The availability of space images appears to have opened new avenues of physiographic research.

RECOMMENDED USE OF ERTS AND SKYLAB IMAGES

It has already been suggested that the approach to interpretation of space images is basically the same as the approach to geologic interpretation of aerial photographs. However, several factors must be considered if maximum use is to be made of ERTS imagery and Skylab photography:

1. scale
2. format
3. spectral band
4. conditions of acquisition
5. sensor systems

SCALE

Both ERTS and Skylab images contain more geologic information than can be interpreted at the original film scales. Consequently, direct interpretation of the images is not efficient, and magnification is necessary. The most effective

method of interpretation is through high quality optical systems, rather than photographically enlarging the originals and using enlarged prints or transparencies; this avoids another generation or two of film degradation. Standard ERTS images (9in x 9in) are at a scale of 1:1,000,000; for interpretation, ERTS transparencies can be magnified to about 1:250,000 without significant image degradation. Skylab S190A photographs have an original scale of about 1:2,850,000; 12X seems to be about the maximum magnification, to a scale of about 1:240,000. Skylab S190B photos will take similar magnification, from an original scale of 1:950,000 to about 1:80,000. The Richards MIM light tables, with a Bausch & Lomb 240R zoom stereoscope, are ideally suited to magnified stereoscopic and monoscopic photointerpretation.

FORMAT

As ERTS and Skylab films contain more geologic information than can be interpreted at original scales, they likewise contain more information than can be graphically represented at original scales. Therefore, photographic enlargements are also required to map the interpreted information, either directly onto the enlargements or onto clear overlays. A good method we have used entails interpretation of low-generation contact positive transparencies under stereo (where available) magnification, with interpretive results transferred to clear overlays on enlarged transparencies or prints. The annotated images can then be transferred to topographic maps with the Bausch & Lomb zoom transfer scope.

At whatever enlargement, or under whatever magnification, the quality of film transparencies is superior to that of paper prints. However, in the ultimate interpretation step - field checking - transparencies are difficult to use, and prints are far handier (and cheaper). A good compromise is to annotate onto clear overlays, which can then be put onto prints for field use.

The use of stereoscopic viewing cannot be overemphasized. One of the ideas developed in previous sections is that topography is the dominant surface phenomenon used in geologic interpretation of space images, and it obviously follows that stereo viewing is required to use this to optimum advantage. Full stereo coverage (endlap) was obtained by Skylab cameras on many of the EREP passes, and ERTS imagery provides some stereo sidelap (about 35% at Colorado latitudes, providing stereo coverage for about 70% of the ground).

SPECTRAL BANDS

In areas covered by both Skylab and ERTS, the geologist is faced with an array of spectral data from both cameras and multispectral scanners (not to mention thermal infrared and microwave radiometry and spectrometry, which we will not mention). Thus, a few comments are warranted on the choice of spectral bands for interpretation.

Of the ERTS MSS bands, there is no overall "best". Each band has proved best for some geologic feature, under certain conditions. The interrelationships here are complex; suffice it to say that Band 5 (red) has found more use in our area.

Of the Skylab S190A black and white photographs, the red band appears best. Both of the IR bands have very poor resolution, obvious graininess and low contrast. The green band is considerably better, but tends to lack the sharp contrast of the red band. Resolution of the red and green bands appears about the same, but the higher contrast of the red band probably stems from (a) darker shadows due to less red light in shadows, (b) less red light contributed by the atmospheric path, and (c) greater band reflectance differences between vegetation and rock/soil due to the red chlorophyll absorption band.

GEOLOGIC INFORMATION FROM SATELLITE IMAGES

It is possible to produce "true" color and false color composites using the ERTS multiband imagery. In some cases these color composites serve to enhance subtle tonal changes present between lithologic units. The most useful color composite for lithologic mapping appears to be a nearly "true" color rendition made by projecting the green and red bands with green and red light, respectively. However, color composites constructed in this manner using an I^2S color additive viewer are inferior in resolution and general image quality to the individual black and white bands. Color IR composites made by EROS and by General Electric Corp. also appear to be inferior to single band black and white transparencies in resolution and image quality. In short, the use of color additive viewing appears to produce an esthetically more pleasing image at the expense of image quality. As with color photographs, color additive viewing or the purchase of commercial color composites can be an expensive proposition and should be considered only if color additive viewing facilities are readily available or if the actual color of rock units can be used to identify the mapping units. The latter is particularly useful in areas where redbeds are interstratified with light colored (brown, gray, tan, light-green) sedimentary units. In most other types of rock sequences, color composites are of minor usefulness, although other examples could probably be cited.

Color and color IR Skylab photos commonly are better for lithologic discrimination than simultaneously acquired multiband photos (S190A) where changes in rock color are important at lithologic boundaries. However, color photos are more expensive than black and white (multiband) photos, and most geologists on limited budgets must keep this in mind. In addition, lithologic contacts defined by color differences of the rock units are relatively rare in some areas; color differences caused by other factors (e.g. - vegetation, topographic effects) may be equally detectable and mappable on black and white photos. Color photos

are no better than black and white photos in snow-covered scenes.

CONDITIONS OF ACQUISITION

The consideration of time of day and time of year that space data are acquired may be extremely important. The former can be translated directly to solar elevation, or the incidence angle of scene illumination; the latter may involve both illumination angle and azimuth, as well as snow cover and different stages of plant growth.

As was pointed out in previous sections, topography, and thus geology, may be more easily interpreted when illuminated at low elevation angles. Not only are many subtle features enhanced, but some features (notably high-angle linear slopes) are selectively enhanced as a function of their orientation (Sawatzky and Lee, this publ.). The optimum sun angle obviously is a function of relief, and cannot be defined here without more study, but we suggest that, for areas like the Rocky Mountains, approximately 10° may be best.

For a given sun angle, azimuth will vary seasonally. For a given time of day, both azimuth and sun angle will also vary seasonally. In the case of the ERTS satellite, with its fixed time of overpass, obtaining imagery from different times of the year is the only way to vary sun angle. During the study of structures in NW Colorado (shown in Fig. 18), initial interpretation of ERTS imagery taken with a 42 degree sun angle revealed 10 folds; the final interpretation of 63 folds was made on ERTS imagery with a sun angle of 21 degrees.

The use of winter images in Colorado must contend with nearly-complete snow cover. The effect of the snow is mixed; it tends to obscure differences in rock reflectance, but it may enhance topographic and forest/non-forest contrasts. Snow probably hinders more than helps lithologic

discrimination, and is, overall, most beneficial for structural interpretations

As discussed under Lithology, the maximum amount of geologic information can be obtained by using as many images as possible, acquired under as many different conditions as possible. This has obvious practical limitations, but we think obtaining at least early summer and early winter images is worthwhile. The consideration of time of year is generally of lesser importance for Skylab photos than for ERTS images, simply because the number of Skylab data passes over a given area was limited - commonly to one.

SENSOR SYSTEMS

The advantages and disadvantages of the sensors aboard the ERTS and Skylab satellites should be considered. For practical use of space data by professional geologists, we are discussing imaging systems only; the use of non-imaging systems is restricted at present to research-oriented groups.

The ERTS imaging system (MSS) has several advantages compared to Skylab:

1. Coverage over nearly the entire earth's surface is possible. Coverage right now is complete over the United States, so any area of interest has imagery available. The coverage by Skylab is very limited, and photography of a given area may well not exist.
2. Coverage by the ERTS satellite is repetitive. This characteristic offers not only the capability for studying time-variant phenomena, but a greater probability of obtaining images under near-optimum conditions. The limited opportunities of Skylab precluded acquisition of cloud-free photographs over even some of the priority target areas.

3. ERTS images are generally available at lower sun angles than Skylab photos (though perhaps not low enough). Even though Skylab photos could theoretically be acquired at optimally low sun angles, they in fact were not.
4. ERTS data are suited to automatic processing, whereas Skylab photographs are not. For geologic purposes, however, this apparent advantage is more theoretical than real, since, to date, no practical advantage of this capability has been demonstrated. (Skylab's S192 multispectral scanner data have not yet been properly evaluated.)

The Skylab camera systems have several advantages compared to ERTS:

1. The resolution of Skylab cameras is far superior to the resolution of the ERTS scanner, providing far more scene detail. This is particularly true of the S190B camera, with its 18-inch focal length.
2. Both Skylab camera systems provided color photographs, obviating the need for color-additive viewers or color reconstitution, with their attendant degradation.
3. Full stereo coverage is possible along the ground track, although sufficient endlap was not always acquired.
4. Not only could Skylab obtain photography with optimally low sun angle, but the whole range of southwest illumination azimuths was available.

A distillation of the above comparisons would suggest that advantage should be taken of both systems, where possible, under as many different conditions as possible. Where good, cloud-free, S190B color photography with full endlap stereo is available, it will provide the most geologic information.

GEOLOGIC INFORMATION FROM SATELLITE IMAGES

APPLICATIONS OF SPACE DATA

Images from ERTS and Skylab are merely interesting curiosities unless skillful, enterprising geoscientists extract and use the basic geologic information in the data. In this respect, space data are not different from aircraft photography; only the scale and detail of the available information are more regional in scope.

Prior to the acquisition of space data, great effort was made to produce mosaics covering large areas to get the regional overview. Often this was the only way to obtain an understanding of the regional geologic framework. Mosaics were used during the initial stages of geologic investigation to pinpoint areas of interest, and later were used to check, extend, and correlate geologic information from field studies. Space images serve this purpose even better.

ERTS and Skylab images exist over many parts of the world for which aircraft photography does not exist and, hence, are the only available images. They can be effectively applied to many geologic problems, and they become even more powerful when combined with aircraft photography and field investigations. Some examples of the broad applications of space images are discussed below.

TECTONIC ANALYSIS

ERTS and Skylab images provide a tool by which the geoscientist can probe into the tectonic evolution of large regions of the earth's crust. Tectonic analysis may utilize geologic maps constructed from space images or it may involve specially-prepared maps showing only the major structures of a region. In either case, tectonic analysis may be geared toward more specialized problems, such as mineral or petroleum exploration.

A good example of tectonic analysis using ERTS imagery is the work of Dr. R.J. Weimer of the

Colorado School of Mines (CSM) in the area of the Raton Basin of south-central Colorado (Fig. 17).

Figure 17: ERTS image 1189-17091 of the Raton basin area of south-central Colorado. Major lithologic contacts and structures are shown. S, intrusive body at Spanish Peaks with radiating dike swarm; C, cinder cone in the San Luis Valley; F, basaltic lava flows of Raton Mesa; A, anticline.

On the ERTS image, certain key lithologic units were mapped to show the basin and mountain-flank structures in the area. A stratigraphic section was developed that could be traced throughout the area. The intrabasinal anticline (a possible oil trap) found on the imagery (Fig. 17,A) is one

example of the potential of tectonic analysis of ERTS imagery for petroleum exploration. This structure has been drilled, but it is not a producer.

Intrusive igneous rocks have invaded the sedimentary rocks at S, and numerous radiating dikes can be seen associated with the intrusive bodies. From this relatively simple tectonic map, a sequence of geologic events can be interpreted.

1. Basining and sedimentation
2. Folding
3. Intrusion
4. Erosion

Although this analysis did not produce much "new information" in this area because many ground investigations had already been conducted, this same type of analysis would be valuable in less well-known part of the world. However, the potential of discovering new tectonic relationships even in relatively well-known areas exists because of the regional overview provided by ERTS and Skylab images. It is in the capability of discovering "new information" and the isolation of critical areas for more detailed geologic study that the real worth of space images will ultimately be measured.

PETROLEUM EXPLORATION

Today the search for petroleum has attained a premier position. Geologic studies of ERTS imagery of northwestern Colorado by Dr. D.W. Trexler of Colorado School of Mines (reported in Knepper, 1973) suggests that space images may be useful tools in exploring for new petroleum reserves.

ERTS imagery of a highly petroliferous area of northwestern Colorado (Fig. 18) was studied to determine if numerous folds in the area could be mapped. The troughlines and crestlines of 63 folds were mapped and most of these correlate with known

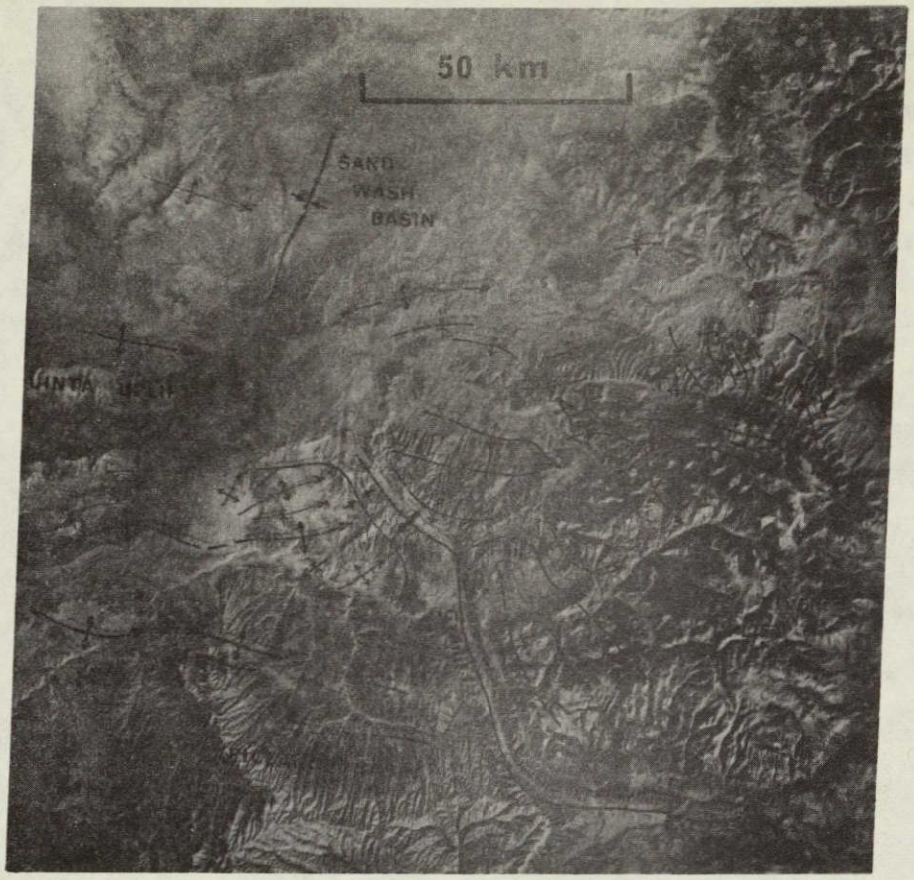

Figure 18: ERTS image 1156-17253-7 of northwestern Colorado showing major folds of the region. Structural symbols displaced slightly so as not to obscure image expression (shadows of symbols at proper location).

folds in the area, several of which are producing or have produced oil. Several folds were mapped on the ERTS imagery that do not correlate with known folds in the area. These "new" folds have not been verified in the field, but the good correlation of the other ERTS-mapped folds with known structures suggests that the "new" folds are surely worthy of more study. The fact that potential structural traps can be mapped on ERTS imagery indicates that the use of ERTS or Skylab images will increase the efficiency of oil exploration in other parts of the world.

MINERAL EXPLORATION

Linear patterns suggesting fractures or fracture zones (lineaments) are commonly the most abundant geologic information that can be extracted easily from ERTS and Skylab images. Analysis of these lineaments can take a variety of directions, depending on the specific geologic problem that is being investigated. One of the more interesting and potentially useful methods of applying this type of fracture information was demonstrated by S.M. Nicolais at the Third ERTS-1 Principal Investigator's Symposium. The study showed that analysis of specific lineament patterns, combined with frequency of intersections, can be a fairly reliable guide to areas of metallic mineralization in central Colorado. The method and results of this investigation are briefly summarized below--see Nicolais (1973) and Knepper (1973) for detailed discussions.

Well-defined lineaments, poorly- to moderately-expressed lineaments, and circular or strongly curved lineaments were mapped on a 1:1,000,000 positive transparency of an ERTS image of central Colorado (Fig. 19A,B). Under the assumptions that metallic mineralization is controlled by fractures and shear zones, and that mineralization is usually associated with intrusive and volcanic centers, 10 circular areas of 14 km diameter were chosen as potential sites of metallic mineralization (Fig. 19B). Priorities were assigned to each of the 10 target areas based on 1) frequency of lineament intersections and 2) types of lineaments. Areas of high density of lineament intersections, associated with circular lineaments suggestive of intrusive or volcanic centers, were considered the most promising areas for exploration.

The target areas picked from the ERTS lineament map were compared to the known mineral producing areas of the ERTS image (Fig. 19C). Five of the ten target areas together included the Breckenridge, Leadville-Climax-Alma, Tomichi, Bonanza, and Cripple Creek mining districts, which

A. ERTS image

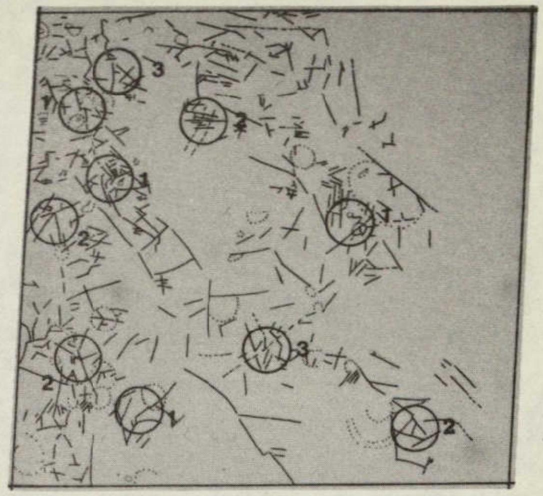

B. Lineament map.

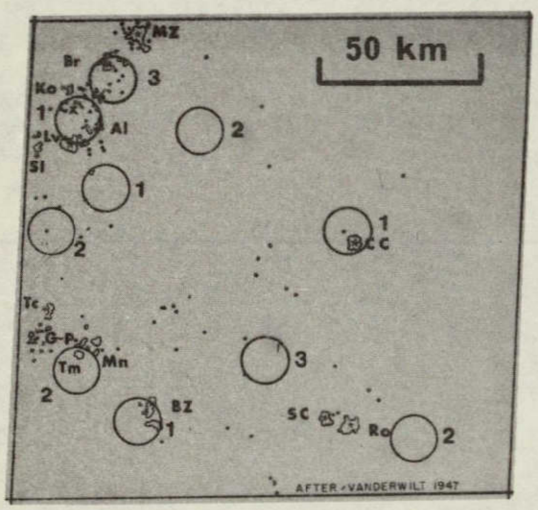

C. Mineral districts

MZ - Montezuma
Br - Breckenridge
Ko - Kokomo
Cx - Climax
Al - Alma
Lv - Leadville
SL - Sugarloaf
Tc - Tincup
G-P - Goldbrick-Pitkin
Mn - Monarch
Tm - Tomichi
BZ - Bonanza
SC - Silver Cliff
Ro - Rosita
CC - Cripple Creek

Figure 19: ERTS imagery applied to metallic mineral exploration in central Colorado. Numbered circles are target area selections and their priority (1, highest, etc.). Irregular, starred areas are major mineral districts; small dots are areas of minor production.

have a combined metallic mineral production of \$2,438,328,722 (Marsh and Queen, 1973). Even more significantly, three of the four target areas given the highest priority rating included the Leadville-Climax-Alma, Bonanza and Cripple Creek mining districts, which together have produced \$2,374,399,283, or 97% of the total mineral production within the areas outlined by the 10 original target areas.

Because these results were much better than had been anticipated, it was suspected that the photo-interpreter's prior knowledge of the location of many of the mineral districts may have unduly biased his original 10 target area selections. To check this, mis-oriented copies of the lineament overlay (only) were distributed to 15 geology professors and graduate students at the Colorado School of Mines. Each member of the group was asked to outline 10 circular target areas of 14 km diameter that they believed held potential for metallic mineralization. The results of the test group's selections are shown in Table 1.

Without knowing where the test area was or having the benefit of the ERTS image to study, a large percentage of the test group chose the same target areas as did the original photo-interpreter. This indicates that prior geologic knowledge had little influence on the selection of the original ten target areas and increases the credibility of using ERTS photo-lineament information as a guide to mineral exploration.

Since the structural control and intrusive and volcanic associations of metallic mineral deposits are not unique to central Colorado, this technique should be applicable to less well known regions of the world. The real application of this technique is not to directly find mineralization from ERTS or Skylab images, but to restrict the areas of search to primary target areas that would have to be studied in more detail, both from

aircraft photography and in the field. To this end, the technique appears to be very effective.

MINERAL DISTRICTS	A	B	C	D	E	F	G	H	I	J	K	L	M	N	O	P	%
MONTEZUMA																	
BRECKENRIDGE												X				0	13
KOKOMO				X	X	X							X		X		31
CLIMAX	X			X	X	X	X	X		X	X		X	X	X	0	75
LEADVILLE	X		X	X	X	X	X	X	X	X	X			X		0	75
ALMA	X		X	X	X	X	X	X		X	X		X	X	X	0	81
SUGARLOAF																	
TINCUP									X								6
GOLDBRICK-PITKIN					X												6
TOMICHI			X		X	X		X			X	X		X	X	0	56
MONARCH	X	X			X	X	X			X				X			44
BONANZA	X					X	X	X		X				X		0	44
SILVER CLIFF																	
ROSITA																	
CRIPPLE CREEK			X	X		X	X	X	X	X		X	X	X	X	0	75

Table 1. Test group results. Each letter across the top corresponds to a member of the test group. X's identify mineral districts included in target area selections; O's identify mineral districts included in original target area selections. The last column shows the percent of group selecting each mineral district.

SUMMARY

We have discussed briefly several geologic applications for which ERTS and Skylab images can be used--many more can be imagined. However, the geologic applications of space images will be largely limited to problems for which regional geologic relationships and the general geology of large areas must be determined. Furthermore, there are but a few types of geologic problems for which analysis of ERTS or Skylab images will produce the ultimate solution; more commonly, detailed studies of selected areas by aircraft photography and ground investigations will be necessary to

provide the final answers. In areas of the world where the geology is not well known, particularly in the underdeveloped countries, ERTS and Skylab images may be applied with a high probability of producing beneficial new information. Even in relatively well-known areas, such as the continental U.S., new information may be found on space images, but finding it will be more difficult.

We have shown some examples where the extraction and analysis of basic geologic information derived from ERTS and Skylab can be applied to specific geologic problems. Further applications will be developed by innovative geoscientists capable of treating this new type of geologic information. At this stage, therefore, it is difficult to place firm limits on the applicability of ERTS and Skylab images to geologic studies--the avenues to potential applications have barely been opened.

CONCLUSIONS

1. Satellite images contain the same geologic information as do conventional aerial photographs - basically lithology, structure, and landforms.

2. The fundamental differences between satellite images and aircraft aerial photographs are scale and resolution. The main effect of smaller scale is to portray regional geologic features in a new, synoptic perspective; poorer ground resolution tends to smooth out (average) minor variations.

3. As with conventional air photos, the geologic interpretation of space images is based on deduction from surface phenomena. Topography is the single most important surface expression interpreted.

4. In the deductive interpretation, the geologist-interpreter is necessary.

5. Skylab S190B color photography, where available, provides more geologic information than any other single satellite sensor. Maximum geologic information is derived from images of different sensors acquired under differing conditions.

6. More geologic information is contained in space images than can be interpreted or mapped at original scales. Interpretation should be conducted under magnification of low-generation contact transparencies and mapping carried out on enlarged prints or transparencies.

7. All interpretations of space images must be verified by field checking, perhaps more so than interpretations of air photos, due to our lack of familiarity with these new forms of data.

8. Maximum geologic information will be extracted through an iterative process of image interpretation and field checking.

9. Space images are an excellent buy for geologists. NASA has already acquired them, and the only cost to the user is for copies.

ACKNOWLEDGMENTS

This research was conducted at the Colorado School of Mines with financial support from the National Aeronautics and Space Administration (Grant NGL-06-001-015 and Contracts NAS9-13394 and NAS5-21778). Some of the results presented here are derived from research conducted by Dr. Robert J. Weimer, Dr. David W. Trexler and Mr. Stephen M. Nicolais.

REFERENCES

Knepper, D.H., 1973, Geologic and mineral and water resources investigations in western Colorado using ERTS-1 data: Progress Report IX: Colo. School of Mines Remote Sensing Report 73-5, 53 p.

Marsh, W.R. and Queen, R.W., 1973, Map showing localities and amounts of metallic mineral production in Colorado: U.S. Geol. Survey Open-file Report, 6 p.

Nicolais, S.M., 1973, Mineral exploration with ERTS imagery: in Proceedings of the Third ERTS Symposium, Mineral Resources, Geologic Structure and Landform Surveys section (in press).

Raines, G.L., and Lee, Keenan, 1974, An evaluation of multiband photography for rock discrimination: this publication.

Sawatzky, D.L., and Lee, Keenan, 1974, New uses of shadow enhancement: this publication.

Vanderwilt, J.W., 1947, Mineral resources of Colorado: Colorado Mineral Resources Board, Denver, 547 p.

INDEX OF SKYLAB DATA
AVAILABLE AT
COLORADO SCHOOL OF MINES

EREP Investigations 380

Contract NAS-13394

Geology Department
Colorado School of Mines
Golden, Colorado 80401

Remote Sensing Report 74-8

31 October 1974

REMOTE SENSING PROJECTS

INDEX OF SKYLAB DATA AVAILABLE AT COLORADO SCHOOL OF MINES

Gary L. Prost

Remote Sensing Report 74-8

31 October 1974

CONTENTS

Page

INDEX OF SKYLAB DATA

AVAILABLE AT

COLORADO SCHOOL OF MINES

EXPLANATION

This index is organized according to

I. Mission
   A. Sensor
      1. Track; date (or orbit; GMT start, stop)
         a. Format (including size, pos. or neg., spectral band, transparency or print, roll and frames, and cloud and snow information)

For each mission (Skylab 2,3, or 4) there is a page indexing each individual sensor, followed by a map showing the approximate coverage over Colorado for the sensor. The photography has endlap varying from zero to sixty percent.

'S190-A' refers to the Skylab 6-camera multiband system, where each camera has a six-inch focal length. Frames are 88 naut. mi. per side.

'S190-B' refers to the Skylab high-resolution earth terrain camera, which has an 18 inch focal length. Frames are 59 naut. mi. per side.

'S191' refers to analog tape and tracking film.

'S192' refers to a 13-channel multispectral scanner.

The scale of a 70mm (2.25 inch per side) S190-A frame is approximately 1:2,800,000; for a 9x9 inch S190-A frame it is ~1:700,000. The scale for the 4½x4½ inch S190-B frames is ~1:950,000; for a 9x9 inch S190-B frame it is ~1:475,000.

The S190-A spectral bands referred to as 'photo-IR, photo-IR, CIR, color, red, green' correspond to the wavelengths '700-830nm, >790nm, color-infrared, color, 600-700nm, and 490-600nm' respectively.

Channels 2,7, and 11 on the S192 correspond to the wavelengths 460-510nm, 780-880nm, and 1.55 to 1.75μm, respectively.

The term 'roll' followed by a number is the NASA film magazine identification.

The term 'orbit' means the same as the term 'pass'.

GMT (Greenwhich Mean Time) start a:b:c:d or GMT stop a:b:c:d refers to the time that a pass started and ended. The 'a' refers to the day of the year (begin counting at Jan. 1=1), 'b' refers to the hour of the day (0 = midnight), 'c' refers to the minute, and 'd' refers to the second. Mountain Standard Time is equal to G.M.T. minus 7 hours; Mountain Daylight Time is G.M.T. minus 6 hours.

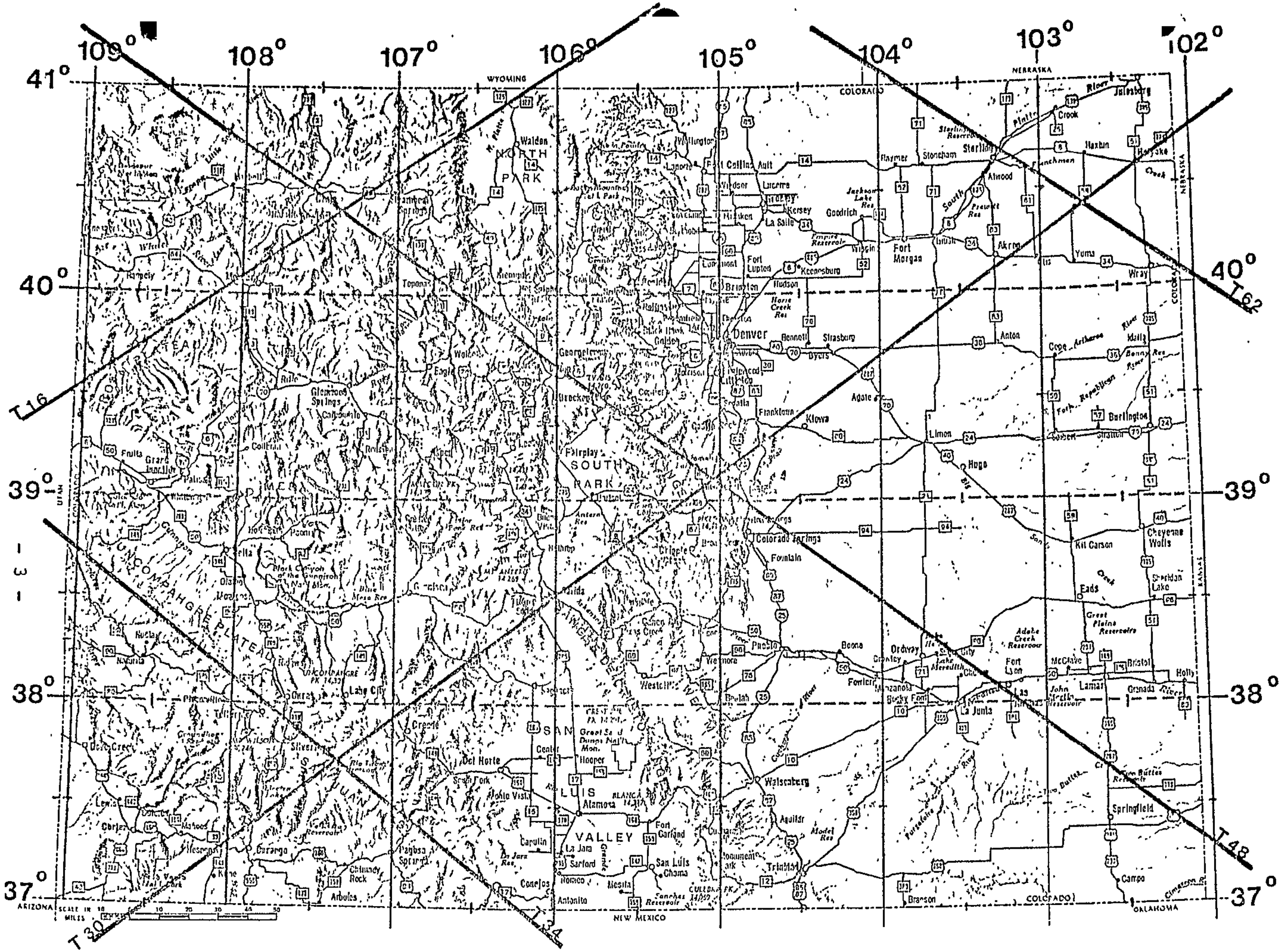

Skylab Ground Track

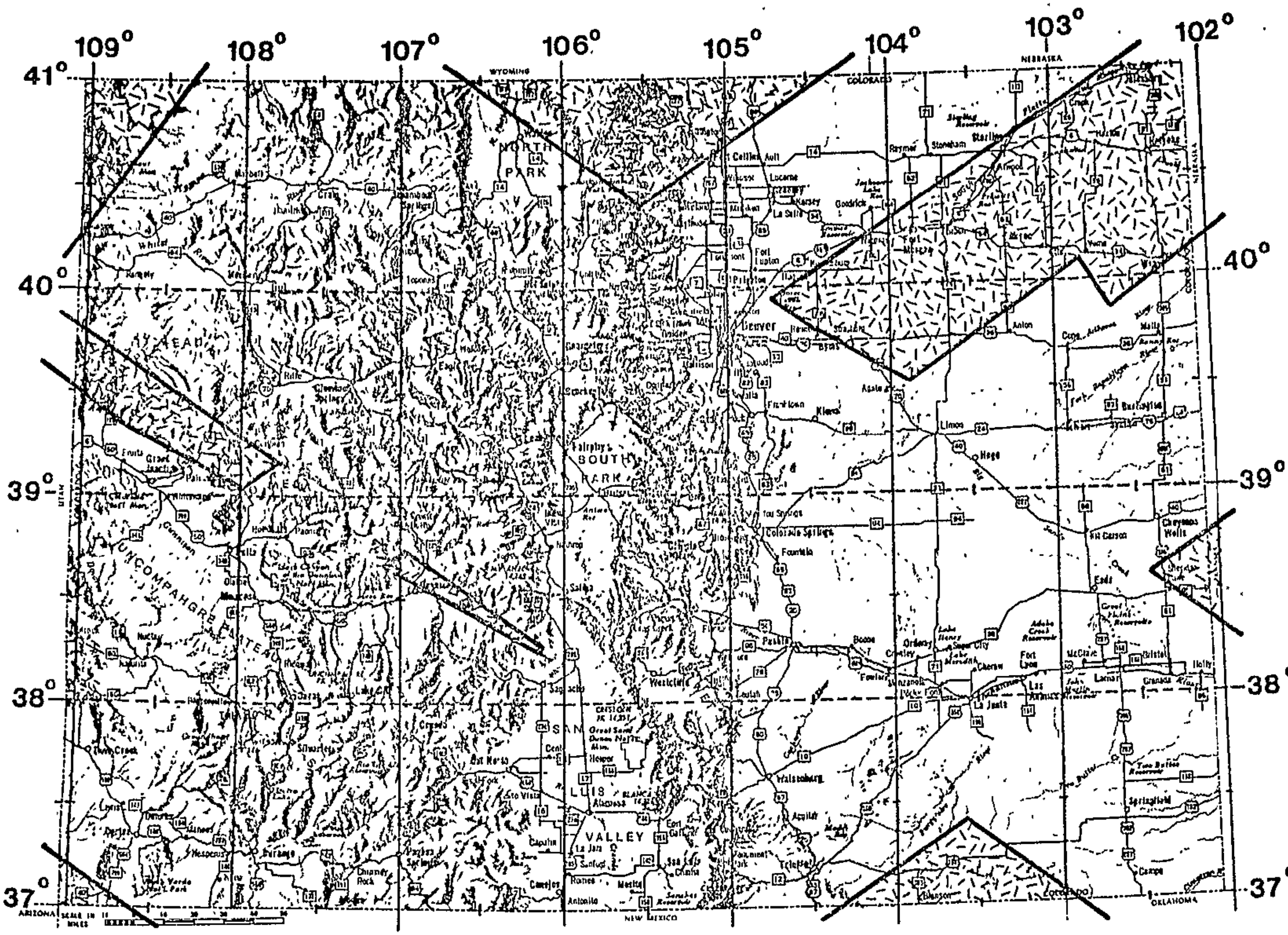

TOTAL SKYLAB

DATA COVERAGE

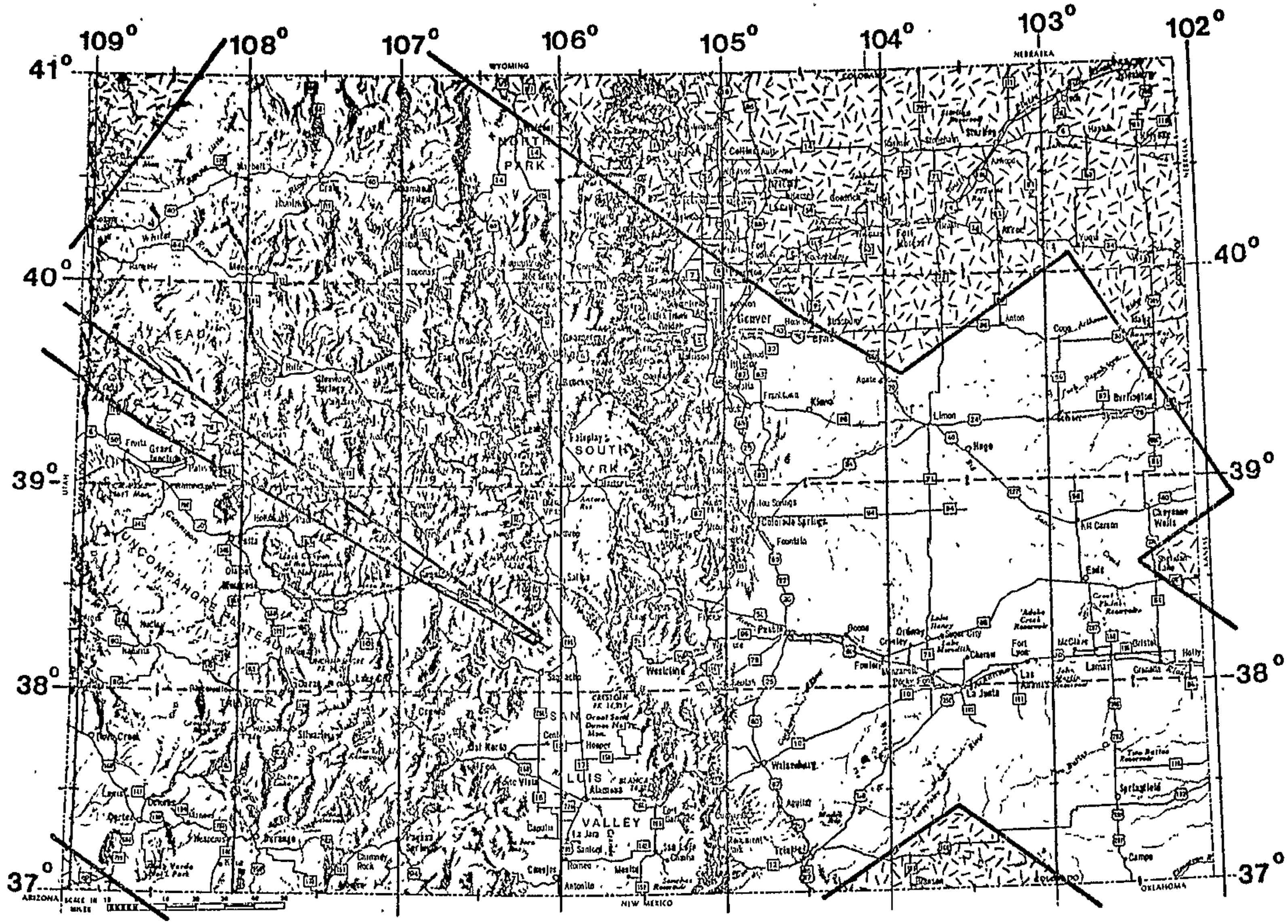

TOTAL SKYLAB

S190-A PHOTOGRAPHY

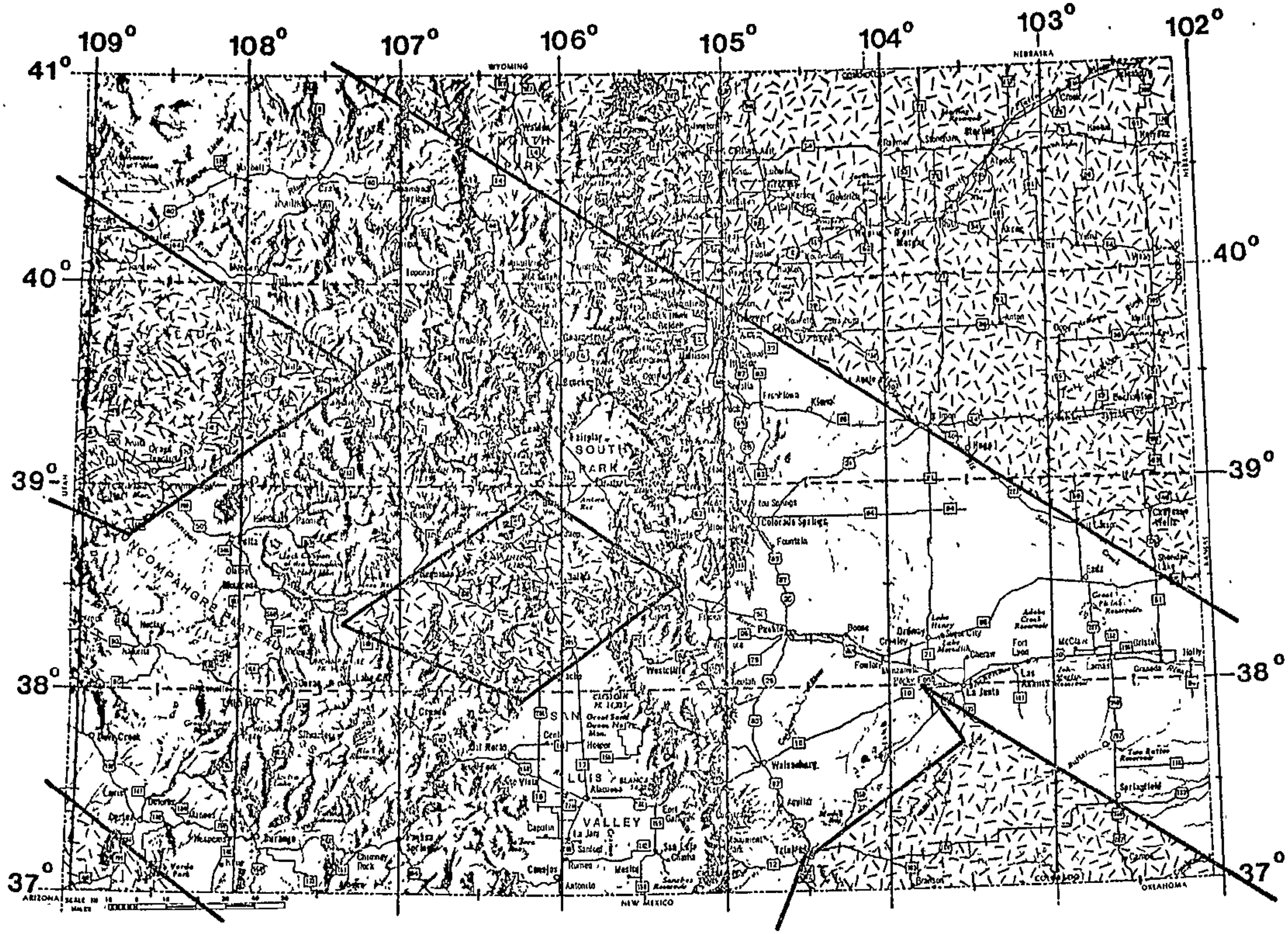

TOTAL SKYLAB

S-190B PHOTOGRAPHY

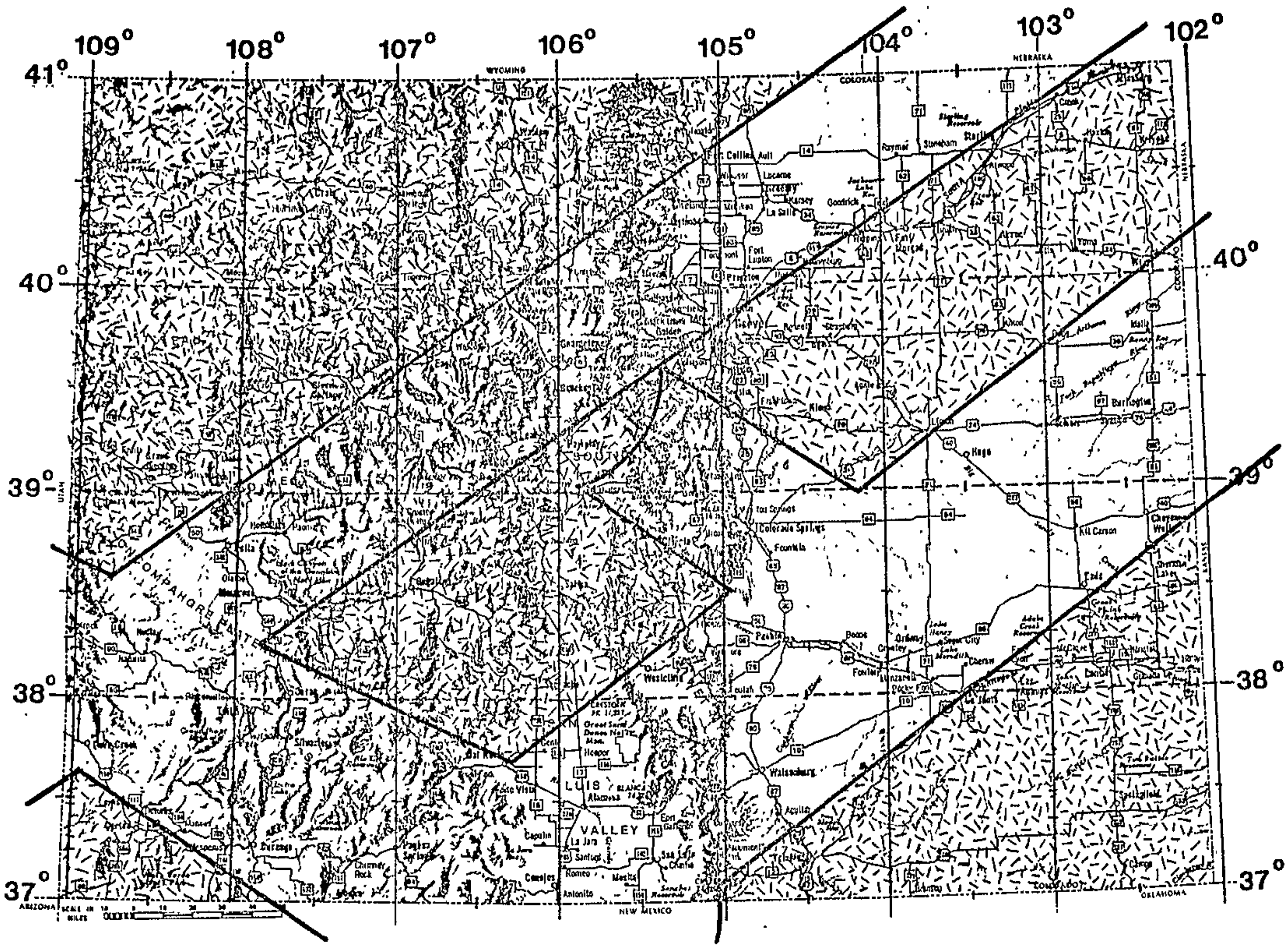

TOTAL SKYLAB

S-192 IMAGERY

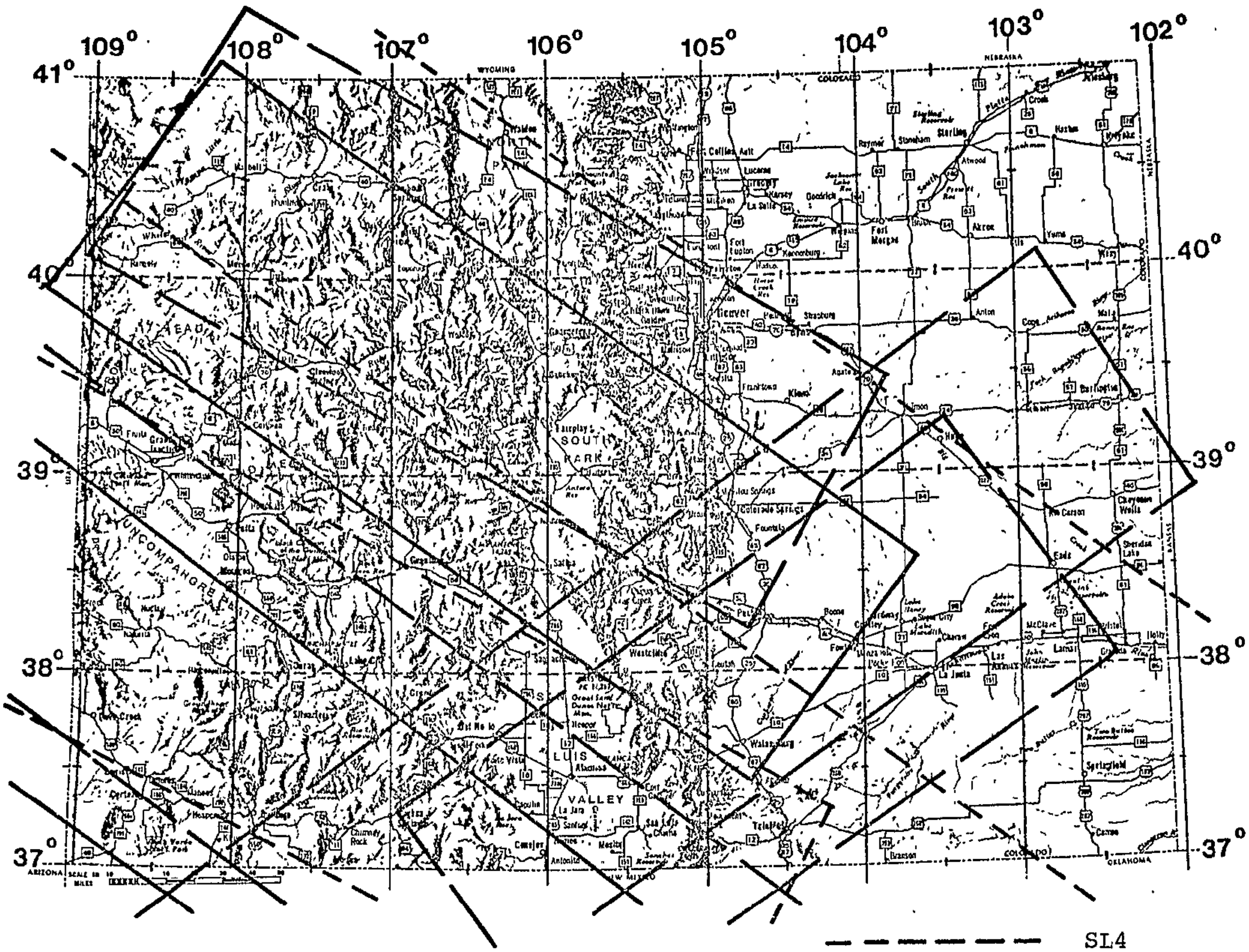

S-190A PHOTOGRAPHY

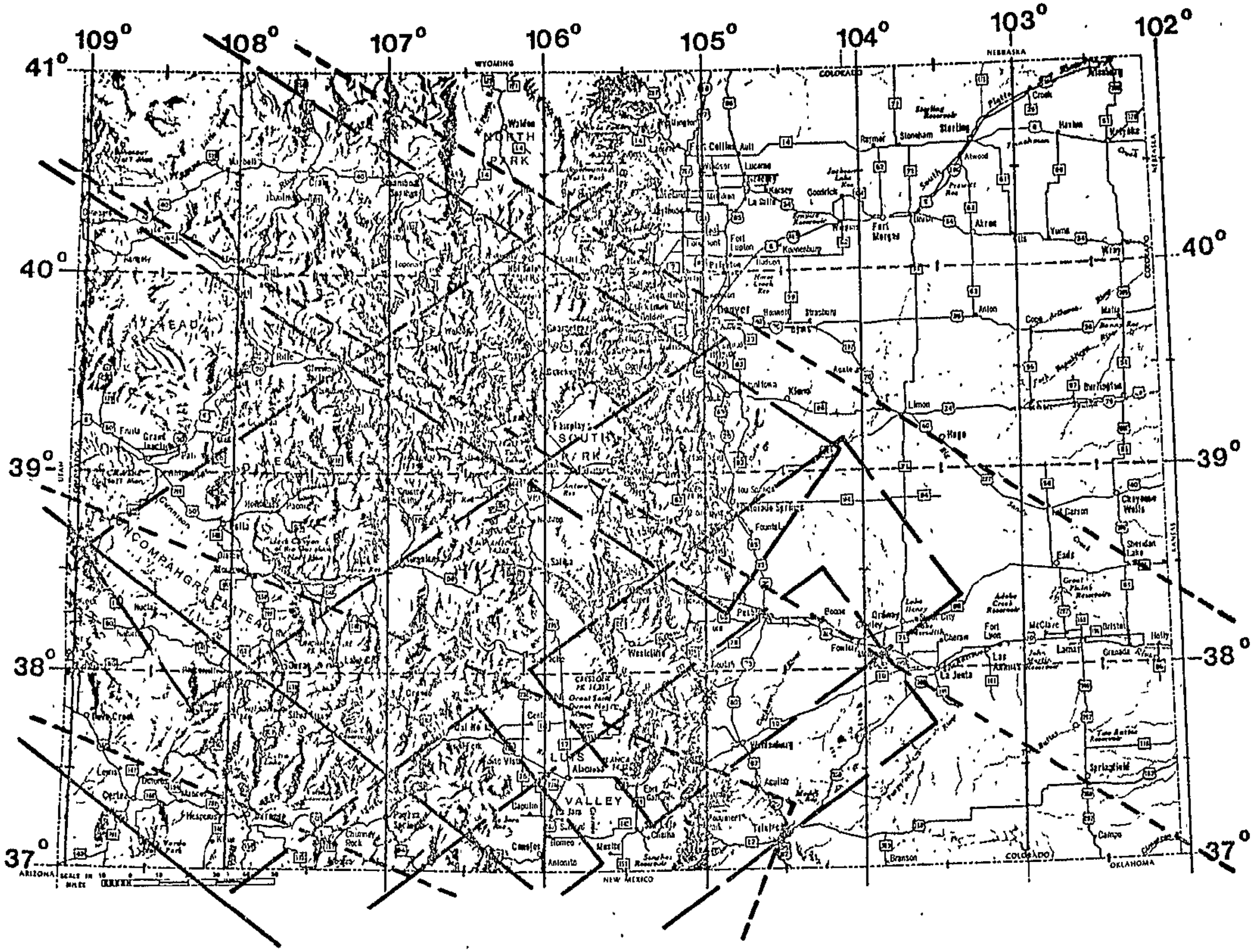

S-190B PHOTOGRAPHY

SL4

SL3

SL2

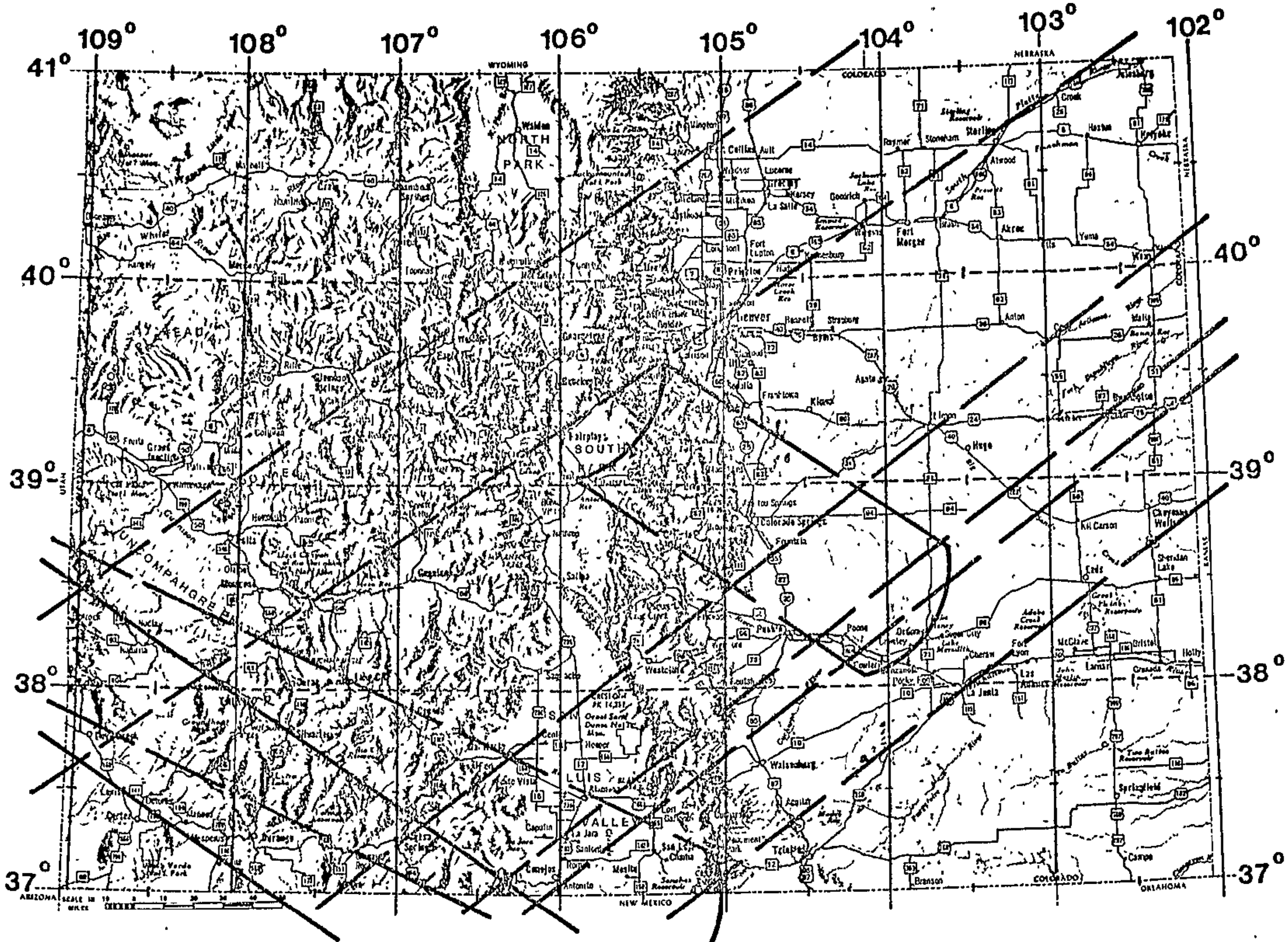

S-191 IMAGERY

SL4

SL3

SL2

I.A. SKYLAB 2 S-190A

1. Track 34, 5 June 73

   a. 70mm pos. & neg. transparencies, rolls 7,8,9,10,11, and 12 (photo-IR, photo-IR, CIR, color, red, and green bands respectively), frames 12-20. Snow-covered above 11,000 ft. About 10% cloud cover.

   b. 7x8" B/W, color, CIR prints of rolls 7-12.

   c. 9x9" pos. & neg. trans. of rolls 7-12. 2 each of color & CIR.

2. Track 48, 11 June 73

   a. 70mm pos. & neg. trans., rolls 13-18 (photo-IR, photo-IR, CIR, color, red, green, respectively), frames 11-28. Snow-covered above 11,000 ft. About 10% patchy clouds.

   b. 7x8" B/W, color, CIR prints of rolls 13-18.

   c. 9x9" pos. & neg. trans. of rolls 13-18. 2 each of color & CIR.

   d. 9x9" pos. print; 18x18" pos. print; 27x27" pos. print, roll 17, frame 17 (enlargements of central Colorado area).

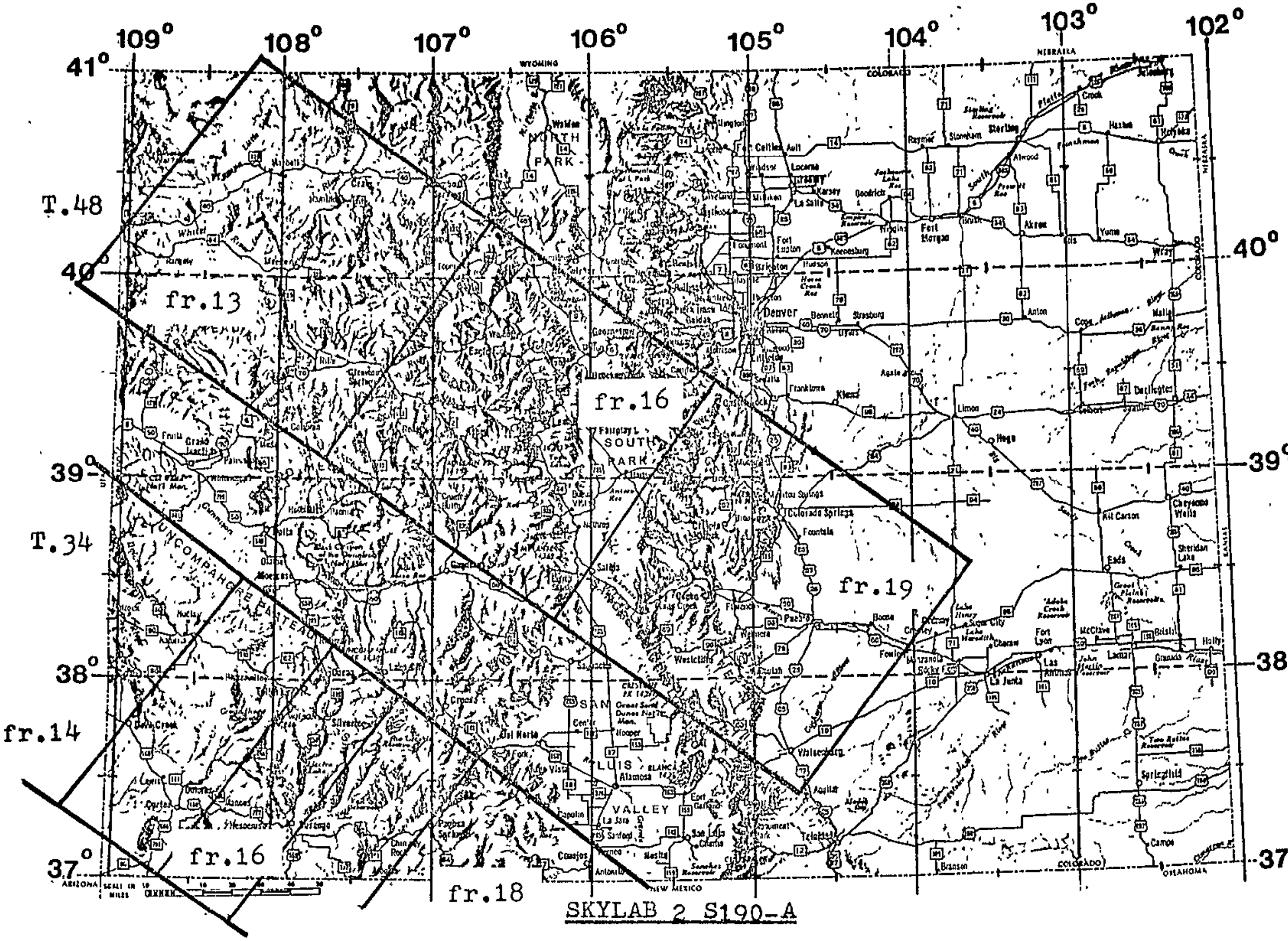

SKYLAB 2 S190-A

T.34, 5 Jn 73, rolls 7-12, fr.12-20. Snow above 11,000 ft.; about 10% cloud cover.
T.48, 11 Jn 73, rolls 13-18, fr.11-28. " " " ; " " " ".

I.B. SKYLAB 2 S-190B

1. Track 34, 5 June 73

   a. $4\frac{1}{2}$x$4\frac{1}{2}$" pos. trans., color, roll 81, frames 16-27. Snow over 11,000 ft. About 10% cloud cover.

   b. 9x9" pos. trans., color, 2 each.

   c. 9x9" pos. prints, color.

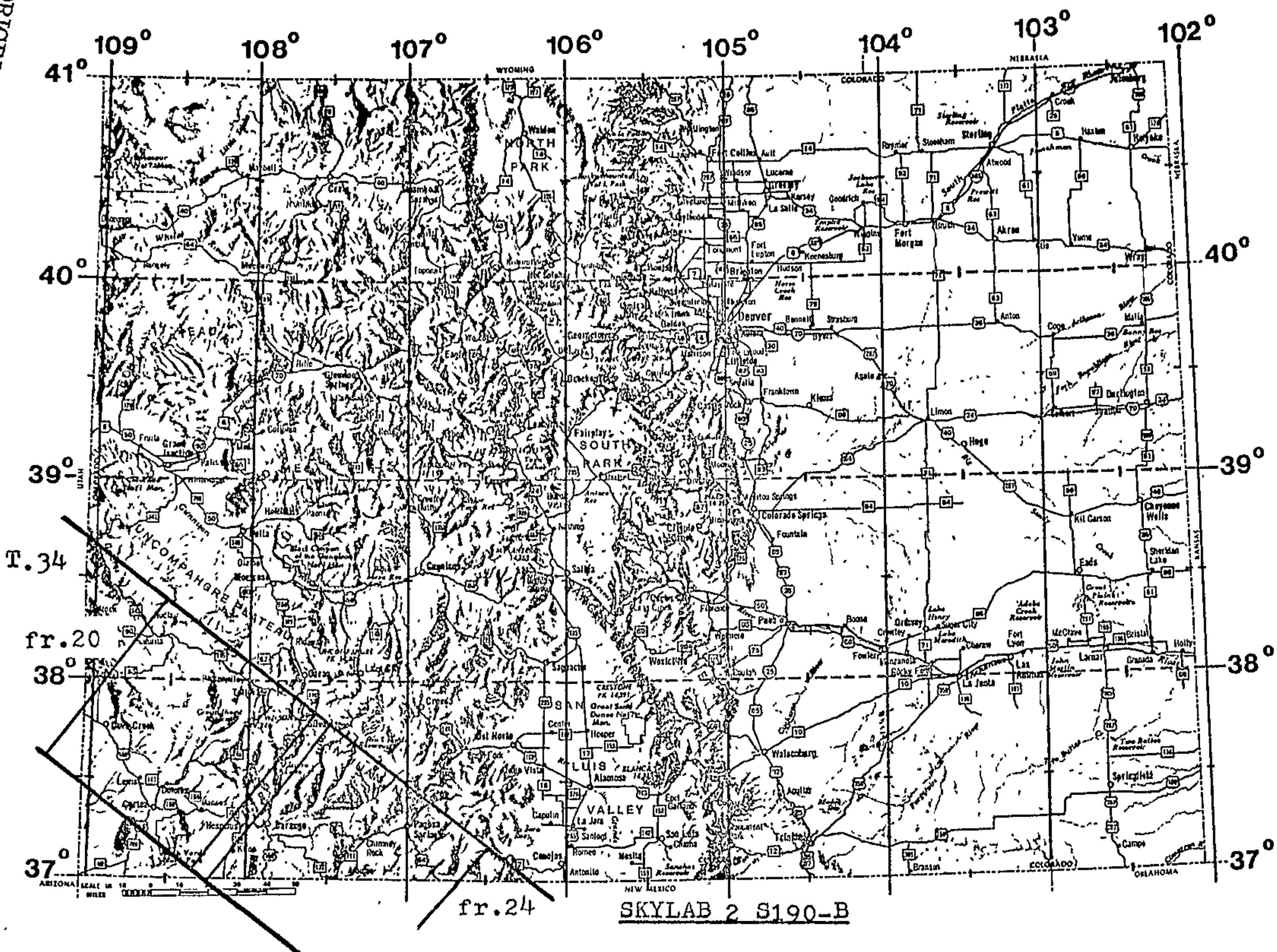

T.34, 5 Jn 73, roll 81, fr.16-27. Snow above 11,000 ft.; about 10% cloud cover.

I.C. SKYLAB 2 S-192

1. Track 34, 5 June 73, Orbit 5; GMT start 156:17:57:02, GMT stop 156:18:02:52.

   a. 1x6" pos. trans. "screening film", channels 2,7, and 11. Snow above 11,000 ft. About 10% cloud cover.

   b. 8x10" pos. prints, "screening film", channels 2, 7, and 11.

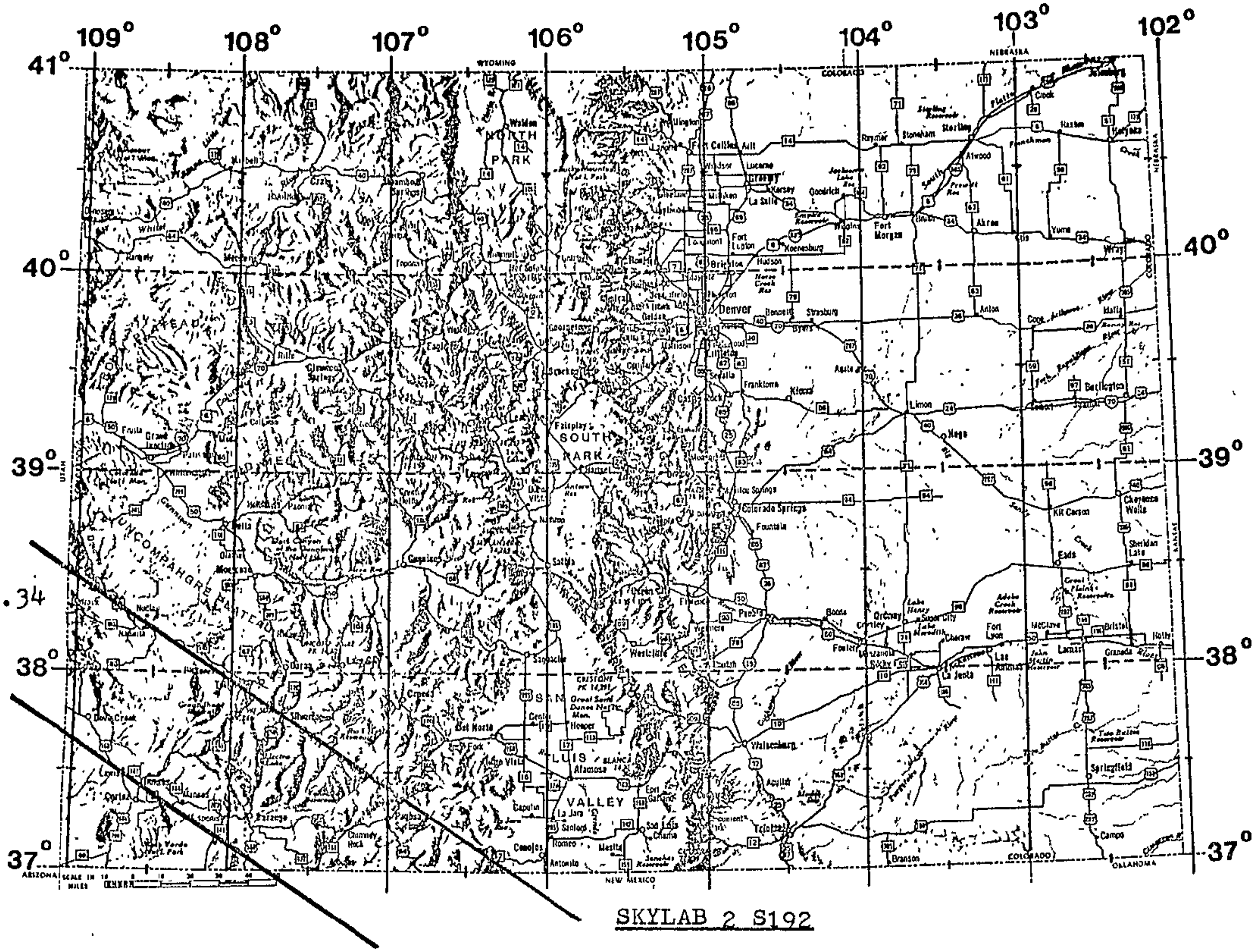

T.34, 5 Jn 73, Orbit (Pass) 5, GMT start 156:18:02:52, GMT stop 156:17:57:02.
Snow above 11,000 ft.; about 10% cloud cover.

II.A. <u>SKYLAB 3 S-190A</u>

1. Track 30, 6 Sept. 73

   a. 70mm pos. & neg. trans., rolls 31-36 (photo-IR, photo-IR, CIR, color, red, green, respectively), frames 248-256. No snow. About 25% cloud cover east of Colo. Spgs.

   b. 9x9" pos. trans., rolls 31-36. 2 each of color and CIR.

   c. 9x9" pos. prints, 2 each of all rolls.

2. Track 30, 16 Sept. 73

   a. 70mm pos. & neg. trans., rolls 43-48 (photo-IR, photo-IR, CIR, color, red, green, respectively), frames 61-73. No snow. Totally cloud-covered east of Pueblo.

   b. 9x9" pos. trans., rolls 43-48. 2 each of color and CIR.

   c. 9x9" pos. prints, 2 each of all rolls.

3. Track 34, 3 Aug. 73

   a. 70mm pos. & neg. trans., rolls 19-24 (photo-IR, photo-IR, CIR, color, red, green, respectively), frames 1-9. No snow. About 20% patchy clouds over San Juans.

   b. 9x9" pos. trans., rolls 19-24. 2 each of color and CIR.

   c. 9x9" pos. prints, 2 each of all rolls.

4. Track 48, 4 Aug. 73

   a. 70mm pos. & neg. trans., rolls 19-24 (photo-IR, photo-IR, CIR, color, red, green, respectively), frames 102-113. Minor snow. About 20-40% patchy clouds over mountains.

   b. 9x9" pos. trans., rolls 19-24. 2 each of color and CIR.

   c. 9x9" pos. prints, 2 each of all rolls.

5. Track ?, Date ?, Cape Mendocino, Calif.

   a. 70mm pos. & neg. trans., rolls 31-36 (photo-IR, photo-IR, CIR, color, red, green, respectively), frames 336-345. Clouds over coast.

   b. 9x9" pos. trans., rolls 31-36. 2 each of color and CIR.

   c. 9x9" pos. prints, 2 each of all rolls.

ORIGINAL PAGE IS
OF POOR QUALITY

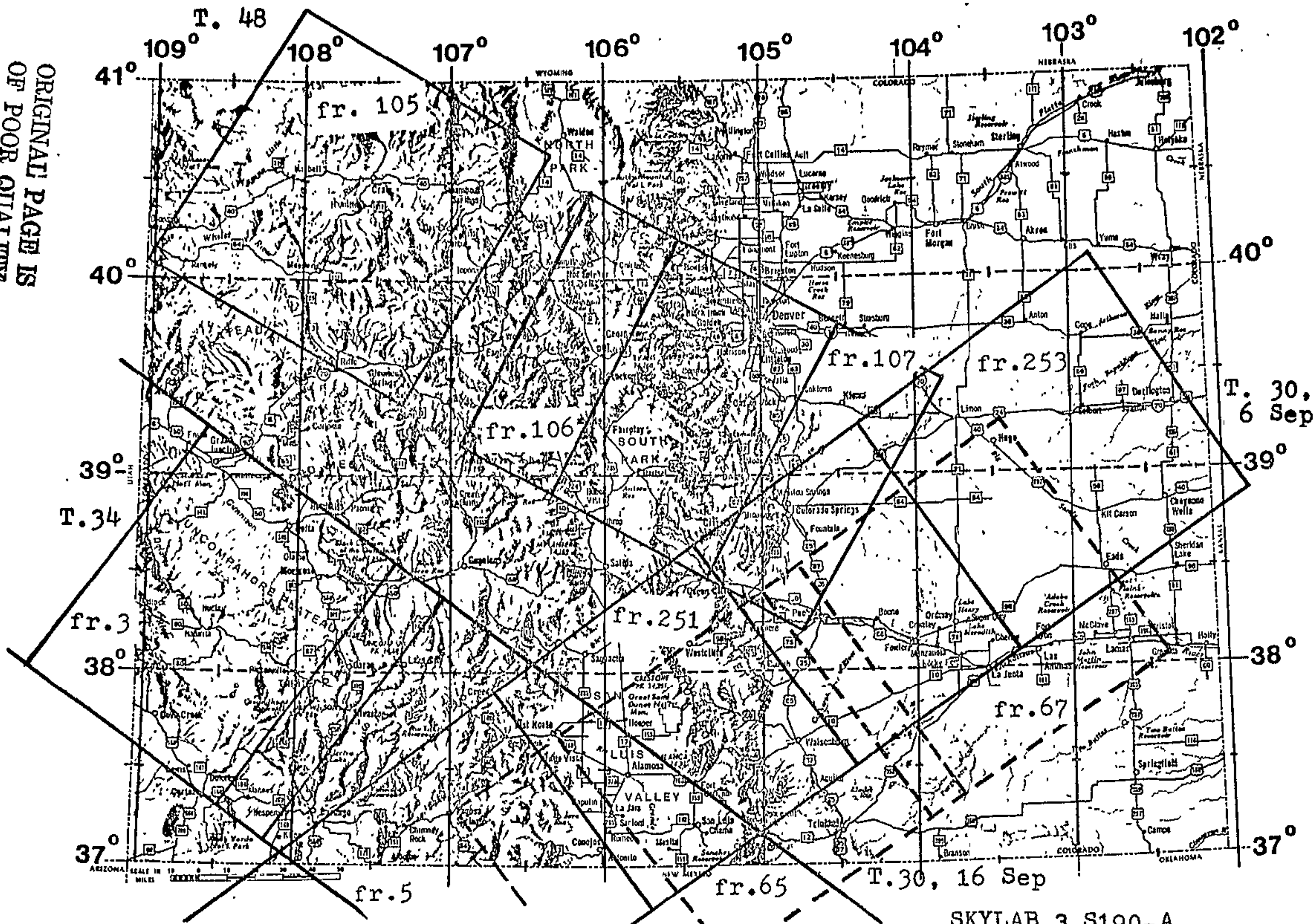

SKYLAB 3 S190-A

T.30, 6 Sep 73, rolls 31-36, fr.248-256. No snow; about 25% cloud cover east of Colo. Spgs.
T.30, 16 Sep 73, rolls 43-48, fr. 61- 73. " " ; 100% clouds east of Pueblo.
T.34, 3 Aug 73, rolls 19-24, fr. 01-09. " " ; patchy clouds over San Juans.
T.48, 4 Aug 73, rolls 19-24, fr.102-113. " " ; 20-40% clouds over mountains.

II.B. <u>SKYLAB 3 S-190B</u>

1. Track 16, 15 Sept. 73

   a. 4½x4½" pos. trans., CIR, roll 87, frames 117-127. No snow. 100% cloud cover east of Kremmling/Georgetown.

   b. 9x9" pos. prints, CIR, 2 each.

2. Track 30, 6 Sept. 73

   a. 4½x4½" pos. trans., color, roll 86, frames 19-28. No snow. About 25% clouds east of Colo. Spgs. Gap over San Luis Valley.

   b. 9x9" pos. prints, color, 2 each.

3. Track 30, 16 Sept. 73

   a. 4½x4½" pos. trans., color, roll 88, frames 103-123. No snow. 100% cloud cover east of Pueblo.

   b. 9x9" pos. prints, color, 2 each.

4. Track 48, 4 Aug. 73

   a. 4½x4½" pos. trans., color, roll 83, frames 33-45. Minor Snow. 30-50% patchy clouds.

   b. 9x9" pos. prints, color, 2 each.

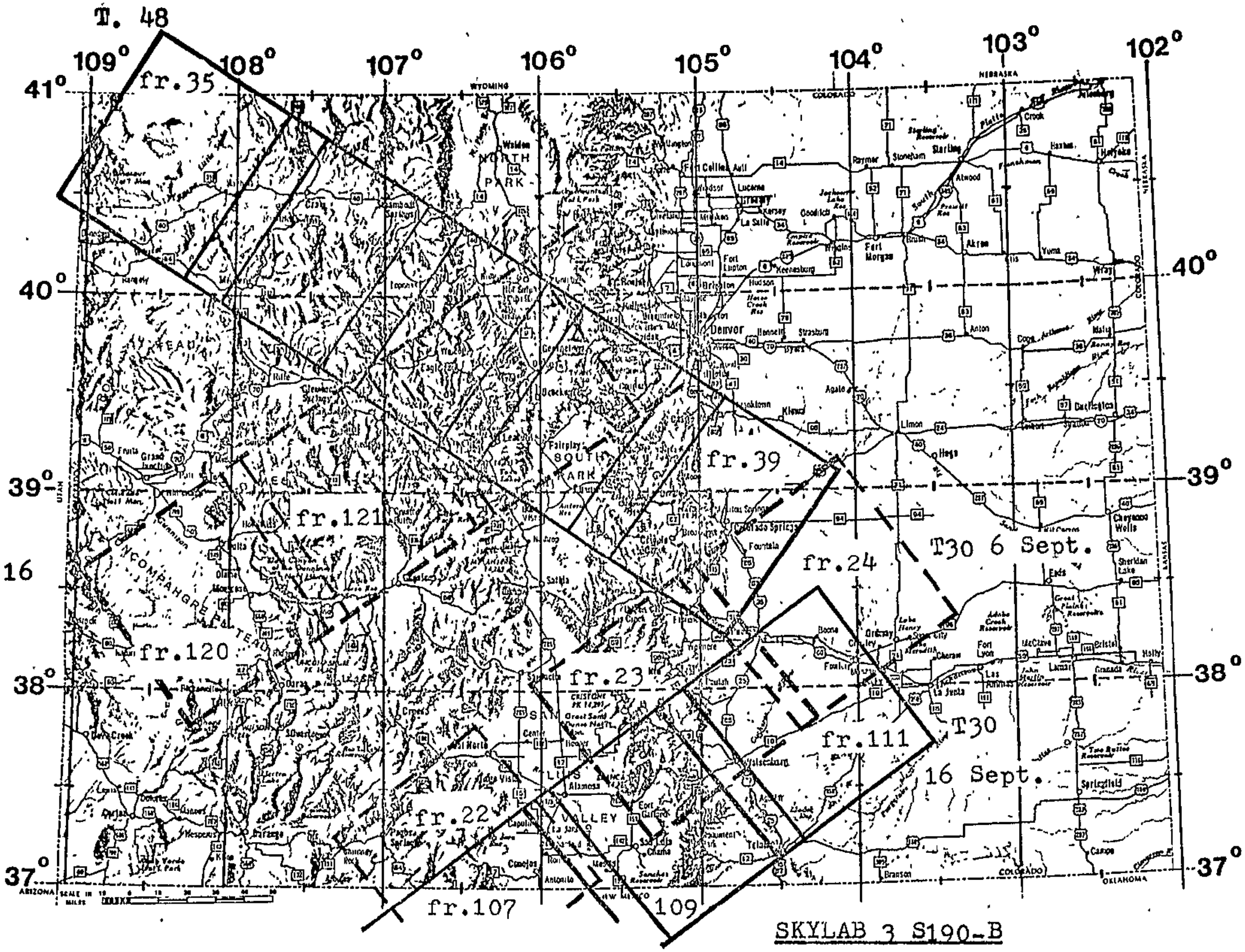

T.16, 15 Sep 73, roll 87, fr.117-127. No snow; 100% clouds east of Kremmling/Georgetown.
T.30, 6 Sep 73, roll 86, fr. 19- 28. No snow; about 25% cloud cover east of Colo. Spgs.
T.30, 16 Sep 73, roll 88, fr.103-123. No snow; 100% cloud cover east of Pueblo.
T.48, 4 Aug 73, roll 83, fr. 33- 45. Minor snow; 30-50% patchy clouds.

II.C. SKYLAB 3 S-191

1. Track 30, 16 Sept. 73, Orbit 45; GMT start 259:17:22:09, GMT stop 259:17:27:04.

   a. Analog tape and 16mm tracking film, Great Sand Dunes. No snow, no clouds.

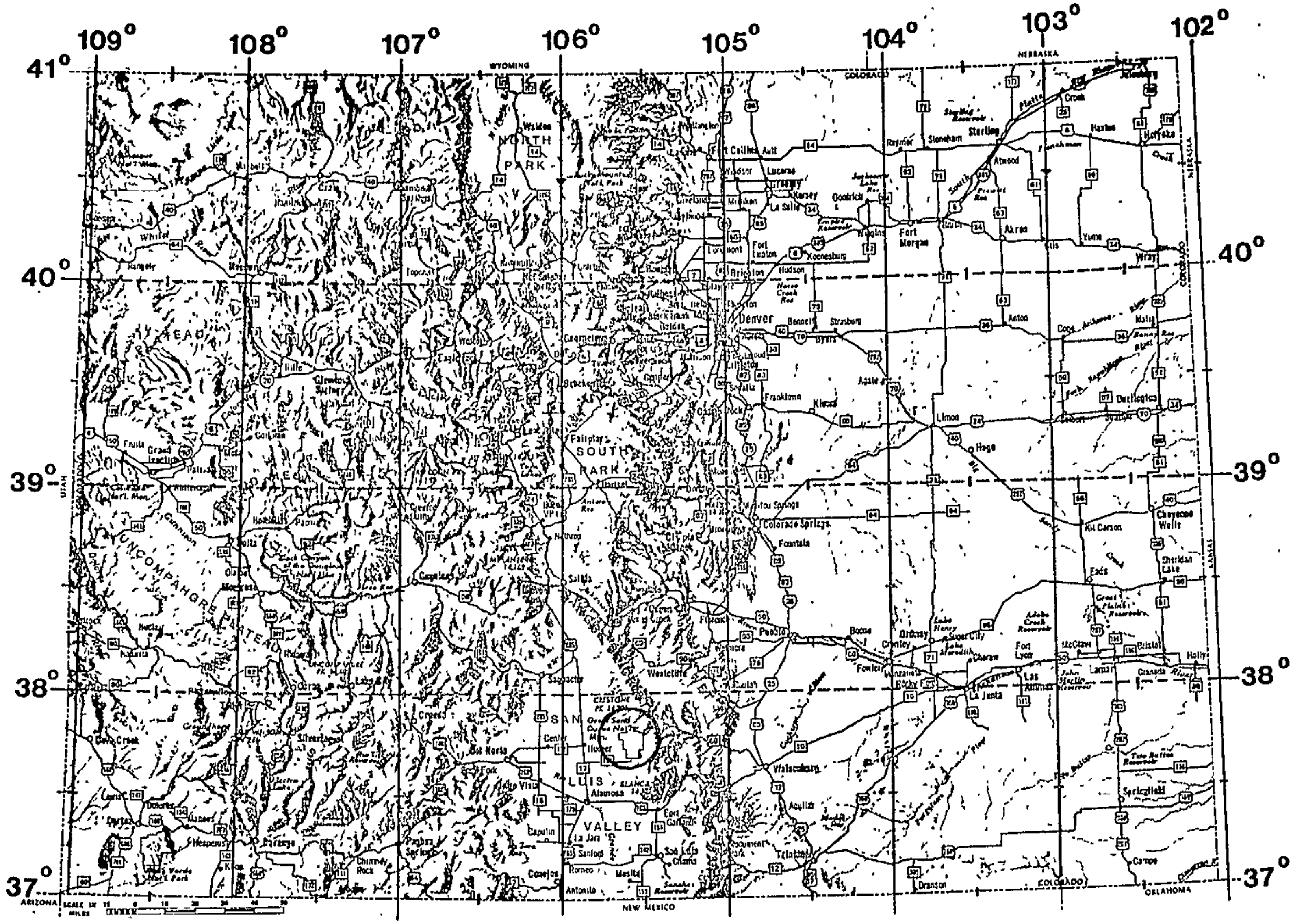

SKYLAB 3 S191

Orbit (Pass) 45, 16 Sep 73. Great Sand Dunes. No snow; no clouds.

II.D. SKYLAB 3 S-192

1. Track 16, 21 Sept. 73, Orbit 43; GMT start 264:18:06:50, GMT stop 264:18:08:31.

    a. 4" wide roll, pos. trans., channels 2,7,11, uncorrected "screening film". No snow. No clouds.

2. Track 30, 6 Sept. 73, Orbit 27; GMT start 249:21:26:14, GMT stop 249:21:27:38.

    a. 4" wide roll, pos. trans., channels 2,7,11, uncorrected "screening film". No snow. About 25% clouds east of Colo. Spgs.

3. Track 30, 16 Sept. 73, Orbit 45; GMT start 259:17:23:29, GMT stop 259:17:25:04.

    a. 4" wide roll, pos. trans., channels 2,7,11, uncorrected "screening film". No snow. 100% clouds east of Pueblo.

4. Track 34, 3 Aug. 73, Orbit 12; GMT start 215:18:02:21, GMT stop 215:18:04:05.

    a. 4" wide roll, pos. trans., channels 2,7,11, uncorrected "screening film". No snow. About 25% patch clouds over San Juans.

5. Track 48, 4 Aug. 73, Orbit 13; GMT start 216:17:19:30, GMT stop 216:17:20:05.

    a. 4" wide roll, pos. trans., channels 2,7,11, uncorrected "screening film". Minor snow. Patchy clouds over mountains.

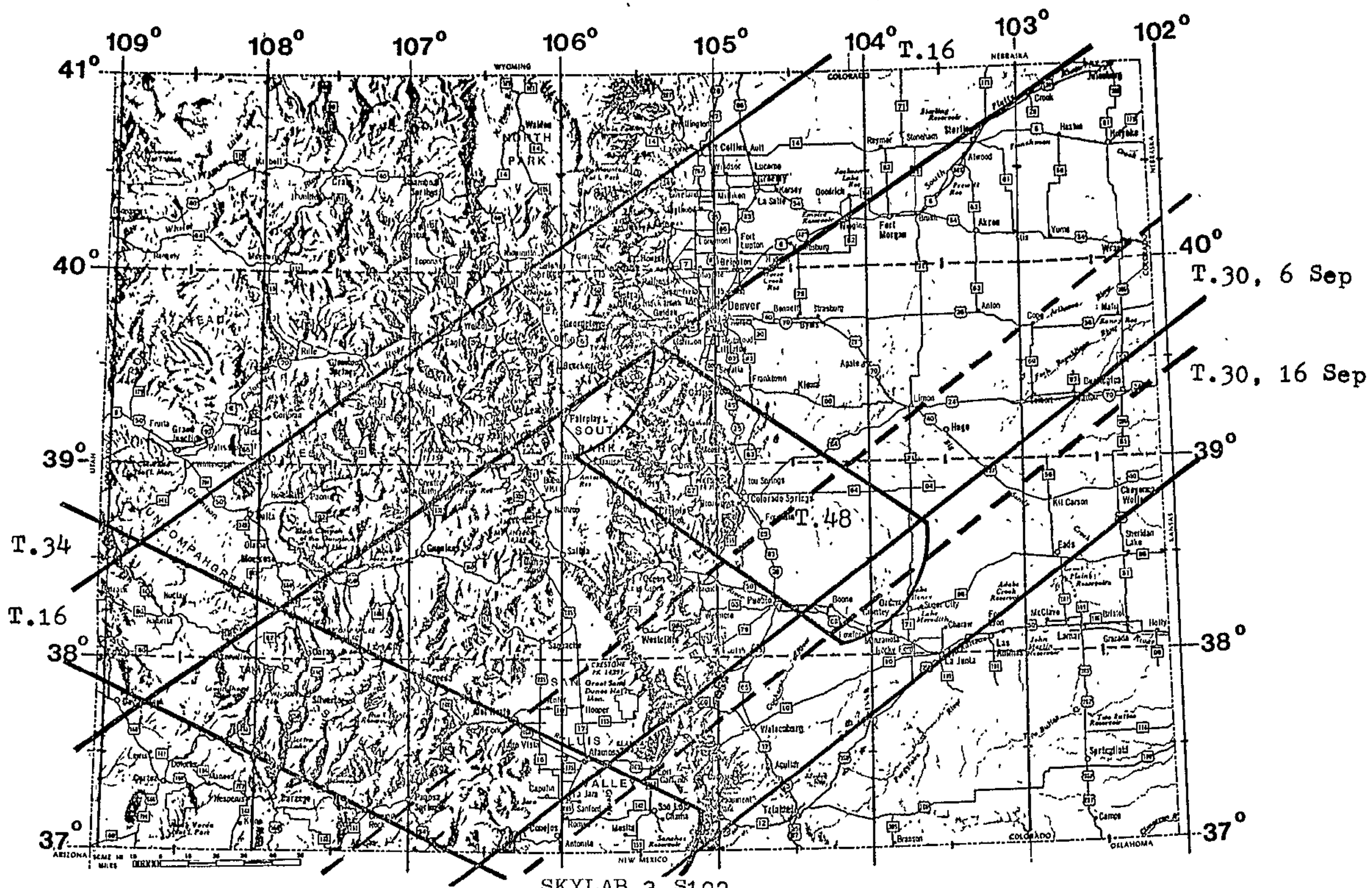

SKYLAB 3 S192

T.16, 21 Sep 73, Orbit 43, GMT start 264:18:06:50, GMT stop 264:18:08:31. No snow; no clouds.
T.30, 6 Sep 73, Orbit 27, GMT start 249:21:26:14, GMT stop 249:21:27:38. No snow; 25% " , Colo. Spg.
T.30, 16 Sep 73, Orbit 45, GMT start 259:17:23:29, GMT stop 259:17:25:04. No snow; 100% " , Pueblo.
T.34, 3 Aug 73, Orbit 12, GMT start 215:18:02:21, GMT stop 215:18:04:05. No snow; 25% patchy clouds.
T.48, 4 Aug 73, Orbit 13, GMT start 216:17:19:30, GMT stop 216:17:20:05. Minor snow; " " .

III.A. SKYLAB 4 S-190A

1. Track 34, Jan. 74

   a. 70mm pos. & neg. trans., rolls 73-78 (photo-IR, photo-IR, CIR, color, red, green, respectively), frames 350-356. Snow-covered above 7,000 ft. 0-20% clouds.

   b. 9x9" pos. trans., rolls 73-78, frames 350-356. Two each of color and CIR.

2. Track 48, Jan. 74

   a. 70mm pos. & neg. trans., rolls A1-6 (photo-IR, photo-IR, CIR, color, red, green, respectively), frames 176-188. Snow-covered above 7,000 ft. Up to 60% patchy and wispy clouds in places.

   b. 9x9" pos. trans., rolls A1-6, frames 176-188. Two each of color and CIR

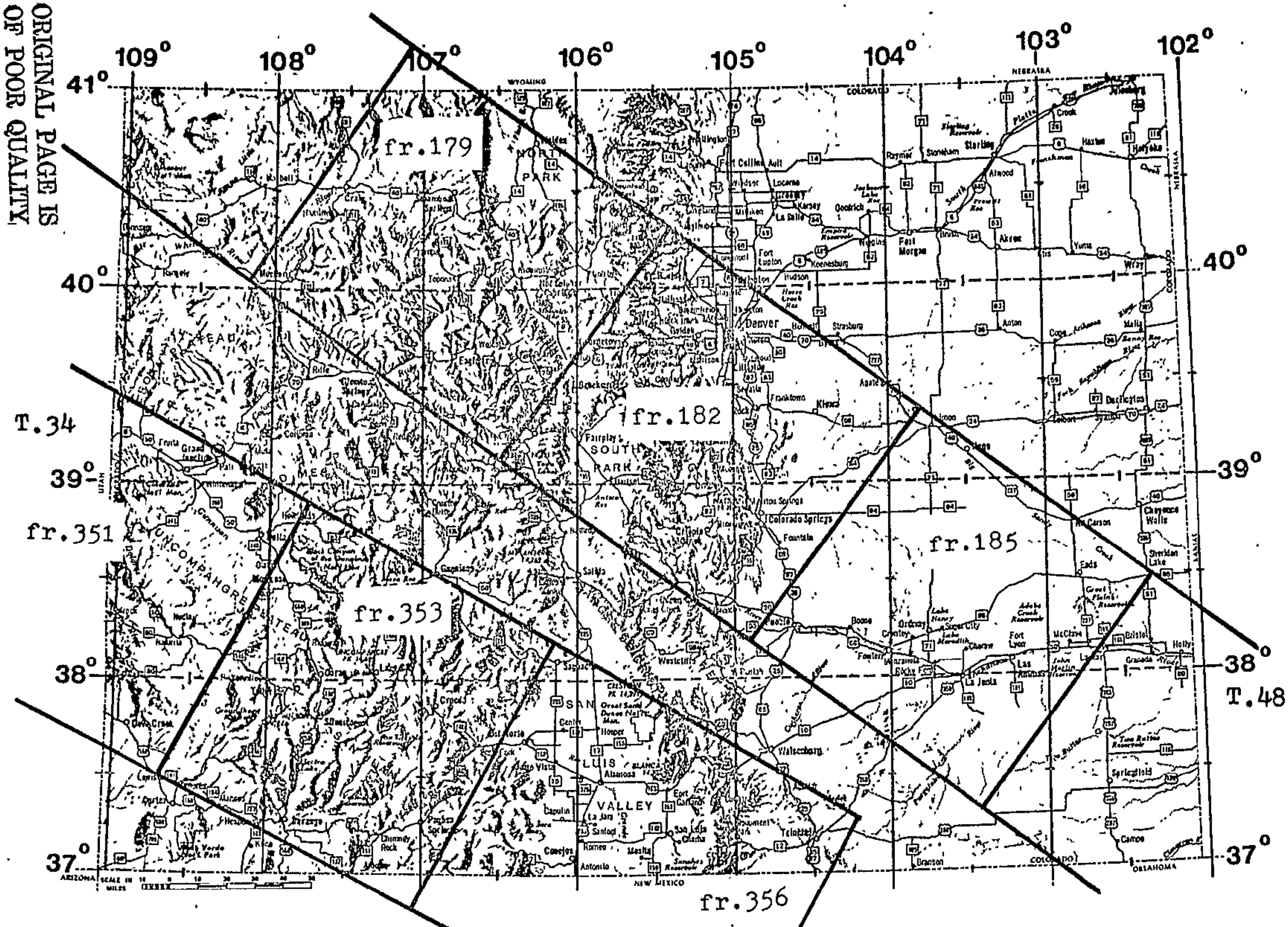

SKYLAB 4 S190-A

T.34, Jan 74, rolls 73-78, fr. 350-356. Snow above 7,000 ft.; 0-20% clouds.
T.48, Jan 74, rolls A1- 6, fr. 176-188. Snow above 7,000 ft.; up to 60% patchy clouds.

III.B. <u>SKYLAB 4 S-190B</u>

1. Track 34, Jan. 74

    a. 4½x4½" pos. trans., color, roll 94, frames 90-101. Snow over 7,000 ft. 0-20% clouds.

    b. 9x9" pos. prints, color, 2 each.

2. Track 48, Jan. 74

    a. 4½x4½" pos. trans., color, roll 94, frames 151-168. Snow over 7,000 ft. Up to 60% local clouds.

    b. 9x9" pos. prints, color, 2 each.

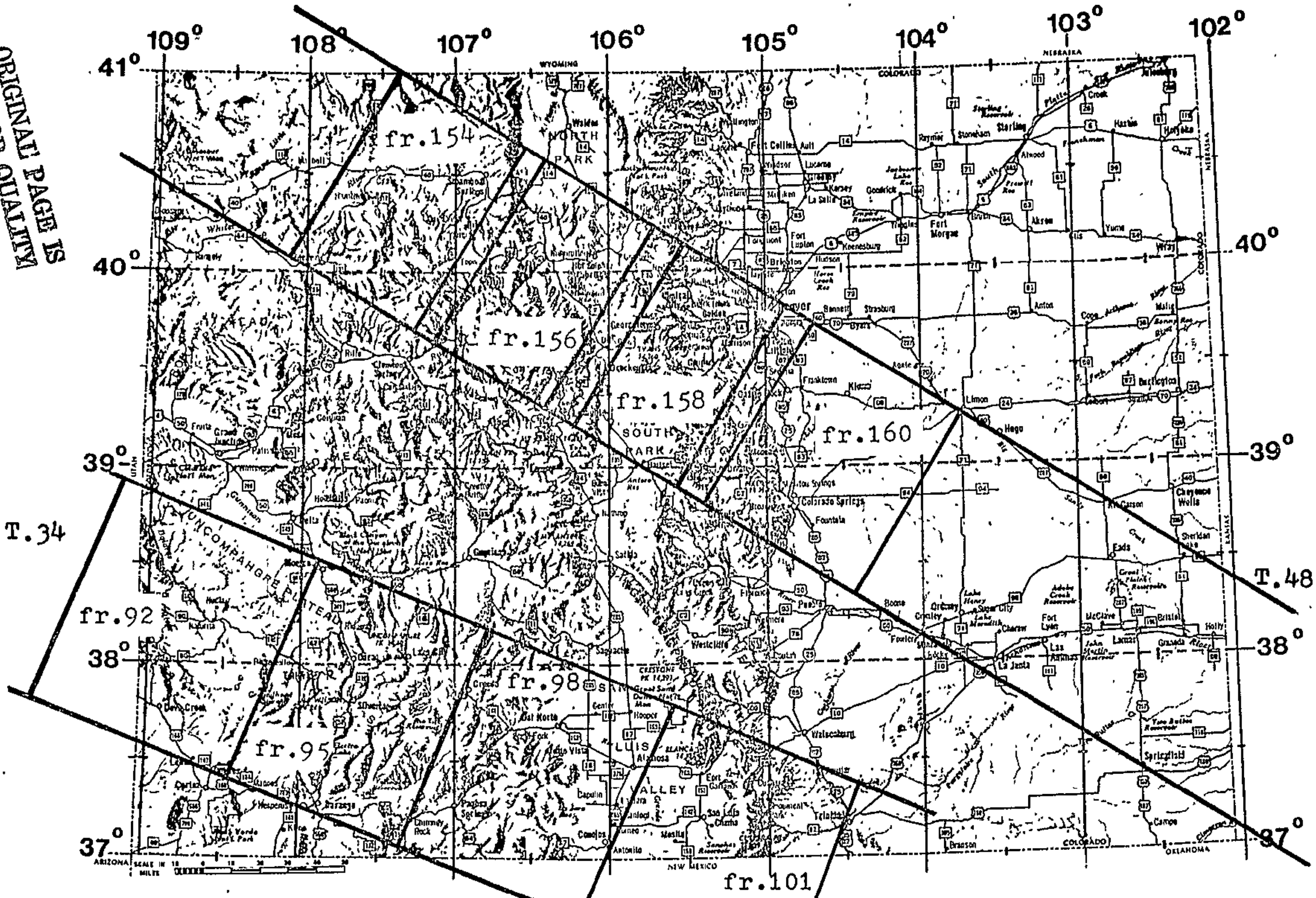

<u>SKYLAB 4 S190-B</u>

T.34, Jan 74, roll 94, fr.90-101. Snow above 7,000 ft.; 0-20% clouds.
T.48, Jan 74, roll 94, fr.151-168. Snow above 7,000 ft.; up to 60% patchy clouds.

EVALUATION OF SKYLAB S190-A PHOTOS
FOR ROCK DISCRIMINATION
AND COMPARISON WITH ERTS IMAGERY

by

Daniel H. Knepper

Remote Sensing Report 75-4

EREP Investigations 380

Contract NAS9-13394

National Aeronautics and Space Administration

December 1975

REMOTE SENSING PROJECTS

DEPARTMENT OF GEOLOGY

COLORADO SCHOOL OF MINES GOLDEN, COLORADO

EVALUATION OF SKYLAB S190-A PHOTOS
FOR ROCK DISCRIMINATION
AND COMPARISON WITH ERTS IMAGERY

by

Daniel H. Knepper

Remote Sensing Report 75-4

Remote Sensing Projects
Department of Geology
Colorado School of Mines
Golden, Colorado

NASA Contract NAS9-13394

National Aeronautics and Space Administration

Approved for Publication: ______________________
Keenan Lee
Principal Investigator

December 1975

ABSTRACT

A suite of 12 lithologic contacts was studied on ERTS images, Skylab S190-A photographs, and high altitude color aerial photography to determine the information content and detectability of contacts on each type of image. The study shows that some criteria can be used for selection of optimum space images for geologic interpretation. With ERTS imagery, band 5 is the overall "best" band, and maximum information comes from band 5 images from combined summer and winter scenes. Of the Skylab S190-A photography, color photos are best and the season is not important. Skylab photographs are better than ERTS images for both information content and ease of interpretation.

CONTENTS

INTRODUCTION

Photographs acquired on the three Skylab Missions and multispectral scanner imagery from the ERTS (now Landsat) satellites are an abundant source of information for the geoscientist. Choosing data from this vast storehouse can be an expensive and time-consuming job if there are no criteria on which to base a selection. The purpose of this study is to determine if there are optimum images and photographs for discriminating lithologies.

A study was previously conducted to determine if band and time of year of ERTS imagery are significant factors in the ability of a photointerpreter to detect lithologic contacts, and, if possible, to determine which bands and times of year produce the best results. This study was described in Knepper (1974, p. 39-79).

The method used in the ERTS study was easily adopted to evaluating the detectability of lithologic contacts on Skylab S190-A photos, and, because of the methods used, a direct semi-quantitative comparison could be made between the detectabilities of lithologic contacts on these two types of remote sensor data. The results reported here may aid practicing geoscientists in intelligently choosing the most appropriate type of imagery and photographs for lithologic mapping.

METHOD AND APPROACH

Twenty-four known lithologic contacts in the Canon City region, central Colorado, were selected for study and evaluation on ERTS imagery. Of these twenty-four, twelve were selected for identical study and evaluation on Skylab S190-A photos to reduce the time consumed in the overall analysis procedure.

Each contact, or a specific portion of a contact, was defined and located on small-scale (1:100,000) positive color transparencies (Fig. 1), and the detectability (how easily seen) of each of the contacts on the photos was arbitrarily given a value of 1.0. This operation formed a common base reference for comparing detectabilities on ERTS images and Skylab S190-A photos directly.

The defined contacts were then studied on each band of 4 sets of ERTS imagery and 3 sets of Skylab S190-A photos acquired at different times of year (Table 1), and the detectability of each contact was evaluated relative to the reference color photos. These detectability values were always less than or equal to 1.0.

Neither the ERTS imagery nor the Skylab S190A photos were studied in stereo, since lack of stereo is the general case for much of the areal coverage of these data. Experience suggests that where stereo is available, the detectability values would be significantly higher than without stereo.

Figure 1. Reproduction of one of the small-scale color photos (NASA Mx 211, 31-0009) used to define geologic contacts for this study. Some contacts are identified. Each contact, by definition, has a detectability of 1.0 on this photography.

C.3

Table 1. ERTS imagery and Skylab S190-A photos of central Colorado evaluated in this study.

ERTS IMAGERY

	IMAGE I.D.	DATE ACQUIRED	BANDS
1.	1172-17141	11 Jan. 1973	4,5,6,7
2.	1028-17135	20 Aug. 1972	"
3.	1154-17143	24 Dec. 1972	"
4.	1334-17142	22 June 1973	"

SKYLAB S190-A PHOTOS

	MX	TRACK	DATE	FRAME	BANDS
1.	SL2	34	5 June 1973	014	Color, Color IR,
2.	SL3	34	3 Aug. 1973	003	Red, Green, IR 1 and
3.	SL4	34	29 Jan. 1974	351	IR 2 on all sets.

Evaluation of the detectabilities was performed on the 10" x 10" positive ERTS transparencies and the 70mm Skylab S190-A positive transparencies using a 1X to 7X magnifying glass and a 10X hand lens. The 4 sets of ERTS imagery were laid out in stacks on a light table according to image set. One image was chosen from each stack and the 4 images were evaluated relative to the color reference photo and to each other. Next, all four bands of one image set were evaluated relative to the color reference photo and to each other. Finally, the remaining images in each set were evaluated using the color reference photo and the previous evaluations as a guide. The same procedure was used to

evaluate the Skylab S190-A photos. All the evaluations were performed without intentionally knowing the specific image or photo set and band being evaluated in order to try to reduce any conscious or unconscious bias in the evaluation procedure.

Occasional adjustments in the values of detectabilities for a given contact were necessary during the evaluation process. This occurred when a contact was found to have a detectability in between two previously evaluated images, but the two previous evaluations only differed by 0.1 (i.e.- no value to give the new image). The adjustments consisted of sliding the higher or lower detectabilities up or down, respectively, by a value of 0.1 in order to make room for the in-between image, rather than use fractions of a detectability point.

Table 2 is an example of a portion of the type of evaluation matrix that was constructed for the ERTS and Skylab data.

Table 2. Partial evaluation matrix generated during evaluation of detectability of lithologic contacts on ERTS imagery. J, January; A, August; D, December; Ju, June.

	CONTACT											
	1				2				3			
ERTS IMAGE	J	A	D	Ju	J	A	D	Ju	J	A	D	Ju
BAND												
4	0	.7	.1	.9	0	.4	.3	.7	0	.2	0	.1
5	0	.6	0	.8	0	.3	.3	.9	0	.4	0	.3
6	0	.4	0	.3	0	.6	.2	.8	0	.1	0	.2
7	0	.4	0	.2	0	.3	.1	.8	0	.1	0	.1

RELIABILITY OF DETECTABILITY EVALUATIONS

To test the reliability of the detectability evaluations, a second investigator was asked to produce a detectability matrix of the 12 lithologic contacts on the 3 sets of Skylab S190-A photos using the same monoscopic evaluation technique. When the matrix was completed, the detectability values for each corresponding photoset-contact-band were plotted as paired points and the best-fitting straight line was constructed using the least squares method (Fig. 2).

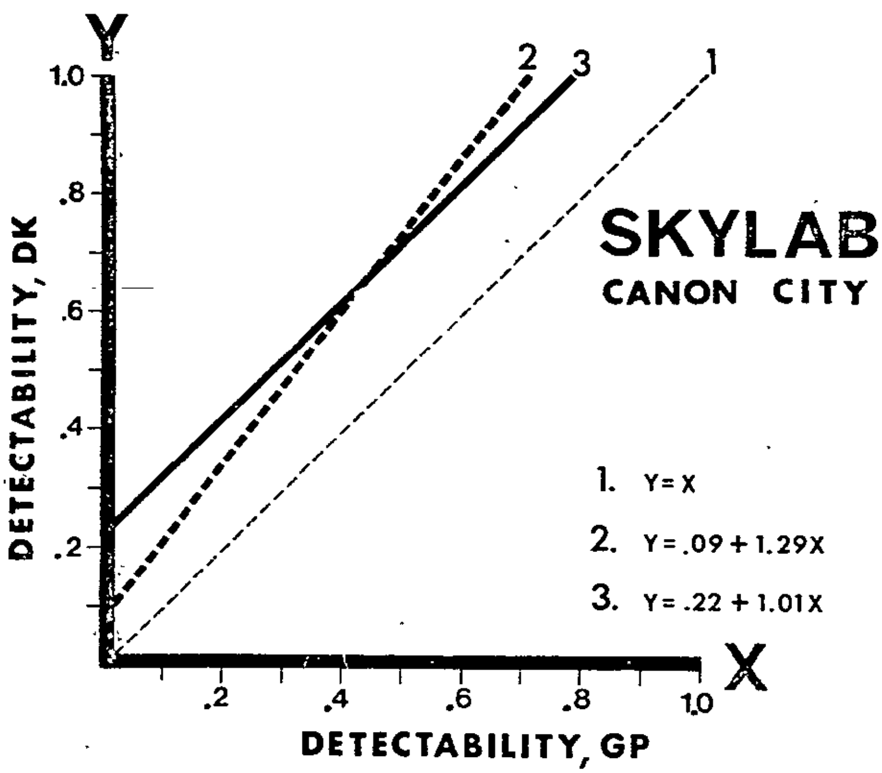

Figure 2. Least squares lines constructed for the detectability evaluations of the same contacts and photos made by two independent investigators, DK and GP. See text for explanation.

Line 1 is the line that would indicate perfect agreement between the two sets of evaluations; line 2 is the least squares line first constructed. Inspection of the plot indicated that something less than perfect agreement existed in the two sets of evaluations, so the two data matrices were re-examined to locate the major differences. The points of major disagreement were found where detectability values are very small, specifically, where a decision had to be made as to whether the lithologic contact was not detectable (detectability = 0.0) or barely detectable (detectability - 0.1).

To test this, all of the detectability data points where one of the data sets had a value of 0.0 or 0.1 were excluded from the data matrix and a new least squares line (line 3 in Figure 2) was constructed. The line (line 3) shows that there is very good relative agreement (slope nearly equal to 1), but a constant difference in detectability value of 0.22 between the two sets of evaluations.

The results of this test for reliability in detectability evaluations indicate that:

1. Except where the evaluators are forced to make a decision as to whether a lithologic contact is or is not detectable, good relative agreement can be obtained from two independent evaluators using the evaluation method described.

2. Evaluations made by two independent investigators can be directly compared if the detectability data are normalized.

STATISTICAL TESTS

After all the detectability evaluations were completed for the lithologic contacts, statistical tests were run on various subsets of the resulting data matrices. These tests compare the mean detectability of a data subset with the mean detectability of another subset, producing information as to whether the means are statistically different at a given level of significance (α value). Three types of tests were used:

1) Standard F-test at $\alpha = 0.05$
2) Confidence intervals at $\alpha = 0.05$
3) Duncan multiple-range test at $\alpha = 0.05$

The standard F-test and the Duncan multiple-range test are relatively rigorous statistical tests. Confidence intervals are useful in visualizing the variability between a large number of populations (Miller and Freund, 1965).

Inspection of the completed Skylab detectability data matrix and the mean values of detectability for the six bands of photography showed that detectabilities in the two black and white photo-infrared bands are so inferior to both ERTS imagery and the remaining Skylab bands, that further statistical testing was unnecessary. They are, therefore, excluded from the statistical analyses discussed below.

Six different subsets of the data matrices were analyzed:

(1) Overall band--to compare the relative usefulness of the bands

(2) Overall image set--to determine if the time of year the imagery or photography was acquired affects the detectability of contacts, regardless of band

(3) Overall contact--to determine if some contacts are easier to detect than others, regardless of band and time of year

(4) Contact/band--to determine if specific contacts are best detected on any particular band

(5) Contact/image or photo set--to determine if specific contacts are best detected on any particular image or photo set (time of year).

(6) Band/image or photo set--to determine if any particular band is best for a given image or photo set (time of year)

OVERALL BAND DETECTABILITY

The initial step in data analysis was to test the mean detectability (of lithologic contacts) between the four bands of ERTS MSS imagery and between the four bands of Skylab S190-A photography. The results of these tests are summarized in Figures 3 and 4. Initial F-testing was conducted to determine if statistical differences exist; further F-testing was used to determine where the statistical differences occur.

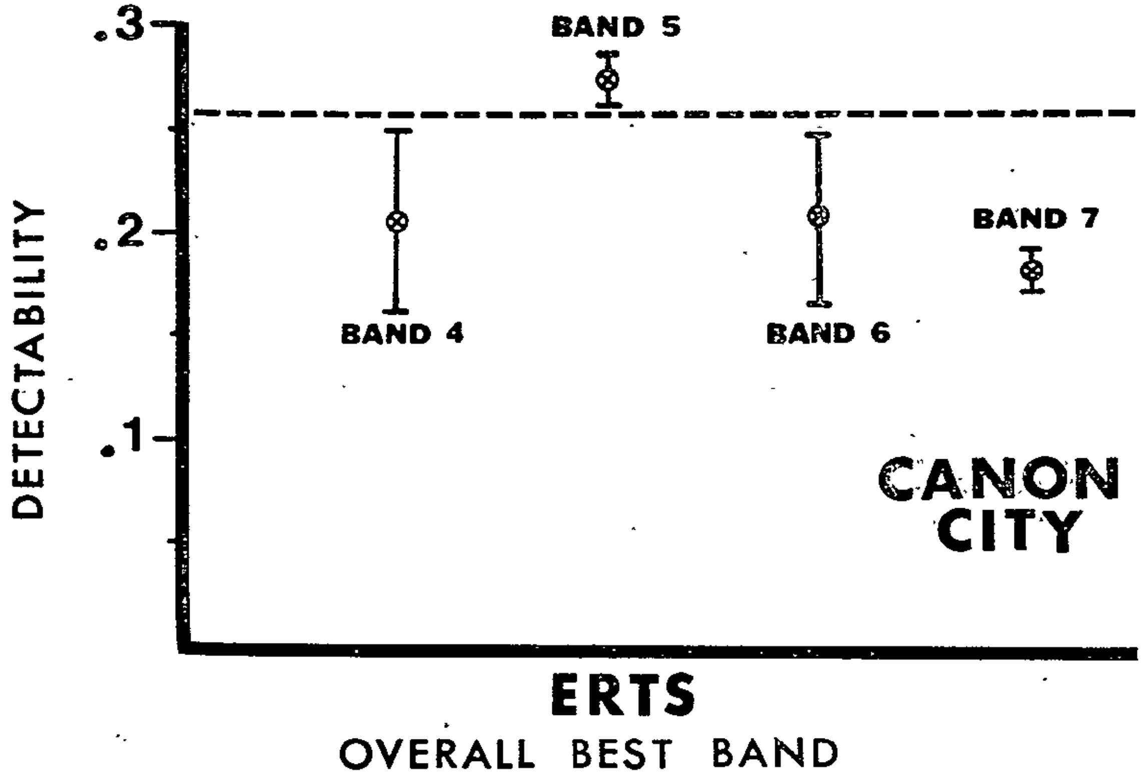

Figure 3. Confidence intervals of mean band detectability of ERTS images studied. Dashed lines indicate statistically separable bands at $\alpha = 0.05$.

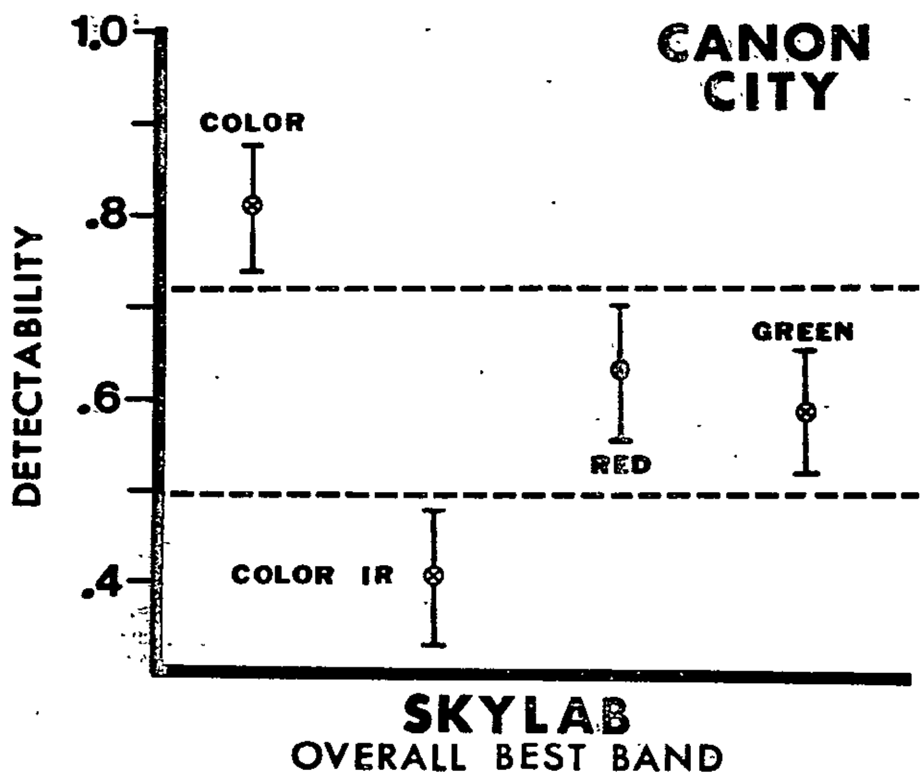

Figure 4. Confidence intervals of mean band detectability of Skylab S190-A photos studied. Dashed lines indicate statistically separable bands at $\alpha = 0.05$.

It is clear from these tests that the band of imagery and photography must influence the detectability of lithologic contacts. Band 5 (red) appears to be singly the "best" band for overall detection of lithologic contacts on ERTS imagery, while the remaining 3 bands are not statistically separable. S190-A color photography ranked the highest of the Skylab photos studied, with the red and green band photos in a statistically separable group below the color, but above the color infrared photography.

A moderate degree of caution should be exercised before extrapolating these results too far, since they represent only the general case. That is, all influences of image or photo set (time of year) and individual lithologic contacts are confounded in the analysis.

OVERALL IMAGE SET DETECTABILITY

It might be anticipated that the detectability of lithologic contacts in central Colorado would be highly sensitive to the time of year that the data were acquired, since the time of year affects many factors including sun azimuth and elevation, vegetation, snow cover, and soil moisture. The results of F-testing shown in Figures 5 and 6 indicate, however, that the time of year has no significant effect on the detectability on either ERTS images or Skylab S190-A photos. These relatively surprising results are

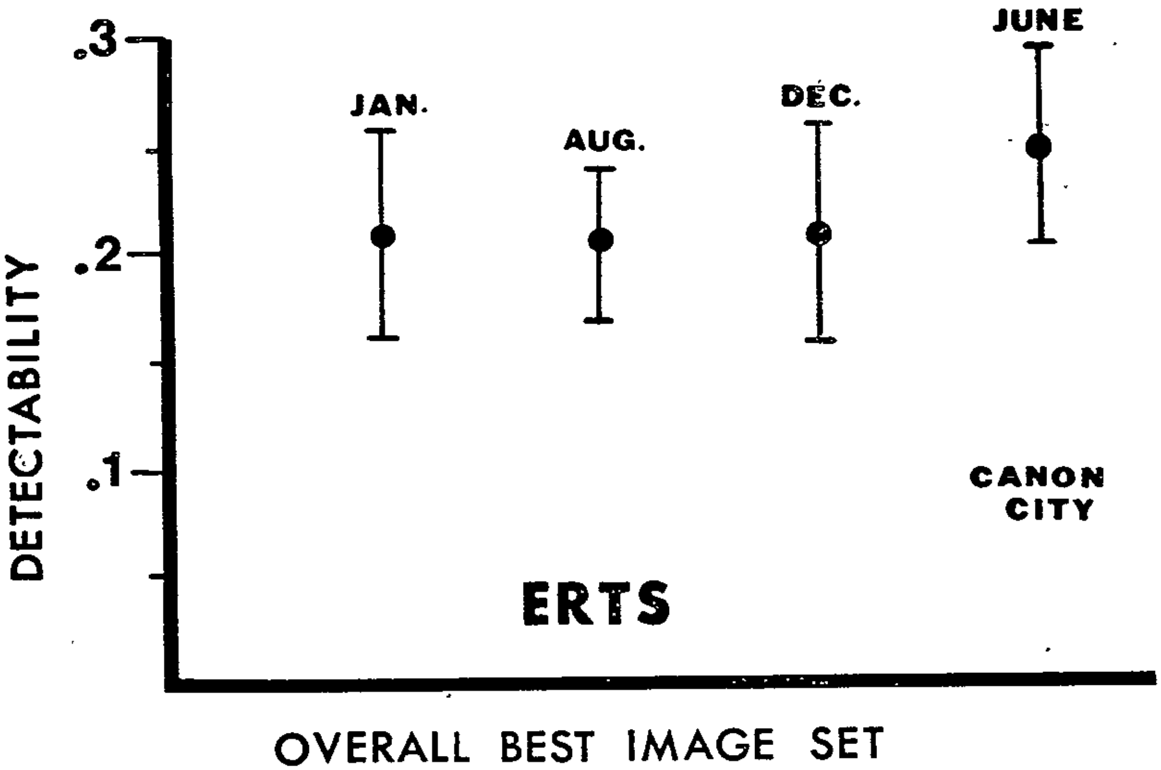

Figure 5. Confidence intervals of mean image set detectabilities of ERTS images studied. There are no statistical differences at $\alpha = 0.05$.

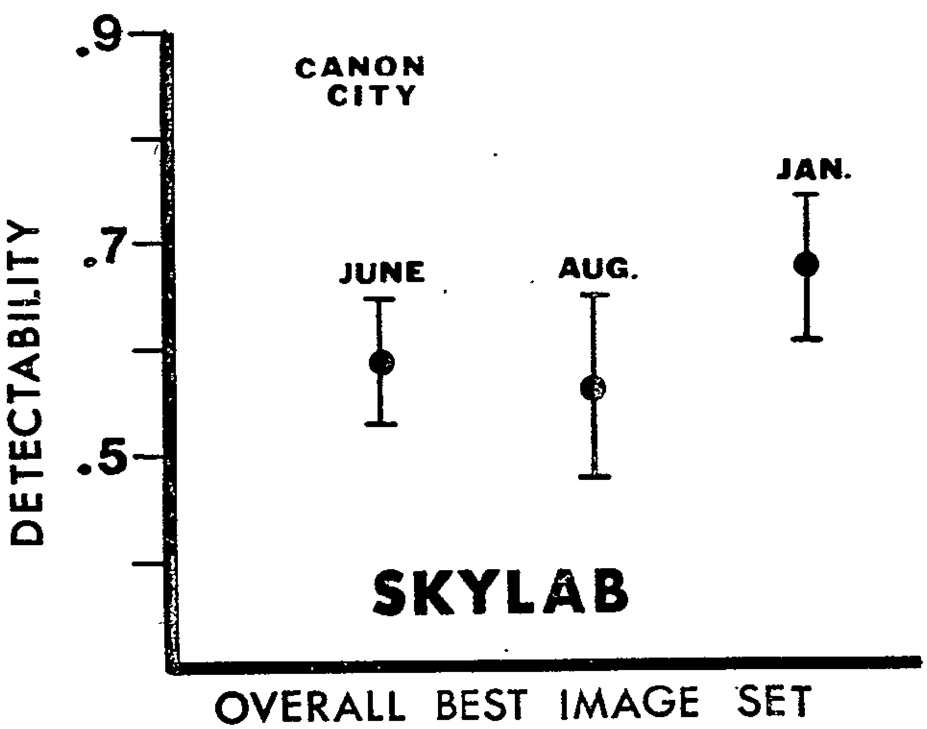

Figure 6. Confidence intervals of mean image set detectabilities of Skylab S190-A photos studied. There are no statistical differences at $\alpha = 0.05$.

discussed and, perhaps, explained in a later series of tests that compare the detectability of individual contacts as a function of time of year.

OVERALL CONTACT DETECTABILITY

Confidence intervals of the mean detectability of the lithologic contacts were constructed to examine their variation in detectability. The confidence intervals for those contacts studied on both ERTS and Skylab data are shown in Figure 7.

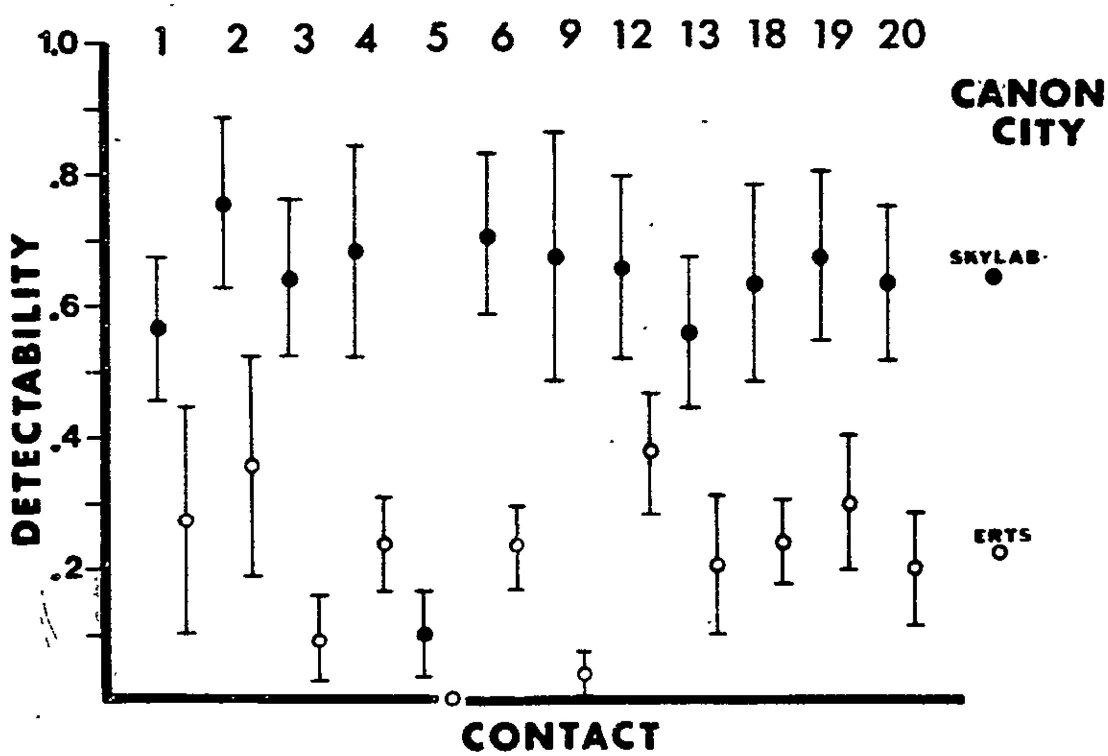

Figure 7. Confidence intervals of mean detectability of the 12 common lithologic contacts studied on both ERTS and Skylab imagery. $\alpha = 0.05$.

It is difficult to draw many conclusions from the plot in Figure 7, with the notable exception that detectabilities on the Skylab photography are consistently higher than on the ERTS imagery. The variations of mean contact detectabilities within the ERTS and the Skylab groups appear to be similar suggesting that some contacts are, indeed, more difficult or easier to detect than others. However, when the confidence intervals are replotted in order of decreasing $\bar{X}$, the order of the contacts is not the same for ERTS and Skylab S190-A (Fig. 8). The shifts are, by and large, minor and contacts

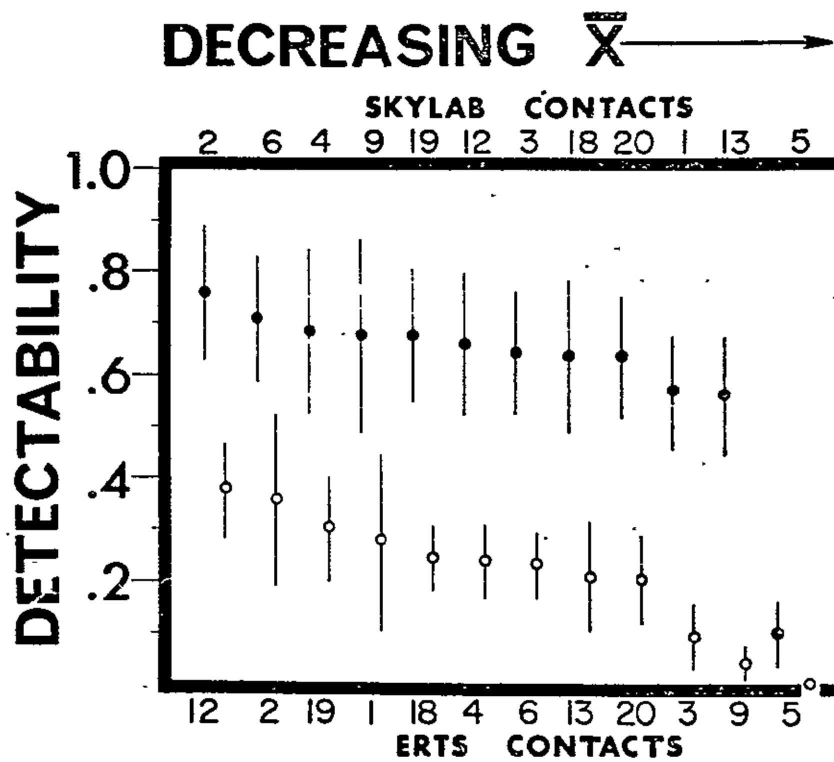

Figure 8. Confidence intervals of mean detectability of the 12 common lithologic contacts studied on both ERTS and Skylab S190-A imagery plotted in order of decreasing $\bar{X}$. $\alpha = 0.05$.

that are easy or difficult to detect on ERTS are also generally easy or hard to detect on Skylab S190-A. It should be noted that the range of the means, particularly those of intermediate value, is fairly small so that small variations in the original detectability evaluations could easily result in a shift in position of 4 or 5 positions.

INDIVIDUAL CONTACT DETECTABILITY

The mean detectability of each of the 12 contacts was statistically analyzed with respect to band and to month using the Duncan multiple-range test (Miller and Freund, 1965). This test can be used (1) to determine whether statistical differences exist between the measurements from several different populations and (2) to determine the relative order of the population measurements (best to worst; highest to lowest, etc.) where statistical differences exist. Similar results can be obtained by repeatedly testing pairs of measurements using the simple F-test, but the individual tests are not independent; a constant level of significance is maintained using the Duncan multiple-range test and the analysis takes less time.

CONTACT/BAND

The results of analyzing contact detectability as a function of band is shown in Table 3. None of the 12 contacts

Table 3. Number of contacts that are statistically more detectable on each band of ERTS and Skylab S190-A. Several contacts were found to be more detectable on statistically unseparable bands of Skylab S190-A photos.

BEST BAND FOR
EACH CONTACT

ERTS	SKYLAB
1. NONE = 12	1. COLOR = 2 2. COLOR, RED AND GREEN = 6 3. COLOR AND RED = 1 4. NONE = 3

is statistically easier to detect on a specific band of ERTS imagery; band does not appear to be important in contact detectability. But, in the test of overall band detectability previously described, band 5 was found to be statistically better. This discrepency is probably due to the difference in the number of observations (sample size) used in the respective tests. To analyze the effect of band on each individual contact, only 4 observations were used (1 from each image set). However, in analyzing the overall effect of band, a total of 96 observations of each band were available for analysis (4 image sets X 24 original contacts studied on ERTS only). In each test of individual contacts, the mean detectability in band 5 was consistently higher than the mean detectabilities in the remaining 3 bands, but this difference did not become statistically significant except when 96 observations were used.

Analysis of the Skylab S190-A photo detectabilities showed results similar to the overall band test (Table 3). 9 of the 12 contacts were statistically more detectable on 1 or more bands, and it is particularly significant that all of these contacts showed color photos in the highest rating.

CONTACT/MONTH

The results of analyzing contact detectability as a function of image set (month) is shown in Table 4. 9 of the

Table 4. Number of contacts that are statistically more detectable on each image set of ERTS and Skylab S190-A. Several contacts were found to be more detectable on statistically unseparable sets of ERTS imagery.

BEST MISSION FOR EACH CONTACT

ERTS	SKYLAB
1. JUNE = 2 2. JUNE OR AUGUST = 2 3. JANUARY = 4 4. DECEMBER = 1 5. NONE = 3	1. NONE = 12

12 contacts are statistically more detectable on one (or more) of the ERTS image sets. These results are interpreted as meaning that the surface expression (and image expression) of some of the contacts is best developed at one time of year, whereas other contacts are better seen at different times

of year. If these contacts and image sets are considered together, as was done in the overall image set analysis, these differences cancel out, indicating that there is no best image set (i.e. - not statistically separable).

Skylab S190-A photo detectabilities, however, apparently are not affected by image set (month) according to both the overall and individual contact analyses. An explanation of the dependence of ERTS and the independence of Skylab S190-A on image set may be contained in the spacial resolution differences between the two systems. The higher spacial resolution of Skylab S190-A photos may allow the subtle surface expression of contacts to be readily detected even at less than optimum times; the low resolution ERTS system may not be able to show these subdued contacts adequately.

INFORMATION CONTENT

Analysis of the detectabilities of the lithologic contacts does not tell anything about the information content of the various possible combinations of band(s) and image or photo set(s). Conceivably, an image with relatively low detectabilities may contain more lithologic information (more contacts detectable) than an image with high detectabilities. Therefore, the information content of the images and photos must be considered if the optimum imagery (most information with least number of images) is to be determined.

The detectability data contain a crude estimate of information content as follows:

(1) If a contact is detectable on a given image or photo (detectability greater than zero), then the information content of that image, for that contact, is plus one.

(2) If a contact is not detectable on the image or photo (detectability equals 0), the information content of that image or photo, for that contact, is zero.

The detectability data matrices can be converted to information content data matrices using the above criteria. Once the detectability data are converted, various subsets of the new matrices can be studied to determine the relative amounts of information that may be extracted using various combinations of band(s) and image set(s).

BAND/ALL IMAGE SETS

The information content of each band of imagery and photography shown in Table 5 is expressed in percentage of the 12 contacts that are detectable.

Table 5. Percentage of contacts studied that can be detected if a given band of imagery is studied in all the available image sets. Four ERTS images and three Skylab S190-A photos must be studied for each band.

ERTS	
Band 4	92
Band 5	92
Band 6	92
Band 7	92

SKYLAB S190-A	
Green	100
Red	100
Color	100
Color IR	100

Clearly, if an interpreter studied all the Skylab S190-A photos from a single band, he could have detected all of the 12 contacts studied. On ERTS imagery, however, only 92% of the contacts (11/12) could be detected from a single band of imagery. In addition, the interpretation of all 16 images (all bands in all image sets) would still allow only 92% of the contacts to be detected; one contact was not detected on any of the ERTS images, probably because of its small areal extent.

IMAGE SET/ALL BANDS

The information content of each set of imagery shown in Table 6 is expressed in percentage of the 12 contacts studied that are detectable.

Table 6. Percentage of contacts studied that can be detected if all the data from a given image set are interpreted. Four images must be interpreted in each image set.

ERTS

January	50
August	75
June	75
December	75

SKYLAB S190-A

January	100
August	100
June	100

The amount of information extracted by an interpreter decreases if ERTS imagery from only a single time of year is

analyzed, however, the maximum amount of information (100%) can still be extracted if only a single set of Skylab S190-A photos are studied.

BAND/IMAGE SET

Obviously, the maximum amount of available lithologic information will be gained if each band of each image set is analyzed. But can this same information be found if only 1 or 2 specific images or photos are studied? To check this, matrices showing the information content of each ERTS image and Skylab S190-A photo were prepared (Tables 7 and 8) and the percentage of the contacts that can be seen on each image was computed.

Table 7. Percent contacts detected on single ERTS images.

PERCENT CONTACTS DETECTED ON SINGLE

ERTS IMAGES

	BAND 4 GN	BAND 5 RD	BAND 6 IR	BAND 7 IR
JAN	50	58	58	58
AUG	83	83	83	83
DEC	75	67	58	58
JUNE	83	83	83	67

ALL BANDS + ALL IMAGE SETS = 92%

Table 8. Percent contacts detected on single Skylab S190-A photos.

PERCENT CONTACTS DETECTED ON SINGLE

SKYLAB PHOTOS

	GN	RD	C	CIR
SL2 (JUNE)	100	92	100	100
SL3 (AUG)	100	92	100	83
SL4 (JAN)	92	100	100	100

The maximum amount of information that can be extracted from a single ERTS image is 83% (all bands of August and bands 4, 5, and 6 of June). 8 of the 12 Skylab S190-A photos provide 100% information content and, most notably, color photos provide 100% information on all 3 of the image sets. These results indicate that satisfactory lithologic mapping might be conducted using a single Skylab S190-A photo, while less than satisfactory results could be expected if only a single ERTS image was used. Clearly, the fewer the number of images it is necessary to study to gain the maximum amount of available information, the greater the savings in time and expense.

In order to check whether it may be possible to gain the maximum amount of information using only 2 specific ERTS images, the percent of contacts found considering each permutation of band and image set was computed. It was found that there were 37 pairs of images that would give 92% of the contacts studied--this is the same as when all 16 of the images were studied (i.e.- the maximum amount using these particular image sets). And significantly, each pair of images was a combination of a wintertime and a summertime image, thus pointing up, again, the dependence of the detectability of specific contacts on ERTS imagery to time of year (image set).

SUMMARY AND CONCLUSIONS

Interpretation of the results of the statistical analyses performed in this study cannot be casually extrapolated to all ERTS and Skylab S190-A data in all areas of the world for all lithologic contacts. To the contrary, these results pertain to only those lithologic contacts studied on the specific imagery and photos used. Indeed, it is not conclusively known whether the results apply equally well to all of central Colorado, even though a variety of types of contacts were studied. Agreement with empirical analyses of ERTS and Skylab S190-A data of central and western Colorado, however, suggest that the results are, at least, representative of this area.

The results of this investigation seem to warrant the following conclusions:

(1) The capability of a photointerpreter to detect lithologic contacts is consistently better on Skylab S190-A photos than on ERTS imagery. And of these photos, color photos seem to produce the most consistently good results.

(2) Overall, band 5 (red) seems to be best for detecting lithologic contacts on ERTS imagery. However, on a contact for contact basis, band of imagery seems to be of little importance.

(3) Overall, band is not important in detecting lithologic contacts on Skylab S190-A photos, except for the multiband photo-infrared photos which are extremely poor. On a contact for contact basis, however, detectabilities are somewhat better on the color, red, or green bands; no contacts appeared "better" on the color infrared photos.

(4) Detectabilities of lithologic contacts are sensitive to the time of year the ERTS images are acquired. Some contacts, according to their specific topographic, spectral, and vegetation characteristics, are selectively enhanced or subdued at certain times of year. The maximum amount of information can be gained by studying images from two contrasting times of year (summer and winter).

(5) Individual contact detectability appears to be insensitive to time of year on Skylab S190-A photos. Contrary to ERTS imagery, Skylab S190-A spacial resolution is good

enough that even subdued lithologic contacts, not detectable or poorly detectable on ERTS imagery, are readily detectable at less than optimum times of year.

(6) As few as 2 ERTS images may be studied to gain the maximum amount of information available. One image must be high sun-angle, snow-free and one must be at least low sun-angle. Even then, it is probable that all contacts detectable on Skylab S190-A photos of the same area will not be detected.

(7) A single Skylab S190-A photo, judiciously chosen, will provide as much information as several photos. Color photos seem to be the best choice, although other bands of Skylab S190-A photos may produce the same results; color infrared photography seems to be the worst choice (except for the black and white photo-infrared multiband photos).

REFERENCES

Knepper, D.H., 1974, Geologic and mineral and water resources investigations in western Colorado using ERTS-1 data: final report: Colorado School of Mines Remote Sensing Rept. 75-1, 212 p.

Miller, Irwin, and Freund, J.E., 1965, Probability and statistics for engineers: Prentice-Hall, Englewood Cliffs, N.J., 432 p.

APPENDIX E

GEOLOGICAL SIGNIFICANCE OF FEATURES OBSERVED IN COLORADO FROM ORBITAL ALTITUDES

Don L. Sawatzky, Gary Prost, Keenan Lee, and D.H. Knepper

Geology Department, Colorado School of Mines, Golden, Colorado

ABSTRACT

Three major investigations using LANDSAT and Skylab imagery were concerned with analyses of color anomalies and linear features of central Colorado.

Skylab S190A and S190B photographs over central Colorado, covering approximately 47,000 sq km of the Rocky Mountains, were analyzed to determine which features associated with known mining districts are recognizable on space images. This analysis indicates that visible features associated with mineralization include high densities of linears, complex linear intersections, red-ocher and light color (alteration) anomalies, and perhaps vegetation patterns unique to mineralized areas. It was assumed that linears designate ore-controlling fractures, and that color anomalies are gossans or hydrothermally-bleached intrusives.

The Skylab photographs were then studied to locate indicators of mineralization. Two target areas were chosen where several features coincide; a primary study area (32.5 sq km) at Weston Pass, and a secondary area (130 sq km) at Dome Rock. Ground truth, obtained at the primary target by geologic mapping at a scale of 1:12,000, was used to identify the features seen on photography and to evaluate orbital imagery as a tool in mineral exploration. The secondary target was briefly field-checked by identifying the indicators of mineralization in a reconnaissance fashion. The secondary site was evaluated to determine if indicators of mineralization are consistent throughout the region.

Field work indicates the original assumptions are incomplete. Red-ocher colors may result from features other than weathered sulfides, and light-colored units need not be intrusive sills. Linear patterns may not be unique to an area, nor are high densities and intersections of regional linears the only structural controls on mineralization. Distinctive vegetation patterns associated with mineralization were not observed because vegetation is influenced more by other factors.

Orbital imagery in itself is inadequate to fulfill exploration needs; it may, however, be a powerful tool when used in conjunction with aerial photography and field work.

The second investigation was concerned with the structural information available in a LANDSAT image of central Colorado and has revealed several

techniques that extract much of that information.

The techniques include selecting an image with maximum linear enhancement, preparation of a relatively unbiased linear map, measurement of lengths and azimuths of the linears, selection of all linears of supermodal length, generation of strike-frequency diagrams, and selection of significant structural trends.

A length-versus-frequency graph of the linears is prepared from which is determined the modal length. Azimuth-versus-frequency curves suggest that the short linears of less than modal length have a large part of the uniformly distributed azimuths. On the other hand, comparisons with structural trends indicate that linears greater than modal length contain most of the structural information. A length-weighted strike-frequency diagram of super-modal linears combines the two features and reveals structural information in close correlation to structural trends.

Four major trends are present in the LANDSAT imagery of the central Colorado test site. The test site contains sedimentary terrains (South Park, Denver Basin, and Canon City Embayment) surrounding the metamorphic and igneous terrains of the southern Front Range. In addition is a Tertiary volcanic terrain superposed on a metamorphic terrain south of South Park. A N.25W. trend is an important trend which is manifest as a pervasive fracture trend in the uplifted mountain block and as the trends of Laramide folds and faults in the sedimentary terrains. In the northern part of the test site these structures have the prominent N.0-10E. trend. The N.65E. trend is parallel to a fracture trend orthogonal to the other fracture trend. The fourth trend N.85E. appears only in the length-weighted analysis and occurs in the Tertiary volcanic terrain. It is a manifestation of long pre-volcanism drainage channels which have been enhanced by differential erosion.

The third investigation was concerned with those anomalous megalinears and their associated geologic lineaments that transect major tectonic features in central Colorado. They are anomalous relative to the major known lineaments that essentially bound and parallel the major features. These anomalous megalinears have not been studied extensively because a synoptic view has not been available heretofore.

The transecting megalinears are equally as detectable in an image as the more structurally consistent lineaments. Their associated lineaments are composites of anticlines, synclines, drag folds, monoclines, faults, crush zones, shear zones, and rock joints. The variability of structure types along the trend of a lineament is very dependent upon the lithologic terrains in which they are developed. It is this variability as well as the transecting nature of the lineaments that presents a somewhat confusing structural picture, and perhaps has slowed the recognition of these major anomalous structural features.

In LANDSAT and Skylab images the normal tectonic elements and their marginal structures are recognizable. In addition are four concentric features and several transecting megalinears. Of the concentric features, the most prominent one is the Pikes Peak intrusive center of the Pikes Peak batholith. Two volcanic centers, the Thirtynine Mile and one in Wet Mountain Valley, are also recognizable. Three transecting megalinears are in the Rampart Range portion of the Front Range, and three are in part of the Front Range south of Pikes Peak.

The structural evidence associated with the transecting megalinears of the Front Range uplift points to a more complex involvement of the crystalline basement in the regional tectonic deformations. These deformations consist not only of the familiar ones of uplifts decoupled from the basins along flank thrusts and monoclines but also independent or subsequent, continuous cross-cutting deformations that have the spatial unity of a lineament, yet are manifest in different structural features along that lineament. Further study of these features may add considerably to our knowledge of the tectonic histories and kinematics of regions.

INTRODUCTION

The results of three independent investigations of LANDSAT and SKYLAB imagery of central Colorado are reported in this paper in three sections. These studies are concerned with, through the use of extensive ground observations, the geological significance of spectral and spatial features on the images. The first investigation analyzed and evaluated color anomalies in SKYLAB photographs for locating indicators of mineralization. The second investigation determined the relationships of all linear features in a LANDSAT image to the rock joint systems and the detectible larger geologic structures and indicates techniques to extract that geologic information. The third investigation analyzed some anomalous megalinear features in LANDSAT and SKYLAB images that transect major structures and described their associated geologic features.

PART 1: LOCATING INDICATORS OF MINERALIZATION

Introduction

The objective of this research has been to evaluate and utilize Skylab EREP (Earth Resource Experiment Package) and, to a lesser extent, LANDSAT and aircraft imagery, for their value in locating indicators of mineralization in central Colorado. The reason for such a study is that it is economically more desirable to survey large areas for potential ore deposits by remote sensing than by conventional ground surveys. Advantages of satellite imagery, both photography and scanned imagery, include a synoptic view, repetitive coverage, accessibility to remote areas, and relatively low cost to the user. Despite the desirability of locating targets quickly and inexpensively, it must be stressed that field work is essential as verification. It is merely hoped that needless field work may be eliminated.

This research began with an evaluation of two mining districts considered typical of those in central Colorado. A literature study of the Leadville and Cripple Creek districts was undertaken to determine which geologic features are associated with mineralization. Satellite photos over these areas were studied and compared with published geologic maps. It was determined that color (alteration) anomalies and structural density and intersections were the most obvious indicators of mineralization in the two areas, and it was assumed these criteria would be valid for the central Colorado region.

Limited Skylab coverage over Colorado restricted research to the area outlined in figure 1. This area is covered by frame 17, track 48, Skylab 2 S190A taken on 11 June 1973; by frames 106 and 107, track 48, Skylab 3 S190A and frames 38 and 39, track 48, Skylab 3 S190B taken on 4 August 1973; by frames 181 and 182, track 48, Skylab 4 S190A and frames 57 and 58, track 48, Skylab 4 S190B taken on 30 January 1974. Skylab 4 photography was delivered too late to be used in target selection. The area is also covered by frame 1172-17141, LANDSAT imagery from 11 January 1973; by frame 1154-17143, LANDSAT imagery from 24 December 1972; and by several aircraft underflights, including NASA Missions 184, 211, and 235. The entire study area covers approximately 46,800 square kilometers (18,000 square miles) in central Colorado

The central Colorado area was studied to locate indicators of mineralization. Structure targets were chosen in areas of high linear density or at complex linear intersections. Target areas were ranked from most to least favorable according to the degree of association of color anomalies (each a "color" target) with structure targets.

Evaluation of the primary target at Weston Pass consisted of mapping from satellite and aerial photography and in the field (scale 1:12,000) to determine the origin of color anomalies and linears, and to discern the relationship of these features to mineral deposits. The secondary test site, at Dome Rock, was briefly investigated in the field to identify the indicators of mineralization.

The relationship between satellite, aircraft, and field mapping was determined, and the usefulness of Skylab in locating indicators of mineralization in Colorado was evaluated.

Skylab Evaluation

Remote sensing studies have been conducted on various aspects of the geology over both the Weston Pass and Dome Rock targets. In a study of controls on mineralization in the Colorado mineral belt, (1) noted that "areas of high density of lineament intersections, associated with circular lineaments...are considered the most promising areas for exploration." Linear overlays of LANDSAT imagery led him to select ten targets in central Colorado. Five of these covered major mineral districts; the highest priority target that did not correspond to a major mining district covered the Weston Pass-Buffalo Peaks area.

Lineament studies over central Colorado using both LANDSAT (2) and Skylab (3) indicate linear trends correlate well with known regional joint sets and fault patterns. Linears are most abundant in areas of crystalline basement, and linears with greater relief (as in the Dome Rock area) are visible because erosion has exposed the otherwise buried basement.

Prior to field work, Skylab photography was compared to LANDSAT and aircraft imagery over central Colorado. The comparison indicates that LANDSAT multiband imagery is superior to Skylab S190A multiband photography in the photographic-infrared (photo-IR) range, and that LANDSAT imagery in the red and green bands is comparable in quality (contrast and resolution) to the Skylab red and green bands. In general, the simulated color on LANDSAT imagery is comparable to Skylab, but system resolution is inferior to Skylab.

Cloud-free LANDSAT images are available during various seasons, while cloud-free Skylab photography is not, due to lack of repetitive coverage. In all cases the Skylab S190B product is superior to LANDSAT and S190A because of its greater resolutions.

Advantages of Skylab photography over LANDSAT imagery include greater resolution, stereo coverage, and the availability of colored films (both true color and color infrared), eliminating the need for color composites. Disadvantages include the general lack of repetitive coverage, the time necessary to retrieve and process film, and a restricted ground track.

Aircraft photography has equal or lower system resolution but greater scale than Skylab photography. Therefore more detail, and consequently more geology, can be mapped.

Advantages of satellite over aircraft photography include the synoptic view, the ability to see regional linear features, easier access to remote areas, and relatively low cost to the user. Disadvantages include over-flight times that cannot be varied to take advantage of changing surface conditions (weather), slow film retrieval, and smaller scale. Surprisingly, the color rendition of the S190B film (SO-242) allowed detection of color anomalies that were not obvious on aircraft photography. Among airphotos, color film at a scale of 1:20,000 proved most useful for detailed photointerpretation.

The primary objective of field work was to obtain ground truth to determine the origin of anomalous colors, linear features, and vegetation patterns. A common surface indicator of ore at depth is the gossan, an outcrop of leached and oxidized iron sulfides (4). Where unobscured, the characteristic red-ocher color should be easily seen on color photography. In addition, intrusive rhyolite porphyries should be obvious as light-colored anomalies where intruded into darker sediments. Areas of complex structural intersection have also long been considered favorable to ore deposition. It is hoped that linear features seen on satellite photography are structures (faults, joints, shear zones). Many researchers have suggested that vegetation patterns near ore deposits should be influenced by unique soil characteristics (5, 6, 7, 8). It was assumed that such patterns should be easily seen on satellite and aircraft photography, providing an additional indicator of mineralization. The Weston Pass and Dome Rock study areas were evaluated with these indicators in mind.

Red-ocher color anomalies can be caused not only by a gossan, but also by red sedimentary rocks, such as the Maroon Formation, which are probably the most visible red features in central Colorado, and by microcline-rich crystalline rocks and grus, commonly found in Precambrian units. Rocks appearing red-ocher on satellite and aerial photography in the Weston Pass study area are exposed as talus or outcrops and contain microcline and/or iron oxides. The most obvious color anomaly, on the west slope of Weston Peak (fig. 2), contains both microcline- and hematite/limonite-rich granite talus. One less visible anomaly consists of microcline-rich granite outcrop and grus; another comprises limonite-stained dolomite talus overlying a white quartzite. The extensively limonitized ore horizons at Weston Pass were not visible on orbital photography because of limited outcrops and extensive vegetation and soil cover.

Outcrops, talus, and minimal soil and vegetation cover provide optimum visibility. This limits most anomalies in central Colorado to talus slopes or areas above timberline. Mapping indicates that color anomalies in the Precambrian units generally are due to greater than thirty percent 'pink minerals' (potassium feldspars and iron oxides) in outcrops, talus, or grus, regardless of unit (figs. 3,4,5,6). Red color is not obvious in every place these conditions are met; an explanation may be indirect illumination, or differences in films or processing.

Light color anomalies (none was seen on satellite images in the primary study area) may be caused by light sedimentary units such as the Sawatch Quartzite or quartz-rich pegmatites, as well as by light-colored, altered intrusives. Light-colored intrusives are visible on aircraft photography because of their color contrast with adjacent rocks. They have often been emplaced as sills between dark dolomites and shales, and sometimes there is a change in vegetation growing on the unit (this change in vegetation is inconsistent from place to place). It is not possible to distinguish the sills where there is a lack of contrast, such as within the Sawatch.

Photography at a scale of 1:20,000 was most useful for discriminating colors and attempting to determine their origins. Even at this scale, however, distinguishing between microcline-rich talus and limonitically-altered talus is difficult, and identification is a matter of speculation.

Regional lineaments were assumed to be the expression of structure, and lineament density and complex intersections were important criteria in target selection. Field work revealed that linear objects may be accidentally aligned or geologically aligned streams and saddles, ridges, vegetation alignments, cultural features such as fences, roads, powerlines, or airplane contrails, as well as geologic features such as dikes, contacts, shear zones, joints, and faults. Within the Weston Pass area, 22 lineaments were mapped from Skylab photography (fig. 7). A comparison with faults mapped by (9) (modified within the study area) shows that seven mapped lineaments, or 32%, correspond closely to known faults (Fig. 8). One lineament was correlated to a cultural feature (powerline), and the remainder are thought to be structurally-controlled drainage or vegetation alignments. A comparison of 53 linear drainage azimuths with 239 joint measurements suggests that one drainage trend is directly controlled by jointing, and that another trend is a consequence of drainages formed on dip slopes normal to fracturing.

The indicators of mineralization did lead to an old mining district at Weston Pass, where lead and zinc sulfides formed manto deposits in the Leadville Formation. The ore is thought to have originated either in nearby porphyry sills or in a batholith at depth, and to have migrated along fissures adjacent to large, regional, gouge-filled fractures such as the Weston fault.

Reconnaissance field work in the Dome Rock area indicates that lineaments and color anomalies mapped using Skylab 3 S190B photos (fig. 9) are generally related to geologic or geomorphic features. Lineaments were found to be the topographic expressions of weathering along faults, joints, lithologic contacts, folds, and paleovalleys (R.B. Taylor, oral comm., 1974). Major linear orientations do coincide with fault and fracture trends in the

Precambrian Pikes Peak granite, the dominant rock in the area (R.M. Hutchinson, oral comm., 1974). It has been suggested that the fracture pattern in the study area is not unique, but rather is a local exposure of the regional basement pattern. Comparison to fracture orientations throughout the region confirms this (10,11)

The color anomaly in the secondary test site is Pikes Peak granite and grus. The rock is a pink to red-brown biotite granite with associated aplite and pegmatite. Pink minerals compose approximately forty to sixty percent of the rock, and are dominantly microcline. The color is particularly obvious where it is vegetation-free (at Dome Rock, Balanced Rock, and Sheep Rock).

The main source of potentially economic minerals in the Pikes Peak batholith is pegmatite; minerals include feldspars, mica, beryl, topaz, cassiterite, and lithium minerals. The position, shape, and size of pegmatites are controlled by structure. Primary fractures, such as cross joints, longitudinal joints, diagonal joints, and flat-lying joints, as well as marginal fissures and fissure intersections, may be used by pegmatitic solutions escaping a magma, and may become filled with pegmatite. Pikes Peak pegmatites are tabular, lenticular, or highly irregular in shape, and range in size to one kilometer in length, and up to 60 meters in width (12). Pegmatites in the Pikes Peak region have been uneconomic.

Interpretation of Skylab photos identified no pegmatites, probably because they are vegetation- or soil-covered, or lack unique color or weathering characteristics.

Results of this study suggest the original assumptions are incomplete. Red-ocher colors in central Colorado may result from sedimentary red-beds, microcline-rich crystalline rock, iron-oxide alteration, or combinations of these. Light color anomalies were attributed to quartz-rich pegmatites, light-colored sedimentary units, as well as to altered intrusives.

Linear features have been identified as aligned or straight streams, ridges, vegetation, cultural features, and geologic features including faults, joints, shear zones, dikes, contacts, folds, and paleovalleys. Where a linear pattern is obviously structural, such as jointing in the Pikes Peak granite, what is seen may be just a local manifestation of a regional pattern, enhanced in the particular area by unique aspect angle, or weathering or erosional characteristics.

Intersections and high densities of regional lineaments are not the only structural controls on mineralization. Regional faults with large displacements may be filled with gouge. Relatively small auxiliary fractures are often equally important. Intrusive centers, sometimes related to "circular features," frequently supply metallizing fluids. Changes of foliation in crystalline rocks have been cited as controls on ore deposition. Identification of reactive units, such as the dolomites of central Colorado, would facilitate locating mineralized strata. Recognition that a reactive unit had been intruded would increase its prospects as a host. Many of these features, however, are not visible on satellite photos at available resolutions.

Vegetation assemblages in the two target areas were found to be influenced more by moisture, slope steepness and direction, season, and altitude than by composition of the substrata.

Conclusions

Skylab photography can cover large areas quickly and inexpensively, and there are some surface features in any given region that are indicators of mineralization. Photolineaments and color anomalies may be important indicators of mineralization in central Colorado, but positive identification of these features is not possible. A thorough evaluation of assumptions and detailed field work are mandatory. Also, areas that are extensively covered by soil, vegetation, clouds, or snow, no matter how favorable, are incapable of being evaluated. Areas where orbital photography would be most useful in the search for mineral deposits include desert mountains or snow-free alpine mountains. Orbital photography in itself is considered inadequate to fulfill exploration needs. It is useful in reducing the size of an exploration area to potentially favorable targets; like other remote sensing techniques, it is a powerful tool only when used in conjunction with detailed field work.

PART 2: LINEAR FEATURES IN LANDSAT IMAGERY

Two LANDSAT images of central Colorado, E-1172-17141 (Figure 10) and E-1154-17143, were selected for analysis of linear geologic structure information content. The two images were selected for their excellent expression of linear features. Their main attributes are low sun elevation and near maximum snow cover. Since a significant proportion of linears is the result of shadow enhancement of topographic features, the lowest sun elevation was selected; it was the minimum available nearest the winter solstice, approximately 23 degrees. This sun elevation is not the optimum for maximum shadow enhancement of the topography in central Colorado, because slopes less than this are not shadow enhanced. In addition to this restriction, there is selective shadow enhancement of linears as a function of deviation from the sun azimuth, which was approximately S.30W. (13). On the other hand, some linear features, especially those which are the margins of dark areas or are long linear dark areas, were enhanced by the snow cover. Snow cover enhances the dark-area margins (particularly between coniferous forests and dormant grassland) and shadow margins by increasing the contrast between the dark and light areas. Furthermore, the snow decreases the contrasts in illuminated areas and provides a uniform high reflectance in areas of otherwise variable reflectance. On the contrary, snow cover might obliterate some linears by smoothing low topographic features. All things considered, when imagery from other seasons was subjectively evaluated, information content and detectability of linears were found to be very much less, which discouraged further analysis for new information not available in snow-covered imagery.

The image that has the more widespread and deeper snow cover, E-1174-17141, also has the greater detectability. The reason seems to be in the greater contrasts as explained above. However, despite some cloud cover, E-1154-17143 has more information (more linears) compared to the other image.

Band 6 images seem to have the greatest detectability of all the LANDSAT bands. In these winter scenes, contrasts between vegetation types and

between vegetated and less vegetated areas are the least and are further diminished by snow cover. In addition, detectability is improved in Band 6 because shadows are darker because of low radiance in this bandwidth as compared to other bandwidths.

There is little doubt that the linear trends in images are not always a true representation of linear trends determined from fault maps and/or rock joint trend maps. Other studies have shown that less than half the linears in one photograph can be related to known structures. Not all geologic linears are represented as linears on the image, say, for example, as vegetation or topographic linears. This may be due to preferential enhancement of some trends by geomorphic processes. Some linears parallel to streams seem not to be controlled so much by lithology or structure, but by direction of drainage evolution, determinable by the line from the local headwaters to the local outflow area of the stream. It seems very probable that stream patterns contribute a great deal of randomness to strike frequency distributions, while structurally controlled trends provide less information. Thus, the "signal-to-noise" ratio is low. The detrimental effects of snow cover and sun attitude have already been discussed.

Strike-Frequency Analysis

The purpose of the strike-frequency analysis was to determine the dominant azimuthal trends of the linears measured on the imagery in order to study the geographical distributions of the trends and their geologic origins. Firstly, linears were marked and traced on a clear overlay of a 9 in. by 9 in. positive transparency (scale - 1:1,000,000) viewed in transmitted light (Figure 11). Only linears of obviously cultural origin were not entered into the analysis. As will be demonstrated, there may be some valid bases for being more selective of linears to be entered into the analyses and, thereby, the possibility of improving correlations between two or more data sets.

Following preparation of the overlay, the linears were hand digitized for length and azimuth to the nearest degree. When lengths of linears were measured, they were grouped into length classes of 0.254mm (0.1 inch) with a maximum of 5cm (2 inches) being found. Strike-frequency histograms of the azimuths of the linears and their length-weighted azimuths were made with the aid of a computer program developed for the study. Azimuthal trends were selected at those azimuths where maxima in the strike-frequency histogram occurred. In addition, to aid in the selection of trends, significance values were calculated for the frequency maxima.

Various degrees of smoothing of the frequency histograms were performed by the method of moving sums as even large data sets had very irregular histograms. Because of the loss of information in the summing process, various summing intervals were investigated for optimum enhancement of dominant trends. Maxima and minima of the histogram constitute an irregular wave form, and where two maxima or two minima are closer together than the summing interval, they are merged into one and some information is lost or filtered out (Figure 12). It should be noted that the summing interval for the original data set is 1 degree of azimuth.

In the discussion that follows, strike frequency histograms have significance values plotted on the ordinate and azimuths on the abscissa as in Figure 12. Relative frequency values determined by moving averages at each degree of azimuth were converted to significance values. Two smoothing intervals were selected for emphasizing the trends found in the histograms. An 18-degree interval (10% of azimuth half-circle) was selected to emphasize broader trends. A 5-degree trend (3%) was selected to emphasize trends of narrower azimuthal range.

Selection of trends was not easy nor entirely consistent because of the irregularity of the frequency histograms. However, the procedure of selecting trends was to associate them with significant maxima surrounded by significant minima. Thus, in the worst case, a trend or significant maxima might consist of numerous significant "spikes" surrounded by values of low significance. A study of some randomly generated linears indicated that such data sets have fewer maxima above the 90 percent significance value than real data sets. In this study, if a real data set fell short of producing 99-percent maxima then 90-percent maxima were used for trend selection.

It was found that the "signal-to-noise" ratio of the histogram is considerably increased by length weighting linears before entering them into the strike-frequency analysis. Thus, where any azimuth had a frequency value of one, in the unweighted analysis, this value became the value of the length class (increasing from 1 in steps of 1). This method provided no new trends over the non-length weighted analysis, but did enhance the trends; that is, increased the "signal-to-noise" and improved their significance values (Figure 13). While no new trends appeared as a result of length weighting, it is very possible for a few long linears to produce a trend in a length-weighted analysis, but none in an unweighted analysis.

Azimuth Trends in the Whole Images

Approximately 300 linears were measured in each of the two images studied. Strike-frequency histograms at unweighted azimuths for each image are shown in Figure 14 and for the combined images in Figure 15. The larger interval of smoothing (18 degrees) was used for Figure 14 and two intervals (5 and 18 degrees) in Figure 15. The trend in Figure 15a is a very broad and significant one ranging from N.40E. to N.35W. and corresponds to the major structural and topographic trends in central Colorado (Figure 16). Figure 15b reveals that at the smaller smoothing interval there may be 5 to 7 closely grouped trends constituting the broader trend. The trends are wholely in counterclockwise deviation to the sun azimuth of N.30W., indicating that there are relatively fewer slopes, as well as other linears, with trends in the west-northwest and east-northeast quadrants.

Areal Distributions of Trends

Inspection of the areal subdivisions of the linear map (Figure 11) indicates that each contains one or more distinct and easily detectable trends, more so than in the greater imaged area. Also, the trends in each subdivision are not part of image-wide trends but of trends localized to that subdivision and a few neighboring ones.

The local trends of each of the 10 subdivisions are plotted in Figure 17. The frequency of local trends for each 10 degree interval of azimuth for the combined images is shown in the histogram in the figure. The frequency histograms for each image are nearly the same. The result is that the local trends, while spread across the azimuth half-circle, do emphasize four major trends: N.20-40W., N.0-10E., N.20-50E., and N.60-70E. When the occurrence of the local trends within the major trends is plotted areally, as in Figure 18, a correspondence to the major structural features in Figure 16 can be made. The N.20-40W. and N.0-10E. trends are associated within the Cenozoic folds and faults of South Park and Canon City Embayment and in the older igneous and metamorphic terrains of the Front Range. The N.20-50E. trend is predominant in the southeast quarter of the area. The N.60-70E. trend is associated with the Cenozoic volcanic terrain and is also dominant in the Front Range in the north part of the image. In the volcanic terrain, there is a definite control of topography by volcano-depositional features (14). In the north, the area is of high relief associated with the Tarryall Mtns. and the North Fork of the South Platte River. Generally, local trends occur in no more than about 40 percent of the area.

Lengths of Linears

All linears of E-1172-17141 that lie within the area of the Pueblo, Colorado, Quadrangle plastic relief map (scale 1:250,000) were grouped by length. For comparison, a linear map of the relief map was made and the linears were also grouped by length. Frequency distributions of linear lengths in the two data sets are shown in Table 1.

TABLE 1. FREQUENCY OF LINEARS FOR EACH LENGTH CLASS CONVERTED TO KILOMETERS FOR LANDSAT IMAGE E-1172-17141 (IN AREA OF RELIEF MAP) AND FOR PUEBLO RELIEF MAP.

E-1172	1			1					4	5	8	7	25	26	31	46	32

Relief Map	1									2	1	4	2	6	11	22	33	118	279	174

45— 40— 35— 30— 25— 20— 15— 10— 5— 0—

LENGTH - km

The LANDSAT linears consist of topographic and non-topographic linears illuminated at a sun elevation of 23° and azimuth of N.28W. in a heavily snow-covered scene. The Pueblo linears are essentially high-relief topographic linears illuminated at a sun elevation equivalent to 15 degrees

and accumulated at illuminations from four directions, S.45E., South, S.45W., and West. The relief map was painted white to remove tonal contrasts not due to illumination angle. Thus, the relief map linears were mapped under optimum conditions.

The scale of the LANDSAT image studied is 1:1,000,000 and that of the photograph of the Pueblo Relief Map is 1:800,000. Smaller features are detectable in the LANDSAT scene that in the relief map photograph because the resolution of the relief map itself is lower.

Over three times as many linears were extracted from the relief map as from the LANDSAT scene. While the modal and longest lengths are nearly the same between the two sources of data, the LANDSAT images yielded a greater average and median length (Table 2). It is believed that the higher

TABLE 2. STATISTICS OF LENGTHS OF LINEARS IN E-1172-17141 AND PUEBLO RELIEF MAP IN KILOMETERS.

Source	No.	Total Length	Average Length	Median Length	Modal Length	Longest
E-1172-17141	186	1417	7.6	6	3	42
Pueblo Relief Map	653	2561	3.9	3	3	42

resolution of the LANDSAT images permits the connection of what would be disconnected line segments on the relief map in the range greater than the modal length and less than the greatest length.

Length and Trend

The two data sets discussed in the previous section were analysed for length preference as a function of azimuth. Length trends (of length-weighted azimuths) are shown in Figure 19b and 20b. Comparison of the length trends with the azimuthal trends in Figure 19a and 20a indicates that no new trends occur as a result of length-weighting of linears, but enhancement of the maxima and minima does occur. Figures 21a and 21b show the frequencies of length as a function of azimuth. In both data sets there is a preference of long linears (length greater than the modal values) in the range of N.10-40W. and a weaker preference at N.20E., N.60E. and N.85E. It is concluded that within a trend the frequencies at the modal length of the data are greater than in non-trend areas, and that lengths greater than the modal length occur much more frequently at azimuths within the major trends. Hypothetically, the best way to extract structural information from LANDSAT linears is to determine modal values from data sets of all linears and then determine structural trends by analyzing the trends of the linears of length greater than the modal length (super-modal linears).

A frequency analysis of the super-modal linears (length class greater than 2) of E-1172-17141 yields 4 significance trends: (I) N.20-40W.,

(II) N.5-20E., (III) N.40-50E., and (IV) N.85E.-N.70W. These trends are plotted for the image subdivisions in Figure 22. They are also extrapolated to subdivisions outside the area of the Pueblo relief map. They are further extrapolated to the local linear trends of E-1154-17143. Trends I and II are associated with the trends of the large folds and faults of the central Colorado area (Figure 16). Subdivisions 22, 32, 33, 34 are underlain mostly by Precambrian rocks which contain trends I and II. Subdivisions 23, 24 and 42 are underlain by younger sedimentary rocks folded at least by Cenozoic diastrophism. In subdivision 22 Cenozoic volcanic rocks lie upon Precambrian metamorphic rocks and Paleozoic and Mesozoic sedimentary rocks.

Subdivisions 22 and 32 also contain trend IV which is dominant in the Cenozoic volcanic terrains. This trend may be ascribed to non-topographic linears discussed in the following section. Trend IV is also found in subdivision 24 outside the area of the length-trend analysis. In this subdivision, the trend can be ascribed to deep topographic valleys in the Tarryall Mountains and the area of the North Fork of South Platte River.

Topographic and Non-topographic Linears

Analysis of the Pueblo relief map was done primarily to evaluate the dominance of topographic linears in LANDSAT imagery over other linears. To make the trend sampling as complete as possible, and diminish the azimuthal filtering effect, linear azimuths and lengths from four illumination directions were collected. The results of the analyses of all linears and super-modal linears is shown in Figures 20 and 23. Trends I, II, III, IV appear in Figure 20a, though trend IV is weak. In the length-weighted data (Figure 20b), trend IV is not present, indicating that long linears are few in this trend. The same is true for the super-modal trends (Figure 23). Thus, trends I, II, and III contain much of the total length of linears while trend IV does not. A comparison of Figures 20b and 23 would indicate that trend IV contains a large proportion of linears of length 2 or less and few longer linears.

The non-length-weighted histogram of E-1172-17141 (Figure 19a) is similar to Figure 20a. The length-weighted trends (Figure 20b) are all strong. The enhancement of trends II and IV is due to length-weighting. Trend IV enhancement is due to length-weighting of a few long linears as further indicated by the super-modal trends in Figure 24.

Because the LANDSAT image records non-topographic linears (these will include topographic linears of low relief) as well as topographic linears (mostly moderate to high relief), comparison of LANDSAT and relief map trend analyses should indicate the relative proportions of the two types of linears in LANDSAT imagery. A hypothetical comparison will be given here as no corroboration by study of other sources of data has been done. Hypothetically then, LANDSAT trends IV could consist mainly of non-topographic linears. Trends I, II, and III could contain large numbers of topographic linears. The idea could be extended further to compare the trends of snow-free and snow-covered scenes of an area in the same season. The snow-covered scene would approximate the painted relief map in the enhancement of topographic linears.

Linears and Joints

Measurements of attitudes of joints from the area of subdivisions 32, 42, 33, 24, and 34 were also analyzed for trends. Many of the joints were provided by Dr. Robert M. Hutchinson of Colorado School of Mines from uncompleted research and were available only in synoptic form. The following discussion considers the correspondence of joints for the entire data set covering the five subdivisions and for a data set from the southern Front Range south of Pikes Peak.

Figure 25 shows that the dominant trends in the two groups of joints are N.0-30W. and N.55-90E; they are approximately orthogonal. In the southern Front Range, the LANDSAT trends are I, II, and III, (Figure 22a), but not IV since the area lies outside the Cenozoic volcanic terrain. The correspondence of the joints trends with the orthogonal LANDSAT trends I and III is the most favorable one but is 20 degrees out of register for both. Nevertheless, the tendency is to correlate the NNW joint trend with the major structural trend (Trend I) in favor of topographic control by joints. The ENE joint trend correlates with the major faults that transect the southern Front Range, again in favor of topographic control by joints.

The LANDSAT trends for the larger area of joint coverage are dominated by the local trends of the subdivisions, trends I and II (Figure 25b). The major structures parallel these trends, as does the NNW joint trend. However, the ENE joint trend does not seem to strongly affect topography and enhance or produce trend III. A joint analysis in the Devil's Head Quadrangle (1:24,000) is subdivision 34 by (15) indicates two strong trends: N-S and E-W. The latter trend does appear on E-1154-17143 in subdivision 34 (Figure 22). Three major faults in the Rampart Range parallel trend II and do have fault-line topography (Figure 16). It is entirely possible that in this area trend II contains a large percentage of topographic linears. Comparison of LANDSAT trends with relief map trends and length-weighted analyses could be done for this area as was done to the south.

Summary and Conclusions

Method of Analysis

1. Estimating azimuth data to nearest degree, smoothing over 15-20 degree moving intervals and plotting in strike frequency histograms is an effective way to determine azimuthal trends of linears.

2. The method used for determining significance values provides a measure of the likelihood of non-random origin of the frequency values in a trend.

3. Detectability of linears and trends in LANDSAT images varies greatly between image generations and depends on sun attitude and surficial tonal contrasts due to seasonal vegetation effects, snow cover, etc.

4. The high resolution of LANDSAT imagery allows detection and connection of longer linear features than is possible with relief maps or topographic maps.

5. Length-weighted linears produce more distinct trends, and can reveal trends based on a few, very long linears.

6. Short linears contribute a large number of random azimuths and, as a result, decrease the signal (trend)-to-noise ratio.

7. More distinct trends can be produced from length-weighted linears greater in length than the modal length.

Data Characteristics

1. The strike-frequency histogram of linears from the total imaged area is not isotropic, but contains one distinct broad trend.

2. In subsets of the imaged area based on geologic distinctions 4 trends exist.

3. Trends are localized to less than 50 percent of the total area and are related to large geologic features.

4. In small areas of the image, the existence of only one or two trends is typical.

Correspondence with Geologic Trends

1. The analysis was confined to a portion of the imaged area of two LANDSAT images of central Colorado and four linear trends were found.

2. An overall broad trend reflects a change from south to north of the trends in major geologic structures from N.40W. to N.10E.

3. All four linear trends have geologic trends associated with them.

4. Trend I (N.20-40W.) and II (N.5-20E.) correspond to the trends of the major geologic folds and faults as well as one regional joint set.

5. Trend III (N.40-50E.) corresponds to a second regional joint set (perpendicular to the other) and several major faults.

6. Trend IV (N.85E.-N.70W.) corresponds to a few long, linear depositional features in a volcanic terrain.

7. The localization of trends in smaller areas is strongly related to the underlying major lithologic terrains.

Speculations

1. Trends of linears of length greater than modal length may yield the most information about geologic trends.

2. All geologic trends are not expressed as linear trends in a given small area, but might be on opposite sides of the area. In other words, all geologic trends are expressed somewhere as linear trends.

3. Intersections of linear trends in an image do not necessarily indicate a localized or unique intersection of geologic trends.

4. The trends of geologic structures in younger sedimentary strata strongly parallel linear trends in older metamorphic and igneous terrains.

PART 3: MEGALINEARS AND LINEAMENTS

Linears are here defined as any essentially unidimensional straight or continuously curved features in an image. They are defined on combinations of infinitesimally small picture elements and not on the real things they represent. Megalinears are defined as features which are essentially unidimensional groups of linears that are parallel, en echelon, overlapping, or end-to-end. Lineaments are the groups of geologic structures, often diverse in type, that are associated with the linear elements of a megalinear. The lineaments of this section are those that have structural elements that appear only to have the same kinematic movement plan and subparallel trends.

Included in the discussion of linears are closed or open, curved or polygonal features. These often consist of concentric groupings of short linears. They are frequently associated with plutonic igneous or volcanic activity as well as other structural deformation. They will be called concentric features.

This investigation is concerned with those anomalous megalinears and their associated lineaments that transect major tectonic features in central Colorado. They are anomalous relative to the major known lineaments that essentially bound and parallel the tectonic features. These anomalous megalinears have not been studied extensively before now because a synoptic view has not been available. Furthermore, most earlier geologic investigations have been circumscribed by the margins of major tectonic features, and synoptic evaluations have been thus restricted.

Transecting megalinears are nearly as detectible in an image as the more structurally consistent lineaments. Their associated lineaments are composites of anticlines, synclines, drag folds, monoclines, faults, crush zones, shear zones, and rock joint sets. Structure type along the trend of a lineament is very dependent upon the lithologic terrains in which they are developed. It is this variability as well as the transecting nature of the lineaments that presents a somewhat confusing structural picture, and perhaps has slowed the recognition of these major anomalous structural features.

The anomalous transecting megalinears are part of a regional tectonic framework as follows. The major structural elements of the central Colorado test site (Figure 16) are the southern Front Range, a block mountain uplift bounded by typical mountain flank structures; the Denver Basin on the east;

South Park on the west; Canon City Embayment on the south; the Wet Mountains, a block mountain uplift; and Wet Mountain Valley. The basins are downfolded Cenozoic and older sedimentary rocks. The block mountains are Precambrian metamorphic and plutonic igneous rocks which also underly the basins. Between South Park and Wet Mountain Valley, the Tertiary Thirtynine Mile volcanic field lies upon metamorphic rocks.

The flank structures of the block mountains consist of major high-angle thrust faults and associated monoclines (Figures 26, 27). The Rampart Range and Ute Pass thrusts lie along the eastern margin of the Front Range; the Elkhorn and Oil Creek thrusts along the western margin. The eastern margin of the Wet Mountains is bounded by the Wet Mountain thrust and monoclines.

In LANDSAT and Skylab images of central Colorado the normal tectonic elements and their marginal structures are recognizable. In addition, there are four concentric features and several of the transecting megalinears (Figure 28). Of the concentric features the most prominent one is the Pikes Peak intrusive center of the Pikes Peak batholith. Two other centers of the batholith are not recognizable. The Lake George stock also is very prominent. Two volcanic centers, the Thirtynine-Mile and one in Wet Mountain Valley, are also recognizable (Figure 28).

Three transecting megalinears are in the Rampart Range portion of the Front Range and three are in part of the Front Range south of Pikes Peak.

In the Rampart Range (Figure 29), the Manitou Park megalinear is associated with the Ute Pass fault on the south, which passes into the Ute Pass thrust west of Manitou Park, and northward in Pikes Peak granite into the Bear Creek shear zone. The one singular feature of this lineament is that the fault zones have been intruded with sandstone dikes throughout the length of 125 kilometers. The Manitou Park "graben" of sedimentary rocks is bounded on three sides by this large crescent-shaped lineament.

East of this lineament is the Jackson Creek megalinear associated with the Jackson Creek fault which also has been intruded by sandstone dikes. This lineament transects the Rampart Range and offsets the flank structures on the east and passes into the flank structure of Manitou Park on the west. A third unnamed megalinear is associated with a long prominent escarpment that trends into the flank structure on the east and a shear zone in the flank structure of Manitou Park on the west.

The three large lineaments of the Rampart Range are continuations of or are involved with long known structural features. On the west, they are continuations of the major thrust fault and the monocline of the Manitou Park structures. These lineaments extend northward across the Range and become involved in the major thrust fault on the eastern side of the block uplift. The Rampart Range thrust is offset in the places where two of the megalinears pass into the flank structure. A new interpretation of this block uplift is that it consists of three giant imbricated plates with two thrust faults at the outer margins and two normal faults between the plates.

South of Pikes Peak (Figure 30), the Milsap Creek megalinear trends S. 10W. from the Pikes Peak intrusive center across Garden Park syncline, Royal Gorge Arch and into the Wet Mountain Valley. The associated structures consist of mafic intruded crushed zones in the metamorphic terrain of the

Front Range, a major offset of the mountain flank structure on the western margin, a gentle drape fold in Garden Park, and Mikesell Gulch fault. The latter fault passes into intensely folded and fault sedimentary rocks west of Royal Gorge arch and southwestward into metamorphic rocks. The total length is 35 kilometers.

Two other megalinears are the Adelaide and Peck's Camp features. The latter is a mineralized mafic-intruded crushed zone. The Adelaide megalinear is associated with a major fault that transects the block mountain range and involves faulted sedimentary rocks in the flank structure on both margins of the range.

The structural evidence associated with the transecting megalinears of the Front Range uplift points to a more complex involvement of the crystalline basement in the regional tectonic deformations. These deformations consist not only of the familiar ones of uplifts decoupled from basins along flank thrusts and monoclines but also independent or subsequent, continuous cross-cutting deformations that have the spatial unity of a lineament, yet are manifest in different structural features along that lineament. Further study of these features may add considerably to our knowledge of tectonic history and kinematics of regions.

ACKNOWLEDGEMENTS

These investigations were carried out at the Department of Geology at Colorado School of Mines under LANDSAT contract NAS5-21778 and Skylab contract NAS9-13394. Data collected under Bonanza Project contract NGL-06-001-015 were also used.

REFERENCES

1. Nicolais, S.M., 1974, Mineral exploration with ERTS imagery: in Third Earth Resource Technology Satellite-1 Symposium, v. 1, Sec. B, Goddard Space Flight Center, Washington, D.C., p. 785-796.

2. Knepper, D.H. (ed.), 1973, Geologic and mineral and water resources investigations in western Colorado using ERTS-1 data: Progress report 9: Colorado School Mines Remote Sensing Rept. 73-5, 53 p.

3. Lee, Keenan, Knepper, D.H., and Sawatzky, D.L., 1974, Geologic information from satellite images: Colorado School Mines Remote Sensing Rept. 74-3, 37 p.

4. Blanchard, Roland, 1968, Interpretation of leached outcrops: Nevada Bur. Mines, Bull. 66, p. 89-91.

5. Carlisle, Donald, and Cleveland, G.B., Plants as a guide to mineralization: California Div. Mines Spec. Rept. 50, 31 p.

6. Cannon, H.L., 1960, Botannical prospecting for ore deposits: Science, v. 132, p. 591-598.

7. __________ 1971, The use of plant indicators in ground water surveys, geologic mapping, and mineral prospecting: Taxon, v. 20, p. 227-256.

8. Canney, F.C., 1969, Remote detection of geochemical soil anomalies, in Second Annual Earth Resources Aircraft Program Status Review: NASA, v. 1, p. 7-1 to 7-8.

9. Tweto, O.L., 1974, Reconnaissance geologic map of the Fairplay West, Mount Sherman, South Peak, and Jones Hill 7½-minute quadrangles, Park, Lake, and Chaffee Counties, Colorado: U.S. Geol. Survey map MF-555, 1:62,500.

10. Sawatzky, D.L., 1973, Photolinears, in Knepper, D.H. (ed.), Geologic and mineral and water resources investigations in western Colorado using ERTS-1 data: Progress report 9: Colorado School Mines Remote Sensing Rept. 73-5, 53 p.

11. __________ 1974, Geologic structures, in Lee, Keenan (ed.), Geologic and mineral and water resource investigations in western Colorado using Skylab EREP data: Colorado School Mines Remote Sensing Rept. 74-6, p. 18-27.

12. Hanley, J.B., Heinrich, E.W., and Page, L.R., 1950, Pegmatite investigations in central Colorado, Wyoming, and Utah, 1942-1944: U.S. Geol. Survey Prof. Paper 227, 125 p.

13. Sawatzky, D.L., and Lee, Keenan, 1974, New uses of shadow enhancement. Remote Sensing of Earth Resources, v. 3, p. 1-18.

14. Epis, R.C., Scott, G.R., and Taylor, R.B., 1973, Petrologic, tectonic, and geomorphic history of central Colorado: Geol. Soc. America, Rocky Mtn. Section, Guidebook for Field Trip 8, 22 p.

15. Johnson, D.H., 1961, Geology of the Devil's Head quadrangle, Douglas County, Colorado: Unpublished Colorado School Mines D.S. Thesis.

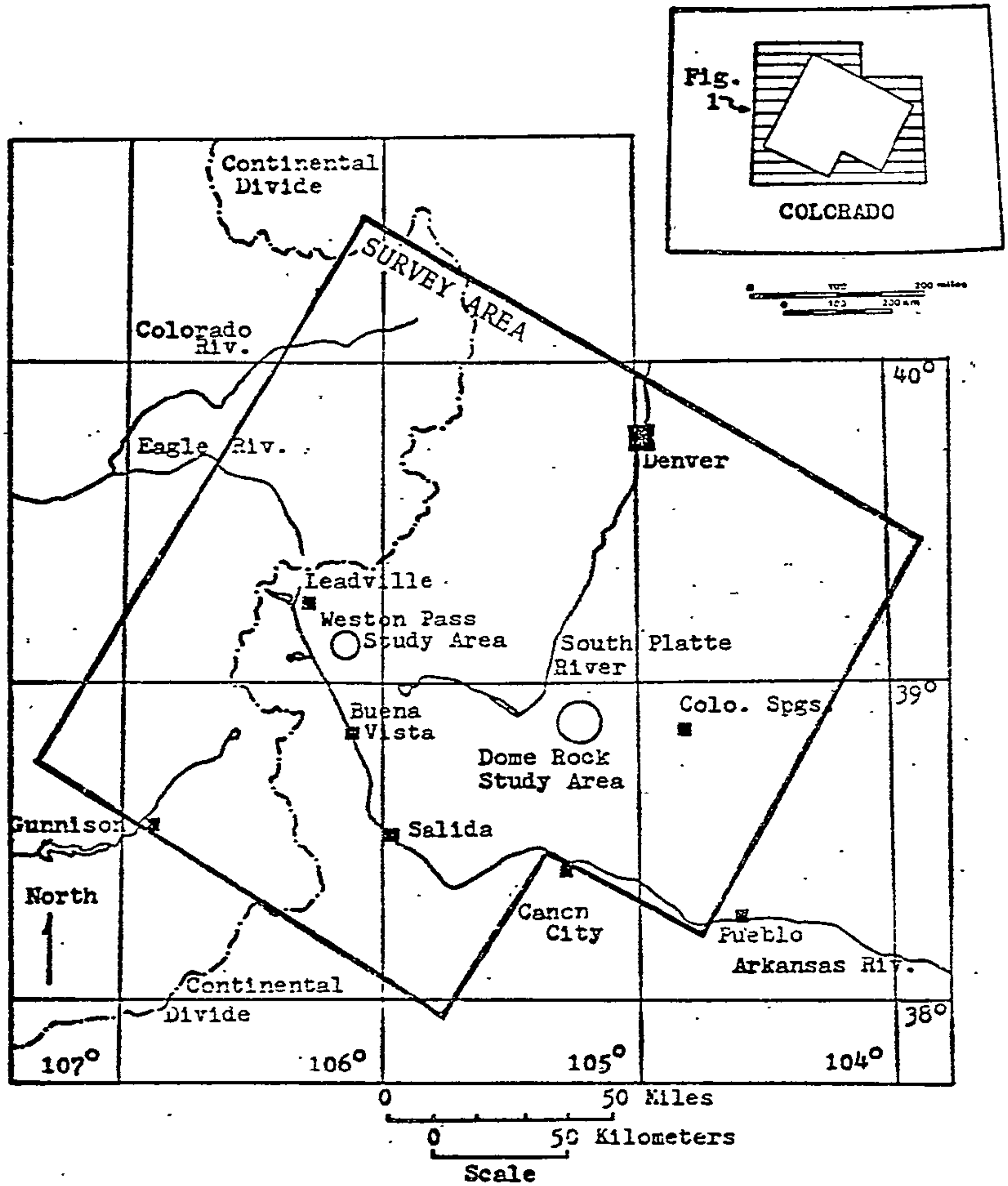

Figure 1: Central Colorado study area.

WESTON PASS PRIMARY TARGET STUDY AREA

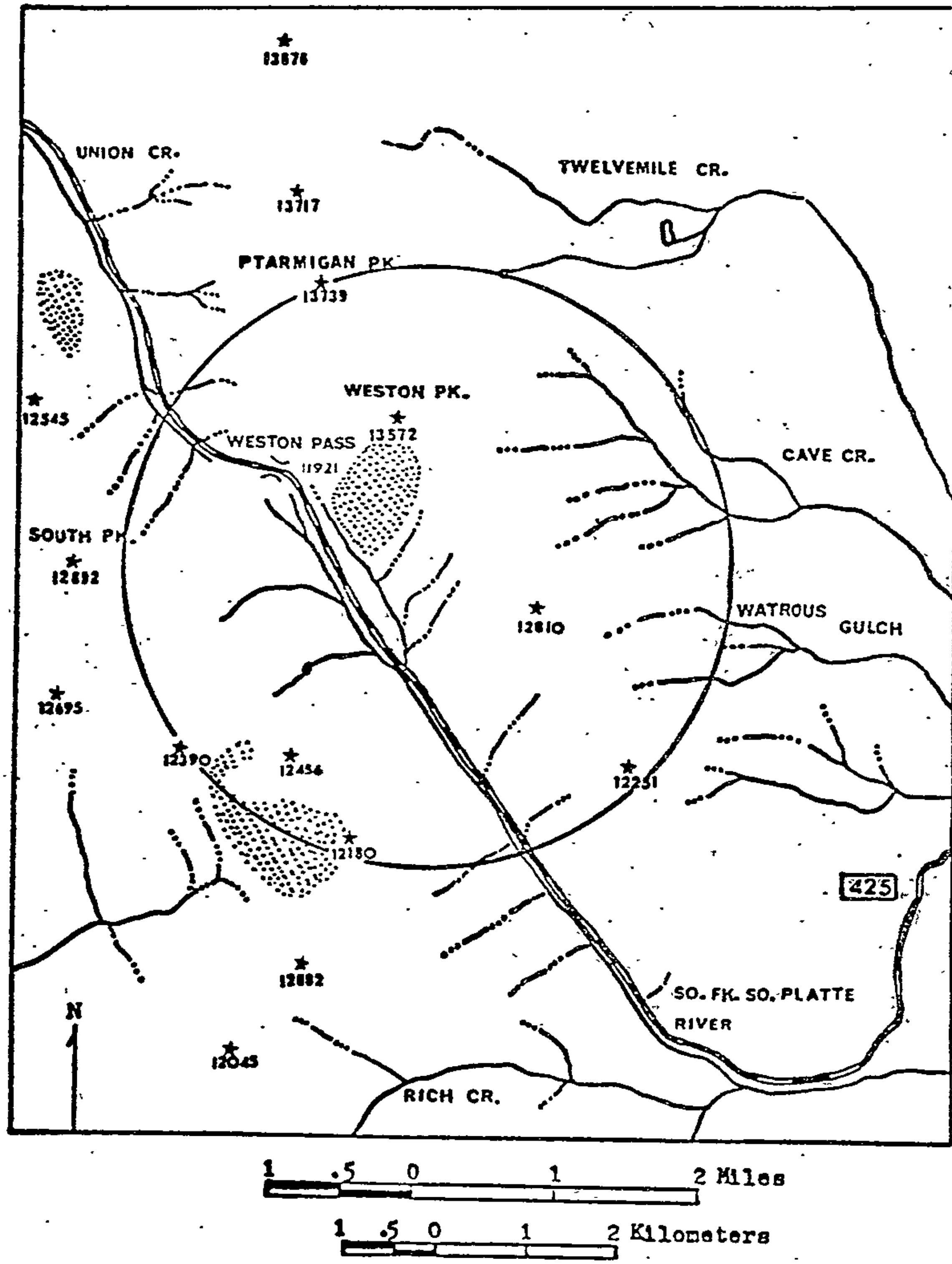

Figure 2 : Red-ocher color anomaly targets, mapped from Skylab 3 S190B, track 48, frame 38, 4 August 1973.

Anomalous colors.

WESTON PASS PRIMARY TARGET STUDY AREA

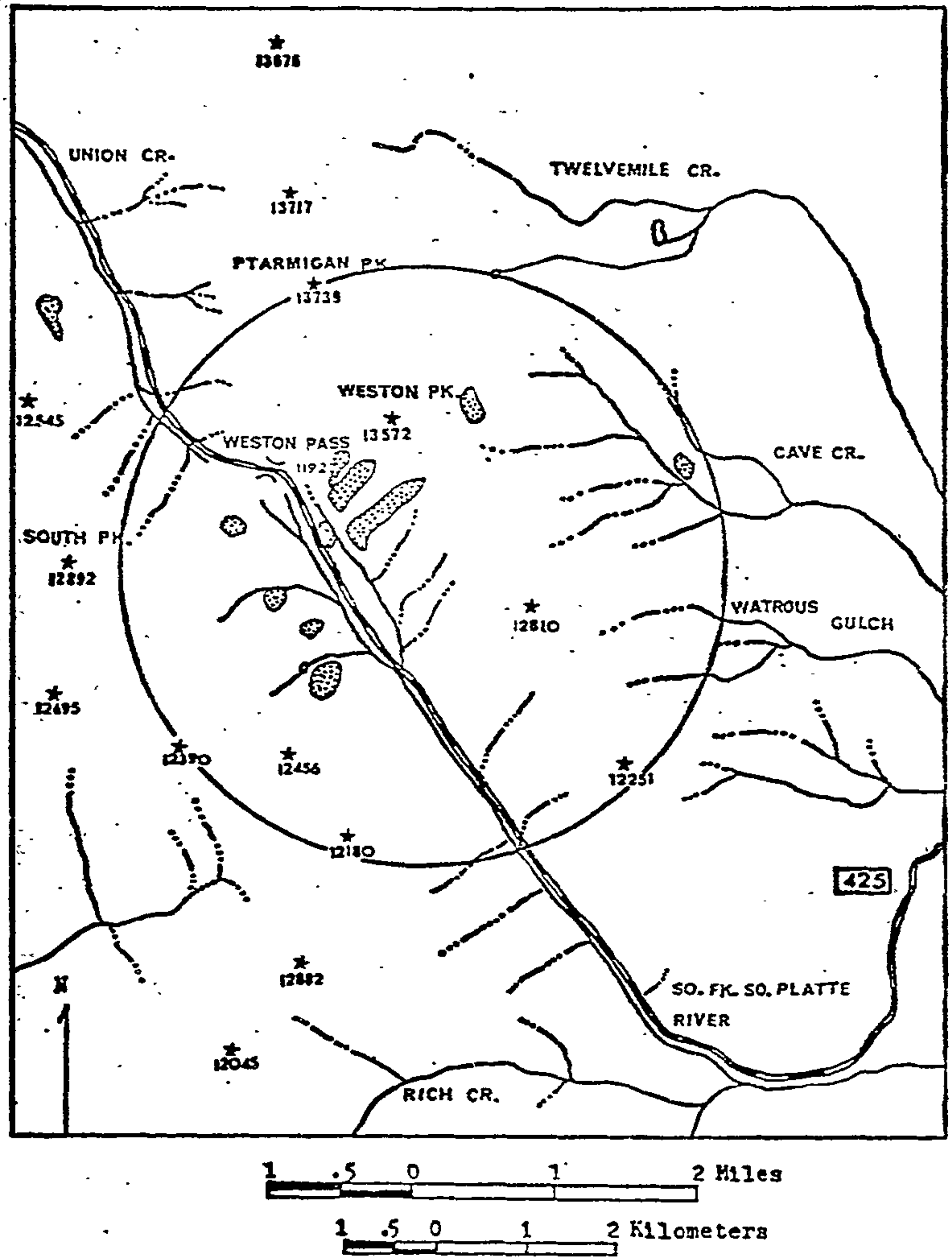

Figure 3: Distribution of limonitic alteration.

Limonitic alteration.

WESTON PASS PRIMARY TARGET STUDY AREA

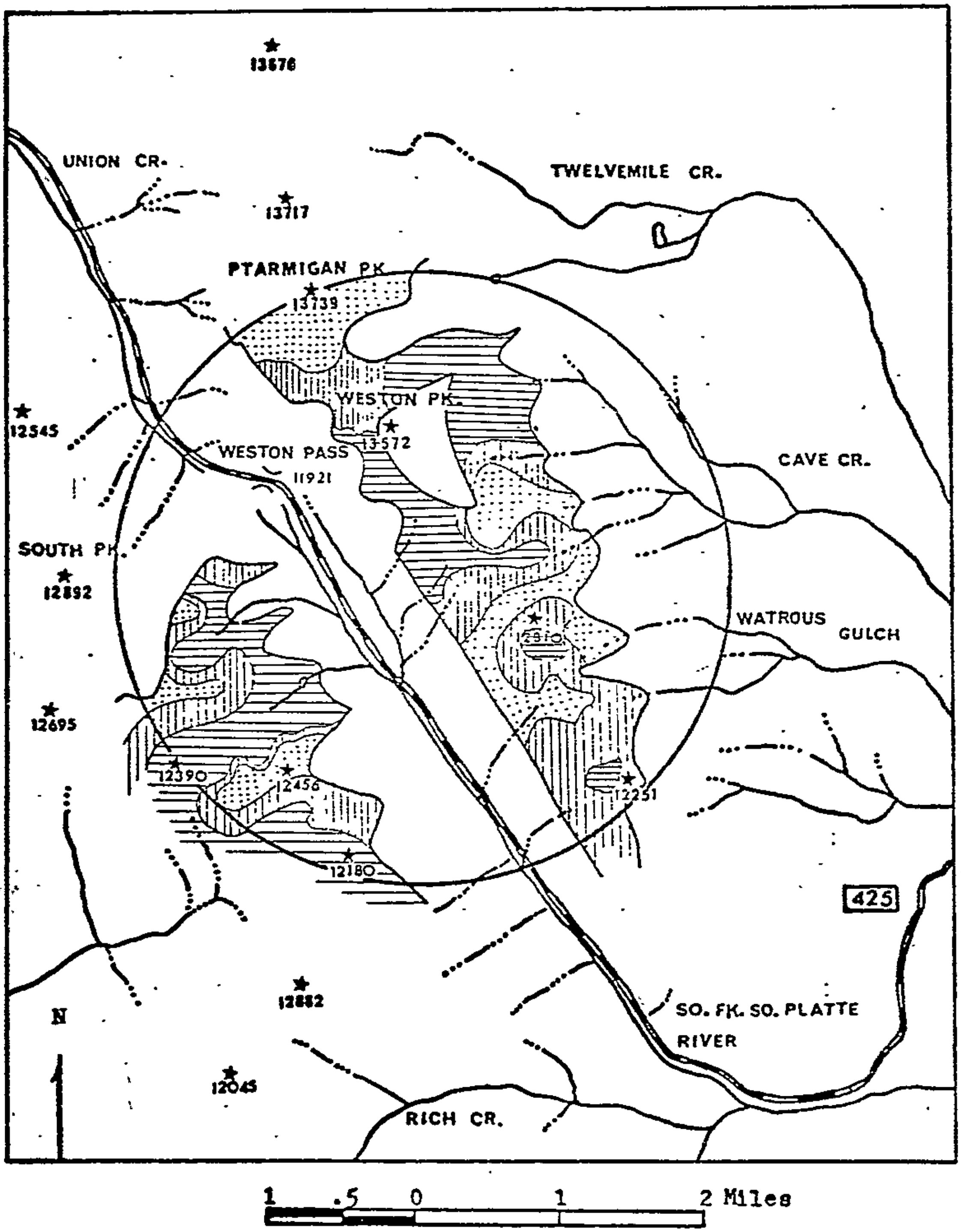

Figure 4: Distribution of 'pink minerals' (volume percent) in Precambrian units.
0-15% 16-30% greater than 30%

WESTON PASS PRIMARY TARGET STUDY AREA

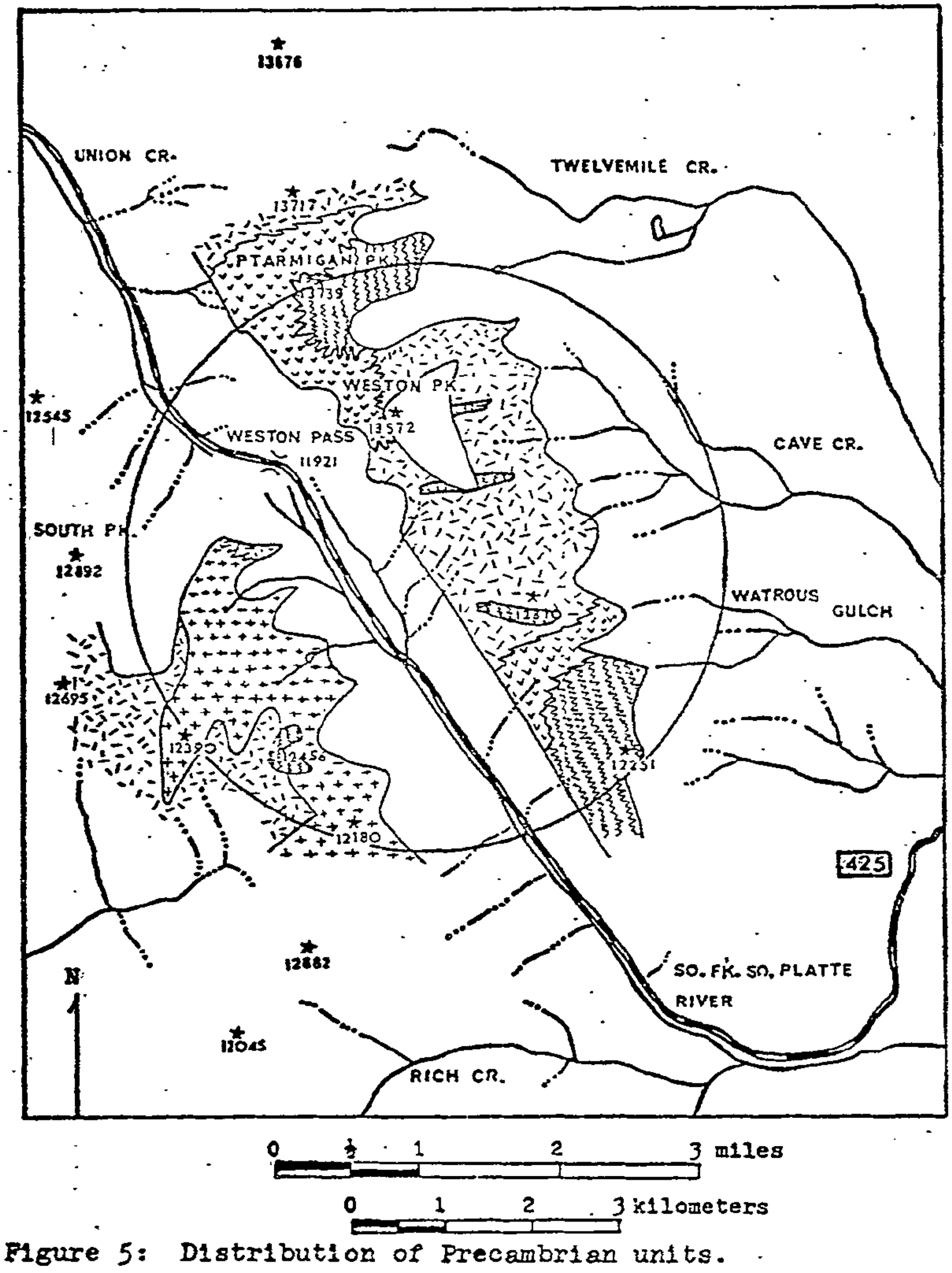

Figure 5: Distribution of Precambrian units.

Silver Plume-Type Granite

Trout Creek Augen Gneiss

Biotite Gneiss

Injection Gneiss

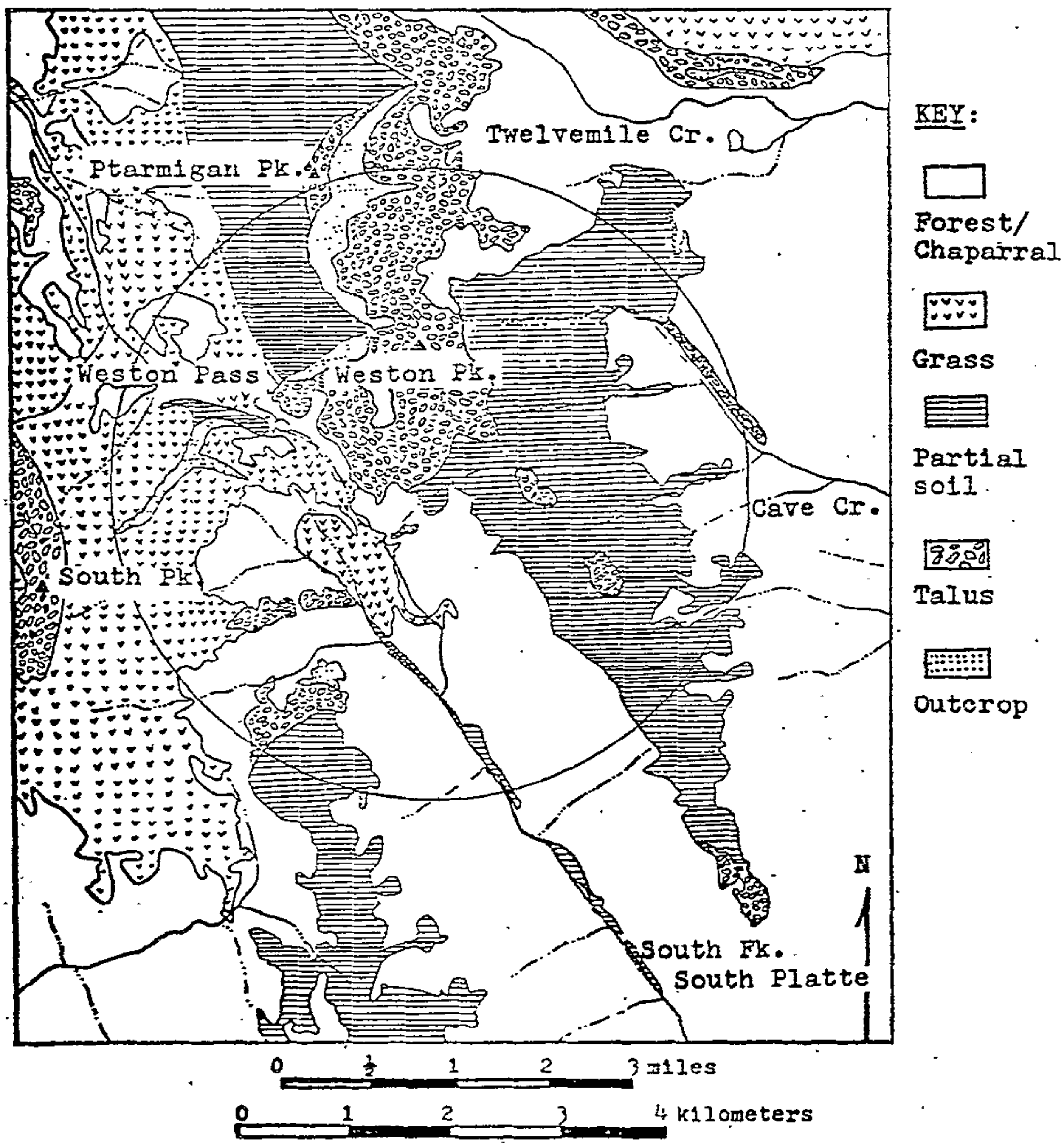

Figure 6: Ground cover map, Weston Pass and vicinity.

WESTON PASS PRIMARY TARGET STUDY AREA

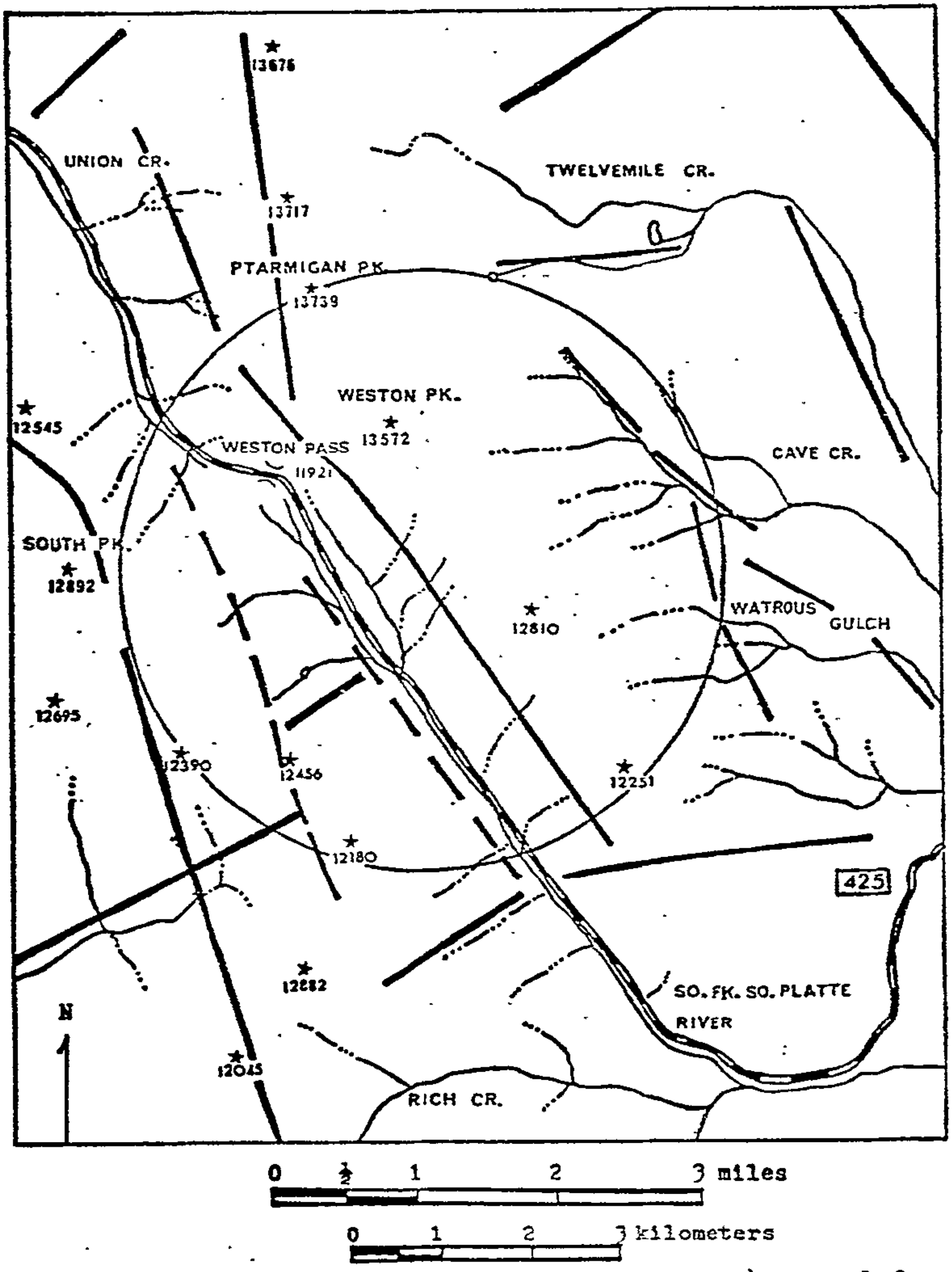

Figure 7: Lineaments (dashed where uncertain) mapped from Skylab 2 S190A, track 48 frame 17, 11 June 1973, and Skylab 3 S190A, track 48 frames 106 and 107, 4 August 1973.

WESTON PASS PRIMARY TARGET STUDY AREA

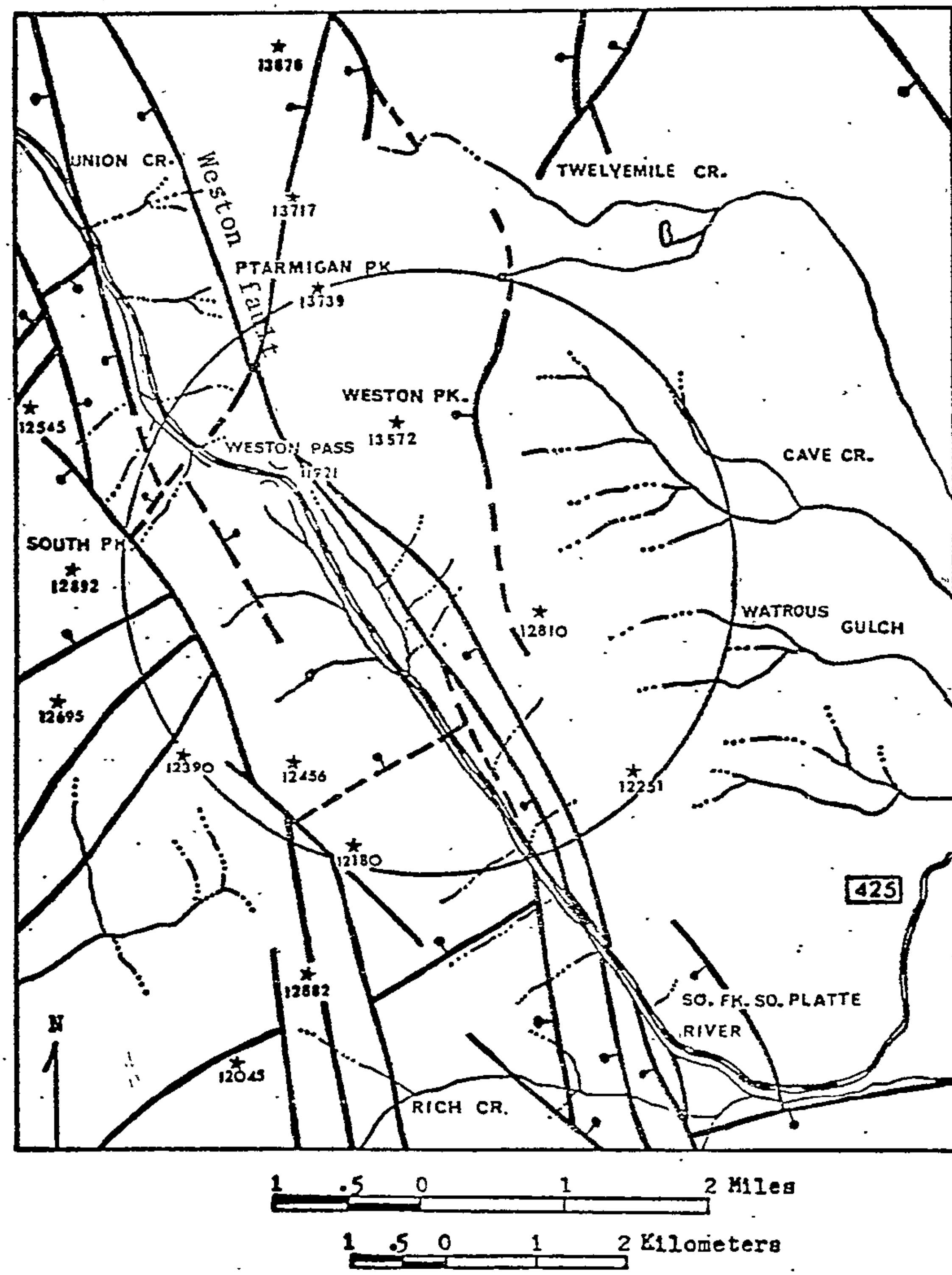

Figure 8: Regional structure, modified after Tweto, 1974. Bar and ball on downthrown side of fault.

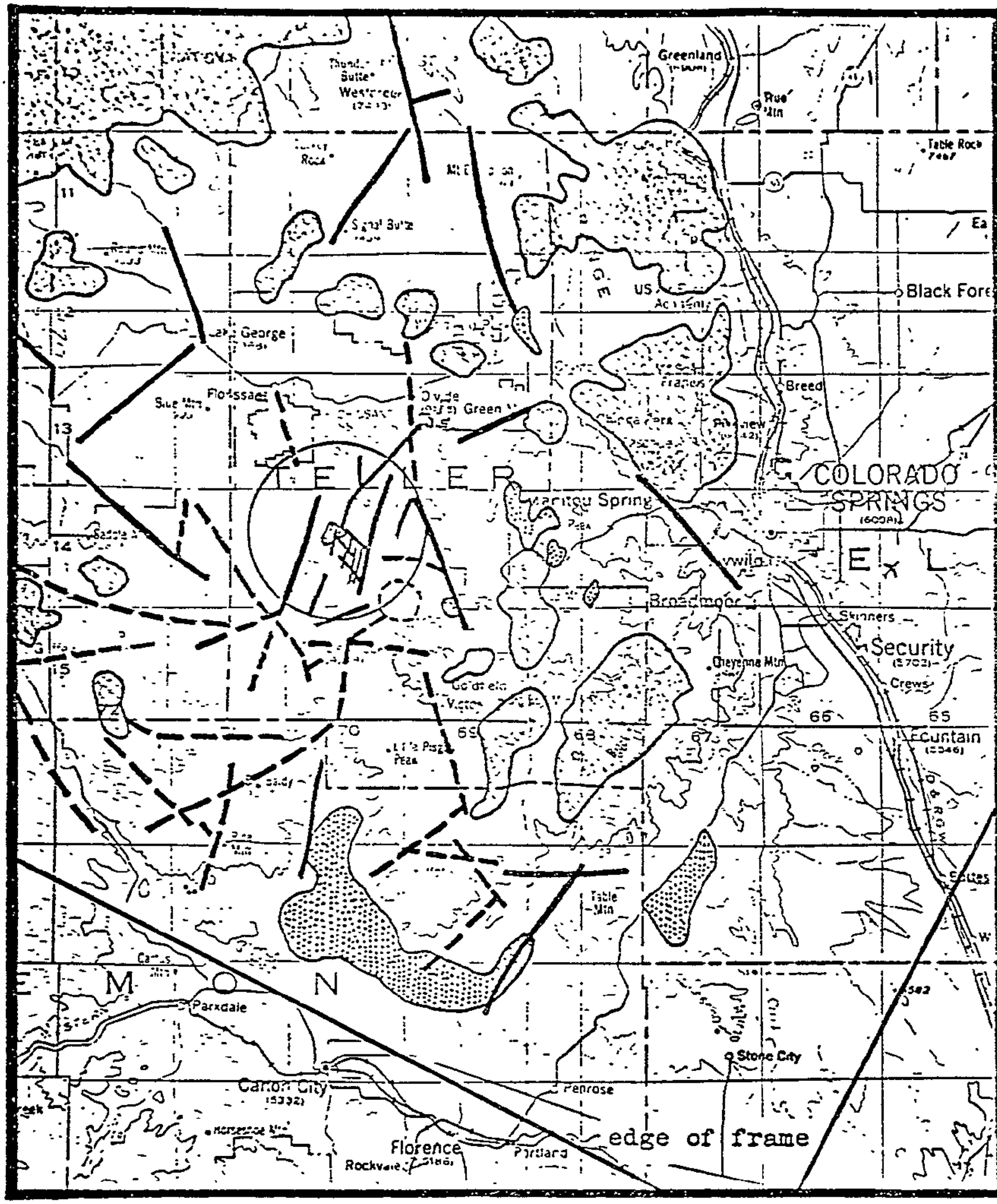

0 4 8 16 miles

0 5 10 20 kilometers

Figure 9: Linear diagram. Skylab 3 S190-B, track 48 frame 39. 4 August 1973. Study area at Dome Rock is circled.

—— – – Linears, dashed where existence questioned.

Color anomalies.

Clouds.

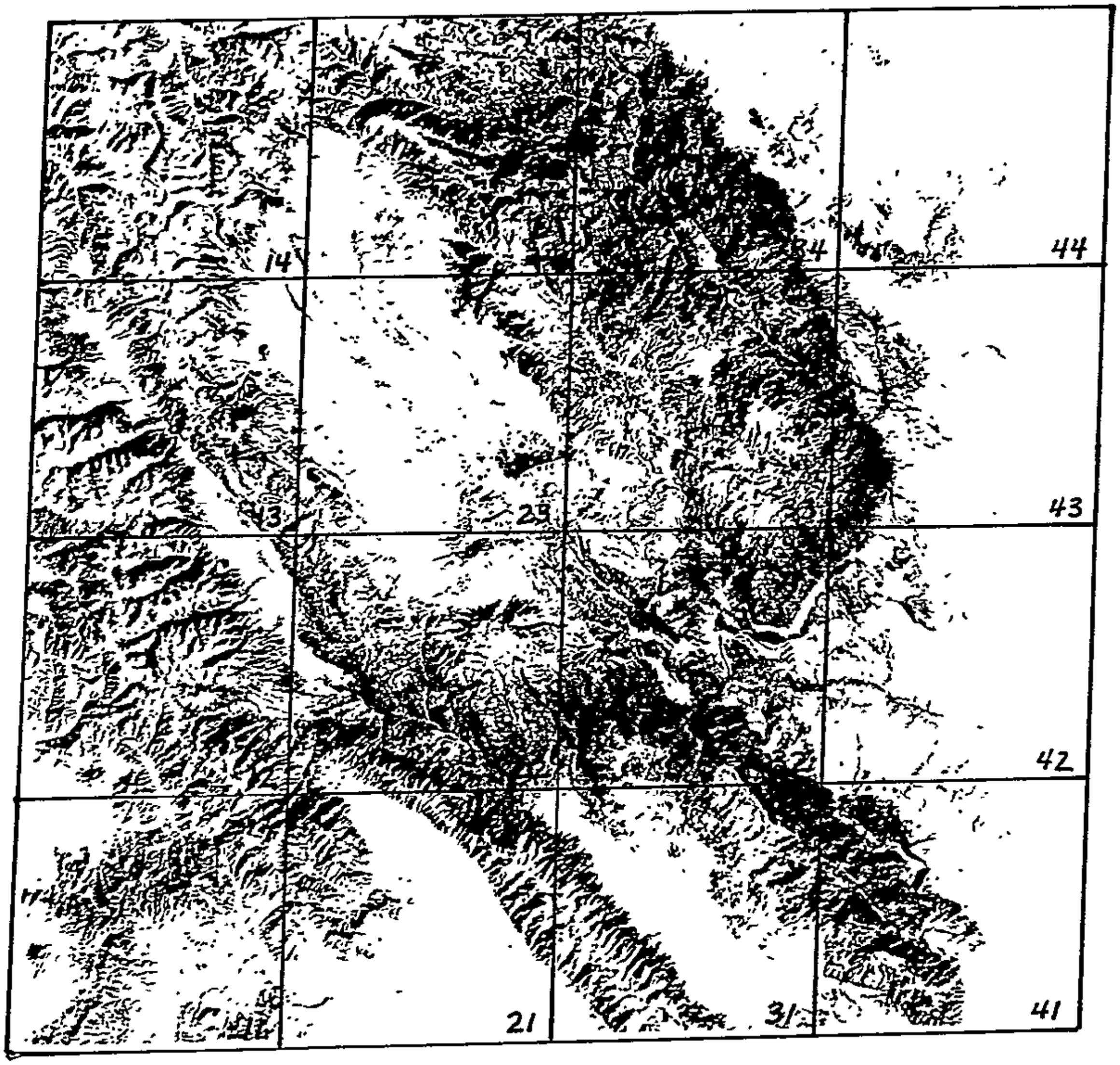

ORIGINAL PAGE IS
OF POOR QUALITY

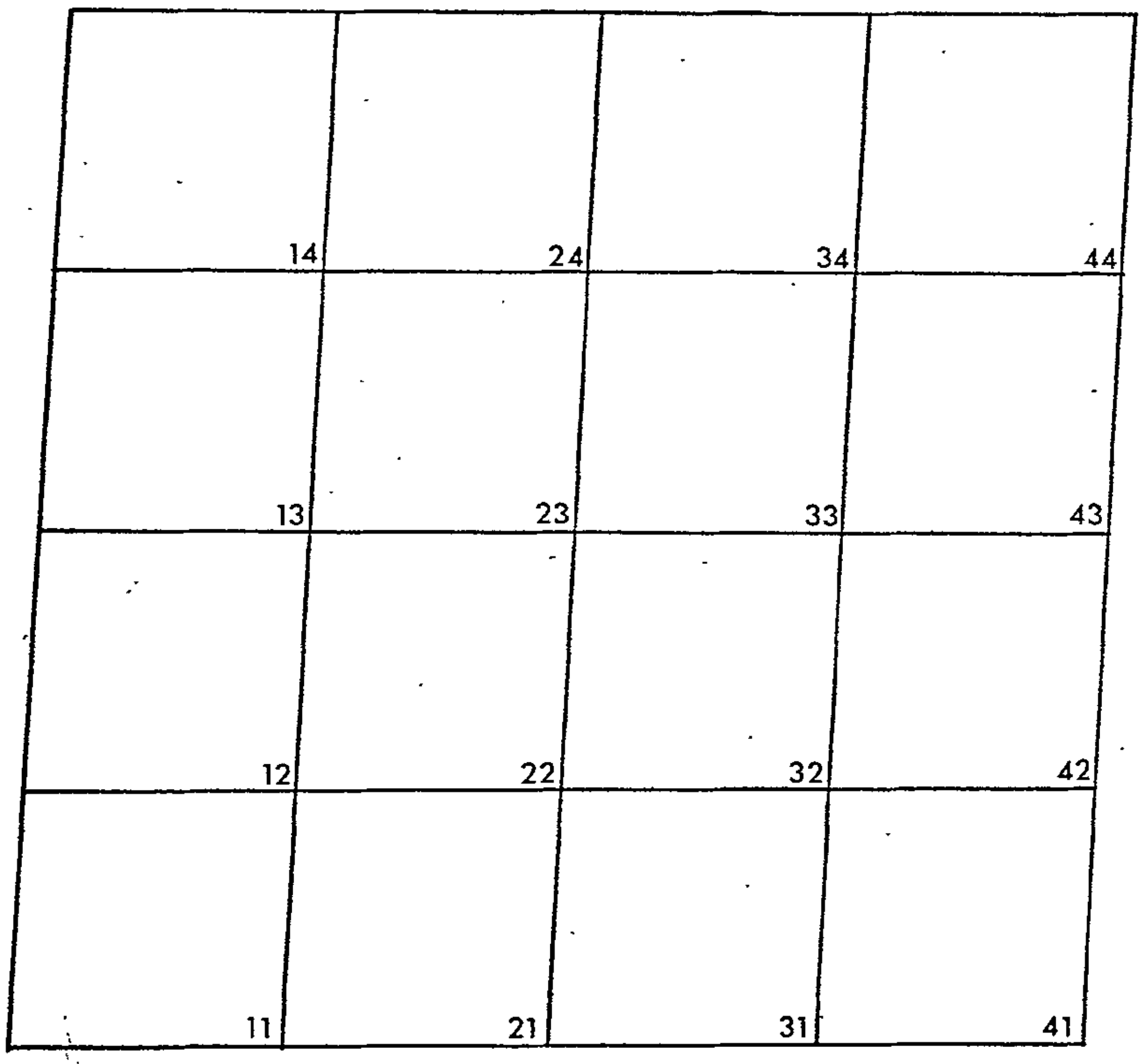

Figure 10. ERTS image, E-1172-17141, of central Colorado. Date January 11, 1973, sun elevation is 23 degrees, sun azimuth is 150 degrees. Grid subdivisions will be referred to in the text.

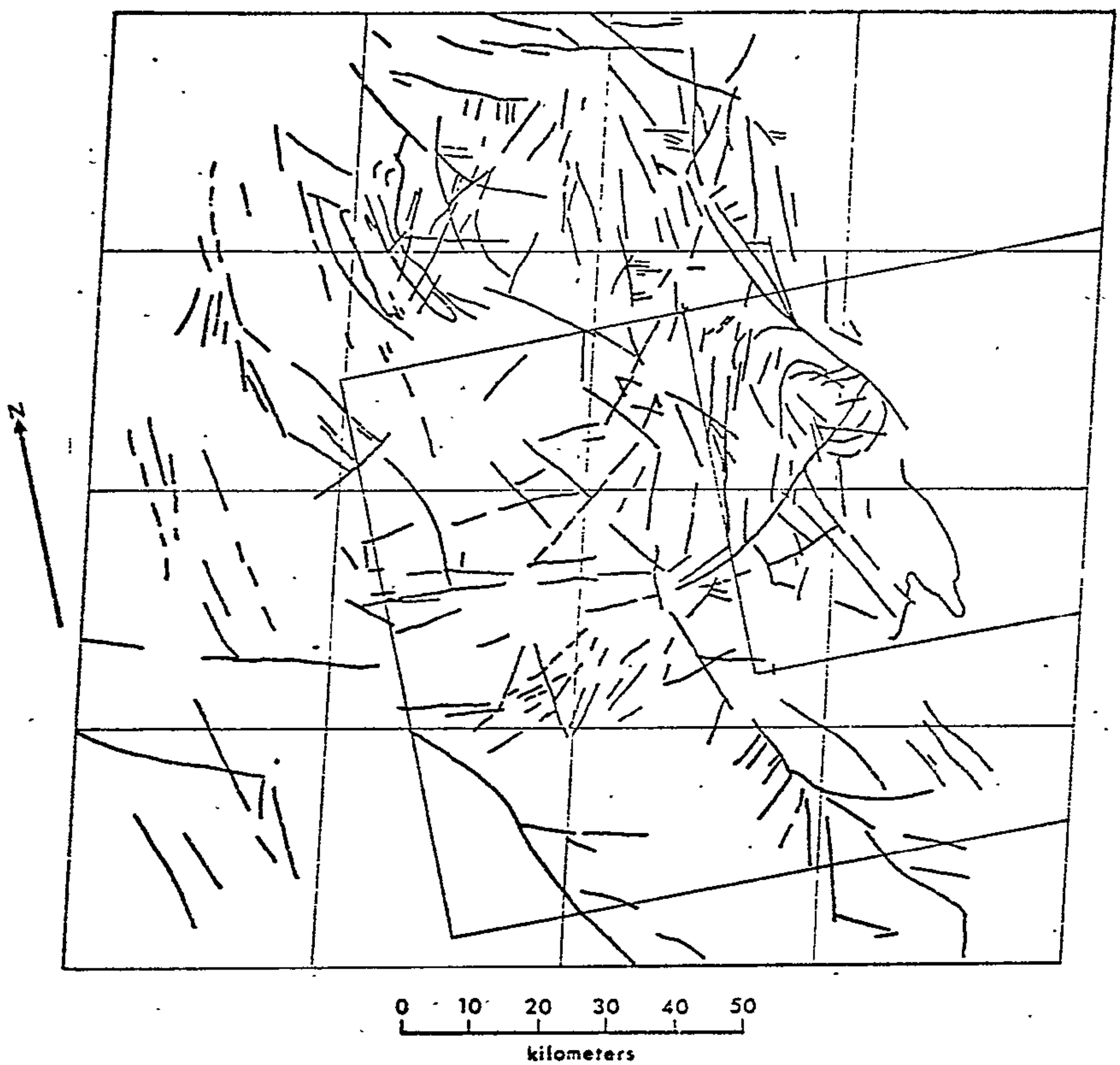

Figure 11. Linears traced from ERTS image E-1172-17141. Gridded areas are as in Figure 10. Larger rectangular subarea is of the Pueblo relief map. Smaller subarea is of the Southern Front Range.

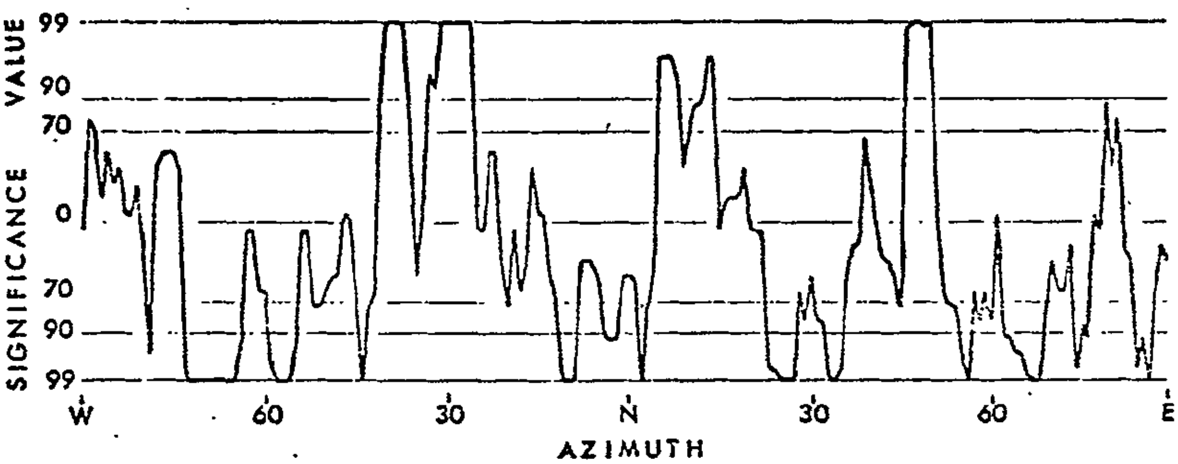

(a) Smoothing interval is 5 degrees of azimuth.

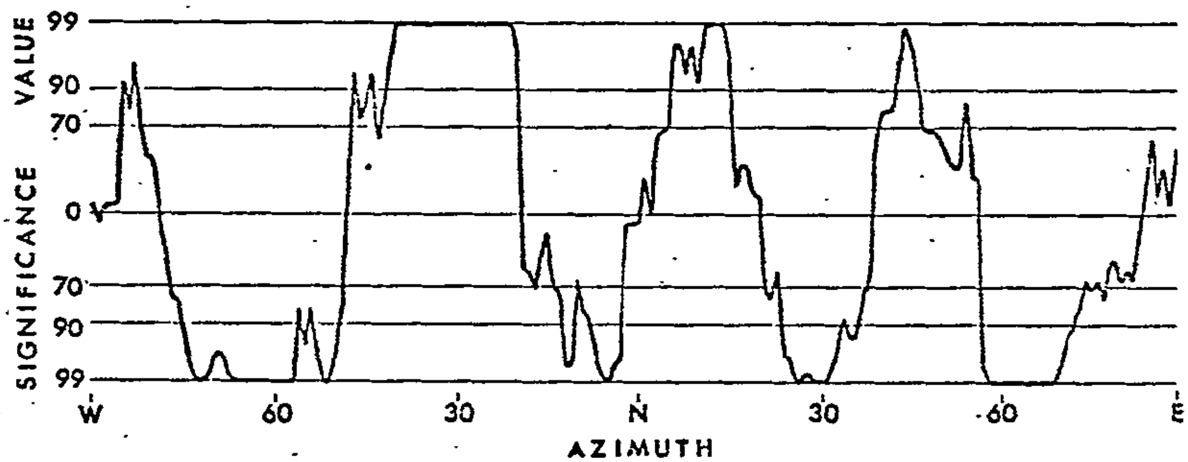

(b) Smoothing interval is 18 degrees of azimuth

Figure 12. Example of merging of narrow maxima and minima by increasing the azimuthal summing or smoothing interval.

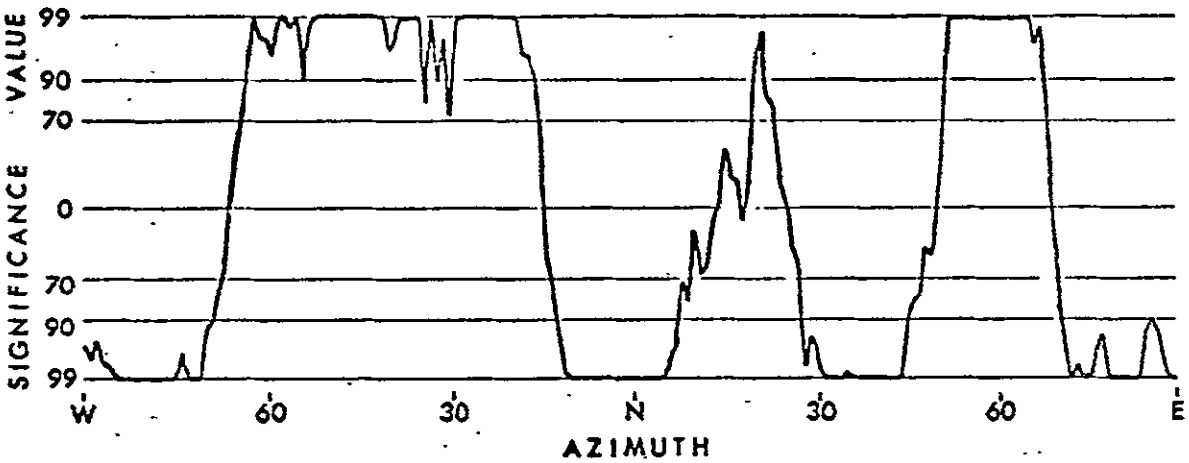

(a) Length-weighted azimuthal data

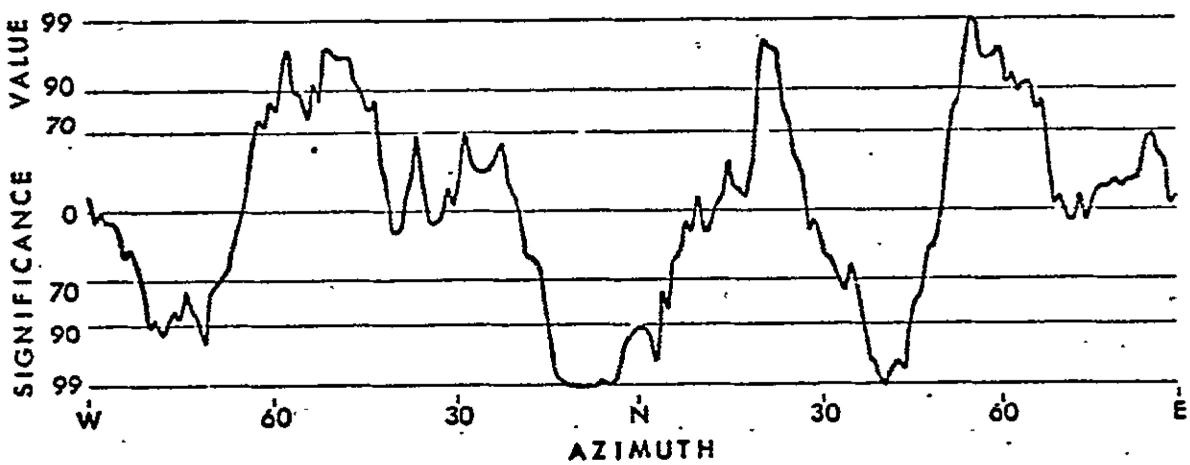

(b) Unweighted azimuthal data

Figure 13. Illustration of effect of length-weighting on significance of trends in strike-frequency histograms, 18-degree smoothing.

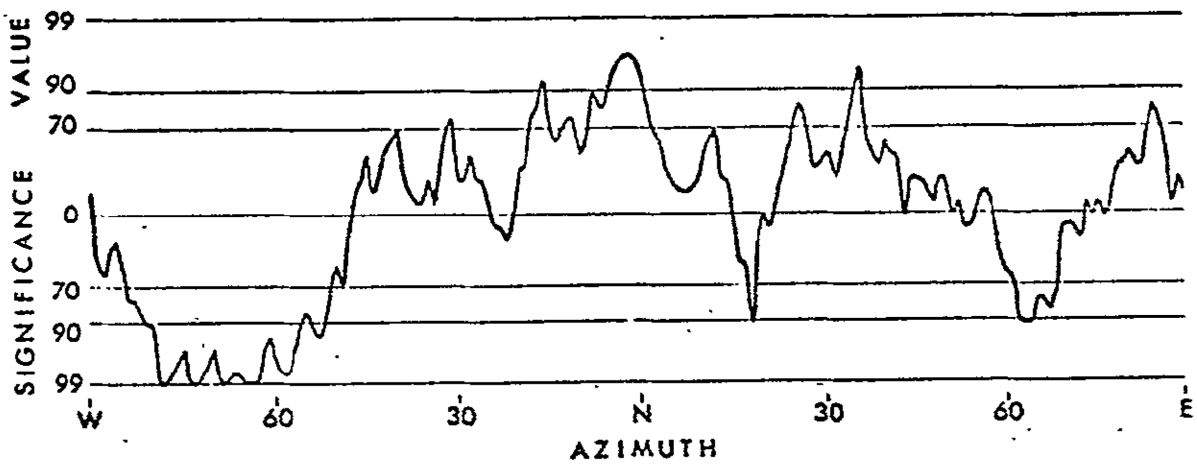

(a) E-1154-17143

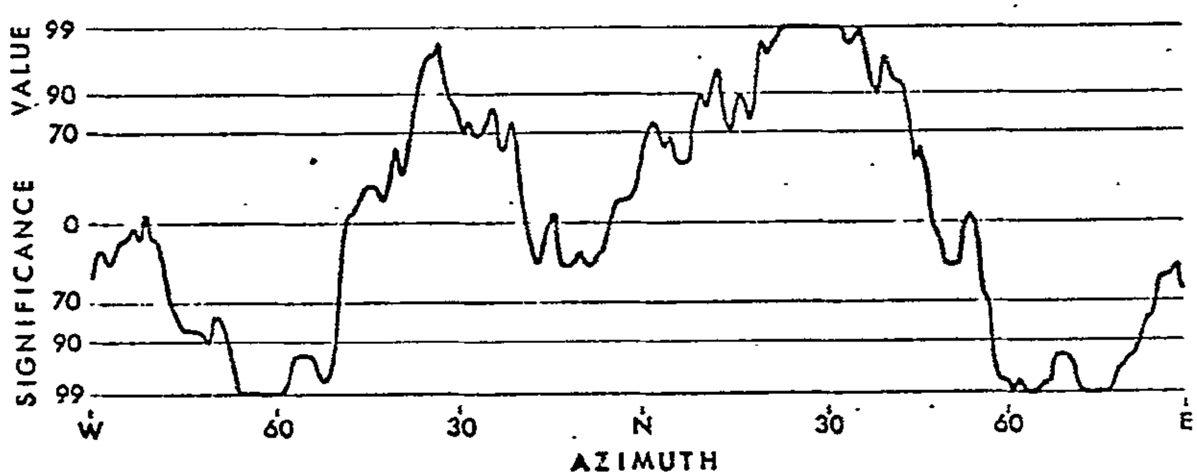

(b) E-1172-17141

Figure 14. Strike-frequency histograms of linears in two ERTS images of central Colorado. The area covered is shown in Figures 2 and 7.

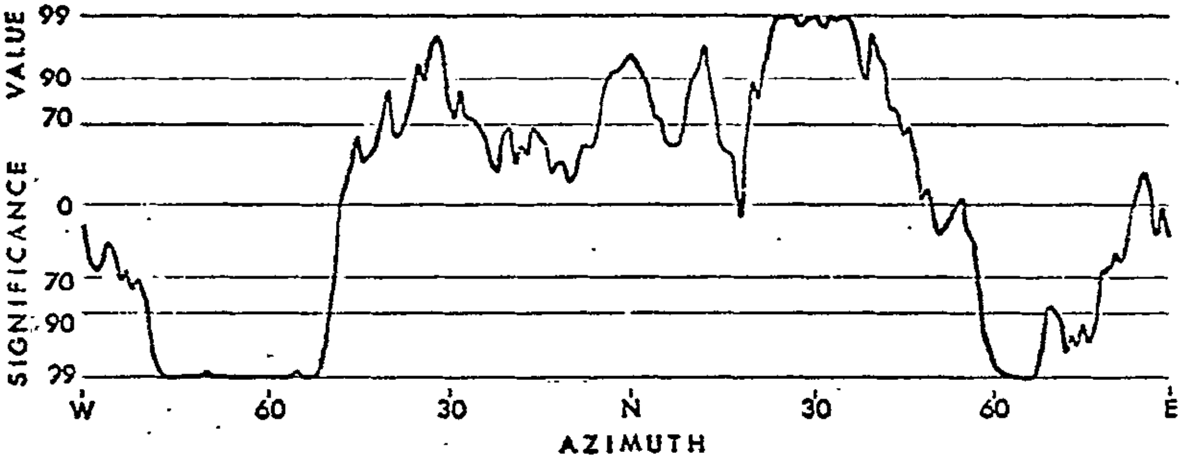

(a) Smoothing interval is 18 degrees.

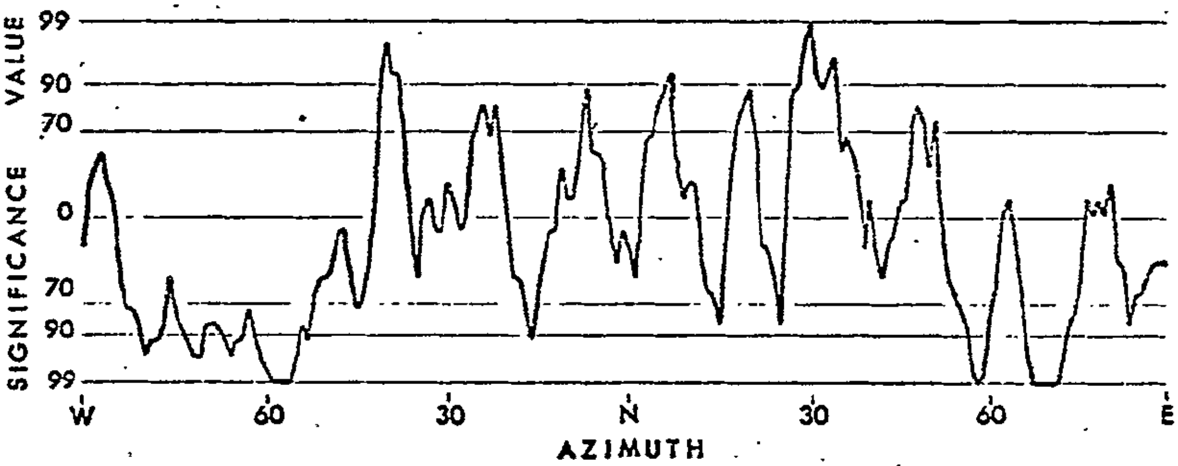

(b) Smoothing interval is 5 degrees.

Figure 15. Strike-frequency histograms of linears combined from both ERTS images, E-1154-17143 and E-1172-17141.

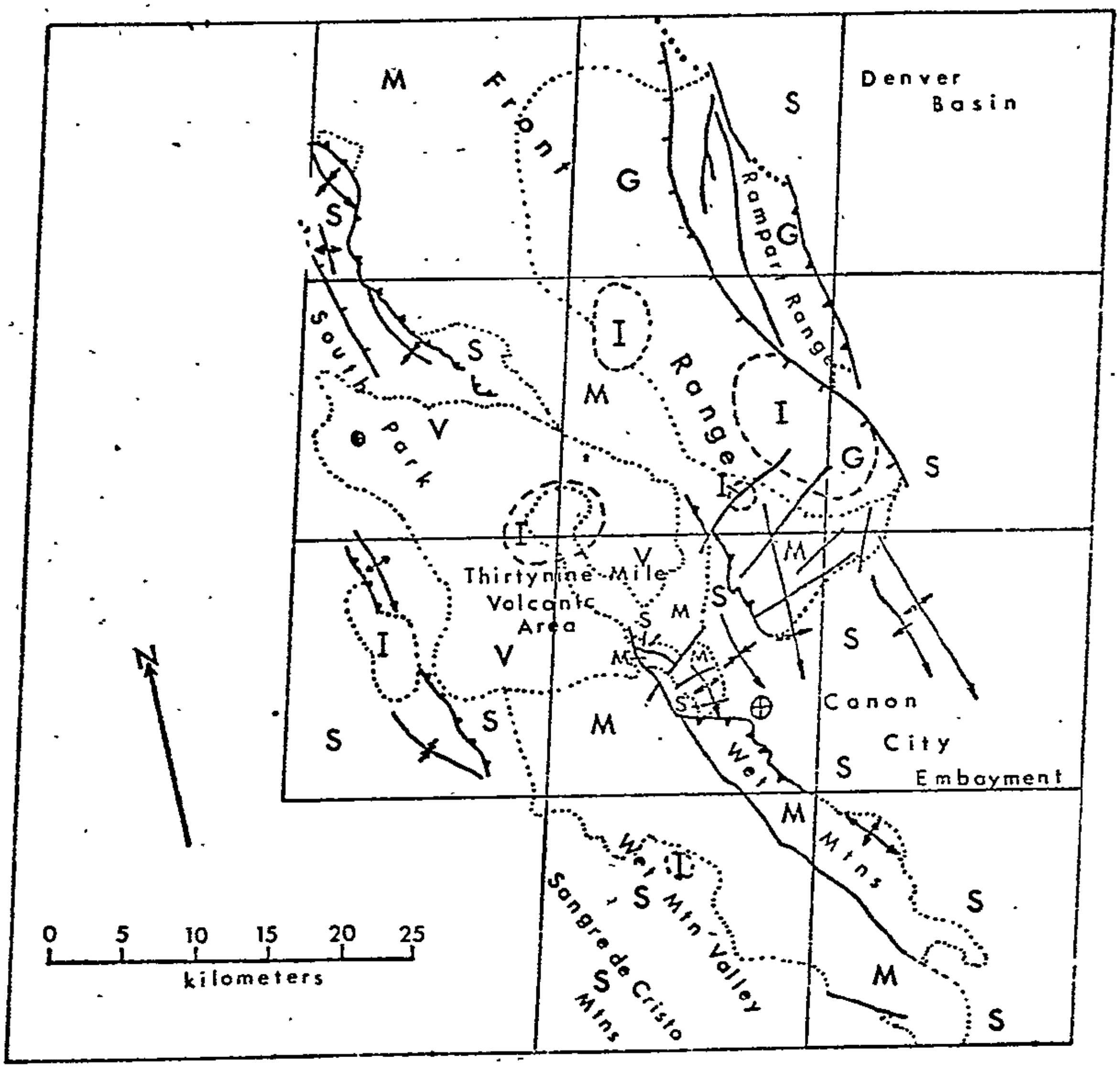

Figure 16. Geologic map of imaged area showing major faults and folds and gross lithologic terrains. Plain, hachured, and toothed lines are faults. Hachures indicate reverse faults, teeth indicate thrust faults. Lines with arrows are folds. Lithologic terrains are defined by dotted lines and are sedimentary (S), metamorphic (M), granitic igneous (G), volcanic (V), igneous or volcanic intrusive centers (I).

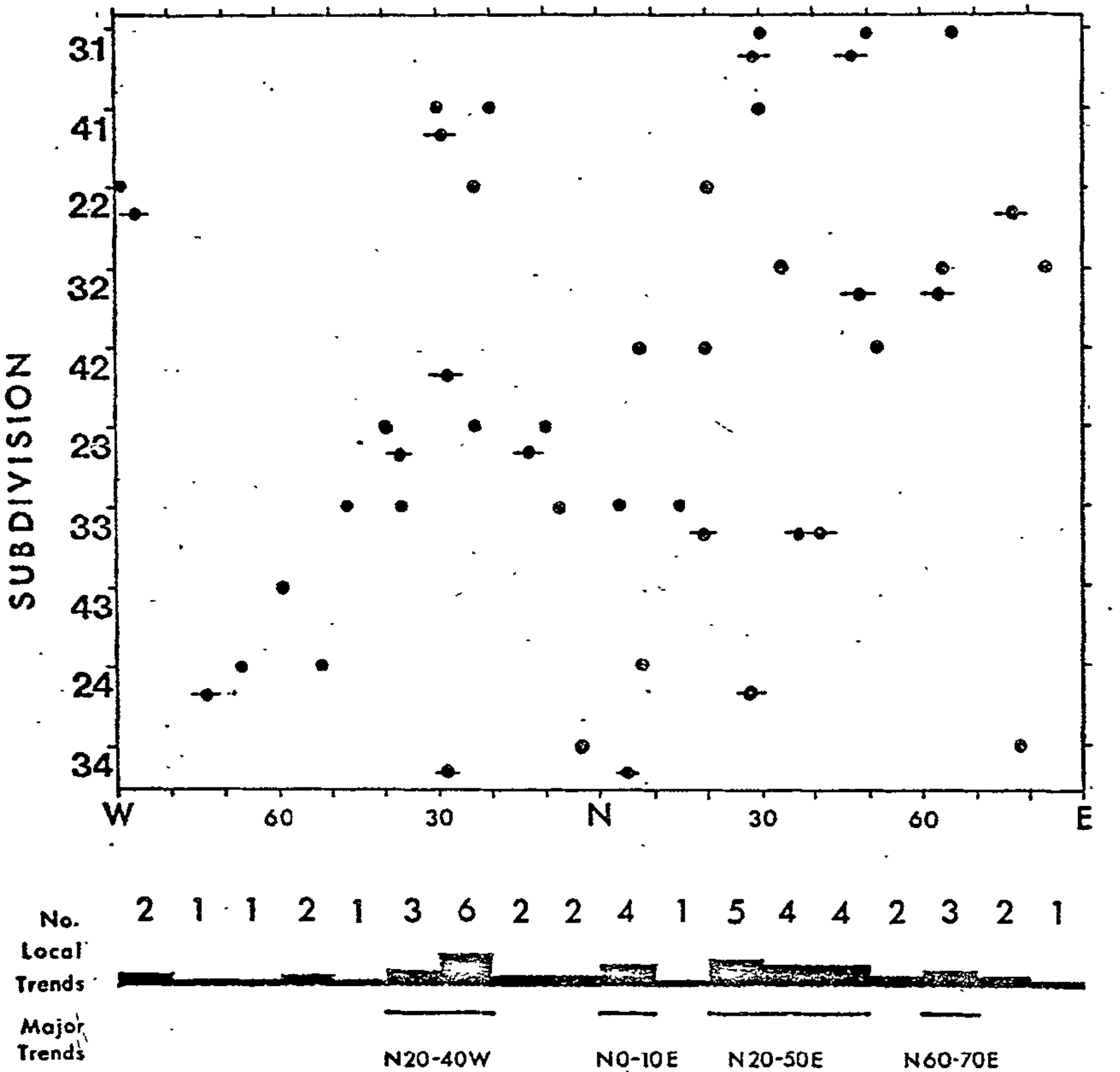

Figure 17. Areal distribution of local trends in 10 subdivisions of E-1172-17141 (barred dots) and E-1154-17143 (plain dots). Histogram shows number of trends for both images per 10 degree sector of azimuth. Heavy lines below histogram indicate 4 prominent trends for total area of all subdivisions.

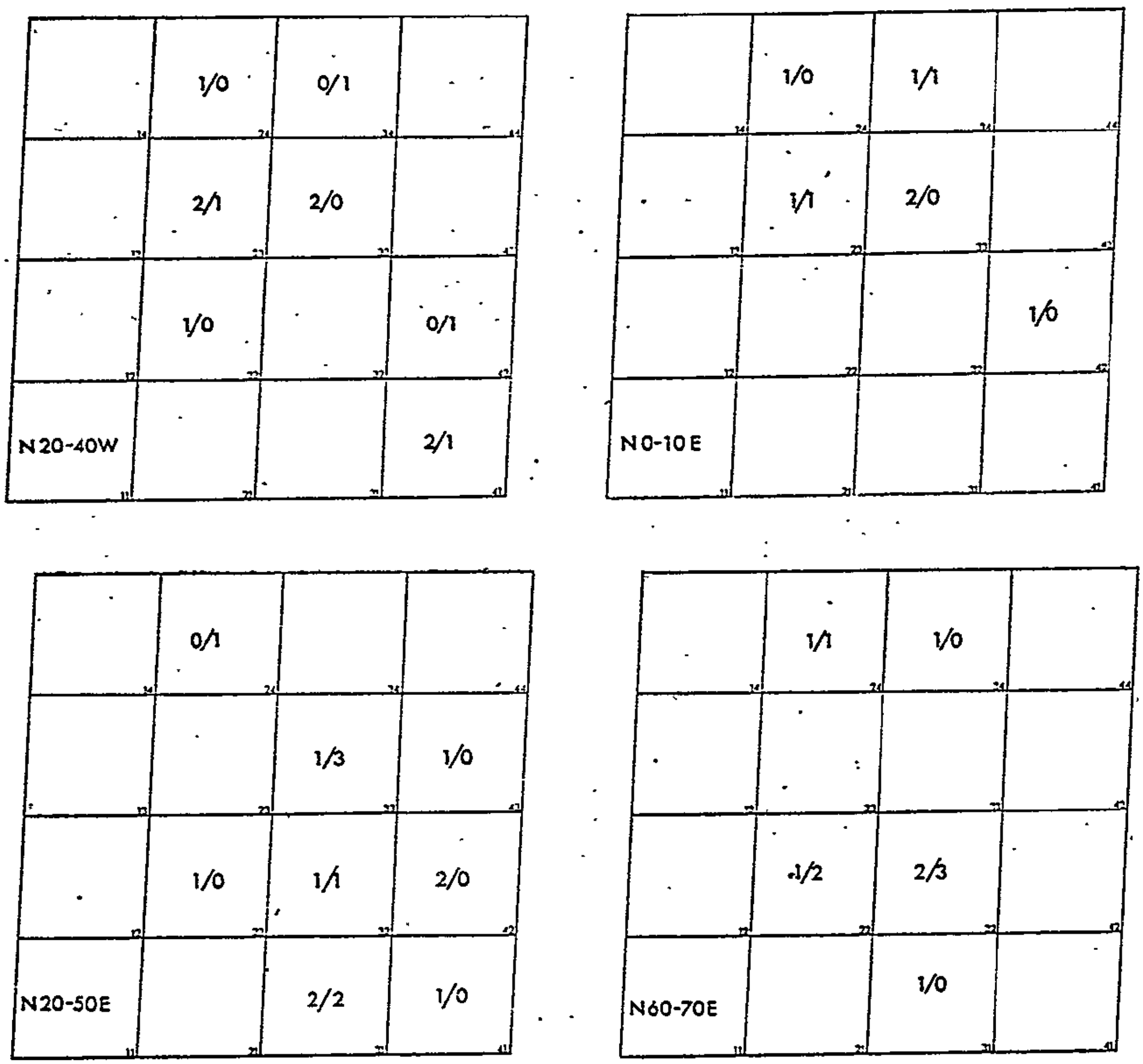

Figure 18. Number of local trends within each subdivision that falls within the four major trends of Figure 8. Numerator is for E-1154-17143 and denominator is for E-1172-17141.

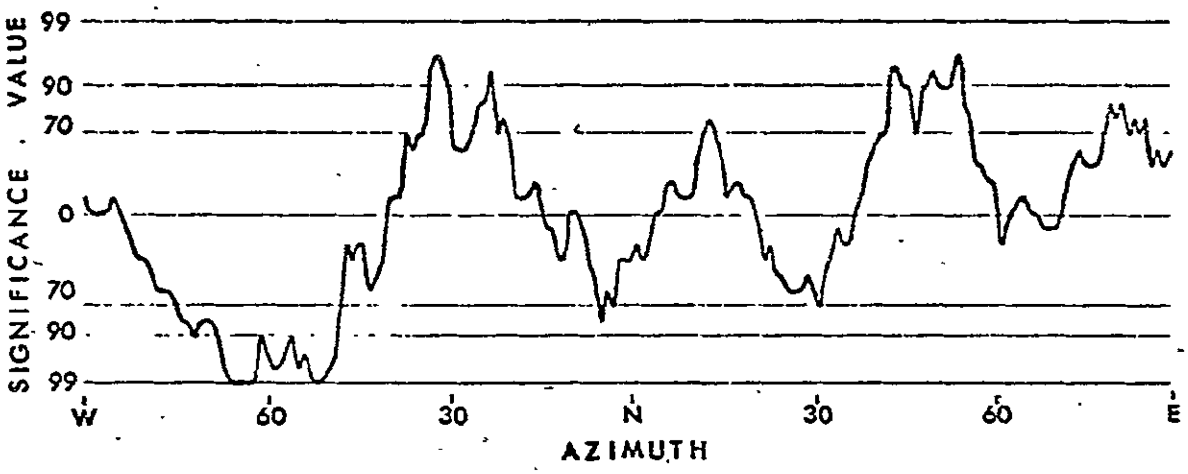

(a) unweighted azimuthal trends

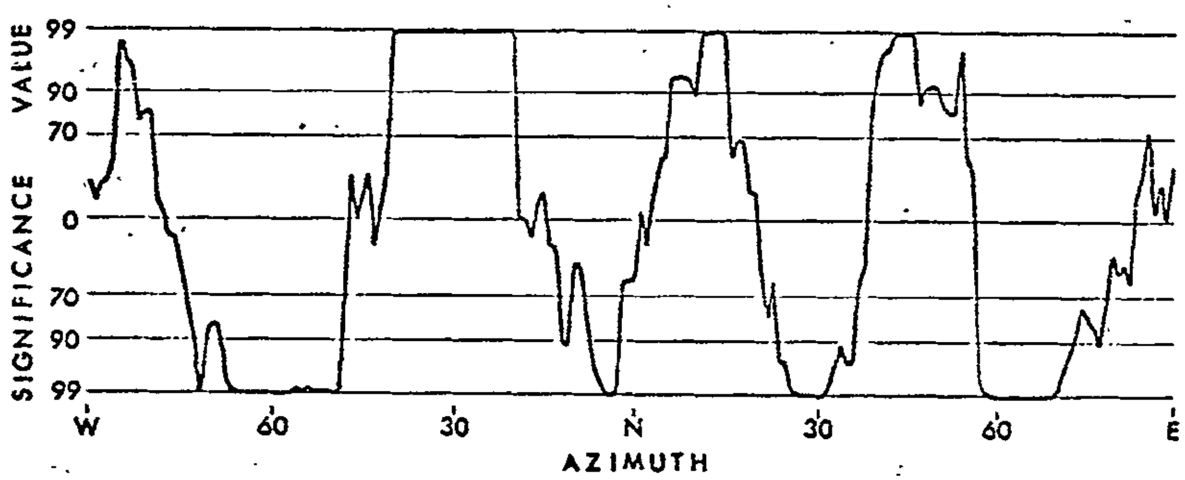

(b) length-weighted azimuthal trends

Figure 19. Linear trends in ERTS image E-1172-17141 for area of Pueblo relief map as outlined in Figure 2, 18 degree smoothing.

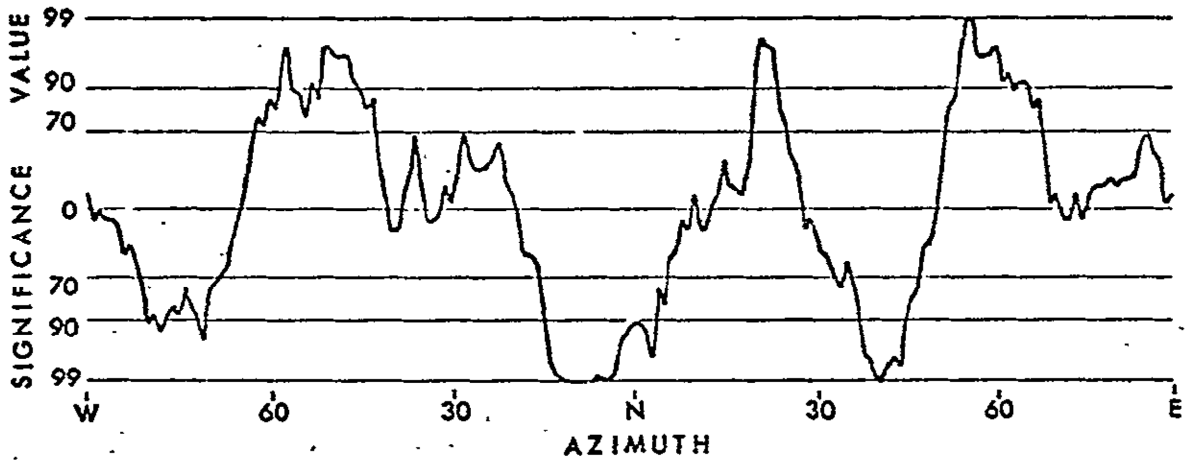

(a) Unweighted azimuthal trends

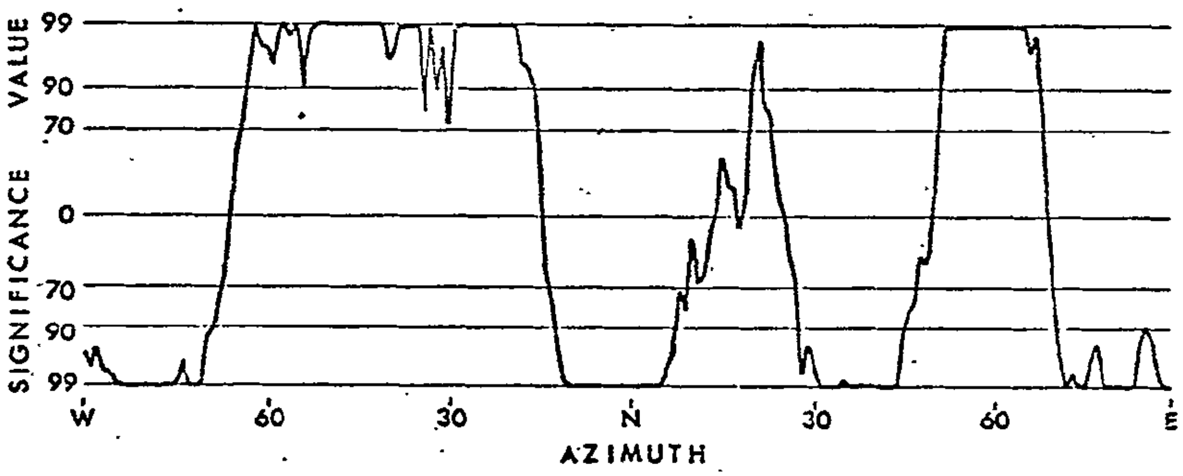

(b) Length-weighted azimuthal trends

Figure 20. Histograms of linears in Pueblo relief map as outlined in Figure 2, 18 degree smoothing.

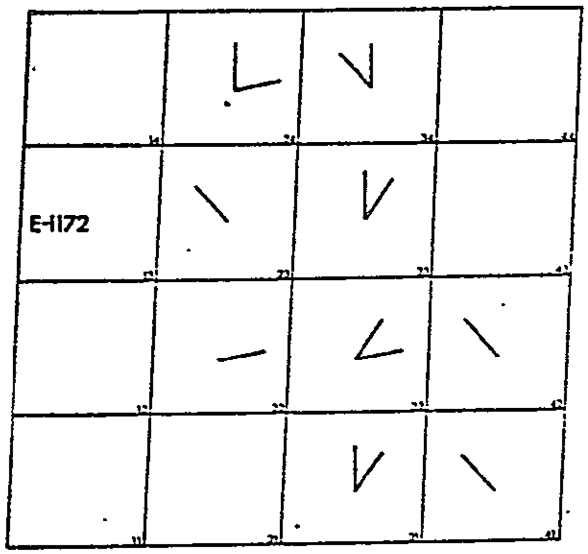

(a) ERTS image E-1172-17141

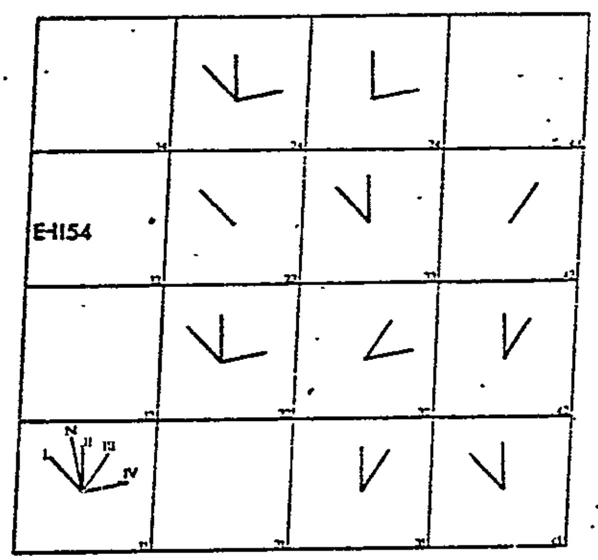

(b) ERTS image E-1154-17154

Figure 22. Occurrence in areal subdivisions of four super-modal trends of length-weighted linears

PRECEDING PAGE BLANK NOT FILMED

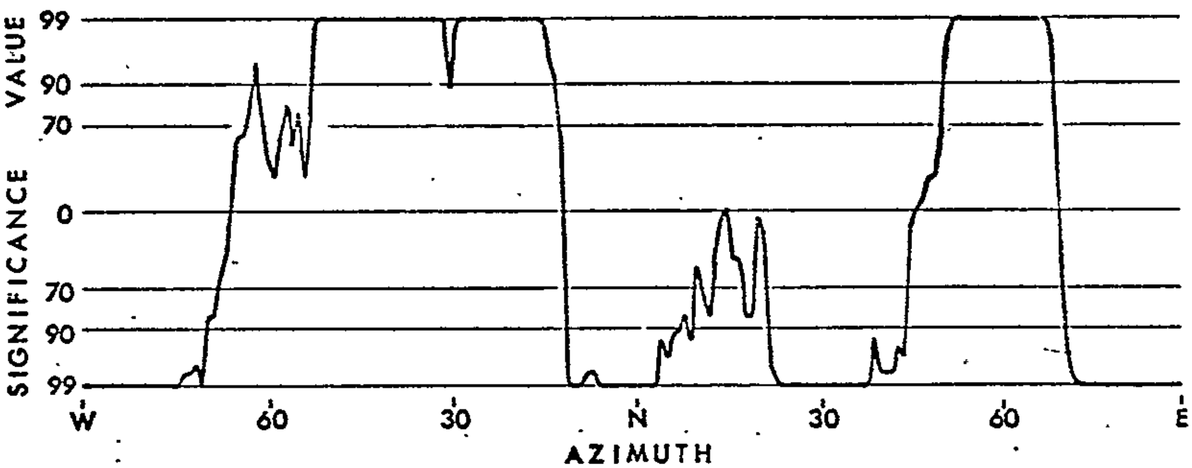

Figure 23. Length-weighted, super-modal linear trends in Pueblo relief map.

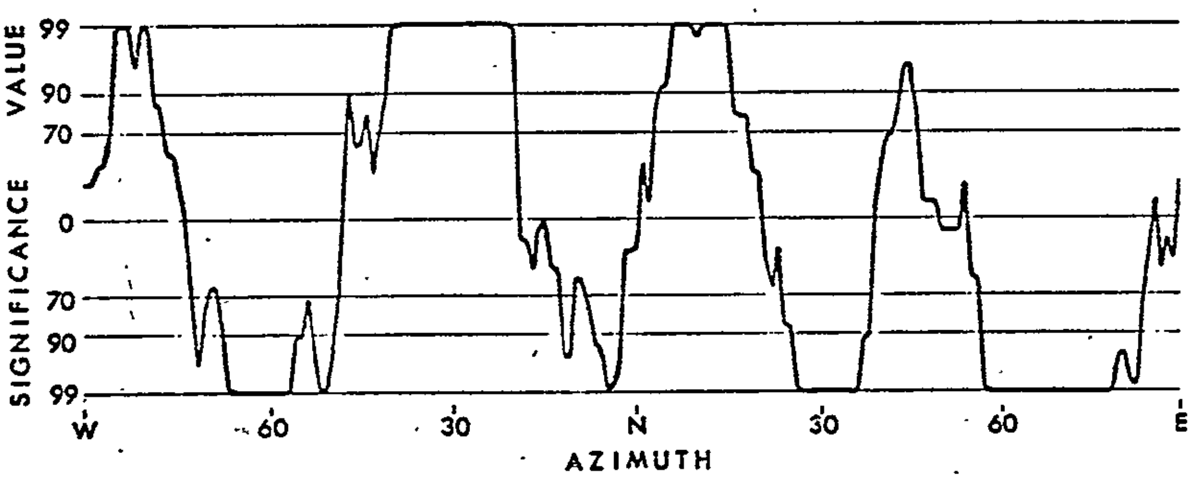

Figure 24. Length-weighted, super-modal linear trends in E-1172-17141 for area of Pueblo relief map.

PRECEDING PAGE BLANK NOT FILMED

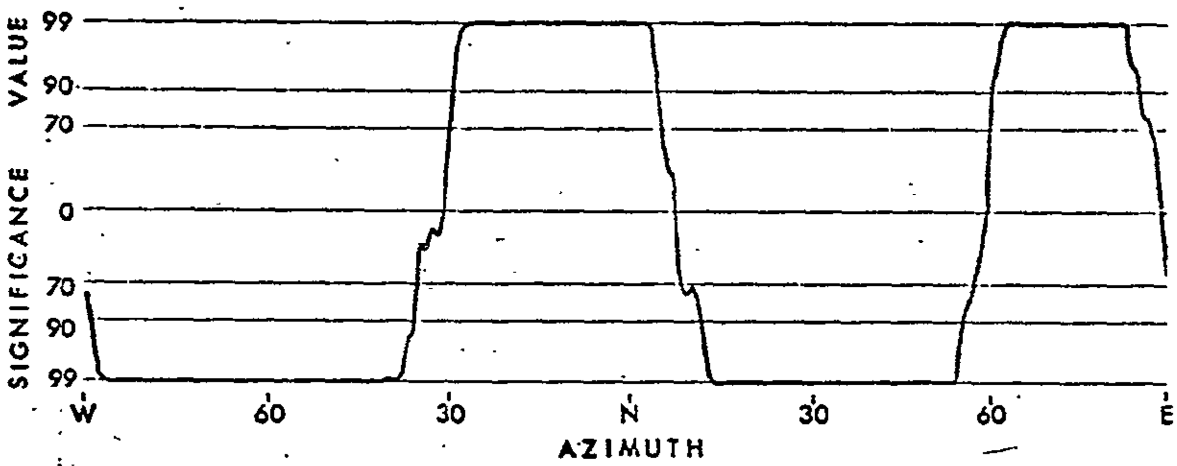

(a) Southern Front Range south of Pikes Peak, 18 degree smoothing

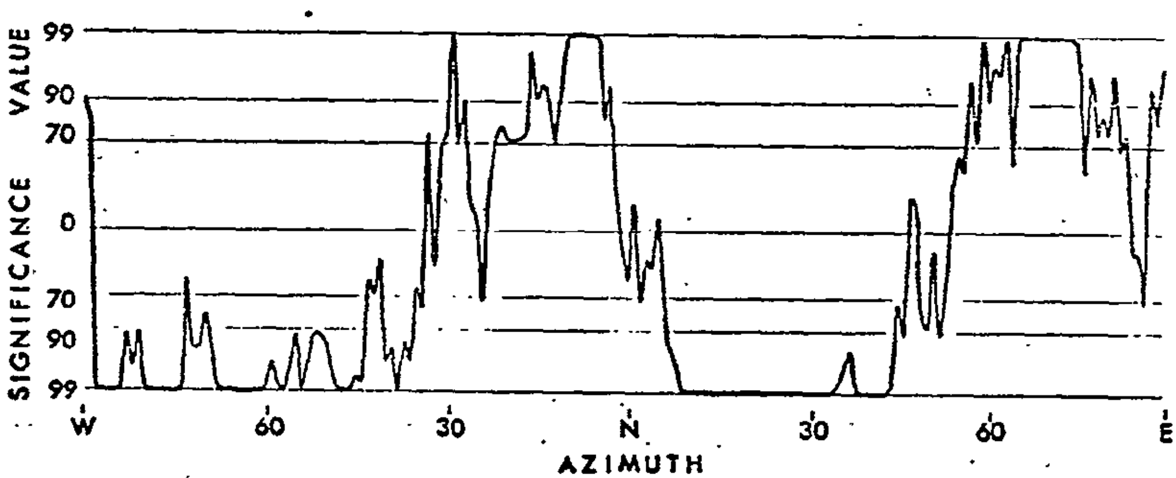

(b) Subdivisions 32, 42, 33, 24, and 34 of imaged area of E-1172-17141, 5 degree smoothing.

Figure 25. Azimuth trends of joints in area of central Colorado.

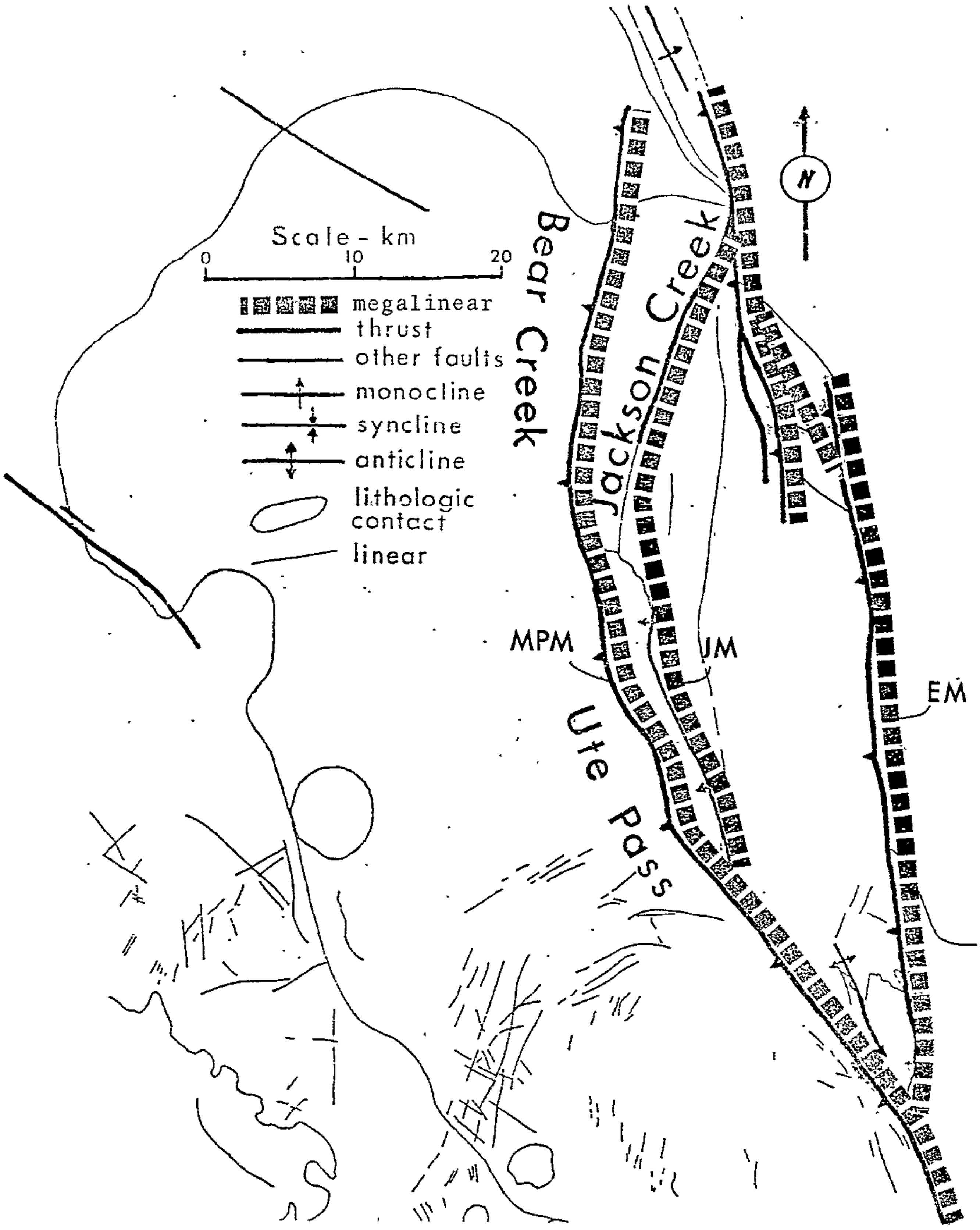

Figure 26. Geologic structure map of Rampart Range, central Colorado, showing named anomalous megalinears. (MPM, Manitou Park megalinear; JM, Jackson Creek megalinear; EM, eastern megalinear).

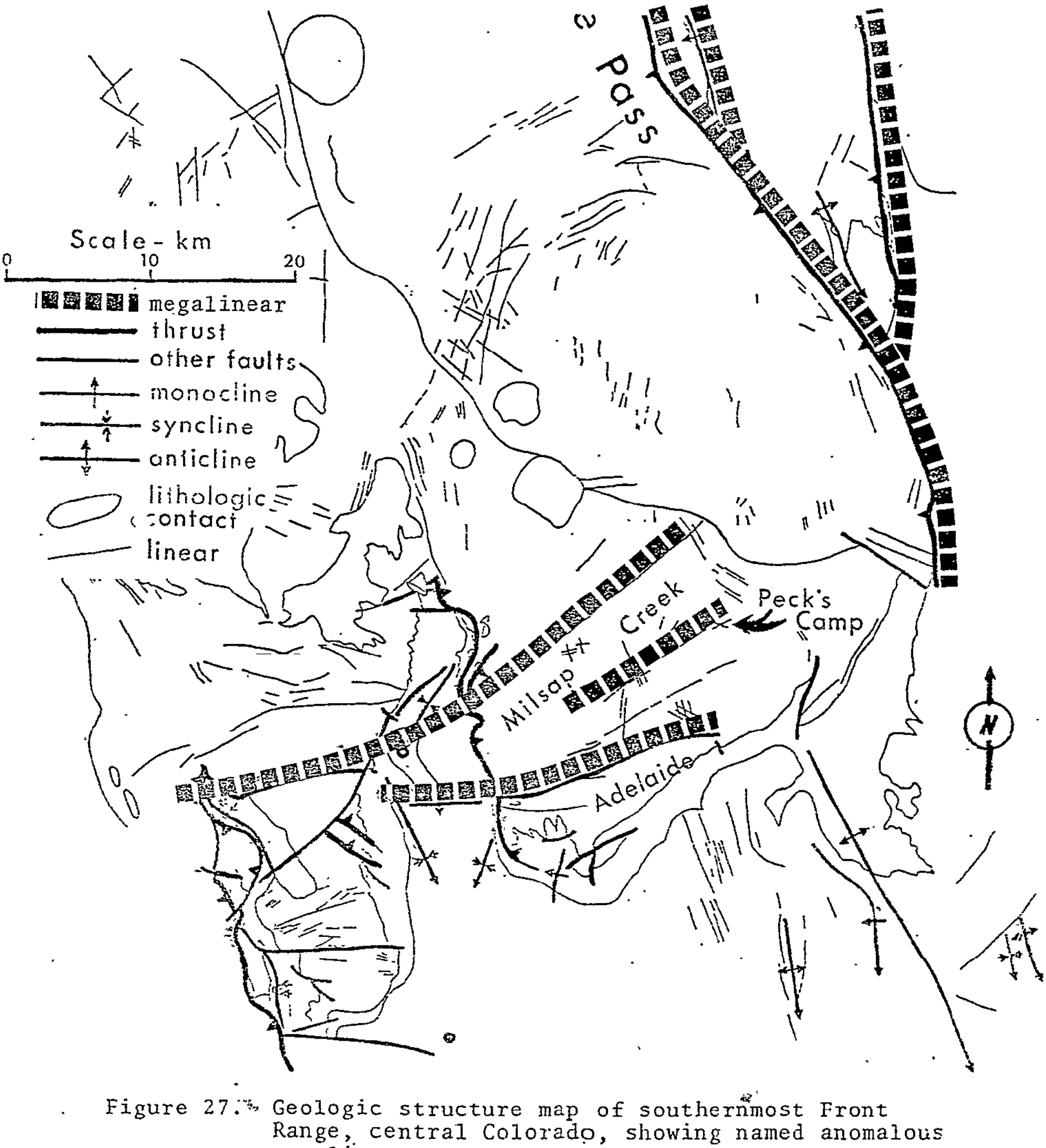

Figure 27. Geologic structure map of southernmost Front Range, central Colorado, showing named anomalous megalinears.

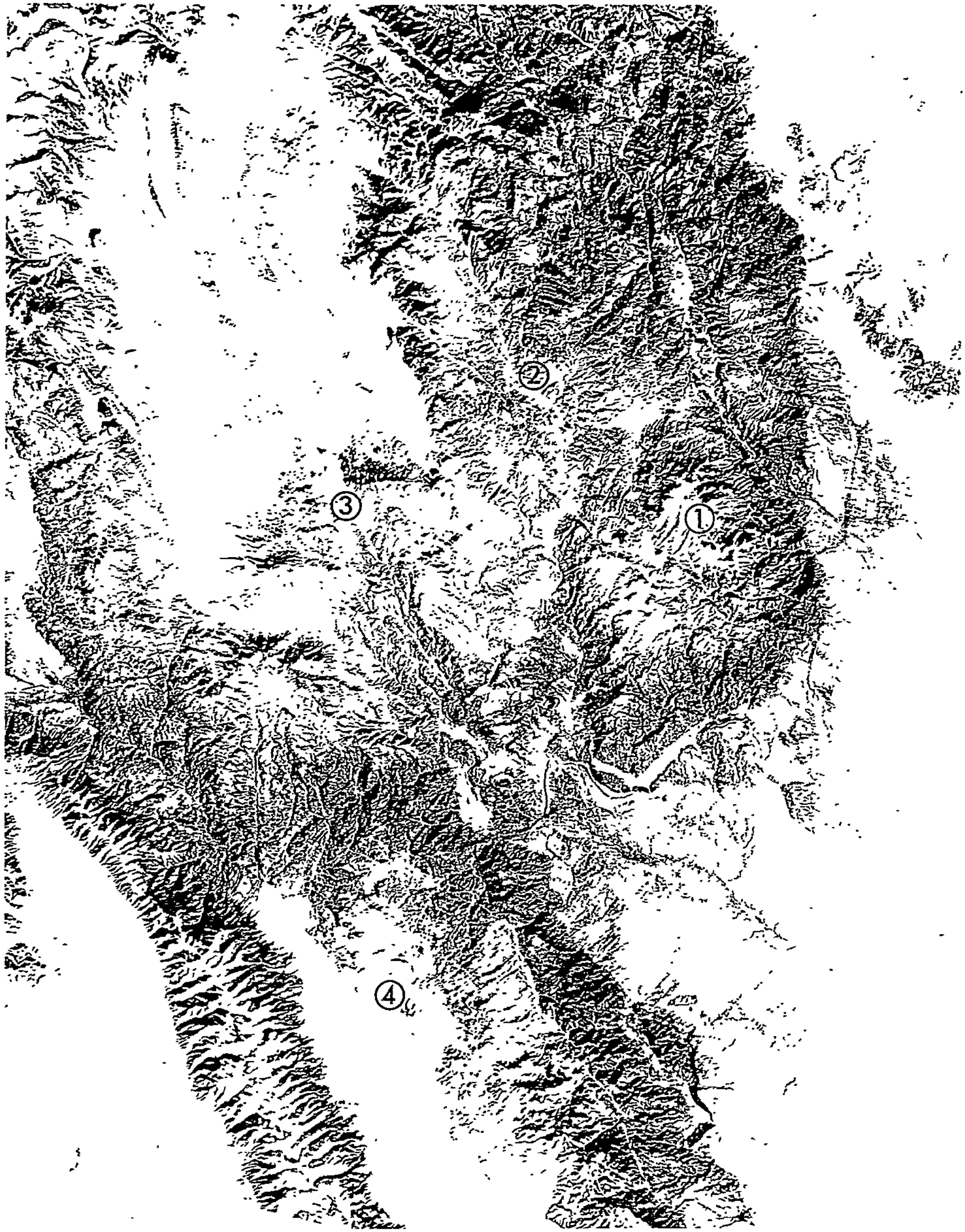

2
3
1
4

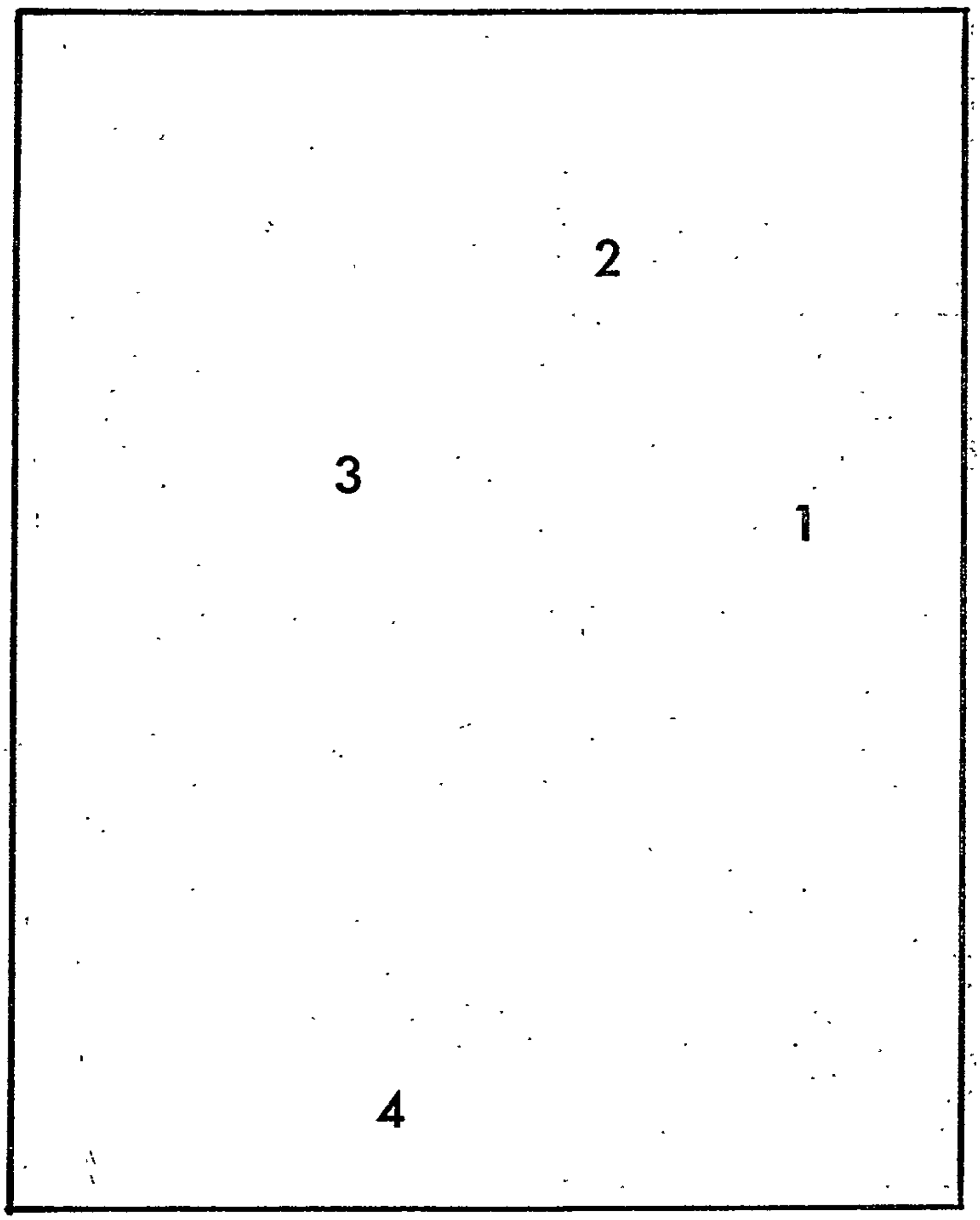

Figure 28. Concentric features in LANDSAT image E-1172-17141 described in Figure 10. 1-Pikes Peak intrusive center of Pikes Peak batholith, 2-Lake George stock, 3-Thirtynine Mile volcanic field, 4-Wet Mountain Valley volcanic field.

Figure 29. Linear features of the Rampart Range in snow-enhanced LANDSAT image E-1550-17102. Sun azimuth is 147. Sun elevation is 25. Date is January 24, 1974. Scale is same as Figure 26.

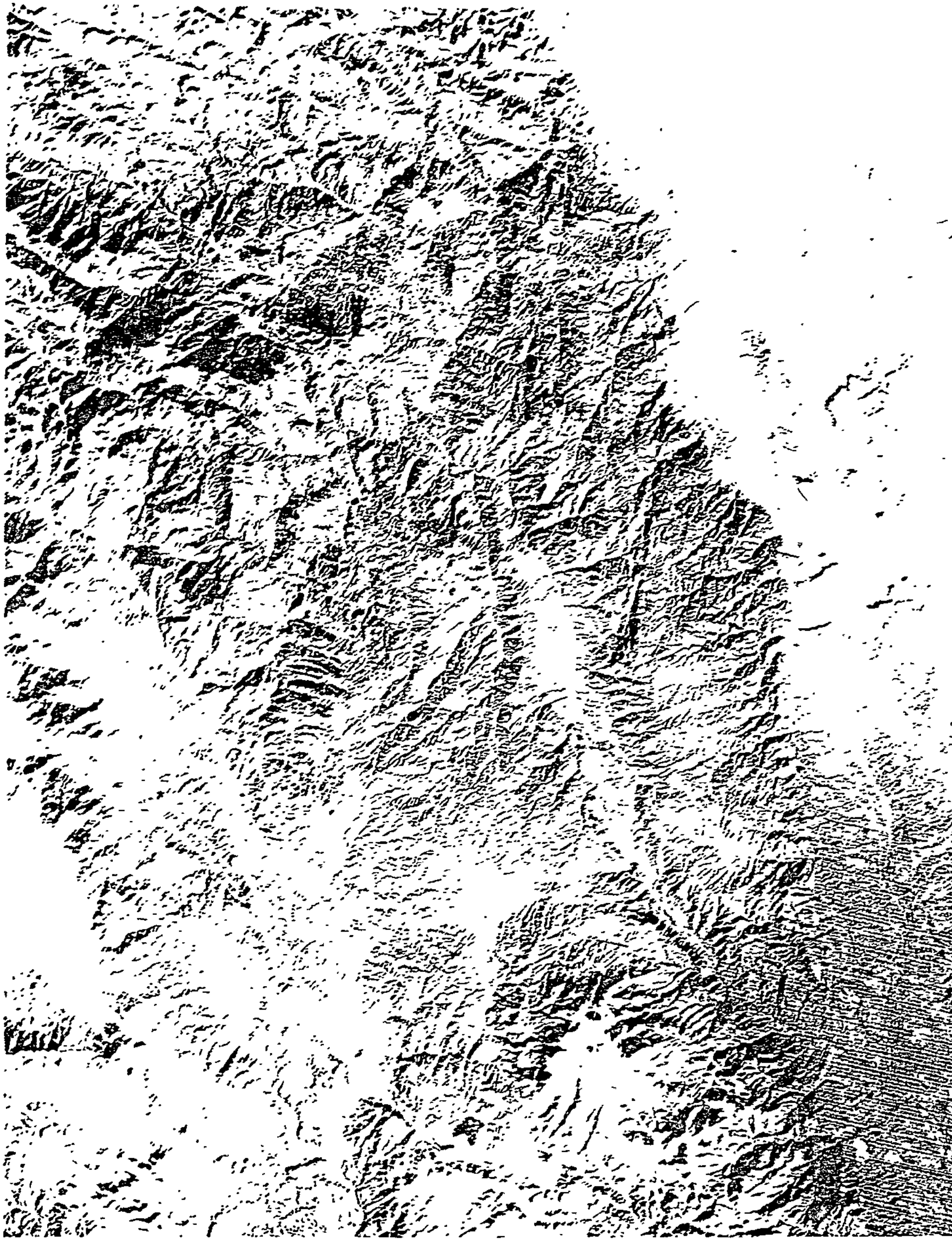

APPENDIX G

EVALUATION OF SKYLAB PHOTOGRAPHS OVER CENTRAL COLORADO FOR LOCATING INDICATORS OF MINERALIZATION

by

Gary L. Prost

Remote Sensing Report 75-3

EREP Investigations 380

Contract NAS9-13394

9 May 1975

REMOTE SENSING PROJECTS

DEPARTMENT OF GEOLOGY

COLORADO SCHOOL OF MINES ◇ GOLDEN, COLORADO

EVALUATION OF SKYLAB PHOTOGRAPHS OVER CENTRAL COLORADO FOR LOCATING INDICATORS OF MINERALIZATION

by

Gary L. Prost

Remote Sensing Report 75-3

Remote Sensing Projects
Department of Geology
Colorado School of Mines
Golden, Colorado

NASA Contract NAS9-13394

Approved for Publication:

Keenan Lee
Principal Investigator

June 1975

ABSTRACT

Skylab S190A and S190B photographs over central Colorado, covering approximately 47000 square kilometers of the Rocky Mountains, were analyzed to determine which features associated with known mining districts are recognizable on space images. Results of this analysis indicate that visible features associated with mineralization include high densities of linears, complex linear intersections, red-ocher and light color (alteration) anomalies, and perhaps vegetation patterns unique to mineralized areas. It was assumed that linears designate prospective ore-controlling faults and fissures, and that color anomalies are related to gossans or hydrothermally-bleached intrusives.

The Skylab photographs (taken 11 June and 4 August 1973) were then studied in an attempt to locate the features indicative of mineralization. Two target areas were chosen where several favorable features coincided; a primary study area (32.5 km^2) was established at Weston Pass, and a secondary area (130 km^2) was located at Dome Rock. Ground truth, obtained at the primary target area by geologic mapping at a scale of 1:12000, was used to identify the features seen on the photography and to evaluate orbital imagery as a tool in mineral exploration. The secondary target was briefly field checked by identifying the sources of color anomalies and linear features in a reconnaissance

fashion. The purpose of evaluating a secondary site was to determine if indicators of mineralization are consistent throughout the region.

Results of field work indicate the original assumptions were incomplete. Linear features may be attributed to aligned or straight streams, ridges, vegetation, and cultural features such as roads, fences, powerlines, and contrails, as well as geologic features including faults, joints, shear zones, dikes, contacts, and paleovalleys. Local linear patterns may not be unique to a given area, nor are high densities and intersections of regional linears the only structural controls on mineralization.

Red-ocher colors in central Colorado may result from sedimentary red-beds, microcline-rich crystalline rock or grus, iron-oxide alteration, or combinations of these. Light color anomalies were attributed to quartz-rich pegmatites, light-colored sedimentary units or talus, as well as to altered intrusives.

Vegetation was found to be influenced more by moisture, slope steepness and direction, season, and altitude, than by composition of the substrate.

Orbital photography in itself is considered inadequate to fulfill exploration needs; like other remote sensing techniques, it may be a powerful tool when used in conjunction with detailed field work.

CONTENTS

Illustrations

Page

INTRODUCTION

The Skylab orbiting laboratory (Skylab 1) was launched on 14 May 1973, and three subsequent manned missions, known as Skylab 2, 3, and 4, continued until the last three-man crew returned on 8 February 1974. The space station orbits the earth fourteen times each day at an altitude of approximately 380 kilometers (234 nautical miles) and covers the same point on the earth's surface at five-day intervals. Each repeat pass is about two hours earlier than the previous pass over a given point. The Skylab groundtrack lies between 50° north and 50° south latitude.

Under NASA contract NAS 9-13394, several satellite sensor experiments are being evaluated with respect to earth resource surveys. The S190A sensor system is a multiband array of six six-inch focal length cameras, each boresighted to photograph the same scene simultaneously. The bands, or wavelength ranges of the cameras, are: true color (0.4-0.7 μm), color-infrared (CIR; 0.50-0.88 μm), the green portion of the spectrum (0.49-0.60 μm), red (0.60-0.70 μm), photographic-infrared 1 (0.70-0.83 μm), and photo-IR 2 (0.70-0.90 μm). Each frame covers approximately 140 kilometers (88 nautical miles) per side, or an area about 20000 square kilometers (7750 square miles).

The S190B, called the "earth terrain camera," is an eighteen-inch focal length camera and takes color or CIR

photographs. Each frame is 95 kilometers (59 nautical miles) per side, covering about 9000 square kilometers (3500 square miles). This is the high-resolution camera on Skylab.

The objective of this research is to utilize and evaluate Skylab EREP (Earth Resource Experiment Package) and, to a lesser extent, ERTS (Earth Resource Technology Satellite) and aircraft imagery, for their value in locating indicators of mineralization in central Colorado. The reason for such a study is that it is economically more desirable to survey large areas for potential ore deposits by remote sensing than by conventional ground surveys. Advantages of satellite imagery, both photography and scanned imagery, include a synoptic view, repetitive coverage, accessibility to remote areas, and relatively low cost. Despite the desirability of locating potentially economic targets quickly and inexpensively, it must be stressed that field work is essential as verification. It is merely hoped that needless field work may be eliminated.

This research began with an evaluation of two mining districts considered typical of those in central Colorado. A literature study of the Leadville and Cripple Creek districts was undertaken to determine which geologic features are indicative of mineralization. Satellite photos over these areas were then studied in search of such features. It was determined that color anomalies and structural density and intersections were the most obvious indicators of

mineralization in the two areas, and it was assumed these criteria would be valid for the central Colorado region.

Limited Skylab coverage over Colorado restricted research to the area outlined in figure 1. This area is covered by frame 17, track 48, Skylab 2 S190A taken on 11 June 1973; by frames 106 and 107, track 48, Skylab 3 S190A and frames 38 and 39, track 48, Skylab 3 S190B taken on 4 August 1973; by frames 181 and 182, track 48, Skylab 4 S190A and frames 57 and 58, track 48, Skylab 4 S190B taken on 30 January 1974. Skylab 4 photography was delivered too late to be used in target selection. The area is also covered by frame 172-17141, ERTS-1 imagery from 11 January 1973; by frame 154-17143, ERTS-1 imagery from 24 December 1972; and by several aircraft underflights, most notably NASA Missions 184, 211, and 235. The entire survey area covers approximately 46,800 square kilometers (18,000 square miles) in central Colorado (fig. 2).

The central Colorado survey area was studied to locate indicators of mineralization. Various techniques were used to enhance both linears and colors. Structure targets were chosen in areas of high linear densities or at complex linear intersections; structure subtargets, located within each target, were designated in the event that the target had been previously mapped at a smaller scale. Target areas were ranked from most to least favorable according to the degree of association of color anomalies (each a "color"

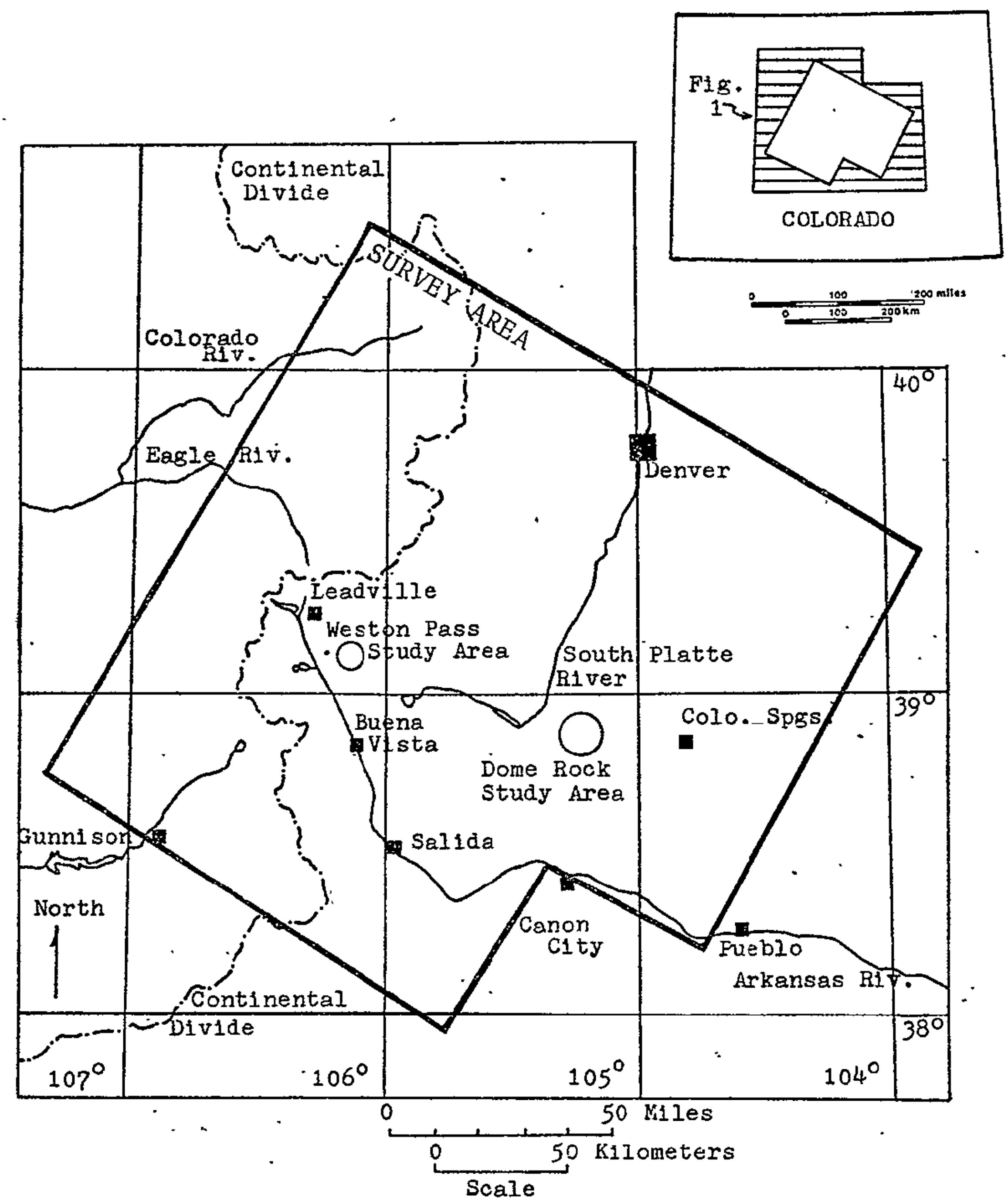

Figure 1: Central Colorado study area.

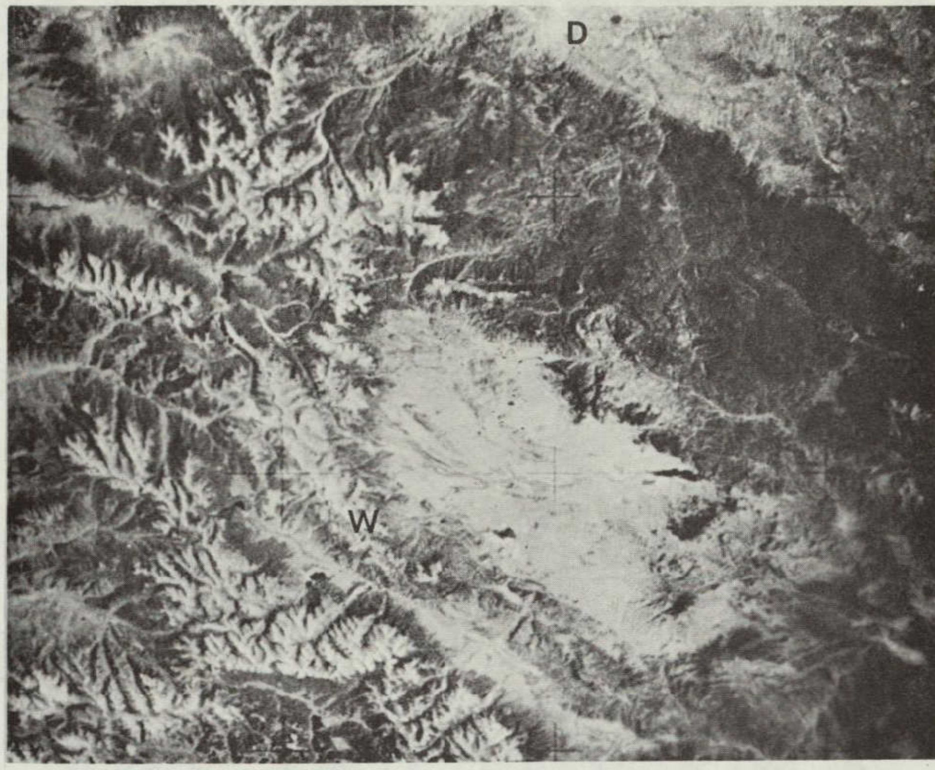

Figure 2: Skylab view to the northeast over Colorado. D = Denver; W = Weston Pass (for source, see Appendix A).

target) with structure targets. The most favorable target/ subtarget became the prime experimental area for this study. The second most favorable target was briefly evaluated to determine whether two areas some distance apart do indeed contain the same indicators of mineralization.

Evaluation of the primary target at Weston Pass consisted of mapping from satellite and aerial photography and in the field to determine the origin of color anomalies and linears, and to discern the relationship of these features to mineral deposits. The secondary test site, at Dome Rock,

was briefly investigated in the field to determine if indicators of mineralization are consistent throughout the region.

Lab work involved determining the relationship between satellite, aircraft, and field mapping; comparison of various satellite sensors, formats, and enhancement techniques; discerning the controls on mineralization, and evaluating the usefulness of Skylab in locating indicators of mineralization.

This report is taken exclusively from Prost (1975). Several of the photographs used in this report may be seen in color in Prost (1975).

Previous Work

Remote sensing studies have been conducted on various aspects of the geology over both the Weston Pass and Dome Rock targets. Bruns (1972) chose the Weston Pass area as a training site to test the ability of low-, medium-, and high-altitude color, CIR, and side-looking airborne radar (SLAR) to map stratigraphy, structure, and alteration. He concluded SLAR would have been more useful had better imagery been available; CIR was most useful for mapping faults, and color photography proved best for mapping lithologies. Three areas of possible hydrothermal alteration were located, although the sensor used was not mentioned.

In a remote sensing study of controls on mineralization in the Colorado mineral belt, Nicolais (1974) noted that "areas of high density of lineament intersections, associated with circular lineaments...are considered the most promising

areas for exploration." Linear overlays of ERTS imagery led him to select ten targets in central Colorado. Five of these covered major mineral districts; the highest priority target that did not correspond to a major mining district covered the Weston Pass-Buffalo Peaks area.

Lineament studies over central Colorado using both ERTS (Knepper, 1973) and Skylab (Lee and others, 1974) indicate linear trends correlate well with known regional joint sets and fault patterns. Linears are most abundant in areas of crystalline basement, and linears with greater relief (as in the Dome Rock area) are visible because erosion has exposed the otherwise buried basement.

The first geologic description of the Weston Pass area was by Emmons (1886), and was accompanied by a map (1:31,680) that included the northern half of the present study area. A study by Behre (1932) included a geologic map of about three square kilometers at Weston Pass (1:12000) and a discussion of lithology, structure, ore, and controls on mineralization. Behre concluded that ore solutions migrated along Weston and auxiliary faults until encountering and depositing minerals along a layer in the Leadville Formation that had been shattered by bedding-plane slip (later workers believe this shattered layer is a karst solution zone). An association of the ore to deposits at Leadville was proposed in 1934 (Laughlin and Behre), under the assumption that mineralization in the region was zoned with

respect to the Breece Hill Stock, and that outlying districts, including Weston Pass, had characteristics unique to epithermal deposits. These characteristics include galena as primary ore, sphalerite, minor silver, absence of gold, and a gangue of dolomite and jasperoid. An excellent summary of earlier works was presented by Behre in 1954, and another review by Chronic (1964) is accompanied by a geologic map (1:70000). Detailed lithologic descriptions of local units are given by Johnson (1934), Bloom (1965), Valdes (1967), and De Voto (1971). Valdes mapped that portion of the study area lying in the Jones Hill Quadrangle (1:24000). Gravity and magnetic features of the region were surveyed by Tweto and Case (1972; scale 1:125,000), and a gravity low in the area is thought to be the expression of a Upper Cretaceous and Tertiary granodiorite-quartz monzonite batholith 24 to 32 kilometers (15-20 miles) wide, up to 16 kilometers (ten miles) deep, and lying within a few thousand meters of the surface. This batholith is a postulated source of the hypabyssal intrusives and associated ore deposits in the region. The most recent work in the area combines airphoto interpretation and map compilations. Bruns (1972, scale 1:12,000; 1974, 1:24,000) and Tweto (1974, scale 1:62,500) both relied heavily on aerial photography.

There are no published studies describing the geology of the Dome Rock area.

Acknowledgements

This research was supported by NASA and the Colorado School of Mines through contract NAS 9-13394. Discussions with Dr. Sawatzky, Dick Taylor, and Dr. Tweto at the U.S. Geological Survey (Federal Center, Denver), Don Gould (retired), Dr. Carpenter, Dr. De Voto, Dr. Hutchinson, and Dr. Lee (Colorado School of Mines, Geology) proved invaluable in formulating and carrying out the research program.

ANALYSIS OF SKYLAB PHOTOGRAPHY

System and Band

Fourth-generation 2.25-inch by 2.25-inch positive transparencies of S190A photography (fig. 3) were studied in stereoscopic mode using Richards MIM light tables and a Bausch and Lomb 240R zoom stereoscope at magnifications from three to fourteen power. At 3X magnification all the photos have good resolution and contrast and are properly exposed. Reproduction quality is good. This holds at 14X except that the two photo-IR bands have low contrast and are grainy at this magnification. The S190A photographs at fourteen power can discriminate objects such as clusters of buildings (a speckled appearance), two-lane roads (Interstate 24 through South Park) and airport runways (Leadville runway, 1600 meters long, 60 meters wide), and objects as small as Golden Reservoir (300 meters diameter) and Interstate 70 (about 70 meters wide) can be identified. Linear objects are generally easier to see than equidimensional objects of equal contrast.

The photo-IR bands are best for outlining bodies of water or large streams, and the photo-IR 2 band shows good topographic contrast in heavily snow-covered areas. They also separate forested bedrock highland areas from grass-covered alluvial lowlands, and snow-covered from snow-free areas. CIR has excellent detail for distinguishing verdant from

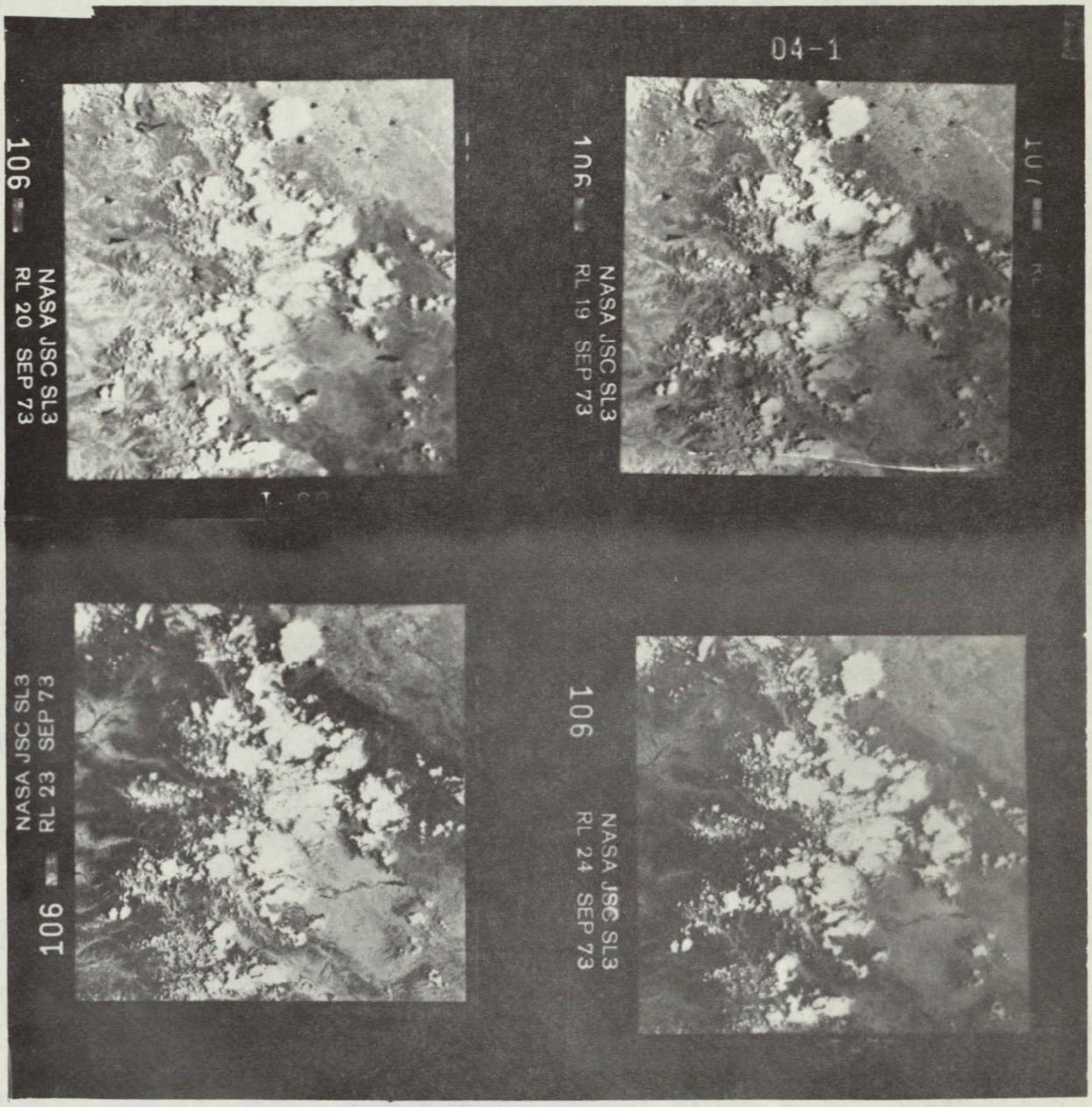

N

Figure 3: Skylab 3 S190A multiband photography of frame 106, track 48, taken 4 August 1973. Roll 19 = photo-IR 1, roll 20 = photo-IR 2, roll 23 = red band, and roll 24 = green band. Color and CIR not shown. Each frame is 140 kilometers on a side.

water-stressed fields, fields from grasslands, grasslands and fields from forested areas, vegetation-covered from non-vegetated rock, and bedrock from alluvium. It does not, however, separate snow from clouds from light-colored barren rock, and color rendition varies with exposure and processing. Bodies of water are easily distinguished as black where relatively deep (Dillon Reservoir), blue where shallow (Cherry Creek Reservoir), and mottled when there is suspended sediment (Elevenmile Reservoir).

The color band discriminates the same types of features as the CIR, but it is difficult to distinguish between kinds of vegetation. Color photos are best for discriminating barren rock of different colors, and only color film shows the subtle color differences between clouds, snow, and light-colored rocks.

The red band easily discriminates snow, clouds, field patterns, cultural and non-cultural areas, forest/bedrock, and grass-covered alluvial material. The green band is equivalent to the red band in resolution, but its lower contrast may be due to poor processing, or may result from (1) lower shadow contrast due to more green light in shadows, (2) more green light contributed by atmospheric scattering, and (3) lower reflectance differences between vegetation and rock/soil than in the red band (Lee and others, 1974). However, in a study conducted with photography from near Moab, southeast Utah (Skylab 2 S190A, track 34, 5 June 1973),

the green band had good tonal contrast. This may be due to sparse vegetation.

Structural features (faults, joints, folds) are most easily seen on CIR, color, and red bands (bands with best contrast).

Third-generation 4.5-inch by 4.5-inch positive color transparencies of S190B photography (fig. 4) were studied

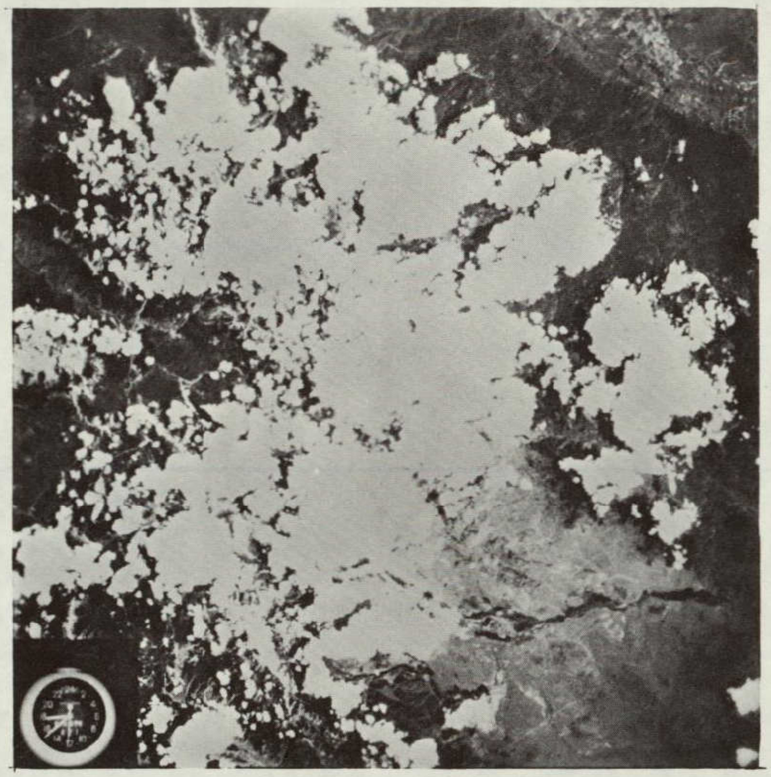

Figure 4: A black and white example of S190B color photography; frame 38, track 48, Skylab 3.

both in monoscopic and stereoscopic modes (depending on endlap). S190B photography over central Colorado has a maximum of ten percent endlap, causing a loss of stereo

viewing that is either an unfortunate accident or a thoughtless oversight in mission planning. The S190B photos are easily viewed at three to fourteen magnifications, have good contrast, and are properly exposed. Reproduction quality is excellent. S190B photography at fourteen power can discriminate clusters of buildings, large isolated buildings (Carleton gold mill at Cripple Creek, with an aluminum roof approximately 100 by 200 meters), and unimproved roads (power plant road east of Leadville, about ten meters wide, including shoulders). Tailings piles and color anomalies several hundred meters in diameter (tailings at Alma, Climax, or Cripple Creek; weathered pyrite at Sweet Home mine, Buckskin Gulch near Alma), islands as small as 100 meters in diameter (in Elevenmile Reservoir), and linear features such as the paved portion of the runway at Leadville (24 by 1600 meters), improved roads (Interstate 285 between South Park and Morrison, about seventeen meters wide including shoulders), or structural features (if they are large enough, - i.e., prolongued lateral extent, juxtaposition of contrasting rock types, moderate to high relief, etc.) can be identified.

The high-resolution color photography gives excellent discrimination of fields from grasslands, grasslands and fields from forested areas, vegetation-covered from barren rock, bedrock from alluvium, rocks and soils of varying

colors, bedded from non-bedded rock, fractured from non-fractured rock, snow and clouds from light-colored rock, and bodies of water. Large throughgoing (regional) structures are best observed at three power magnification, while fairly small structures (fractures in granite) are easily seen at fourteen power.

Format

Skylab S190A originals are 2.25-inch by 2.25-inch and have a scale of about 1:2,850,000. These frames are easiest to work with when they are enlarged four times (nine by nine-inch) to a scale of about 1:700,000. The limits of resolution appear to be at about twelve magnifications of the original (high-resolution SO-356 color film has a dynamic resolution of 23.4 meters; the lowest resolution S190A film, photo-IR EK-2424, has a resolution of 67 meters). Such magnification is best achieved using optical systems. Annotation is greatly simplified on a print enlarged twelve times (27 by 27 inches; scale 1:240,000), and features that may have been overlooked at a smaller scale become noticeable. However, resolution is degraded by another photographic generation, and the ability to use stereo is lost.

The S190B originals are 4.5-inch by 4.5-inch frames and have a scale of about 1:950,000. Two-time enlargements are easiest to work with, at a scale of about 1:475,000. These enlargements can be optically magnified another ten times (to 20X; scale 1:50,000) before the limits of resolution are

reached. The highest resolution S190B film, SO-242 color film, has a resolution of 15 meters, while low-resolution EK-3443 film has a resolution of 33 meters (Potter, 1974).

Positives and negatives both contain the same information, but positives are easier to work with because the interpreter is familiar with what is seen.

All bands contain the same geologic information, but some bands are easier to interpret because of better film resolution and contrast. This supports the work of Raines and Lee (1975), who concluded that rock spectral reflectance differences do not contribute unique information to any band. It is suggested that, where economically feasible, color photography is the easiest and fastest to use, because of interpreter familiarity with natural colors. Also, it is easier to find red-ocher colors on true color photography than on false color photography, where the desired colors may appear yellow, green, or light blue against a blue-green background.

In all cases, transparencies were superior to prints with respect to resolution. However, as has been often noted, transparencies are clumsy and prints are more convenient for field work.

Stereoscopic viewing is also far preferable to monoscopic photointerpretation, for in the ability to see relief lies the interpretation of geologic information. Such information includes the estimation of dips, recognition of fault displacements and geomorphic features, the distinction between topographic linears and others such as airplane contrails,

C14

and the distinction between clouds and light-colored rock or snow. Skylab stereo coverage varies from sixty percent endlap to occasional gaps in coverage between frames.

Data Acquisition

The time of day and time of year that space photography is acquired is related to factors such as shadows, clouds, snow, soil moisture, and vegetation growth.

Topography, and thus geology, may be enhanced by low sun elevations. In mountain areas the optimum shadowing appears to occur at elevation angles between five and fifteen degrees (Lee and others, 1974). Changes in illumination azimuths tend to emphasize geologic features with different orientations.

Space photography has often been degraded by the presence of clouds. Cloudiness in central Colorado is a function of westerly winds, and is decreased after the passage of a cold front in all seasons (Lee, 1974). From May to August clouds are caused by convective heating of the atmosphere due to long days and high sun angles. For this reason clouds commonly begin to fill a clear sky at midmorning. Clouds form later in the day during the winter.

Cloud-cover statistics for the central Colorado mountains (fig. 5) show that the least average monthly cloud cover during daylight hours occurs during September (40-50% coverage), then October (40-60%), then June (50-60%). Greaves (1970) developed

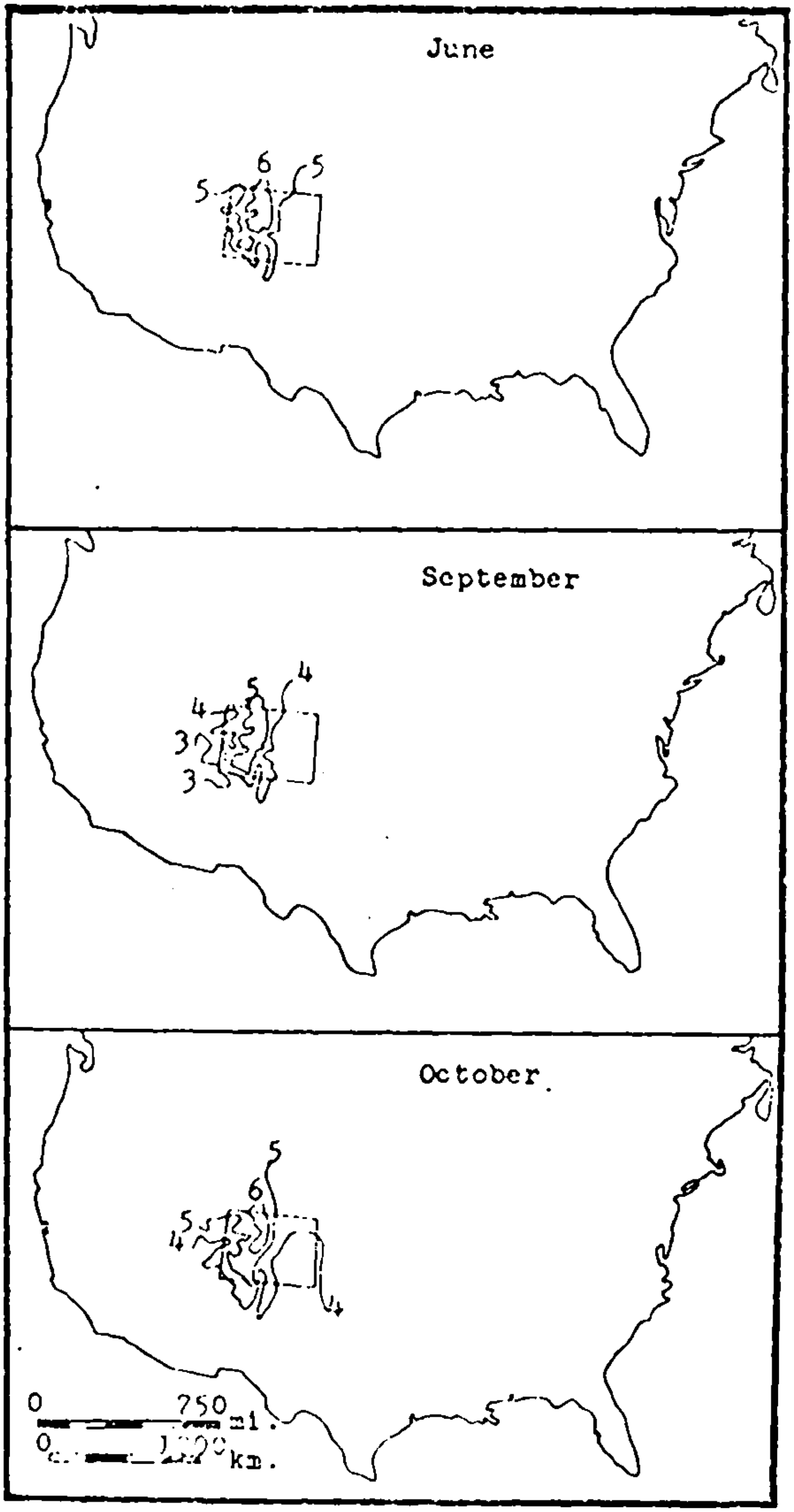

Figure 5: Mean sky cover over Colorado during daylight hours (in tenths). From U.S. Weather Bureau, 1968.

cloud cover curves for the Gulf Stream region off the eastern coast of the United States, and claims the shapes of the curves are typical of those developed elsewhere. These curves indicate that five satellite passes over an area 480 kilometers (300 nautical miles) in diameter have a 95% probability of obtaining 50% cloud-free coverage; twelve passes give a 95% probability of acquiring 90% cloud-free coverage (fig. 6). Cloud cover statistics may be used to minimize cloudiness on earth resource surveys. Minimum cloud cover over central Colorado occurs in the morning during September or after passage of a cold front. Repetitive coverage increases the probability of a cloud-free survey.

During the winter, snow is found at almost all elevations in central Colorado. Snow obscures rock colors, but may enhance topographic features of moderate to high relief. Weather statistics for the Rocky Mountains, gathered by the United States Weather Bureau over the last thirty years, indicate the best time for universal snow cover is from December to February, and the best time for uniform snow-free coverage is July through August (Table 1). In the Weston Pass area, snow-free coverage should be available from July to August (fig. 7).

Soil moisture and vegetation growth are both greatest in late spring and early summer, a result of snowmelt. Variations in soil moisture, generally observed in alluvial material, may indicate changes in composition, porosity, permeability, etc., of the soil or substrate. Vegetation is influenced by slope

Gulf Stream area, off eastern coast of the United States

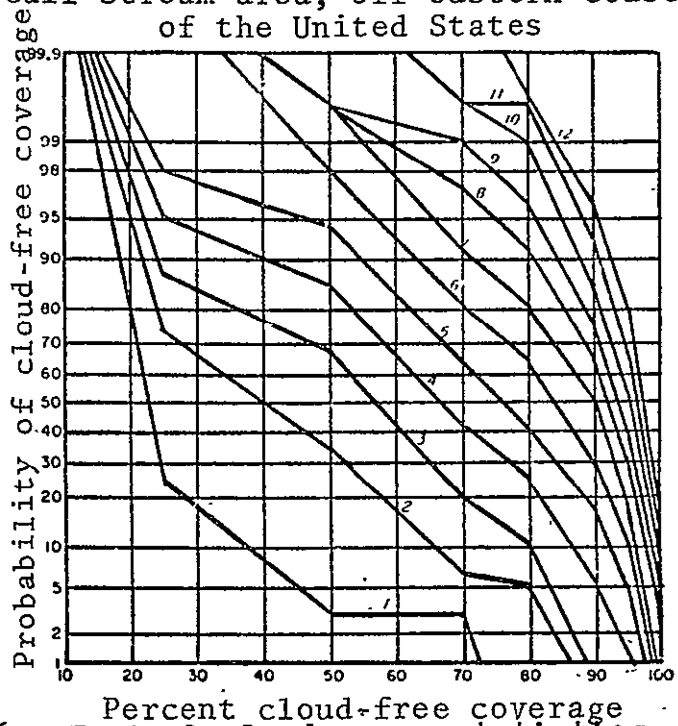

Figure 6: Typical cloud cover statistics. Curve numbers indicate the number of passes necessary to obtain a specific probability of the desired cloud-free coverage (percent). After Greaves, and others, 1970).

direction and steepness, moisture, and altitude, as well as by season and the soil it grows on.

Comparison with ERTS and Aircraft Imagery

Prior to field work, Skylab photography was compared with ERTS and aircraft imagery over the central Colorado area. The comparison indicates that ERTS multiband imagery is superior to Skylab S190A multiband photography in the photo-IR range, that ERTS imagery in the red and green bands

ORIGINAL PAGE IS OF POOR QUALITY

CITY	ELEV.	# YRS. RECORD	MONTH											
			J	F	M	A	M	J	J	A	S	O	N	D
Aspen	7913	26	28.9	25.8	24.9	12.1	2.2	0.6	0	0	0.9	4.6	18.7	22.2
Boulder	5385	30	10.9	10.8	17.3	14.3	2.8	0.1	0	0	1.0	4.3	11.5	8.0
Buena Vista	7954	26	5.8	7.4	6.4	9.3	2.6	T	0	T	1.2	1.8	4.9	4.0
Canon City	5343	29	6.3	5.6	6.2	5.2	0.5	0	0	0	0.8	0.9	4.9	4.6
Colo. Spgs.	6098	28	3.8	5.5	6.5	3.5	0.4	0.1	0	0	0.5	0.8	2.9	3.9
Craig	6280	18	15.8	10.2	11.8	5.1	0.8	T	0	0	1.1	1.0	7.8	12.9
Crested Butte	8855	30	37.8	34.6	31.0	15.1	4.5	0.4	0	0	1.3	6.8	19.7	29.3
Del Norte	7884	30	7.9	4.7	5.4	4.6	1.1	T	0	0	0.4	2.0	4.8	5.4
Dillon	9065	30	25.4	25.4	30.0	23.4	7.4	0.6	0	0	1.4	6.8	16.7	20.2
Durango	6550	29	16.4	13.8	9.6	3.7	0.3	0	0	0	T	0.6	4.2	14.5
Estes Park	7497	19	7.9	13.7	14.2	18.8	5.4	0.5	0	0	0.9	4.6	9.2	8.5
Fraser	8560	30	25.1	25.0	22.6	19.1	4.6	0.4	0	T	0.9	6.6	16.2	16.6
Georgetown	8500	23	8.0	9.3	13.3	14.8	5.8	0.3	0	0	3.6	5.6	10.5	5.7
Glenwood Spgs.	5823	28	21.6	15.2	7.6	1.9	0.2	T	0	0	0	0.8	5.0	17.8
Grand Lake (#1)	8576	30	24.6	20.0	19.8	18.2	3.3	0.1	T	T	1.3	6.7	11.6	22.8
Gunnison	7694	28	14.5	13.5	8.1	3.8	0.5	T	0	0	0.3	0.9	5.9	10.4
Lake George	8500	5	6.3	11.6	11.5	11.1	1.4	T	0	0	3.3	4.9	8.3	6.1
Lakewood	5450	30	7.0	8.2	10.3	7.9	1.1	0	0	0	0.4	2.0	6.5	5.4
Leadville	10177	26	18.0	20.8	21.4	18.0	6.2	1.0	0	T	1.9	9.8	14.7	16.4
Northdale	6693	28	14.8	9.0	7.7	1.9	T	0	0	0	0.2	1.1	4.7	12.0
Paradox	5309	20	8.0	5.3	2.1	0.5	T	0	0	0	0	T	1.9	5.8
Salida	7060	30	5.6	6.5	8.4	8.4	2.6	0	0	0	1.6	5.0	6.0	5.3
Telluride	8756	30	33.2	27.7	29.3	22.0	4.6	0.4	0	0	1.0	7.3	16.1	23.4

Table 1: MEAN DEPTH OF SNOW/SLEET (inches), CENTRAL AND WESTERN COLORADO
T - Trace amount, too small to measure. U.S. Dept. Commerce Weather Bureau, Climatological Summary, Weather Bureau Office, Denver, Colorado.

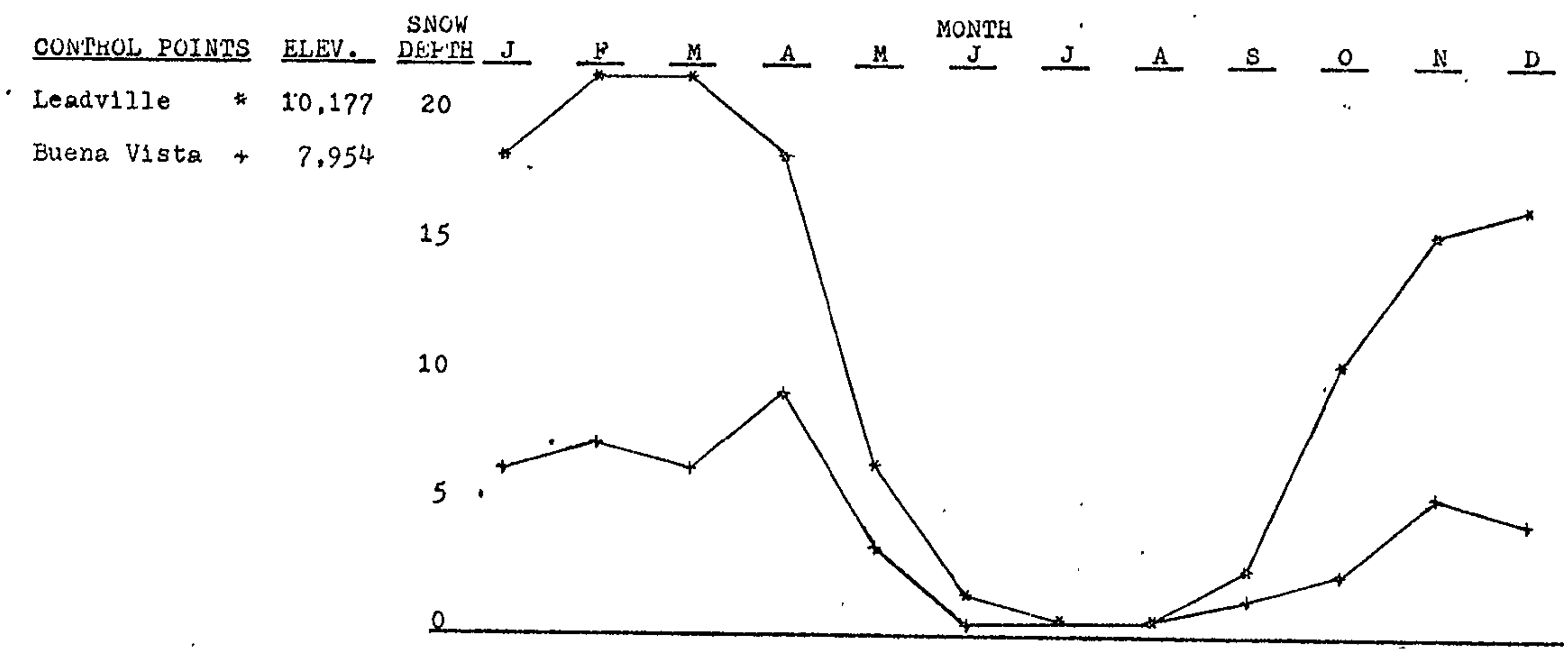

Figure 7: MEAN DEPTH OF SNOW/SLEET (inches), MOSQUITO RANGE, COLORADO

is comparable in quality (contrast and resolution) to the Skylab S190A red and green bands. A comparison of Skylab S190A color photography with ERTS simulated color photography (Knepper, 1973) reveals that the ERTS simulation produces unnaturally blue clouds and terrain shadows. In general, the simulated color on ERTS imagery is comparable to Skylab, but system resolution is inferior to Skylab. ERTS simulated CIR is superior or equal to Skylab S190A CIR in color rendition, since optimum color and contrast may be obtained through manipulation of the multiband film chips, while Skylab S190A CIR has variable color rendition and contrast because of varying exposures, or lack of control during developing. Cloud-free ERTS images are available during various seasons, while cloud-free Skylab photography is not, due to lack of repetitive coverage. In all cases the Skylab S190B product is superior to ERTS and S190A because of its greater resolution.

Advantages of the Skylab photography over ERTS imagery include greater resolution, stereo coverage, and the availability of colored films (both true color and CIR), eliminating the need for color composites. Disadvantages include the general lack of repetitive coverage, the time necessary to retrieve and process film, and a restricted ground track.

In this study the term "linear" refers to any line or alignment of features, straight or slightly curved, with no interpretation involved. "Lineament" refers to a linear of probable geologic origin. Known linear geologic features, such as contacts, joints, and faults, are referred to by name.

A comparison of overlays (fig. 8, plates 3-6) reveals that different lineaments are emphasized on each overlay, and color anomalies are mapped only on the S190B overlay. These variations are probably a result of differing solar azimuth and elevation angles, cloud cover, and original scales.

Aircraft photography has equal or lower system resolution but greater scale than Skylab photography. Therefore more detail, and consequently more geology, can be mapped (figs. 9 and 10).

Advantages of satellite over aircraft photography include the synoptic view, the ability to see regional linear features, easier access to remote areas, and relatively low cost to the user. Disadvantages include overflight times that cannot be varied to take advantage of changing surface conditions (weather), slow film retrieval, and smaller scale. Surprisingly, the color rendition of the S190B film allowed detection of color anomalies that were not obvious on aircraft photography. Airphotos observed over the primary target include color and CIR film taken during NASA Mission (Mx) 184 (scale 1:20,000), Mx 211 (1:55,000 and 1:110,000), and Mx 235 (1:20,000). Among airphotos, color film at a scale of 1:20,000 proved the most useful for detailed photointerpretation.

Problems

The major problems during data acquisition involve non-repetitive coverage and the lack of stereo coverage. Limited

PRIMARY TARGET: WESTON PASS STUDY AREA

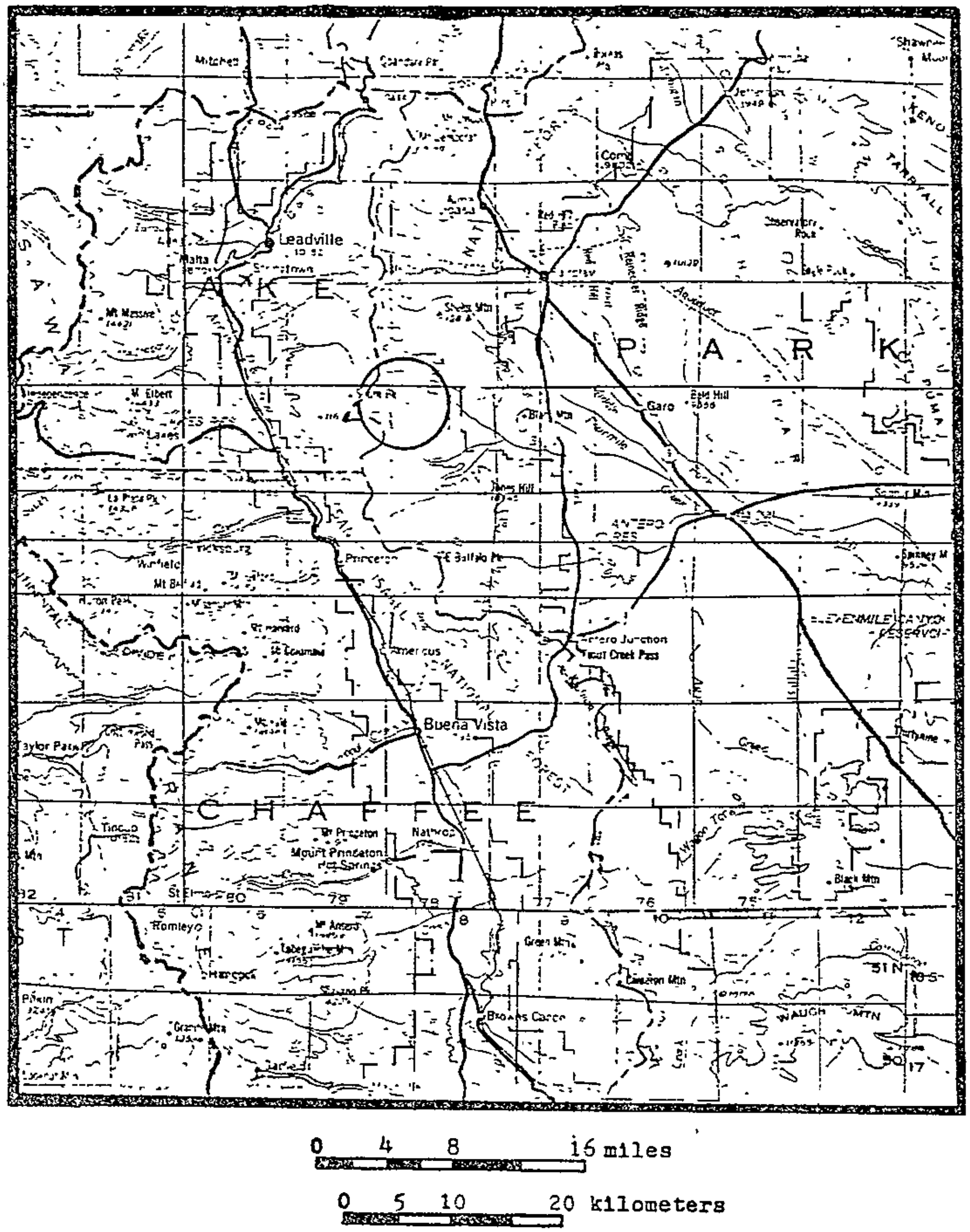

Figure 8 (to be used with plates 1-4): Base map of area around Weston Pass. Study area circled. On some overlays the edge of the Skylab frame is shown.

Linears, dashed where existence questioned.
Color anomalies.
Clouds.

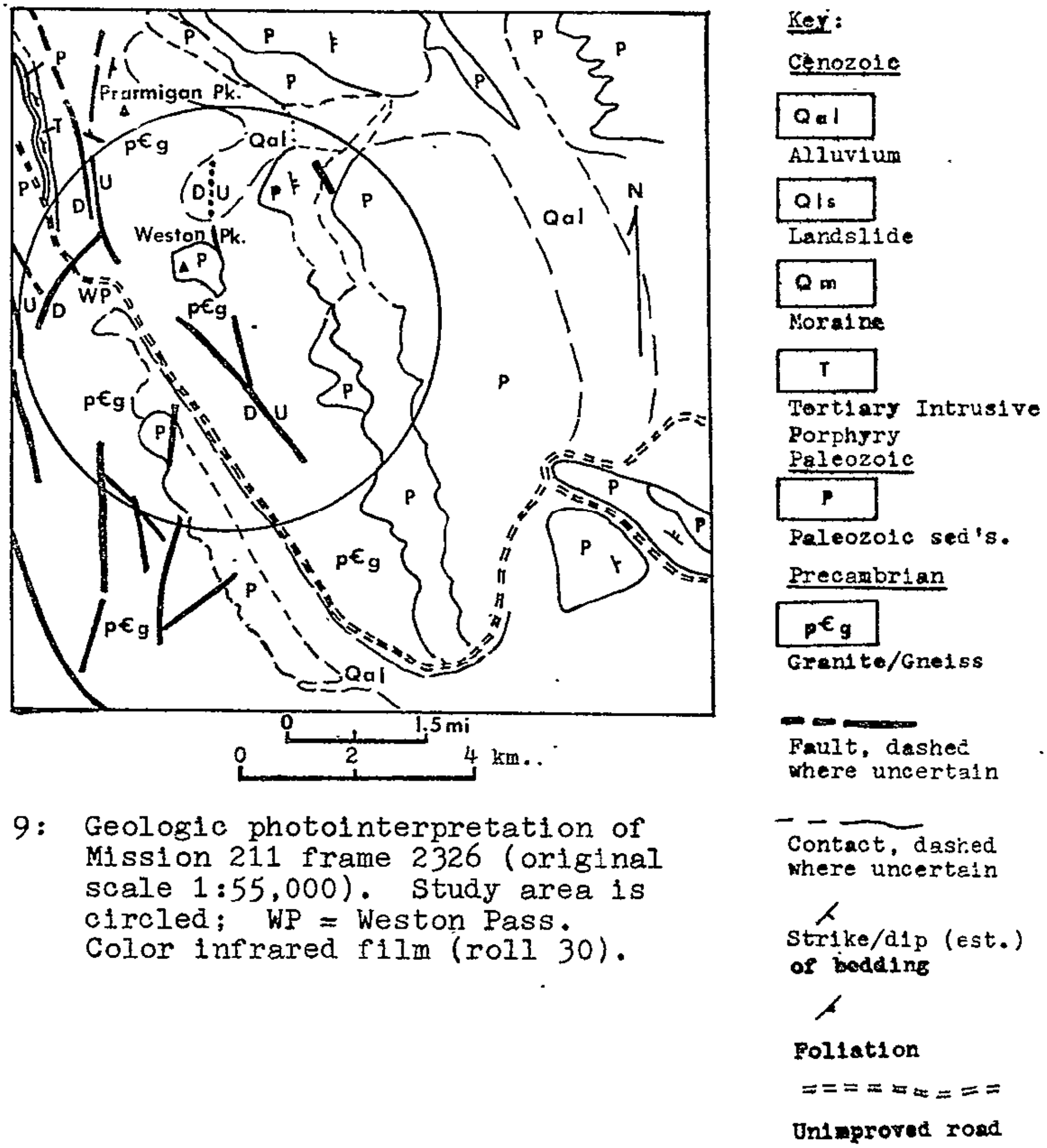

Figure 9: Geologic photointerpretation of Mission 211 frame 2326 (original scale 1:55,000). Study area is circled; WP = Weston Pass. Color infrared film (roll 30).

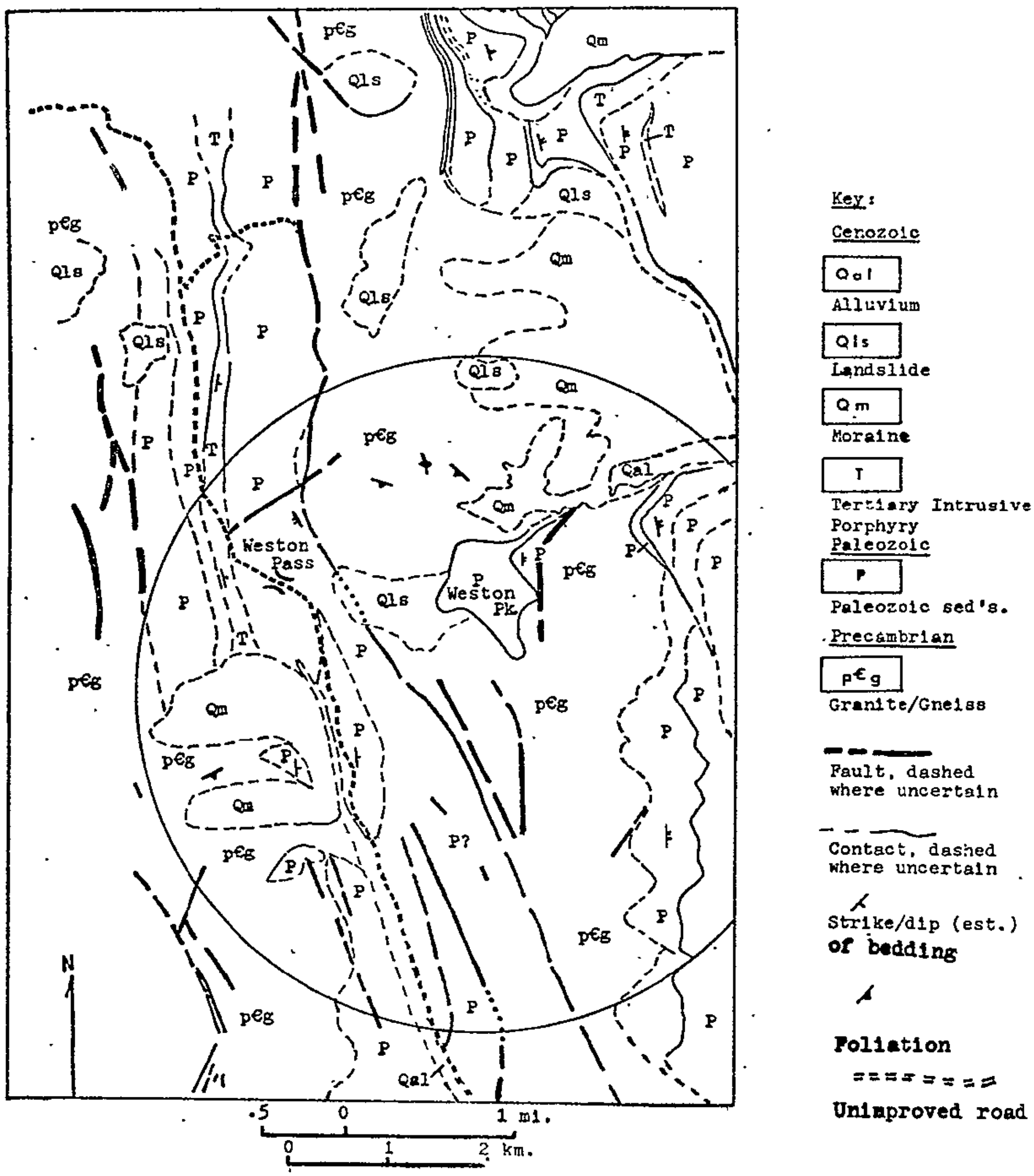

Figure 10: Geologic photointerpretation of Mission 184 frames 1096 to 1101 (original scale 1:20,000). Study area is circled. True color film (roll 28).

coverage is largely responsible for extensive snow or cloud cover on available film, and for limited solar illumination angles and spotty ground coverage. The lack of stereo coverage and occassional complete gap in ground coverage decreases confidence in photointerpretation.

Processing problems encountered include variable color rendition, especially in CIR film (may be due to varying exposures or lack of control during developing), red specks on S190A CIR film (caused by abrasion and emulsion lifting), scratches, emulsion on the underside of film (causing scratches when unrolling film), reversal of stereo-sequence (in a continuous sequence each frame has been rotated 180 degrees, making stereo viewing of adjacent frames difficult), and the excessive amount of time necessary for processing and delivery (more than one year for some enlargements).

Enhancement Techniques

The simplest types of data enhancement involve enlarging originals or increasing contrasts. Enlargements may be obtained photographically or using optical systems. Contrast is increased by using high contrast copy film or by increasing developing time. Other enhancement techniques evaluated include slip masking, direct overlay masking, color-additive viewing, and cumulative density slicing.

Slip Masking

Positive-negative slip masking (Lee, 1972; 1973) is an enhancement technique where a direct overlay (mask) of a

positive and negative transparency is offset, or "slipped," in a given direction. Linear features that trend from approximately twenty to ninety degrees from the slip direction can be enhanced. Comparison of photolinears from a positive-negative slip mask with an original positive shows that some significant linears may be found, but that many are overlooked or misplaced because of the blurring that accompanies slipping (fig. 11).

Direct Overlay Masking

Direct overlay positive-negative masking was undertaken using nine by nine-inch positive and negative transparencies of frame 17, track 48, Skylab 2 S190A taken in June, 1973. Transparencies of the photo-IR 1, photo-IR 2, red, and green bands were available. Each positive was masked with the negative of the three other bands, and each negative was masked with positives of the other bands, 12 combinations in all. The most obvious features on these masks are clouds, snow, bodies of water, verdant vegetation (irrigated fields, phreatophytes), grass-covered alluvial material, and forested bedrock.

Fair contrast of features other than geology is seen by masking the positive of the photo-IR 2 band with the negative of photo-IR 1 (fig. 12a.). Topography is eliminated, grasslands and alluvium are light gray, snow and clouds are medium gray, forests and bedrock are dark gray, and water bodies are black.

Good contrast of features is seen when masking the positive of photo-IR 2 with the negative of the red band (fig. 12b.).

Figure 11: Examples of positive-negative slip masks. The original is given for comparison. Arrows at the top of masks show slip direction.

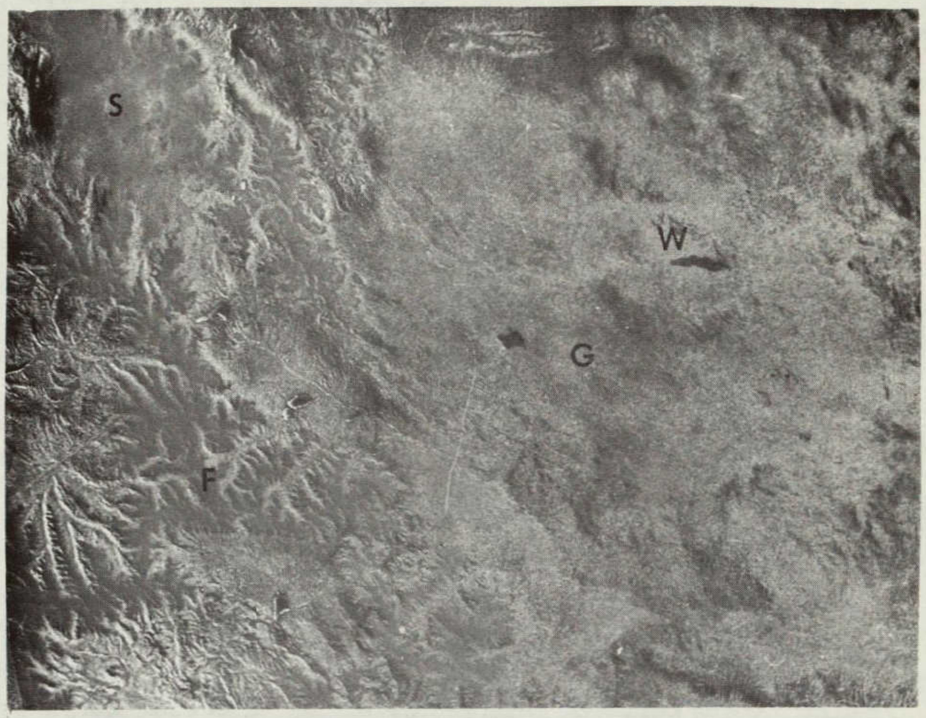

a.

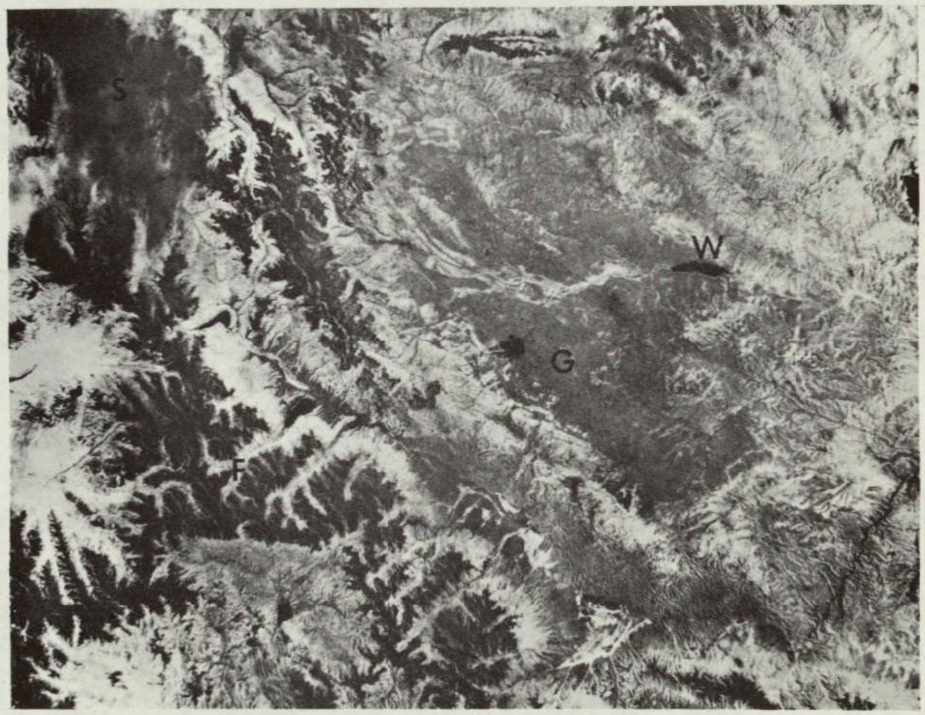

b.

Figure 12: Direct overlay masks of the central Colorado area. (see text for descriptions) W = water, G = grasslands/alluvium, F = forest/ bedrock, S = snow/cloud.

Snow, clouds, and water bodies are black, verdant vegetation is nearly white, grasslands and alluvium are medium gray, while forests and bedrock are dark gray (the red band negative gives the same information, except water bodies are white).

Direct overlay positive-negative masking provides no significant geologic information.

Color-Additive Viewing

Color-additive viewing was used in an attempt to enhance color anomalies. The International Imaging Systems Mini-Addcol Additive Color Viewer was used with frames 106 and 107 from track 48, Skylab 3 S190A, taken in August 1973. Film chips used were the 2.25-inch positive and negative transparencies of the two photo-IR bands and the red and green bands, and positives of the color and CIR bands.

Three alternatives were investigated for enhancing red-ocher color anomalies. In the first (fig. 13a.), the color positive was illuminated with white light at an intensity of 9 (on a scale of 0 to 9, with 9 maximum), the positive of the CIR band with blue light at 7, and the negative of the red band with white light at 9. The second combination (fig. 13b.) used the positive of the color band with white light at 9, the negative of the green band with green light at 6, the negative of the photo-IR 1 with blue light at 9, and the positive of the red band with red light at 5, which makes all bedrock/alluvium varying shades of red. This alternative allows easy discrimination of forests and fields from bedrock and alluvium, but makes it difficult to find red-ocher anomalies.

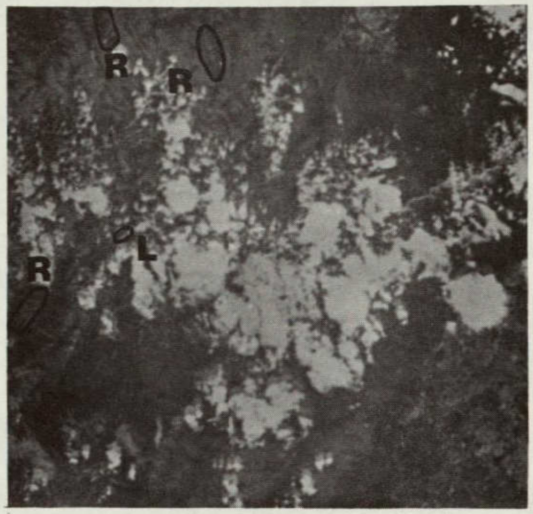

a.

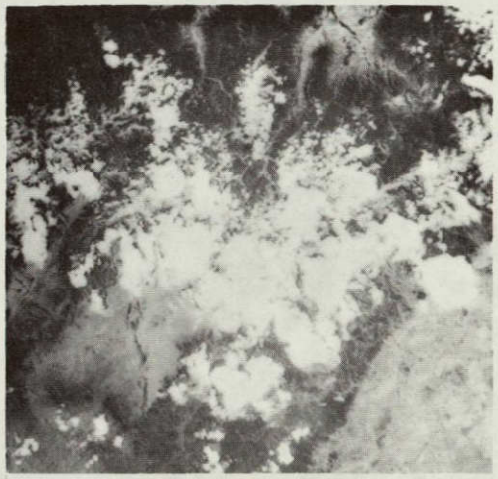

b.

Figure 13: Color-additive viewing alternatives one and two. Red-ocher anomalies are labeled "R"; light-colored anomalies are labeled "L". (see text for explanation) For color originals, see Prost (1975).

The third alternative was true color (fig. 4). True color and alternative one are best for locating red-ocher anomalies, although neither located all areas of red rock. Color targets were chosen using these two alternatives.

A true-color composite suggested for ERTS may also be applicable to Skylab multiband. Knepper (1973) claims to have achieved a true-color composite by projecting band 4 (green) with green light, band 5 (red) with red, band 6 (photo-IR) with green, and the negative of band 7 (photo-IR) with blue light.

Some color anomalies are a result of light-colored rock in an area of darker rocks (Tertiary sills in Permo-Pennsylvanian sediments in the Mosquito Range). The first and third techniques above do a fair job of isolating light-colored rock.

Color additive viewing (alternative one) may help locate both red-ocher and light-colored anomalies that are not obvious on true color photos. Neither will locate all areas of red or light-colored rock, and each may indicate different areas for a particular color anomaly. This is probably a result of vignetting in the original photography and in the copying process. It is suggested that color additive viewing be used in conjunction with true color photos to obtain the maximum useful information.

Density Slicing

Cumulative density slices of positive and negative transparencies were produced in an attempt to isolate light or dark color anomalies (red areas are usually medium gray on black and white transparencies of the red and green bands, and are not anomalous). In this process, all film densities above or below a given level are color-coded.

Diazo color-additive density slicing was tried on Skylab 2 S190A photos of frame 17, track 48, taken June 1973. Contact negative transparencies were made from the positive of the red band, and densities were "sliced" using high contrast film and varying the lens opening on an enlarger, with exposure time and developing time held constant. A lens opening of f/5.6 gave the darkest, and f/22 gave the lightest negative density slices. The diazo process produces color in the dense (dark) areas of the transparency. A four-colored image was produced using the negatives (fig. 14a).

Black and white negatives were made from frame 39, track 48, Skylab 3 S190B color transparencies taken in August 1973. Normal contrast contact positives were produced from the darkest negative. The density slice color-code scheme is shown in figure 14b. A six-color image was produced using both positives and negatives. Additional densities may be sliced by varying the exposure and developing times.

Color-coding of density slices gives inconsistent results because of the change in radiance of an object corresponding to changes in the geometric relationship (aspect angle) between

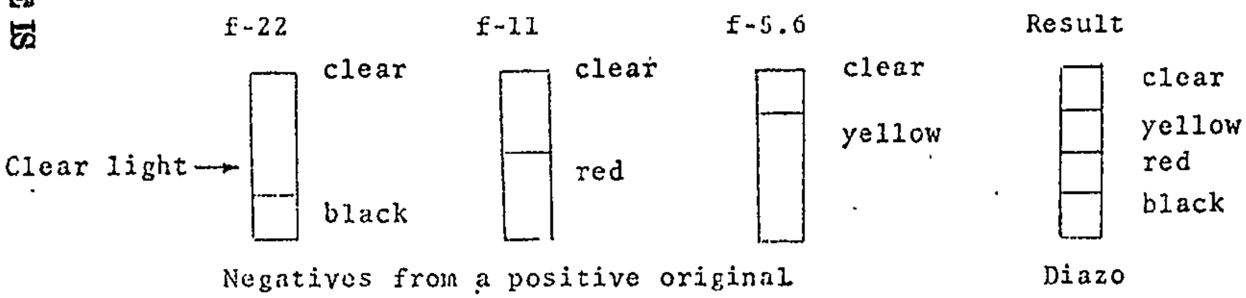

a. Schematic of a diazo four-color density slice image produced from negative transparencies.

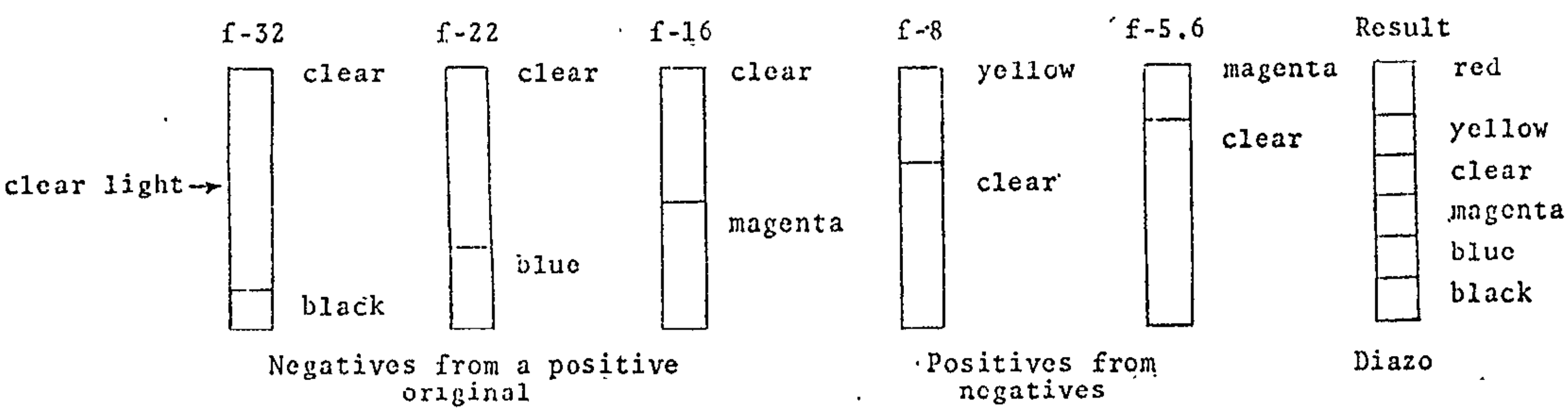

b. Schematic of a diazo six-color density slice image produced from negative and positive transparencies.

Figure 14: Diazo cumulative density slice color schemes.

the camera, object, and illumination source (fig. 15). Because

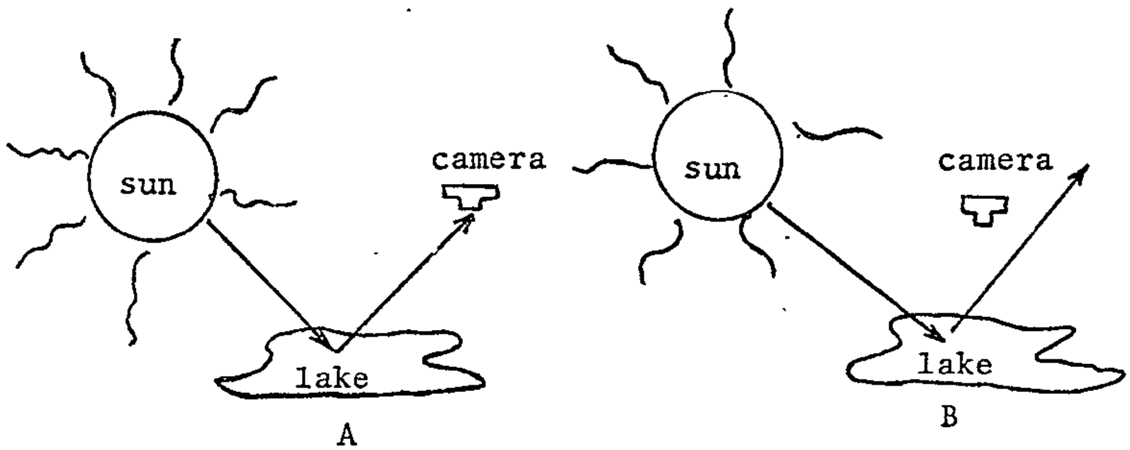

Figure 15: Change in radiance of a lake corresponding to a change in the geometric relationship between camera, object, and illumination source. In A the lake appears bright, while in B the lake appears dark.

of this relationship, bodies of water were sliced at three densities. The same principle, although opposite in sense, applies to rough surfaces (Lee, 1974). In central Colorado, sandstones of the Maroon Formation near Antero Reservoir were on one slice, while outcrops of the same red sandstone near Ruedi Reservoir were on another slice. It is also obvious that one density slice can contain several objects. For example, the Maroon Formation near Antero Reservoir was in the same slice as the water in Elevenmile Reservoir and most of the grassland in South Park.

Another density-slicing technique, where one or more individual density ranges are isolated and color-coded, has been discussed by Janda (1971) and Awald (1974). Janda used a Philco-Ford instrument to make seventeen "intensity splits"

from an original color photo (1:5000) over the Olympic coast of Washington. He concludes:

> applications of the light intensity separation techniques to the Cape Alava-Ozette Island area is of only limited utility; the technique does enhance some features, but it also obscures other features of equal significance.... Enhancing light intensity differences on color photographs does not generate significantly more useful information than can be obtained from the original photograph.

Awald used a Video Image Processor to isolate and color-code density slices that allegedly correlate to ground-mapped geochemical anomalies. This density-slicing technique was not attempted due to lack of the necessary instruments.

Density slicing techniques used in this study provided no geologic information. It is impossible to identify a feature by a code color because assigned colors indicate different features from place to place on an image.

PRELIMINARY EVALUATION AND TARGET SELECTION

Results of Preliminary Studies

The geology of the Leadville and Cripple Creek mining districts was studied as typical of mineralization occurring in central Colorado. Simultaneously, Skylab photos covering these areas were studied, and geology was correlated between maps and the photographs. Each area was field-checked to identify exactly what was seen on the photography. The two control districts were analyzed to determine the geologic features characteristic of mineralized areas that are visible on orbital photography. Enhancement techniques (previously described) were used in an attempt to make all the indicators of mineralization obvious.

A literature study of the Leadville district reveals that ore deposits occur chiefly in fissure zones, karst collapse breccias, or as replacement mantos in dolomites intruded by Upper Cretaceous or lower Tertiary felsic to intermediate porphyries. Major faults contain ore in few places, while auxiliary faults and fissures have served as feeder channels and are often mineralized. Alteration includes local hydrothermal bleaching of porphyries (decomposition of feldspars to sericite and kaolinite) and weathering of disseminated pyrite to hydrous iron oxides. Indicators of mineralization for this district are faulting, intrusion of sedimentary strata by light-colored porphyries, and weathered

pyrite. Field checks verified the ability to see some faulting on all orbital photography, and alteration colors were visible on S190B photos (see Appendix B).

At the Cripple Creek district, ore deposits lie within or near the margins of a steep, fault-caused basin (caldera?, breccia pipe?) filled with Miocene breccia and phonolite and surrounded by Precambrian granite, gneiss, and schist. The basin, approximately three by six kilometers (two by four miles), is filled with non-volcanic as well as volcanic debris, and is crosscut by dikes of phonolite and lamprophyre. Gold mineralization followed intermittent fissuring and is most commonly found as veins associated with quartz and pyrite gangue (Koschmann, 1949). Indicators of mineralization that are visible on satellite imagery are faulting and alteration of pyrite. Weathered pyrite is seen only on mine dumps; red-ochre colors in this area are more likely a result of an abundance of microcline in the local granite and derivative grus.

Results of this study over known mineral deposits lead to the assumption that indicators of mineralization visible on Skylab photography over central Colorado are faulting (intersections and high density of lineaments), weathering of pyrite ("red-ocher" color anomalies), and hydrothermally-bleached intrusives ("light" color anomalies). Breccia-filled basins cut by dikes were not recognized because of a lack of

color contrast or unique topographic or vegetation features. Karst horizons and mantos were not visible because of limited stratigraphic extent and frequent soil and vegetation cover. Distinctive vegetation patterns associated with mineralization were not observed because vegetation appears to be influenced more strongly by other environmental factors.

Target Selection

Indicators of mineralization that can be seen on satellite photography are lineaments and anomalous colors. "Anomalous," in reference to colors, means a local color that deviates from regional uniformity.

Skylab photos of the central Colorado survey area (fig. 1) were studied to find all indicators of mineralization. Structure targets were located by mapping linears as guides to faults, joints, and shear zones. Circular or curvilinear features, related to ore-generating intrusive centers, were not mapped. The preliminary study indicates that such features are not substantially related to mineralization in the two areas considered typical of central Colorado districts (the Cripple Creek basin is not visible on space photography, although unmineralized Rhyolite Mountain, a prominent local circular feature, is quite obvious north of the basin). It seems that (1) there is a real problem defining what a curved or circular feature should look like on photography, and (2)

such features may be related to volcanic cones, domes, or gently-curved glacial valleys as well as to potentially mineralized cauldron subsidence. It has been demonstrated that multiple intrusion and cauldron subsidence is associated with high density radial faulting (Schwarz, 1967; Burbank, 1941), while volcanic piles, anticlinal uplifts, and erosion should be associated with considerably less faulting.

Four lineament diagrams were made, one for each of the following:

(1) a nine-by-nine inch positive CIR transparency of frame 17, track 48, Skylab 2 S190A,

(2) a seven-by-seven inch negative CIR print of frame 106, and a seven-by-seven inch negative red band print of frame 107, track 48, Skylab 3 S190A,

(3) nine-by-nine inch color prints of frames 38 and 39, track 48, Skylab 3 S190B, and

(4) a seven-by-seven inch print of positive-negative slip masks made from the red band transparencies of frame 17, track 48, Skylab 2 S190A, and frames 106 and 107, track 48, Skylab 3 S190A.

An example of such a diagram (diagram 1 above) is provided to illustrate the target selection process (fig. 16). On these diagrams, obvious linear features are marked as a solid line, while questionable linears are dotted. Care was taken to avoid man-made or cloud-caused linears.

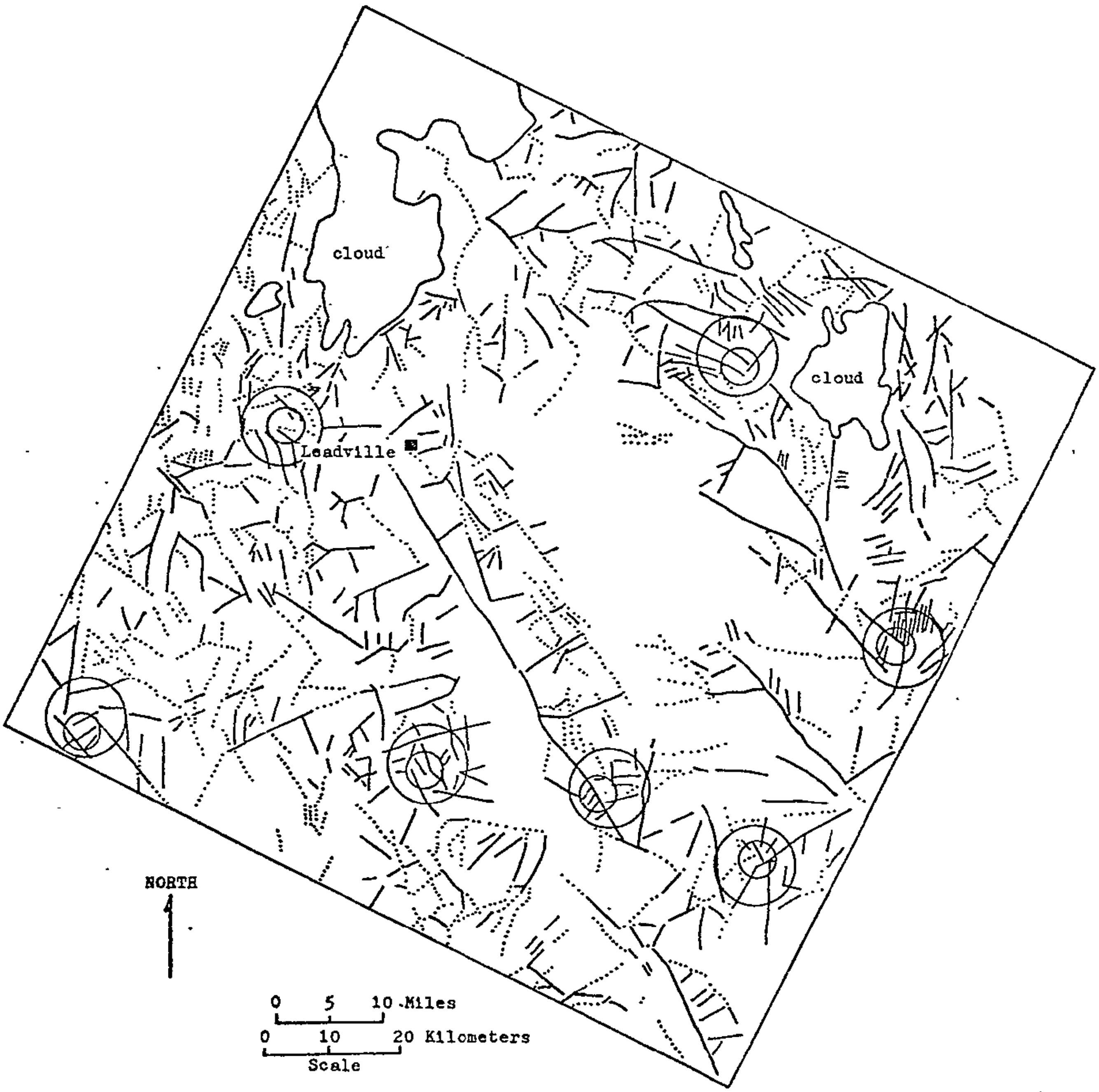

Figure 16 : Linear overlay mapped from Skylab 2 S190-A, track 48 frame 17, 11 June 1973.
Circles indicate structure targets.
Solid lines represent obvious lineaments; dotted lines are questionable lineaments.

Structure targets are those areas with a high density of linears or linear intersections. These targets were arbitrarily designated as circular areas covering 130 km^2 (50 mi^2, or radius of four miles), the primary target to be field-checked by mapping at a scale of 1:24,000. Within each structure target is an alternate subtarget, covering 32.5 km^2 (12.5 mi^2, or radius of two miles), to be mapped at a scale of 1:12,000 in the event the target had been mapped previously at the smaller scale.

Color targets were found by mapping anomalous colors as guides to intrusion and alteration. Anomalous colors were observed by color-additive viewing of frames 106 and 107, track 48, Skylab 3 S190A (Skylab 2 photography is snow-covered) and by viewing frames 38 and 39, track 48, Skylab 3 S190B (fig. 17). Few color anomalies were seen on unenhanced S190A photos and none was noticed on the diazo color-coded density slices. The two possible color anomalies were designated (1) red-ocher, and (2) light rock surrounded by darker rock. Each color anomaly was a color target.

Areas were considered favorable if they contained both color anomalies and structure targets (fig. 18). The most favorable target/subtarget, located at Weston Pass, became the primary study area. Mapping was undertaken at a scale of 1:12,000 because the area had been mapped previously at smaller scales. The next most favorable target, at Dome Rock, was

Figure in pocket

b.

Figure 17: Skylab 3 S190B enlargements.
a. Weston Pass area. Arrow points to anomaly.
b. Dome Rock area. D = Dome Rock; R = Rhyolite Mountain.

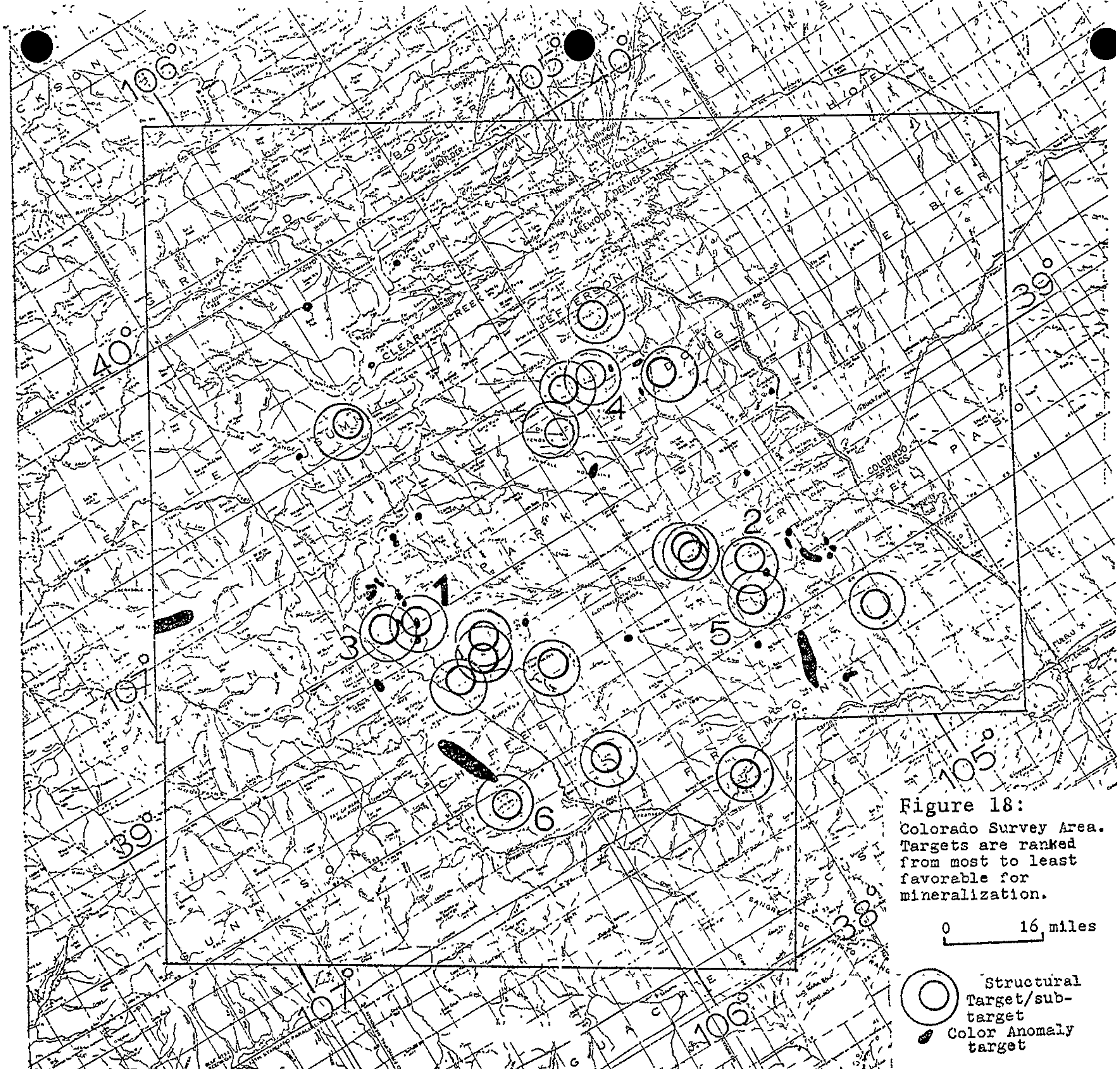

Figure 18: Colorado Survey Area. Targets are ranked from most to least favorable for mineralization.

briefly examined in the field to identify the indicators of mineralization.

It is logical to wonder why proven mining districts such as Alma, Breckenridge, and Climax were not chosen as the primary target. Cloud cover is a major factor in the case of Climax and Breckenridge. Many districts are heavily forested, and color anomalies are visible only in areas of sparse vegetation, which in central Colorado restricts the search to talus slopes and areas above timberline. Also, the basic assumption that favorable areas are structurally complex and associated with color anomalies may be wrong or incomplete. The two most favorable targets were evaluated to answer these questions.

TARGET EVALUATION - WESTON PASS

Indicators of Mineralization

The primary objective of field work was to obtain ground truth to determine the origin of anomalous colors, linear features, and vegetation patterns. A common surface indicator of ore at depth is the gossan (fig. 19), an outcrop of leached and oxidized iron sulfides (Blanchard, 1968). Where unobscured, the characteristic red-ocher color should be easily seen on color photography. In addition, intrusive rhyolitic porphyries should be obvious as light-colored anomalies where intruded into darker sediments. Areas of complex structural intersection have also long been considered favorable to ore deposition (Newhouse, 1942). It is hoped that linear features seen on satellite photography are related to structures (faults, joints, shear zones). Many researchers have suggested that vegetation patterns near ore deposits should be influenced by unique soil characteristics (Carlisle and Cleveland, 1958; Cannon, 1960, 1971; Canney, 1969). It was assumed that such patterns should be easily seen on satellite or aircraft photography, providing an additional indicator of mineralization. The Weston Pass and Dome Rock study areas were evaluated with these indicators in mind.

Red-ocher color anomalies can be caused not only by a gossan, but also by red sedimentary rocks, such as the Maroon Formation (fig. 20), which are probably the most visible

Figure 19: Gossan visible on S190B. Located above Sweet Home mine, Buckskin Gulch, Alma. For color original, see Prost (1975).

Figure 20: Red sedimentary rocks visible on S190A and S190B. Maroon Formation, South Park. For color original, Prost (1975).

red features in central Colorado, and by microcline-rich crystalline rocks and grus, commonly found in Precambrian units. Rocks appearing red-ocher on satellite and aerial photography over the Weston Pass study area are exposed as talus or outcrops and contain microcline and/or iron oxides (figure 21, plates 5 and 6). The most obvious color anomaly, on the west slope of Weston Peak (figs. 17 and 21), contains both microcline- and hematite/limonite-rich granite talus. One less visible anomaly consists of microcline-rich granite outcrop and grus; another comprises limonite-stained dolomite talus overlying white quartzite. The extensively limonitized ore horizons at Weston Pass were not visible on orbital photography because of limited outcrops and extensive vegetation and soil cover (Fig. 23).

Outcrops, talus, and minimal soil and vegetation cover provide optimum visibility. This limits most anomalies in central Colorado to talus slopes or areas above timberline. Mapping indicates that color anomalies in the Precambrian units generally are due to greater than thirty percent pink minerals (potassium feldspars and iron oxides) in outcrops, talus, or grus, regardless of unit (fig. 22, plate 6). Red color is not obvious in every place these conditions are met; an explanation may be indirect illumination, or differences in films or processing. Bloom (1965) attributed hue to the size of phenocrysts. Red coloration in alkali-feldspars is a result of inclusions of hematite formed by exsolution where

WESTON PASS PRIMARY TARGET STUDY AREA

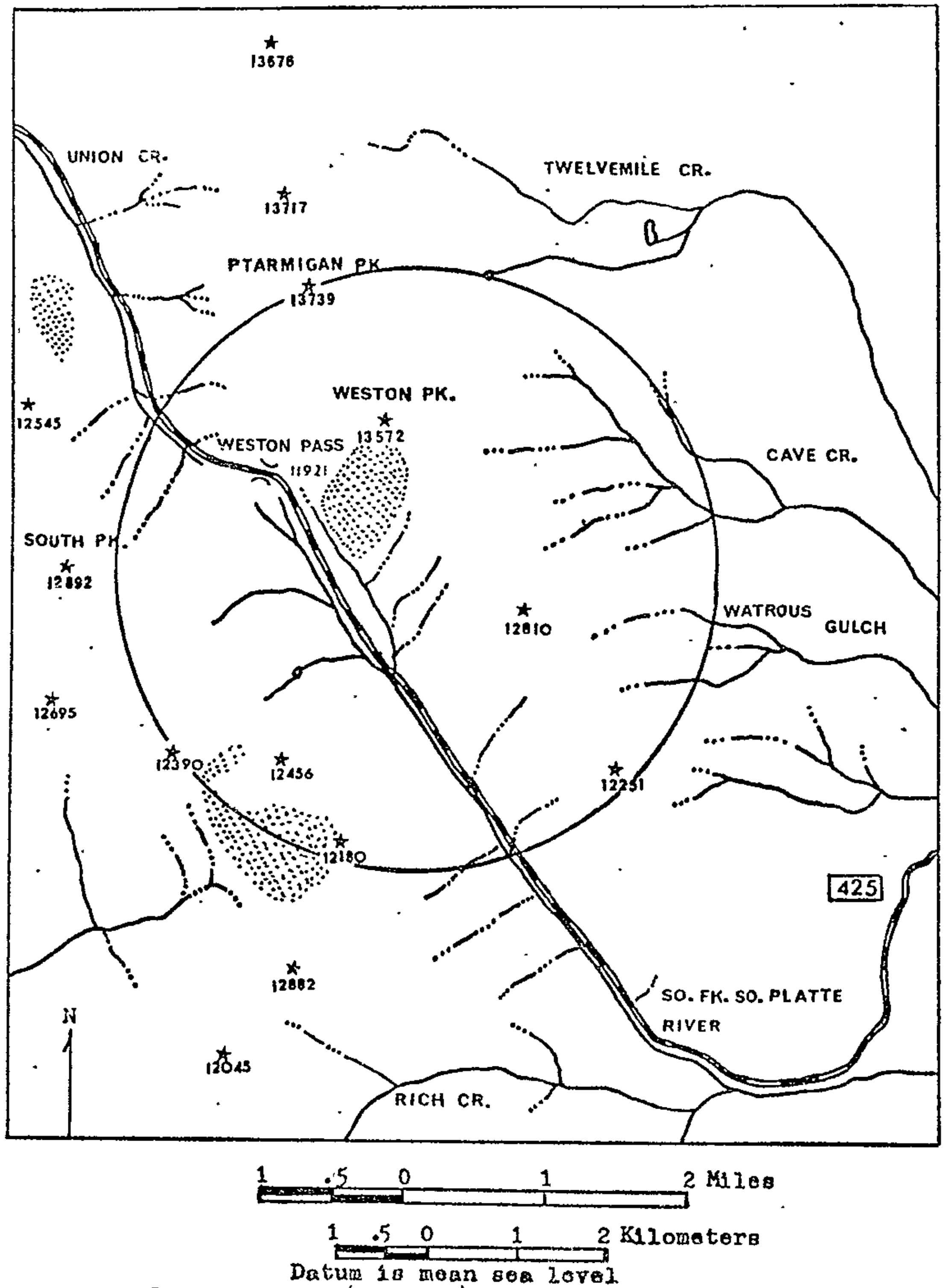

Figure 21: Color anomaly (reddish) targets, mapped from Skylab 3 S190-B, track 48, frame 38, 4 Aug. 1973. Anomalous colors.

WESTON PASS PRIMARY TARGET STUDY AREA

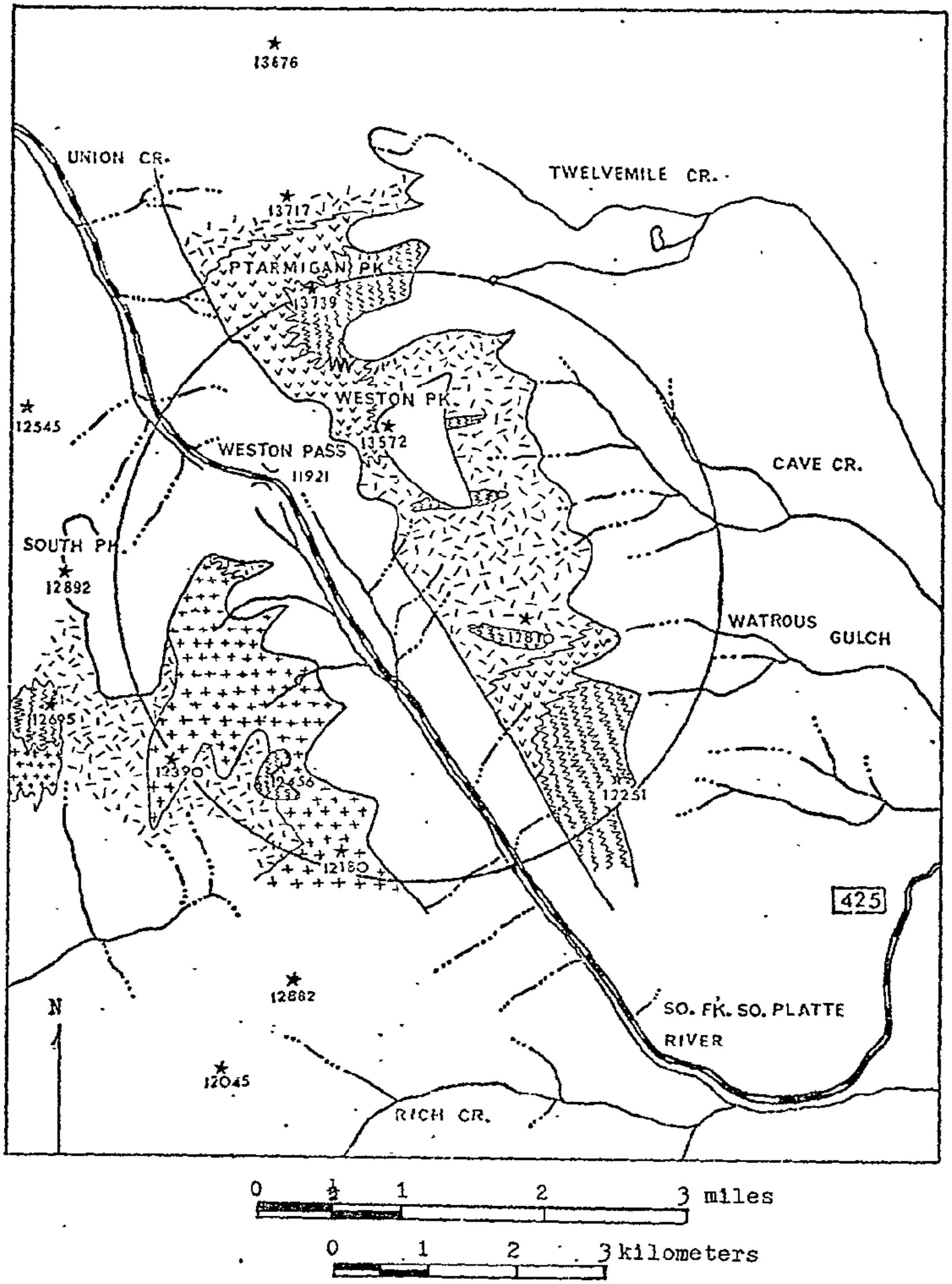

Fig. 22 : Distribution of Precambrian units.
Silver Plume. Trout Creek Augen Gneiss.
Biotite Gneiss. Injection Gneiss.

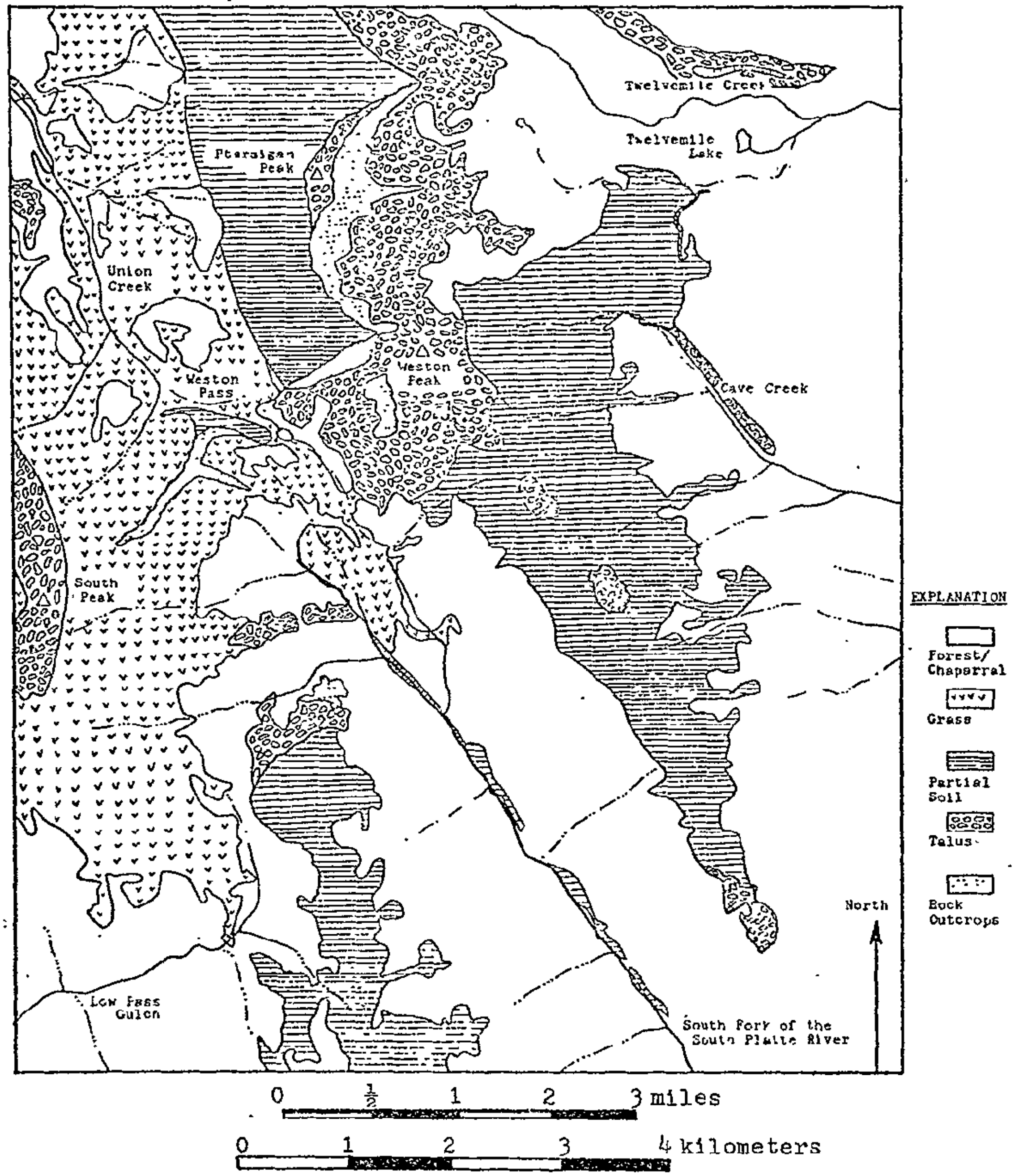

Fig. 23 . Ground cover map, Weston Pass study area and vicinity.

aluminum is replaced by iron in the crystal lattice (Niggli, 1954).

Light color anomalies (none was seen on satellite images in the primary study area) may be caused by light sedimentary units such as the Sawatch Quarzite or quartz-rich pegmatites, as well as by light-colored, altered intrusives. Light-colored intrusives were visible on aircraft photography both because of their color contrast with the adjacent rocks, as they have often been emplaced as sills between dark dolomites and shales, and because of a decrease or change in vegetation type growing on the unit (this change in vegetation is inconsistent from place to place). It is not possible to distinguish the sills where there is a lack of contrast, such as within the Sawatch.

Photography at a scale of 1:20,000 was most useful for discriminating colors and attempting to determine their origins. Even at this scale, however, distinguishing between microcline-rich talus and limonitically-altered talus is difficult, and identification is a matter of speculation.

Regional linears were assumed to be the expression of structures, and linear density and complex intersections were important criteria in target selection. Field work revealed that linear objects may be aligned streams and saddles, ridges, vegetation alignments, cultural features such as fences, roads, power lines, or airplane contrails, as well as geologic features such as dikes, contacts, paleovalleys, shear zones, joints,

and faults. Within the Weston Pass study area, 22 lineaments were mapped from Skylab photography (fig. 24). A comparison with faults mapped by Tweto (1974; modified within the study area) shows that seven mapped linears, or 32%, correspond closely to known faults (fig. 25). One linear was correlated to a cultural feature (powerline), and the remainder are thought to be structurally-controlled drainage or vegetation alignments. To determine the influence of structure on drainages, a rose diagram (fig. 26) was prepared showing the azimuths of 53 linear drainages or drainage segments longer than 1.6 kilometers (1 mile), and this diagram was compared to a pole-normal contour diagram of 139 post-Precambrian joint azimuths (fig. 27) and with another diagram of 100 Precambrian joint measurements (fig. 28). The comparison reveals that the N30E to N40E drainage trend is directly controlled by jointing, and that the major N60E to east trend is a consequence of drainages formed on dip slopes normal to the north to N30W joint trend.

Within the study area there are several throughgoing near-vertical faults trending generally N20W to N30W. One obvious misinterpretation of the S190A photography was the plotting of a linear along the east side of the valley south of Weston Pass. Upon inspection of S190B, and then low altitude photography, this was found to be a powerline right-of-way cut through the forest (fig. 29). Ironically, the right-of-way is linear because the valley is linear, a result

WESTON PASS PRIMARY TARGET STUDY AREA

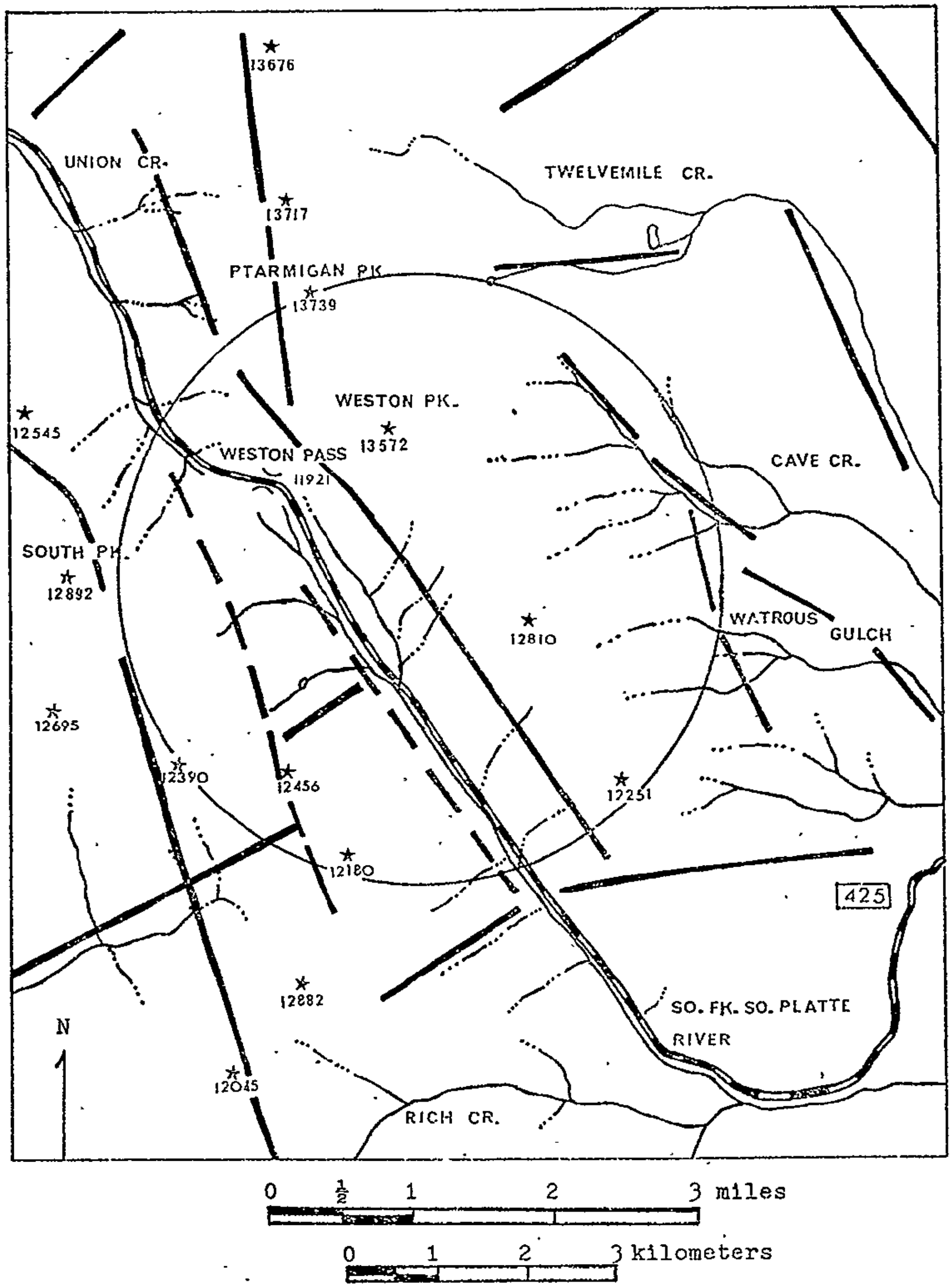

Fig. 24: Area of convergence of regional structures. Lineaments mapped from Skylab 2 S190-A, track 48 frame 17, 11 June 1973, and Skylab 3 S190-A, track 48 frames 106 & 107, 4 August 1973. Linears dashed where uncertain.

WESTON PASS PRIMARY TARGET STUDY AREA

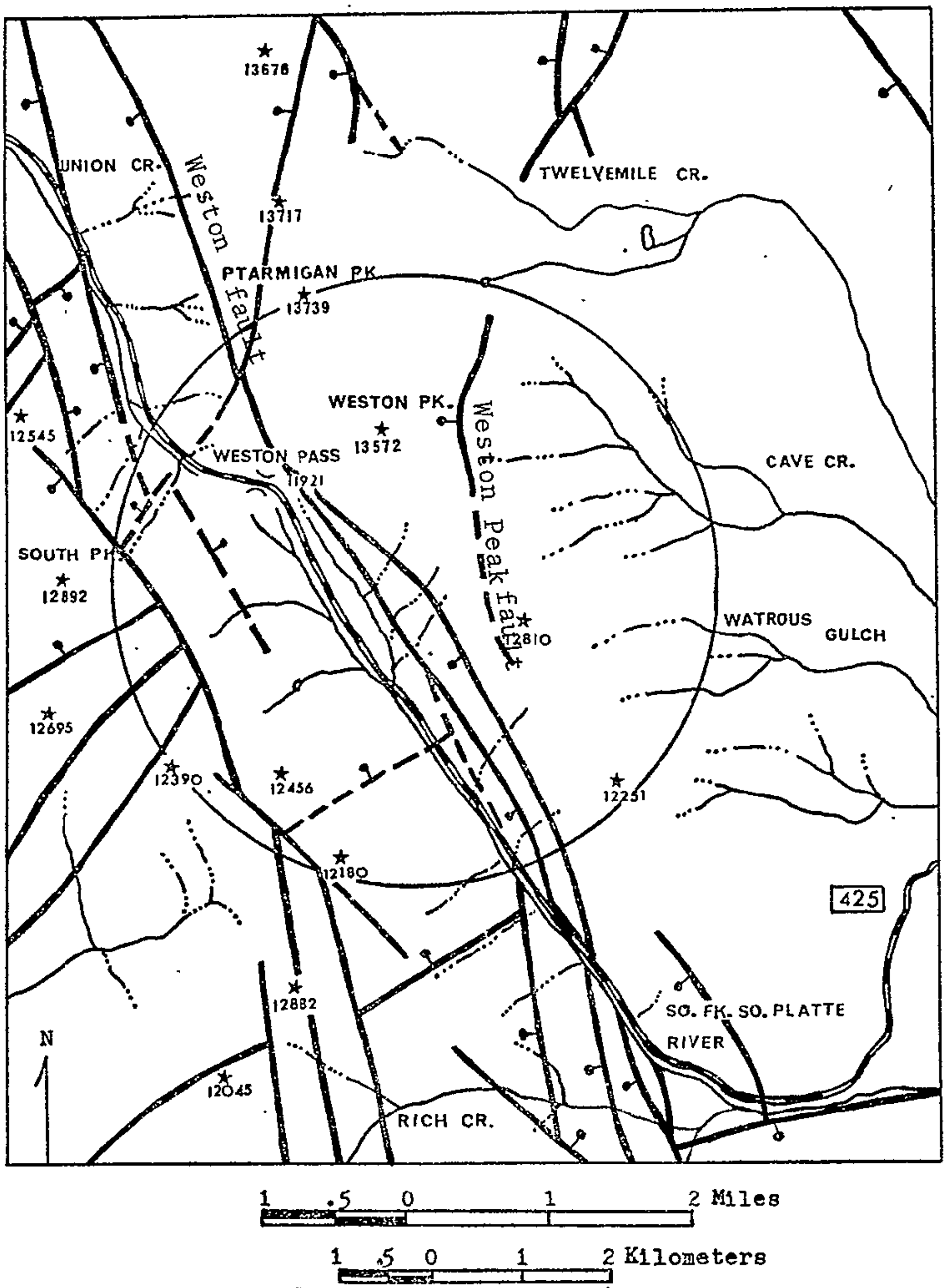

Datum is mean sea level

Fig. 25: Area of convergence of regional structures. Modified after Tweto, 1974. Bar and ball on downthrown side of fault.

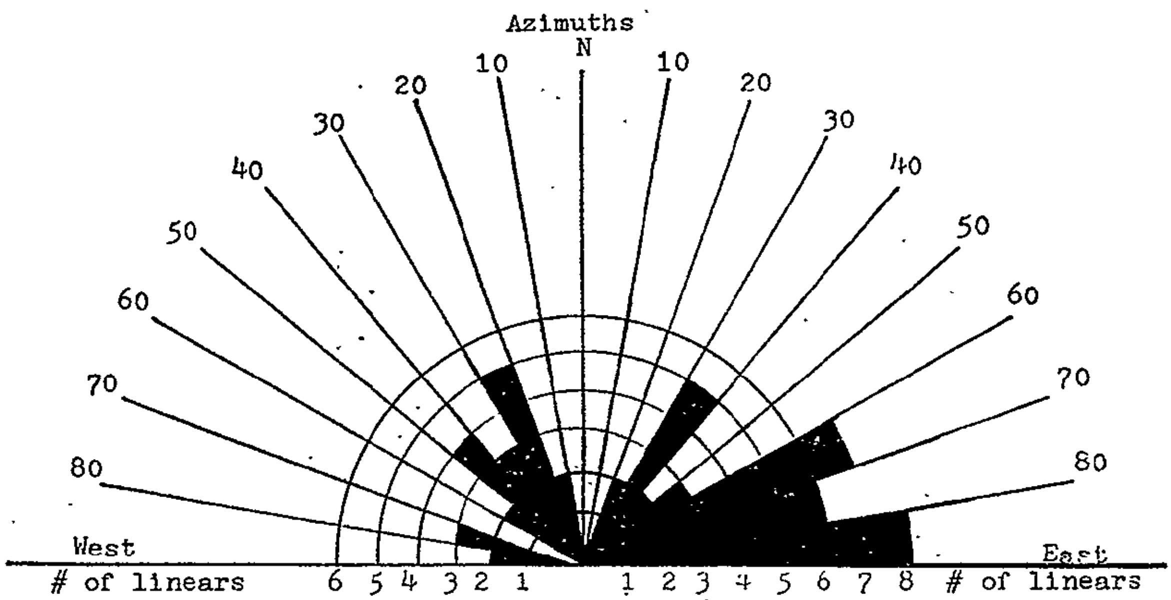

Figure 26: Rose Diagram of 53 linear drainages or portions of drainages over one mile in length, Weston Pass area.

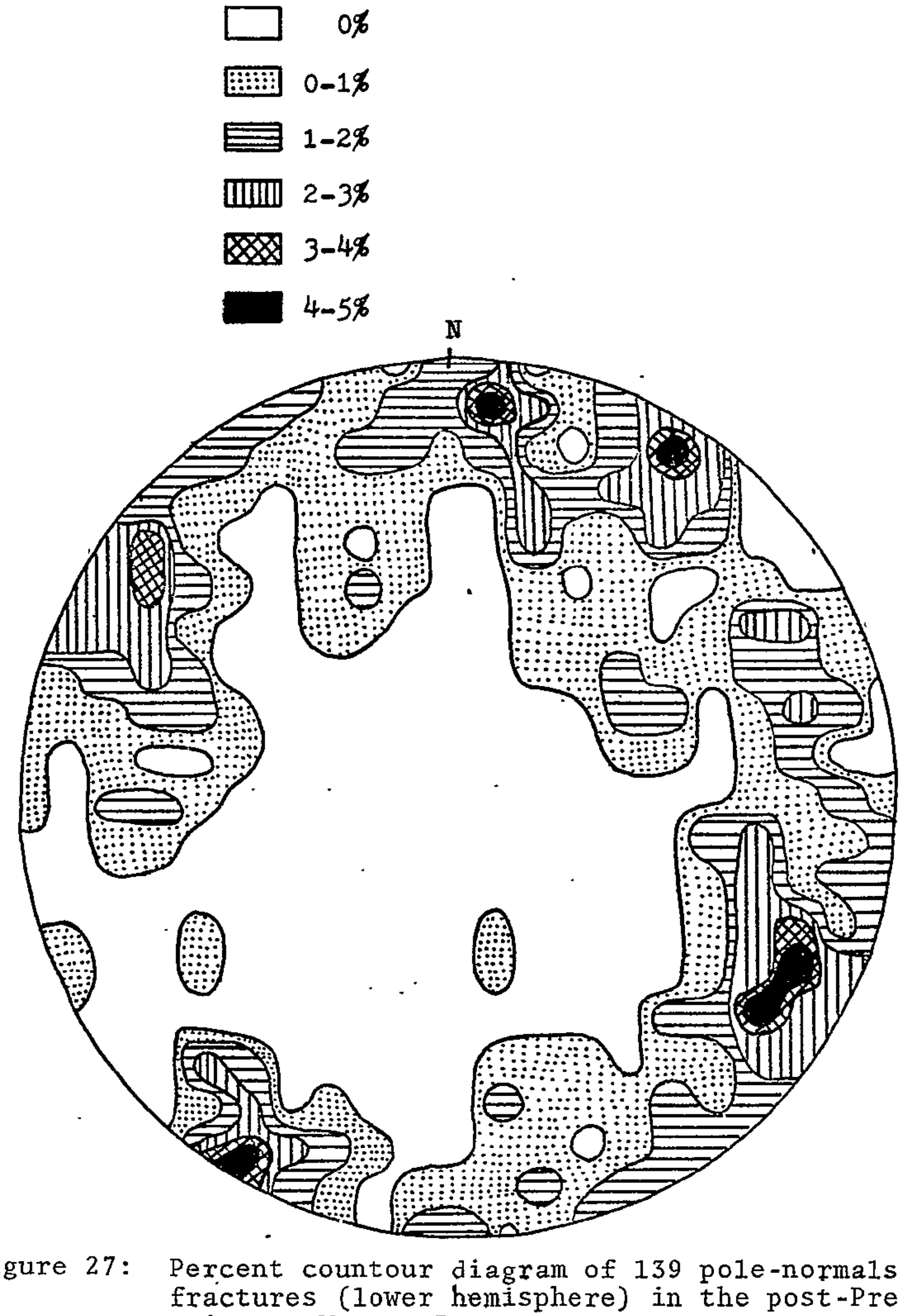

Figure 27: Percent countour diagram of 139 pole-normals to fractures (lower hemisphere) in the post-Precambrian units at Weston Pass.

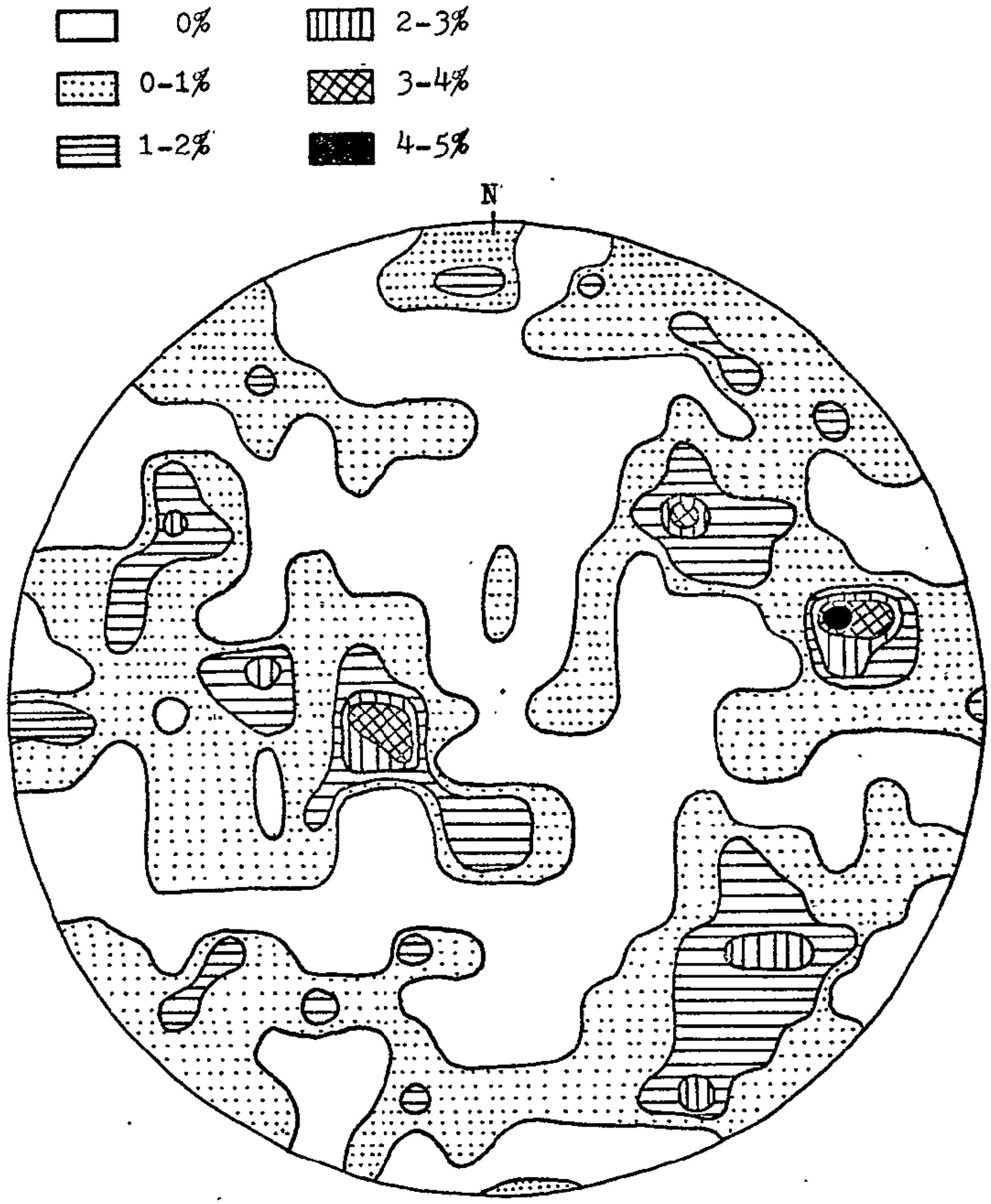

Figure 28: Percent countour diagram of 100 pole-normals to fractures (lower hemisphere) in the Precambrian units at Weston Pass.

Figure 29: Powerline right-of-way through Weston Pass area. View is south from Weston Pass.

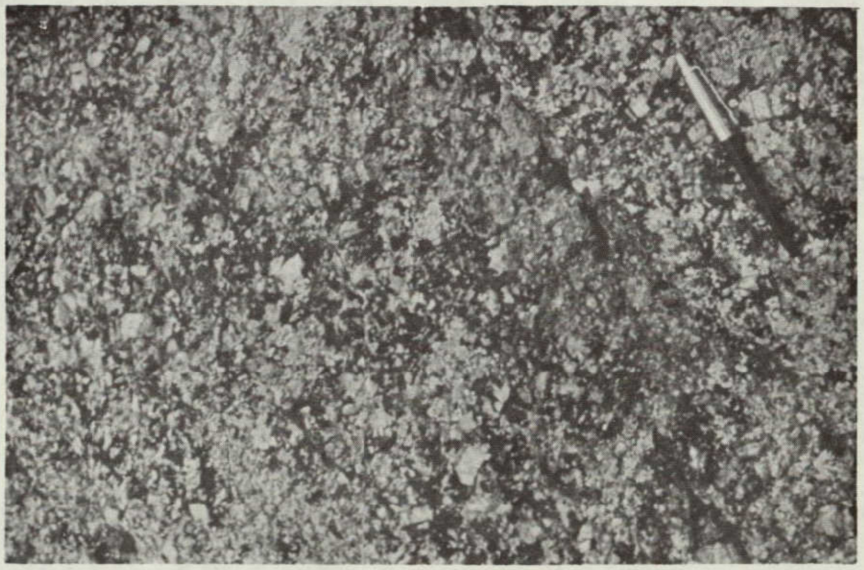

Figure 30: Trout Creek Augen Gneiss. For color original, see Prost (1975).

of the Weston fault zone.

Valdes (1967) noted that a boundary between coniferous forest and aspen coincides with the contact between the Leadville Formation and the Belden Shale in the Jones Hill Quadrangle, and he used this relationship to aid in mapping the contact on airphotos. This relationship does not exist in the area of the present study. The only vegetation-lithology associations noted are a decrease and change in vegetation associated with intrusive porphyries, and locally a slight decrease in the abundance of alpine grasses as one crosses the contact from the Belden Shale to the Leadville Formation above timberline.

Stratigraphy

Precambrian Rocks

The oldest Precambrian rock in the area is a black, foliated, fine to medium-grained, muscovite-garnet-sillimanite-quartz-biotite schist and gneiss with garnet porphyroblasts. This unit has been referred to as Idaho Springs Formation (Chronic, 1964), Idaho Springs Equivalent (Valdes, 1967), and Xb biotite gneiss (Tweto, 1974), dated approximately 1.7 billion years old.

The above unit is intruded by a gray to pink, hypidiomorphic-inequigranular, medium to coarse-grained, seriate, quartz monzonite with oligoclase and microcline porphyroblasts (fig. 30). This augen gneiss has been referred to as Pikes Peak granite (?) (Behre, 1953; Chronic, 1964), Cripple Creek

augen gneiss (Valdes, 1967), and Xg granite (Tweto, 1974), dated at 1.7 billion years. In this report it is referred to as Trout Creek augen gneiss (Hutchinson, 1974, oral comm.).

The youngest major Precambrian unit is a gray to pink hypidiomorphic-inequigranular, medium to coarse-grained, porphyritic granite to quartz monzonite (fig. 31). Referred to here as Silver Plume-Type granite, it is also classified as Yg granite (Tweto, 1974), and has an age of 1.4 billion years. This unit is both massive and trachytoid; alignment of tabular feldspars may result from magma flow during crystallization or from later deformation.

In some areas the Precambrian units are in intimate contact; here they are mapped as injection gneiss (migmatite).

Pegmatite and aplite dikes are numerous and may be found in all the Precambrian units. Composition is dominantly quartz, microcline, and muscovite.

Figure 31: Silver Plume-Type granite. For color original, see Prost (1975).

Cambrian Rocks

The Cambrian section in the study area varies from 48 to 55 meters (158-180 feet) thick (Behre, 1932, measured 49 meters at Weston Pass). The Sawatch Quartzite lies unconformably on Precambrian rocks with an erosion surface that has several centimeters of relief. Locally, a quartz-pebble conglomerate up to 0.3 meter (one foot) thick lies on this surface. The lower 27 meters (90 feet) of the Sawatch is a white (with local light green or light purple), medium-grained, subangular and subrounded, well-sorted, quartz sandstone with silica cement, containing beds five centimeters to one meter (two inches to three feet) thick, local trough cross-beds, and is highly fractured. This grades into eleven meters (35 feet) of brown, medium-grained, well-rounded, well-sorted, quartz sandstone which has dolomite cement and is trough cross-bedded and highly fractured. The upper Sawatch is nine meters (thirty feet) of purple and brown, medium to coarse-grained, well-rounded, fairly well-sorted, quartz sandstone with dolomite cement increasing higher in the unit, beds one to two centimeters (one-half to one inch) thick, and containing burrows or casts. The sands within the Sawatch get finer grained upward in the section and grade into the Peerless Shale. The Peerless Shale is two meters (six feet) thick, light to dark brown, fine-grained, subangular and subround, fairly well-sorted, quartz sandstone which has dolomite cement and is laminated to thinly-bedded, with green shale interbeds distributed at random throughout the unit. Occasionally this

unit contains thin-bedded, green and red shales with what appear to be mud chip casts (red- and green-cast beds). Trilobites, graptolites, and brachiopods indicate a Late Cambrian age for the Sawatch and Peerless formations (Johnson, 1934; Chronic, 1964; Bloom, 1965).

A west to east marine transgression over central Colorado deposited the Sawatch at or near shore, and the Peerless near or offshore (De Voto, 1971).

Ordovician Rocks

The Manitou Formation is approximately 63 meters (205 feet) thick in the study area (Behre, 1932, measured only 31 meters). The lower contact is gradational with the Peerless, and the lower part of the unit is a gray to light yellow-brown, sandy, medium to finely-crystalline dolomite (locally a silicified and dolomitized sandy limestone) with randomly distributed coarse to fine-grained, well-rounded, quartz sandstone inter-laminae. Beds are laminated to one meter (three feet) thick. The upper part of the unit is characterized by gray to yellow-brown, medium to finely-crystalline dolomite containing white and orange chert pods, generally parallel to bedding and up to several centimeters in diameter. The upper six meters (twenty feet) contain dark gray, coarsely-crystalline pisolites up to one centimeter (one-half inch) in diameter in a calcite matrix. These have been described as algal pellets, probably *Girvanella* (Chronic, 1964). An Early Ordovician age is indicated by trilobites and brachiopods (Chronic, 1964; Bloom, 1965).

After local regressions of the Late Cambrian sea, central Colorado was inundated in Early Ordovician time, and the shallow-water, algal-bearing lime muds of the Manitou Formation were deposited (De Voto, 1971).

Devonian Rocks

The Devonian Chaffee Formation in the Mosquito Range is divided into the Parting Quartzite (lower) and Dyer Dolomite (upper) members. Some confusion exists concerning identification of sands and shales overlying the Manitou in the study area. The Ordovician Harding Formation, south of Buffalo Peaks, is nearly identical to the lower Parting Quartzite, described in and north of the study area. Ordovician fish plates *Astraspis* and *Eriptichius* were not found, so the unit will be considered Parting, as others have done (Emmons, et al., 1927; Behre, 1932, 1953; Johnson, 1934; Chronic, 1964).

Twenty-four meters (eighty feet) of Parting Quartzite were measured in the study area (Behre, 1932, measured 19 meters at Weston Pass). Locally, a light brown, sandy, cross-bedded conglomerate overlies an erosional base. This grades up to red and green shales, then to a yellow-brown, limy conglomerate containing medium-grained, subrounded and subangular, quartz sand and pebbles of white quartz, black chert, and brown mud-stone. Above this lies a white, massive section of subrounded and subangular, well-sorted, fine and medium-grained, trough cross-bedded, quartz sandstone with silica and some hematite cement. White to tan, well-sorted, medium-grained, trough

cross-bedded, quartz sandstone with silica and dolomite cement tops the unit, with an upper contact gradational to the Dyer Dolomite.

The unconformity at the base of the Parting indicates erosion of the Middle Ordovician to Upper Devonian section. The Parting Quartzite was deposited in transitional and shallow environments as a Late Devonian sea moved east into Colorado (De Voto, 1971).

The Dyer Dolomite varies from 7 to 49 meters (24-160 feet) within the study area (Behre, 1932, measured 23 meters at Weston Pass). Rapid thickness variations of the Dyer Dolomite occur throughout the region. Valdes (1967) measured less than 12 meters (38 feet) in the Jones Hill Quadrangle, Bloom (1965) measured 15 to 31 meters (50 to 100 feet) in the Horseshoe basin, and Johnson (1934) mentions that thickness varies rapidly from zero to 29 meters (zero to 95 feet) in the Leadville district. The base of the unit is a brown-gray, sandy, coarsely-crystalline dolomite with one meter (three feet) thick beds, then an interval of dark dolomite breccia in a light gray dolomite matrix. This is overlain by a two meter (seven feet) thick, brown sandstone similar to the top of the Parting. A light gray, finely-crystalline dolomite with beds two centimeters to one meter (one inch to three feet) thick and containing dark-brown "webby" chert and wavy laminae of coarse-grained, hematite-stained, quartz grains tops the unit. A Late Devonian Syringopora dates this unit (Johnson, 1934).

The Dyer carbonates were deposited offshore as the Late Devonian sea moved east. Less detrital material was deposited, and carbonates formed in shallow water. Local erosion occurred in latest Devonian (De Voto, 1971).

Mississippian Rocks

The Gilman Sandstone, 30 centimeters to 5 meters (one to fifteen feet) thick, and described by Bloom (1965) as yellow-brown, fine and medium-grained sandstone interbedded with sandy dolomite breccia (40% quartz, 55% dolomite), was mapped in the Horseshoe district, and none was found in the Jones Hill Quadrangle (Valdes, 1967). Within the present study area, a hydrothermally decomposed, or "sanded" dolomite, containing chert pods parallel to bedding, occurs locally above the Dyer Dolomite, and here is classified as part of the Leadville Formation. This unit is probably what Behre (1953) referred to when stating the Gilman has been identified with certainty at Weston Pass. All contacts appear to be gradational.

Behre (1932) measured 113 meters (370 feet) of Leadville Formation at Weston Pass, but later (1953) reported only 49 meters (160 feet). The inconsistency is due both to rapid local thickness variations and to measurements on a talus-covered dip slope at the pass. A thickness of 110 meters (361 feet) was calculated during this study for the Weston Pass section (see plates 1 and 2). The unit comprises a yellow-brown dolomite at the base, grading up to a light gray and yellow, silicified and limonitized breccia, which is in turn

overlain by light gray dolomite and a mineralized replacement horizon. Above this is a dark gray to black dolomite containing black chert pods, and at the top of the unit is a light gray dolomite containing light gray chert.

Good outcrops of Leadville Formation occur north of Twelvemile Lake, where 86 meters (281 feet) were measured. Here the base is dark and light gray,

thin to thickly-bedded, finely-crystalline dolomite containing two to five centimeter (one to two inch) black chert nodules parallel to bedding. An ocher limonite/dolomite-cemented, medium-grained, well-sorted, subrounded quartz-sandstone unit one-third to two meters (one to seven feet) thick and containing light gray dolomite breccia occurs 32 meters (106 feet) above the base. Lenses of this sand are also found in the overlying black finely-crystalline highly-fractured dolomite. Farther up the black dolomite contains zebra stripes and vugs filled with quartz and calcite crystals. Near the top of the unit this grades into a light gray sandy dolomite, and is overlain by a meter (three feet) thick, white limestone containing black zebra-striped dolomite clasts. The top of the unit is a thinly-bedded, black, finely-crystalline dolomite with random zebra stripes, vugs, and black chert all increasing upward.

Many origins have been postulated for the discontinuous intraformational breccias, which may have controlled

mineralization. Behre (1932) suggested a specific bed was shattered by bedding-plane slip accompanying movement of the Weston fault. He later (1953) suggested the breccia resulted from accumulation of debris at the base of upfaulted cliffs of Dyer and Manitou that were being cut by waves of the advancing Mississippian sea. Posada (1973) suggested karst collapse as the origin of breccias, and such an origin is not uncommon (mineralized karst collapse breccias in Puerto Rico reported by Sweeting, 1973, p. 171). The discontinuous nature of the breccias in the study area, as well as some breccias containing material from overlying units, supports a karst collapse origin.

The origin of dolomites in the Leadville Formation has also been the subject of debate. Posada (1973) presented three possibilities: (1) diagenetic dolomite produced in a zone of contact between brackish and fresh underground water, with magnesium derived from ocean water or reflux brines during sea level changes, (2) hydrothermal dolomitization, and least likely (3) dolomite produced by seepage reflux or evaporite pumping in a supratidal closed shelf or lagoon. Tweto (1968) favors a hydrothermal origin related to mineralization locally, but allows that origin probably varies with locality. De Voto (oral comm., 1975) favors Posada's first alternative. Dolomite may have formed at the fresh water/sea water interface as the shoreline transgressed, while a humid coastal climate caused karsting and solution of silica at the surface and redeposition of silica at depth.

Thin-section analysis reveals the subparallel bands known as "zebra stripes" are alternating zones of light, coarse crystals and darker, fine crystals of the same composition, either calcite or dolomite (fig. 32). Proposed

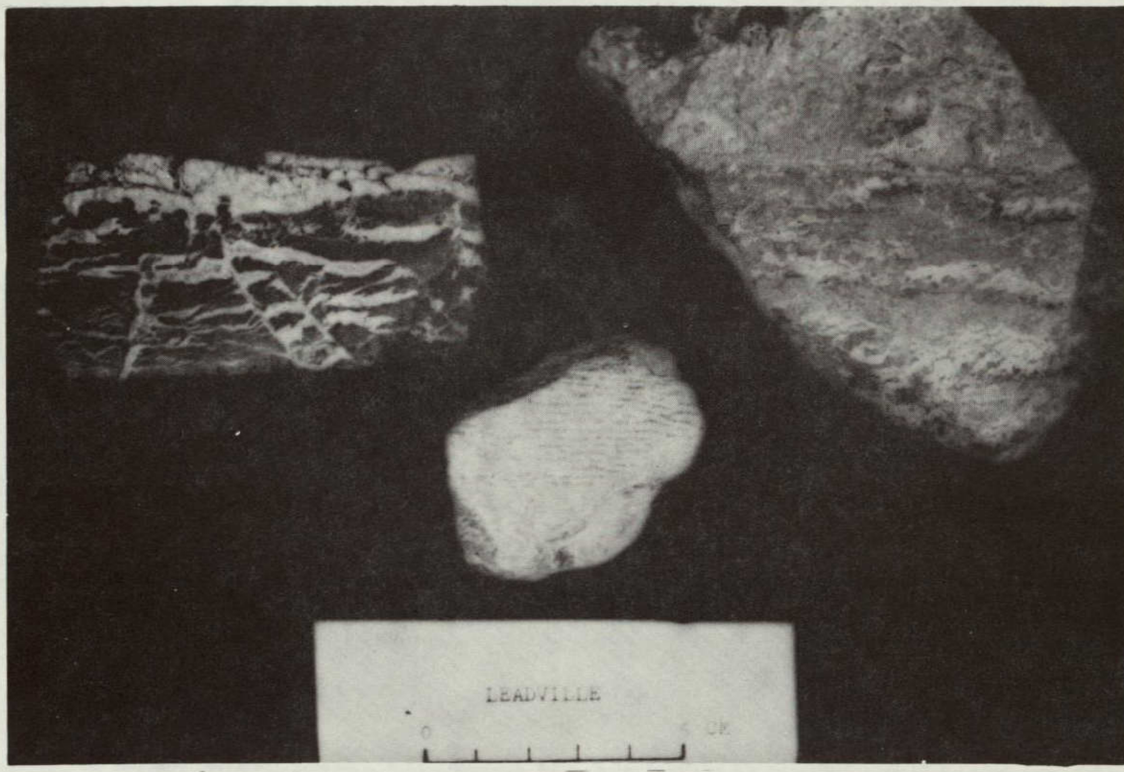

Fig. 32: Examples of "zebra-striped" Leadville Formation.

origins include hydrothermal filling of shear planes by white calcite or dolomite (Chronic, 1964), or contact metamorphic replacement along bedding or fractures (Behre, 1953). A study by Bloom (1965) reveals the zebra-striped dolomite is chemically identical to normal dolomite. It appears, however, that impurities (clay, carbon, pyrite) are concentrated in the

darker bands. A statistical analysis of fractures shows the orientation of black and white layers varies between thrust fractures and bedding planes. The coarse crystals are euhedral, while fine crystals are anhedral, lending support to strain recrystallization in response to stresses unrelieved by fissuring. Increased permeability accompanying recrystallization may have influenced localization of ore.

An Early Mississippian sea deposited the carbonate muds of the Leadville Formation as a result of biogenic activity in sheltered environments such as shallow lagoons and bays (Nadeau, 1972). The age of the Leadville Formation has been determined by Foraminifera and brachiopods (Johnson, 1934; Nadeau, 1972). During this study a brachiopod thought to be *Punctospirifer solidirostris* or *Spirifer bifurcatus* was found near the top of the Leadville on the east slope of Weston Peak.

Pennsylvanian Rocks

About 113 meters (372 feet) of Belden Formation were measured on the east slope of Weston Peak. This compares with 153 meters (500 feet) measured by Bloom (1965) in the Horseshoe basin, and between 320 and 520 meters (1051-1700 feet) at Weston Pass (De Voto, 1972). The base of the Belden is marked by a porphyry sill, and immediately above this is a zone of black chert breccia in a white silicified quartzite, originally a black sandstone that was bleached by contact

metamorphism (Behre, 1953). Above this are six to nine meters (twenty to thirty feet) of alternating white, powdery, contorted gypsum in beds one centimeter to three meters (one-half inch to ten feet) thick and thin-bedded black limestones. Cave Creek was named for solution cavities in this unit. Above this lies an angular to subrounded well-sorted, pyritic, quartz sandstone with silica and hematite/limonite cement, grading up to gray micaceous shales containing abundant biotite. Near the top of the section is a brown shale grading up to a gray, poorly-sorted, angular, coarse-grained, conglomeratic arkose that may be part of the Coffman Formation (Tweto, 1974, oral comm., prefers to call this unit the Minturn). A modern erosion surface tops the section. An Early Pennsylvanian age is indicated by over 100 fossils listed in Johnson (1934), Brill (1952), and Behre (1953).

Regional uplift and erosion during Late Mississippian developed a karst topography on the Leadville Formation, which was covered by an Early Pennsylvanian sea advancing from the northwest at the same time the Ancestral Front Range and Uncompahgre Highland were being formed. Thick calcareous shales indicate a marine environment, while carbonaceous shales accumulated on the lower delta salt marshes and fresh-water swamps (De Voto, 1972). Coal at Weston Pass indicates a paludal environment, while up to nine meters (thirty feet) of gypsum at the head of Cave Creek may have formed in fault-controlled basins with an evaporite environment

(Chronic, 1964). Sandstones and conglomerates near the top are probably related to alluvial channel and associated deltaic deposits of the Coffman Formation (De Voto, 1972).

Cenozoic Rocks

Three Cenozoic porphyries are within the study area. The Pando Porphyry, a light gray to white, holocrystalline, hypidiomorphic-inequigranular, porphyritic-aphanitic, heavily sericitized, muscovite rhyolite to quartz latite, dated at 70 million years (Pearson, et al., 1962), occurs as a sill between the Leadville and Belden formations north of Weston Pass and south of Twelvemile Lake. The sill north of the pass is about twelve meters (fourty feet) thick; south of Twelvemile Lake it thins from about 185 meters (600 feet) to zero in five kilometers (three miles).

The Little Union Quartz Latite (?) is a gray, holocrystalline, hypidiomorphic-inequigranular, and allotriomorphic-inequigranular, porphyritic-aphanitic, sericitized and kaolinized, quartz latite and quartz trachyte (non-aligned). This unit occurs as a sill within the Sawatch Quartzite west of Weston Pass (about nine meters thick) and east of Weston Peak (about three meters thick). The unit is believed to be upper Tertiary (Tweto, 1968).

A dike of Rhyolite Porphyry (?) of late Tertiary or early Quaternary age (Tweto, 1968), appears to have been localized along the Weston fault, cutting the Leadville

Formation about five kilometers (three miles) southeast of Weston Pass. This intrusive is a light gray holocrystalline hypidiomorphic-inequigranular porphyritic-aphanitic kaolinized rhyolite. Covered contacts prevent thickness determination.

A plug of what appears to be rhyolite porphyry occurs in the Precambrian about 2.5 kilometers (1.5 miles) southeast of South Peak, and a dike of the same (?) rock occurs in the Precambrian approximately the same distance southeast of Weston Peak. Porphyry intrusions in general are thought related to the dominant northwest fault trends (Stark and others, 1949).

Pleistocene till covers much of the ground between Weston Pass and South Peak, and glacial materials form lateral and terminal moraines near the mouths of gulches south of the pass. The most recent units are landslides, alluvium, and talus.

Structure and Structural History

The earliest structural event recognized in the study area is the Boulder Creek orogeny, approximately 1.7 billion years ago, which deformed detrital sediments and interbedded basalts. Intrusion of Trout Creek augen gneiss accompanied deformation. About 1.4 billion years ago the Silver Plume-Type granite intruded the area, causing further metamorphism and extensive migmatization. Shear zones trending N55E and N65W developed during the Precambrian in a region that would

later become the Colorado mineral belt (Tweto and Sims, 1963). A major Precambrian fault trend was N75W to N30W (Badgley, 1960). In Horseshoe Amphitheater, three kilometers (two miles) north of the study area, Precambrian sills, dikes, and foliation planes trend N29W and N14W (Bloom, 1965). The two strongest foliation directions within the study area are N10W to N20E and N70W to N80E. The only joint orientation unique to the Precambrian in the study area is N5W to N10W. The orientations of these features indicate compressive stresses oriented N80E to east.

During the early Paleozoic, occasional epeirogenic uplifts occurred throughout central Colorado, which for the most part was relatively stable. The Front Range Uplift began in Late Devonian, and an uplifted area must have been located north of South Park, contributing coarse detritus to the Parting sea. Uplift in Early Mississippian provided the basal limestone conglomerates of parts of the Leadville Formation (Baars, 1972). Uplift continued into Late Mississippian, exposing the formation to weathering.

Tectonic activity associated with formation of the Ancestral Front Range and Uncompahgre Uplifts was intense throughout the Pennsylvanian and Early Permian, as indicated by abrupt thickness and facies variations in Pennsylvanian and Permian rocks. The north-northwest trending Weston fault had an estimated east-side-up displacement of 1500

meters (5000 feet) during Permo-Pennsylvanian time in the Antero Reservoir Quadrangle. Active uplift decreased during the Permian, and the lack of Upper Permian to Lower Jurassic rocks indicates erosion during this period (De Voto, 1971).

The Laramide orogeny began during the Late Cretaceous, with large-scale warping producing uplifts such as the Sawatch anticline and the Front Range (Tweto, 1973). Faulting occurred (?) in Late Cretaceous and early Tertiary time. In the Mosquito Range, faulting was most intense within a six million year interval between intrusion of the Pando (70 million years) and Lincoln (64 million years) porphyries (Tweto, 1968). Laramide magma emplacement appears confined to intersections of north-south with northeast fractures, or areas where north-trending fractures are sharply bent. Melting may have been caused by a release of pressure associated with deep faulting, and magmas then localized where fracturing was extensive. Magmas may have used faults as channelways, penetrating formations and forming sills at susceptible horizons, as at the top of the Leadville.

Emmons and others (1927) believed folds and reverse faults in the Mosquito Range (Fig. 25) were developed by compression in an east-northeast to east direction. Badgley (1960) found the principal Laramide stress in this area oriented approximately N84E. A structural analysis by Bloom (1965) indicated compression along two axes, N55E and N80W. A dominant

N20W to N30W fault trend developed as a result of these stresses, with variations usually caused by a strong pre-existing Precambrian fabric. The chief Laramide longitudinal joint direction in the Mosquito Range is N20W, and an east-west cross-joint direction is common. Shear joints trending N57E and N65W are a direct result of the N84E stress direction. These shear joint directions are also the major trend of mineralized veins and faults. Major Laramide joint trends within the present study area are (1) N55W to N65W, which coincides with reactivated Precambrian faults and shears, and (2) N35E to N45E, a Laramide shear joint indicating a N80E stress direction.

Erosion occurred in central Colorado from mid- to late Eocene. The Buffalo Peaks andesites, tuffs, and lahars were extruded in early Oligocene, as was the major portion of the Thirtynine Mile volcanic field. Erosion continued in South Park through early Miocene.

Graben downfaulting of the upper Arkansas River Valley began around early Oligocene time. Although local Cenozoic structures followed late Paleozoic and Laramide trends, the tectonic framework of the upper Arkansas Valley, an _en echelon_ segment of the Rio Grande rift zone, is indicative of taphrogeny, or crustal extension (Knepper, 1974). Faults in the upper Arkansas graben show decreasing Laramide movement from west to east, become increasingly complex, and normal faults steepen progressively eastward until they are high-angle reverse

faults upthrust to the east along the crest of the Mosquito Range. Chapin (1971) proposed rifting may result from continental crust drifting at varying rates over a mantle blister. Several workers have expressed the opinion that these faults are currently active. Tweto (1961) noted faults parallel to the valley axis have displaced Pleistocene gravel and stream deposits, with displacement down toward the valley center. Knepper (1974) describes photolineaments in Pleistocene gravels suggestive of recent faulting in the upper Arkansas valley. Recent movement is suggested on that portion of the Weston fault at Weston Pass, where a prominent topographic break (approximately six meters) extends approximately one kilometer (1/2 mile) north of the pass in an otherwise glacially smoothed terrain.

The main structural feature north and south of Weston Pass is the Weston fault zone, one or more subparallel reverse faults dipping approximately sixty degrees to the east and cutting the common limb of an anticlinal-synclinal fold. This fault, upthrown to the east, bifurcates immediately south of the pass and extends south of the study area as a steplike fault zone. Beds between the two fault segments have been deformed into an S-shaped fold .
At the pass the fold is constricted,
with subsequent crumpling and tight folding of Paleozoic strata in the synclinal portion of the fold. Emmons (1886) estimated the Weston fault had a displacement of 1070 meters

(3500 feet) at Weston Pass. Behre (1932) calculated at least 386 meters (1265 feet) of displacement, and Tweto (1968) described the fault as near vertical, locally normal and locally reverse, with the west side downdropped 915 to 1525 meters (3000-5000 feet). The cross-section of the pass area (cross section B) indicates a stratigraphic separation on the order of 400 meters (1200 feet). Separation along the parallel branches of the Weston fault about five kilometers (three miles) south of the pass is probably less than 107 meters (350 feet) for the fault cutting the Leadville, and greater than 180 meters (600 feet) for the fault juxtaposing Leadville and Precambrian rocks.

An east-northeast plunging assymetric anticline, probably fault-controlled, is located between Weston Pass and South Peak.

On the east slope of Weston Peak another reverse fault, here called the Weston Peak fault, is upthrown on the east on the order of 250 meters (800 feet), is lost in the Precambrian to the south, and appears to die out under glacial deposits near the headwaters of Twelvemile Creek

A near-vertical, east-northeast-trending, down-to-the-north fault intersects and displaces the Weston fault about one kilometer (1/2 mile) north of Weston Pass.

Faults in the study area tend to be high-angle and alternate between normal and reverse along strike and perhaps along dip.

Ore Deposits

The earliest mining in the Weston Pass district dates to 1890, and most of the activity occurred between 1902 and 1916. No more than $125,000 worth of ore was produced. After analyzing several samples of the ore, Behre (1932) believed that large-scale mining might yield three percent lead, one-half percent zinc, and a trace of silver. The Ruby mine once shipped high-grade ore assaying thirty to forty percent zinc, forty percent lead, and fifteen ounces of silver per ton.

Hypogene ore consisted of disseminated masses of pyrite and galena with minor sphalerite, and supergene ores occurred as punky or massive cerussite, anglesite, native silver, smithsonite, hemimorphite, hematite, limonite, and goethite. Gangue minerals included calcite, dolomite, quartz, and jasperoid. Late Tertiary climates favored oxidation and leaching, but Pleistocene glaciation seems to have removed much of the oxidized zone.

Hydrothermal alteration is associated with ore deposition. Alteration within porphyries includes sericitization and albitization. Intrusives become poorer in silica, lead, zinc, silver, manganese, and chromium with increasing alteration. In some cases porphyries are resilicified (Bloom, 1965).

Hydrothermal alteration halos (up to several meters in extent) in Precambrian units are generally intermediate argillic,

characterized by kaolinite, sericite, and brown and green biotite, and become increasingly sericitic (sericite-quartz-pyrite) as fissures are approached. Paleozoic sandstone and shale units show the same type of alteration; secondary silica, as cement, and limonitic pyrite pseudomorphs were found in the Parting Quartzite and in the lower Belden Formation. In addition, contact metamorphism bleached quartzites in the lower Belden Formation, and probably caused the recrystallization and alignment of micas in shales elsewhere in the formation.

Alteration in the carbonates is more diverse. Silica, possibly derived from nearby porphyries, preceded mineralization and commonly filled open spaces. Silica was often accompanied by limonite; a distinctive breccia thus altered is located within the lower 27 meters (90 feet) of the Leadville Formation at Weston Pass. Local leaching and disaggregation of dolomite, contemporaneous with porphyry intrusion, resulted in local "sanded" dolomites. Widespread recrystallization of dolomites has been attributed to solution and recrystallization, heat, and stress. Some skarn minerals, chiefly grossularite, have been observed in thin sections of altered carbonates adjacent to porphyries. Finally, dolomites themselves are thought by some to be alteration products.

The deposits at Weston Pass are epithermal. Calcite and dolomite gangue indicate a maximum temperature of formation at 300°C, and the lead-silver association indicates a maximum at about 250°C. Fluid inclusion studies show zebra stripes

formed between 200 and 300°C (Tweto, 1968). The relatively low-temperature minerals led early workers (Behre, 1932; Laughlin and Behre, 1934) to assume Weston Pass deposits are a "distant facies" of the Leadville district, since all deposits in the region were thought zoned concentrically around the Breece Hill stock at Leadville. Bloom (1965) noted there is little basis to assume all ore in the region has the same source; varying lead isotopes may indicate numerous sources. Porphyry dikes and plugs, possible sources of mineralizing solutions, were mapped in the Weston Pass area for the first time during the present study.

Controls of mineralization may include structure, stratigraphy, chemistry, and mineralogy.

Tectonic setting has been critical in the emplacement of porphyries and ore. Northeast to northwest-trending fractures, active since Precambrian, localized deposits during the Laramide orogeny, especially where northwest-trending faults cross-cut regional foliation or intersect northeast-trending faults (Badgley, 1960; Tweto and Sims, 1963).

Locally, deep-seated faults may have tapped sources of ore fluids, but contain little ore because of gouge. Auxiliary fractures served as feeder channels. Joints stained by transported iron oxides have been observed in every unit, both at outcrop and in thin section, and often reveal feeder channels (fig. 33). Deposition of ore was favored by fracture intersections (Emmons and others, 1927; Bloom, 1965). "The

Fig. 33: Limonitic alteration halo around fracture (feeder channel) in sericitized Silver Plume-Type granite at Weston Pass. For color original, see Prost (1975).

junction of two veins is universally regarded by miners as favorable to the occurrance of an ore shoot" (Lovering, 1942). Bloom (1965) noted fracturing increases as ore is approached, and ore bodies tend to form northeast-trending elongate pods. Behre (1932) remarked, however, that northeast-trending gouge-filled pre-mineral fissures had no apparent genetic relation to ore. Intrusion of dikes along faults demonstrates a structural control (plumbing system) of potential sources of ore (both magmas and magmatic fluids). Northeast fracture systems controlled jointing in the Leadville along which solution caves were developed. Karst caves formed during Late Mississippian and later collapsed,

producing extremely permeable and reactive breccias, perhaps the most important factor in ore localization (Posada, 1973). The ore at Weston Pass may also have been localized along the crest of a small plunging anticline.

Stratigraphic controls include damming of fluids at contacts, the effects of permeable or reactive horizons, and the proximity of intrusive porphyry. Ore-bearing fluids appear to have been dammed below impervious layers such as the Belden shales or porphyry sills. Permeable zones, such as karst collapse horizons, served as solution conduits, often reacting with solutions to precipitate ore. At Weston Pass, however, the horizon was silicified and is barren. The nearness of a sill above the Leadville in the Horseshoe district is considered an important factor in the stratigraphic control of ore, yet in the Jones Hill Quadrangle the porphyry apparently has had no influence on the mineralization in the Leadville Formation (Valdes, 1967).

Chemical and mineralogical features have also been variously interpreted. Limestones are more soluble, so should be more reactive to ore than dolomites (Park and MacDiarmid, 1970), yet dolomites are considered by some (Krynine and Judd, 1957) to be more porous and permeable than limestones, and therefore should be the better host. Bloom (1965) noted the recrystallized zebra stripes had greater permeability and greater tendency to be mineralized. Yet Posada (1973) remarked that rock texture had no effect on mineralization. Except

for a higher manganese content in the upper seventeen meters (55 feet), the mineralized upper and barren lower Leadville in the Horseshoe district is chemically identical (Bloom, 1965).

Contrasting observations probably result from local differences. Controlling factors noted during the present study include presence of a major fault and feeder channels, a plunging anticline, proximity of porphyries, presence of limy units, the greater permeability of recrystallized and sanded dolomites, and karst collapse breccias.

Several theories exist concerning the local origin of ore and ore solutions. Emmons (1886) originally believed ore solutions emanated from sills, but later he and others (1927) decided the ore was deposited by ascending fluids that had escaped from a deep magma during late-stage fissuring. A cupola contributing solutions that rose along the Weston fault and penetrated rock along permeable horizons was postulated by Behre (1932; 1953) as the source of deposits at Weston Pass. Tweto (oral communication, 1974) also believes mineralization is not necessarily related to porphyries, but that both ultimately share a common source. Chloride-and sulfide-rich, moderate-temperature, acidic solutions transported ore metals and deposited them as temperatures and pressures lowered and as the solution neutralized by reaction with the carbonates.

Bloom (1965) re-examined sills as a possible source and noticed the sill above the Leadville became depleted in silica,

lead, zinc, silver, manganese, and chromium as it was increasingly altered. Calculations demonstrated that the amount of metal that this sill may have contributed exceeds five times the total production of the Horseshoe district. Dilute sulfide-chloride solutions are thought to have sericitized silicates in the cooling porphyry, in the process becoming enriched in silica, iron, sodium, calcium, magnesium, and metals as chloride complexes. These moved through fractures into reactive formations and were deposited. It is noted that such solutions passing through the Belden could also be enriched in lead, zinc, copper, and silver.

Both deep and shallow magmatic sources of ores and fluids are feasible within the Weston Pass area.

After ore deposition, supergene oxidation and leaching replaced some galena with anglesite, cerussite, and native silver, dissolved sphalerite and reprecipitated smithsonite and hemimorphite, and altered pyrite to hematite, limonite, and goethite. Paragenetic relationships are indicated in figure 34.

Suggestions to prospectors include looking for (1) igneous centers, (2) major faults and related minor faults, (3) intersections of fractures with the Leadville-porphyry contact, (4) intersections of reactive units with steep-dipping N30W to N30E-trending faults, especially reverse, (5) recrystallized or zebra-striped rock, (6) sanded dolomite, (7) the upper part of the Leadville, (8) local thinning of the Leadville that may indicate karst collapse breccias, and (9) an increase in fracturing, leaching, alteration, and iron-staining.

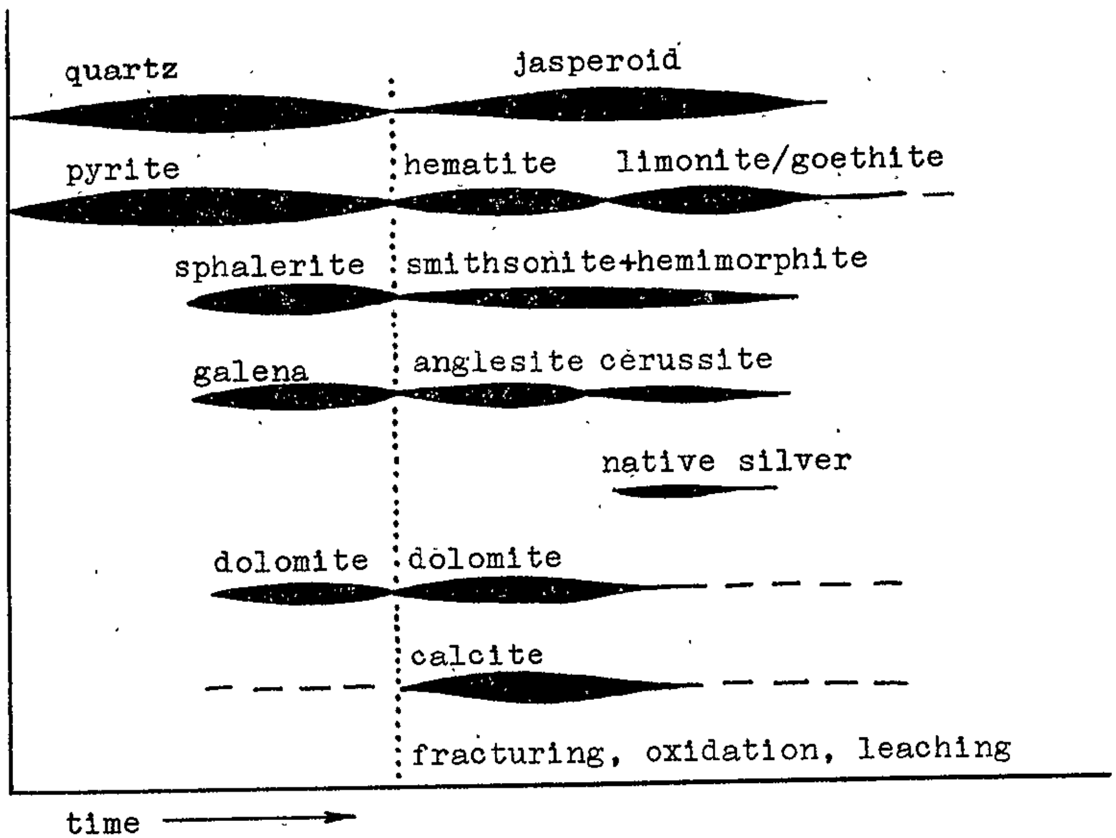

Figure 34: Paragenetic relationships of ore and gangue minerals. Based on work done by Emmons and others, 1927; Behre, 1932, 1953; Laughlin and Behre, 1934, 1947; and Bloom, 1965.

A combination of these favorable features exists one kilometer (1/2 mile) north of Weston Pass, where an east-northeast trending auxiliary fault intersects the northwest-trending Weston reverse fault. At this point the porphyry sill caps the Leadville karst, which should lie 200 to 500 meters (660-1650 feet) below the surface (fig. 35).

Another favorable area may be within the Leadville Formation east of the Weston fault. If the fault was active during Mississippian and Pennsylvanian time, and if movement was up-to-the-east, this portion of the Leadville may have been exposed to karsting. This would explain a thickness about 30 meters (100 feet) less than at Weston Pass, and would provide a permeable and reactive zone for mineralization.

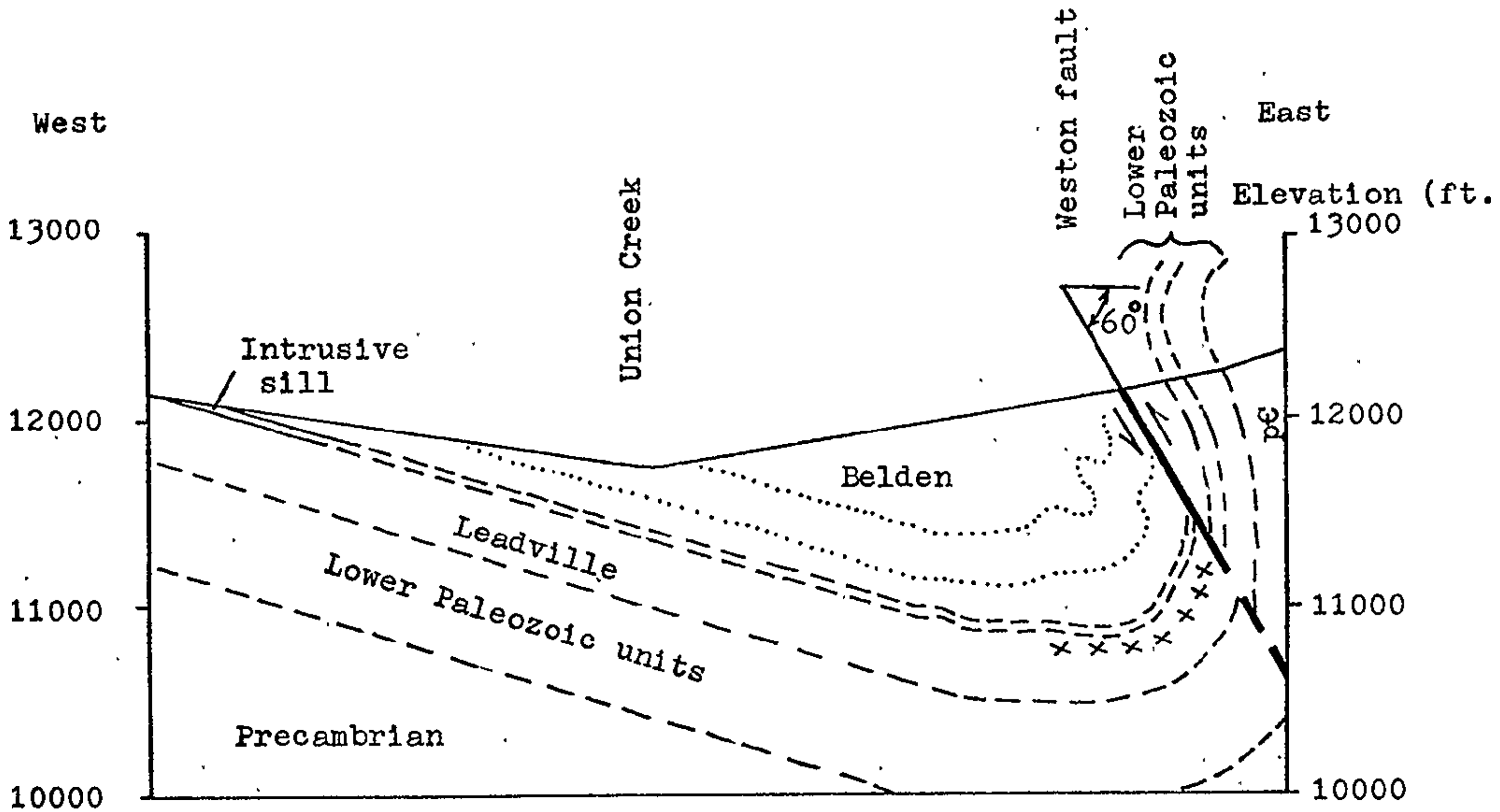

Figure 35: Cross-section along auxiliary fault located one kilometer north of Weston Pass (looking north). This area incorporates several features favorable to mineralization. "x" indicates potentially mineralized horizon. Drawn to scale (1:12,000).

TARGET EVALUATION - DOME ROCK

Indicators of Mineralization

Reconnaissance field work in the Dome Rock area indicates that linears and color anomalies mapped using Skylab 3 S190B photos (fig. 36) are generally related to geologic or geomorphic features. Linears were found to be the topographic expressions of weathering along faults, joints, lithologic contacts, and paleovalleys (R.B. Taylor, oral communication, 1974). Major linear orientations (fig. 37) do coincide with fault and fracture trends in the Precambrian Pikes Peak granite, the dominant rock in the area (D.L. Sawatzky, R.M. Hutchinson, oral comm., 1974). It has been suggested (D.L. Sawatzky, oral communication, 1974) that the fracture pattern in the study area is not unique, but rather is a local exposure of the regional basement pattern. Comparison to fracture orientation measurements throughout the region confirms this (Sawatzky, 1973; 1974).

The color anomaly in the secondary test site is caused by Pikes Peak granite and grus (fig. 38). The rock is a pink to red-brown, holocrystalline, hypidiomorphic-granular, medium to coarse-grained, seriate, biotite granite with associated aplite and pegmatite. Pink minerals compose approximately forty to sixty percent of the rock, and are dominantly microcline. The color is particularly obvious where it is vegetation-free (at Dome Rock, Balanced Rock, and Sheep Rock).

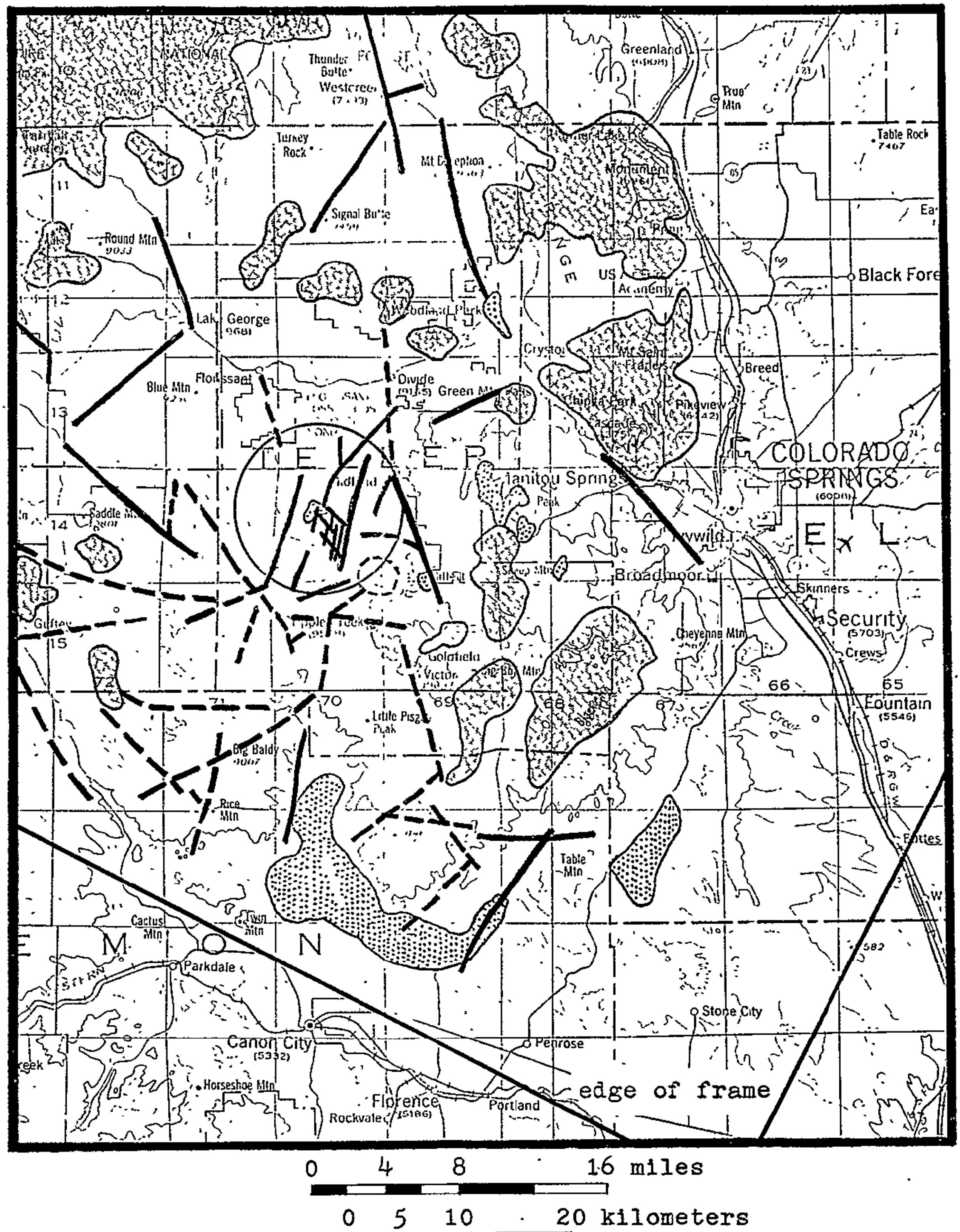

Figure 36: Linear diagram, Skylab 3 S190-B, track 48 frame 39, 4 August 1973. Study area at Dome Rock is circled.

Linears, dashed where existence questioned.

Color anomalies.

Clouds.

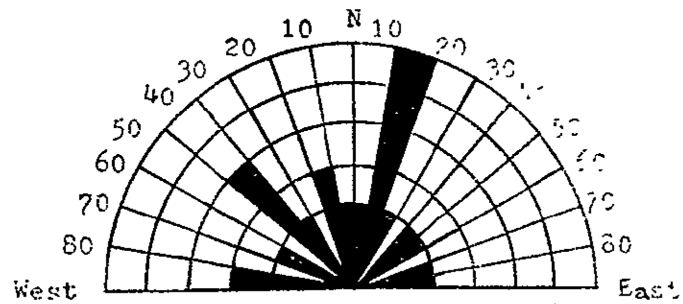

Fig. 37: Orientations of linears mapped from Skylab 3 S190-B in or immediately adjacent to the Dome Rock secondary test site. Twenty-one linears were mapped.

Ore Deposits

The main source of potentially economic minerals in the Pikes Peak batholith is pegmatite; minerals include feldspars, mica, beryl, topaz, cassiterite, and lithium minerals (Schaller, 1933; Colo. State Plan. Comm., 1960). Pegmatites are products of granite differentiation, and their positions, shape, and size are controlled by structure. Primary fractures, such as cross joints, longitudinal joints, diagonal joints, and flat-lying joints, as well as marginal fissures and fissure intersections, may be used by pegmatitic solutions escaping the magma, and may become filled with pegmatite (Landes, 1942). Intrusions of granite pegmatite into gneisses commonly parallel foliation. Pikes Peak pegmatites are in an outer zone of the batholith, about 1.6 kilometer (one mile) wide, where they were emplaced in marginal fissures that dip inward 24 to 70 degrees. Pegmatites also occur in an intermediate zone where they occupy flat-lying (sheet) joints dipping eight to 27 degrees outward (Hutchinson, 1958). These pegmatites are tabular,

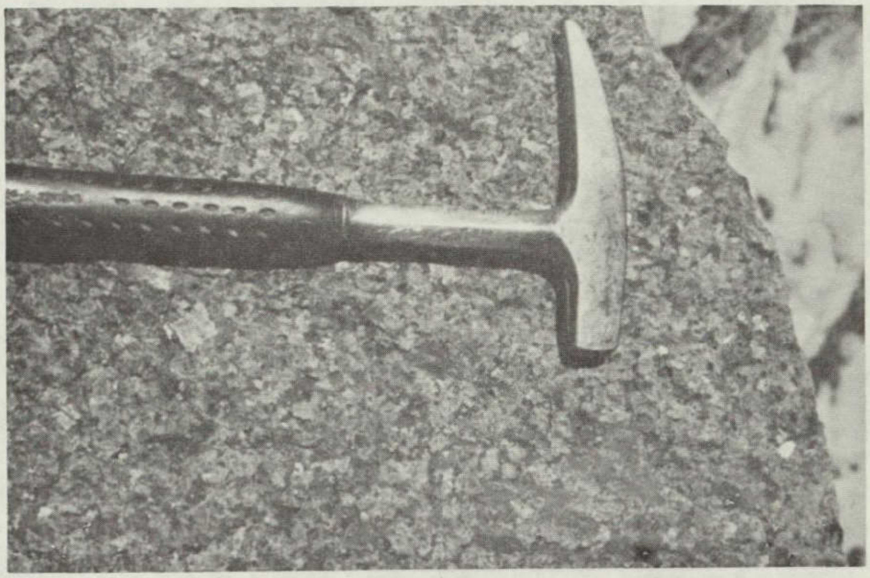

Figure 38: Pikes Peak granite. For color original, see Prost (1975

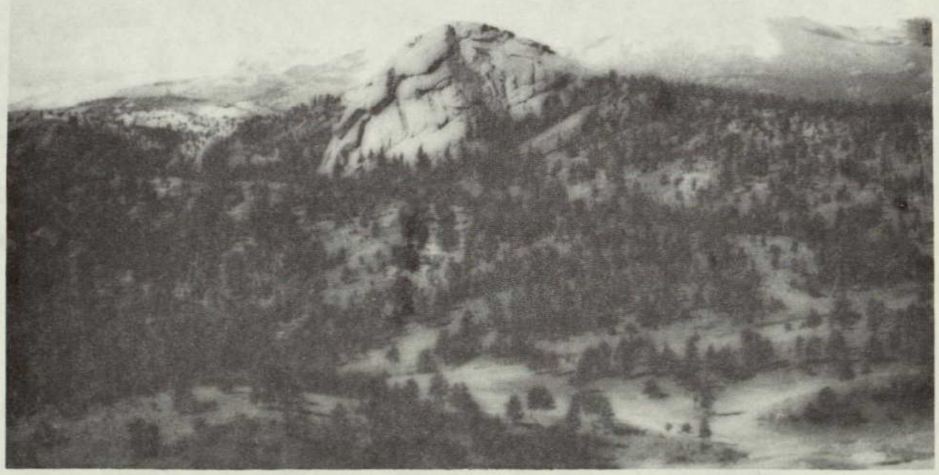

Figure 39: Dome Rock and fracture-controlled linear valleys.

lenticular, or highly irregular in shape, and range from a few meters to one kilometer (1/2 mile) in length, and up to 61 meters (200 feet) in width (Hanley and others, 1950). Pegmatites in the Pikes Peak region have been uneconomic.

Interpretation of Skylab photos identified no pegmatites, probably because they are vegetation-or soil-covered, or lack unique color or weathering characteristics.

CONCLUSIONS AND RECOMMENDATIONS

Effectiveness of Skylab in Locating Indicators of Mineralization

Of the three indicators of mineralization considered in this study - color anomalies, linear densities and intersections, and vegetation patterns - only the first two were useful in locating targets using satellite photography.

One out of four red-ocher color anomalies found in or near the two studied targets was caused exclusively by iron-oxide mineralization: one other was a combination of iron-staining and microcline-rich granite, and the other two were attributed to greater than thirty percent potassium feldspar content.

Skylab S190B photography is most effective in sensing colors, and rock colors are most visible on outcrops and vegetation-free talus, with minimal soil cover. Even under these conditions, however, all areas of red-ocher color are not obvious, and enhancement techniques such as color-additive viewing may locate some anomalies not obvious on true color photography. The inability to transmit true colors to the S190B film may be a function of indirect illumination, atmospheric haze, film, processing methods, or the number of film generations involved in the available prints and transparencies.

Thirty-two percent of the linears mapped from Skylab photos over the primary target correspond to known faults. Of the

three major linear trends in the Weston Pass area, one is directly related to joint orientations, and another results from drainages formed on dip slopes normal to a joint trend. In the Dome Rock area, only one of the eight regional joint orientations (Sawatzky, 1973; 1974) correspond well to a linear trend, although there is general agreement that the Dome Rock linears are chiefly a reflection of basement fractures.

Linears are most often expressed topographically, then by tone, color, vegetation, or cultural features. Skylab photos are effective in discriminating linear features, and the photography may be enhanced by snow, low sun angles, and stereo viewing. Techniques such as positive-negative slip masking may enhance some linears, but others become blurred and location of features becomes difficult.

Evaluation of Original Assumptions

Results of this study suggest the original assumptions are incomplete. Red-ocher colors in central Colorado may result from sedimentary red-beds, microcline-rich crystalline rock or grus, iron-oxide alteration, or combinations of these. Light color anomalies were attributed to quartz-rich pegmatites, light colored sedimentary units or talus, as well as to altered intrusives.

Linear features have been identified as aligned or straight streams, ridges, vegetation, and cultural features such as roads, fences, powerlines, and contrails, as well as geologic features

including faults, joints, shear zones, dikes, contacts, folds, and paleovalleys. Where a linear pattern is obviously structural, such as jointing in the Pikes Peak granite, what is seen may be just a local manifestation of a regional pattern, enhanced in the particular area by unique aspect angle, or weathering or erosional conditions.

Intersections and high densities of regional linears are not the only structural controls on mineralization. Regional faults with large displacement may be filled with gouge. Relatively small auxiliary fractures are often equally important. Intrusive centers, often related to "circular features," frequently supply metallizing fluids. Changes of foliation in crystalline rocks have been cited as controls on ore deposition. Identification of reactive units, such as the dolomites of central Colorado, would facilitate locating mineralized strata. Recognition that a reactive unit had been intruded would increase its prospects as a host. Many of these features, however, are not visible on satellite photos at available resolutions.

Vegetation assemblages were found to be influenced more by moisture, slope steepness and direction, season, and altitude than by composition of the substrate.

Recommendations

S190B color photography proved the most useful system and band for geologic photointerpretation. The trade-off

between areal coverage and resolution is insignificant, since large areas are still covered. The high resolution and contrast of the S190B photography are vital in discriminating and possibly identifying details of geology. Quality photography can be degraded when discrimination of regional features is desired; the reverse is not true. Color film used in taking Skylab photos over Colorado has the best resolution and contrast available, and is most familiar to the interpreter, making it easiest and fastest to use. Repetitive coverage and speedy processing and delivery are recommended.

The best format for lab work is low-generation nine-by-nine inch positive transparencies. These are large enough to permit annotation while allowing stereo interpretation. Stereo coverage is essential in enhancing topography, which often reveals geology.

The optimum format for field work is low-generation nine-by-nine inch positive prints. Prints have lower resolution and contrast than transparencies, but are more convenient to handle in the field.

The easiest and most successful photographic enhancement is optical magnification. Increased contrast, a function of film, exposure, and development, is often helpful. Color-coding and linear enhancement techniques have been of marginal value.

The best time for data acquisition over central Colorado is during the morning in autumn, or after passage of a cold front. This provides minimal snow and cloud cover, yet good shadowing. Maximum topographic enhancement by shadowing occurs in mid-winter with uniform snow cover. Repetitive coverage increases the probability of acquiring coverage under a desired set of conditions.

This study presents one practical approach to the interpretation of space photography. High resolution color photos with stereo coverage over an area of interest are obtained from NASA, and a literature study of known deposits in the area is undertaken. Geologic features associated with mining districts are noted, observed on the satellite photography, and field-checked to verify authenticity. All assumptions regarding indicators of mineralization should be thoroughly examined in light of available ground truth. The region is then scanned in search of these features. Optical enlargement is used with transparent overlays to map color anomalies, linears, or other geologic information. Targets containing several of the desired indicators are selected, and low-altitude aerial photography over each target area is obtained, if possible. These areas are then subjected to conventional photogeologic interpretation, and are re-evaluated in light of any new information. Detailed field maps are then prepared with the aid of photography and overlays.

Conclusions

Skylab photography can cover large areas quickly and inexpensively, and there are some surface features in any given region that are indicators of mineralization. Photolineaments and color anomalies may be important indicators of mineralization in central Colorado, but positive identification of these features is not possible. A thorough evaluation of assumptions and detailed field work are mandatory. Also, areas that are extensively covered by soil, vegetation, clouds, or snow, no matter how favorable, are incapable of being evaluated. Areas where orbital photography would be most useful in the search for mineral deposits include desert mountains or snow-free alpine mountains. Orbital photography in itself is considered inadequate to fulfill exploration needs. It is useful in reducing the size of an exploration area to potentially favorable targets; like other remote sensing techniques, it is a powerful tool only when used in conjunction with detailed field work.

Appendix A: Sources of Skylab Photos

All photos were received from NASA through Lyndon B. Johnson Space Flight Center, Houston, Texas.

Figure	Mission	Sensor	Photo Date	Roll (band)	Track & Frame
2	S.L. 3	Hasselblad		CX-27-122	2583
3	S.L. 3	S190A	4 Aug. 1973	19, 20, 23, 24	48; 107
4	S.L. 3	S190B	4 Aug. 1973	83	48; 38
11	S.L. 3	S190A	4 Aug. 1973	23	48; 107
12	S.L. 2	S190A	11 June 1973	13, 14, 17	48; 17
13	S.L. 3	S190A	4 Aug. 1973	21, 22, 23, 24	48; 107
17	S.L. 3	S190B	4 Aug. 1973	83	48; 107, 108
40	S.L. 3	S190B	4 Aug. 1973	83	48; 107
41	S.L. 3	S190B	4 Aug. 1973	83	48; 108

Appendix B: Annotated Photos

Figure 40 is a photo of the Leadville region enlarged from Skylab 3 S190B. Geologic annotation may be correlated to Tweto (1972; 1974). Shown on this photo are faults (heavy solid lines), intrusive porphyry sills (outlined and labeled P), and red-ocher color anomalies (outlined and labeled R). Leadville is labeled L. The scale is approximately 1:300,000.

Figure 41 is a photo of the Cripple Creek district enlarged from Skylab 3 S190B. Annotation may be correlated to Koschmann (1949). Shown on this photo are fractures (heavy solid lines), red-ocher color anomalies (continuous outline, labeled R), and the Cripple Creek basin (dotted outline). Cripple Creek is labeled C, Victor is labeled V, and the Carleton gold mill is labeled M. Scale is approximately 1:150,000.

These figures are meant to show that geology can be correlated between geologic maps and satellite photographic features.

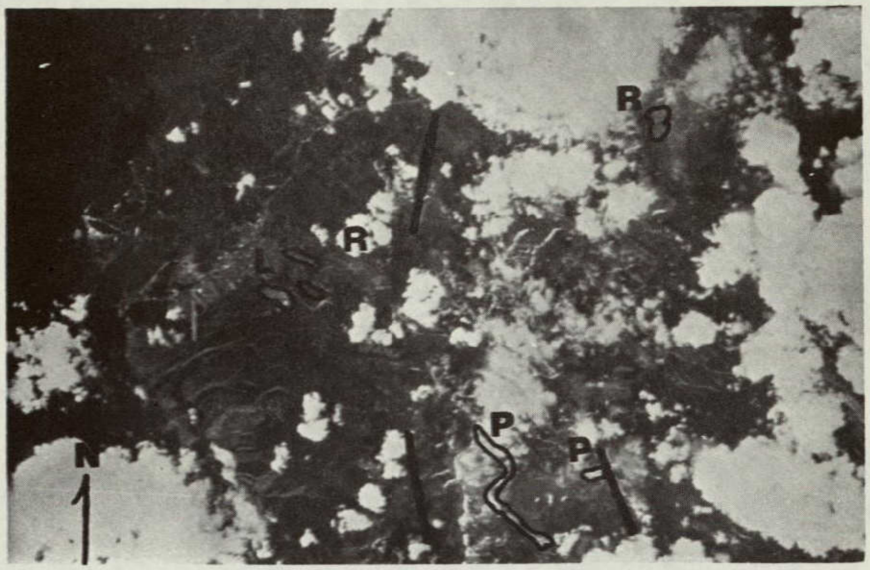

Figure 40: Annotated photo of the Leadville district. For color original, see Prost (1975).

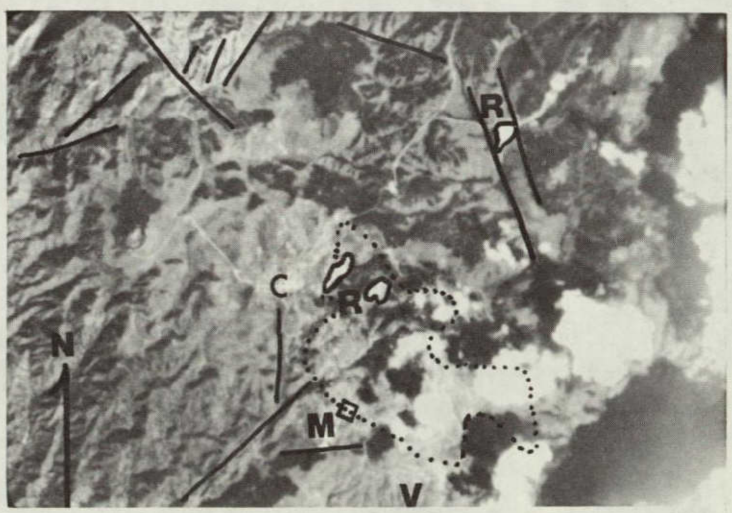

Figure 41: Annotated photo of the Cripple Creek district. For color original, see Prost (1975).

Appendix C

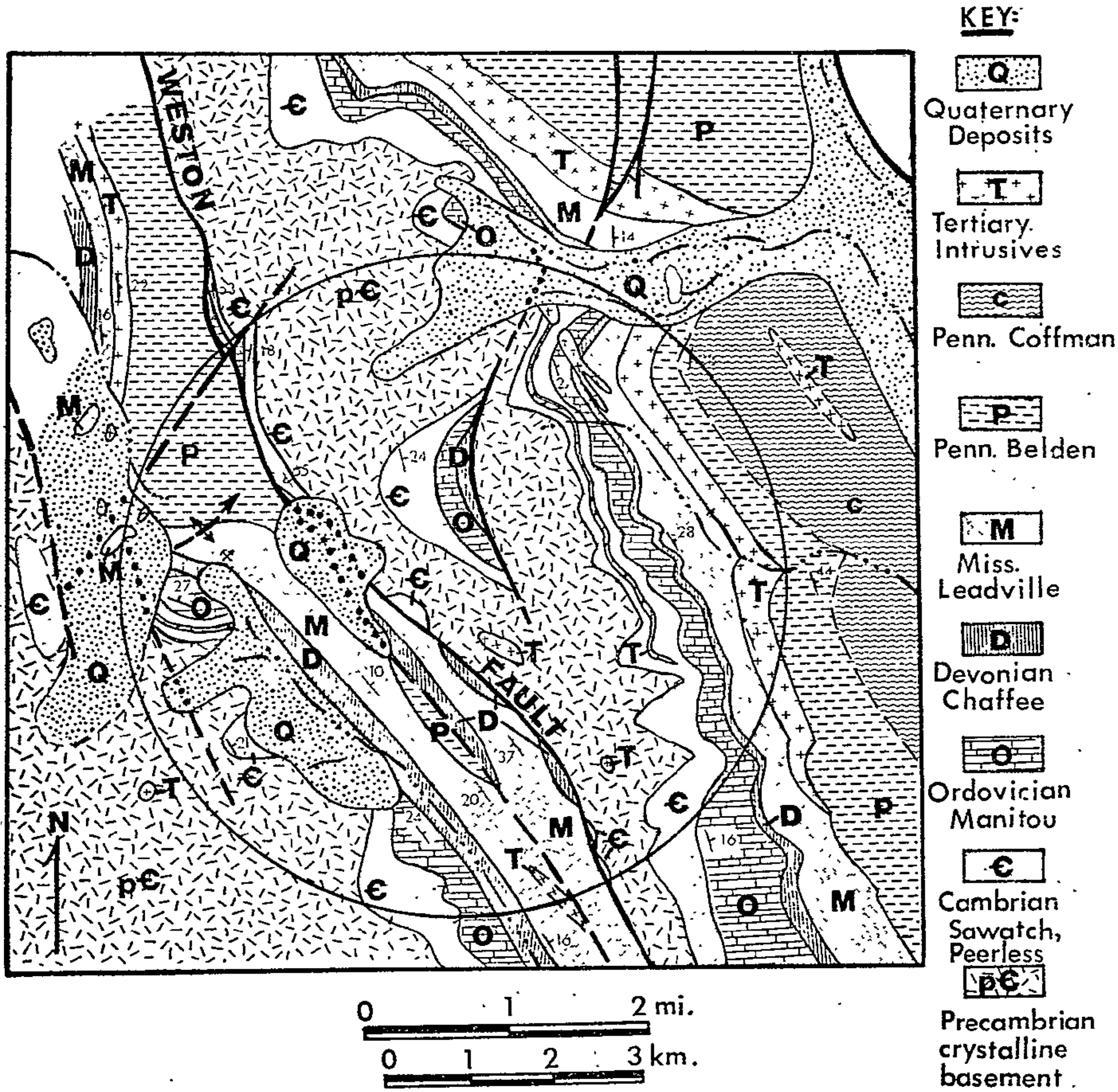

Simplified Geologic Map, Weston Pass Area. Study area circled.

REFERENCES

Awald, J.T., 1974, A technology to renovate the search for new mineral deposits: Photog. Eng., v. 40, p. 1173-1186.

Baars, D.L., 1972, Pre-Pennsylvanian paleotectonic framework of the ancestral Rockies of Colorado (abs.), in De Voto, R.H., (ed.), Paleozoic stratigraphy and structural evolution of Colorado: Mines Quart., v. 67, no. 4, p. 137.

Badgley, P.C., 1960, Tectonic relationships in central Colorado, in Weimer, R.J., and Haun, J.D., (eds.), Guide to the geology of Colorado: Geol. Soc. America, Rocky Mtn. Assoc. Geol., Colorado Sci. Soc., p. 165-169.

Barnes, F.F., 1935, Precambrian rocks of the Sawatch Range, Colorado: Colorado Sci. Soc. Proc., v. 13, no. 8, p. 467-480.

Behre, C.H., 1932, Weston Pass mining district, Lake and Park Counties, Colorado: Colorado Sci. Soc. Proc., v. 13, no. 3, p. 53-75.

______ 1953, Geology and ore deposits of the west slope of the Mosquito Range: U.S. Geol. Survey Prof. Paper 235, 176 p.

Billings, M.P., 1972, Structural geology: Englewood Cliffs, Prentice-Hall, 606 p.

Blanchard, Roland, 1968, Interpretation of leached outcrops: Nevada Bur. Mines, Bull. 66, p. 89-91.

Bloom, D.N., 1965, Geology of the Horseshoe district and ore deposits of the Hilltop mine, Park County, Colorado: Colorado School of Mines PhD. dissertation, T-1019, 211 p.

Brill, K.G., Jr., 1952, Stratigraphy in the Permo-Pennsylvanian zeugogeosyncline of Colorado and northern New Mexico: Geol. Soc. America Bull., v. 63, p. 809-880.

Brooks, R.R., 1972, Geobotany and biogeochemistry in mineral exploration: New York, Harper and Row, 290 p.

Bruns, D.L., 1972, Research activities, in Reeves, R.G. (ed.), Applications of remote sensor data to geologic and economic analysis of the Bonanza test site, Colorado: Colorado School Mines Remote Sensing Rept. 72-4, p. B1-B7.

______ 1974, Reconnaissance geology of the South Peak and Mount Sherman quadrangles: unpub., 1:24,000.

Burbank, W.S., 1941, Structural control of ore deposition in the Red Mountain, Sneffels, and Telluride districts of the San Juan Mountains, Colorado: Colorado Sci. Soc. Proc., v. 14, no. 5, p. 148-161.

Butler, B.S., 1942, Some inter-relations of structure, mineralogy, and associations with intrusive bodies in ore deposits, in Newhouse, W.H. (ed.), Ore Deposits as Related to Structural Features, p. 3-5.

Canney, F.C., 1969, Remote detection of geochemical soil anomalies, in Second Annual Earth Resources Aircraft Program Status Review: NASA, v. 1, p. 7-1 to 7-8.

Cannon, H.L., 1960, Botannical prospecting for ore deposits: Science, v. 132, p. 591-598.

_______ 1971, The use of plant indicators in ground water surveys, geologic mapping, and mineral prospecting: Taxon, v. 20, p. 227-256.

Carlisle, Donald, and Cleveland, G.B., 1958, Plants as a guide to mineralization: California Div. Mines Spec. Rept. 50, 31 p.

Chapin, C.E., 1971, The Rio Grande Rift, Part 1: modifications and additions, in James, H.L. (ed.), Guidebook of the New Mexico Geol. Soc., p. 191-201.

Chronic, John, 1964, Geology of the southern Mosquito Range, Colorado: Mountain Geologist, v. 1, no. 3, p. 103-113.

Colorado State Planning Commission, 1960, Teller County, in Mineral Resources of Colorado: p. 296-300.

De Voto, R.H., 1961, Geology of southwestern South Park, Park and Chaffee Counties, Colorado: Colorado School Mines PhD. dissertation, 323 p.

_______ 1971, Geologic history of South Park and geology of the Antero Reservoir Quadrangle, Colorado: Mines Quart., v. 66, 90 p.

_______ 1972, Pennsylvanian and Permian stratigraphy and tectonism in central Colorado: Mines Quart., v. 67, no. 4, p. 139-185.

Eardley, A.J., 1962, Structural geology of North America: New York, Harper and Row, 743 p.

Edwards, Jonathan, Jr., 1966, Petrology and structure of the buried Precambrian basement of Colorado: Mines Quart., v. 61, no. 4, 436 p.

Emmons, S.F., 1886, Geology and mining industry of Leadville, Colorado: U.S. Geol. Survey Mon. 12, 770 p.

Emmons, S.F., Irving, J.D., and Laughlin, G.F., 1927, Geology and ore deposits of the Leadville mining district, Colorado: U.S. Geol. Survey Prof. Paper 148, 368 p.

Epis, R.C., 1968, Cenozoic volcanism in the southern Rocky Mountains: Mines Quart., v. 63, no. 3, 287 p.

Gould, D.B., 1935, Stratigraphy and structure of Pennsylvanian and Permian rocks in the Salt Creek area, Mosquito Range, Colorado: Am. Assoc. Petroleum Geologists Bull., v. 19, no. 7, p. 971-1004.

Greaves, J.R., Sherr, P.E., and Glaser, A.H., 1970, Cloud cover statistics and their use in the planning of remote sensing missions: Remote Sensing Environ., v. 1, p. 95-101.

Hanley, J.B., Heinrich, E.W., and Page, L.R., 1950, Pegmatite investigations in central Colorado, Wyoming, and Utah, 1942-1944: U.S. Geol. Survey Prof. Paper 227, 125 p.

Howard, J.A., Watson, R.D., and Hessin, T.D., 1971, Spectral reflectance properties of Pinus Ponderosa in relation to copper content in the soil - Malachite mine, Jefferson County, Colorado: Remote Sens. Environ. Proc., 7th, Ann Arbor, p. 285-298.

Hutchinson, R.M., 1956, Structure and petrology of the Enchanted Rock batholith, Llano and Gillespie Counties, Texas: Geol. Soc. America Bull., v. 67, p. 763-806.

__________, 1958, Structure and petrology of northernmost end of Pikes Peak batholith, Jefferson and Douglas Counties, Colorado (abs.): Geol. Soc. America Bull., v. 69, no. 12, p. 1731.

Hyndman, D.W., 1972, Petrology of igneous and metamorphic rocks: New York, McGraw-Hill, 533 p.

Jackson, K.C., 1970, Textbook of lithology: New York, McGraw-Hill, 553 p.

Janda, R.J., 1971, Evaluation of light intensity differences on color aerial photographs and thermal infrared imagery for the Ozette Island - Cape Alava area of the Olympic Coast of western Washington: U.S. Geol. Survey Interagency Rept., USGS-187, 34 p.

Johnson, J.H., 1934, Paleozoic formations of the Mosquito Range, Colorado: U.S. Geol. Survey Prof. Paper 185-B, p. 15-33.

Knepper, D.H. (ed.), 1973, Geologic and mineral and water resources investigations in western Colorado using ERTS-1 data: Progress report 9: Colorado School Mines Remote Sensing Rept. 73-5, 53 p.

__________, 1974, Tectonic analysis of the Rio Grande Rift Zone, central Colorado: Colorado School Mines Ph.D. dissertation, T-1593, 237 p.

Koschmann, A.H., 1949, Structural control of the gold deposits of the Cripple Creek district, Teller County, Colorado: U.S. Geol. Survey Bull. 955-B, p. 387-395.

__________, 1960, Cripple Creek district, in Weimer, R.J. and Haun, J.D. (eds.), Guide to the Geology of Colorado: Geol. Soc. America, Rocky Mtn. Assoc. Geol., Colorado Sci. Soc., p. 185-188.

__________, 1960, Cripple Creek district, Teller County, in Colorado State Planning Commission, Mineral Resources of Colorado: p. 387-395.

Krynine, D.P., and Judd, W.R., 1957, Principles of engineering geology and geotechnics: New York, McGraw-Hill, 730 p.

Landes, K.K., 1942, Effects of structure on intrusion of pegmatites, in Ore deposits as related to structural features, Newhouse, W.H. (ed.), p. 140-143.

Laughlin, G.F., and Behre, C.H., 1934, Zoning of ore deposits in and adjoining the Leadville district, Colorado: Econ. Geology, v. 29, no. 3, p. 215-224.

__________, 1947, Leadville mining district, Lake County, Colorado in Vanderwilt J.W. (ed.), Mineral resources of Colorado, p. 350-370.

Lee, Keenan (ed.), 1972, Application of remote sensor data to geologic analysis of the Bonanza test site, Colorado; Semi-annual progress report: Colorado School Mines Remote Sensing Rept. 72-7, 34 p.

__________, 1973, Application of remote sensor data to geologic analysis of the Bonanza test site, Colorado; Semi-annual progress report: Colorado School Mines Remote Sensing Rept. 73-2, 51 p.

__________, 1974, Geologic and mineral and water resources investigations in western Colorado using Skylab EREP data; Monthly progress reports: Colorado School Mines Remote Sensing Rept. 74-6, 60 p.

Lee, Keenan, Knepper, D.H., and Sawatzky, D.L., 1974, Geologic information from satellite images: Colorado School Mines Remote Sensing Rept. 74-3, 37 p.

Lovering, T.S., 1942, Physical factors in the localization of ore, in Newhouse, W.H. (ed.), Ore deposits as related to structural features, p. 5-9.

Nadeau, J.E., 1972, Mississippian stratigraphy of central Colorado, in De Voto, R.H. (ed.), Paleozoic stratigraphy and structural evolution of Colorado: Mines Quart., v. 67, no. 4, p. 77-102.

NASA-JSC, 1973, EREP investigators' information book: Houston, L.B.J. Space Center, Rept. MSC-07874.

__________, 1974, Skylab EREP principal investigators data meeting: Houston, L.B.J. Space Center, 182 p.

Nicolais, S.M., 1974, Mineral exploration with ERTS imagery, in Third Earth Resource Technology Satellite-1 Symposium, v. 1, Sec. B, Goddard Space Flight Center, Washington, D.C., p. 785-796.

Niggli, Paul, 1954, Rocks and mineral deposits: San Francisco, W.H. Freeman.

Park, C.F., and MacDiarmid, R.A., 1970, Ore deposits: San Francisco, W.H. Freman, 522 p.

Pearson, R.C., Tweto, O.L., Stern, T.W., and Thomas, H.H., 1962, Age of Laramide porphyries near Leadville, Colorado: U.S. Geol. Survey Prof. Paper 450-C, p. C78-C80.

Posada, J.H., 1973, Karst related features and controls on ore mineralization in the Leadville Formation, central Colorado: Colorado School Mines MSc. thesis, T-1568, 107 p.

Potter, A.E., et al., 1974, Summary of flight performance of the Skylab Earth Resource Experiment Package (EREP): NASA-JSC, Houston, 44 p.

Prost, G.L., 1975, Evaluation of Skylab photography for locating indicators of mineralization: Colorado School Mines MSc. thesis, T-1736, 111 p.

Raines, G.L., and Lee, Keenan, 1975 In Situ rock reflectance: Photog. Eng., v. 41, no. 2, p. 189-198.

Reuss, R.L., 1974, Precambrian quartzite-schist sequence in Wilson Park, Fremont County, Colorado: Mountain Geologist, v. 11, no. 2, p. 45-58.

Rosenberg, Paul, 1971, Resolution, detectability, and recognizability: Photog. Eng., v. 37, no. 12, p. 1255-1258.

Ross, D.S., 1969, Image-tone enhancement: American Soc. Photogram. Ann. Mtg., Washingotn, D.C., 19 p.

Sage, R.P., 1966, Geology and mineralogy of the Cripple Creek syenite stock, Teller County, Colorado: Colorado School Mines MSc. thesis T-1066, 236 p.

Sawatzky, D.L., 1973, Photolinears, in Knepper, D.H. (ed.) Geologic and mineral and water resource investigations in western Colorado using ERTS-1 data; Progress Rept. 9: Colorado School Mines Remote Sensing Rept. 73-5, p. 9-14.

_____________, 1974, Geologic structures, in Lee, Keenan (ed.), Geologic and mineral and water resource investigations in western Colorado using Skylab EREP data: Colorado School Mines Remote Sensing Rept. 74-6, p. 18-27.

Sawatzky, D.L., and Lee, Keenan, 1974, New uses of shadow enhancement: Colorado School Mines Remote Sensing Rept. 74-5, 18 p.

Schaller, W.T., 1933, Pegmatites, in Lindgren volume, Ore deposits of the United States: New York, American Institute of Mining, Metallurgical, and Petroleum Engineers, p. 144-151.

Schwarz, F.P., 1967, Geology and ore deposits of Minnie Gulch, San Juan County, Colorado: Colorado School Mines MSc. thesis, T-1115, p. 93-103.

Stark, J.T., 1934, Reverse faulting in the Sawatch Range: Geol. Soc. America Bull., v. 45, p. 1001-1016.

Stark, J.T., and Barnes, F.F., 1935, Geology of the Sawatch Range, Colorado: Colorado Sci. Soc. Proc., v. 13, p. 468-479.

Stark, J.T., et al., 1949, Geology and origin of South Park, Colorado: Geol. Soc. America Mem. 33, 188 p.

Sweeting, M.M., 1973, Karst landforms: Columbia Univ. Press, 362 p.

Taylor, R.B., 1973, Upper Tertiary tectonism and deposits in south-central Colorado (abs.): Geol. Soc. America Abstracts with Programs, p. 518-519.

Tweto, O.L., 1961, Late Cenozoic events of the Leadville district and upper Arkansas Valley, Colorado: U.S. Geol. Survey Prof. Paper 424-B, p. B133-B135.

__________, 1968, Geologic setting and interrelationships of mineral deposits in the mountain province of Colorado and south-central Wyoming, in Graton-Sales volume, Ore deposits of the United States: New York, American Institute of Mining, Metallurgical, and Petroleum Engineers, p. 551-558.

__________, 1968, Leadville district, Colorado, in Graton-Sales volume, Ore deposits of the United States: New York, American Institute of Mining, Metallurgical, and Petroleum Engineers, p. 681-705.

__________, 1973, Summary of Laramide orogeny in the southern Rocky Mountains (abs.): Geol. Soc. America Abstracts with Programs, p. 521.

__________, 1974, Reconnaissance geologic map of the Fairplay West, Mount Sherman, South Peak, and Jones Hill 7 1/2-minute quadrangles, Park, Lake, and Chaffee Counties, Colorado: U.S. Geol. Survey map MF-555, 1:62,500.

Tweto, O.L., and Case, J.F., 1972, Gravity and Magnetic features as related to geology in the Leadville 30-minute quadrangle: U.S. Geol. Survey Prof. Paper 726-C, 31 p., map 1:125,000.

Tweto, O.L., and Pearson, R.C., 1964, Saint Kevin granite, Sawatch Range, Colorado: U.S. Geol. Survey Prof. Paper 475-D, p. D28-D32.

Tweto, O.L., and Sims, P.K., 1963, Precambrian ancestry of the Colorado mineral belt: Geol. Soc. America Bull., v. 74, p. 991-1014.

U.S. Dept. Commerce (Weather Bureau), 1968, Climatic atlas of the United States: p. 71-72.

Valdes, G.E., 1967, Geology of the Jone Hill quadrangle, South Park, Park County, Colorado: Colorado School Mines MSc. thesis T-1140, p. 13-63.

Vanderwilt, J.W. (ed.), 1947, Mineral resources of Colorado: Denver, Colorado Mining Association, 547 p.

Weber, W.A., 1972, Rocky Mountain flora: Colorado Assoc. Univ. Press, 438 p.

Yost, Edward, 1971, The reflectance spectra of mineralized trees, in Remote Sens. Environ. Proc., 7th, Ann Arbor, p. 269.

PLATE 1: ERTS frames 1407-17190 and 1424-17125, taken Sept., 1973. Band 5 (red).

PLATE 2: Skylab 2 S190A, track 48 frame 17, 11 June 1973. True color.

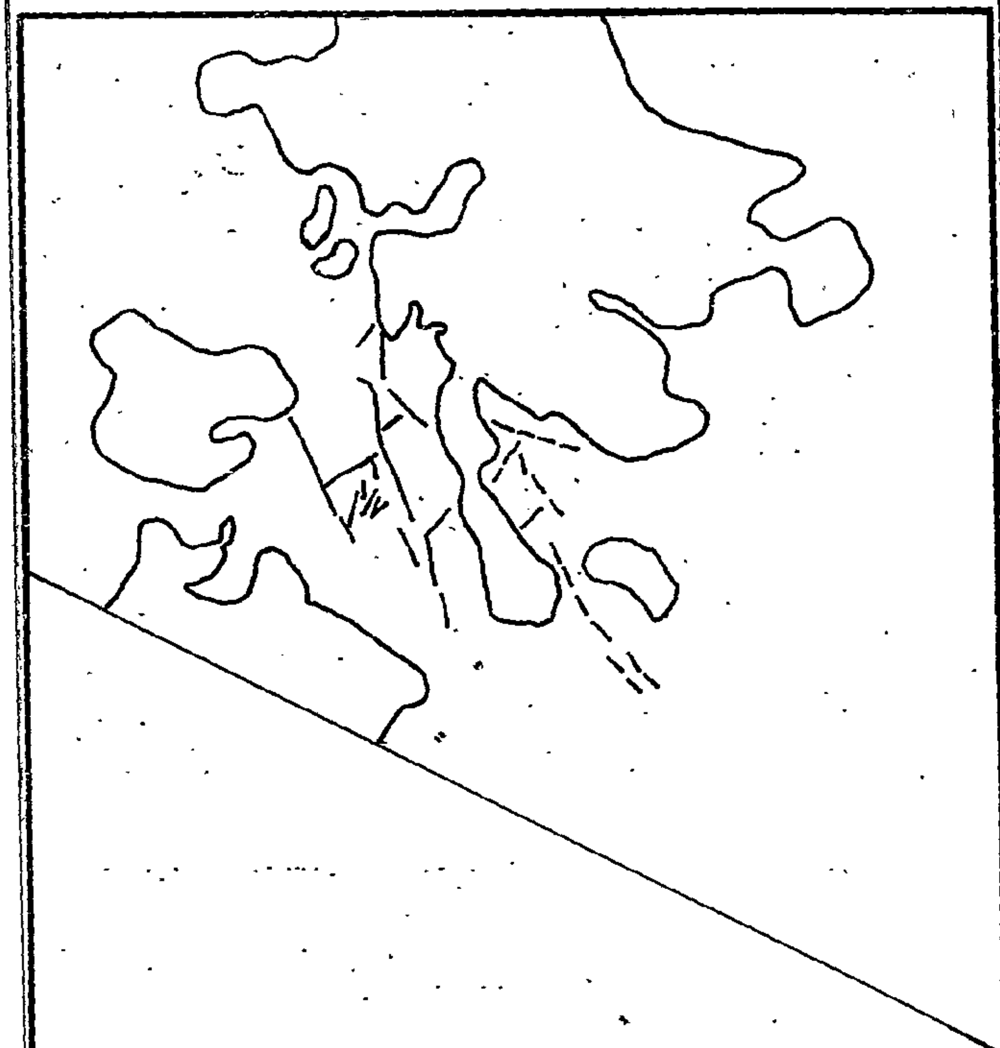

PLATE 3: Skylab 3 S190A, track 48 frames 106 and 107, 4 Aug. 1973. True color.

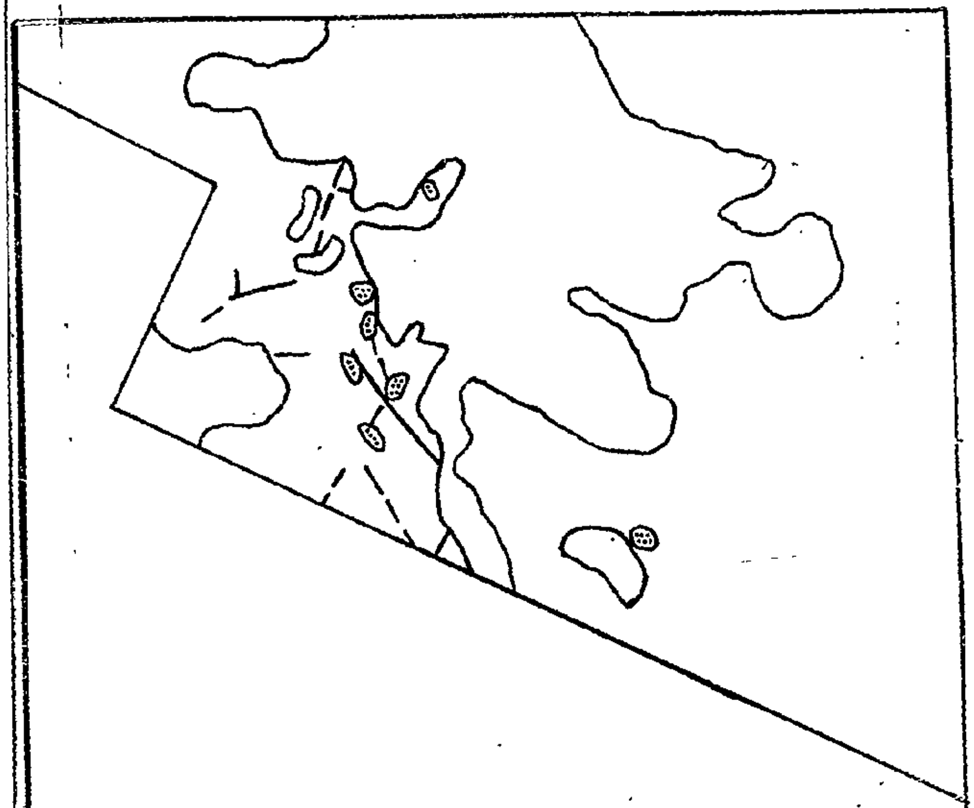

PLATE 4: Skylab 3 S190B, track 48 frame 38.
4 Aug. 1973. True color.

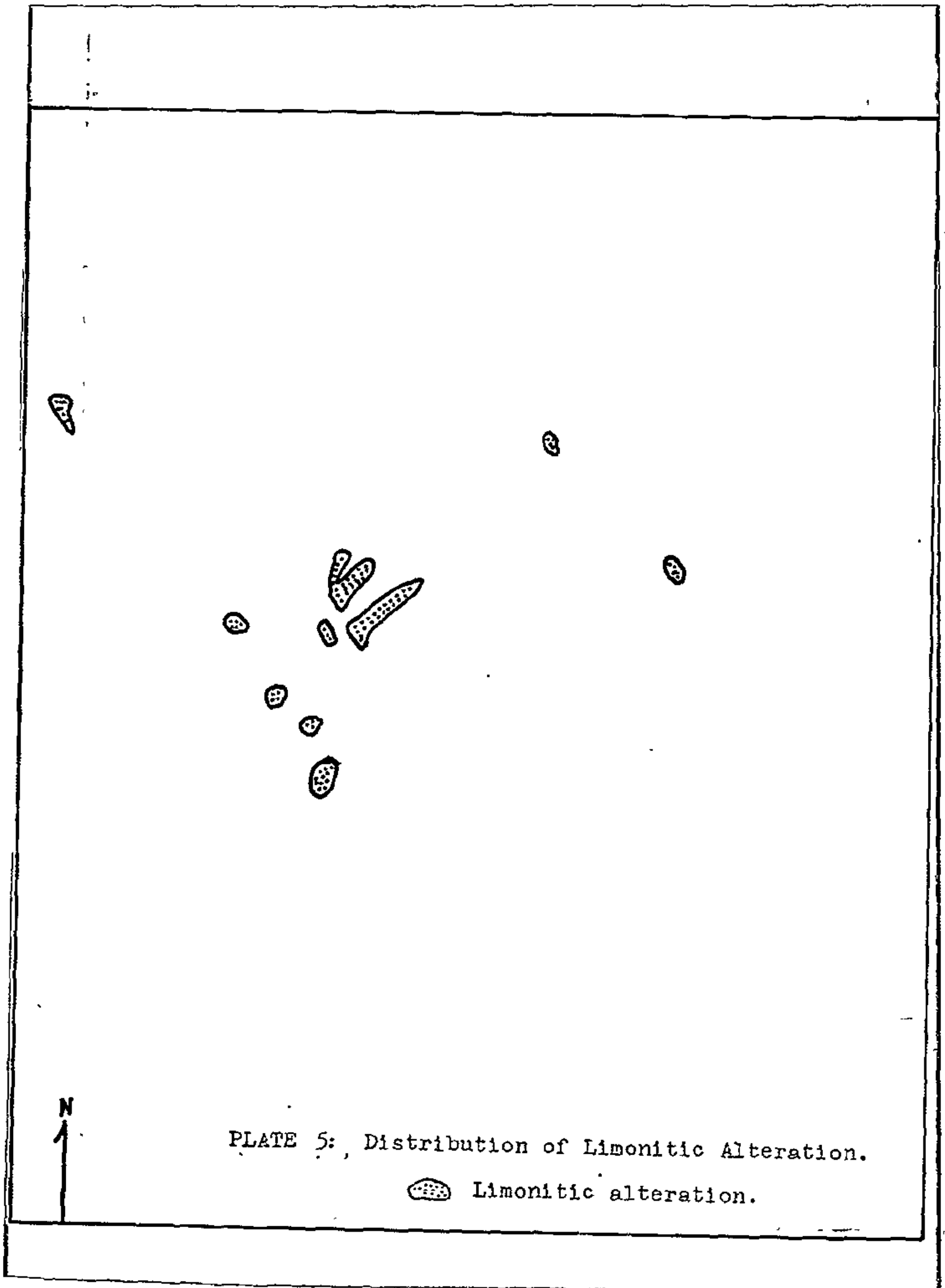

PLATE 5: Distribution of Limonitic Alteration.

Limonitic alteration.

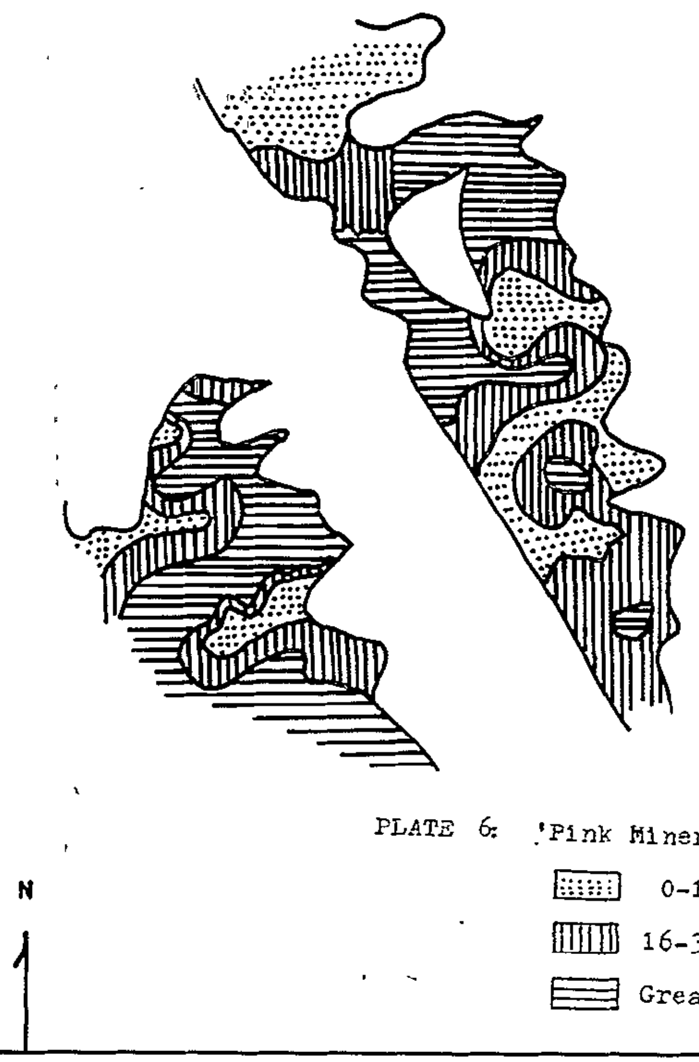

PLATE 6. 'Pink Mineral' Distribution.

0-15%

16-30%

Greater than 30%


D
R

PRINT
MADE
BY
KODAK

Kodak

JUNE [illegible]

EVALUATION OF SKYLAB PHOTOGRAPHY

FOR

WATER RESOURCES

SAN LUIS VALLEY, COLORADO

by

David Huntley

Remote Sensing Report 75-5

EREP Investigations 380

Contract NAS9-13394

National Aeronautics and Space Administration

C.5

December 1975

REMOTE SENSING PROJECTS

DEPARTMENT OF GEOLOGY

COLORADO SCHOOL OF MINES GOLDEN, COLORADO

EVALUATION OF SKYLAB PHOTOGRAPHY

FOR

WATER RESOURCES

SAN LUIS VALLEY, COLORADO

by

David Huntley

Remote Sensing Report 75-5

Remote Sensing Projects
Department of Geology
Colorado School of Mines
Golden, Colorado

NASA Contract NAS9-13394

National Aeronautics and Space Administration

Approved for Publication: ______________________
Keenan Lee
Principal Investigator

December 1975

ABSTRACT

Skylab S190-A and S190-B photography, covering the northern closed basin of San Luis Valley, Colorado, was evaluated with respect to regional water resource studies. Resolution is the most important factor limiting the photography in its use for mapping of surface drainages and hydrologically significant rock units and geologic structures. At the regional level, S190-A stereo photography is sufficient for defining drainage divides and patterns, but is insufficient for hydrogeologic mapping. S190-B photography has adequate resolution to map the hydrogeology in some cases, but aircraft photography is a necessity for most studies and field work is a necessity for all studies, even at the regional level.

Studies of the distribution of vegetation type and saline soils suggest correlation with ground water depth. Narrowleaf cottonwood (*Populus angustifolia*) trees and willow (*Salix* spp.) are found where saturated sediments are present within five meters of the ground surface. The distribution of these two vegetation types is best mapped on color-infrared photography. Saline soils are present where the ground water is simultaneously shallow, of relatively high salinity, and potential (head) increases with depth.

Laboratory and field reflectance measurements suggest that band ratioing would not aid in discriminating between moist and dry non-saline soils, but the technique may aid in discriminating saline from non-saline soils.

CONTENTS

FIGURES

TABLES

INTRODUCTION

The northern closed basin of San Luis Valley is a major ground and surface water basin of southern Colorado (Fig. 1). Precipitation varies from less than 200mm in the valley to greater than 1200mm in portions of the surrounding mountains. Because of abundant ground water, the San Luis Valley is a major agricultural area of Colorado. The area is currently undergoing extensive exploration for geothermal energy.

Skylab photography of the closed basin was studied to evaluate the potential use of satellite photography as a tool in regional surface and ground water studies. Specifically, the study evaluated the ability of a photo-interpreter, using only Skylab products, to map:

1) surface water divides and drainages,
2) distribution of hydrogeologically-significant rock and alluvial units, as well as significant structures,
3) depth to the ground water table,
4) zones of ground water recharge and discharge, and
5) areas of relatively high evapotranspirative discharge.

All interpretations were checked by either field work or comparison with ongoing work by the author and work in the San Luis Valley by the U.S. Geological Survey (Emery and others, 1973). All available photography that covered the study area

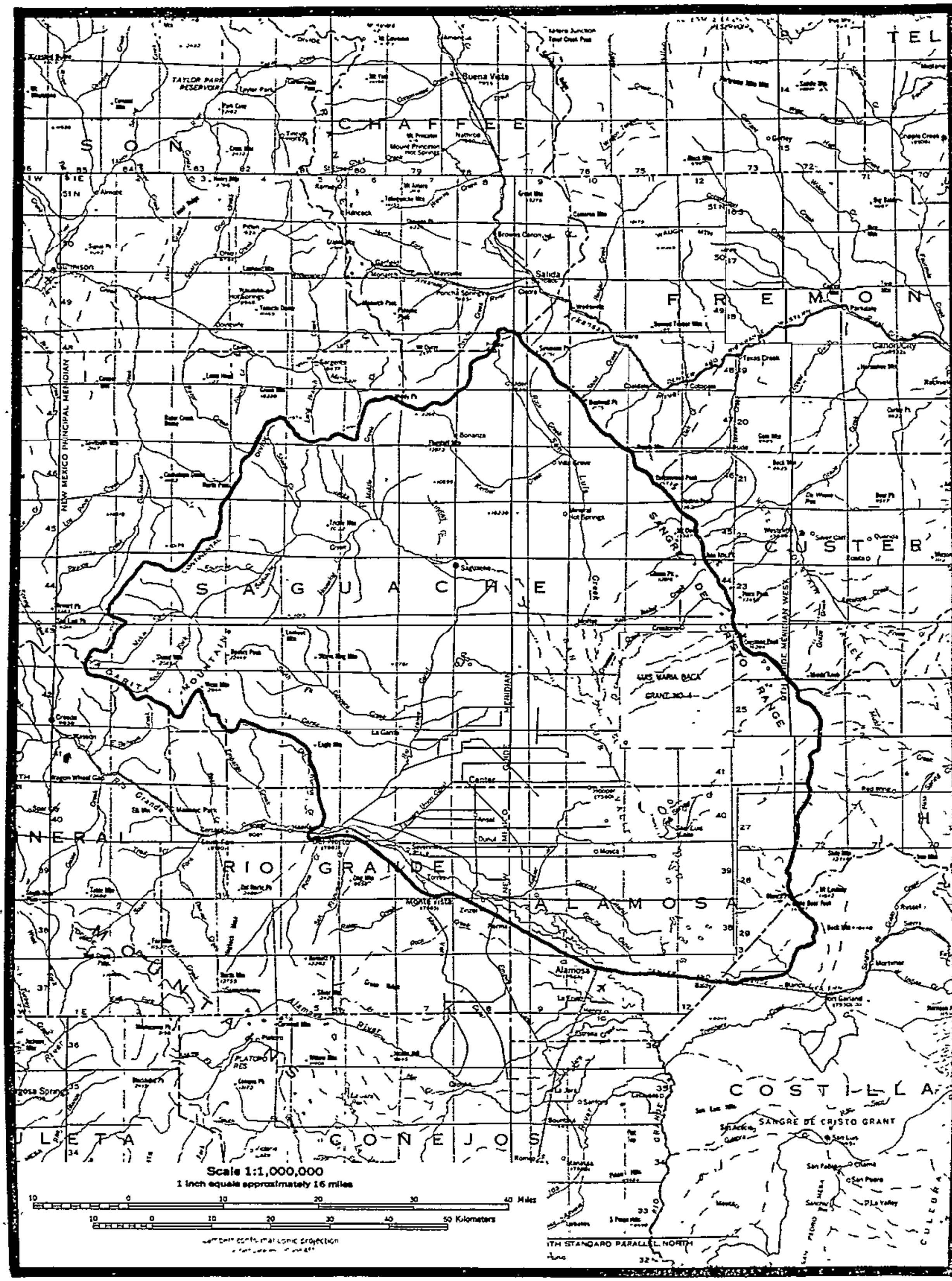

Figure 1. Outline of water resources study area, northern San Luis Valley, Colorado

ORIGINAL PAGE IS
OF POOR QUALITY

from Skylab 2, 3, and 4 was interpreted as part of this study and is listed in Table 1.

TABLE 1

Skylab Photography of San Luis Valley

Mission	Date of Acquisition	Track	Frames	Camera System	Comment
Skylab 2	11 June 1973	48	19	S190A	Good
Skylab 3	6 Sept. 1973	30	251	S190A	No stereo coverage
Skylab 3	6 Sept. 1973	30	23	S190B	No stereo coverage
Skylab 3	16 Sept. 1973	30	65	S190A	Cloud covered
Skylab 4	Jan. 1974	34	353,356	S190A	Snow covered
Skylab 4	Jan. 1974	34	98	S190B	Snow covered

SURFACE DRAINAGE

Some of the most important, and certainly some of the most obvious, features observable on Skylab photography are the positions of the major surface water divides and drainages. Figure 2 shows a drainage map of the northeastern part of the study area, as interpreted from Skylab 2 S190A photography. Comparison with Figure 1 shows that the Skylab-prepared drainage map is much more detailed than the existing 1:1,000,000 scale map of the area. Accuracy of the mapped position of the surface water divide is comparable to that of the existing 1:250,000 scale topographic map. The detail of the drainage

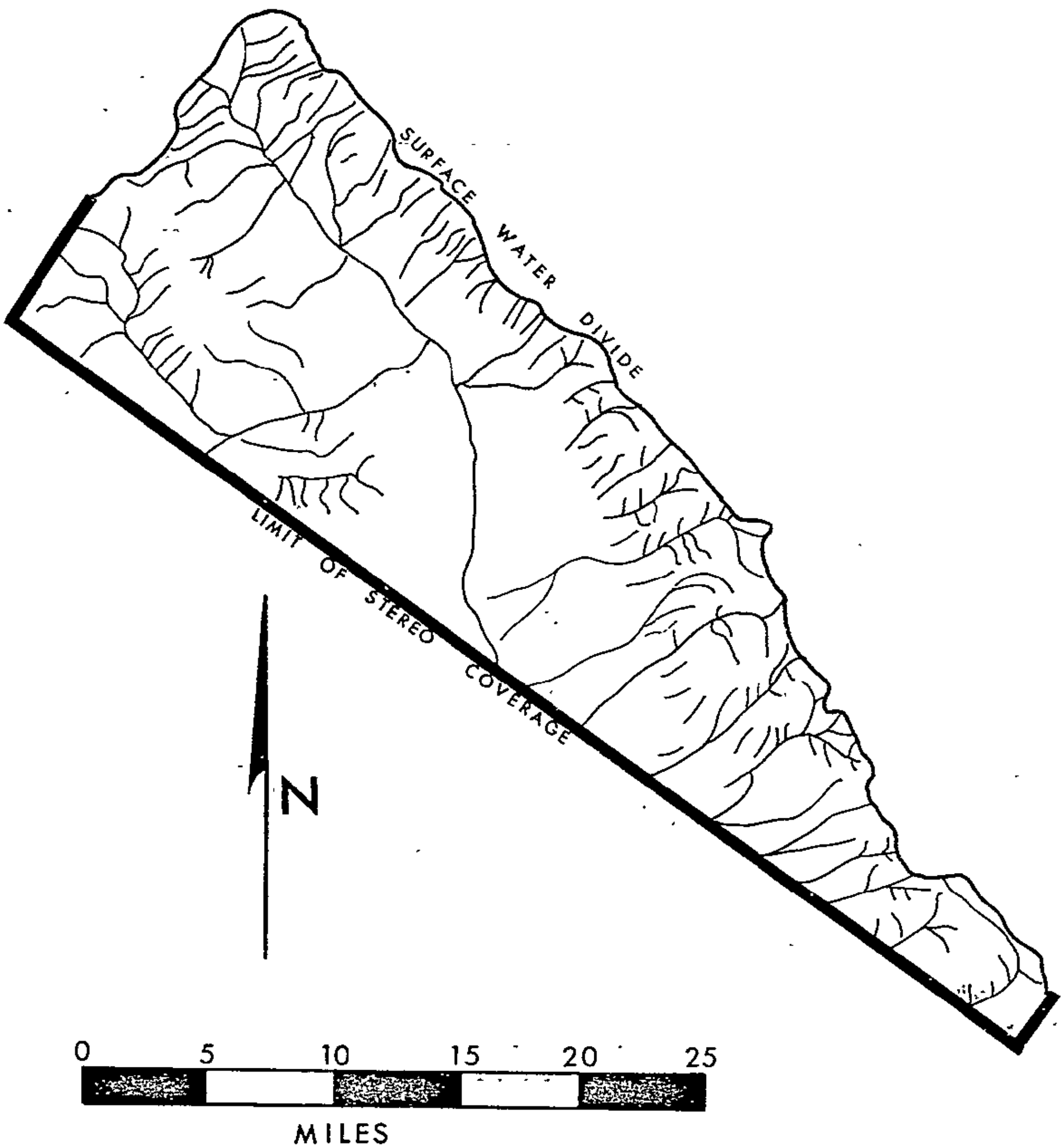

Figure 2. Drainage map of northeastern San Luis Valley drainage basin, as interpreted from Skylab S190A photography.

network, however, is inferior to existing 1:250,000 scale maps. Mapping of the drainage network is best accomplished using color-infrared photography, because streams within the alluvial portion of the basin are best defined by the presence of deciduous vegetation along their course.

Knowledge of the positions of the surface water divide and the drainages is significant not only in the evaluation of surface water flow directions and boundaries, but, in most cases, it helps define the boundaries of ground water movement. In most terrains, the ground water table forms a subdued replica of the topography. Ground water recharge often occurs at topographic highs, and discharge is found at topographic lows (Fig. 3). In a homogeneous medium, or in an inhomogeneous medium of horizontal units, the surface water divides and major drainages will act as impermeable boundaries, and there will be no flow across them. This condition is approached in the San Luis Basin, where rocks west of the valley are near-horizontal, alluvium within the valley is near-horizontal, and indurated rocks east of the valley are fractured in a homogeneous manner. Because these conditions are met, the surface water divide shown in Figure 2 also acts as a ground water divide and the fourth-order stream shown (where a first-order stream is defined as one with no tributaries) is the center of discharge for both the unconfined and confined aquifers present within San Luis Valley. In addition, both Toth (1963) and Freeze (1969)

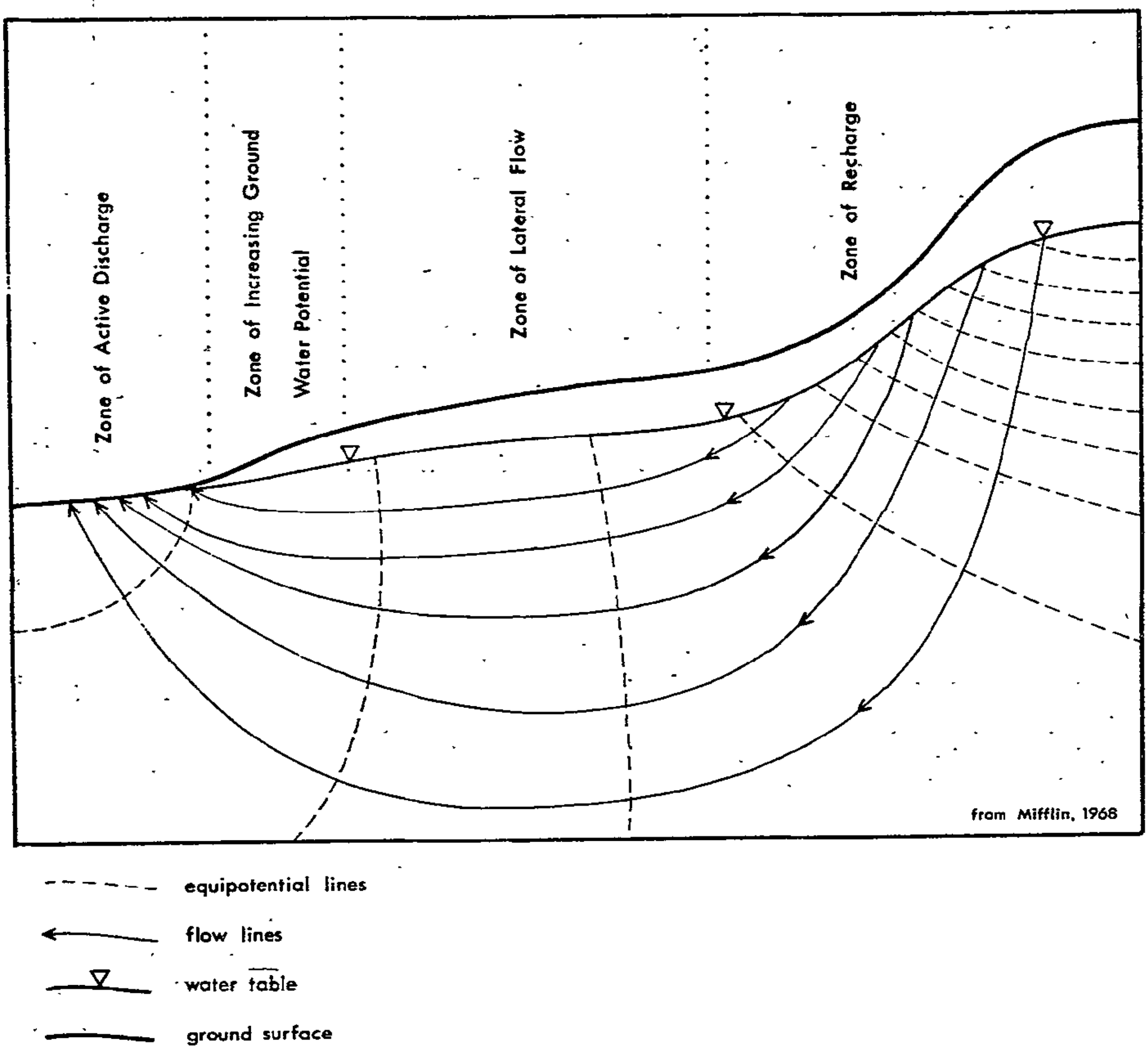

Figure 3. Typical ground water flow patterns.

have shown that lower-order streams may define areas of discharge for more local ground water flow systems. Figure 4 shows the influence of ground water table irregularities on the flow system. A local flow system is one whose areas of recharge and discharge are immediately adjacent.

In summary, the resolution of Skylab S190A photography is adequate to define the major drainage divides and streams, as well as several lower-orders of streams. If the rocks of the region can be approximated as either a homogeneous medium or a horizontally-bedded, inhomogeneous medium, and if the water table configuration follows topography, then the drainage information available on Skylab photography defines ground water flow boundaries and the extremeties of the regional and local recharge/discharge system. It can be seen that the first assumption can be evaluated by mapping the significant hydrogeologic units.

HYDROGEOLOGIC MAPPING

Lithology

Rock types in the San Luis Basin include fractured Precambrian igneous and metamorphic rocks and Paleozoic sedimentary rocks of the Sangre de Cristo Mountains, Tertiary volcanic rocks of the La Garita Mountains, and extensive Quaternary alluvial deposits lying on a thick section of Tertiary sediments and volcanics in the San Luis Valley. A

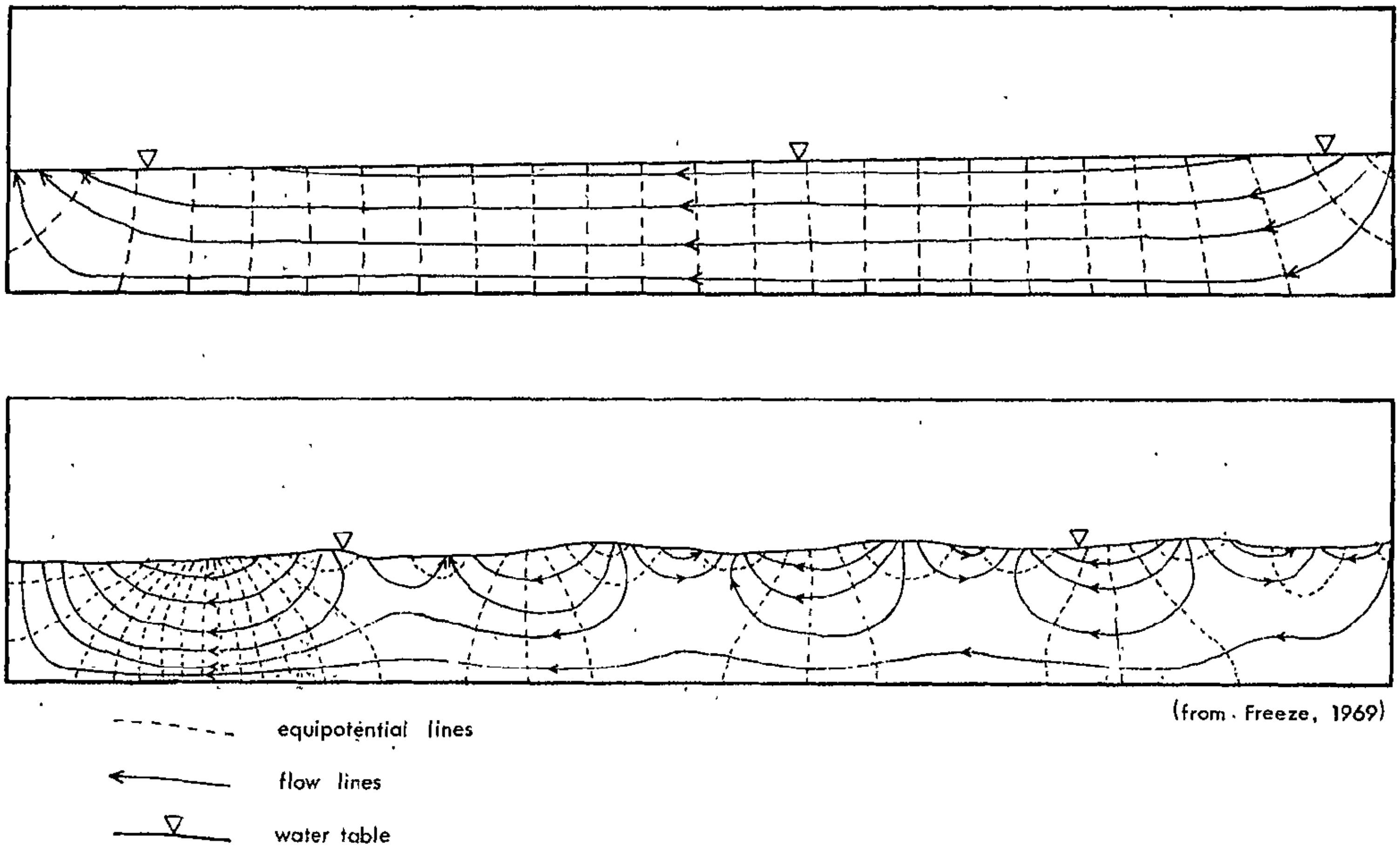

Figure 4. Effect of irregularities of the water table on local and regional flow systems.

description of the hydrogeologic properties of these rocks is presented in Table 2.

Skylab 2 S190A photography covering the northeastern part of San Luis Valley was chosen for the most complete hydrogeologic photointerpretation because it is the only cloud-free, snow-free photography with stereo coverage over the area. Other photography was interpreted in a less complete fashion and will be discussed later. Figure 5 shows the hydrogeologic photointerpretation. For comparison, Figure 6 shows the completed hydrogeologic map covering a portion of the same area as Figure 5. The towns of Villa Grove and Crestone are on both maps for location. The completed hydrogeologic map is the result of interpretation of satellite photography and imagery, aircraft high-and low-altitude photography and imagery, and extensive field work.

Drainage patterns and topographic expression are the most important features used to discriminate rock and alluvial units in the basin. With the exception of the most recent stream deposits, which are identified by their associated deciduous vegetation, spectral differences between units is unimportant in discrimination. Resolution is therefore the most important film characteristic in hydrogeologic mapping of the region. Because of the arid climate of San Luis Valley, drainage patterns on the alluvial fans are relatively small-scale, and are generally below the resolution of both the S190A color and color infrared photos. Alluvial fan units

TABLE 2

Hydrogeologic Units of Northern San Luis Valley

Hydrogeologic Unit		Description	Type of Permeability	Hydraulic Conductivity (Darcys)
Recent stream Deposits		Ranges in texture from silt-size through cobble and boulder-size. Permeability varies downstream and with age of alluvial unit it crosses.	Intergranular	0.001-60
Eolian Sands		Moderately well-sorted to well-sorted sands forming both active and stabilized dunes.	Intergranular	5-20
Quaternary Alluvial Fans	4	Small, steeply sloped, most recent fan. Poorly sorted with continuous grain-size gradation of silt through cobble.	Intergranular	0.1-5
	3	Relatively well-sorted deposits with grain size varying from fine-sand to cobble-size. Largest of the alluvial fans.	Intergranular	12-40
	2	Medium to coarse-grained, poorly to moderately well-sorted. The slope is intermediate between units 1 and 3 and is moderately dissected.	Intergranular	30-60
	1	Oldest alluvial fan unit in sequence; Very steep and highly dissected. Caliche layer near top of unit is very coarse-grained.	Intergranular	55
Valley Fill		Wide range of textures, grain-sizes, degrees of cementation.	Intergranular	<0.00001-60
Youngest Volcanics		Andesite and basalt flows.	Fracture, constant with depth.	0.9-100
Uppermost Ash-flow Sequence		Quartz latite to rhyolite ash-flow tuffs. Degrees of welding vary from unwelded to highly welded. Permeability is greatest in highly welded portions. Permeability is strongly anisotropic.	Fracture, constant with depth.	30-60
Middle Ash-flow Sequence		Includes Carpenter Ridge Tuff (Rhyolite), Fish Canyon Tuff (Quartz latite), and thin andesite flow. Permeability is strongly anisotropic and is greatest in highly welded tuffs.	Fracture, constant with depth.	1-100
Upper Air-fall/Water-laid Tuff		Fine grained, unwelded tuffs.	Intergranular	0.00001-0.01
Sapinero Mesa Tuff		Rhyolite ash-flow tuff.	Fracture, constant with depth	30-40
Lower Air-fall/Water-laid Tuff		Fine grained, unwelded tuffs.	Intergranular	0.00001-0.01
Conejos Formation		Rhyolite to basalt (dominantly andesite) flows, flow breccias, air-fall/water laid tuffs, laharic breccias.	Intergranular and fracture, constant at depth	0.00001-3
Tertiary Intrusives		Intermediate to silicic intrusives of early Tertiary age.	Fracture	0.001-0.01
Basement		Paleozoic sandstones, shales, conglomerates, limestones, all very well indurated, and Precambrian schists, gneisses, and granodiorite intrusives.	Fracture, decreasing with depth	0.001-0.1

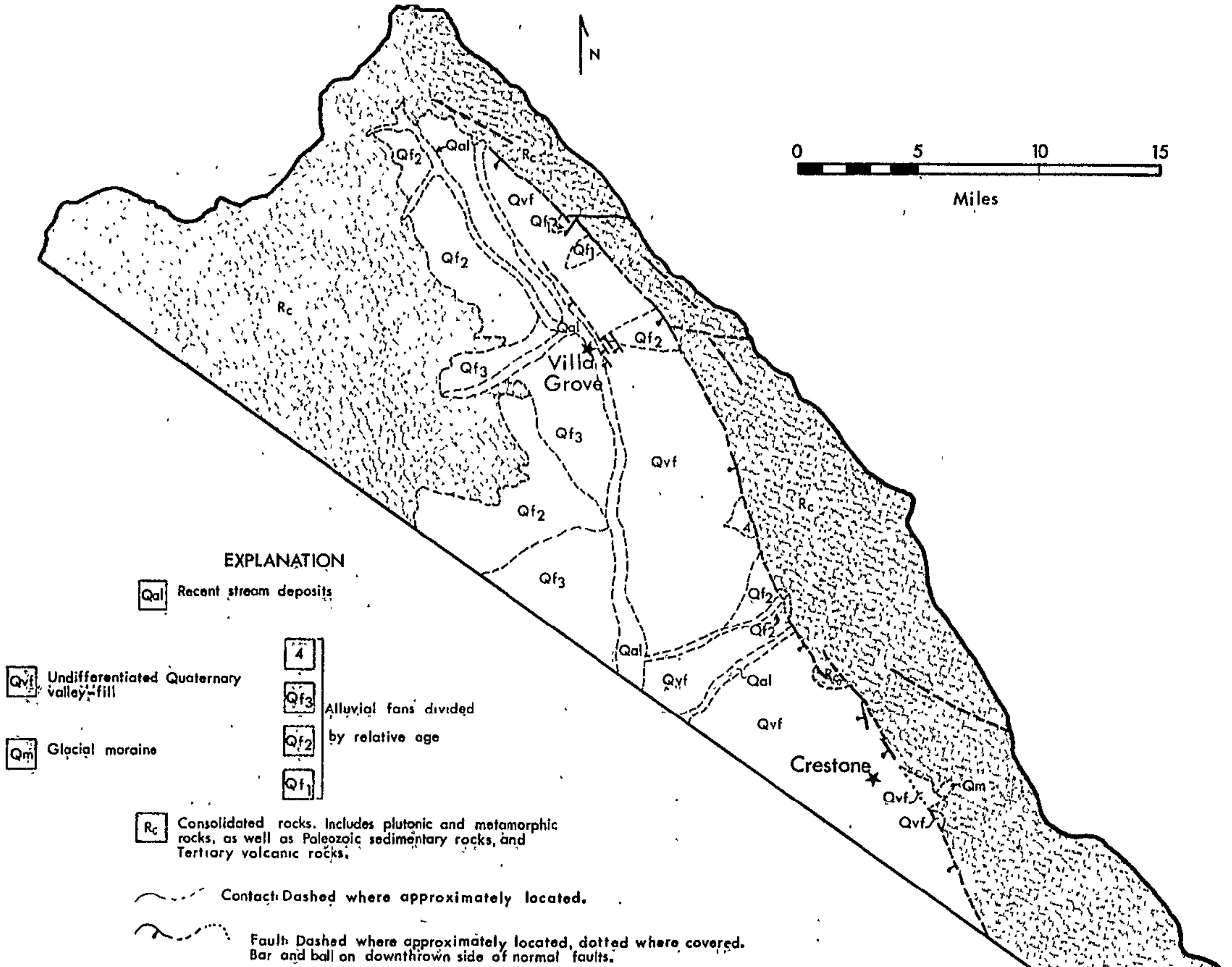

Figure 5. Hydrogeologic map of a selected portion of San Luis Valley, interpreted from Skylab S190A photography.

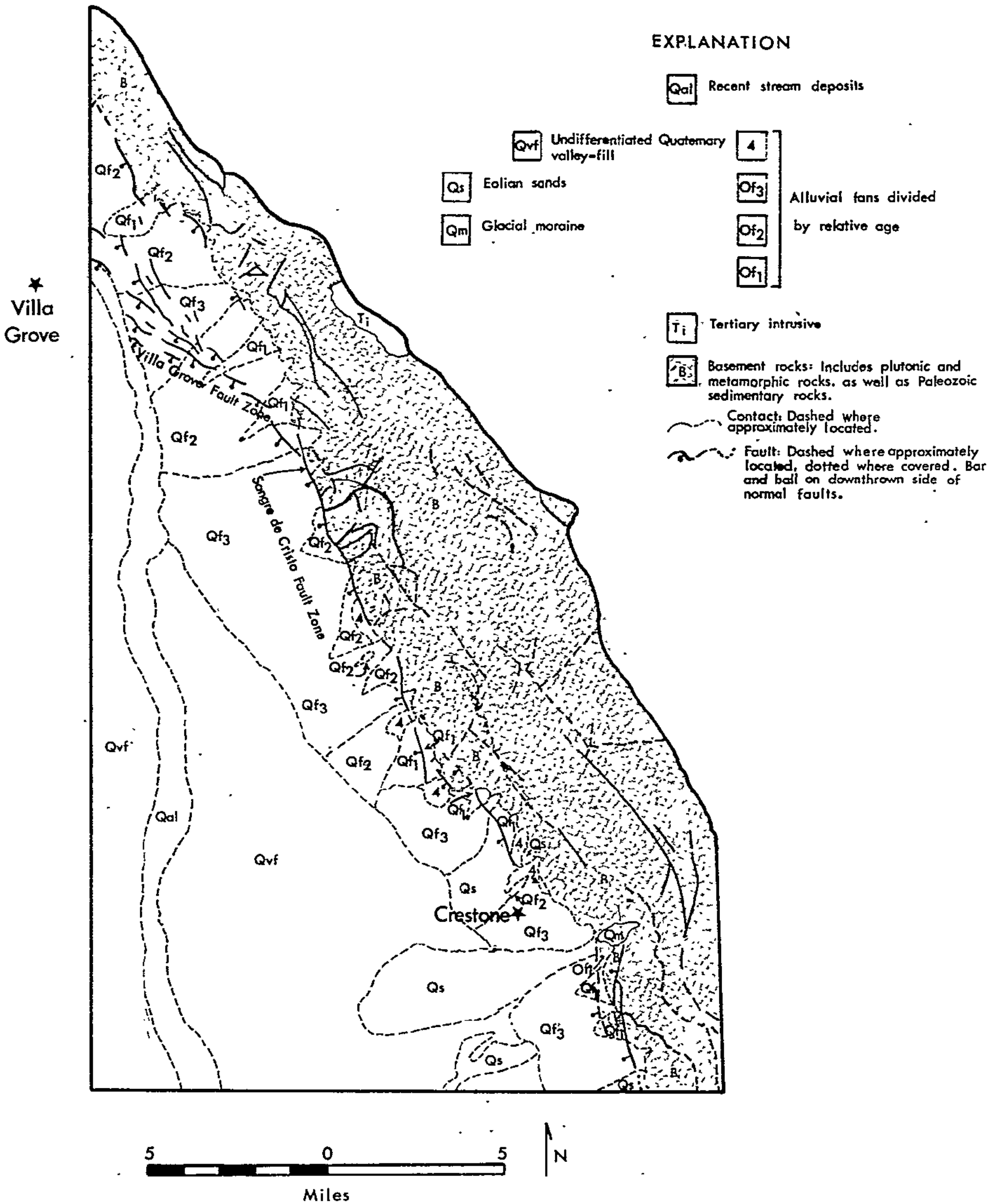

Figure 6. Hydrogeologic map of a selected portion of the San Luis Valley.

can be discriminated only where differences in extent and slope are detectable. Stabilized eolian deposits similarly are not discriminable from other low-lying alluvial units because the sand dunes (visible on larger-scale photography) are below the resolution capability of the S190A camera system. Though no stereo coverage exists for the Skylab 3 S190B September photos, it is nonetheless apparent that the increased resolution of the system increases information content. Drainage textures on the alluvial fans south of Crestone are well within the resolution capability of the S190B. It is very likely that, with stereo coverage, a complete subdivision of alluvial units would be possible, suggesting that mapping at reconnaissance-level accuracy could be achieved in alluvial areas using only S190B photography.

Discrimination between the basement sequence of fractured crystalline and sedimentary rocks and Tertiary volcanic rocks of the Conejos Formation is not possible with any of the S190A photos. This is due largely to the thick stands of coniferous vegetation in both the Sangre de Cristo Mountains and the La Garita Mountains/Bonanza area. Bedding within the Conejos Formation is below the resolution capability of the S190A system, and so cannot be used as a basis for discrimination. Drainage density may be somewhat greater in the basement complex than within the Conejos Formation, but the relationship is by no means consistent.

Only snow-covered photography is available to study terrain covered by post-Conejos Formation volcanic rocks. In general, terrain underlain by ash-flows can be recognized by the flat-top plateaus and the regular joint patterns developed in the welded ash-flows. The only unit within this sequence that can actually be identified relatively consistently is the Fish Canyon Tuff. It should be noted, however, that many of the same comments can be made about conventional low- and medium-altitude aircraft photography.

Volcanic units in this region lack any distinctive spectral contrasts and can be mapped only by their topographic expression. Correlation based on topographic expression is extremely tenuous because of the control of pre-existing topography on the distribution of volcanic rocks. Any mapping of volcanic rocks is likely to require extensive field work. Resolution is again the major factor in the interpretation of the volcanic units; S190B photography permits a more detailed subdivision of rock units than does the S190A photography.

Structures

Geologic structure, particularly faults, exerts a strong influence on ground water movement in the San Luis Basin. Fractures provide the most significant permeability in the marginal bedrock units, and fractures are much more closely spaced and more pervasive in the vicinity of faults, despite the fact that the faults themselves may exhibit little or no

permeability because of gouge developed from relative shear motion. Faults within the alluvial sequence of San Luis Valley often are ground water barriers, probably because of the development of gouge along the fault plane.

Faults within the Sangre de Cristo Mountains and the Bonanza area can be interpreted only by the presence of linear topographic depressions, or the linear alignment of discontinuous topographic depressions, such as ridge saddles. The capability of mapping stratigraphic units in sufficient detail to delineate fault separations is simply not present using S190A system photography. The majority of faults in the basement complex shown in Figure 6 have been mapped on the basis of stratigraphic information, and are therefore not delineated in Figure 5, the Skylab S190A interpretation. All faults shown in Figure 5 can be correlated with real faults in the field, although often a single fault mapped on Skylab photography correlates with a complex series of faults on the ground.

The two major fault zones in the area are the Sangre de Cristo fault zone, trending northwest and separating the basement complex from the Quaternary alluvium, and the Villa Grove fault zone, trending northwest between Villa Grove and and Sangre de Cristo fault zone. Both zones are a series of en echelon normal faults. Fault scarps within the alluvium of up to 10m in height are found along both fault zones. Comparison between the interpretation of S190A photography (Fig. 5) and the final hydrogeologic map (Fig. 6) shows that

interpretation of the Sangre de Cristo fault zone on Skylab photography is generalized, and interpretation of the Villa Grove fault zone is nearly absent. This difference is solely a function of the resolution of the photographic system. The mapping of the Sangre de Cristo fault zone is not based on the presence of fault scarps in the alluvium except along isolated segments. The photointerpretation of the fault is based primarily on the position of the sharp, linear break between the basement complex and the alluvium of San Luis Valley. Only the segment of the Sangre de Cristo fault due north of Crestone is visible on S190A photography as an alluvial fault scarp. It should be noted that it is only visible on the color and red-band photography, because of the superior resolution of these systems.

The Villa Grove fault zone is visible only near the town of Villa Grove, and is interpretable there only because of the heavy deciduous vegetation developed on the up-gradient side of the fault in response to ground water ponding. Without the capability to map fault-scarps in the alluvium, however, there is little to suggest the continuation of a fault zone between Villa Grove and the Sangre de Cristo fault.

Summary and General Remarks

Resolution of the film/camera system is the most important factor determining the amount of hydrogeologic information that can be interpreted. The S190A system does not have sufficient

resolution for more than a cursory examination of the distribution of rock and alluvial units. Though no stereo coverage was available for the S190B system, it is still obvious that much more information results from the greater resolution. Interpretation of stereo S190B photographs would probably produce a map comparable to that of an interpretation of high-altitude aircraft photography, sufficient for a reconnaissance-level, regional ground water study. Because resolution is the most important factor in interpretability, the films with the greatest resolution contain the most information, except where vegetation information is important (such as the fault scarps near Villa Grove). The red and green bands of the S190A contain the same information as the color band, though the resolution of the red band may be somewhat superior to that of the green band. Both of the infrared bands and the color infrared band have inferior resolution. The color infrared film is useful for vegetation-related rock distribution or structure, while the black and and white infrared bands contain little useful information because of the extreme graininess of the film.

GROUND WATER

Two approaches were followed in an attempt to determine ground water depth and quality using Skylab photography. The first approach consists of determining the relationship between vegetation type and density and ground water depth and

quality, and then evaluating the minimum contrast between vegetation zones that is identifiable using S190A color or color infrared photography. The second approach is an attempt at relating saline soils, which appear as areas of high reflectance on photography, to ground water depth and quality.

Vegetation Indicators

Previous studies (Huntley, 1973) in the San Luis Valley have indicated several relationships between ground water depths and vegetation type and density. These relationships are observable both in the field and on low-altitude color-infrared photography, and include:

1) Thick stands of narrowleaf cottonwood (*Populus angustifolia*) trees where the water table is less than five meters from the surface, and thin stands of narrowleaf cottonwood trees that are restricted to the immediate vicinity of an active stream where the ground water table is greater than five meters deep and where shallow, water-saturated sediments are restricted to the stream bank sediments. Narrowleaf cottonwood trees are restricted to areas of good water quality.

2) Growths of willow (*Salix* spp.) occur under the same conditions as narrowleaf cottonwood trees, but they are not restricted to areas of high water quality.

3) The density of rabbitbrush (*Chrysothamnus nauseosus*) can sometimes, but not consistently, be correlated with ground water depth. Dense growths usually are related to ground water depths of less than seven meters, but shallow ground water may exist without a dense growth of rabbitbrush.

4) Wiregrass (*Juncus balticus*) commonly is found in areas where the water table is less than one meter from the surface and periodically reaches the surface.

5) Other brush-type vegetation, such as saltbush (*Atriplex canescens*) and greasewood (*Sarcobatus vermiculatus*), have an irregular and unpredictable relation with ground water depth. High density often is related to shallow ground water, but the converse is not consistently true.

Of the above relations, only the first two are observable on Skylab photography, because of their high photo-infrared reflectance. Figure 7 shows a vegetation/land use map derived from interpretation of Skylab 3 S190A color-infrared photography, and Figure 8 shows a ground water depth map from Emery and others (1973). Throughout much of the area, a fairly strong correlation exists between shallow ground water (<2m) and the stream-associated vegetation. The correlation breaks down where agricultural practices have eliminated the natural vegetation or where water quality is very poor.

Unfortunately, the vegetation associations of narrowleaf cottonwood and willow also exist in areas where the water

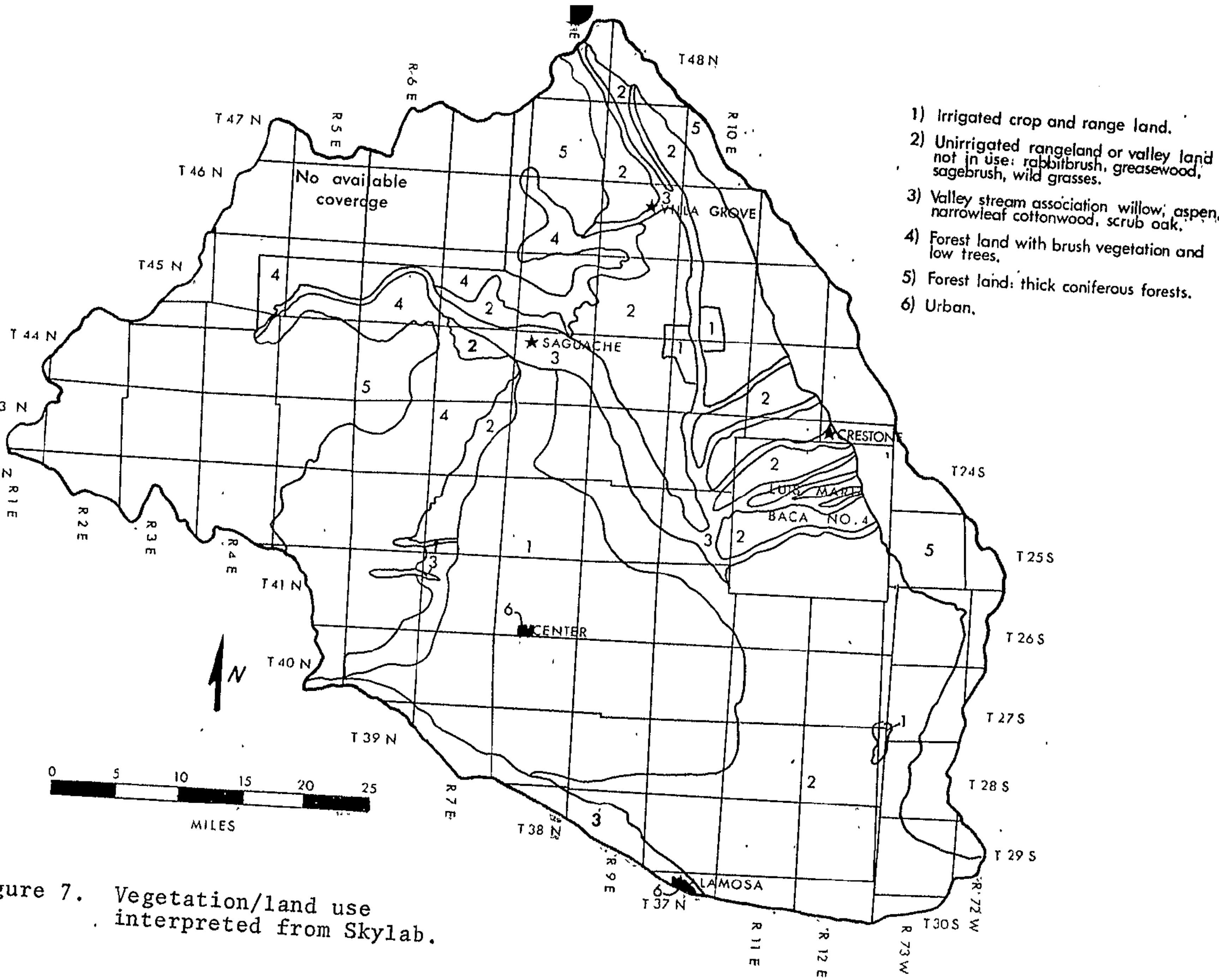

Figure 7. Vegetation/land use interpreted from Skylab.

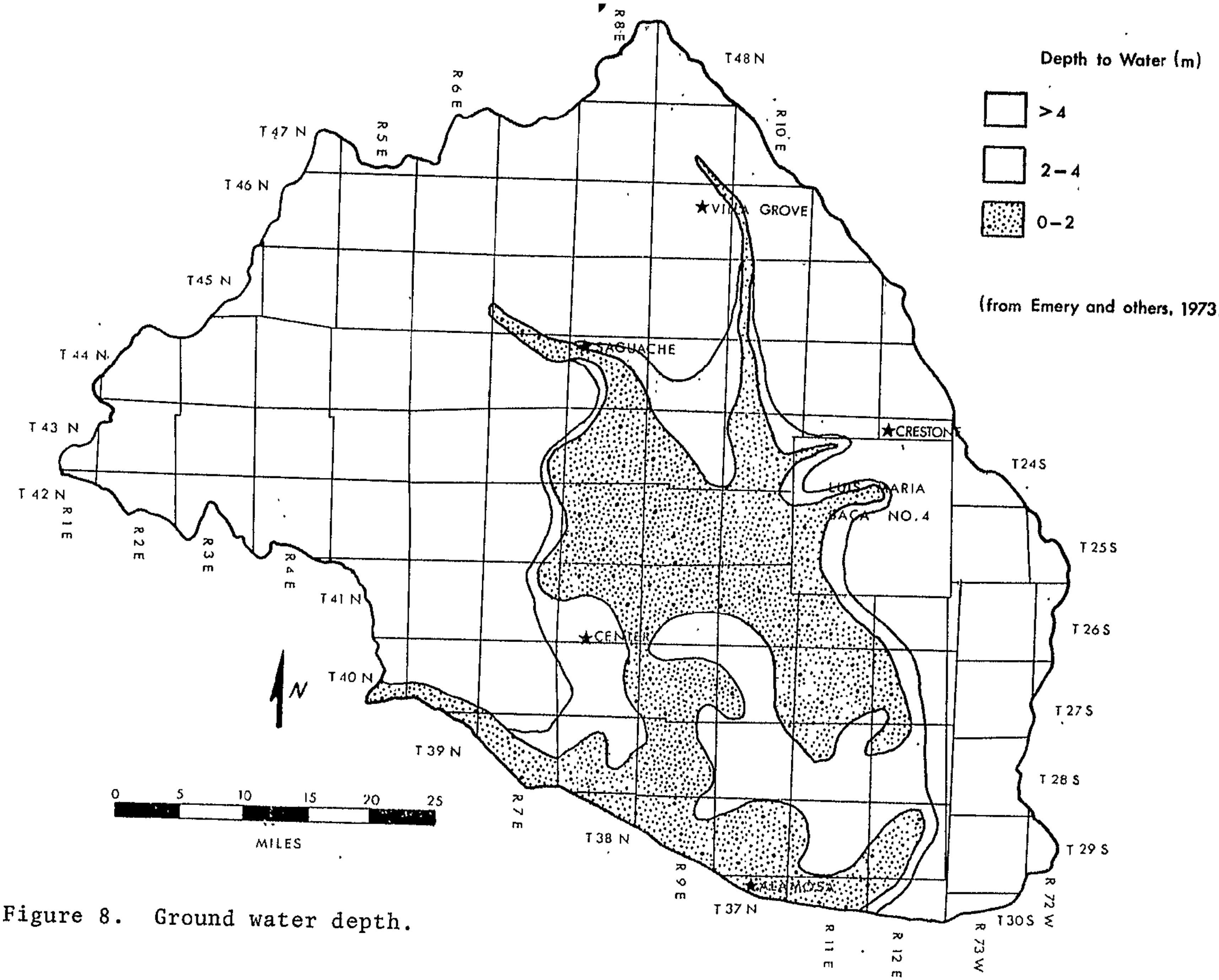

Figure 8. Ground water depth.

table is greater than 4m, as indicated by Emery and others (1973). This occurs in areas where stream flow is high enough throughout the year to keep stream bank sediments saturated, and where perched water tables exist. Areas of perched water tables cannot be discriminated from areas where the real water table is shallow, but the above two often can be discriminated from areas where only the stream banks are saturated by examining the distance that the vegetation has grown away from streams.

Density variations within the brush-type vegetation are not observable with the available resolution of the S190A system.

<u>Saline Soil Indicators</u>

Possible relations between saline soil and ground water depth were first observed on LANDSAT imagery and studied in more detail on Skylab 3 S190A photography. The distribution of saline soils was mapped from S190-A photography (Fig. 9) and was studied to determine its relation to ground water depth, quality, and direction of flow. Reflectances of dry saline soils and moist and dry non-saline soils were measured to determine the best method for isolating the saline soils on photography.

Comparison of the interpreted soil salinity (Fig. 9) with ground water depth (Fig. 8) shows that saline soils develop only where the ground water is relatively shallow, but that saline soils are not present everywhere the ground

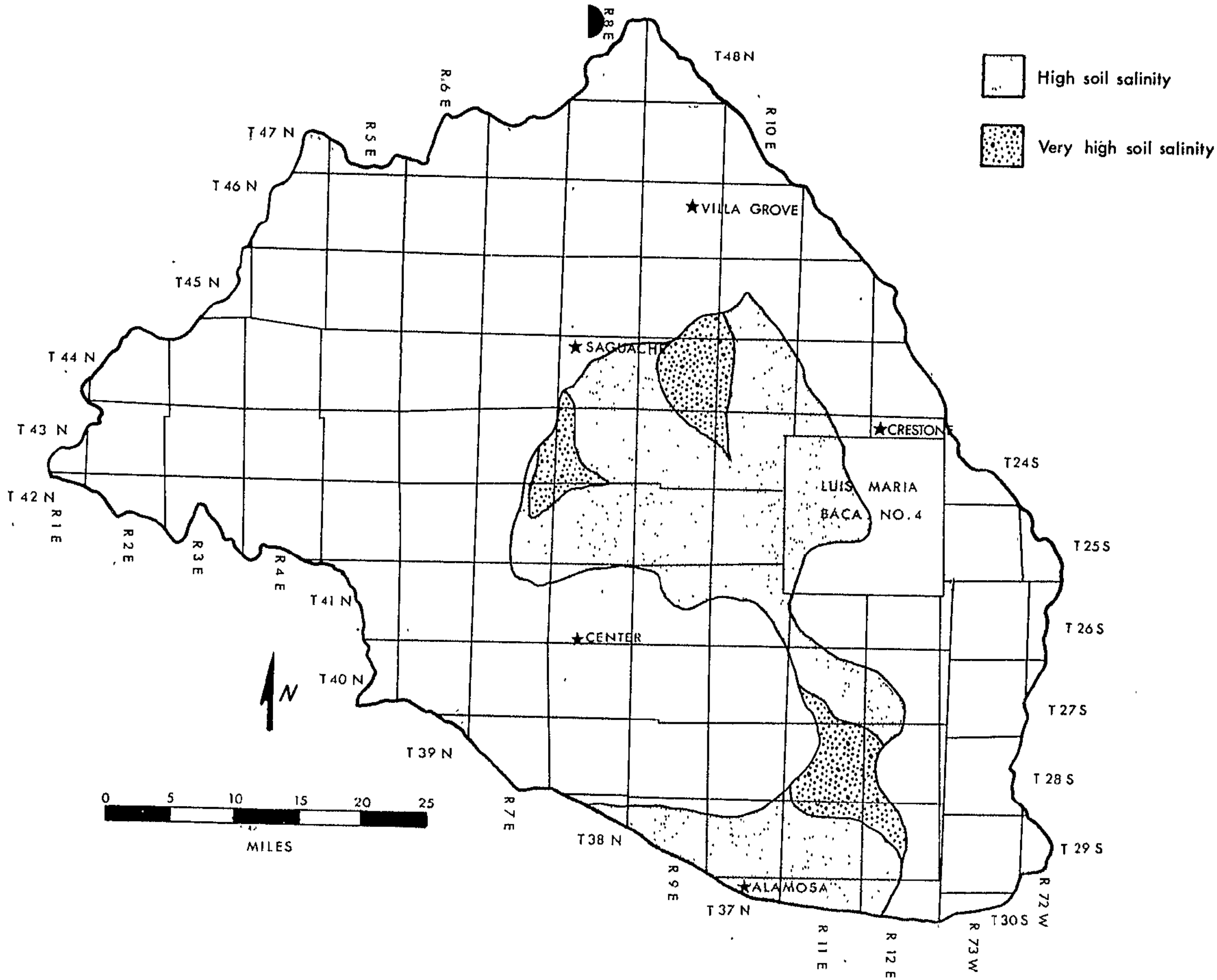

Figure 9. Soil salinity distribution interpreted from Skylab.

water table is near the surface. Saline soils are not present, or are masked, in areas of agricultural land use, as seen when the saline soils distribution is compared with the vegetation/land use map (Fig. 7). Overhead irrigation in agricultural areas tends to rinse the soil free of heavy surface accumulations of salts and, at the same time, the agricultural crops tend to hide soils at the resolution of satellite photography.

The presence of shallow ground water associated with non-saline soils indicates that at least one additional parameter limits the distribution of saline soils. Water quality, and the position of the saline soils within the ground water recharge/discharge system were both considered. Figure 10 shows the limit of artesian wells in San Luis Valley. As artesian conditions are produced by an increasing ground water potential (or head) with depth, flowing wells are found only in areas of potential ground water discharge. The confined and unconfined aquifers of San Luis Valley exhibit a great deal of interaquifer communication, and it is likely that the boundary of the area of potential ground water discharge for the confined aquifer is nearly coincident with the boundary of potential ground water discharge for the shallow, unconfined aquifer. All areas of high soil salinity can be represented as areas of shallow ground water within the zone of potential discharge. The northern and eastern boundaries of shallow ground water and ground water discharge

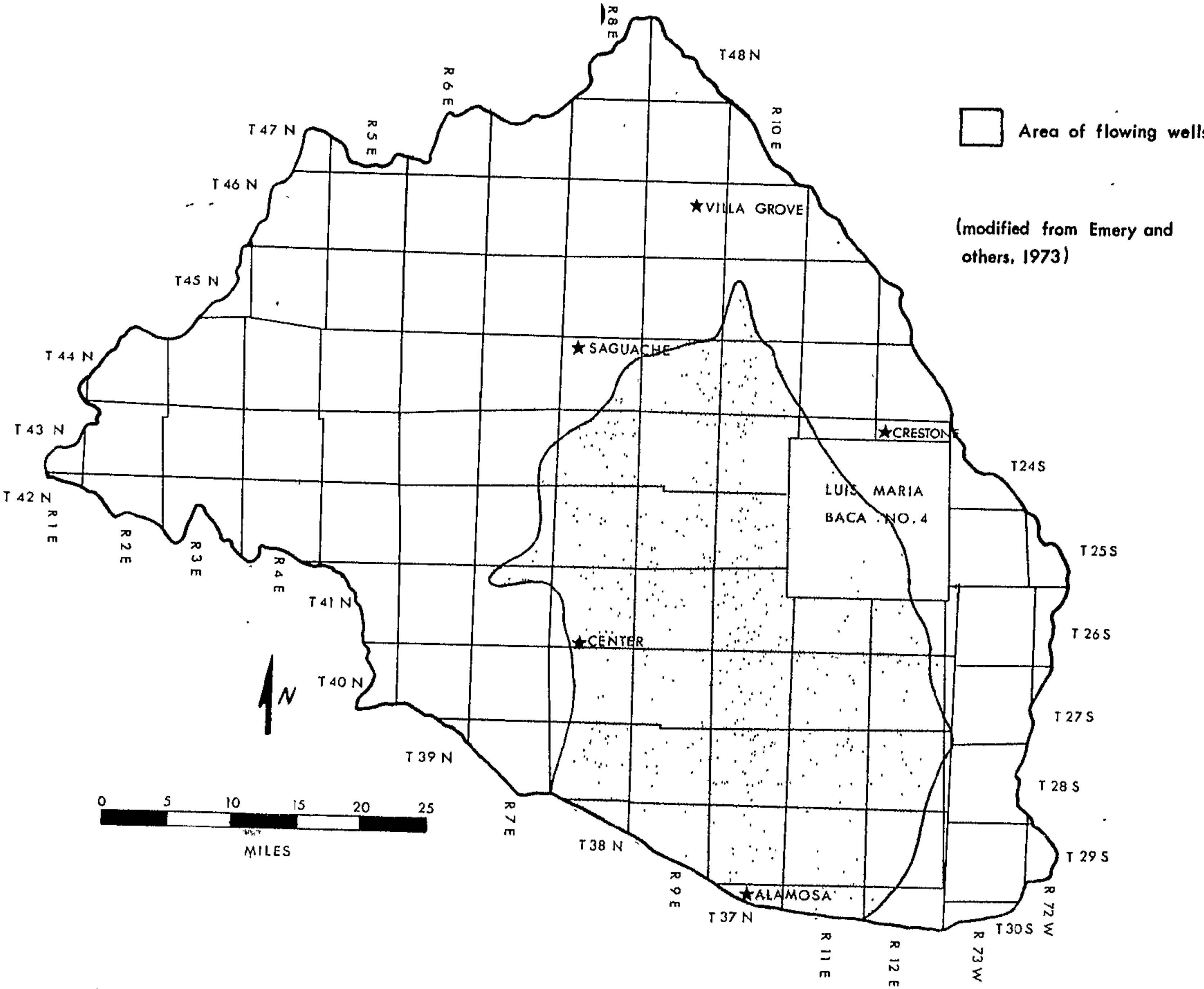

Figure 10. Limit of artesian wells.

correlate particularly well with the limits of soil salinity. The areas of very high soil salinity and the eastern boundary of soil salinity are not explained by even a combination of potential ground water discharge and shallowness.

Figure 11 through 14 show the distribution of salinity and sodium hazard for both the confined and unconfined ground waters of San Luis Valley. The area of very high soil salinity centered on T.39N., R.11E. is in the center of the closed basin sump, the central area of ground water discharge for the closed basin. Salinity and sodium hazards for the unconfined aquifer are extremely high in this area, and evaporation of this water produces soils of extremely high salinity. The area of very high soil salinity centered on T.43N., R.8E. is a region of surface springs and heavy artesian well usage. Evapotranspiration is heavy in this region, and accumulation of salts in the soil results. The area of very high soil salinity centered on T.44N., R.9E. is an area where evaporation from the water table (at a depth of 2-4m) is minimal, but artesian wells are used heavily and evaporation from accumulated surface water is substantial. The westward flexture of the soil salinity boundary near the southern boundary of the Luis Maria Baca No. 4 correlates well with areas of relatively high water quality in both the unconfined and confined aquifers.

Areas of high soil salinity appear to correlate relatively well with areas of shallow, discharging ground water that

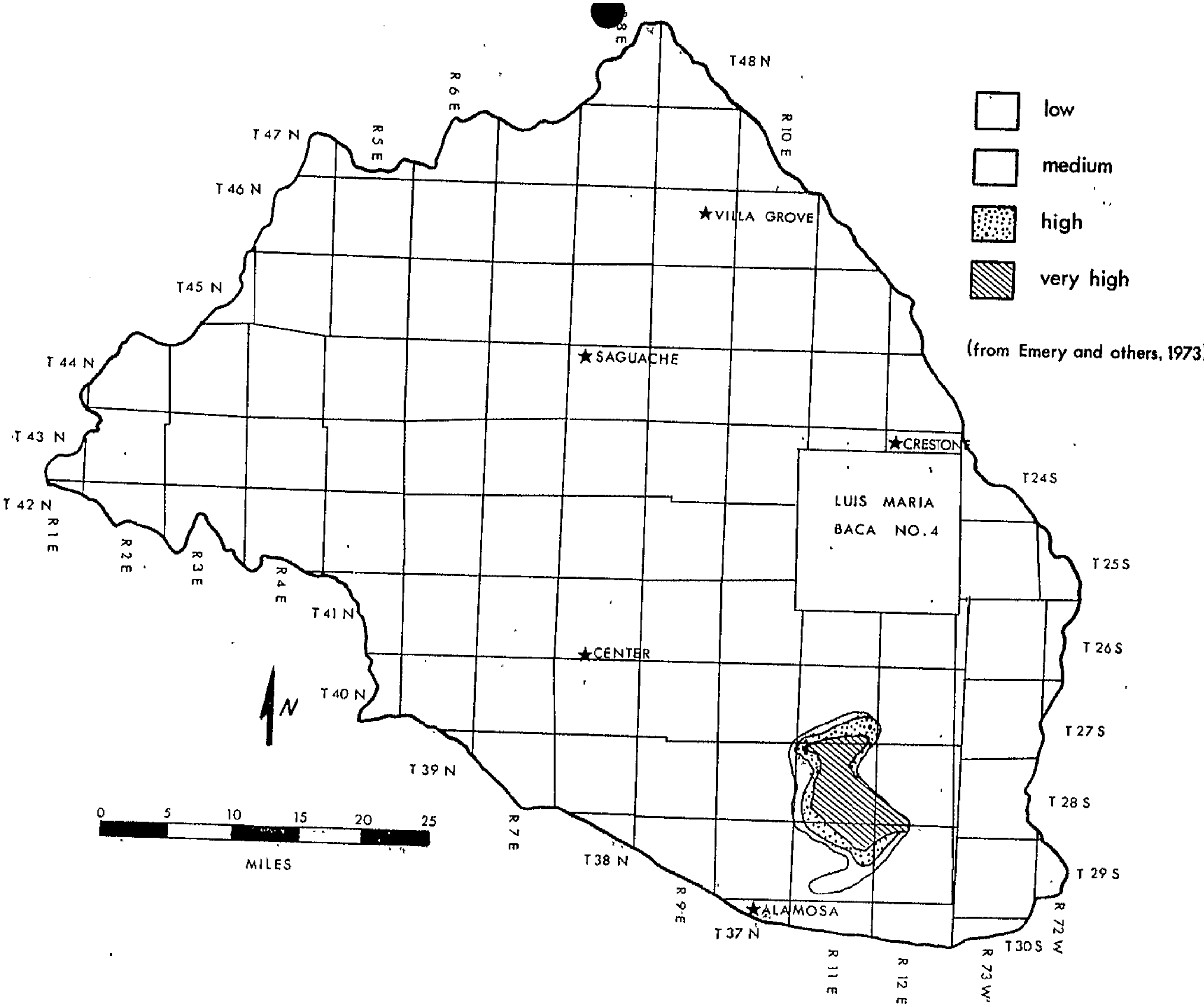

Figure 11. Sodium (alkali) hazard, unconfined aquifer.

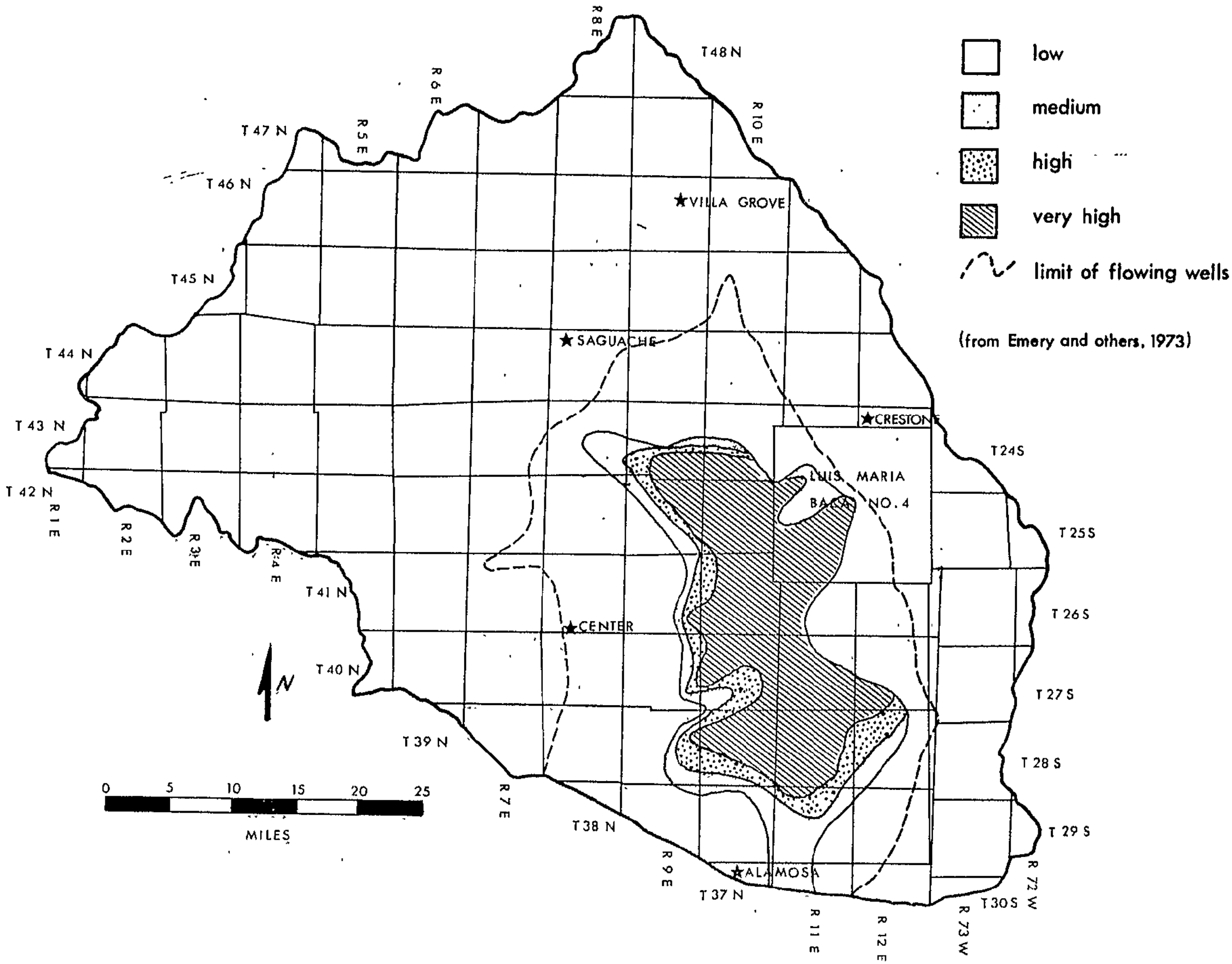

Figure 12. Sodium (alkali) hazard, confined aquifer.

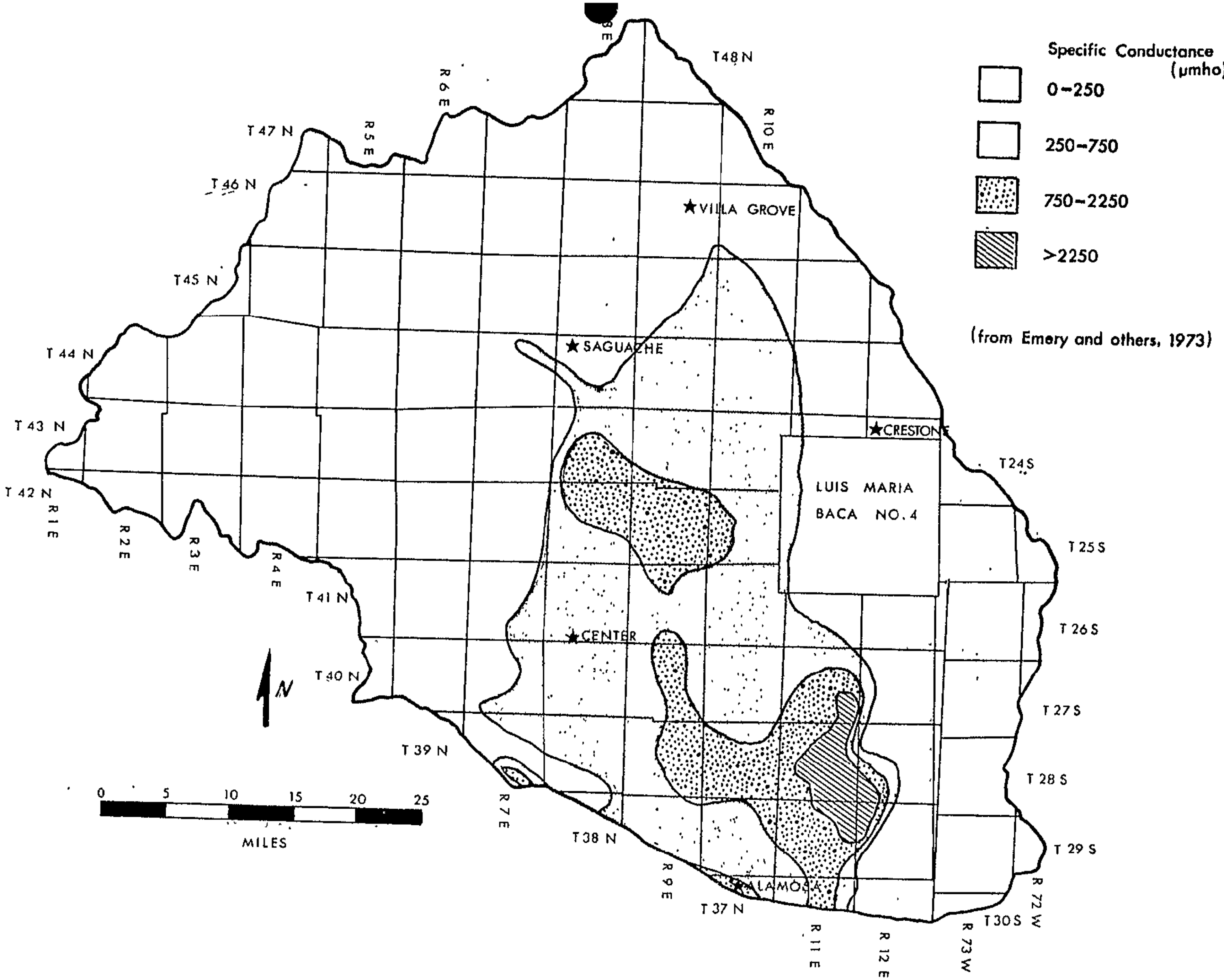

Figure 13. Salinity hazard, unconfined aquifer.

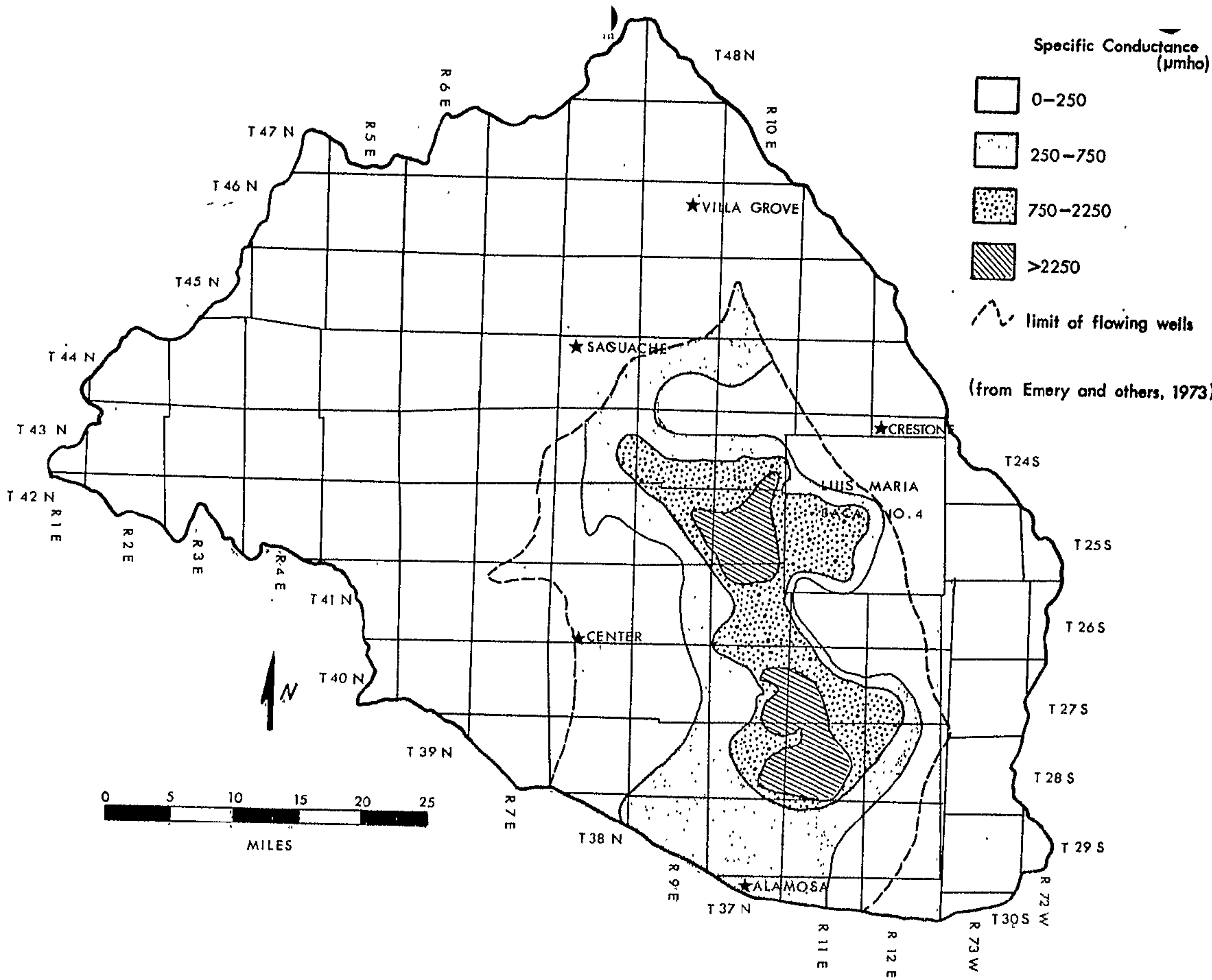

Figure 14. Salinity hazard, confined aquifer.

contains at least a moderate concentration of salts. The use of soil salinity in the interpretation of ground water depth appears to be more dependable than vegetation, if interpreted with care. With this in mind, examination of the spectral reflectance of the saline soils was undertaken to attempt to better delineate these soils.

Saline soil reflectances were measured in the field only, while dry and moist non-saline soil reflectances were measured in both the laboratory and field. The saline soils are dominantly very fine-grained silts and clays, while the non-saline soils range from clay through wind-blown sands, organic-rich peats, and cobble-strewn alluvium.

Reflectance measurements were made using the filter wheel photometer described by Raines and Lee (1974). Measurements were made in 13 spectral bands covering the photographic region (Fig. 15). To determine if band ratioing (Raines and Lee, 1975) might be a successful technique, the data were computed as normalized band reflectances by dividing all band reflectances values by the corresponding no-filter band reflectance value. This technique shows whether there is any significant difference in the shape of the spectral reflectance curve from unit to unit that might be used in band ratioing techniques. It is particularly useful in this analysis, because the dry and moist non-saline soils show quite a range of absolute reflectances, but a relatively uniform normalized reflectance curve (Fig. 16).

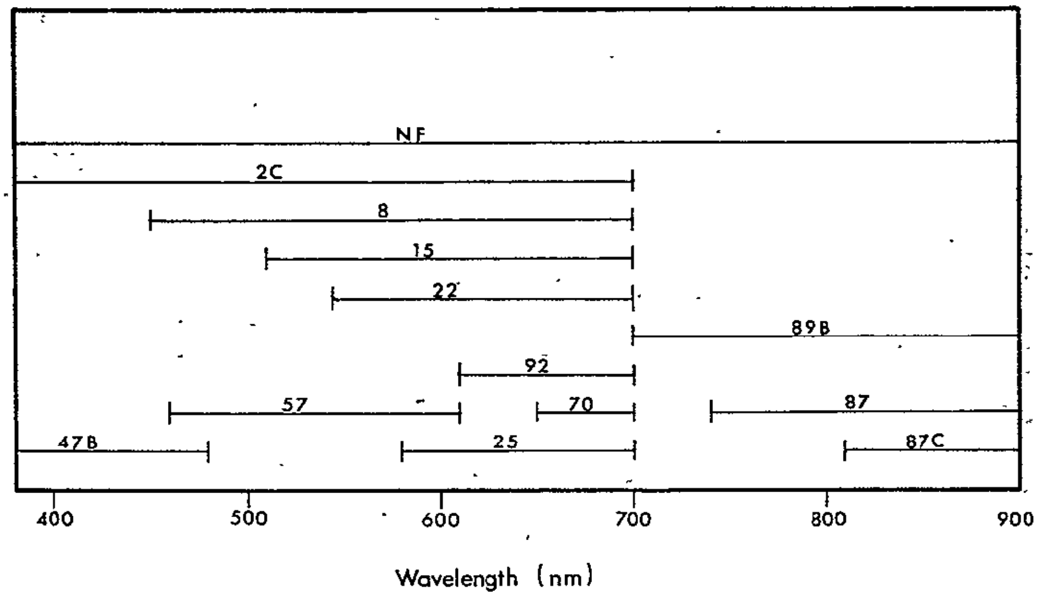

Figure 15. Bandpass filters used in spectral reflectance measurements.

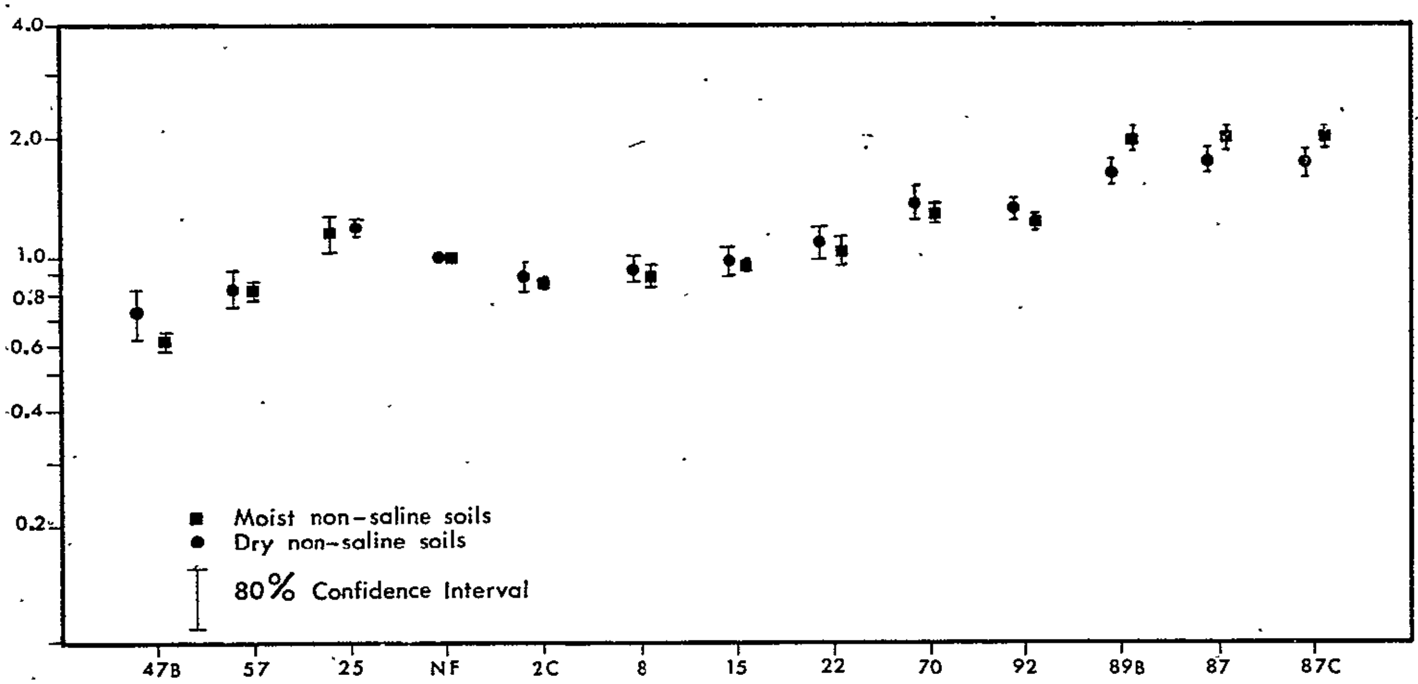

Figure 16. Normalized band reflectance of dry and moist non-saline soils.

Figure 17 shows the normalized band reflectance plots for saline soils compared with moist and dry non-saline soils separately. Only the 47B (blue) band, the 2C (minus UV) band, and the 89B, 87B, 87C (photo-infrared) band show significant separations at the 80% confidence interval. The same effect in the infrared bands is observed in the plot of dry versus moist non-saline soils (Fig. 16), and it is suggested that saline soils having a high average reflectance show a reduced slope of increased reflectance towards the infrared region. These observations indicate that ratioing may help increase the contrast between high reflectance units, such as saline soils, from soils having the usual range of intermediate reflectances. This has not been tested in application.

A plot of absolute band reflectances for dry non-saline and saline soils is shown in Figure 18. There is separation of the ranges in the photo-infrared bands, the deep red bands, the minus-blue band, and the no-filter band. These observations contradict the subjective evaluation of S190A photography, where the infrared bands show the least contrast. One possible explanation for this, aside from the generally poor quality of the infrared bands, is that the photography is not contrasting non-saline with saline soils, but is contrasting vegetation with saline soils. Vegetation typically exhibits a high photo-infrared reflectance, which would show a low contrast with saline soils, and exhibits a much lower green-band reflectance than that measured for the saline soils. This may well affect the conclusions reached above concerning band ratioing.

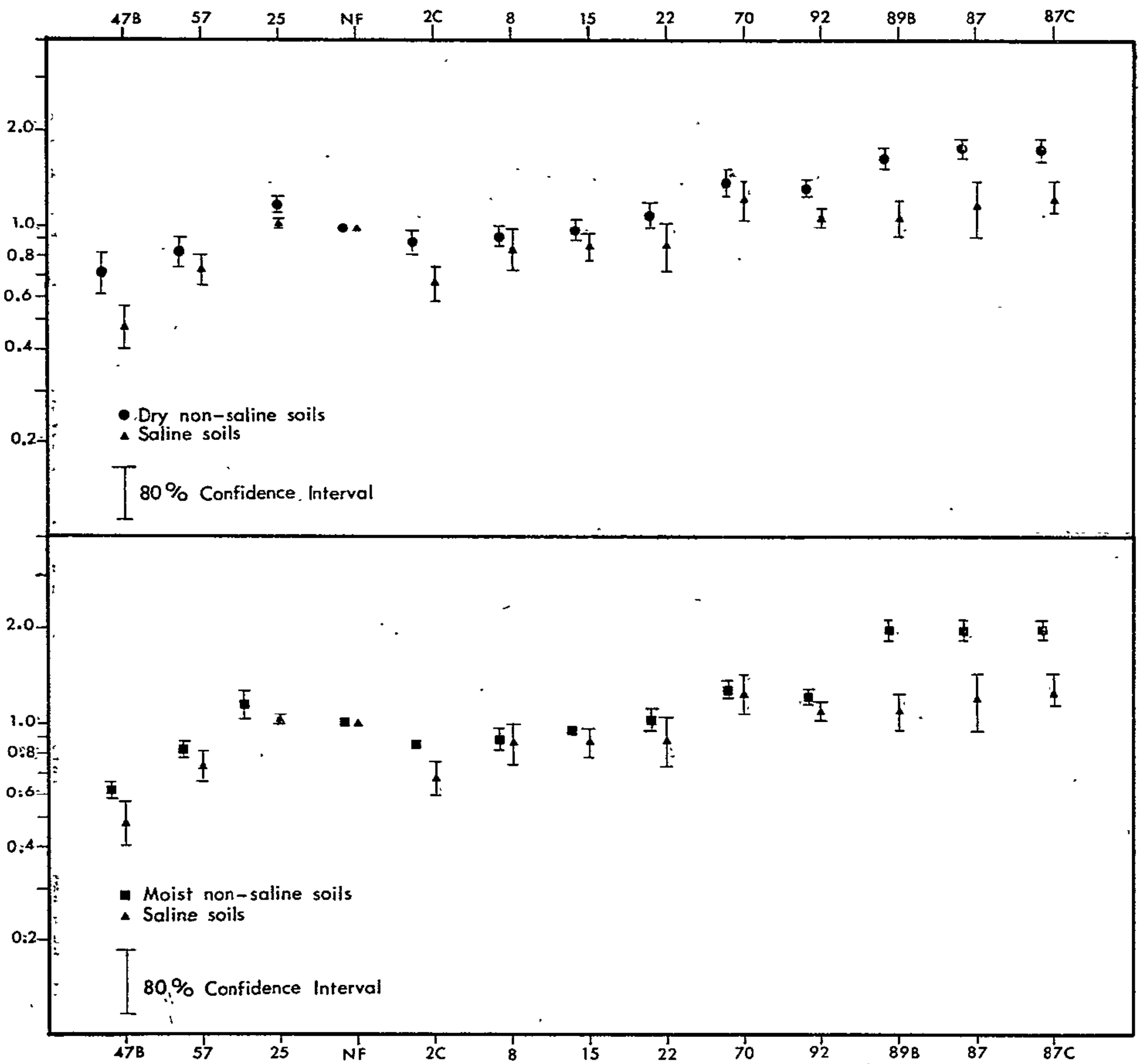

Figure 17. Normalized band reflectance of saline soils, and moist and dry non-saline soils.

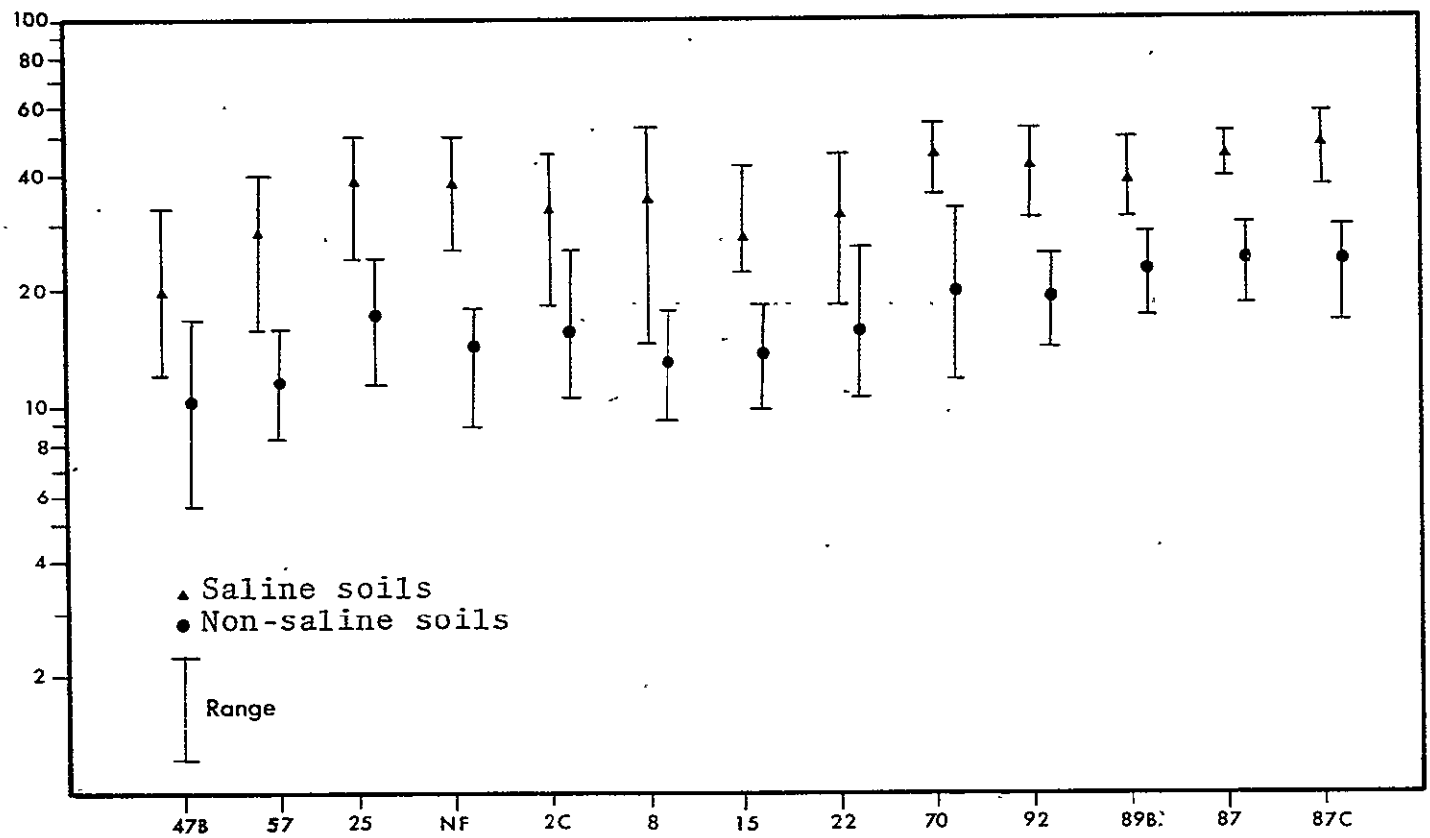

Figure 18. Absolute band reflectance (in percent) of saline and non-saline soils.

Summary and General Remarks

Narrowleaf cottonwood trees and willows are present only where water saturated material is present within 4m of the surface. This condition is met both where the water table is shallow and where streams have sufficient flow to maintain saturated bank sediments throughout the year, with either a shallow or deep water-table. Where the vegetation extends away from streams a good distance, the ground water table is likely shallow.

The presence of saline soil more reliably indicates shallow ground water, but it also is dependent upon the position within the regional flow system and the ground water quality. If non-saline and saline soils are being mapped, band ratioing may increase contrast. If vegetation and saline soils are being compared, as appears likely at satellite resolution, the green band shows better contrast than the other available bands.

EVAPOTRANSPIRATIVE DISCHARGE

Rates of evapotranspirative discharge from the water table depend upon vegetation density and type, ground water depth, and climate. The vegetation/land use map (Fig. 7) contains the essential vegetation information. This information, combined with ground water depth information (as discussed in the previous section) and climatic information,

allows a computation of evapotranspiration rates of an accuracy sufficient for most regional ground water studies. For this computation, both vegetation and soil salinity should be used as indicators of depth to a saturated zone, because evapotranspirative rates are equal for a shallow water table, a perched water table, and saturated stream bank sediments well above the water table.

CONCLUSIONS

1) Resolution is the single most important factor in determining the potential application of Skylab photography to hydrogeologic investigations.

2) Skylab S190A photography used in a stereo mode is sufficient for defining the drainage divides and drainage patterns at the regional level. This information, combined with geologic information, defines the boundaries and distribution of ground water recharge and discharge areas within the basin.

3) Only Skylab S190B photography has sufficient resolution to adequately map more than the most obvious hydrogeologic units and structures, and in some cases may be sufficient for regional studies. In most regions, however, aircraft photography is still a necessity to produce an accurate and useful hydrogeologic map. Field work is a necessity for all studies.

4) Both vegetation and soil salinity are useful indicators of shallow ground water, but both must be interpreted carefully.

5) Evapotranspirative rates can be interpreted through knowledge of the climate and use of vegetation and ground water depth information interpreted from Skylab photography.

REFERENCES

Emery, P.A., Snipes, R.J., Dumeyer, J.M., and Klein, J.M., 1973, Water in the San Luis Valley, south-central Colorado: Colorado Water Conserv. Board Water Resources Circ. 18, 26 p.

Freeze, R.A., 1969, Theoretical analysis of regional groundwater flow: Inland Waters Branch Scientific Series No. 3, Canadian Dept. of Energy, Mines, and Resources. 147 p.

Huntley, David, 1973, Hydrogeology of the Crestone quadrangle area, Colorado: unpublished summary of research, Colorado School of Mines. 29 p.

Mifflin, M.D., 1968, Delineation of groundwater flow systems in Nevada: Desert Research Institute, Univ. of Nevada, Tech. Rept. #4., 110 p.

Raines, G.L., and Lee, Keenan, 1974, Spectral reflectance measurements: Photogrammetric Eng., v. 40, no. 5, p. 547-550.

__________, 1975, In situ rock reflectance: Photogrammetric Eng., v. 41, no. 2, p. 189-198.

Toth, J., 1963, A theoretical analysis of groundwater flow in small drainage basins: Jour. of Geophysical Research, v. 68, no. 16, p. 4795-4813.

GEOLOGIC AND MINERAL AND WATER RESOURCES INVESTIGATIONS IN WESTERN COLORADO, USING SKYLAB EREP DATA

FINAL REPORT

by

Keenan Lee
Gary L. Prost
Daniel H. Knepper
Don L. Sawatzky
David Huntley
Robert J. Weimer

Remote Sensing Report 75-7

Remote Sensing Projects
Department of Geology
Colorado School of Mines
Golden, Colorado

National Aeronautics and Space Administration

NASA Contract NAS9-13394

December 1975

SIGNIFICANT RESULTS

Skylab photographs are superior to ERTS images for photogeologic interpretation, primarily because of improved resolution. Similarly, S190B photos provide more geologic information than do S190A photos. Multiband photography shows no apparent advantage over good color photography; S190B stereo color photos, where available, provide maximum geologic information.

Lithologic contacts can be detected consistently better on Skylab S190A photos than on ERTS images. Color photos are best; red and green band photos are somewhat better than color-infrared photos; infrared band photos are worst. With S190B color photos, all stratigraphic units at or above formation-rank can be mapped in this area, and many formations can be effectively subdivided into members. Conjunctive use of topo maps permits estimation of section thicknesses and lateral thickness changes. Stratigraphic pinch-outs, intertonguing sedimentation, and lateral facies changes have been accurately mapped with S190B photos.

All major geologic structures can be recognized on Skylab photographs. Large folds, even those with very gentle flexures, can be mapped accurately and with confidence. Bedding attitudes of only a few degrees are recognized; vertical exaggeration factor is about 2.5X. Faulting is

recognized more easily, but with less reliability, than folds. Fractures as short as 1 km are seen on S190B photos, as are joint spacings of less than 200 m. Anomalous megalineaments are recognized that transect regional tectonic elements. By recognizing and tracing stratigraphic units in detailed mapping, major uplifts can be demonstrated to have recurrent structural movement.

Mineral deposits in Central Colorado may be indicated on Skylab photos by lineaments and color anomalies, but positive identification of these features is not possible. High densities of lineaments may indicate complex fractures that exert controls on mineralization, but they may represent many other types of structures as well. Color anomalies may indicate gossans or hydrothermal bleaching associated with mineralization, but they may also represent sedimentary redbeds and pink, microcline-rich granitic rocks. Orbital photography alone is inadequate to fulfill mineral exploration needs. It is useful in reducing the size of an exploration area to potentially favorable targets, but it is a powerful tool only when used in conjunction with detailed field work.

Water resource studies can use Skylab photography for interpretation of drainage, hydrogeology and ground water flow. S190A stereo color photography is adequate for defining drainage divides that in turn define the boundaries and distribution of ground water recharge and discharge areas

within a basin. Skylab S190B stereo photography has sufficient resolution to map hydrogeologic units and structures that may be sufficient for regional studies. Aircraft photography and field work are still necessary to produce an accurate hydrogeologic map. Both vegetation and soil salinity are surface phenomena capable of being interpreted on Skylab photos that are indicators of shallow ground water.

Regional geologic mapping using Skylab photography is best done by photointerpretation, a deductive process best carried out by a geologist-interpreter. Using S190B photographs, photogeologic mapping at a scale of 1:24,000 is not feasible, and 1:250,000 is, in some cases, too small a scale. Optimum scale for photogeologic mapping is in the range of 1:62,500 to 1:250,000.

Skylab photography will add little new geologic information in areas where 1:250,000 scale geologic maps are available. In such areas, however, the photography should prove useful for re-examining the geology in the light of new concepts or hypotheses. Photogeologic mapping from Skylab S190B color photography can provide invaluable geologic information in areas that are geologically unknown or poorly known.

CONTENTS

INTRODUCTION

This report summarizes the research conducted by the Colorado School of Mines under NASA Contract NAS 9-13394 for the purpose of evaluating Skylab remote sensing data for geologic and mineral and water resources in western Colorado. The primary objectives of the investigation were to:

- assist NASA/JSC in mission planning activities,
- screen all EREP data obtained over Colorado and select frames for detailed study,
- prepare photogeologic maps using selected S190 photographs and analyze them to determine what geologic information may be contained in them,
- compare the geological interpretations to interpretations obtained from S-192 imagery and to interpretations made from ERTS-1 imagery,
- verify the geological interpretations by means of interpretation of aerial photographs, published geological reports, and field observations, and
- prepare recommendations for the optimum imagery to be used for studies of regional geology and exploration for mineral deposits and water resources.

Because EREP is an experimental program, research efforts were directed largely toward evaluations rather than applications.

Research on the Skylab Project was conducted by faculty and graduate students of the Colorado School of Mines. Over the duration of the project, the following geologists contributed to the research: Rebecca Dodge, David Huntley,

Robert Hutchinson, Harry Kent, Daniel Knepper, Keenan Lee, Gary Prost, Don Sawatzky, Robert Spoelhof, John Thigpen, David Trexler and Robert Weimer.

The authors of this report thank Rebecca Dodge, Rosemary Lee and Jean Mbok for their help in preparing the report. Kitty Huntley's assistance was not only valuable - it was critical to the completion of the Project.

The format of this final report is stratified, with three strata being (1) Significant Results, (2) the text of this report, Chapters 2 through 7, and (3) the appendices. This format was designed such that Significant Results is a listing of results; the text of the report is a short, narrative discussion of our results, without any supporting material; and the appendices contain the full arguments, details and evidence. Recommendations are a reflection of the Principal Investigator's opinions and prejudices.

SKYLAB DATA

Five of the six Skylab ground tracks across Colorado were designated EREP passes (App. C, p. 3). Four of these tracks (16, 30, 34, and 48) traversed what was originally defined as the primary test site, and each of these tracks was photographed at least once, although only one was photographed under very good conditions.

Maps have been compiled that show the total Skylab data coverage of Colorado (App. C, p. 4), total coverage by each sensor (App. C, p. 7), and individual frame index maps (App. C., p. 8 ff.). The maps are used for location reference only; the photography must be examined to determine clouds, snow, etc., over any given location. In general, good clear continuous stereo coverage is available only in the southern part of Colorado and southeastern Utah.

Skylab S190A original-scale transparencies are 57 mm square and have a scale of about 1:2,850,000. These frames are easiest to work with when they are enlarged four times, to a scale of about 1:700,000, with limits of resolution at about twelve magnifications of the original. The S190A photographs can discriminate objects such as clusters of buildings, two-lane roads, and airport runways, and objects as small as Golden Reservoir (300 m diameter) and Interstate 70 (about 70 m wide) can be identified.

The S190B original-scale transparencies are 115 mm square frames and have a scale of about 1:950,000. Two-time enlargements are easiest to work with, at a scale of about 1:475,000, with optical magnification limits similar to the S190A photos. The S190B photography can discriminate clusters of buildings, large isolated buildings (Carleton gold mill at Cripple Creek, with an aluminum roof approximately 100 by 200 meters), and unimproved roads about ten meters wide.

The major data problems involve non-repetitive coverage and the lack of stereo coverage. Limited coverage is largely responsible for extensive snow or cloud cover on available film, and for limited solar illumination angles and spotty ground coverage. The frequent lack of stereo coverage and occasional complete gaps in ground coverage decrease confidence in photointerpretation.

Processing problems encountered include occasional variable color rendition, especially in CIR film, red specks on S190A CIR film (caused by abrasion and emulsion lifting), scratches, emulsion on the underside of the duping film (causing scratches when unrolling film), and reversal of stereo-sequence (in a continuous sequence each frame has been rotated 180 degrees, making stereo viewing of adjacent frames difficult). In general, the data processing quality is excellent.

EVALUATION OF SKYLAB PHOTOGRAPHY

FOR

LITHOLOGY

The utility of Skylab photography for lithologic discrimination was evaluated in two ways. One appraoch was a semi-quantitative study of the detectability of a group of specific formation contacts on different types of photographs (and ERTS images). Detectability was rated, and information content was estimated. The results of this study provide a fairly objective measure of the capabilities and limitations of the different bands of photography. The second approach is qualitative, and consists of the observations made by several geologists who interpreted the photography and correlated these interpretations with ground observations.

Semi-Quantitative Study

The purpose of the semi-quantitative study was to determine if there are optimum bands of photography for discriminating lithologies, and what the bands are. Twelve lithologic contacts in the Canon City area of central Colorado were selected for study on Skylab photographs and ERTS images (App. D). Each contact was defined and located on small-scale (1:100,000) aerial color photographs,

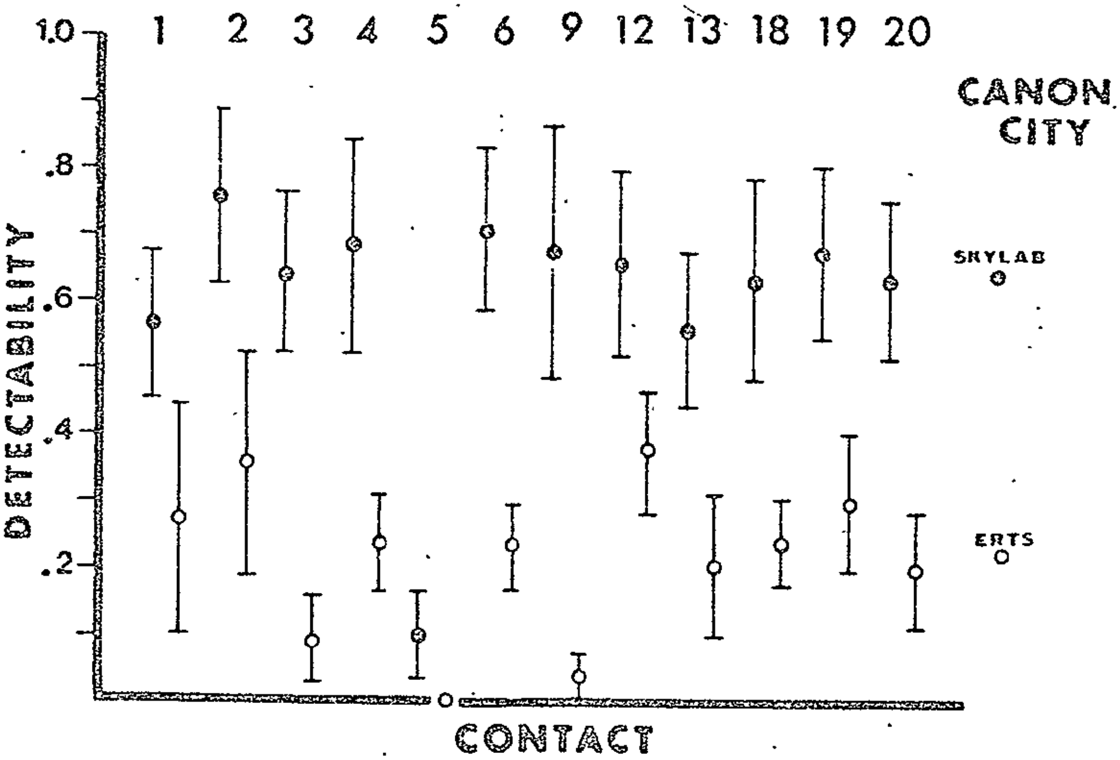

Confidence intervals of mean detectability of the 12 common lithologic contacts studied on both ERTS and Skylab imagery. $\alpha = 0.05$.

Detectabilities of individual contacts on ERTS images are strongly influenced by the time of year the images were recorded, but on Skylab S190A photos there is no significant difference between the June, August and January photos. An explanation for the dependence of ERTS and the independence of Skylab S190A on time of year may be contained in the spacial resolution differences between the two systems. The higher spacial resolution of Skylab S190A photos may allow the subtle surface expression of contacts to be detected even at less than optimum times; the low resolution ERTS system may not be able to show these subdued contacts adequately.

PRECEDING PAGE BLANK NOT FILMED

Analysis of the detectabilities of the lithologic contacts does not measure the information content of the images or photo sets. Therefore, the information content of the images and photos must be considered if the optimum imagery is to be determined.

Obviously, the maximum amount of available lithologic information will be gained if each band of each image set is analyzed. But can this same information be found if only one or two specific images or photos are studied? To check this, matrices showing the information content of each ERTS image and Skylab S190A photo were prepared, and the percentage of the contacts that can be seen on each is as follows:

	ERTS				Skylab S190A			
	Band 4	Band 5	Band 6	Band 7	Green	Red	Color	Color IR
January	50	58	58	58	92	100	100	100
June	83	83	83	67	100	92	100	100
August	83	83	83	83	100	92	100	83

A single ERTS image selected for photogeologic interpretation, might provide as much as 83% of the available information (number of lithologic contacts mapped) or it might provide as little as 50%. A single Skylab color photo would yield 100%.

CONCLUSIONS

Lithologic contacts can be detected consistently better on Skylab S190A photos than on ERTS images.

Color photos are best; red and green band photos are somewhat better than color-infrared photos; infrared band photos are worst.

Detection of contacts on ERTS images is sensitive to time of year, whereas Skylab photos are able to detect contacts under poor conditions, probably because of higher resolution.

Satisfactory lithologic mapping might be realized using a single Skylab S190A photo, but less than satisfactory results should be expected if only a single ERTS image is used.

It might prove risky to extrapolate the results from this study, conducted in Colorado, to all areas of the world for all lithologic contacts.

Qualitative Study

A difficulty arises in attempting to communicate to others the "lithologic information content" of a Skylab photograph. To state that the stratigraphy can be interpreted "in great detail" is insufficient, and good objective criteria are unknown. For this reason, it is important to study critically some of the S190B color photos (App. F,

Pls. 8-10), in stereo, and to compare these with published geologic maps (App. F, Pls. 3, 6 and 7). Alternatively, photogeologic maps derived from S190B photos (App. F, Pls. 2, 4 and 5) should be examined.

The lithologic discrimination capability of S190B color photography is dramatically superior to S190A black-and-white photography and ERTS imagery. The addition of color, combined with the increased ground resolution, markedly increases the ability to subdivide lithologic units. Most of the formations broken out on 1:250,000 scale geologic maps can be discriminated and mapped where scale permits. Whereas the S190A black-and-white photography (red band) permitted the subdivision of one area into five formations, with S190B color photography it was possible to break out (at least in some places) eleven mappable units.

The general ability to map stratigraphic units is significantly increased on 1:125,000 scale (8X) transparencies as compared with 1:500,000 scale (2X) transparencies. A brief comparison of Plates 2 and 5 (App. F) indicates the amount of stratigraphic subdivision possible.

Photogeologic mapping studies were conducted in southwestern Colorado and southeastern Utah to evaluate S190A and S190B photographs. This region is ideal for the study of Skylab photography because of the large percentage of exposed bedrock in the area. Difficulty in recognizing and tracing stratigraphic units was encountered only in the higher terrain covered by vegetation. Maximum stratigraphic

information derived from the S190B photos was obtained in the Canyonlands National Park area south of Moab, Utah.

Results of the stratigraphic subdivision in this area are shown in the figure on the following page. Inspection of this figure forcibly brings out one salient feature of the photointerpretation: not only can formations and members be interpreted from the EREP photographs, but stratigraphic lateral variations can be determined as well.

Using the base of the Wingate Sandstone as a datum, the figure clearly shows stratigraphic thickening toward the southwest. Almost all of this thickening can be accounted for by changes within the Permian Cutler Formation, but this relationship persists into the Triassic, as evidenced by the pinch-out/facies change of the White Rim Sandstone and Keybed 2 in a northeasterly direction.

The ability to determine stratigraphic thicknesses is quite good. Obviously this capability stems from, and is dependent upon, the conjunctive use of accurate topographic base maps. As an illustration of thickness determination, the stratigraphic section below the Wingate Sandstone and above the Hermosa Formation was estimated to be about 500 m thick in the northeast and about 670 m in the southwest. Interpolation of measured stratigraphic sections by McKnight (1940) gives corresponding thicknesses of about 525 m and 730 m, suggesting the photointerpretive studies are in error by about 4 percent and 8 percent respectively.

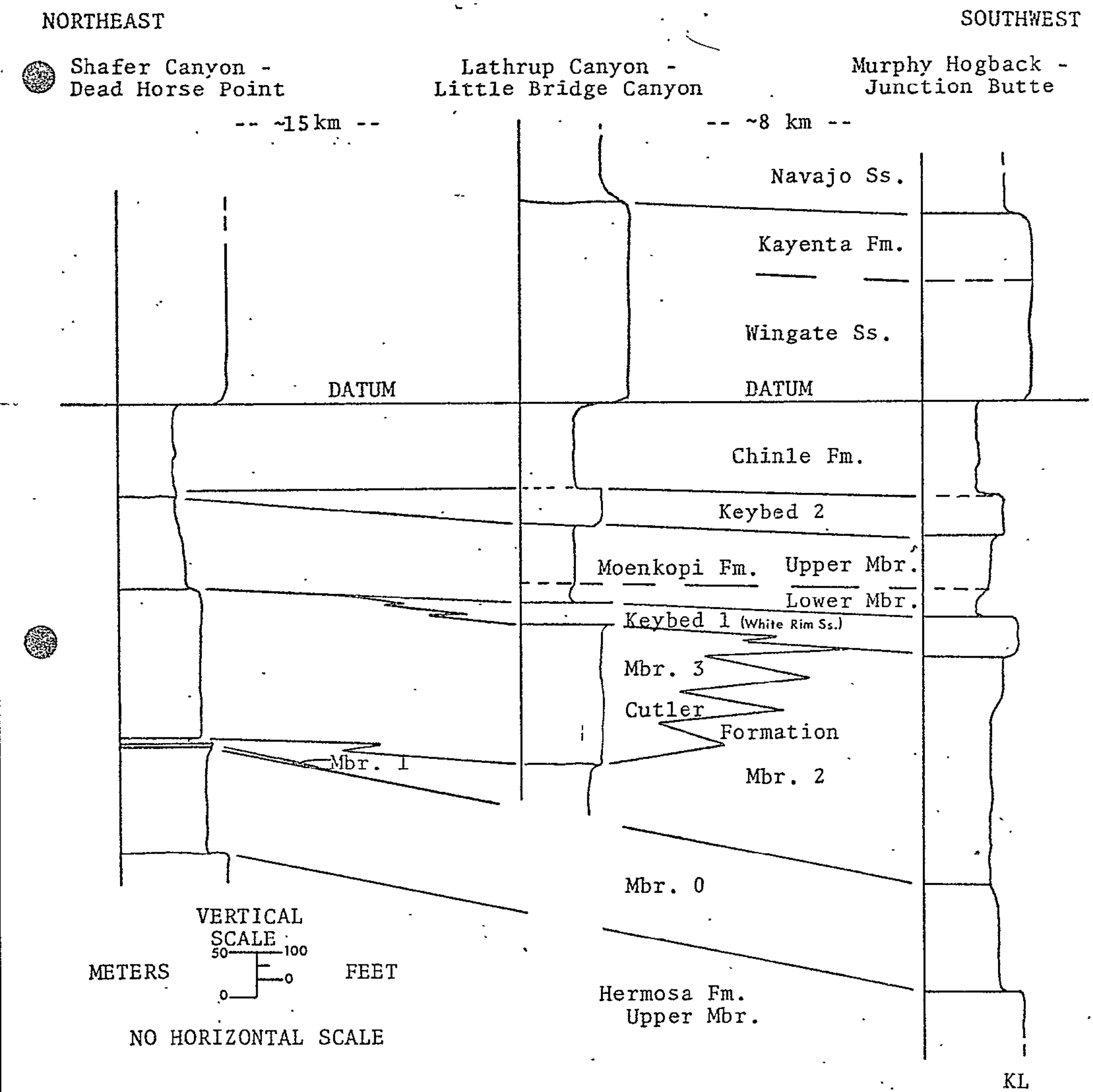

Generalized stratigraphic sections and correlations based on photointerpretation of Skylab S190-B photographs, Moab South area, Utah.

To illustrate the detail of stratigraphic information available in the S190B photos, the following section describes one of the lithologic formations mapped in this area and compares photo observations of the formation with published descriptions.

The Cutler Formation in this area is quite complex. Initial photointerpretation of the Cutler subdivided the formation into three members, called simply Member 1, Member 2 and Member 3. Later photointerpretation broke out a lower unit, which was then called Member 0, and the prominent keybed (k1) at the top of the Cutler Formation was subsequently identified as the White Rim Sandstone and included in the Cutler Formation. Thus, the Cutler Formation, as used here, consists of five members, Members 0 through 3, plus Keybed 1.

Member 0 is differentiated from the underlying Hermosa and from the overlying Member 1 by its red color and lower resistance. Thickness of Member 0 is estimated at about 120 m, compared with an estimate of 177 m by McKnight (1940), but McKnight's section also included what is here designated as Member 1 and part of what is here designated as Member 2.

Member 1 is a very resistant, grey, carbonate unit among the Cutler redbeds. Although the unit is only about 3 m thick, because of its resistance it forms benches and ledges such that it is exposed over fairly wide areas. Field examination shows this unit to be a somewhat rubbly,

brachiopodal crinoidal lime wackestone (Elephant Canyon Formation of Baars, 1975).

Member 2 is very thin in the north part of the area (12 m) and thickens to about 260 m in the south, although it cannot be shown conclusively that this is one continuous unit. Member 2 is characterized by a pink to red to red-brown color and relative non-resistance to erosion.

Member 3 is differentiated from Member 2 by a darker red to a maroon color and by being relatively more resistant.

The relationship between Member 3 and Member 2 is not entirely clear; this photointerpretation suggests that the two members are at least in part facies equivalents. Member 2 appears to correspond to the Cedar Mesa Sandstone Member of Williams (1964) and Baars (1975) and to a transition zone where the Cedar Mesa Sandstone Member interfingers with an unnamed arkose and arkose conglomerate. Member 3 appears to correspond well with Williams' unnamed arkose and arkosic conglomerate and Baars' "Cutler arkosic red beds from the east". Both authors consider the arkose and the Cedar Mesa Sandstone Member to be facies equivalents.

Keybed 1 is an excellent marker bed throughout its area of outcrop. It forms a prominent and conspicuous white ledge that stands out sharply against the red-brown units beneath and above it. This member is relatively thin, yet forms extensive areas of outcrop because of its high resistance to erosion. Keybed 1 is the White Rim Sandstone, considered

by most authors to be the uppermost member of the Cutler Formation.

The White Rim Sandstone was estimated to be about 45 m thick in the southwest part of the map area, which does not compare well with McKnight's (1940) measurement of about 17 m, but agrees well with Baars' (1975) isopach thickness of 30-45 m. The sandstone thins continuously toward the northeast, where it pinches out. It is significant that the point of pinchout of this member could not be more accurately mapped from observations in the field than it was determined from interpretation of the S190B photographs.

CONCLUSIONS

All of the stratigraphic units at formation rank and above that appear on the published geologic map (1:250,000) are recognized on the Skylab photography. In some cases, individual formations were mapped together, but this was done because their contacts were not resolvable at the map scales because of their exposure on cliff faces.

In many cases, stratigraphic units of ranks below formation level could be established. As a result, the study area was mapped to a large extent at member level; seventeen members were mapped.

Not only can vertical variations in the lithology be interpreted, as evidenced by subdividing rock units into formations and members, but some lateral variations can be interpreted as well. The Navajo Sandstone, present throughout

most of the map area, is shown to pinch out to the northeast. Several members of the Cutler Formation are shown to have limited areal distribution; the uppermost member pinches out entirely to the northeast, and Member 2 and Member 3 appear to be lateral facies equivalents.

Intertonguing of gray marine shales with sandstones is recognized and mapped. From this mapping, the direction of more continuous marine sedimentation can be determined.

By recognizing and tracing stratigraphic units in detailed mapping, major uplifts can be demonstrated to have recurrent structural movement. Pennsylvanian and Permian strata are absent on some uplifts, indicating late Paleozoic or early Mesozoic uplifts, with the present structural relief due to Cenozoic structural movement.

References

Baars, D.L., 1975, The Permian System of Canyonlands Country, in Fassett, J.E., ed., Canyonlands Country: Four Corners Geol. Soc. 8th Field Conf. Guidebook, p. 123-127.

McKnight, E.T., 1940, Geology of area between Green and Colorado rivers, Grand and San Juan counties, Utah: U.S. Geol. Survey Bull. 908, 147 p.

Williams, P.L., 1964, Geology, structure, and uranium deposits of the Moab Quadrangle, Colorado and Utah: U.S. Geol, Survey, Misc. Geol. Investigations Map I-360 (1:250,000).

EVALUATION OF SKYLAB PHOTOGRAPHY FOR GEOLOGIC STRUCTURES

Evaluation of EREP data as a source of structural geologic information was carried out by simultaneous evaluation of interpretive techniques, sensors, and information extracted. Interpretation used widely-known photo-interpretation techniques and simple instruments such as magnifiers, stereoscopes, light tables, and devices such as tracing overlays. Sensor evaluation was done for S190A and S190B, considering band stereoscopic availability, resolution and the upper and lower limits of detectability within frames. Information evaluation was concerned with the ability to recognize known geologic structures and to map contiguous or related structures.

The best sensors are those that enhance the linear and curvilinear qualities of most geologic structures in images. This enhancement is due primarily to sharp color or tonal contrasts on the film, so the best characteristics are color and stereoscopic viewing. Secondarily, sensors in red bands and infrared bands bring about enhancement of many linear features by increasing shadow contrast. Color is superior to color IR in the interpretation of folds along the Southern Front Range because of high spectral contrasts of three sedimentary formations involved in the folds. On color IR the spectral contrasts are low and not useful.

Spatial resolution of the elements of structures is important in mapping contiguous structures. The resolution of S190B, as expected, is better than S190A. S190A photographs (red band) revealed a fault about 2 kilometers long; on S190B color photography a fracture 1 kilometer long was observed, as well as joint spacings of less than 200 meters (App. B, p. 17, Fig. 14). Spatial resolution, if high, permits continuation of what could otherwise be unrelated linear segments. Linear features greater than 50 kilometers are frequently observed in satellite photos, though their relationship to geologic structures is often uncertain. However, in the southern Front Range, linear features 35 and 125 kilometers long are related to geologic structures (App. E, p. 17,18).

Few folds are instantly recognized on photos. Most are relatively subtle in expression and must be carefully worked out by determination of opposing dips, with the dip interpretations based largely on the recognition of topographic features. Dip slopes may be directly recognized where stereo viewing is possible. Without stereo, indirect expressions helpful in slope interpretations are shadow relationships and variations of vegetation that are topographically-controlled. Drainage patterns are indicators of slopes, and the rule of V's is the most consistently useful criterion for determination of dips (App. B, Fig. 4,A).

Because the vertical exaggeration factor for the S190B photography has not been reported, a training area southeast

ORIGINAL PAGE IS
OF POOR QUALITY

of Moab, Utah, was used to determine empirically the vertical exaggeration factor using a mirror stereoscope (with no magnification). The estimated factor is about 2.5X. A trial area in the vicinity of Moab was used to test this factor. Twenty-two attitudes were interpreted, with apparent dips of 2-20°. Estimated true dips using the 2.5X vertical exaggeration factor were compared with field measured attitudes and agree within 2°.

Maximum enhancement of topography and structural features occurs for about 60 days before and after the winter solstice. Lower sun elevations bring increased areas of shadows and low reflected irradiance. In addition, during this time there is prevalent uniform snow cover, which further adds to the enhancement increase and uniform image contrasts.

NASA Mission 261 was an underflight in support of Skylab designed for low sun-angle photography. Black-and-white infrared film, Type 2424, was used with a Wratten 25 filter to photograph snow-covered areas from 50,000 ft a.m.t. with a 10 degree sun angle. The conclusion of the study was that steep topographic slopes of azimuth of 20 to 30 degrees deviation from the sun azimuth are selectively enhanced because only steeper slopes are shaded. This effect can be used to quantitatively select the azimuth range of linear features to be studied, and the date and time of day to maximize their enhancement by sun and shadow (App. I).

The effect of sun attitude on Skylab photos is shown where three new north-trending lineaments in the Rampart Range

were discovered on SL-2 photography and not seen on SL-3 photography (App. E). This is attributed to the favorable sun attitude of SL-2, when the sun azimuth was 92° and sun elevation was 40°, whereas for SL-3 the sun azimuth was 132° and the sun elevation was 57°. The reverse was true for lineaments in the Royal Gorge arch, which trend N 80 E. Lineaments with greater relief are visible on both SL-2 and SL-3.

One Skylab and ERTS investigation was concerned with those anomalous megalineaments and their associated structures that transect major tectonic features in central Colorado. These anomalous features have not been studied extensively before now because a synoptic view has not been available.

Lineaments are here defined as any unidimensional straight or continuously curved combination of picture elements that appear on photographs or images and that are thought to have geological significance. Lineaments may be the pictorial representation of faults, folds, shear zones, etc. Groups of lineaments that show elongate parallel trends, either end-to-end, overlapping or en echelon, are here defined as megalineaments ("megalinears" of App. E).

Transecting megalineaments are nearly as detectible in a space photo or image as the more structurally-consistent lineaments. Their associated geologic structures are composites of anticlines, synclines, drag folds, monoclines, faults, crush zones, shear zones, and joint sets. Structure

type along the trend of a megalineament is very dependent upon the lithologic terrains in which it is developed. It is this variability, as well as the transecting nature of the megalineaments, that presents a somewhat confusing structural picture and that has slowed the recognition of these major structural features.

In Skylab and LANDSAT images of central Colorado, the normal tectonic elements and their marginal structures are recognizable, as well as transecting megalineaments. The major structural elements of the central Colorado test site (App. E, Fig. 16) are the southern Front Range, a block mountain uplift bounded by typical mountain-flank structures; the Denver Basin on the east; South Park on the west; Canon City Embayment on the south; the Wet Mountains, a block mountain uplift; and Wet Mountain Valley. The basins are downfolded Cenozoic and older sedimentary rocks. The block mountains are Precambrian metamorphic and plutonic igneous rocks, which also underlie the basins. The trend of all of these major tectonic elements is northwest. Two sets of megalineaments occur in the southern Front Range - a north-trending set of three megalineaments in the Rampart Range area (App. E, Fig. 26) and a northeast-trending set of three megalineaments south of Pikes Peak (App. 3, Fig. 27).

In the Rampart Range (App. E, Fig. 26), the Manitou Park megalineament is associated with the Ute Pass fault on the south, which passes into the Ute Pass thrust and

northward in Pikes Peak granite into the Bear Creek shear zone. The one singular feature of this megalineament is that the fault zones all have been intruded with sandstone dikes throughout the length of 125 kilometers.

The Jackson Creek megalineament transects the Rampart Range and offsets the flank structures on the east. The eastern megalineament is associated with a long prominent escarpment that also trends into the flank structure on the east.

The three megalineaments of the Rampart Range are continuations of, or are involved with, long-known structural features. On the west, they are continuations of a major thrust fault and monocline. On the eastern side of the block uplift, the Rampart Range thrust is offset where two of the megalineaments cross. A new interpretation of this block uplift is that it consists of three giant imbricated plates with two thrust faults at the outer margins and two normal faults between the plates.

South of Pikes Peak (App. E, Fig. 27), the Milsap Creek megalineament trends southwest from the Pikes Peak intrusive center 35 kilometers. The associated structures consist of mafic-intruded crushed zones, a major offset of the mountain flank structure on the western margin, a gentle drape fold, and a fault. Two other megalineaments are the Adelaide and Peck's Camp features.

The structural evidence associated with the transecting megalineaments of the Front Range uplift points to a more complex involvement of the crystalline basement in the regional tectonic deformations. These deformations consist not only of the familiar ones of uplifts decoupled from basins along flank thrusts and monoclines, but also independent, or subsequent, continuous cross-cutting deformations that have the spatial unity of a single geologic structure, yet are manifest in different kinds of structural features along that megalineament. Further study of megalineaments may add considerably to our knowledge of tectonic history and kinematics of regions.

CONCLUSIONS

Resolution, color photography, and stereoscopic endlap coverage are the most important sensor characteristics for structure interpretation.

Fractures as short as one kilometer can be recognized on S190B photos, and joint spacings less than 200 m are resolvable.

Geologic folds can be interpreted with confidence.

Bedding attitudes can be estimated, using a 2.5X vertical exaggeration factor, with accuracies of a few degrees obtained in an area of low dips. Dips of only a few degrees are recognized.

Linear structures are selectively enhanced as a function of solar attitude; three new lineaments were detected this way.

Anomalous megalineaments are seen on space images that transect normal structural trends in the Colorado Front Range. These represent geologic structures that may reflect more complex involvement of the crystalline basement.

The amount and detail of structural information contained in the Skylab photos is difficult to quantify. The best evaluation of this information content is gained by examining S190B stereo color photographs (App. F, Pls. 8, 9, 10) and comparing the photos with published geologic maps (App. F, Pls. 3, 6 and 7). Alternatively, photogeologic maps compiled from the Skylab photos (App. F, Pls. 1, 2, 4 and 5) should be examined.

EVALUATION OF SKYLAB PHOTOGRAPHY

FOR

REGIONAL MAPPING

Two photogeologic mapping studies were conducted along Track 34 (southwestern Colorado and southeastern Utah) using SL-2 and SL-3 color photography. One study used S190A color photos and evaluated their use in reconnaissance structural mapping. The second study mapped mostly from S190B color photos, with the objective of more accurately evaluating the scale limitations and level of geologic detail available from these photos.

S190A

Approximately 40 hours were spent analyzing Skylab 3 S190A color photographs from western Colorado and eastern Utah. The objectives of the study were 1) to prepare a photogeologic map to determine the geologic information content of the S190A photographs, 2) to compare the results of this work with a map of the general area prepared from ERTS imagery, and 3) to determine how accurately and rapidly a large area could be mapped by an experienced geologist with a working knowledge of the geology.

A photogeologic map was prepared for approximately 25,000 square kilometers covering the region of the Uncompahgre Uplift and the northern portion of the Paradox Basin (App. F, Pl. 1).

Four frames of S190A color transparencies (~4X, 1:710,000) with stereoscopic coverage were used to study the geology of the region. The images were observed with a mirror stereoscope and interpretations transferred to a transparent overlay on color prints (~8X, 1:360,000).

The investigator was generally familiar with both the geology and geography of the region from detailed mapping that had been conducted in small areas scattered through the region. The observer was continually amazed at the excellent quality of the color photography, the ease of recognizing stratigraphic units and structural elements, and the accuracy of locating oneself relative to geographic points.

Eight stratigraphic units with widely varying lithologies were selected for mapping purposes based on ease of recognizing mappable contacts throughout the area and sufficient detail to define the structural features. Additional stratigraphic units could have been mapped, but, for the purposes of this project, the time required for mapping greater stratigraphic detail was judged to be inappropriate in achieving the stated objectives.

The largest and most significant structure is the Uncompahgre Uplift. The uplift is a large block approximately 160 km long and 60 km wide that is tilted to the northeast and trends N50W. A thin sedimentary sequence covers the uplift, forming long northeast dip slopes. Precambrian rocks are exposed in deeply eroded canyons and on the north side

of the major fault zone separating the uplift from the Paradox Basin. The major faults are believed to be high angle and are obviously basement-controlled systems.

The northern Paradox Basin contains numerous anticlines formed in Pennsylvanian through Cretaceous strata. Five major anticlinal trends have been delineated by both outcrop patterns and dip of strata. Some of the fold axes can be traced for more than 150 km; the flanks of the folds vary in width from 5 to 10 km.

Many more faults have been mapped on the photos than appear on published maps of similar scale (App. F, Pl. 3). Ground checking may eliminate some of the lineaments, but it is believed that the Skylab S190A photographs show fault trends not heretofore known from published geologic maps of the area.

By tracing stratigraphic units on the Skylab photographs, the history of major structural elements can be reconstructed. The Paradox Basin contains Pennsylvanian and Permian stratigraphic units that are not present on the Uncompahgre Uplift. This indicates the uplift was a high area during the late Paleozoic or that rocks of these ages were deposited and subsequently removed by erosion prior to deposition of the Triassic. Under either interpretation, and because the area is an uplift today, the mapping indicates renewed tectonic movement of the uplift through geologic time.

Photogeologic mapping in this area was conducted by use of both ERTS-1 and Skylab 3 images. Band 6 was used in mapping on an ERTS image, whereas color photography was used on Skylab. The major folds, the general distribution of stratigraphic units, and major fault patterns were similar on both types of images. However, much more detailed and accurate information was available from the Skylab photos. The ERTS imagery does not have continuous stereoscopic coverage, and its use must definitely be classed as a reconnaissance mapping technique. By contrast, the quality of the Skylab S190A photographs permits accurate, detailed mapping in a manner equal or superior to any other system of photogeology where an investigator wishes to map a large area in a short period of time.

S190B

The approach followed in this study was to use a designated training area, in which area each type of satellite image was interpreted in a conjunctive way with published geologic maps. Experience derived from this training area was then used to photointerpret the geology of an unknown area.

Initial photogeologic mapping used 1:500,000 scale photos for annotation and 1:250,000 scale topo base maps for geologic compilation (App. F, Pl. 2). It soon became apparent, however, that the amount of geologic information

was greater than could be compiled effectively at this scale. Most detailed photogeologic mapping, therefore, was done at larger scales.

Photointerpretation was conducted using 4X and 8X enlargement positive transparencies of the S190B photographs. Stereo interpretation used a mirror stereoscope with an effective magnification range of 1-2X, so these positive transparencies were examined at about 1:250,000 to 1:60,000 scale. Where geologic information was apparent on the enlargements, the information was directly annotated; areas of structural complexity or subtle detail were studied concurrently on contact transparencies at high optical magnification.

Geologic information was annotated onto clear acetate overlays on top of the positive transparencies. The interpretations were then transferred from the overlays onto topographic maps (1:62,500) using a zoom transfer scope, and using the topographic information as a secondary control. It was often necessary to go back to the original duplicate positive on the zoom stereoscope for resolving detail and resolving complex structures.

The accuracy and validity of the photointerpretation maps were checked in the field. Field observations consisted of examining areas characteristic of the geology of each map area, as well as investigation of areas where geologic interpretations were complex or where no geologic interpretation could be made from the photographs. Four days were spent field-checking the 1:62,500 photogeologic maps.

This research was conducted so that the photogeologic maps produced represent data products that would be obtained from an application of photointerpretation, using Skylab S190B photography, to areas that are geologically unknown or geologically poorly known. The geologic maps (App. F, Pls. 2, 4 and 5) represent geologic mapping by photointerpretation on Skylab S190B photographs, supplemented by minimal field checking. In general, the correlation between the photogeologic maps and the published geologic maps is excellent, but this can be evaluated only by carefully comparing the maps (App. F, Pl. 2 with Pl. 3; Pl. 4 with Pl. 3; and Pl. 5 with Pls. 3, 6, and 7).

CONCLUSIONS

By viewing large structural features of the earth's crust in one or two images, fault and fold patterns can be interpreted in a perspective not previously possible.

Skylab S190A photos permit rapid and accurate photogeologic mapping in areas of complex folding and faulting, if outcrops are good. Approximately 25,000 square kilometers were mapped at a scale of 1:360,000 in about 40 hours.

In areas of heavy vegetation, mapping accuracy is significantly reduced to a reconnaissance level.

The Skylab photos are superior to ERTS imagery. Skylab maps may be equal to or greater in accuracy than some published geologic maps.

An increase in geologic information is associated with increase in scale when comparing the S190A and S190B photography. System resolution is approximately the same for each camera, but ground resolution of the S190B is superior because of its longer focal length and correspondingly greater scale. There is little doubt that an increase in resolution can be directly translated into an increase in geologic information.

Using S190B photographs, photogeologic mapping at a scale of 1:24,000 is not feasible, and 1:250,000 is, in some cases, too small a scale. Optimum scale for photogeologic mapping is about 1:62,500. This conclusion, however, may be valid only for this area.

Photogeologic mapping from Skylab S190B color photography will add little new geologic information in areas where 1:250,000 scale geologic maps are available. In such areas, however, the photography should prove useful for re-examining the geology in the light of new concepts or hypotheses.

Photogeologic mapping from Skylab S190B color photography would provide invaluable geologic information in areas that are geologically unknown or poorly known, provided only that exposures are good and photo quality is high.

EVALUATION OF SKYLAB PHOTOGRAPHY
FOR
MINERAL DEPOSITS

It is economically more desirable to survey large areas for potential ore deposits by remote sensing than by conventional ground surveys. Advantages of satellite imagery, both photography and scanned imagery, include a synoptic view, repetitive coverage, accessibility to remote areas, and relatively low cost. The objective of this research was to evaluate Skylab EREP photographs and, to a lesser extent, ERTS (LANDSAT) and aircraft images, for their utility in locating indicators of mineralization in central Colorado.

The Leadville and Cripple Creek mining districts are typical of mineralized areas in central Colorado. Skylab photos covering these areas were studied, and geology was correlated between maps and photographs. Each area was field-checked to identify exactly what was seen on the photography, and the two control districts were analyzed to determine the geologic features characteristic of mineralized areas that are visible on orbital photography.

Ore deposits of the Leadville district occur chiefly in fissure zones, karst collapse breccias, or as replacement mantos in dolomites intruded by Upper Cretaceous or lower Tertiary felsic to intermediate porphyries. Major faults

contain ore in few places, while auxiliary faults and fissures have served as feeder channels and often are mineralized. Alteration includes local hydrothermal bleaching of porphyries and weathering of disseminated pyrite to hydrous iron oxides. Indicators of mineralization for this district are faulting, intrusion of sedimentary strata by light-colored porphyries, and weathered pyrite. Field checks verified the ability to see some faulting on all orbital photography, and alteration colors were visible on S190B photos.

At the Cripple Creek district, ore deposits lie within or near the margins of a steep, fault-caused basin (caldera?, breccia pipe?) filled with Miocene breccia and phonolite and surrounded by Precambrian granite, gneiss, and schist. The basin, approximately three by six kilometers (two by four miles), is filled with non-volcanic as well as volcanic debris, and is crosscut by dikes of phonolite and lamprophyre. Gold mineralization followed intermittent fissuring and is most commonly found as veins associated with quartz and pyrite gangue. Indicators of mineralization that are visible on satellite images are faulting and alteration of pyrite. Weathered pyrite is seen only on mine dumps.

Results of the study at the Leadville and Cripple Creek mining districts led to the preliminary conclusion that indicators of mineralization visible on Skylab photography over central Colorado are faults and alteration. Breccia-filled basins could not be recognized on Skylab photos

because of a lack of color contrast or unique topographic or vegetation features. Karst horizons and mantos likewise were not visible because of limited stratigraphic extent and frequent soil and vegetation cover.

Faults and alteration are seen on satellite photography as lineaments and anomalous colors. A "lineament" is any line or alignment of features of probable geologic origin; extensive faulting appears as a high density of lineaments and numerous intersections of lineaments. Alteration produces anomalous colors, or a local color that deviates from regional uniformity. Primary color anomalies associated with alteration are red-ocher colors produced by weathering of pyrite, and light-color areas due to hydrothermally-bleached intrusives.

Skylab photos of the central Colorado survey area were studied to find other areas that show indicators of mineralization. Limited cloud-free Skylab photography somewhat narrowed the study area; the primary site was the area covered by Skylab 2, S190A, Track 48, Frame 17, acquired 11 June 1973 (App. G, Fig. 1). Skylab 2 and Skylab 3 photos were used (Skylab 4 photos were received too late to be included), as well as ERTS images (e.g. - E 1154-17143) and aircraft data (NASA Mxs 184, 211 and 235). The entire study area includes 47,000 square kilometers.

In this study to locate other areas of mineralization, structure targets were chosen in areas of high lineament density or at complex lineament intersections, by mapping lineaments as guides to faults, joints, and shear zones.

It has been demonstrated that multiple intrusions and cauldron subsidence are associated with high density radial faulting, while volcanic piles, anticlinal uplifts, and erosion have considerably less radial faulting, and therefore less complex fault intersections. Areas of complex structural intersection have long been considered favorable to ore deposition. It is expected that linear features seen on satellite photography are fractures (faults, joints, shear zones).

A common surface indicator of ore at depth is the gossan, an outcrop of leached and oxidized iron sulfides. Where unobscured, the characteristic red-ocher color can be seen on color photography. In addition, intrusive rhyolite porphyries should appear as light-colored anomalies where intruded into darker sediments. Surprisingly, the color rendition of the S190B film (SO-242) allowed detection of color anomalies that were not obvious on aircraft photography.

An overlay map of the study area was constructed showing all of the mapped lineaments. From this map, favorable structural targets were picked (App. G, Fig. 16). In a similar way, the color Skylab photos were interpreted for color anomalies, and areas of favorable color were picked (App. G, Fig. 17). From the conjunctive use of these two maps, mineral target areas were defined on the basis of concurrence of structural and color anomaly targets, and these target areas were ranked according to priority. The highest

priority target area occurred at Weston Pass, and this area was subsequently field checked.

Evaluation of the primary target at Weston Pass consisted of mapping from satellite and aerial photography (1:500,000 and 1:20,000, respectively) and in the field (1:12,000) to determine the origin of lineaments and color anomalies, and to discern the relationship of these features to ore deposits.

Twenty-two lineaments were mapped from Skylab photography within the Weston Pass study area (App. G, Fig. 24). Detailed field mapping shows that seven of these lineaments, of 32%, are in fact faults (App. G., Fig. 25). One lineament was correlated to a cultural feature (powerline), and the remainder are vegetation and drainage alignments thought to be strongly influenced by structure. A comparison of 53 linear drainage azimuths with 239 joint measurements suggests that one drainage trend is directly controlled by jointing, and that another trend is a consequence of drainages formed on dip slopes normal to fracturing.

Field mapping revealed that red-ocher color anomalies are caused not only by a gossan, but also by red sedimentary rocks and microcline-rich crystalline rocks and grus. The most obvious color anomaly, on the west slope of Weston Peak (App. G, Fig. 17), contains both microcline and hematite/limonite-rich granite talus. Another less visible anomaly consists of microcline-rich outcrop and grus; another comprises

limonite-stained dolomite talus overlying a white quartzite. Most color anomalies at Weston Pass (App. G, Fig. 21) correspond well with the percentage distribution of microcline in Precambrian basement rocks (App. G, Fig. 22).

Indicators of mineralization did lead to an old mining district at Weston Pass, where lead and zinc sulfides formed manto deposits in the Leadville Formation. The ore is thought to have originated either in nearby porphyry sills or in a batholith at depth, and to have migrated along fissures adjacent to large, regional, gouge-filled fractures such as the Weston fault. The (former) presence of these ores, however, was not directly indicated by the Skylab photographs; the extensively limonitized ore horizons at Weston Pass were not visible on orbital photography because of limited outcrops and extensive vegetation and soil cover.

Results of this study suggest the preliminary conclusions were incomplete. Red-ocher colors in central Colorado may result from sedimentary red-beds, microcline-rich crystalline rock, iron-oxide alteration, or combinations of these. Linear features have been identified as aligned streams and cultural features, as well as geologic features such as faults, joints, shear zones, dikes, contacts, folds, and paleovalleys. Intersections and high densities of regional lineaments, where they in fact represent structures, are not the only structural controls on mineralization.

CONCLUSIONS

Skylab photography can cover large areas quickly and inexpensively, and there are some surface features in any given region that are indicators of mineralization. Photolineaments and color anomalies are important indicators of mineralization in central Colorado, but positive identification of these features is not possible. Areas where orbital photography may be most useful in the search for mineral deposits include the snow-free alpine portion of mountain ranges and in arid regions.

Orbital photography alone is inadequate to fulfill exploration needs. It is useful in reducing the size of an exploration area to potentially favorable targets, but like other remote sensing techniques, it is a powerful tool only when used in conjunction with detailed field work.

EVALUATION OF SKYLAB PHOTOGRAPHY FOR WATER RESOURCES

Skylab S190-A and S190-B photography, covering the northern closed basin of San Luis Valley, Colorado, was evaluated for its use in regional water resource studies. Specifically, the study evaluated the ability of a photo-interpreter, using only Skylab products, to map surface water divides and drainages, zones of ground water recharge and discharge, distribution of hydrogeologically-significant rock and alluvial units and significant structures, and ground water depth and quality. All interpretations were checked by either field work or comparison with published data.

Some of the most obvious features on Skylab photographs are the major surface water divides and drainages. A drainage map of the northeastern part of the study area interpreted from Skylab 2 S190A photography (App. H, Fig. 2) is much more detailed than the existing 1:1,000,000 scale topo map of the area, but inferior to existing 1:250,000 scale maps. Accuracy of the surface water divide from the photos is comparable to that of the existing 1:250,000 scale topographic map. Mapping of drainage is best using color-infrared photography, because streams within the alluvial

portion of the basin are best defined by the presence of deciduous vegetation along their course.

Knowledge of the positions of the surface water divide and the drainages is significant not only in the evaluation of surface water flow directions and boundaries, but, in most cases, it helps define the boundaries of ground water movement. In most terrains, where the water table forms a subdued replica of the topography, ground water recharge often occurs at topographic highs, and discharge is found at topographic lows. In a homogeneous medium, or in an inhomogeneous medium of horizontal units, the surface water divides and major drainages will act as impermeable boundaries, and there will be no flow across them.

Resolution of the film/camera system is the most important factor determining the amount of hydrogeologic information that can be interpreted. The S190A system does not have sufficient resolution for more than a cursory examination of the distribution of rock and alluvial units. Although no stereo coverage was available for the S190B system, it is obvious that much more information results from the greater resolution. Interpretation of stereo S190B photographs would probably produce a map comparable to that of an interpretation of high-altitude aircraft photography, sufficient for a reconnaissance-level, regional ground water study.

Geologic structures, particularly faults, exert a strong influence on ground water movement in the San Luis

Basin. Fractures provide the most significant permeability in the marginal bedrock units, and faults within the alluvial sequence of San Luis Valley often are ground water barriers. Faults within the mountains can be interpreted only by the presence of linear topographic depressions, or the linear alignment of discontinuous topographic depressions; the capability of mapping stratigraphic units in sufficient detail to delineate fault separations is simply not present using S190A system photography. S190B photography has adequate resolution to map the hydrogeology in some cases, but aircraft photography is a necessity for most studies and field work is a necessity for all studies, even at the regional level.

Ground water depth and ground water quality can be estimated from Skylab photographs. Narrowleaf cottonwood trees (<u>Populus angustifolia</u>) and willow (<u>Salix</u> spp.) are found where saturated sediments are within five meters of the ground surface, and both are capable of being seen on the color infrared photography because of their high photo-IR reflectance compared with surrounding xerophytes. Cottonwoods thrive only in areas of good water quality, whereas the willows are more tolerant. Vegetation maps derived from Skylab 3 S190A color infrared photography (App. H, Fig. 7) correlate well with maps of ground water depth (App. H, Fig. 8).

Possible relations between saline soil and ground water depth were first observed on LANDSAT imagery and studied in

more detail on Skylab 3 S190A photography. The distribution of saline soils was mapped from S190A photography and was studied to determine its relation to ground water depth, quality, and direction of flow.

Comparison of the interpreted soil salinity (App. H, Fig. 9) with ground water depth (App. H, Fig. 8) shows that saline soils develop only where the ground water is relatively shallow, but that saline soils are not present everywhere the water table is near the surface. The presence of shallow ground water associated with non-saline soils indicates that at least one additional parameter limits the distribution of saline soils, and this appears to be position within the ground water flow regime. All areas of high soil salinity can be represented as areas of shallow ground water that are within the zone of potential discharge - that is, in areas where ground water potential (head) increases with depth.

Because the use of soil salinity in the interpretation of ground water depth appears to be potentially more dependable than vegetation, examination of the spectral reflectance of the saline soils was undertaken to attempt to better delineate these soils. Reflectances of dry saline soils, and moist and dry non-saline soils were measured to determine the best method for isolating the saline soils on photography.

Saline soil reflectances were measured in the field, and dry and moist non-saline soil reflectances were measured in

both the laboratory and field, using a filter-wheel photometer. The dry and moist non-saline soils show a wide range of absolute reflectances, but a relatively uniform normalized reflectance curve (App. H, Fig. 16), so normalization should be used as a preprocessing step. Saline soils with a high average reflectance do show a reduced slope of increased reflectance towards the infrared region, suggesting that ratioing may help increase the contrast between saline soils and non-saline soils having the usual range of intermediate reflectances. This has not been tested in application.

A plot of absolute band reflectances for non-saline and saline soils (App. H, Fig. 18) shows separation of the ranges in the photo-infrared bands, the deep-red bands, the minus-blue band, and the no-filter band. These observations in part contradict the subjective evaluation of S190A photography, where the infrared bands show the least contrast. One explanation for this is that the photography is not contrasting non-saline with saline soils, but is contrasting vegetation with saline soils. Vegetation typically exhibits a high photo-infrared reflectance, which would show a low contrast with saline soils, but has a much lower visible relfectance than the saline soils. This may well affect the conclusions reached above concerning band ratioing.

C. 6

CONCLUSIONS

Both vegetation and soil salinity are useful indicators of shallow ground water, but both must be interpreted carefully.

Resolution is the single most important factor in the application of Skylab photography to hydrogeologic investigations.

Skylab S190A stereo photography is sufficient for defining drainage divides that in turn define the boundaries and distribution of ground water recharge and discharge areas within the basin.

Skylab S190B stereo photography has sufficient resolution to map hydrogeologic units and structures that may be sufficient for regional studies. Aircraft photography and field work are still necessary to produce an accurate hydrogeologic map.

RECOMMENDATIONS

The Earth Resources Experiment Package was a successful experiment. The photographic part of the package should now be applied.

Photographic sensors should be used to provide reliable, accurate, detailed geologic maps that in turn can be applied to specific programs such as hydrogeology, mineral deposits exploration, petroleum exploration, etc.

This geologic mapping application should be directed toward areas that are poorly-known in a geologic sense - specifically, to areas where geologic maps do not exist at scales as large as 1:250,000 and where exposures are good. Normally, this would direct the application to underdeveloped countries; photogeologic mapping of Colorado from S190 photos is not cost-effective, but for Iran the return should be enormous.

Mineral resource industries should become more involved in the application of Skylab data. Few publications are available to bring Skylab photos to the attention of industry, and at the two main industry-oriented geologic remote sensing meetings of 1975 (U. Kansas, February; EROS Data Center, October), Skylab was little mentioned. It seems that Skylab to date has existed largely in the research lab and university environment, appropriately. But to be applied, industry must begin to use the data. Educate the users rather than use educators.

Geologic applications should emphasize photography and photointerpretation. Computer processing techniques will have specialized uses when they become commonly available, and will require sophisticated equipment. Photointerpretation of space photos requires only minimal re-education of a geologist and builds upon his prior experience.

Future satellite programs should attempt a marriage between ERTS and Skylab. For all geologic uses where we have compared good ERTS data with good Skylab data, there is no doubt that the Skylab photographic data are superior. But the photographs just aren't available for many areas, or they are cloudy. The biggest single advantage of ERTS imagery is that it is there.

Specifically, the global, repetitive coverage of ERTS should be combined with the resolution, stereoscopic capability and color of quality photography. Perhaps an unmanned Skylab, with its huge payload and film storage capability, could use film eject systems, combined with data takes regulated by real-time MSS feedback, to obtain global, cloud-free, stereo, high resolution, color photography.

Sensor improvements in photography should require little effort. Multiband photographs should be de-emphasized; if camera systems have multiple magazine capability, color infrared and panchromatic films would be available for designated uses, and the multiband photography concept has not proved effective. It would be much more desirable to have

multi-focal length (zoom?) cameras, each with 9-inch film format. Consideration should be given to 150 mm, 450 mm and 1500 mm focal lengths that would provide (from 435 km) respectively, ~1:3,000,000 scale photos covering 660 km, ~1:1,000,000 scale photos covering 220 km, and ~1:300,000 scale photos covering 66 km. Parallel MSS systems, especially with sweep detector arrays, could still provide computer-compatible data tapes.

APPENDIX I

NEW USES OF SHADOW ENHANCEMENT

Don L. Sawatzky and Keenan Lee

Remote Sensing Report 74-5

NASA Grant NGL-06-001-015
NASA Contract NAS9-13394
National Aeronautics and Space Administration

27 March 1974

REMOTE SENSING PROJECTS
DEPARTMENT OF GEOLOGY
COLORADO SCHOOL OF MINES ◇ GOLDEN, COLORADO

NEW USES OF SHADOW ENHANCEMENT

Don L. Sawatzky and Keenan Lee

Remote Sensing Report 74-5

NASA Grant NGL-06-001-015
NASA Contract NAS9-13394
National Aeronautics and Space Administration

Paper Presented at the 3rd Annual
Remote Sensing of Earth Resources Conference
University of Tennessee Space Institute
25 March 1974

27 March 1974

NEW USES OF SHADOW ENHANCEMENT

Don L. Sawatzky and Keenan Lee

Department of Geology
Colorado School of Mines
Golden, Colorado

ABSTRACT

Shadow enhancement of topographic linears in photographic or scanner images is a valuable tool for interpretation of geologic structures. Whether linears will be enhanced or subdued depends on sun angle and azimuth. The relationship of the sun's attitude to topographic slopes determines which trends are available for interpretation in existing imagery, and it can be used to select the time of day, surface properties, and film and filter characteristics in planning aircraft flights or satellite orbital passes. The technique of selective shadow enhancement can be applied to all photographic or imaging experiments, but is best for snow-covered scenes, side-looking radar images, and painted relief models.

INTRODUCTION

D.U. Wise (1969) discussed the enhancement of topographic linears produced by low-angle illumination of relief maps from various directions. The technique reveals sets of linears often noticeably aligned within 30 degrees of the illumination direction. Many of these linears are anomalous in that they are unrelated to obvious geologic structural trends and transect major features of different tectonic style.

This paper attempts to explain selective shadow enhancement by developing and extending the

ideas of Wise. The theory of selective shadow enhancement is shown to be useful in the interpretation of linear trends on imagery and photographs, and useful in planning experiments that selectively enhance certain trends.

Shadow enhancement is defined as the exaggeration of topographic linears or alignments of such linears by shadows formed within or along them. The topographic linears may or may not be obvious. Enhancement can be produced by a linear shadow margin or by an elongated shaded area.

The shadow is the result of low irradiance on the area, and is distinguished from illuminated areas of low reflectance. In much imagery and photography the distinction between the two is not always obvious. While both types of dark areas may have strong geologic controls, the shape of a shadow is strongly controlled by the illumination attitude (elevation and direction).

Numerous techniques have been developed to exaggerate linears in imagery and photographs. On the spectrum of enhancement techniques, image enhancement techniques are ternary. Shadow enhancement is secondary, and geomorphic processes, while not under our control, are primary. Image enhancement operates only on the linears available in the image, which are only a subset of all the linears in the object scene. Shadow enhancement is the result of topography and illumination at the time of exposure or scanning. However, it operates variably upon topographic linears, depending on slope attitudes, and may subdue them as well as enhance them (Fig. 1, [A]). Therefore, there will always be some linear features unavailable for enhancement.

Alignment of several linear segments is a puzzling phenomenon that may have psychophysical aspects to it. Little seems to be known about it, and long-winded speculations will not be made here. The phenomenon is puzzling for two reasons. First, very long linear features are often composed of

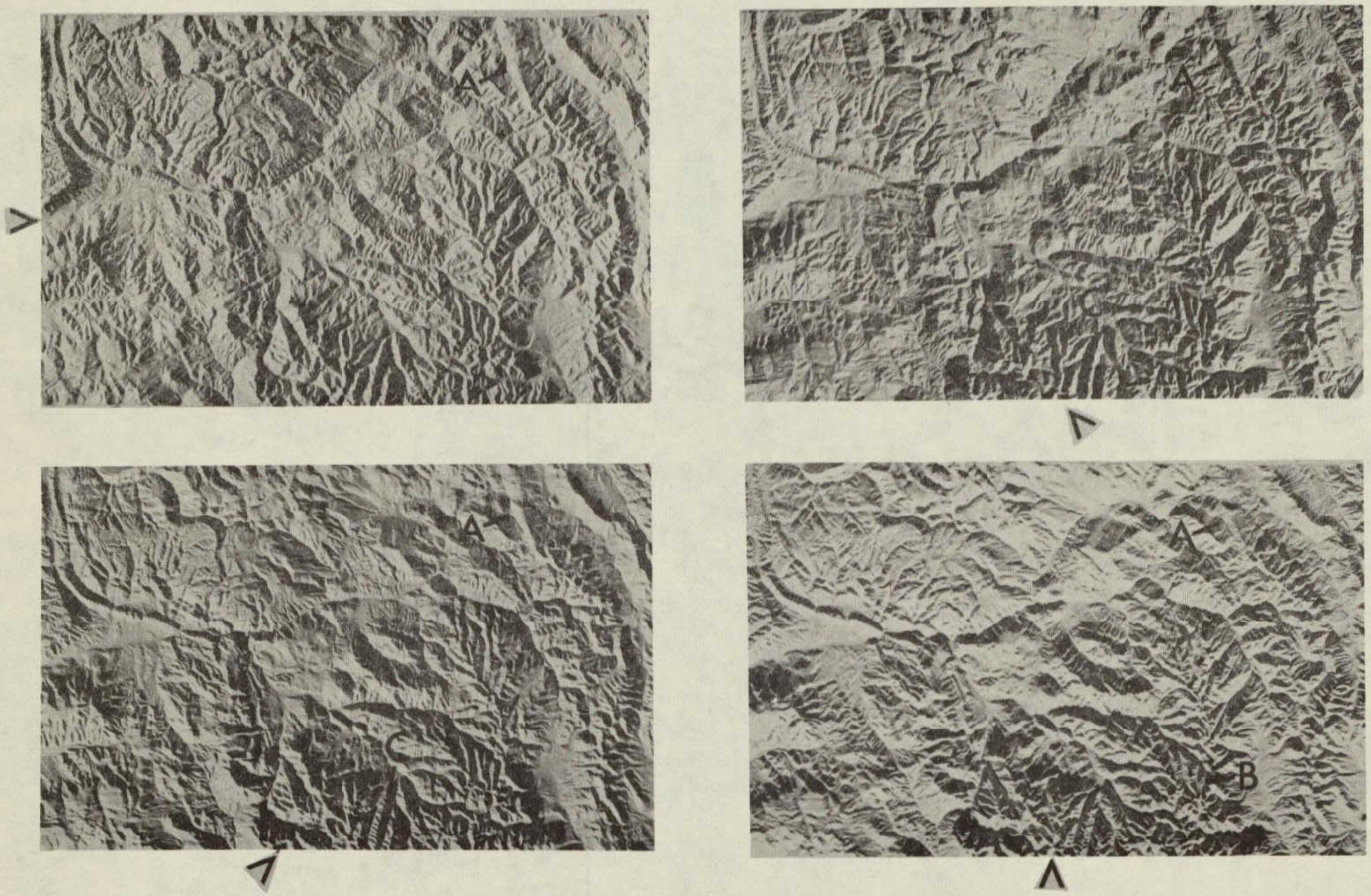

Figure 1: High contrast photographs of a relief model of the Leadville, Colorado, map (original scale = 1:250,000). Arrows indicate the illumination direction. The elevation is 27 degrees.

several segments. They cross major tectonic features without apparent relationship to the tectonic trends. Second, the alignments are near perfect at some illumination directions, but become angular or even non-existent at other directions (Fig. 1, [B]). In our experience, the physical origin of short linears or individual segments can be determined with great probability, but the origin of many of the long alignments cannot be. Some preliminary results of plots of random linears indicate that apparent trends will exist (Fig. 2).

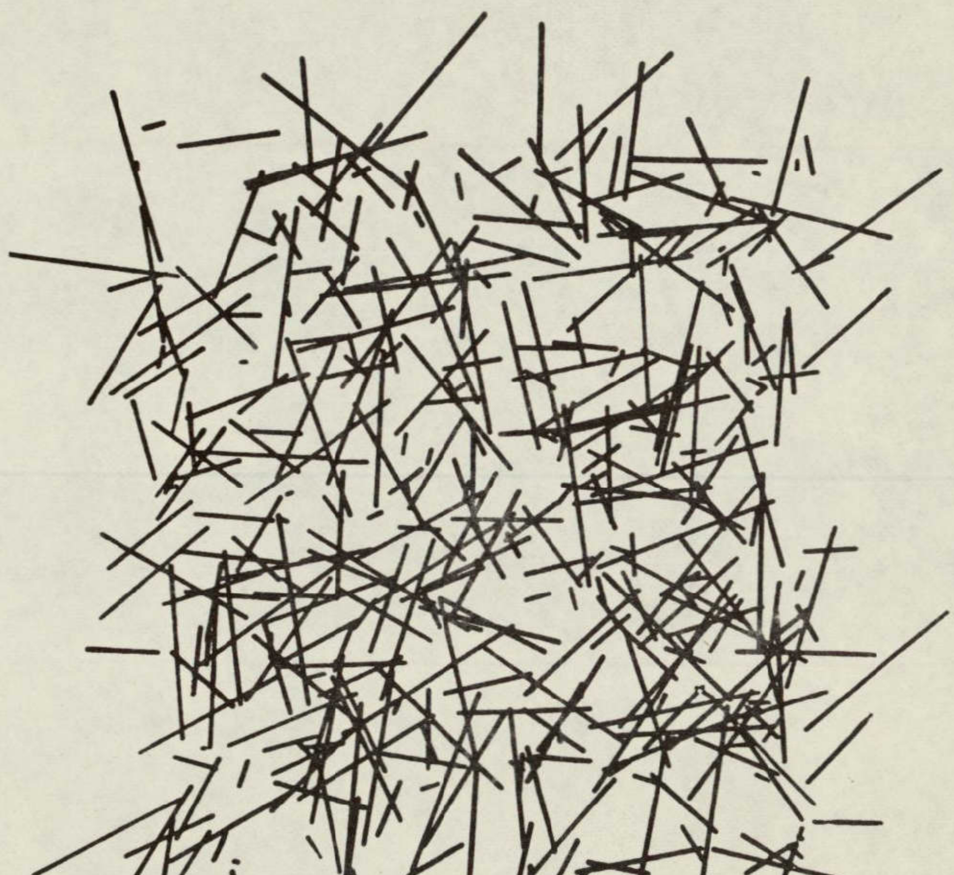

Figure 2: Plot of lines whose position, azimuth, and length have been generated randomly.

Unless such alignments can be identified, they should be considered seriously to be <u>fortuitous</u> alignments.

Applications of shadow enhancement can be made to many types of imagery and photography and relief models. The latter are most effective when painted a uniform light color. Side-looking radar imagery is also effective because of the high contrasts between the illuminated and shaded areas. Photography that has high contrasts can also be effective, for example, a black-and-white positive of a snow-covered scene (Fig. 3). Black-and-white ERTS images or Skylab photographs display abundant linears, many of which are shadow enhanced. In such images, areas of low reflectance are as abundant as shadows and may compete with or enhance shadow trends.

BASIS OF SHADOW ENHANCEMENT

Wise (1969, Fig. 4) reasoned that effective enhancement of linears occurs when the angle between the normal to the slope and the illumination vector is 90 degrees (Fig. 4). Under this condition the slope is shaded, and the distal margin of the shadow (the margin away from the source) lies at the foot of the slope, which could be a valley floor. If the valley floor is a linear feature, it is enhanced by the shadow margin. Thus the condition defined by Wise can account for the enhancement of linears. However, a study of shadows on relief maps reveals that this condition occurs for only a small percentage of shadows, and, under other conditions of shadowing, sets of linears also appear (Fig. 1, [C]).

The equation of Wise can be extended to include all conditions of shadowing. In this general case, the angle between the unit source vector $\overline{S}$ and the unit slope normal $\overline{N}$ is equal to or greater than 90 degrees or, in vector notation, the vector scalar product

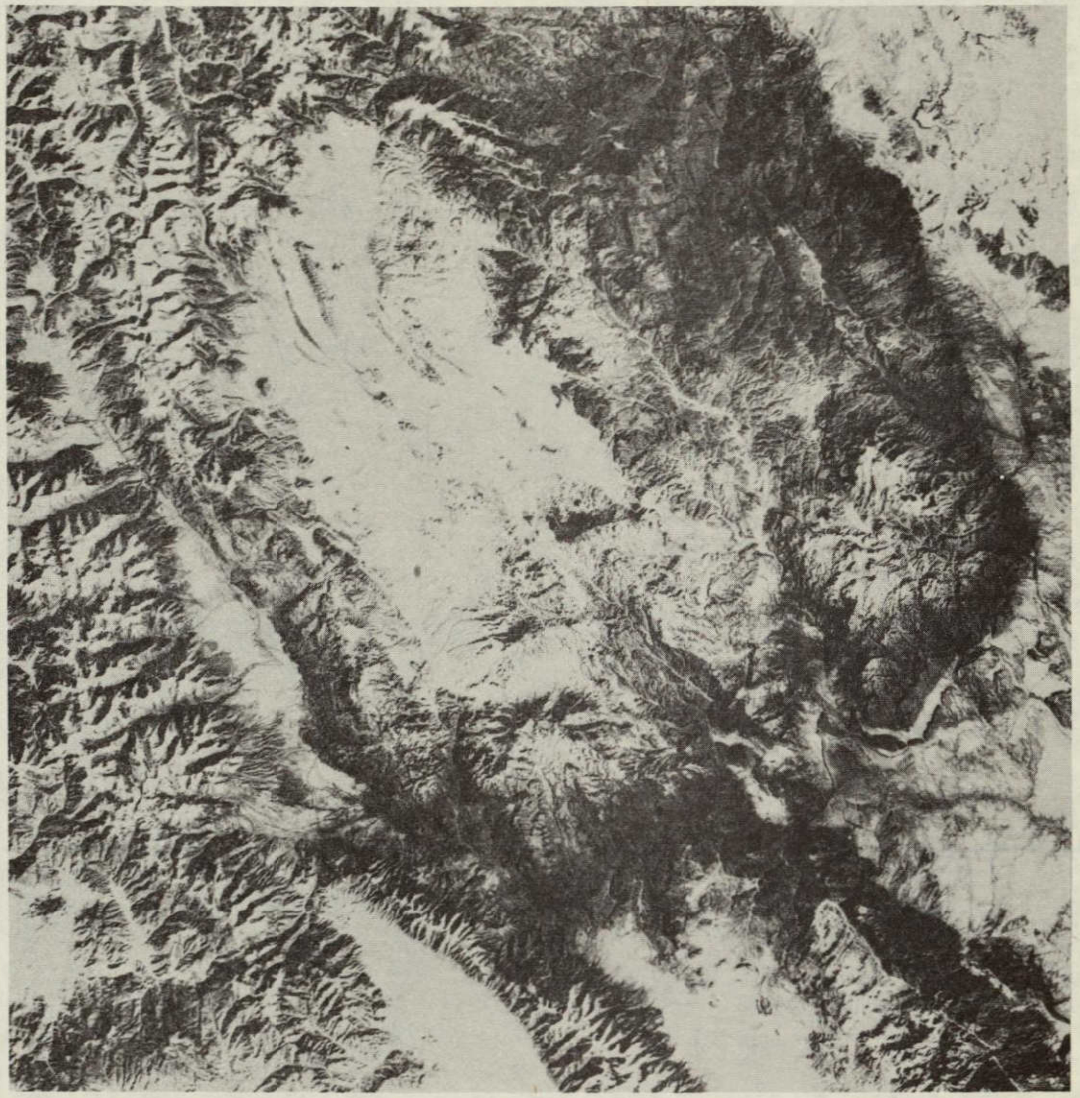

Figure 3: ERTS image (Band 6) of a snow-covered scene in central Colorado. The sun elevation is 23 degrees, azimuth is 150 degrees.

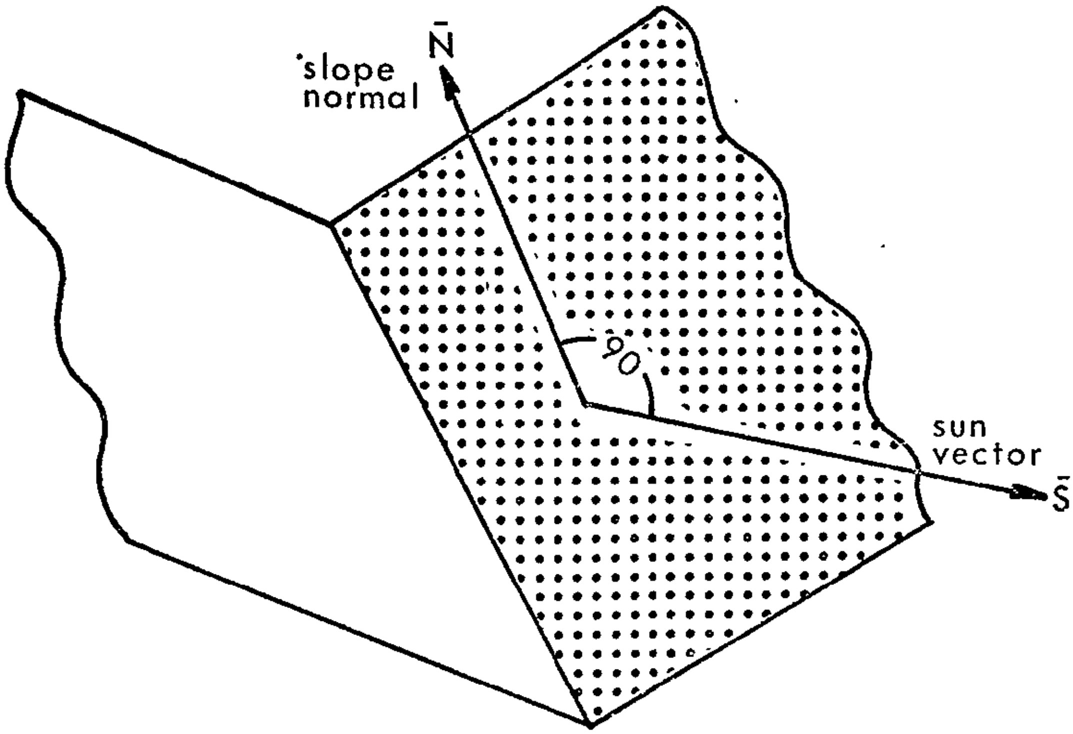

Figure 4: Diagram of Wise's condition of shadow enhancement.

$$\bar{S} \cdot \bar{N} \leq 0. \tag{1}$$

This inequality reduces to

$$\text{SIN(deviation)} \cdot \text{TAN(slope angle)} \geq \text{TAN(elevation)}, \tag{2}$$

where deviation is the acute angle between the illumination direction (e.g., sun azimuth) and the strike of the slope, the slope angle is the true dip of the slope, and the elevation is the vertical angle of the source above the horizon (e.g., sun elevation). See Appendix for details.

Under all conditions of the extended formula (2) are included not only enhancement of the foot of a slope (or a valley bottom) but also enhancement of a ridge line or escarpment rim at the proximal margin of a shadow (nearest the source) (Fig. 5). Parallelism of ridge lines and valley bottoms is a common situation.

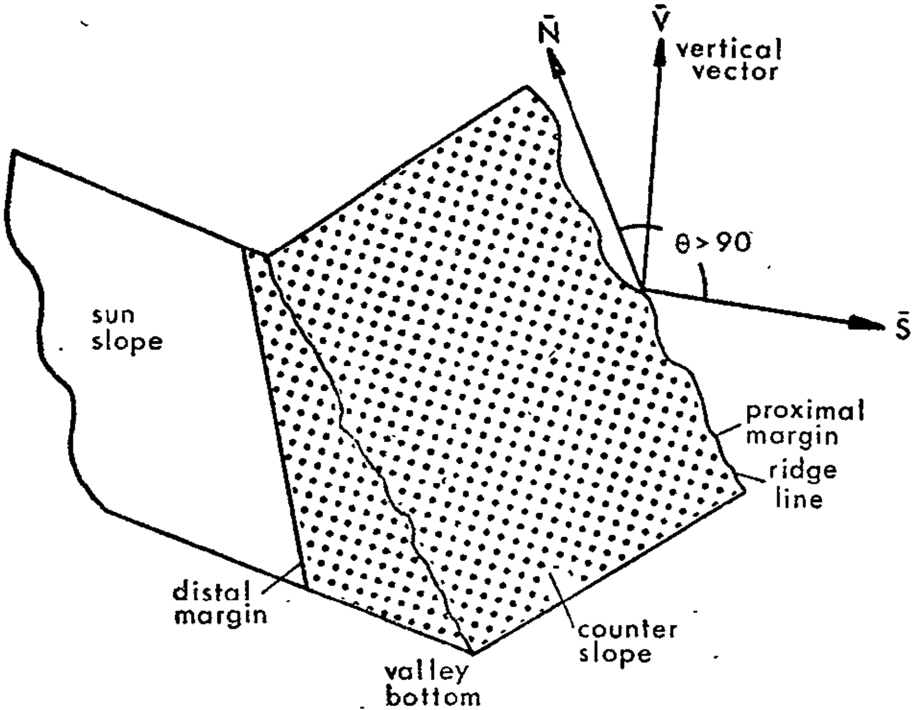

Figure 5: Diagram of extended conditions of shadow enhancement. The symbols are defined in the Appendix.

SELECTIVE ENHANCEMENT

Under the broader definition, shadow enhancement can be thought of as a two-dimensional filter that "cuts on" when the formula (2) is satisfied equally and "passes" information (shade is present) on those combinations of slope angle, deviation, and elevation that satisfy the inequality of (2). These combinations define the pass band of the filter (Fig. 6). In other words, for a given elevation, the cut-on slope angle is inversely proportional to deviation, but always greater than the elevation. It is this last characteristic that provides an explanation of the enhancement of some anomalous linears.

For a wide range of elevations, and in the range of deviations from about 45 to 90 degrees, information is passed (counter slopes are shaded) for nearly the whole range of available slopes (from the illumination elevation through 90

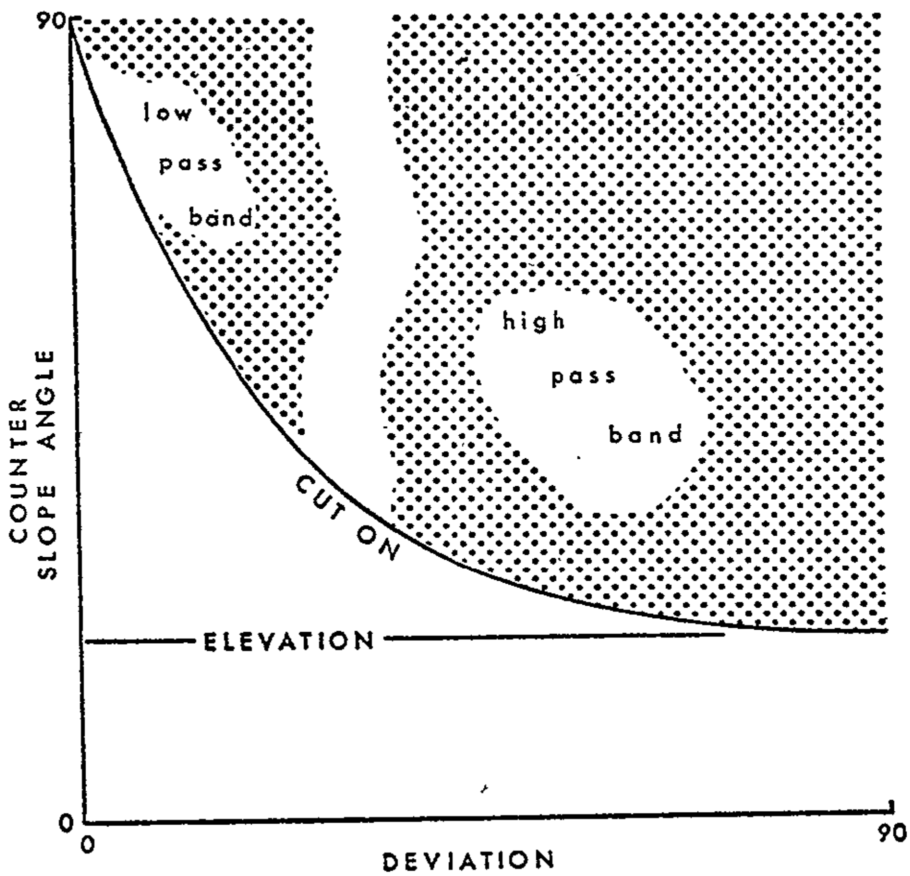

Figure 6: Graph of shadow enhancement filter. The pass band is above the cut-on curve. The cut-on curve is defined by a unique value of elevation.

degrees). These slope angles and deviations are in the high pass band of the filter. In other words, slopes within broad ranges of slope angle and deviation are all shaded. However, for deviations in the range from 0 to about 20 degrees, only slope angles in the range from approximately 20 to 90 degrees are shaded. This is in the low pass band of the filter. Therefore, while shadow enhancement as a filter passes all slopes greater than the elevation at larger deviations, it passes only the steeper slopes at low deviations. This is an important aspect of shadow enhancement, since steep-

sloped topographic features commonly produce the straightest patterns. This is especially important in interpretation of high-angle geologic faults and associated fault-line scarps.

EFFECT OF IRRADIANCE

Another cut-on characteristic of the filter can be defined. In reality there are slopes, outside the pass band, but near the cut-on curve, whose irradiance is low enough so that they can be considered effectively to be shaded. Therefore, the sharpness of the cut-on must be considered.

For the cut-off region of the filter, the irradiance of a slope is a function of the angle of incidence of illumination. (See Appendix.) For near grazing illumination, which usually occurs at low elevations less than about 15 degrees, tonal contrasts between shaded and illuminated slopes may be sufficiently small to make discrimination difficult. The problem will be greater if reflectances are low. If it is desirable to have shadow enhancement at low sun elevations, then it is also desirable to have the reflectances at a uniform and high value. This can be achieved by painting relief models white (Fig. 1) or by photographing snow-covered scenes (Fig. 3). If the photographic process is included in the method of shadow enhancement, the cut-on sharpness can be selectively modified by increasing the gamma of the film. This increases the contrast between shadowed and illuminated slopes. Further increase in contrast is possible by making shadows darker with respect to illuminated areas at the time of exposure. This can be done by using black-and-white infrared film with a Wratten 25 filter (Fig. 7).

APPLICATIONS

Many useful and potentially useful applications of selective shadow enhancement exist. It can be

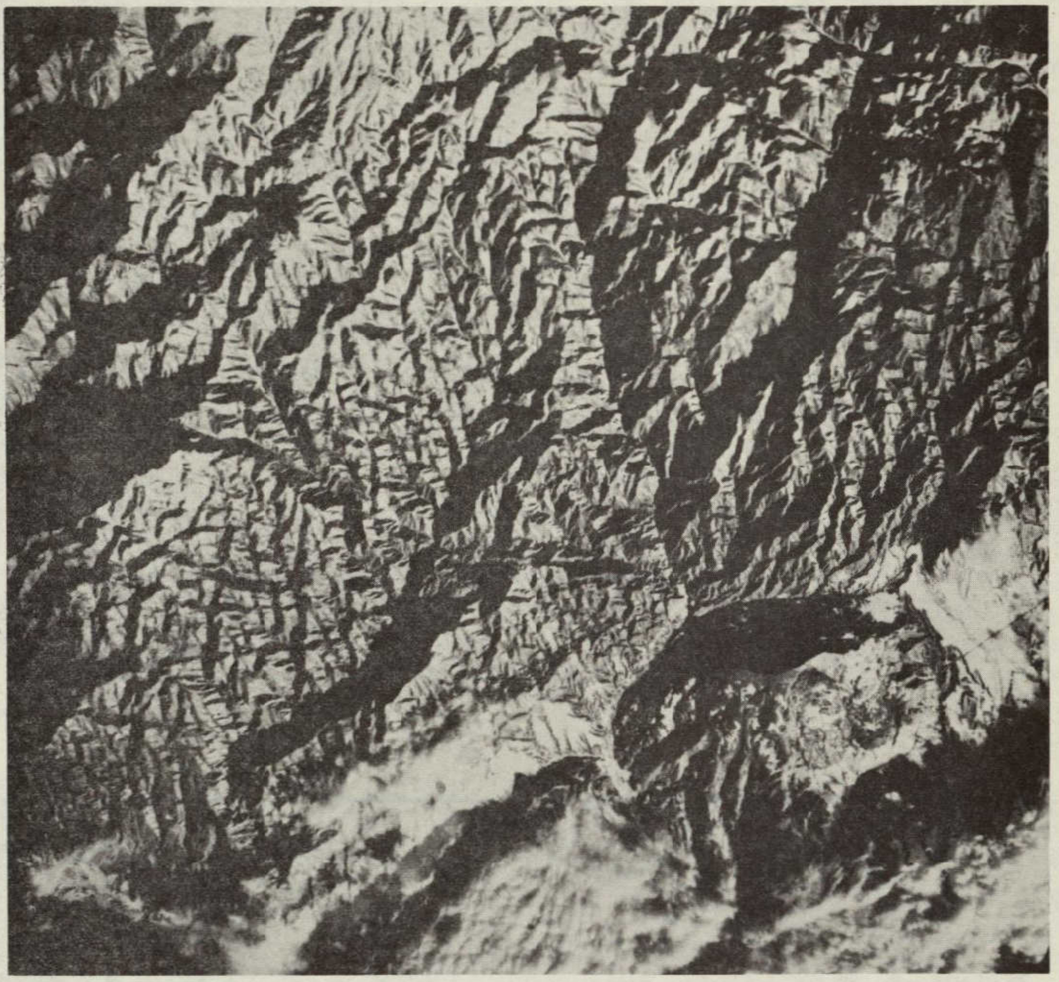

Figure 7: High-altitude, low sun-angle photography of a snow-covered scene in southern Front Range, Colorado. Sun elevation is 10 degrees and sun azimuth is 128 degrees. Black-and-white infrared film was exposed through a Wratten 25 filter and developed for high contrast.

applied in the study of relief maps and in designing aircraft photography flights and satellite orbital passes. The simplest experiment, designed for illumination at fixed elevation and azimuth, cuts off all slopes less than the elevation and selectively cuts off slopes of smaller angle at smaller deviations (Figs. 1,3,7). It is possible to look for linear trends at low deviations to the sun azimuth. These trends will be the straightest ones associated with the steepest slopes. Several experiments could be planned that would enhance trends at several ranges of azimuth.

Low sun-angle photography is included is this simple experiment. The low sun elevation defines a broad pass band for slopes, and therefore, most structurally controlled topography is enhanced (Fig. 7). The low angle also defines a broad pass band for all deviations, and selective passing of very steep slopes occurs at only very small deviations. Low sun elevation also produces broader shadows, which aid discrimination. On the other hand, high sun-angle photography has a narrower, and more selective, slope pass band, but shadows are narrower and discrimination is decreased. This could be overcome by changing the vertical look direction to a high-oblique look direction directly toward the source of illumination.

More complicated experiments involve two illumination directions (Fig. 8). By the following formula,

$$\mathrm{TAN(elevation)} \cdot \mathrm{CTN(slope\ angle)} = \mathrm{SIN(deviation)}, \quad (5)$$

combinations of azimuth and elevation can be determined to selectively shadow enhance slopes in any desired ranges of slope angle and deviation. Desired deviation and slope-angle cut-ons are determined by inspection of Fig. 9, and the optimum sun elevation is calculated from (5). The result is a filter combination as shown in Fig. 10. The band of deviations between the peaks is a slope-

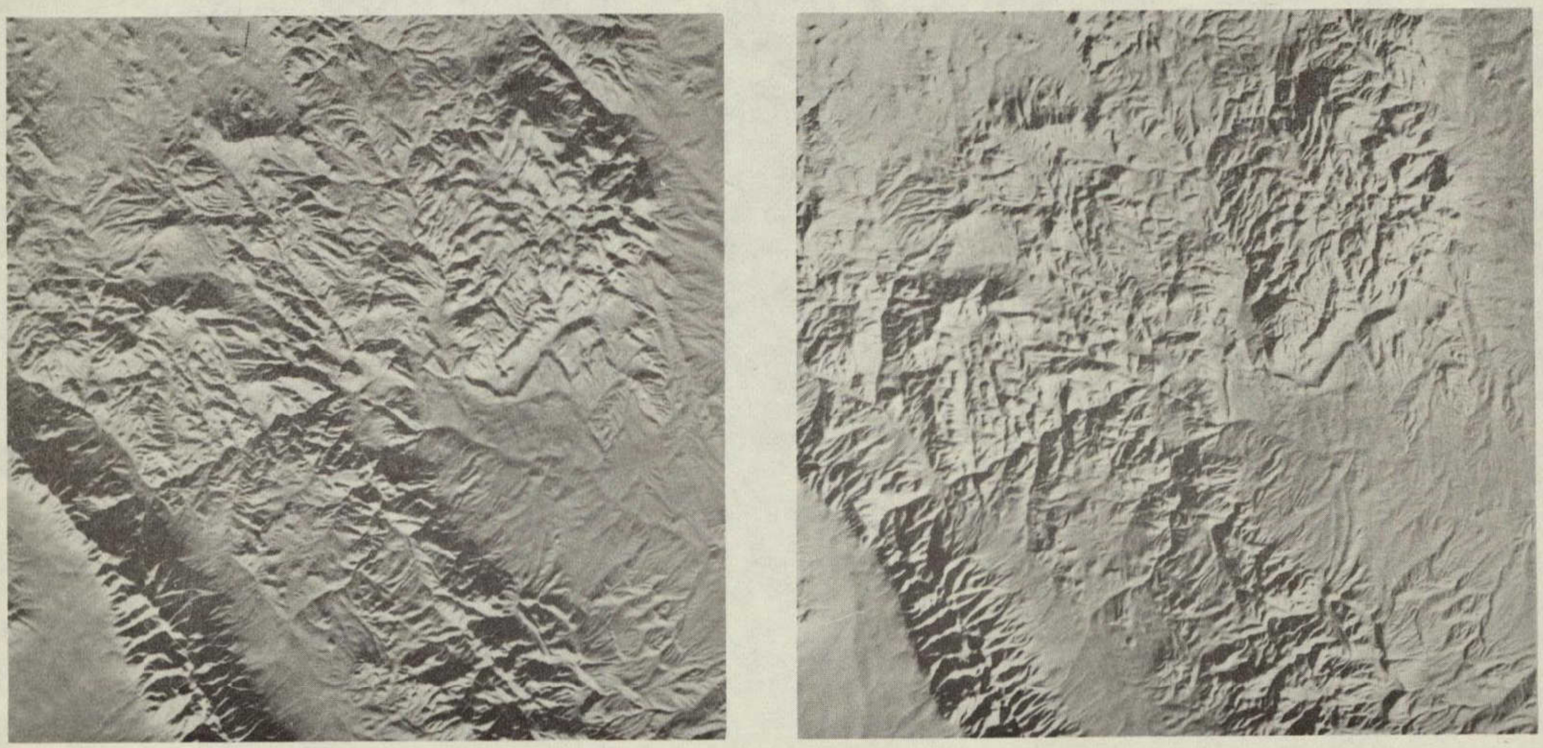

Figure 8: Images of painted relief model taken at two illumination azimuths, shown by arrows. Single filter effect is evidenced in each. The two-filter effect is observed by pseudostereoscopic viewing of the two images. The double pass band is centered on N22½W azimuth.

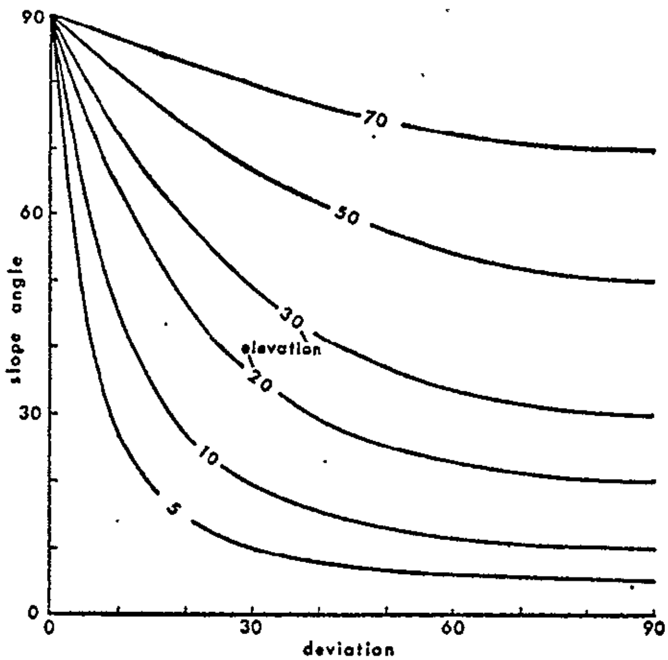

Figure 9: Graph of cut-on curves for various illumination elevations.

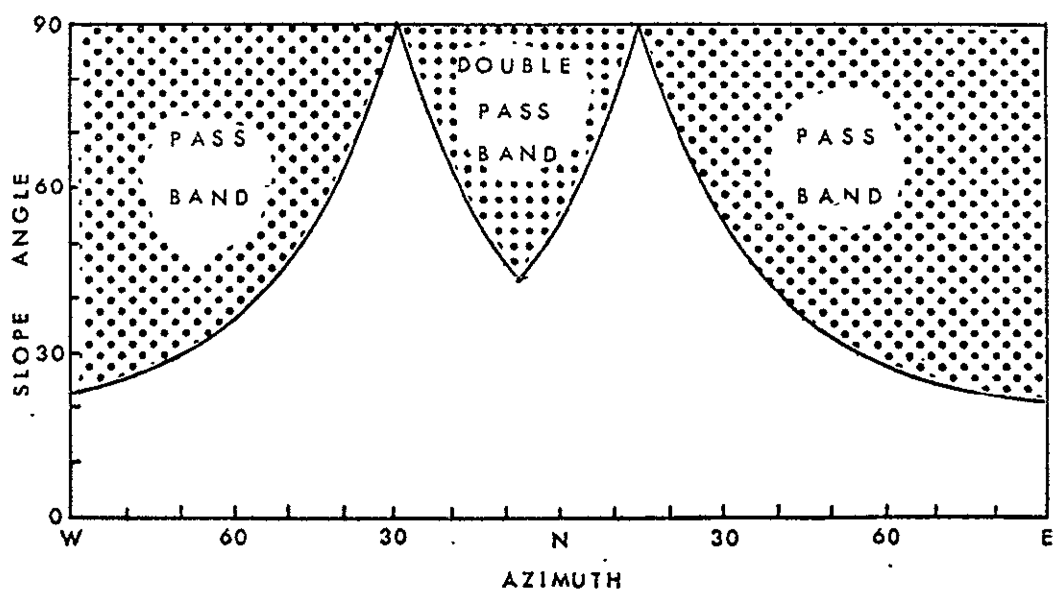

Figure 10: Shadow enhancement pass band for illumination at two azimuths.

angle pass band double that of a single filter. Thus, the selective pass band can be increased by filter combinations. Multiple double pass bands can be used by simply extending the technique to several filters at several azimuths.

A further extension is to have continuous illumination over a band of azimuths. The resulting filter is shown in Fig. 11. The pass band of this filter is just the selective pass band of a double filter. This experiment would be difficult to realize for the earth's surface because of limitations of the sun's attitude. However, the experiment could be set up for relief models or side-looking radar.

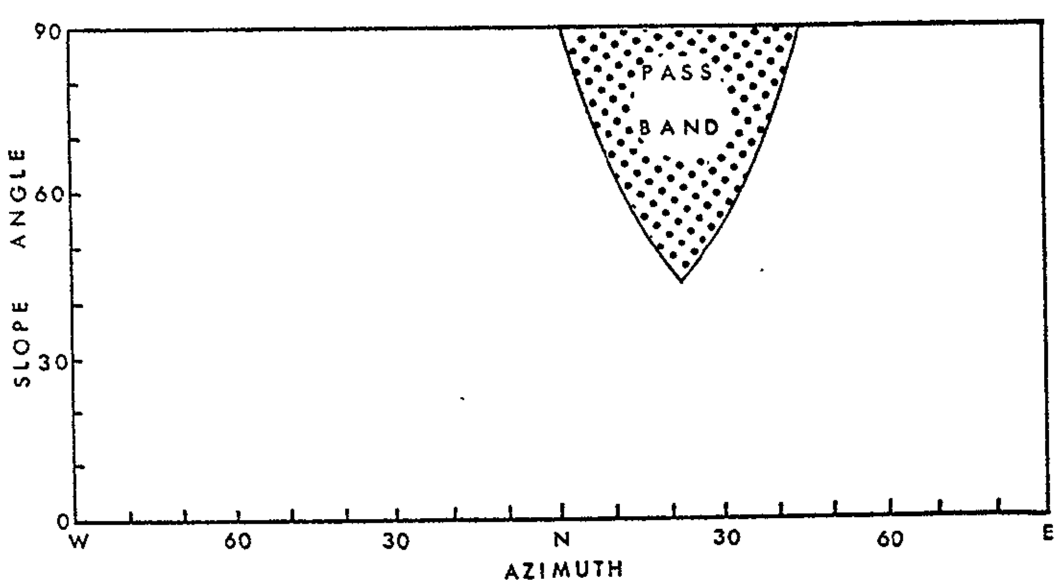

Figure 11: Shadow enhancement pass band for illumination over a continuous band of azimuths.

The ultimate extension is to have a constant illumination over an azimuth band of 180 degrees. The result is a gray level map or image free of deviation information. The gray levels represent different magnitudes of slope angle only. The results are confused when there is extreme shading of sun slopes, but, when most of the slopes are near the value of the sun elevation, the results are best.

CONCLUSIONS AND RECOMMENDATIONS

(1) Shadow enhancement is valuable for the study of geologic folds, faults, and regional fracture systems.

(2) Shadow enhancement is best where the scale of the imagery is small with respect to the size of the features studied.

(3) Painted relief maps, snow-covered scenes, radar imagery, and low sun-angle photography have the best shadow enhancement.

(4) Sun elevation and azimuth determine which trends are enhanced or subdued in images.

(5) Many techniques of image enhancement have been developed. A useful technique that enhances shadows in snow-free ERTS images, where they are confused with areas of low reflectance, involves color reconstitution. A color composite is made with Band 4 in green, Band 5 in red, and negative Band 6 in blue.

(6) It is possible to plan photography in which selective shadow enhancement is optimized to study one or more selected trends.

(7) Optimum enhancement is dependent on the topography. For low sun-angle photography, the sun elevation should be a few degrees less than the predominant slope angle. For mountainous areas, elevations of 10 to 15 degrees seem to be optimum,

while for gentler terrain approximately 5 degrees seems best. Elevations of 22 to 27 degrees seem to be optimum for relief models of mountainous terrain with a vertical exaggeration of 2. The optimum sun elevation should be increased as much as possible for surfaces with low reflectances.

ACKNOWLEDGEMENTS

This investigation was conducted at the Colorado School of Mines with support from the National Aeronautics and Space Administration (Grant NGL 06-001-015 and Contract NAS 9-13394). Daniel H. Knepper, Department of Geology, Colorado School of Mines, provided critical discussions and valuable experience during the investigation.

REFERENCE

Wise, D.U., 1969, Pseudo-radar topographic shadowing for detection of sub-continental sized fracture systems: Proc. 6th Intl. Symp. Remote Sensing of Environment, U. Michigan, Ann Arbor, p. 603-615.

APPENDIX

The sun vector is the directed line taken in the sense toward the sun. The slope normal is the directed line perpendicular to the plane of the slope taken in the sense toward the atmosphere, whether in a model slope or a real one. Overturned slopes are a special case not considered in this discussion. Counter slopes are those whose normals have an angle greater than 90 degrees to the sun vector. Sun slopes have normals that form an angle less than 90 degrees to the sun vector. In the notation of formula (2) discussed earlier, if

$$-1 \leq N \cdot V \leq 1,$$

where $\overline{V}$ is the vertical vector,

then for counter slopes: $\overline{S} \cdot \overline{N} \leq 0$,

and for sun slopes: $\overline{S} \cdot \overline{N} \geq 0$.

The vector equation

$$\overline{S} \cdot \overline{N} = \mathrm{COS}\theta$$

relates two unit vectors to the angle between them. This forms the basis of formulas (1) and (2). The angle θ is the illumination angle of incidence (measured from slope normal) upon the slope surface. The equation can be reduced to a function of slope angle, deviation, and illumination elevation:

$$\overline{S} \cdot \overline{N} = \mathrm{SIN(elev)} \cdot \mathrm{COS(slope\ angle)} - \mathrm{COS(elev)} \cdot \mathrm{SIN(slope\ angle)} \cdot \mathrm{SIN(dev)}.$$

Irradiance E on an illuminated slope is expressed by

$$E = E_o \overline{S} \cdot \overline{N} = E_o \mathrm{COS}\theta ,$$

where E_o is the irradiance on a surface perpendicular to the sun vector.

APPENDIX F

GEOLOGIC INTERPRETATION OF SKYLAB PHOTOGRAPHS

by

Keenan Lee

and

Robert J. Weimer

Remote Sensing Report 75-6

EREP Investigations 380

Contract NAS9-13394

National Aeronautics and Space Administration

December 1975

REMOTE SENSING PROJECTS

DEPARTMENT OF GEOLOGY

COLORADO SCHOOL OF MINES GOLDEN, COLORADO

GEOLOGIC INTERPRETATION OF SKYLAB PHOTOGRAPHS

by

Keenan Lee

and

Robert J. Weimer

Remote Sensing Report 75-6

Remote Sensing Projects
Department of Geology
Colorado School of Mines
Golden, Colorado

NASA Contract NAS9-13394

National Aeronautics and Space Administration

December 1975

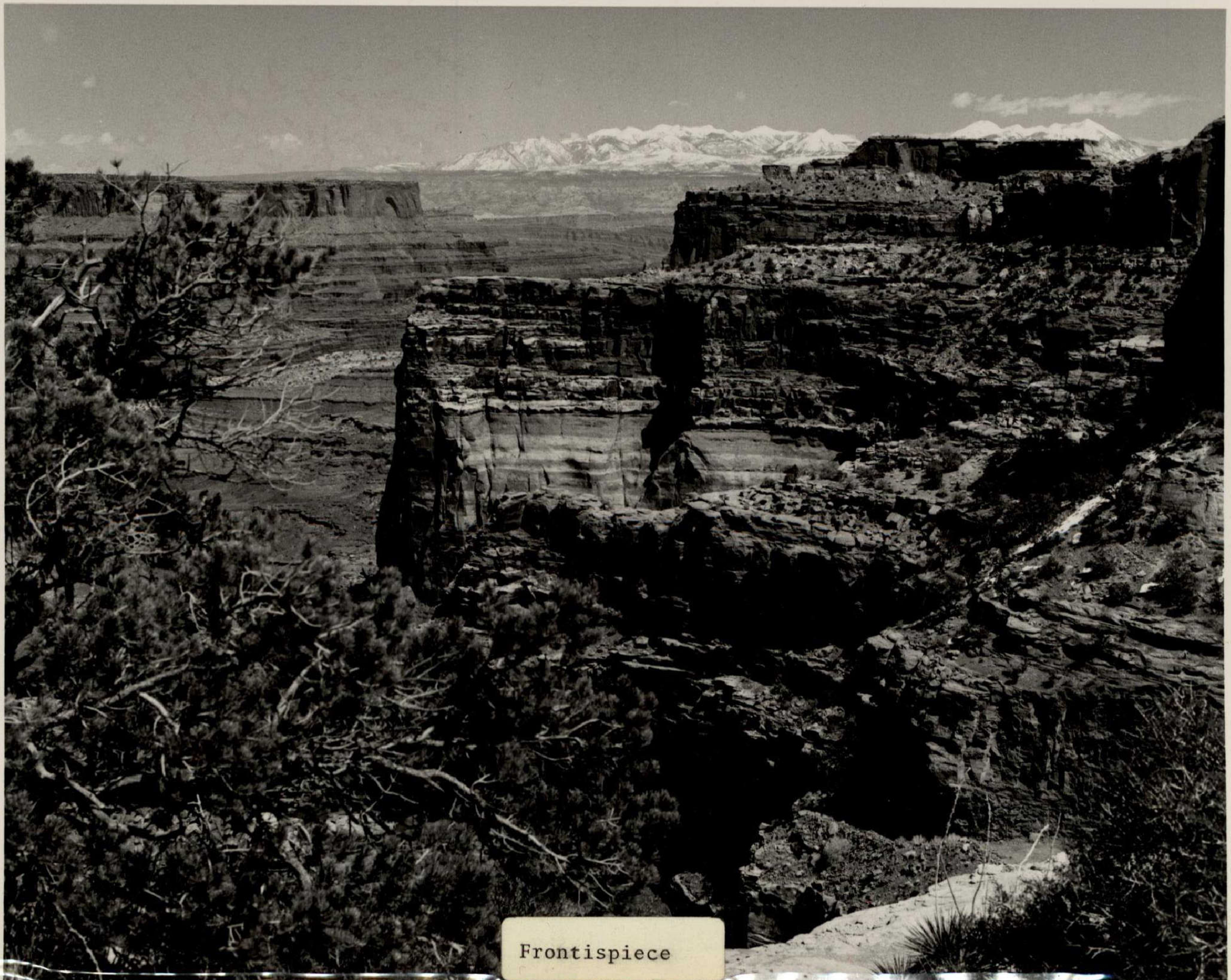

Frontispiece

ABSTRACT

Satellite images contain the same geologic information as do conventional aerial photographs, but at a smaller scale and with correspondingly poorer resolution. As with aerial photographs, maximum geologic information currently is derived from photointerpretation, a deductive process best carried out by a geologist-interpreter.

Skylab photographs are superior to ERTS images for photogeologic interpretation, primarily because of improved resolution. Similarly, S190B photos provide more geologic information than do S190A photos. Multiband photography shows no apparent advantage over good color photography; S190B stereo color photos, where available, provide maximum geologic information.

Topography is the single most important surface phenomenon in photogeologic interpretation. Vegetation, especially coniferous forests, severely limits interpretation. Maximum information is extracted through the iterative process of photointerpretation and field checking.

More geologic information is contained in space images than can be interpreted or mapped at original scales. Interpretation is best with optical magnification of low-generation contact transparencies, with annotations put on

enlarged transparencies. Optimum scale for geologic mapping in this study area is about 1:62,500.

All stratigraphic units at or above formation-rank can be mapped in this area, and many formations can be effectively subdivided into members. Conjunctive use of topo maps permits estimation of section thicknesses and lateral thickness changes. Stratigraphic pinch-outs, intertonguing sedimentation, and lateral facies changes have been accurately mapped with S190B photos.

All major structures in the study area can be recognized on the space photographs. Major folds were mapped accurately, even those with very gentle flexures, as well as several secondary drag folds. Faulting is recognized in considerable detail, both large, fold-bounding faults and subsidiary collapse systems. The ability to interpret detailed stratigraphy and structure allows recognition of recurrent structural movement on some uplifts.

CONTENTS

ILLUSTRATIONS

Figures | Page

Plates (All plates are in pocket)

Page

Plates

TABLE

INTRODUCTION

Because EREP is, by definition, an experimental package, much of the effort here is devoted to evaluating the results of the EREP missions rather than attempting to apply them. This report contains the results of the evaluation of the photographs from S190A and S190B for geologic information.

Early geologic evaluations of space images, from both ERTS and Skylab, have stressed the structural information content of the images, especially lineament interpretations. Whereas lineaments are apparent in all of the Skylab photos, definite attempts were made in this research to evaluate the photos in terms of their lithologic information content.

A difficulty arises in attempting to communicate to others the "lithologic information content" of a Skylab photograph. To state that the stratigraphy can be interpreted "in great detail" is insufficient, and good objective criteria, if they exist, are unknown to the author. For this reason, it is important - it is imperative - that the reader study critically the enclosed geologic maps. The essence of this report is in the maps.

CASE STUDY I: GEOLOGIC INTERPRETATION OF S190A PHOTOGRAPHS

(R.J. Weimer)

INTRODUCTION

Approximately 40 hours were spent analyzing 190A color photographs from Skylab 3 covering an area in western Colorado and eastern Utah. The objectives of the study were 1) to prepare a photogeologic map to determine the geologic information content of the S190A photographs, 2) to compare the results of this work with a map of the general area prepared from ERTS imagery, and 3) to determine how accurately and rapidly a large area could be mapped by an experienced geologist with a working knowledge of the geology.

A photogeologic map was prepared for approximately 25,000 square kilometers covering the region of the Uncompahgre Uplift and the northern portion of the Paradox Basin. The region is bounded by Grand Junction on the north; Green River, Utah, on the west; Ouray, Colorado, on the southeast; and the Black Canyon of the Gunnison River on the northeast.

To facilitate comparison with S190-B photointerpretations and previously published geologic maps, the results of this study (Pl. 1) are plotted on the same base map - the Moab Quadrangle, at a scale of 1:250,000. Some parts of the present study area, therefore, are not shown on Plate 1.

Four frames of S190A color transparencies (~4X, 1:710,000) with stereoscopic coverage were used to study the geology of the region. The images were observed with a mirror stereoscope and interpretations transferred to a transparent overlay on color prints (~8X). The prints were taped together to give one continuous photomosaic of the region at a scale of approximately 1:360,000.

The investigator (RJW) was generally familiar with both the geology and geography of the region. Over a period of several years, detailed mapping had been conducted in small areas scattered throughout the region. Specifically, these areas are the Ridgway-Ouray area, the Salt Valley anticline in the Arches National Monument near Moab, and the Colorado National Monument near Grand Junction. By travel through the region, a good knowledge was acquired of the general geology and the distribution of mappable units (formations).

The observer was continually amazed at the excellent quality of the color photography, the ease of recognizing stratigraphic units and structural elements, and the accuracy of locating oneself relative to geographic points.

LITHOLOGY

Because of the large percentage of exposed bedrock in the area, this region is ideal for the study of Skylab photography. Difficulty in recognizing and tracing stratigraphic units was encountered only in the higher terrain, covered by vegetation.

Eight stratigraphic units with widely varying lithologies were selected for mapping purposes. These are indicated by the legend on Plate 1, and their areal distribution is presented on the photogeologic map. The selection of the units was based on ease of recognizing mappable contacts throughout the area and the mapping of sufficient detail to define the structural features, both folds and faults. Additional stratigraphic units could have been mapped, especially by subdividing the unit labeled Triassic and Jurassic (TJ). However, for the purposes of this project, the time required for mapping greater stratigraphic detail was judged to be inappropriate in achieving the stated objectives.

A general discussion of the stratigraphic units follows.

Precambrian (p€)

Rocks of Precambrian age are exposed in canyons cut through the sedimentary rocks in the Uncompahgre and Black Canyon uplifts (localities are indicated in Fig. 1). Normally, the dark colors of the amphibolite gneisses and schists are easily recognized on the color photography. In some instances, however, shadows may shade the deeper parts of the canyons, or soils and wind-blown sands may cover Precambrian areas, making it difficult to determine if, in fact, the Precambrian is exposed beneath the sedimentary

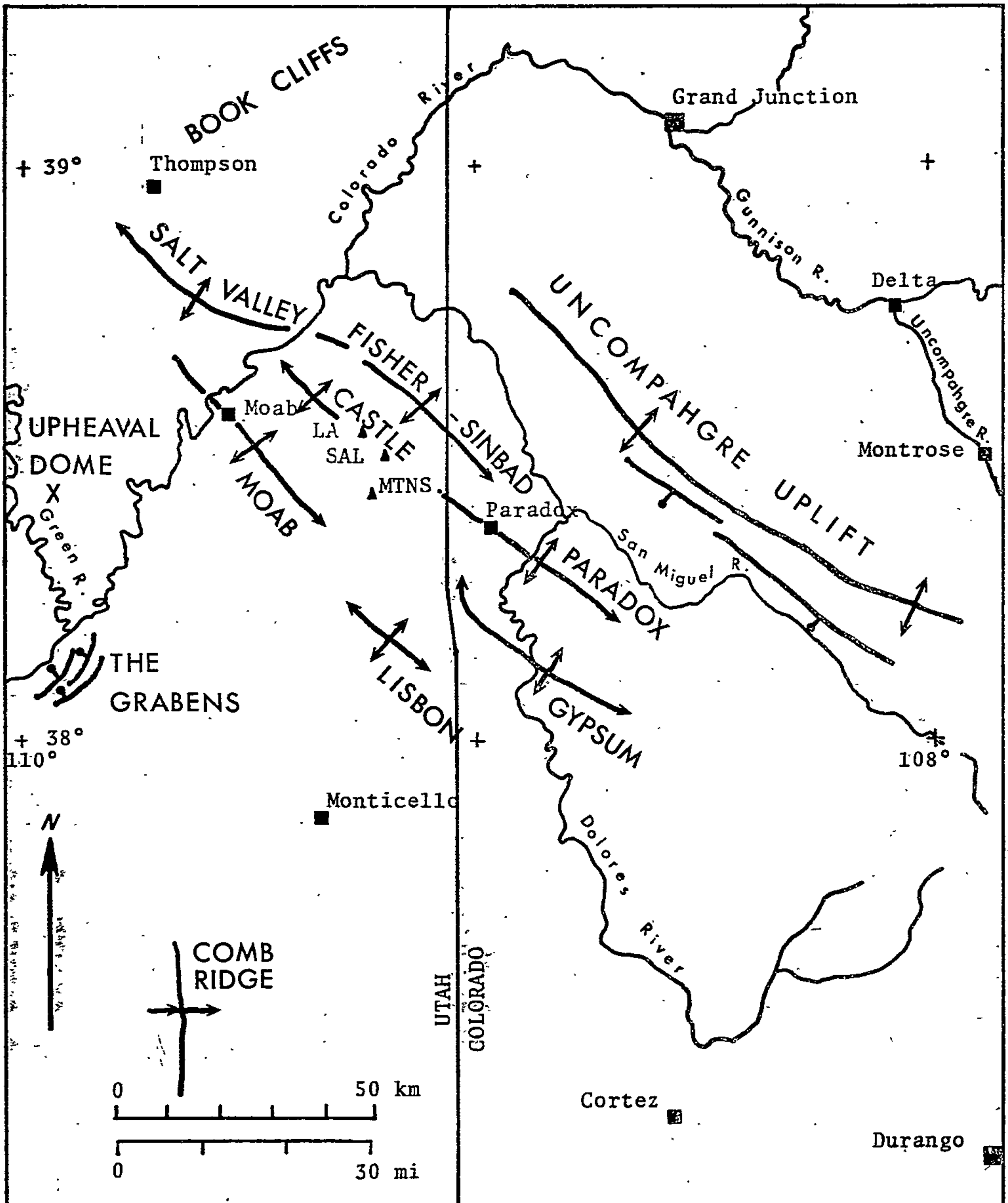

Figure 1. Index map of western Colorado and eastern Utah showing major geologic structures.

sequence. For these reasons, the photointerpretation of areas of Precambrian exposures is probably the least accurate of the map units on Plate 1.

Paradox Formation (₱$_p$)

The northern portion of the Paradox Basin is famous for the long linear "Salt Valley anticlines". The structures are believed to have formed as long, linear, narrow ridges by diapiric movement of evaporites that warped the overlying sedimentary sequence into anticlines with intervening synclines (Fig. 2). Subsequent erosion of the sedimentary rocks from the crests of the anticlines exposed salt, gypsum and associated strata that are collectively referred to as the Paradox Formation. The salt is easily removed by solution, so this material is found only in drill holes.

The Paradox Formation is observed on the color images as light-colored terrain in the core of several anticlines. Because of the diapiric nature of the formation the contact with surrounding units is mapped as a fault contact.

Cutler Formation (Pc)

Overlying the Paradox Formation and underlying the cliff-forming sandstones of the Triassic and Jurassic unit (TJ) is a red, soft-weathering sandstone and shale unit with some limestone. These strata are mapped as the Cutler

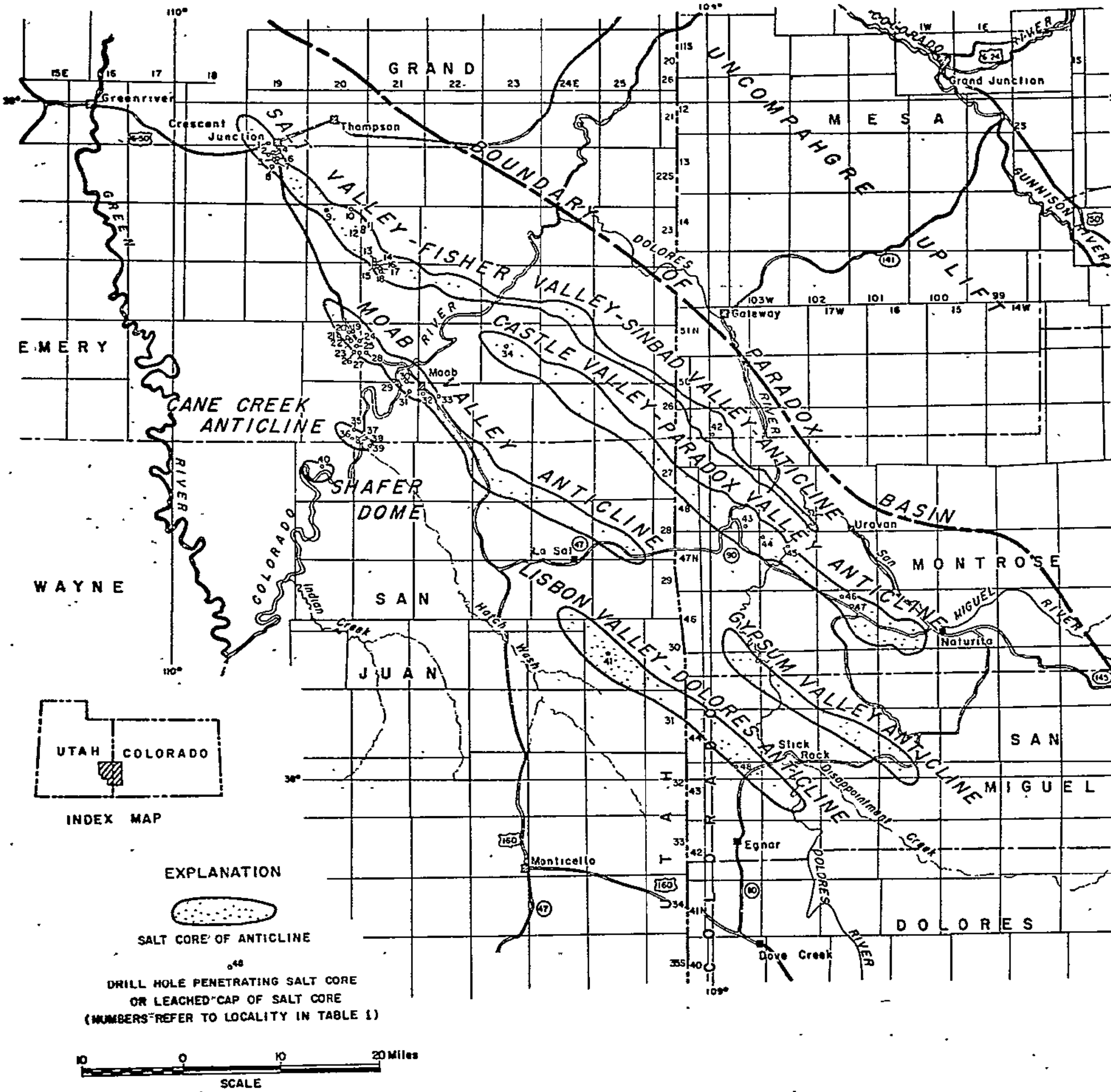

Figure 2. Map of salt cores of anticlines in Paradox Basin (from Shoemaker and others, 1958).

Formation of Pennsylvanian and Permian age. The upper contact may vary slightly from one part of the region to another, but overall the contact can be mapped accurately at the scale used.

Triassic-Jurassic undivided (TJ)

Of all of the selected mapped units, the Triassic-Jurassic undivided contains the most diverse lithologies and the greatest number of formations that are lumped together on Plate 1. The overall lithology is alternating red, cliff-forming sandstone and thin, red, gray and green shales, siltstones and limestones, capped by the soft-weathering shales and sandstones of the Morrison Formation. Although not all are present throughout the area, the following formations, listed in order from oldest to youngest, have been identified somewhere in the area: Moenkopi, Shinarump, Chinle, Wingate, Kayenta, Navajo, Carmel, Entrada, Summerville, and Morrison. Only the Morrison Fm. can be recognized throughout the area, and with time and effort it is possible to map the Morrison separately from the underlying units. This was done in the northwest portion of Plate 1 at the start of the mapping, but the effort was abandoned as too time-consuming and not necessary to define the geologic structure.

Dakota Group (Kd)

One of the most easily recognized stratigraphic units is the Cretaceous Dakota Group, which includes the upper Dakota Sandstone and a lower unit called either the Burro Canyon Formation or the Cedar Mesa Formation. Usually the Dakota Group is a sandstone and shale unit, resistant to weathering, forming hogbacks between the underlying and overlying claystones or shales, or capping mesas or cuestas. The unit can be mapped accurately except in the high terrain of the Uncompahgre Uplift where heavy tree cover masks the formations.

Mancos Shale (Km)

The Mancos Shale of Cretaceous age is a thick homogeneous mass of light-weathering shale that forms a wide outcrop band along the north, northwest and east portions of the region (Pl. 1). Because of the light colors and low topography, the unit is easily recognized and mapped. In the region of the Paradox Basin anticlines, the colors of the Mancos are much like the Paradox Formation; only by mapping the details of the structure and stratigraphic sequence can the two be separated.

Mesaverde Formation (Kmv)

The most impressive topographic feature in the area is the Book Cliffs, held up by the resistant Cretaceous

sandstones of the Mesaverde Formation. The cliffs are present along the northwest portion of Plate 1.

The dark tones and resistant nature of the Mesaverde are in sharp contrast with the lighter-colored Mancos Shale. Because of the sharp contrast, it was possible to map a tongue of the Mancos Shale within the lower portion of Mesaverde Formation in the Book Cliffs. This is indicated on Plate 1 as Kmt -- Mancos Shale tongue, which disappears or thins so it cannot be recognized to the west. The sandstone member of the Mesaverde below the Mancos tongue feathers out to the east, and at the point of pinch out, the Mancos tongue merges with the main body of the Mancos.

Young (1955) mapped a sandstone and overlying Mancos Shale unit in this portion of the Book Cliffs. The sandstone was identified as the eastward extension of the Castlegate Member of the Mesaverde Fm. and the overlying shale as the Buck Tongue of the Mancos Shale.

Tertiary Intrusions (Ti)

The La Sal Mountains, east of Moab, Utah, are formed by Tertiary intrusions that cut the sedimentary sequence of the Paradox Basin. Because the igneous rock is more resistant to erosion than the sedimentary rocks, the intrusions form high topographic features that are heavily forested. The vegetation prevents the accurate mapping of the intrusive contacts with the sedimentary rocks; thus, the outlines of the intrusions on Plate 1 are not precise.

Quaternary Deposits

No effort was made to map Quaternary deposits in the region, although stream terraces, pediments, alluvial fans and other features can be recognized on the color photos. In addition, the volcanic sequence of the western San Juan Mountains was not mapped where it appears along the eastern margin of the region.

STRUCTURES

The relative ease of recognizing and tracing stratigraphic units throughout the area permits accurate mapping of geologic structure. Three major structural elements are recognized as the Uncompahgre Uplift, the Paradox Basin and the Black Canyon Uplift (Fig. 1). Five clearly-defined anticlinal trends, with intervening synclines, were mapped within the Paradox Basin. Both major and minor faults are clearly visible on the photography.

Folds

The largest and most significant structure is the Uncompahgre Uplift. The uplift is a large block approximately 160 km long and 60 km wide that is tilted to the northeast and trends N50W. A thin sedimentary sequence covers the uplift, with the Dakota Group or the

Triassic-Jurassic unit forming long north or northeast dip slopes. Precambrian rocks are exposed in deeply eroded canyons or arroyos (Pl. 1). Along the southern margin of the uplift, Precambrian rocks crop out on the north side of the major fault zone separating the uplift from the Paradox Basin. The major faults that have brought Precambrian rocks to a high structural position are believed to be high angle and are obviously basement-controlled systems.

The Black Canyon Uplift is similar to, but a much smaller fault block uplift than, the Uncompahgre Uplift. The north-tilted block, northeast of Delta, Colorado, was mapped over an area 40 km long and 25 km wide. The south margin of the block is broken by a significant fault zone that places Precambrian rocks in contact with the Cretaceous Mancos Shale. A syncline approximately 25 km wide separates the Black Canyon Uplift from the Uncompahgre Uplift.

The northern Paradox Basin contains numerous anticlines formed in Pennsylvanian through Cretaceous strata. The structural attitude of the sedimentary layers is indicated on Plate 1 by fold axes and direction of fold plunge, rather than by strike and dip symbols. Five major anticlinal trends have been delineated on the map. These are clearly expressed by both outcrop patterns and dip of strata. Some of the fold axes can be traced for more than 150 km.

The flanks of the folds vary in width from 5 to 10 km. Detailed surface observations, geophysical data, and subsurface data from wells indicate that the folds formed as a result of diapiric movement of Pennsylvanian evaporites. The long linear trends result from movement of evaporites into narrow ridges or blade-shaped bodies, probably initiated by basement-controlled faults. Subsequent erosion of the arched sediments over the evaporite ridge and removal of salt by solution caused the collapse of the core of the anticlines. Cliffs of Triassic and Jurassic sandstone now stand in sharp relief on the margin of the flat-floored valleys that mark the crestal region of the anticlines, hence the name "salt valley anticlines".

By tracing the stratigraphic units on the Skylab photographs, the history of the major structural elements can be reconstructed. The Paradox Basin contains Pennsylvanian and Permian stratigraphic units ($\mathbb{P}_p$ and Pc of Pl. 1) that are not present on the Uncompahgre or Black Canyon Uplifts. These observations indicate the uplifts were high areas during the Pennsylvanian and Permian, or that rocks of these ages were deposited and subsequently removed by erosion prior to deposition of the Triassic and Jurassic. Under either interpretation, and because the areas are uplifts today, the mapping indicated renewed tectonic movement of the two uplifts through geologic time.

Faults

The major structural features show numerous lineaments mapped as faults on Plate 1. Minor fault-block segments on the Uncompahgre Uplift are best observed in the region of the Colorado National Monument at the northwest plunge of the uplift. Individual faults trend east-west and northwest, defining blocks that are 5 to 15 km across. These minor faults, like the major ones, are believed to be basement-controlled high-angle faults.

Lineations on the photos were mapped as faults where the following features were observed: 1) Direct offset of strata, 2) omission of a portion of the stratigraphic sequence along a contact, 3) significant change in elevation from one side to another along a lineament, 4) unusually straight outcrop at edge of mesa or hogback, 5) unusually straight stream in anomalous drainage system, 6) lineaments that cross several drainage divides or that cause alignment of portions of different drainage systems, 7) vegetation variation from one side of a lineament to another, or 8) contact around diapiric evaporites in core of "salt valley anticlines" in Paradox Basin. Some of these features can also be caused by joints, paleovalleys, or at lithologic contacts.

Many more faults have been mapped on the photos than appear on published maps of similar scale (Pl. 3). Ground

checking the lineaments may eliminate some of those mapped as faults, but in general, it is believed that the Skylab S190-A photographs show many fault trends not heretofore known from published geologic maps of the area.

COMPARISON WITH ERTS IMAGERY

Photogeologic mapping of the area was conducted by use of both ERTS-1 and Skylab 3 imagery. Band 6 was used in mapping on an ERTS image, whereas color photography was used on Skylab.

The major folds, the general distribution of stratigraphic units, and major fault patterns were similar on both types of images. However, much more detailed and accurate information was available by use of the Skylab data. The ERTS imagery does not have stereoscopic coverage, and its use must definitely be classed as a reconnaissance mapping technique. By contrast, the quality of the Skylab S190-A photographs permits accurate, detailed mapping in a manner equal or superior to any other system of photogeology where an investigator wishes to map a large area in a short period of time.

CONCLUSIONS

1) The Skylab data permit rapid and accurate photogeologic mapping in areas of complex folding and faulting, if

outcrops are good. Approximately 25,000 square kilometers were mapped at a scale of about 1:360,000 in about 40 hours.

2) In areas of heavy vegetation, mapping accuracy is significantly reduced to a reconnaissance level.

3) By viewing large structural features of the earth's crust in one or two images, fault and fold patterns can be interpreted in a perspective not previously possible. As a result, significant photo lineaments have been observed that may represent mapping of new tectonic elements, if field checking confirms the lineaments as faults.

4) The Skylab photos are superior to the ERTS imagery. The Skylab maps may be equal to or greater in accuracy than published geologic maps. Therefore, the Skylab maps may present new data that could be important in mineral exploration programs. By contrast, mapping with the ERTS images is primarily reconnaissance in nature, and is especially useful in areas where there is little or no published information.

5) By recognizing and tracing stratigraphic units in detailed mapping, the major uplifts in the project area can be demonstrated to have recurrent structural movement. Pennsylvanian and Permian strata are absent on the uplifts, indicating Paleozoic or early Mesozoic uplift. The present structural relief in the area results from Cenozoic structural movement.

6) The intertonguing of gray marine shale of the Mancos Formation with sandstones of the Mesaverde Formation is recognized and mapped in the Book Cliffs. From this mapping, the direction of more continuous marine sedimentation is determined to be in an eastward direction. This is an example of the detailed stratigraphic information observable on the Skylab photos.

CASE STUDY II: GEOLOGIC INTERPRETATION OF S190B PHOTOGRAPHS

(Keenan Lee)

INTRODUCTION

The original objectives of this study were to determine the geologic information content of both ERTS and EREP images. The area selected for this common study is the southwestern part of Colorado and the southeastern part of Utah. This area was selected as a study site because it met the following criteria:

(1) the area has good coverage by satellite images from both ERTS and EREP sensors,

(2) bedrock exposures are relatively good,

(3) the area has existing published geologic maps at a scale of 1:250,000,

(4) portions of the study area have published geologic maps at scales as detailed as 1:24,000, and

(5) the principal interpreter (K.L.) had no familiarity with the geology at the beginning of the study.

Some other areas of Colorado met the same criteria (for example, south-central Colorado), but the EREP photography was neither as extensive nor as good as that from the southwestern part of Colorado

The approach followed in the course of this study was to use a designated training area, in which area each type of satellite image was interpreted in a conjunctive way with published geologic maps. Experience derived from this training area was then used to photointerpret the geology of an "unknown" area. Specifically, the study was broken into three phases, as follows:

Phase 1 A training area was defined as the Cortez 2° sheet plus the southern one-third of the Moab 2° sheet. In this training area, ERTS images were first studied in conjunctive use with the published geologic map (1:250,000). Following the ERTS interpretation, the same area was interpreted using EREP S190A photography, followed by study of the EREP S190B photography. This sequence was selected because it was anticipated that each succession of satellite images would provide progressively more geologic information. The results from the initial study of Phase 1 were summarized and published in Lee and others (1974).

Phase 2 A test area was defined as the northern two-thirds of the Moab 2° sheet (Fig. 3). The sequence of images studied in this area also progressed from ERTS images to EREP S190A photographs to EREP S190B photographs. During this phase of the study, it became obvious that the S190B photographs contained considerably more geologic information than the other types of images, and emphasis was duly placed on the interpretation of these photographs. It further became obvious during this study that there was more

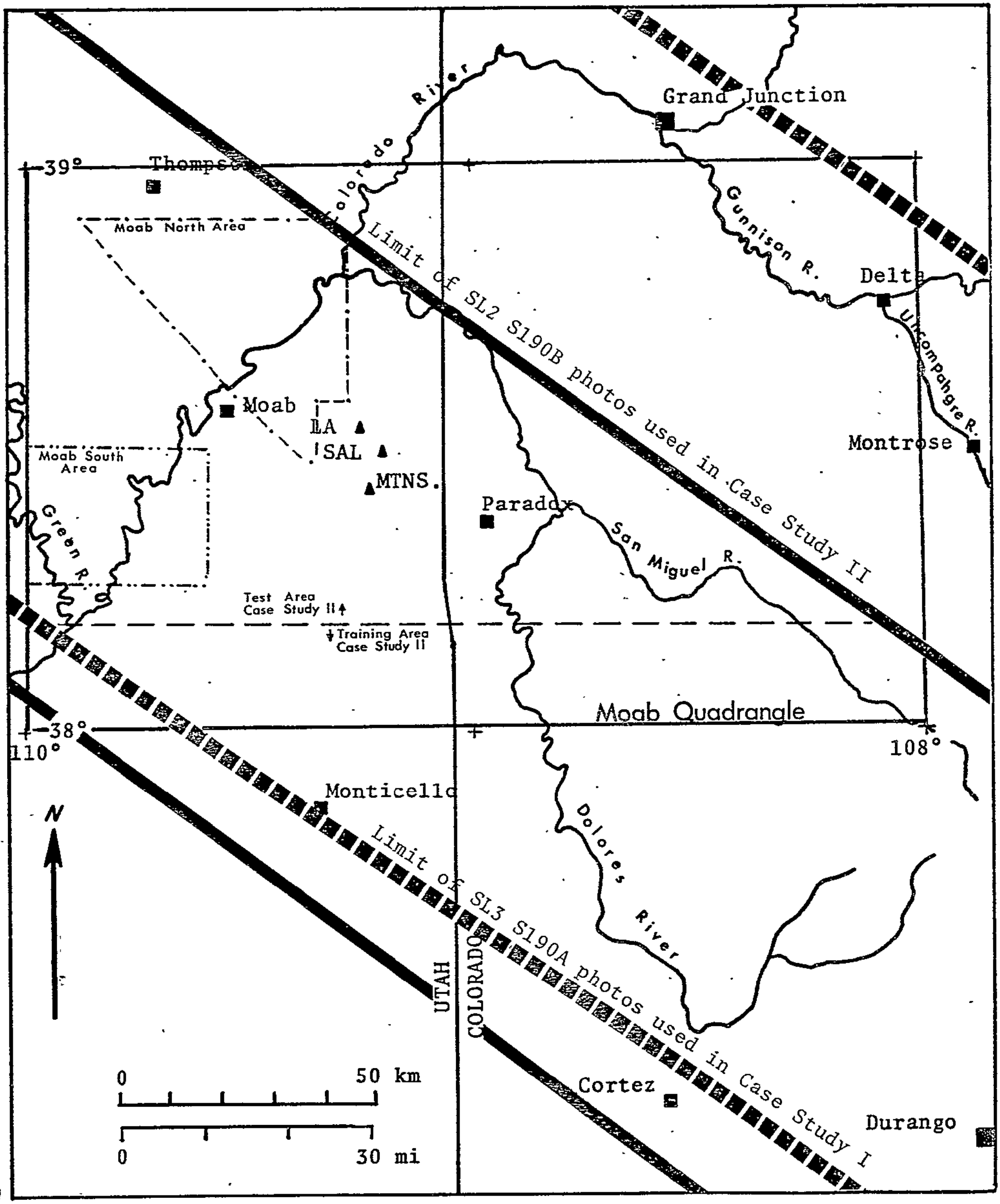

Figure 3. Index map showing Skylab photo coverage and study area.

information in the S190B photographs than could be annotated at the original scales used (1:250,000). A resulting substudy, therefore, was an evaluation of the different scales that could be used for optimum photogeologic interpretation. At the conclusion of the photointerpretation of this unknown area, a field check was scheduled to examine representative areas, complex areas, and areas where the geologic information was not clear on the photographs. At this point of the study, the output data products consisted of geologic maps derived from photointerpretation, along with minimal field checking, of a geologically "unknown" area. These geologic maps (Pls. 2, 4, and 5), therefore, represent what would be an application end product were the EREP photography to be used in a truly unknown area.

Phase 3 The final phase of this study consists of the evaluation of the interpretations made from the space images. The accuracy and completeness of the geologic maps was evaluated mainly by comparison with published geologic maps, with some additional field checking to determine, as best as possible, the "ground truth" in areas where the photo-interpretation maps and the published geologic maps conflict.

The remainder of this report is keyed to discuss these three phases of the study as follows:

Phase 1 - Training area results,

Phase 2 - Test area results, and

Phase 3 - Discussion of results.

Conclusions and recommendations are summarized at the end of the paper.

TRAINING AREA RESULTS

ERTS

ERTS images were studied in conjunction with, and referring to, published geologic maps of the Cortez Quadrangle, Colorado and Utah (Haynes and others, 1972) and the southern third of the Moab Quadrangle, Colorado and Utah (Williams, 1964). The images selected for study were frames 1155-17204-5 and 1156-17262-5, recorded on 25 and 26 December 1972.

The images used for interpretation were positive, black-and-white, 18.5 cm transparencies. The selected frames were imaged with a 23° sun angle, and the area had some snow cover at the time. The positive transparencies were studied on a Richards light table, using a low magnification mirror stereoscope in those areas where stereo side-lap was available.

Lithology

Lithologic discrimination, in general, is poor. Most lithologic discrimination is based on the recognition of topographic differences. Lithologic features amenable to yielding lithologic information are relative resistivity and drainage differences. Resistant vs. nonresistant beds form escarpments that serve to delineate geologic contacts. An

example of this that occurs through large areas of the map is the Cretaceous Dakota-Burro Canyon Fm. overlying the Morrison Formation. Textural differences are occasionally useful for defining drainage density as a function of lithology. The Morrison Formation is discriminable from the underlying Triassic Formations on this basis.

Some lithologic discrimination is based on tonal differences. The Mancos Formation-Dakota Formation contact is an example of a contact recognizable by tonal differences; in this case the Mancos is relatively light. This tonal difference may be an inherent characteristic of the respective formations, but it is also possible that the tonal difference derives from a difference in topography; the relatively non-resistant Mancos Formation forms topographically low areas that often have alluvium and colluvium (or possibly soil) surficial deposits at the surface.

A second tonal phenomenon that serves to discriminate lithologies is along the Quaternary eolian deposits-Dakota Formation contact. Very good discrimination (white vs. light grey) is possible, based on the extent of snow cover. Continuous snow is retained on the eolian deposits, whereas the Dakota Formation shows apparently discontinuous snow cover. This is not a function of elevation, since the snow-free areas occur topographically above and below the snow-covered areas. Possible reasons for the underlying phenomenon may be (1) differential melting due to thermal diffusivity differences,

(2) vegetation differences, with the Dakota supporting more vegetation and the vegetation appearing above the ground snow cover, or (3) surface roughness (macro) differences, with the eolian deposits relatively smooth, and the Dakota irregularly projecting above the snow. Field checks were conducted in the summertime, and as a result, a definitive answer was not available. It seems likely that the vegetation differences would account for the tonal differences on the imagery.

Structures

Major folds could be observed (for example, Paradox structures) on the imagery. Dip-slopes of relatively low dip attitude (4°-10°) could be picked. Very few folds can be recognized by observing a tonal pattern that is immediately associated with a fold, most folds are determined by working out the dips and defining areas of dip reversals.

About 60 percent of the major faults (10-40 km length) are readily observable, and all major faults in the map area were observed except for three. Many small faults (less than 10 km) were observed; the smallest was 3 km in length.

Most faults were delineated by topography, especially escarpments and linear connected drainages. Faults were easiest to see along dip slopes and where escarpments occurred, usually with resistant vs. non-resistant formations across the faults. No faults were picked in areas of high relief; several faults that were traced in low-relief areas were lost as they were

followed into the mountainous areas. Only a very few faults could be picked on the basis of tonal differences.

Seasonal Effects

The images used in the study described above were selected because it was felt they would yield maximum geologic information. To test whether this assumption was, in fact, valid, an ERTS image was selected for interpretation and evaluation that was diametrically opposed to the previous images in seasonal phenomena. ERTS 1317-17204-5, acquired 5 June 1973 with a 62° sun angle and only a trace of remaining snow, was interpreted. The geologic information content was very low compared to the winter images. No advantages were apparent in using this imagery compared to the low sun-angle, snow-covered imagery; many disadvantages were noted.

EREP S190A MULTISPECTRAL PHOTOGRAPHIC CAMERA

Initial photointerpretation studies using EREP photography used the S190-A multiband photography. First studies were conducted with the red band, 4X, positive transparencies. Frames were selected from Skylab 2, Roll 11, Frames 13 through 16, acquired on 5 June 1973. (Note that 5 June 1973 was the date that ERTS imagery was acquired over the same area. Comparative studies of the ERTS images concluded that this time of year was the less favorable time for geologic

interpretation of the space images.) No rigorous comparisons were made between the different bands of the S190A photography, but each band was observed, and no advantage was apparent in any single band. The red band was used most (of the B/W bands) because of its good resolution and high contrast. The transparencies were studied on a light table with a mirror stereoscope.

Lithology

In general, there did not appear to be a significant change in interpreting the S190A black-and-white transparencies as compared with the ERTS images. All comments pertaining to lithologic discrimination from the ERTS study apply to the S190A black-and-white photography as well. One obvious exception is the effect of snow discrimination on the eolian deposits vs. Dakota Formation, but, although this contact is not as easily discriminated as it was with snow cover, there is no difficulty in picking the contact based on tonal differences.

Structures

Comments made previously regarding fold structures are equally applicable here. Fault information on the S190A photography is also similar; about 80 percent of the major faults in the area are readily observable. All faults greater

than 10 km in length were observed except for two. Many faults less than 10 km are seen; the smallest fault noted is about 2 km long. Most of the small faults that are not recognizable on the photographs occur in closely spaced sets parallel to major fault systems. Somewhat more detailed fault information is available on the black-and-white S190A photos than on the ERTS images.

EREP S190B, EARTH TERRAIN CAMERA

The S190B photography studied in conjunction with the geologic maps is color photography (Skylab 2, Roll 81, Frame 19) acquired 5 June 1973 (simultaneously with the S190A photography described above). 2X positive transparencies were studied stereoscopically on the light table with a mirror stereoscope.

Lithology

The lithologic discrimination capability of S190B color photography is dramatically superior to S190A black-and-white photography and ERTS imagery. The addition of color, combined with the increased ground resolution, markedly increases the ability to subdivide lithologic units. Most of the formations broken out on the 1:250,000 scale geologic maps can be discriminated and mapped where scale/resolution permits. Whereas the S190A black-and-white photography (red

band) permitted the subdivision of the map area into five formations, with S190B color photography it was possible to break out (at least in some places) eleven mappable units:

S190B COLOR	S190A B & W
Qe, Qa	Q
Kmv	Km
Km	Kdb
Kdb	J
Jsm	TR
TRJne	
TRkw	
TRc	
TRm	
Pc	
IPh	

For an explanation of these map symbols, see the Explanation on Plate 2.

Even though the increase in lithologic information is great, in that eleven map units were cappable of geing detailed vs. five map units, this does not represent the full potential of the S190B color photography. As will be seen in subsequent portions of this report, many of the map units listed above could be further subdivided.

Structures

All comments made above regarding structural interpretation of ERTS and S190A black-and-white photography apply here as well. In addition, many more structures were mapped because of the high resolution (ground resolution is difficult to describe; some roads were easily seen that are on the order of 10 m wide, some narrow outcrop patterns were seen that are about 200 m wide, and joint spacings of less than 200 m are readily apparent). Much more dip information is available because of the fine topographic detail seen. Whereas on ERTS images and S190A black-and-white photos all large folds could be interpretated, they were sometimes difficult to work out. The same interpretations were much easier on this photography. Folds are also easier to interpret because of the addition of much more information on lithologic distribution (described above).

About 95 percent of all major faults were observed. All faults greater than 10 km in length were seen except for two. The results of interpretation of faults less than 10 km long were about like the S190A photos described above; the smallest observed fault is about 2 km long. In one area of high density fracturing, individual fractures about 1 km long can be seen that have a joint frequency of about 200 m or less.

TEST AREA RESULTS

The initial procedure involved in photointerpretation of the test area consisted of establishing the photointerpretation keys used for discriminating the different geologic map units. On the basis of the appearance of each of the mappable units in the training area, these interpretive keys were compiled and are shown here as Table 1. It is apparent when observing the final geologic maps that the interpretive keys described in this table were used only as rough guidelines. Nonetheless, these keys served well to establish the basic stratigraphic sequence in the unknown area.

1:250,000 MAPPING - MOAB QUADRANGLE

Photointerpretation was conducted using 2X enlargement positive transparencies of the S190B photographs. Geologic information was annotated directly onto clear acetate overlays on top of the positive transparencies, using a 00 rapidograph pen. Stereo interpretation was conducted with a mirror stereoscope with an effective magnification range of 1-2X, so these positive transparencies were examined at about 1:500,000 to 1:250,000 scale. During photointerpretation of these transparencies, the original-scale (~1:1,000,000) contact duplicate transparencies were kept on another light table with a zoom stereoscope. Where geologic information

TABLE 1

PHOTOINTERPRETATION KEYS - MOAB-CORTEZ AREA

S190B PHOTOGRAPHS

Formation	Color	Texture	Drainage	Topography	Erosional Resistance →	Distinguishing Features
Dakota	medium brown	fairly uniform, fine	coarse	secondary hogback		uniform texture
Burro Canyon	dark brown-grey	mottled	moderately coarse	hogback		resistant, light at base
Morrison-Summerville	dark brown-grey	mottled end faces, dark dip slopes	fine dendritic	slopes with central ledge		position, color
Entrada	very light tan	fine light lines		cliff		color, fine lines
Navajo	very light tan	banded-mottled	coarse, occ. parallel	hummocks		light mottled color
Kayenta	dark brown	dark mottled	coarse	ledgy		dark brown, ledgy
Wingate	light brown	irregularly mottled	coarse dendritic	cliff		topography
Chinle	dark red brown			slope		position
Moenkopi	red-brown			weak ledge		position
Cutler	dark red-brown	finely banded	medium coarse dendritic	irregular ledges		color, fine bands
Upper Hermosa Mbr.	medium brown-grey	coarse banded		hogback		position (rarely seen)
Paradox Member	very light tan	mottled	fine dendritic	hummocks		anticlinal cores

was apparent on the 2X enlargements, the information was directly annotated; areas of structural complexity or subtle detail were studied concurrently on the contact transparencies at high optical magnification.

Geologic interpretations were transferred from the clear acetate overlays onto topographic maps (1:250,000) of the Moab Quadrangle using a zoom transfer scope for the 200% scale change. Annotations were transferred to the topographic map in pencil, and a 00 rapidograph pen was then used to finalize the location of the contacts and structures using the topographic information as a secondary control. It was often necessary to go back to the original duplicate positive on the zoom stereoscope for resolving detail and resolving complex structures. It was sometimes necessary to annotate interpretations from the zoom stereoscope onto 4X (1:250,000 scale) positive prints with a clear acetate overlay.

Hand-coloring of the photointerpreted geologic map in many cases pointed out problem areas. In almost all cases, these problem areas were resolved (where resolution was possible) using the zoom stereoscope and the original-scale contact transparencies.

Lithology

All of the formation-rank units that are shown on the published 1:250,000 scale geologic map were recognized on the S190B photographs, at least in some areas. Several of

the formations, however, are not readily distinguishable from contiguous formations, and subsequently were mapped as combined units. For example, the Kayenta and Wingate formations were easily separated (Pls. 9, 10*) where their dip was fairly steep, such as in Lisbon Valley anticline (65.7/422.8 on Pl. 2**), but in most of the map area where dip attitudes are relatively low and these formations form nearly vertical cliffs, the two formations were mapped as a single undifferentiated unit. On the other hand, there were several instances where individual formations could be subdivided into member-rank units. Such an example would be the Morrison Formation, where it is separable into the Salt Wash Member and the Brushy Basin Member in the highlands area north of Arches National Park (63/430, Pl. 2).

Whereas relative thicknesses of stratigraphic units could be estimated on the S190B photographs, lack of experience with photographs at this extremely small scale (compared to conventional photointerpretation scales)

* Plates 8, 9 and 10 are color prints of S190B photographs. Reference will be made to these photos throughout the report. So as not to obscure features on these photos, they are not annotated and features on the photos will be referenced by giving their location on the corresponding map. There is sufficient detail on these photos so the reader should have no difficulty in correlating maps and photos.

** Geographic references for Plates 1-3 are given in UTM grid numbers. For example, Moab is at 62.7/427.1.

precluded determining absolute thicknesses. When formation contacts were transferred to the topographic maps, however, the topographic information provided sufficient control for at least rough estimates of formation thicknesses.

In some cases, surprisingly detailed stratigraphic information was available in the S190B photographs. One surprising capability demonstrated was the ability to delineate the horizontal extent of formations, suggesting lateral stratigraphic changes either by facies change or by pinch-out. For example, the Triassic-Jurassic Navajo Sandstone appears to be absent in the Paradox Valley area (68/425, Pl. 2) and the area immediately to the east and northeast of the Paradox Valley. A similar case of stratigraphic pinch-out occurs in the southwestern part of the Moab Quadrangle, where a key bed at the top of the Cutler Formation, the White Rim Sandstone Member, pinches out toward the northeast (60.6/425, Pl. 2).

Figure 4 shows a composite stratigraphic column of the Moab area that was derived from photointerpretation of the S190B photographs at a scale of 1:500,000. Rather than describe each formation in detail, this figure is offered to show the amount and detail of stratigraphic information available in the photographs.

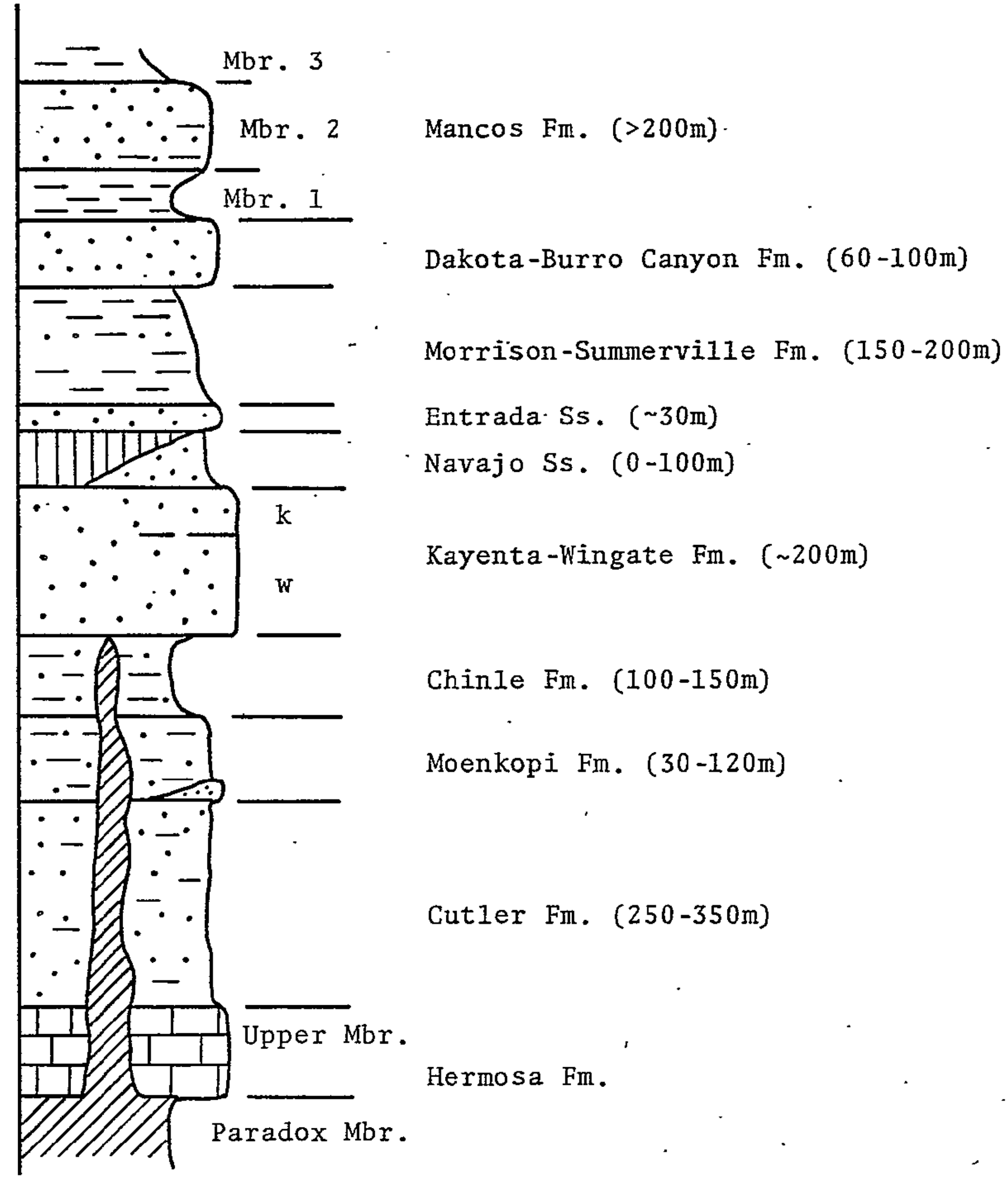

Figure 4. Composite stratigraphic column of Moab Quadrangle from photointerpretation of S190B photos at 1:500,000.

Structure

All of the major structures of the Moab area were interpreted during this part of the study, as well as many secondary structures. Because the map area includes two different structural provinces, discussion will be separated into two parts: the area southwest of Spanish Valley-Lisbon Valley (63/427 to 67/422, Pl. 2) and the area north and east of this line. Southwest of the Spanish Valley-Lisbon Valley trend, the stratigraphic units are largely flat-lying, with dips throughout large portions of this area averaging less than 3°. Some structures diverging from this homocline are the following:

Courthouse-Arth's Pasture Syncline (61/428 to 63/426, Pl. 2) - an asymmetric syncline with a gentle northeast limb and a very gentle southwest limb; ends in a fault towards the northwest;

Shafer Basin - Big Flat Anticline (61.5/426, Pl. 2) - very gentle upwarp, with slightly steeper northeast limb; the anticline appears locally doubly plunging (northwest-southeast at the Colorado River; and

Upheaval Dome (59.4/425.4, Pl. 2) - this anomalous, circular dome area is immediately obvious on the photography. Interpretation of the geology during this phase of the study indicated a definite dome, although the center of the structure was not clearly identified.

A structural anomaly noted in this whole region of the map is the noticeable absence of faulting. The only faults

mapped anywhere in the area were at the extreme southwest part of the map (59.8/422.4, Pl. 2) at the northeastern end of the grabens area, a series of parallel, slightly arcuate graben structures.

The remainder of the map area north and east of the Spanish Valley-Lisbon Valley trend consists of a series of northwest-trending folds, often with subparallel faulting. Northwest of the La Sal Mountains (65/426, Pl. 2), the structural trend is N40-45°W, whereas southeast of the La Sal Mountains the trend is N50-55°W.

The Moab Anticline (62.6/427.1, Pl. 2) is an asymmetric anticline, fault-bounded on the southwest. The anticline is complexly faulted, especially near the Arches National Park Headquarters. The anticline plunges to the northwest, where it is truncated by a northwest trending fault from Moab to Courthouse Pasture. Faults along the anticlinal structure are post-folding, and presumably are related to collapse of the anticlinal crest.

The Crescent Wash-Courthouse Syncline (60/430 to 64/426.6, Pl. 2) is a symmetrical, northwest plunging syncline. The syncline becomes slightly asymmetrical to the southeast with the southwest limb being more steeply dipping. The axis of the syncline may coincide with a fault to the northwest.

The Salt Valley-Cache Valley Anticline (61/430 to 63/428.8, Pl. 2) is a fairly symmetrical anticline at its northwestern end. The northwestern part of the anticline

appears to have a fairly simple, subparallel collapse fault system. Where the Salt Valley turns more easterly to connect with the Cache Valley, the boundary faults appear to be at a high angle to the anticlinal trend, at least on the north side of the structure. In the Cache Valley, the anticline, if it is present, is much more subtle. The main structure in the Cache Valley area seems to be the collapse structures of the subparallel bounding faults. The relationship of the Salt Valley-Cache Valley structure to structures east and south of the Colorado River is problemmatical. The photo-interpretation during this phase of the study was inconclusive as to whether this structure trended to the southeast, through Dry Mesa, connecting with the Castle Valley Anticline (64/427.7, Pl. 2), or whether the structure continued more easterly and connected with the Fisher Valley Anticline (65/428.4, Pl. 2). A corollary of accepting the former interpretation is that the apparent areas of Hermosa Formation in Professor Valley and Fisher Valley (64.3/428.4 and 65/428.4, Pl. 2) would be interpreted as intrusive bodies rather than as structurally located and exposed formations.

The Castle Valley Anticline is a simple anticline that either plunges very gently to the northwest or continues through Dry Mesa and joins the Salt Valley Anticline. Round Mountain is a circular anomaly whose interpretation is questionable.

The Mary Jane Syncline (65/427.7, Pl. 2) is a very gentle, symmetrical syncline of only local extent.

In the Yellow Cat Flat-Highlands area (63/430, Pl. 2), the strata are very gently flexed into a northwest trending anticline and northwest trending syncline. These very gentle, open folds trend about N20-30°W.

The Cottonwood Canyon Graben (66/428.8, Pl. 2) and the Salt Creek Canyon Graben (68/427, Pl. 2) are similar graben structures that trend N51-53°E. These grabens are anomalous in that they are about perpendicular to the regional structural trend. Since both drainages head in Paleozoic anticlines, the grabens may be simply a collapse response to removal of subsurface evaporites. The Sinbad Valley Anticline (67.5/426.4, Pl. 2) is a simple, doubly-plunging anticline, faulted on the northeast flank. The anticline appears to have an intrusive center along the northwest part of the structure. The trend of the anticline, N40-45°W, matches structures to the northwest of the La Sal Mountains more than the closer Paradox structures.

The Paradox Valley Anticline-Syncline (68/425, Pl. 2) is a classic example of the salt anticline structure. The anticlinal nature of the structure is best seen by examining the outcrop patterns away from the bounding faults along the core of the structure. These dip slopes clearly indicate a large, more-or-less symmetrical anticline. Bedding attitudes within the valley-bounding faults, especially at the northwest and southeast ends (67.2/425.2 and 70.8/423.1, Pl. 2) clearly show an opposite - or synclinal - type of structure. This structural anomaly, where a syncline is superposed on an

anticline, produces the curious structural situation where beds on either side of the bounding faults are dipping in opposite directions. Outcrops of the Paradox Member evaporites have a distribution in the core of the structure that definitely suggests an intrusive origin. (In contrast to the geologic maps of Case Study I, where such contacts are shown as fault contacts, these intrusive contacts are shown as normal formational contacts, similar to igneous intrusive contacts).

The Nucla Syncline (71/424, Pl. 2) and the Dry Creek Syncline (69/423, Pl. 2) are subparallel, gentle synclines that flank the Paradox Valley Anticline-Syncline. In both cases, the synclinal structures were defined by photointerpretation of very gentle dips, generally less than 5°.

1:62,500 MAPPING--MOAB NORTH AREA

When it became obvious, during the previously-described study, that there was more geologic information available in the S190B photos than could be annotated at a scale of 1:500,000, additional interpretations were conducted at scales of 1:250,000 and 1:125,000. Whereas the photogeologic interpretation previously described used positive transparencies at a scale of about 1:500,000 and transferred geology onto a topographic map at a scale of 1:250,000, the study described in this section is concerned with photointerpretation on positive transparencies at an enlarged

scale of about 1:250,000 and data transferral onto a topo base map at a scale of 1:62,500. Techniques described in the previous section on photointerpretation apply to this study as well. As in the previous study, continuous referral to the original contact-scale transparency with a zoom stereoscope often was necessary.

Two portions of the Moab Quadrangle were selected for this additional study, areas that are here called Moab North and Moab South (Fig. 3). Moab North was selected because this area includes several complex structures, most of which are associated with salt tectonics.

Lithology

The general ability to subdivide stratigraphic map units is not significantly different on the 1:250,000 positive transparencies. Those units that are mappable at the enlarged scale are similar to the map units used in the 1:500,000 scale photographs, except that the Jurassic section could be more reliably and consistently subdivided. Whereas in many areas of the 1:500,000 transparencies, only one stratigraphic unit was mapped between Kayenta Formation and the Dakota Group, the enlarged photographs permitted subdivision into the Entrada Sandstone, the Summerville Formation, and a subdivision of the Morrison Formation into the Salt Wash Member and the Brushy Basin Member.

Formation contacts were mapped in considerably more detail at the enlarged map scale. Formation thicknesses, as a result, are considerably changed, sometimes dramatically; the thickness of the lower member of the Mancos Formation was estimated at about 100 m on the 1:250,000 map, whereas the enlarged map interpretation gave a thickness of about 25 m. In general, the additional detail available provides more reliability for the interpretation of the contacts and presumably greater accuracy.

The increased accuracy in picking formation contacts provides considerably more detail on actual outcrop distribution. For example, the Dakota-Morrison contact and the Brushy Basin Member/Salt Wash Member contacts are shown in considerably more detail on the 1:62,500 map than on the 1:250,000 map. In order to make this comparison, examine the Poison Strip area (63.2/430.3) on Plate 2 with the same area (T.22S., R.22E.) on Plate 4.

A few significant interpretive changes result from a different interpretation of the formation exposed at the surface. In the Dome Plateau area (NW cor. T.24S., R.23E., Pl. 4), the outcrop is interpreted as the Navajo Formation, whereas on the 1:250,000 map (63.8/428.9, Pl. 2), this area was mapped as undifferentiated Kayenta-Wingate.

A similar difference in assigning formation names occurs in the Parriott Mesa area (SW cor. T.24S., R.23E., Pl. 4; 63.8/428.1, Pl. 2), where a different interpretation centers on differentiating the Moenkopi Formation from the underlying

Cutler Formation. This contact is rather subtle, and cannot always be picked with reliability even in the field.

Structure

Little significant structural information was added concerning the major structural elements. The larger-scale photographs and maps provide more detail on formation contacts, as noted above, that led to improved interpretation of minor, secondary structures and possible refinement of attitude estimations.

The actual differences in structural interpretation between the two different scale maps is relatively minor. Several of the secondary faults mapped, especially along the collapsed anticlines, are somewhat different in orientation, extent, or existance, but do not significantly change a structural interpretation. In most cases, additional information on these minor faults clarifies the structural picture. A good example of this is the faulting along the Moab Anticline near the Arches National Park Headquarters (Sec. 20, T.25S., R.21E., Pl. 4; 62.1/427.5, Pl. 2), where the larger scale map clarifies, rather than changes, the structural interpretation in this area.

None of the folds in this map area were interpreted differently on the larger scale map. The only change between the two maps occurs at the Mary Jane Syncline, whose axis

was shifted somewhat to the southwest on the larger scale map (Sec. 13, T.25S., R.23E., Pl. 4; 64.9/427.7, Pl. 2).

In addition to the minor changes in interpretation going from the small scale to the large scale map, several secondary minor structures were interpreted as new information. Two anticlines were interpreted that appear related to the major salt anticlines as flanking drag structures, probably formed in association with collapse of the central portion of the anticlines. These secondary structures appear at Winter Camp Wash (Sec. 4, T.24S., R.22E., Pl. 4) and at the Arches National Park Headquarters (Sec. 21, T.25S., R.21E., Pl. 4). Another new structure interpreted was the open gentle syncline through Dry Mesa (Sec. 21, 22, T.24S., R.22E., Pl. 4).

The ability to interpret the relatively subtle syncline at Dry Mesa, mentioned above, resolves the question of the structural interpretation at the southeast end of the Salt Valley-Cache Valley Anticline. The structural interpretation compiled on the 1:250,000 map left ambiguous the possible connection of this anticline with either the Castle Valley Anticline or the Fisher Valley Anticline. The existance of the Dry Mesa Syncline effectively negates the possible connection of the Cache Valley structure with the Castle Valley Anticline.

1:62,500 MAPPING - MOAB SOUTH AREA

A second study on the affect of scale differences on interpreting geologic information from EREP photographs was

conducted in an area southwest of Moab, Utah. The S190B color photographs of this area were enlarged about eight times to a scale of approximately 1:125,000. Enlarged transparencies were made of stereo pairs so that continuous stereoscopic interpretation of the area was possible. The procedure followed was similar to that described in preceding sections - that is, the enlarged transparencies were studied with a mirror stereoscope, information was annotated directly onto the enlarged transparencies, and geologic information was then compiled onto a topo base map at 1:62,500. Continuous referral to the original contact-scale transparency with zoom stereo magnification was necessary.

The area chosen for this study was selected because of a relative absence of geologic structures, whereas the area north of Moab was selected for the previous study primarily because of its fairly complex structures. Because the Canyonlands area southwest of Moab has relatively few structures, the area provided a good base for determining the detail of stratigraphic information that was available from the enlarged transparencies.

Lithology

The general ability to discriminate stratigraphic units is significantly increased on the 1:125,000 scale transparencies as compared with the 1:500,000 scale transparencies. A brief comparison of Plates 2 and 5 indicates the amount of

stratigraphic subdivision possible. The following is a brief description of each of the map units that can be interpreted on the S190B color photographs.

Phu The oldest mappable unit exposed in this area is the Upper Member of the Hermosa Formation. Outcrops are restricted to small areas at the south and north parts of the map area where the Colorado River has cut down into positive structures. Limited exposures occur in the center of the Shafer Dome (Secs. 15, 16 and 22, T.27S., R.20E., Pl. 5; Fig. 5) and near the confluence of the Colorado River with the Green River (G.2/9.6, Pl. 5).

Pc0 The distribution of this basal member of the Cutler Formation, and its contact with the underlying Hermosa Formation, are difficult to map accurately because they are exposed only along the very steep canyon walls of the Colorado River. Good outcrops occur at Shafer Basin, (Fig. 5) and in the southern part of the area (as described above for the Hermosa Formation); additional outcrops occur in Lockhart Canyon (Sec. 16, T.28S., R.20E., Pl. 5).

Pc1 This map unit is a resistant bench-former that is seen only in the Shafer Dome area (Fig. 5) and at the mouth of Lockhart Canyon. Although the units above and below it are exposed farther south along the Colorado River, this unit cannot be readily broken out of the Cutler Formation south of Lockhart Canyon. This unit appears grey on the photographs, and during mapping on the 1:500,000 photographs it was questionable as to whether this area would be subdivided as

Figure 30. Linear features of the southernmost Front Range in LANDSAT image E-1550-17102 described in Figure 29. Scale is same as Figure 27.

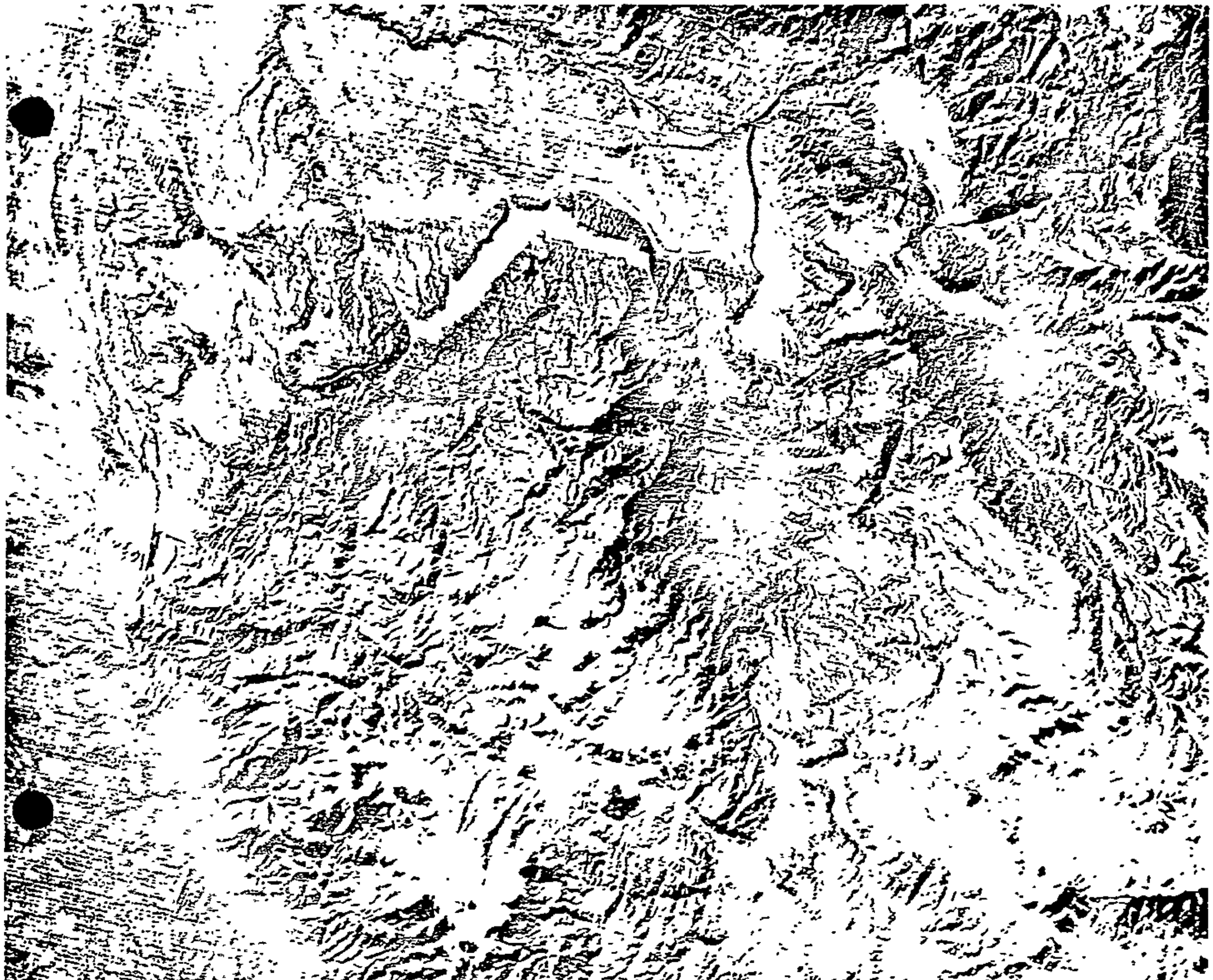

ORIGINAL PAGE IS
OF POOR QUALITY

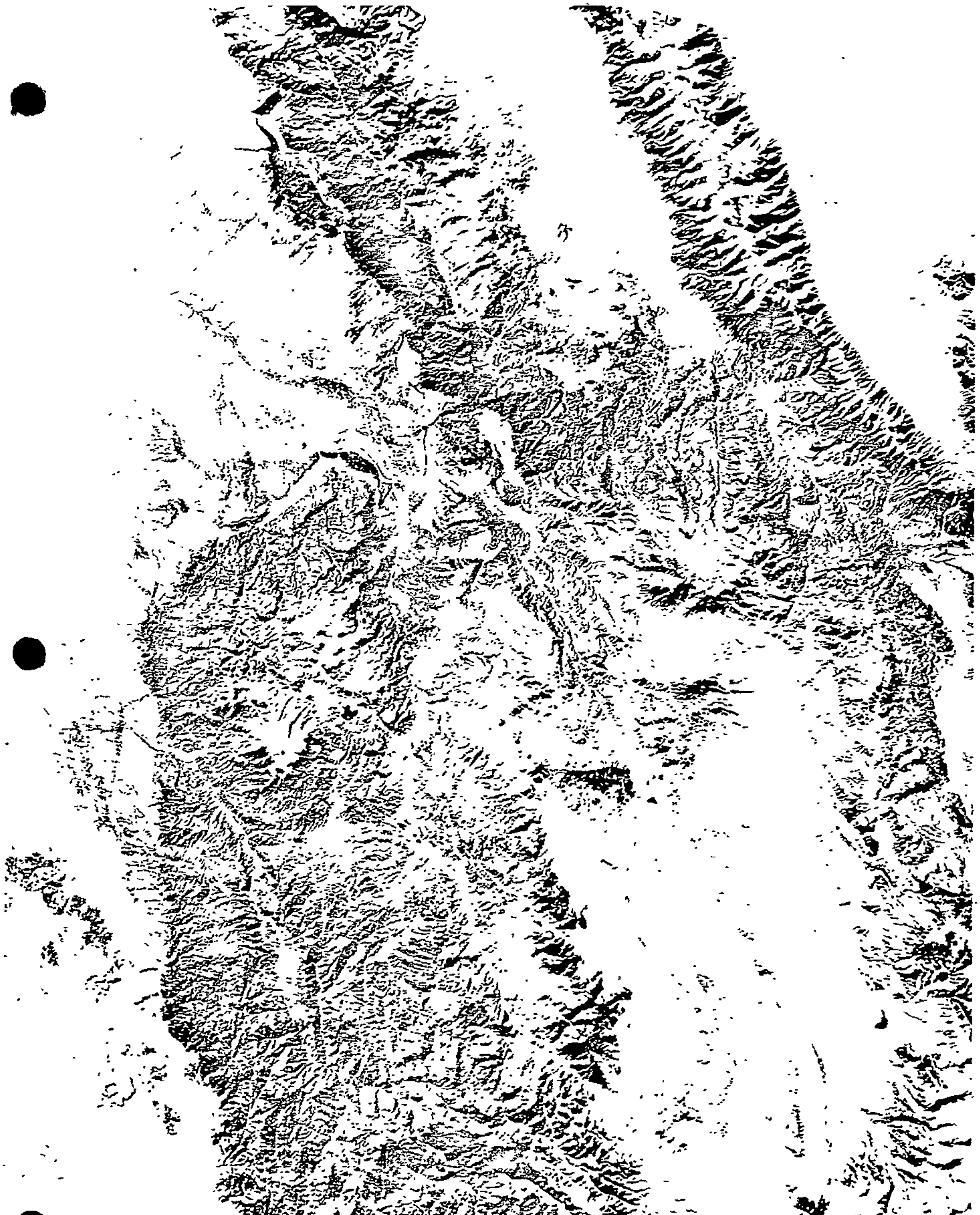

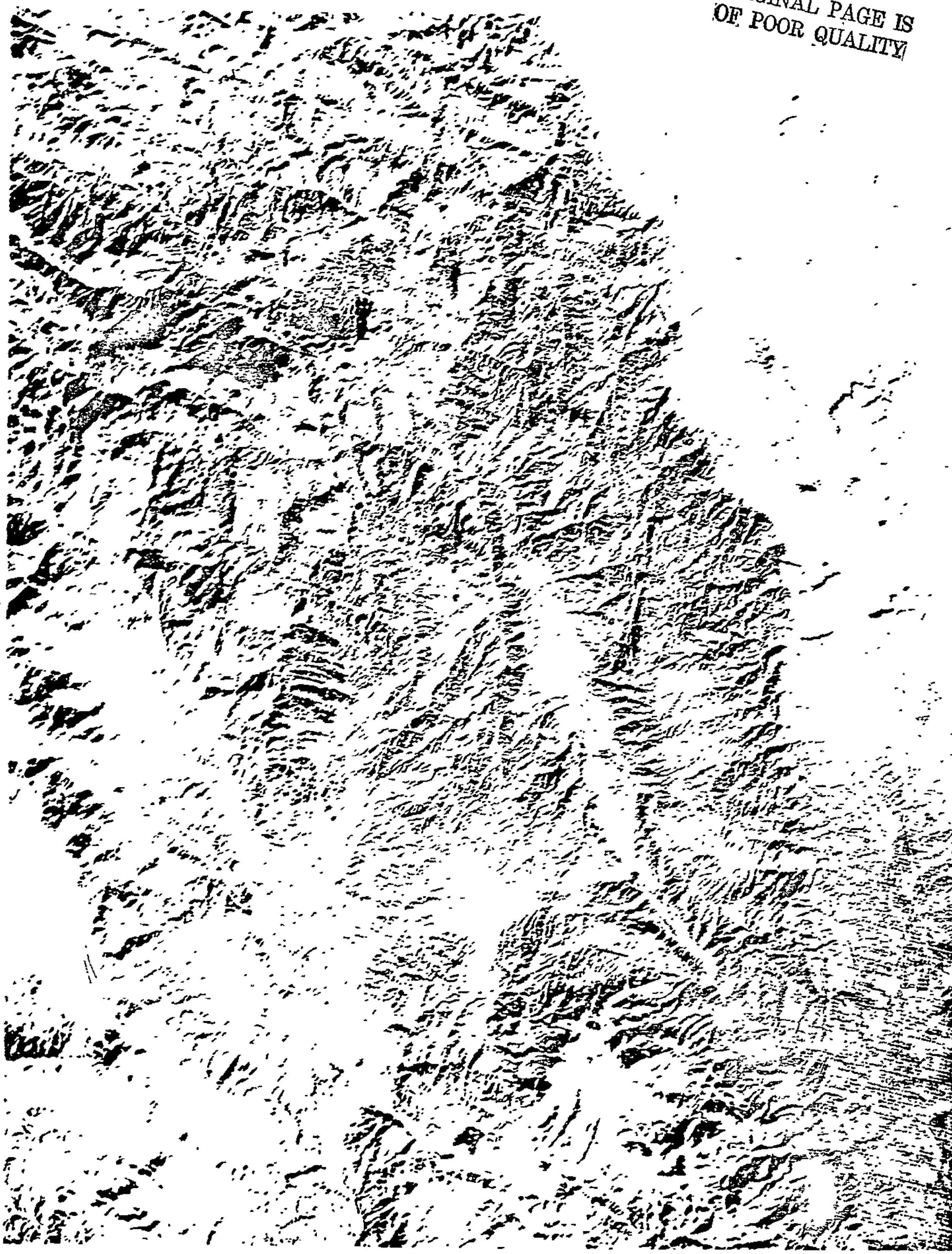

Figure 5. Base of stratigraphic section at Shafer Dome. P_{hu} - Hermosa Fm. P_{co}, P_{cl} - Member 0, Member 1 of Cutler Fm.

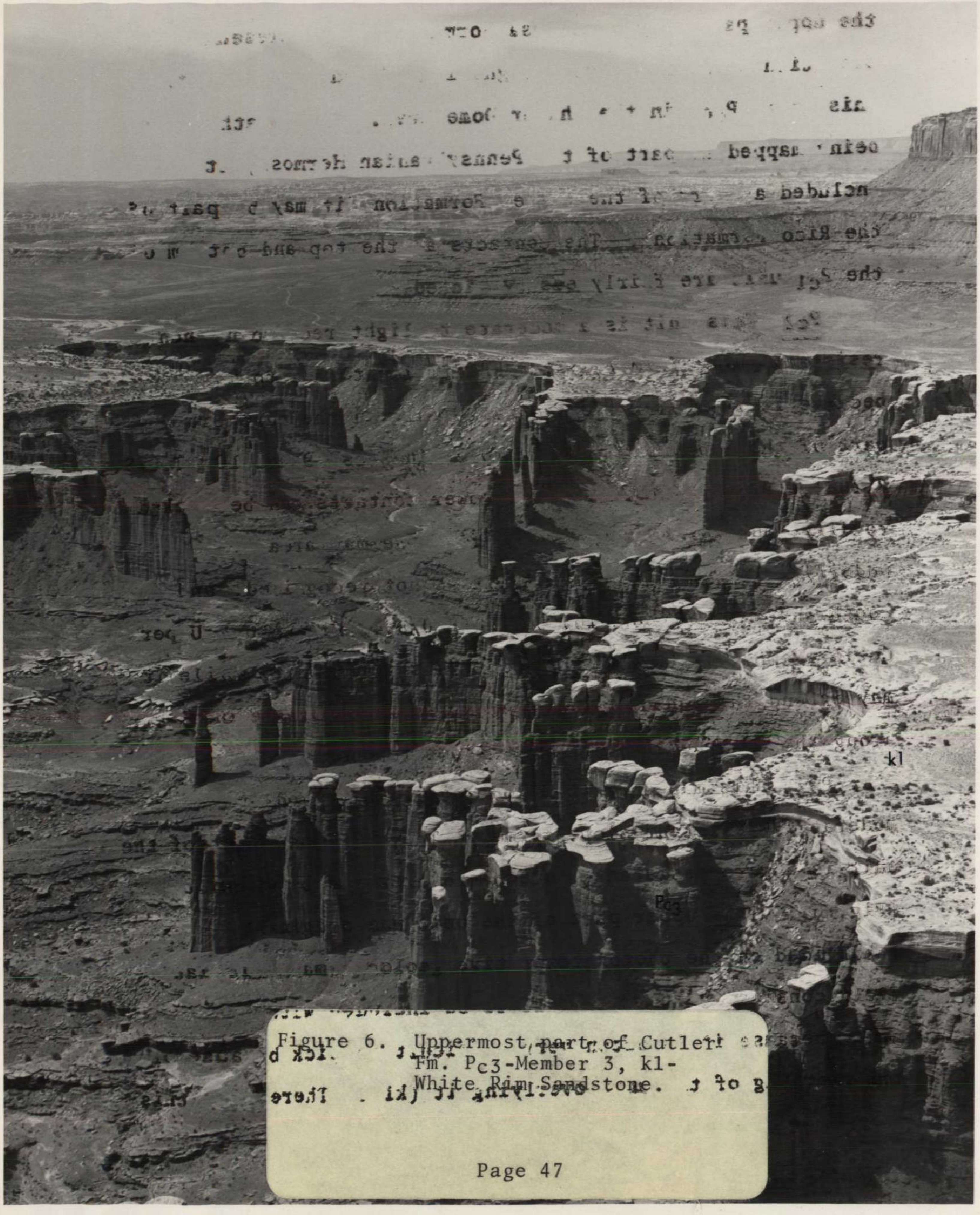

Figure 6. Uppermost part of Cutler Fm. P_{c3}-Member 3, kl-White Rim Sandstone.

the upper part of the Hermosa Formation. The present interpretation stems from the recognition of red beds beneath this unit (P_{c0}) in the Shafer Dome area. Thus, rather than being mapped as part of the Pennsylvanian Hermosa, it is included as part of the Cutler Formation (it may be part of the Rico Formation). The contacts at the top and bottom of the P_{c1} unit are fairly easily picked.

$\underline{P_{c2}}$ This unit is a moderate to light red brown, non-resistant slope former. It is a difficult unit to map because it is clearly recognizable only in the northern part of the map area. For example, in Secs. 9 and 10, T.27S., R.20E., (Pl. 5), its upper and lower contacts can be picked readily, but in the southern half of the map area the underlying P_{c1} ledge-forming unit is not recognized, and south and west of Junction Butte (E.0/8.4, Pl. 5) the Upper Cutler Member is not recognized. Thus, this unit, while it may extend throughout the map area, is recognizable only along the Colorado River in its upper reaches.

$\underline{P_{c3}}$ This map unit is a moderately dark, red-brown, moderately resistant slope former. The uppermost part of the unit is a more resistant, somewhat darker red-brown unit (Fig. 6). This upper part of the unit was originally subdivided on the photointerpretive geologic map, but later field considerations caused it to be included with the P_{c3} unit, because it is often very difficult to pick because of the overhang of the unit overlying it (kl). Therefore, this

key bed, k2. Throughout this region it can be subdivided fairly easily into an upper, somewhat more resistant unit, and a lower, less resistant, thinner member. North of Little Bridge Canyon, where the k2 unit cannot be carried, the Chinle-Moenkopi contact is sometimes difficult to pick.

k2 This key bed is a resistant, light reddish-brown to purplish red-brown, moderately resistant ledge-former or bench-former. The unit forms a prominent marker bed in the southwest part of the area, but cannot be carried with reliability northeast of Little Bridge Canyon. Although this key bed has not been identified east of the Colorado River, it may be correlative with the purplish white, moderately resistant unit in a similar stratigraphic position at Lockhart Basin (Sec. 36, T.28S., R.20E.).

₮c The Chinle Formation is a relatively non-resistant, red slope-former (Fig. 7) that appears uniform in color and texture on the space photography.

₮kw The Kayenta-Wingate unit is a very resistant, red-brown to brown, massive rim rock (Fig. 7). The bottom contact with the Chinle Formation is easy to see on the photography, but difficult to map accurately because of the near-vertical cliffs. The Kayenta-Wingate contact generally cannot be differentiated because the contact occurs on a near-vertical cliff face (Fig. 8), but where moderate dips occur, such as at Upheaval Dome, the contact can be picked easily.

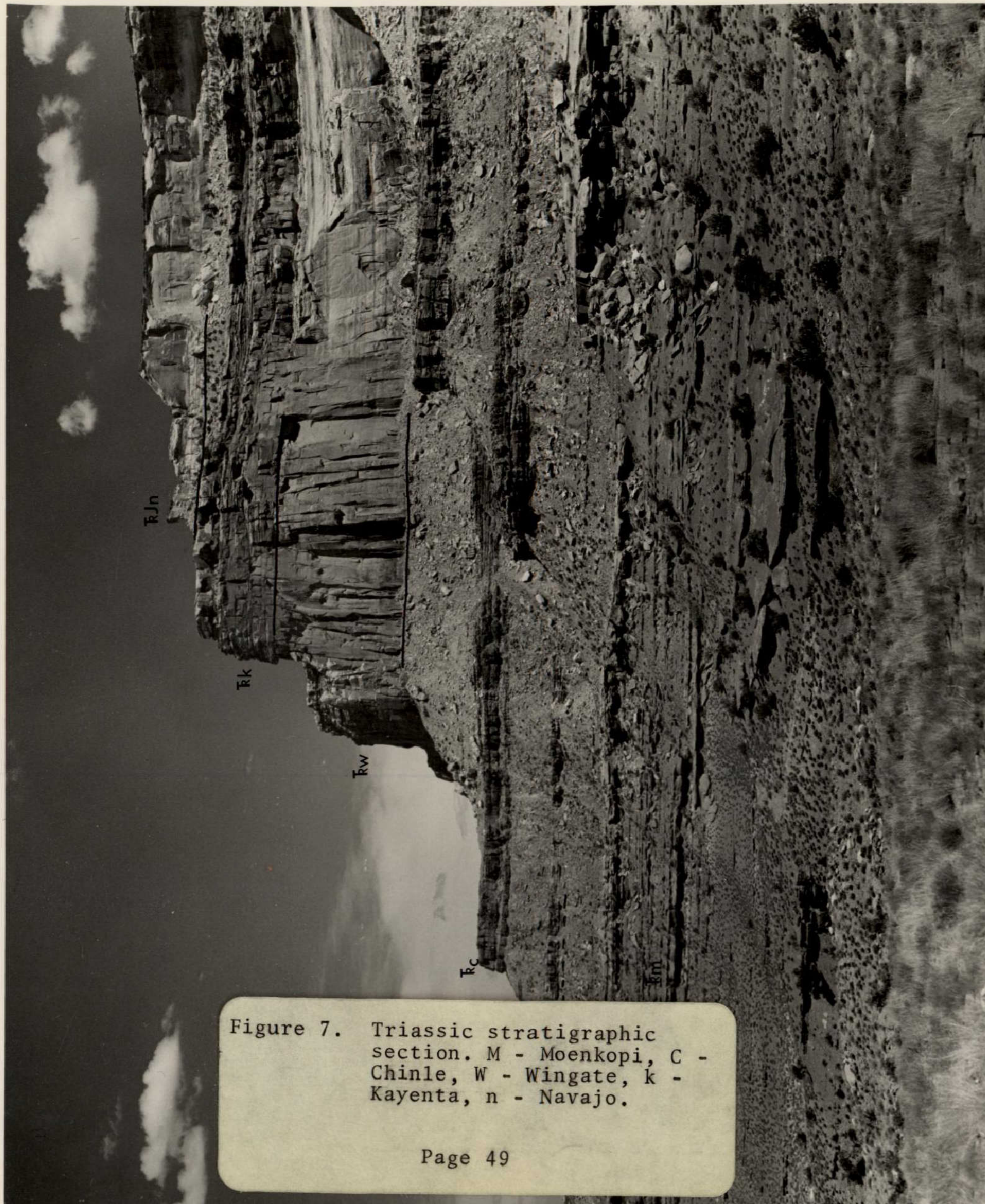

Figure 7. Triassic stratigraphic section. M - Moenkopi, C - Chinle, W - Wingate, k - Kayenta, n - Navajo.

Figure 8. Upper Triassic stratigraphic section. c - Chinle, W - Wingate, k - Kayenta, n - Navajo.

$\overline{R}J_n$ The Navajo Sandstone is a moderately resistant, tan to brown unit (Figs. 7 and 8). Although bedding can sometimes be seen, the unit generally appears massive. The Navajo is present only on the tops of the Canyonlands plateaus, and the bottom contact with the $\overline{R}_{kw}$ is often difficult to pick; both units are relatively resistant, and tone differences must be used.

Structure

A first-order structural approximation of the entire map area would be flat-lying, layer-cake geology. There are only three significant exceptions to this approximation: the Shafer Dome, the Lockhart Basin structures, and Upheaval Dome. The latter was recognized on the small-scale photography, but the latter two represent new structural interpretations.

Shafer Dome This structure (centered on SE cor, Sec. 16, T.27S., R.20E., Pl.5) is clearly a positive structural element, although the exact nature and configuration of the structure is not obvious. It is called a dome because in the simplest sense dips are everywhere away from the center noted. Initial photointerpretation of the structure, however, suggested that the structure more closely resembled two superposed anticlines; one with a trend of approximately N40°E and the second with a N70°W trend. In fact, the

northwest trending structure is so subtle that in its northwestern end it was originally interpreted as a monocline with a southwest flexure. The exact nature and shape of this structure is best observed by studying the outcrop distribution of P_{c1}. One area on the northern part of the structure (Sec. 16, T.27S., R.20E.) shows a fairly steep dip to the northwest on the top of the P_{c1} unit; all other dips off the flank of the structure were interpreted to be relatively gentle, probably less than 10°.

<u>Lockhart Basin Structures</u> Lockhart Basin (southeasternmost T.28S., R.20E.) was interpreted as a northwest-plunging syncline that abruptly changes northwestward into an anticline, with parallel and orthogonal normal faults. The synclinal fold is fairly well established by interpretation of attitudes on the Wingate-Chinle contact. Dips on the southwest flank of the structure are more gentle than the northeast flank. Although the nature of the fold is apparent, the actual location of the surface trace of the synclinal axis cannot be accurately located. The attitude of the bedding can be best estimated by observing the contact between the Chinle and the Moenkopi formations. Although the k2 keybed is not recognized in this area, the same stratigraphic position is occupied by a purplish-white unit previously described.

Four normal faults were originally interpreted in this area. Two of the faults trend northeast, normal to the fold

axis, and define a small graben. The northwesternmost of these two faults (Sec. 25, T.28S., R.20E.) was interpreted with confidence as a normal, down-to-the-east fault. Its northeastward extension on top of Hatch Point, and its southwestern extension on the southwest side of Lockhart Canyon, are questionable interpretations. A subparallel, down-to-the-northwest normal fault is interpreted with somewhat less confidence, as displacement appears to be minor and the fault is not as clear as the previously described one.

The small northwest-trending, down-to-the-northeast normal fault (Secs. 2, 2, T.29S., R.20E) cannot be interpreted with any reliability. The position of this fault is inferred only to account for a lack of clearly interpreted stratigraphy. A longer, northwest-trending, down-to-the southwest fault was originally interpreted northeast of the Kayenta-Wingate contact in Sec. 31, T.28S., R.21E. No surface evidence for this fault was seen at all, but the fault's location and existance were hypothesized to account for the topographically low Wingate Sandstone in the valley. An alternate explanation would be a fairly steep monoclinal flexure in the same position (later field observations suggest the latter interpretation).

Upheaval Dome This structure is one of the most obvious features on any of the Skylab photography in this area. The extreme contrast between very flat-lying strata and this

strongly folded structure make it stand out clearly to even the most casual observer. Upheaval Dome was interpreted correctly in the earlier small-scale study as a dome, and its position and outcrop pattern were fairly accurately mapped. Subsequent photointerpretation of the larger 1:125,000 scale photography, however, significantly reinterpreted the formations that occur in the core of the structure, and more detailed interpretation of their distribution more accurately delimits the domal structure and, for the first time, reveals clearly the presence of a secondary, peripheral rim syncline.

Both the central dome and the peripheral syncline are amazingly symmetrical circular features. This symmetry is well defined by the pattern of the Navajo-Kayenta contact (C.4/3.1, Pl. 5). The doming appears to be somewhat steeper on the south and southwest sides of the structure. The ring syncline is well developed on the north, northeast and southwest flanks, and flattens somewhat on the southeast side. Some concentric, down-to-the-center faulting was interpreted on the northwest side and along the synclinal axis on the southwest side of the structure.

The oldest formation exposed in the center of the dome was interpreted to be Moenkopi. This interpretation differs from that of the small-scale photography in which the core formation was interpreted to be the Paradox Member of the Hermosa Formation. The latter stratigraphic designation was an assumption based on inference from the salt anticlinal

structures to the north; the reinterpretation of the central formation as being Moenkopi is based on more detailed photo-interpretation and delineation of stratigraphic units.

FIELD CHECKS

The accuracy and validity of the photointerpretation maps were checked in the field. Field observations consisted of examining areas characteristic of the geology of each map area, as well as investigation of areas where geologic interpretations were complex or where no geologic interpretation could be made from the photographs. Accessibility in this entire region is very poor, and a large percentage of field time was devoted simply to driving between points to be checked. Accessibility to some key areas was so poor that aircraft observations were required.

The amount of time spent field checking the small-scale 1:250,000 geologic map is difficult to estimate accurately. Because of the nature of this study, considerable time was spent in southern portions of the Moab Quadrangle field checking early photogeologic interpretations of the training area. Additional field time was devoted to establishing photointerpretation keys by field observations in the Paradox-Sinbad Valley areas.

The subsidiary study areas, Moab North and Moab South, were areas in which no geologic observations were made prior to the field check subsequent to photointerpretation. Two days were spent field checking the area north of Moab; and two days were spent in the Moab South area.

DISCUSSION AND EVALUATION

The described research was conducted, and this report was written, so that the data products at this point in the research represent data products that would be obtained from an application of photointerpretation, using Skylab S190B photography, to areas that are geologically unknown or geologically poorly known. Continuous efforts were made throughout the research to help insure that the photointerpreter would not become biased by geologic information from sources other than the EREP photography.

The geologic maps shown as Plates 2, 4 and 5 represent geologic mapping by photointerpretation on Skylab S190B photographs, supplemented by minimal field checking. In general, the correlation between the photogeologic maps and the published geologic maps is excellent. Obviously this is a statement of judgement, and the accuracy or utility of this statement can be evaluated only by carefully comparing the maps (Pl. 2 with Pl. 3; Pl. 4 with Pl. 3; and Pl. 5 with Pls. 3, 6, and 7). It is suggested that the serious reader remove these plates and make a comparison of the geologic interpretations both before and during the discussion that follows.

LITHOLOGY

The maximum amount of stratigraphic information derived from the EREP photographs was obtained in Moab south area. Surprisingly detailed stratigraphic information was available in this area. The following section describes the sedimentary units mapped in the area and compares them with published descriptions of the lithologic units.

The results of the stratigraphic subdivision in Moab South area are shown in Figure 9 (cf. Fig. 4). Even casual inspection of Figure 9 forcibly brings out one salient feature of this photointerpretation: not only can formations and members be interpreted from the EREP photographs, but stratigraphic lateral variations can be determined as well. The generalized stratigraphic sections and correlations illustrate variations from the southwestern part of the map area (Murphy Hogback (sic) - Junction Butte) through the central portion of the map area (Lathrop Canyon - Little Bridge Canyon) to the northeast (Shafer Canyon - Dead Horse Point).

Using the base of the Wingate Sandstone as a datum, Figure 9 clearly shows stratigraphic thickening toward the southwest. Almost all of this thickening can be accounted for by changes within the Permian Cutler Formation, but this relationship persists into the Triassic, as evidenced by the pinch-out/facies change of the White Rim Sandstone and keybed 2 in a northeasterly direction.

The ability to determine stratigraphic thicknesses is quite good. Obviously this capability stems from, and is

c. 7

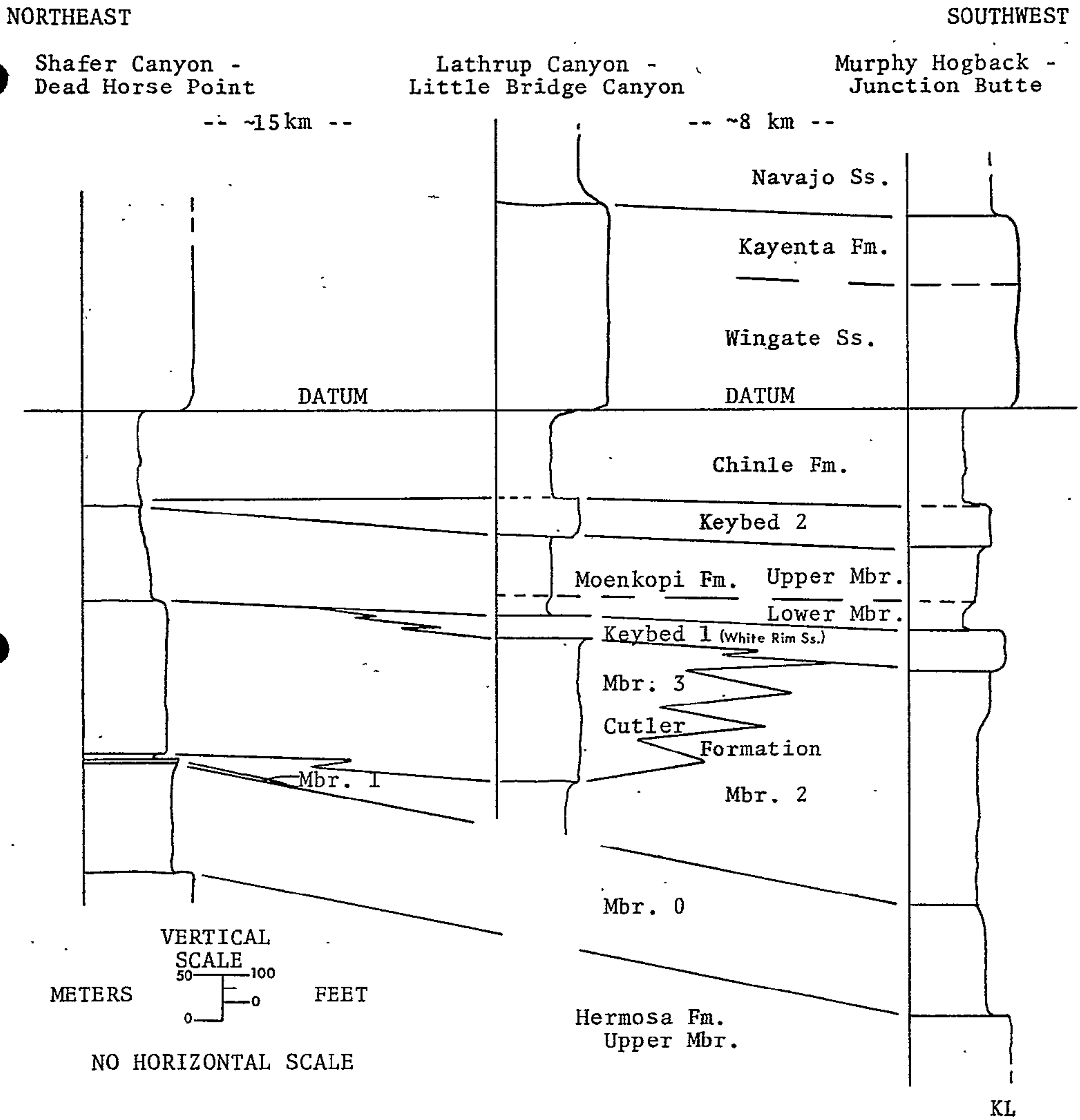

Figure 9. Generalized stratigraphic sections and correlations based on photointerpretation of Skylab S190-B photographs, Moab South area, Utah.

dependent upon, the conjunctive use of accurate topographic base maps. As an illustration of thickness determination, consider the thickness of the stratigraphic section below the Wingate Sandstone and above the Hermosa Formation. In the Shafer Canyon-Dead Horse Point area, this thickness totals about 500 m (1650 ft) and the same section thickens to the southwest to about 670 m (2200 ft). Interpolation of measured stratigraphic sections by McKnight (1940) gives corresponding thicknesses of about 525 m (1720 ft), thickening to 730 m (2403 ft). Using McKnight's data as the true thicknesses, the thicknesses determined from photointerpretive studies are in error by about 4 percent and 8 percent respectively.

Hermosa Formation Upper Member

Outcrops of the Hermosa Formation were interpreted in the Shafer Dome area and in the southernmost part of the map area along the Colorado River. The Hermosa Formation is distinguished from the overlying Cutler Formation by its higher resistance and grey color compared to the red Cutler. The thickness of the Hermosa cannot be determined because the base is covered, but it is greater than about 50 m (160 ft).

Cutler Formation

The Cutler Formation in this area is quite complex, more so than any other stratigraphic unit in the area. Initial

photointerpretation of the Cutler Formation subdivided the formation into three members, called simply Member 1, Member 2 and Member 3. Later photointerpretation in the Shafer Dome area broke out a lower unit which was then called Member 0, and the prominent keybed (k1) at the top of the Cutler Formation was subsequently identified as the White Rim Sandstone and included in the Cutler Formation. Thus, the Cutler Formation, as used here, consists of five members; Members 0 through 3 plus Keybed 1.

Member 0 - Published geologic maps suggest that Member 0 is the Pennsylvanian-Permian Rico Formation (Bates, 1955; Williams, 1964), but there is some doubt that this in fact is the Rico Formation. Its outcrop in this area is confined only to the canyon bottoms, precluding field checking of the unit, and hence the terminology Member 0 of the Cutler Formation is retained. Member 0 is differentiated from the underlying Hermosa by its red color and lower resistance, and it is differentiated from the overlying Member 1 by the same criteria. Thickness of Member 0 is estimated at about 120 m (400 ft). This compares with an estimate of 177 m (580 ft) by McKnight (1940), but McKnight included in the Rico Formation what is here designated as Member 1 and part of what is here designated as Member 2.

Member 1 - Member 1 is a very resistant, grey, carbonate unit among the Cutler redbeds. Although the unit is only about 3 m (10 ft) thick, because of its resistance it forms

benches and ledges such that the member is exposed over fairly wide areas (for example, see Sec. 10, T.27S., R.20E., Pl. 5). Field examination shows this unit to be a somewhat rubbly, brachiopodal crinoidal lime wackestone. Baars (1975) makes a strong case for calling this unit a part of the Elephant Canyon Formation.

Member 2 - Much of the complexity of the Cutler Formation hinges upon the relationship between Member 2 and Member 3. The interpretation derived from this study suggests that Member 2 is very thin in the north part of the area, approximately 12 m (40 ft) thick in the Shafer Dome area where it underlies Member 3, and thickens to about 260 m (850 ft) in the south. It cannot be shown conclusively that this is one continuous unit, however. Member 2 is characterized by a pink to red to red-brown color and relative non-resistance to erosion.

Member 3 - Member 3 is differentiated from Member 2 by having a darker red to a maroon color and by being relatively more resistant. The relationship between Member 3 and Member 2 is not entirely clear; this photointerpretation suggests that the two members are at least in part facies equivalents (Fig. 9). Where the two members are recognized at one location, Member 3 is above Member 2.

Member 2 appears to correspond to the Cedar Mesa Sandstone Member of Williams (1964) and Baars (1975) and to a transition zone where the Cedar Mesa Sandstone Member

interfingers with an unnamed arkose and arkose conglomerate. Member 3 appears to correspond well with Williams' unnamed arkose and arkosic conglomerate and Baars' "Cutler arkosic red beds from the east". The upper dark red part of Member 3 may be part of the Organ Rock Tongue. It is interesting to note that geologic mapping at a scale of 1:62,500 (McKnight, 1940) apparently was unable to subdivide the Cutler Formation effectively. The combined thickness of Members 2 and 3 in the north part of the area is interpreted at about 165 m (550 ft), compared with a measured thickness by McKnight of about 150 m (500 ft). The same stratigraphic interval thickens to the south to an estimated 260 m (850 ft) that compares well with McKnight's measurement of 251 m (823 ft).

Keybed 1 - Keybed 1 is an excellent marker bed throughout its area of outcrop. It forms a prominent and conspicuous white ledge that stands out sharply against the red-brown colors of the units beneath and above it. This member is relatively thin, yet forms extensive areas of outcrop because of its high resistance to erosion (for example, see outcrops of this member in Monument Basin - F.4/8.4, Pl. 5 and Fig. 6).

Keybed 1 is the White Rim Sandstone that is considered by most authors to be the uppermost member of the Cutler Formation. The sandstone was estimated to be about 45 m (150 ft) thick in the southwest part of the map area, which does not compare well with McKnight's measurement of about 17 m (55 ft), but agrees well with Baars (1975) isopach

thickness of 30-45 m. This discrepency probably is due to the difficulty in picking a bottom contact on the vertical cliff exposures of this sandstone. The White Rim Sandstone thins continuously toward the northeast, where it goes to zero thickness at Shafer Canyon (Sec. 7, T.27S., R.20E.).

It is significant to note that the point of pinchout of this member could not be more accurately determined from observations in the field than it was determined from interpretation of the S190B photographs. It is obvious that the nature of the pinchout could not be interpreted from the photographs. McKnight (1940) states that the White Rim Sandstone disappears to the northeast by lateral gradation into the basal two or three meters of the upper brown member of the Cutler Formation (McKnight considered the unit directly above the White Rim Sandstone Member as part of the Cutler Formation, even though he mapped this unit as part of the Moenkopi Formation).

Moenkopi Formation

The Moenkopi Formation consists of about 90 m (300 ft) of brown and reddish-brown siltstones and relatively non-resistant sandstones. The formation is differentiated from the underlying Cutler Formation with ease where the White Rim Sandstone Member is present and with difficulty where this unit is missing. In the southern part of the map area, the Moenkopi Formation can be subdivided into two members,

a relatively non-resistant, thin lower member and a more resistant, thicker upper member. This subdivision becomes unworkable north of Little Bridge Canyon. An estimated thickness of 90 m for the Moenkopi Formation compares well with measured sections by McKnight (1940) of 87 to 114 m (285 to 375 ft).

Chinle Formation

Keybed 2 - The lowermost part of the Chinle Formation can be mapped separately in the southern part of the area. In this area, the keybed is a light red-brown to purple red-brown ledge-former or bench-former. The keybed cannot be carried north and east of Little Bridge Canyon, although it may be correlative with the purplish-white moderately resistant unit at the base of the Chinle Formation in the Lockhart Basin (Sec. 36, T.28S., R.20E., Pl. 5). Although the keybed cannot be carried on the photographs through the northern part of the map area, field observations suggest that it is present, although considerably thinner. This keybed corresponds to what was originally called the Shinarump Conglomerate (McKnight, 1940; Bates, 1955; Detterman, 1955), although later workers (Lowman, 1974; Stewart and others, 1972; O'Sullivan and MacLachlan, 1975) have designated this unit as the Mossback Member of the Chinle Formation.

Above the Shinarump/Mossback keybed, the Chinle Formation consists of red-brown, relatively non-resistant

siltstones and shales. Thickness of the Chinle Formation above Keybed 2 was estimated at 105 to 130 m (350 to 420 ft). This compares well with McKnight's estimate of "about 400 [122 m] feet".

Post-Chinle Stratigraphy

Stratigraphic units younger than the Chinle Formation generally can be recognized and mapped without difficulty. Because the purpose of this report is only to demonstrate the level of geologic detail available in the Skylab S190B photos, a continued description of stratigraphy is not warranted. Reference to the stratigraphic subdivisions contained in the Explanation of Plate 4 or Plate 5, plus continued comparisons of these plates with published geologic maps and literature (e.g., Craig and Shaw, 1975) will provide sufficient information on the younger units.

In areas where bedrock is fairly well exposed, and where structural complexities are not greater than the resolution of the photography, there are few significant differences between the interpreted geology and the published geology. A few notable differences do exist, however, and these warrant some discussion.

In the Dome Plateau area (Sec. 6, T.24S., R.23E., Pl. 4), the southeastward extent of the Navajo Sandstone goes considerably farther on the photogeologic map. It was not possible to field check this area, so a resolution of the

apparent conflict is not possible. An earlier geologic map, however, at a scale of 1:62,500 (Dane, 1935) shows the Navajo Sandstone extending approximately as far southeast as the photogeologic map does.

In the highlands area (for example, sec. 12, T.23S., R.22E., Pl. 4), a very wide outcrop of Summerville Formation is mapped between exposures of the Entrada and Morrison formations. Although the 1:250,000 published geologic map (Pl. 3) does not subdivide the Entrada from the Summerville Formation, the more detailed geologic map of Dane (1935) does subdivide these formations and shows a very narrow Summerville outcrop and a very broad outcrop of the underlying Entrada Sandstone. A field check was made in this area to attempt to resolve the apparent conflict; ground observations show that the area in question is totally covered by a veneer of eolian deposits. Although the eolian cover precludes resolving the question, the actual difference in interpretation is only a matter of a few feet in the vertical stratigraphic sense.

STRUCTURES

As an illustration of the level of detail of structural interpretation possible with the S190B photographs, the following discussion will be keyed to the area north and west of Moab, Utah.

Folds

Interpretation of the major folds of this area on the S190B photographs is excellent. A comparison of Plates 2 and 4 with the published geologic maps (Pl. 3, Sheet 2) shows this correlation clearly. In the area covered by Plate 4 there are three first-order anticlinal trends: the Moab-Spanish Valley Anticline, the Castle Valley Anticline, and the Salt Valley-Cache Valley-Fisher Valley Anticline. The Moab-Spanish Valley Anticline is separated from the Salt Valley Anticline and the Castle Valley Anticline by the prominent Courthouse Syncline. The Castle Valley Anticline is separated from the Fisher Valley Anticline by a very gentle syncline whose axis is shown at Adobe Mesa (Sec. 12, T.25S., R.23E., Pl. 4). This syncline is not named on the published structure map (Pl. 3, Sheet 2), although the structure contour map clearly show its location slightly northeast of Adobe Mesa.

Several second-order folds are also capable of being interpreted on the photography. Two of these, in the northern part of the map area, are broad open folds, trending northwest, parallel to the Sagers Wash Syncline shown on Plate 3, Sheet 2. Although the published map does not name nor show structural axes of these folds, the structure contours accurately delineate the folds. The anticlinal fold in this area (T.23S., R.22E., Pl. 4) is called the Yellow Cat Dome on the published geologic map (T.23S., R.22E., Pl. 3, Sheet 2), even though

the structure contour map shows a definite elongation in a northwest-southeast direction. In fact, an argument could be made for connecting this anticline with the Fisher Valley Anticline to the southeast.

Several second-order folds are located beside and parallel to the major anticlines. Some of these, such as the Dry Mesa Syncline (Secs. 19-22, T.24S., R.22E., Pl. 4) may be a result of the tectonism responsible for the main anticlinal salt structures. Several of the second-order folds, however, appear to be the result of subsequent collapse of the salt anticlines, and appear as drag folds on the distal parts of the anticlines. Examples of this are the Moab Anticline (Secs. 17, 18, 21, T.25S., R.21E., Pl. 4; Pl. 3, Sheet 2), and the Delicate Arch Anticline (Secs. 2-6, 12, T.24S., R.22E., Pl. 4; Pl. 3, Sheet 2).

One small monocline is mapped in the Castle Valley area (Sec. 36, T.24S., R.22E., Pl. 4), but this small fold was observed in the field and was not recognized on the space photography.

Fractures

All of the major first-order faults in the area were defined on the space photography. In general, these faults correspond extremely well with mapped faults, although many of the complexities of the secondary, small faults were not interpretable on the EREP photography.

The Salt Valley-Cache Valley Anticline (T.22S., R.19E. to T.24S., R.22E., Pl. 4) shows a central collapsed portion bounded by normal down-toward-the-axis faults. This structural configuration is clearly shown on the S190B photographs, although due to the close spacing of the faults, many individual faults are not resolved.

A fault was mapped in Cache Valley (NW¼ SE¼, Sec. 9, T.24S., R.22E., Pl. 4) to account for the juxtaposition of the Morrison Formation with the Mancos Formation. This fault does not appear on the published geologic maps, where a normal stratigraphic succession is shown. Interpretation of the fault obviously stems from the inability to recognize the Dakota-Burro Canyon Formation in this area (early mapping in this area (Dane, 1935) did not breakout the Burro Canyon Formation, but included it in the Morrison Formation).

The Professor Creek Graben (Secs. 19-24, T.24S., R.23E., Pl. 4) forms a structural connection between the collapsed portion of the Cache Valley Anticline and the western end of the Fisher Valley Anticline (T.24S., R.23E., Pl. 3). Although the graben as shown does not conflict with the interpretation shown in the published geologic maps, the faulting shown is more extensive and through-going. With the time spent in the field it was not possible to resolve the interpretation of this structure, so the graben is shown with questionable status. It may be that the collapse structures from Cache Valley to Fisher Valley are more accurately seen on the space photography than they are in the field.

SUMMARY

Optimum scale for regional geologic mapping by photointerpretation of Skylab S190B photographs is about 1:62,500. This conclusion, however, may be valid only for this particular study area. Initial study of Skylab photography suggested that photointerpretation at a scale of 1:24,000 was not feasible, and photointerpretation of a large area (Moab Quadrangle) has shown that 1:250,000 is too small a scale.

Significantly more geologic information can be extracted from the Skylab photographs when the photographs are used at an enlarged scale. This increase in geologic information does not come from the larger scale per se, because critical interpretations were always made with the original contact-scale photographs using a zoom stereoscope; the increase in information stems from the attempt and the necessity to force geologic information to match the scale both of the photographic enlargement used for annotation and the topographic base map used for final compilation.

In contrast with the above, however, an increase in geologic information is associated with increase in scale when comparing the S190A and S190B photography. System resolution is approximately the same for each camera, but ground resolution of the S190B is superior because of its longer focal length and correspondingly greater scale. There

is little doubt that an increase in resolution can be directly translated into an increase in geologic information.

All of the stratigraphic units at formation rank and above that were defined in the training area were mapped into the unknown test area. In some cases, individual formations were mapped together, but this was done because their contacts were not resolvable at the map scales due to their exposure on cliff faces.

In many cases, stratigraphic units at ranks below formation level could be established in the test area. Half of the formations that were carried from the training area into the test area were ultimately capable of being subdivided. As a result, the test area was mapped to a large extent at member level; seventeen members were mapped in the test area.

Not only can vertical variations in the lithology be interpreted, as evidenced by subdividing rock units into formations and members, but some lateral variations can be interpreted as well. The Navajo Sandstone, present throughout most of the map area, is shown to pinch out to the northeast. Several members of the Cutler Formation are shown to have limited areal distribution; the uppermost member pinches out entirely to the northeast, and Member 2 and Member 3 appear to be lateral facies equivalents, at least in part.

The area southwest of the Moab Valley is characterized by flat-lying to very gently dipping beds with a few local

domes and normal faults. The area north and east of Moab Valley is characterized by a series of parallel, northwest trending anticlines that show extensive axial collapse structures.

All of the major structures in the study area were recognized on the EREP photographs. In several of the collapsed areas, numerous secondary normal faults were recognized on the S190B photos. Subsequent field checking showed that many of the main boundary faults are actually small en echelon fault systems.

REFERENCES

Baars, D.L., 1975, The Permian System of Canyonlands Country, in Fassett, J.E., ed., Canyonlands Country: Four Corners Geol. Soc. 8th Field Conf. Guidebook, p. 123-127.

Bates, C.E., 1955, Photogeologic map of the Carlisle-3 Quadrangle, San Juan Country, Utah: U.S. Geol. Survey, Misc. Geol. Investigations Map I-68 (1:24,000).

Craig, L.C., and Shawe, D.R., 1975, Jurassic rocks of east-central Utah, in Fassett, J.E., ed., Canyonlands Country: Four Corners Geol. Soc., 8th Field Conf. Guidebook, p. 157-165.

Dane, C.H., 1935, Geology of the Salt Valley Anticline and adjacent areas, Grand County, Utah: U.S. Geol. Survey Bull. 863, 184 p.

Haynes, D.D., Vogel, J.D., and Wyant, D.G., 1972, Geology, structure and uranium deposits of the Cortez Quadrangle, Colorado and Utah: U.S. Geol. Survey, Misc. Geol. Investigations Map I-629 (1:250,000).

Lee, Keenan, Knepper, D.H., and Sawatzky, D.L., 1974, Geologic information from satellite images: Remote Sensing of Earth Resources, U. Tenn. Space Inst., v. 3, p. 411-448.

Lohman, S.W., 1974, The geologic story of Canyonlands National Park: U.S. Geol. Survey Bull. 1327, 126 p.

McKnight, E.T., 1940, Geology of area between Green and Colorado rivers, Grand and San Juan counties, Utah: U.S. Geol. Survey Bull. 908, 147 p.

O'Sullivan, R.B., and MacLachlan, 1975, Triassic rocks of Moab-White Canyon area, southeastern Utah, in Fassett, J.E., ed., Canyonlands Country: Four Corners Geol. Soc., 8th Field Conf. Guidebook, p. 129-141.

Sable, V.H., 1955, Photogeologic map of the Carlisle-4 Quadrangle, Wayne and San Juan counties, Utah: U.S. Geol. Survey, Misc. Geol. Investigations Map I-69 (1:24,000).

Shoemaker, E.M., Case, J.E., and Elston, D.P., 1958, Salt anticlines of the Paradox Basin: Intermount. Assoc. of Petrol. Geol. Guidebook, 9th Ann. Field Conf.

Stewart, J.H., Poole, F.G., and Wilson, R.F., 1972, Stratigraphy and origin of the Chinle Formation and related Upper Triassic strata in the Colorado Plateau region: U.S. Geol. Survey Prof. Paper 690, 336 p.

Williams, P.L., 1964, Geology, structure, and uranium deposits of the Moab Quadrangle, Colorado and Utah: U.S. Geol. Survey, Misc. Geol. Investigations Map I-360 (1:250,000).

Young, R.G., 1955, Sedimentary facies and intertonguing in the Upper Cretaceous of the Book Cliffs, Utah-Colorado: Geol. Soc. Amer. Bull., v. 66, p. 177-202.

DISTRIBUTION

NASA - HEADQUARTERS	Copies
Molloy, M.J.	1
Park, A.B.	1
Vitali, J.A.	1
Sci. & Tech. Information Facility	5
NASA-MSC	
Amsbury, D.L.	1
Charlesworth, C.E.	1
MacDonald, R.B.	1
Miller, M.L.	1
Data Center	5
NASA-GSFC	
Blodget, H.	1
Boeckel, J.H.	1
Freden, S.C.	1
Short, N.M.	1
Stonesifer, G.R.	1
USARO-D	
Bronner, F.E.	1
CGS	
Rogers, W.P.	1
Rold, J.W.	1
CSM	
Bruns, D.L.	1
Bonanza Library	1
Butler, R.W.	1
Copeland, W.D.	1
Fisher, J.C.	1
Gary, J.H.	1
Grose, L.T.	1
Huntley, D.	1
Hutchinson, R.M.	1
Kent, H.C.	1
Knepper, D.H.	1
Lee, K.	1
McBride, G.T.	1
Arthur Lakes Library	1
ORS	1

<u>CSM</u> (cont.)	Copies
Nicolais, S.M.	1
Prost, G.L.	1
Raines, G.L.	1
Sawatzky, D.L.	1
Thigpen, J.B.	1
Trexler, D.W.	1
Weimer, R.J.	1
<u>OTHER</u>	
Asian Inst. of Tech. Library	1
Ballew, G.I.	1
Duskin, D.J.	1
Eichler, R.J.	1
Haas, R.	1
Hulstrom, R.	1
Jefferis, L.H.	1
Lash, T.R.	1
Lyon, R.J.P.	1
Marrs, R.W.	1
Muhm, J.	1
Quade, J.G.	1
Wychgram, D.C.	1

DISTRIBUTION

	Copies
NASA - HEADQUARTERS	
Molloy, M.J.	1
Park, A.B.	1
Vitali, J.A.	1
Sci. & Tech. Information Facility	5
NASA-MSC	
Amsbury, D.L.	1
Charlesworth, C.E.	1
MacDonald, R.B.	1
Miller, M.L.	1
Data Center	5
NASA-GSFC	
Blodget, H.	1
Boeckel, J.H.	1
Freden, S.C.	1
Short, N.M.	1
Stonesifer, G.R.	1
USARO-D	
Bronner, F.E.	1
CGS	
Rogers, W.P.	1
Rold, J.W.	1
CSM	
Bruns, D.L.	1
Bonanza Library	1
Butler, R.W.	1
Copeland, W.D.	1
Fisher, J.C.	1
Gary, J.H.	1
Grose, L.T.	1
Huntley, D.	1
Hutchinson, R.M.	1
Kent, H.C.	1
Knepper, D.H.	1
Lee, K.	1
McBride, G.T.	1
Arthur Lakes Library	1
ORS	1

CSM (cont.)	Copies
Nicolais, S.M.	1
Prost, G.L.	1
Raines, G.L.	1
Sawatzky, D.L.	1
Thigpen, J.B.	1
Trexler, D.W.	1
Weimer, R.J.	1
OTHER	
Asian Inst. of Tech. Library	1
Ballew, G.I.	1
Duskin, D.J.	1
Eichler, R.J.	1
Haas, R.	1
Hulstrom, R.	1
Jefferis, L.H.	1
Lash, T.R.	1
Lyon, R.J.P.	1
Marrs, R.W.	1
Muhm, J.	1
Quade, J.G.	1
Wychgram, D.C.	1

Remote Sensing Report 75-6 Plate 8

81-18

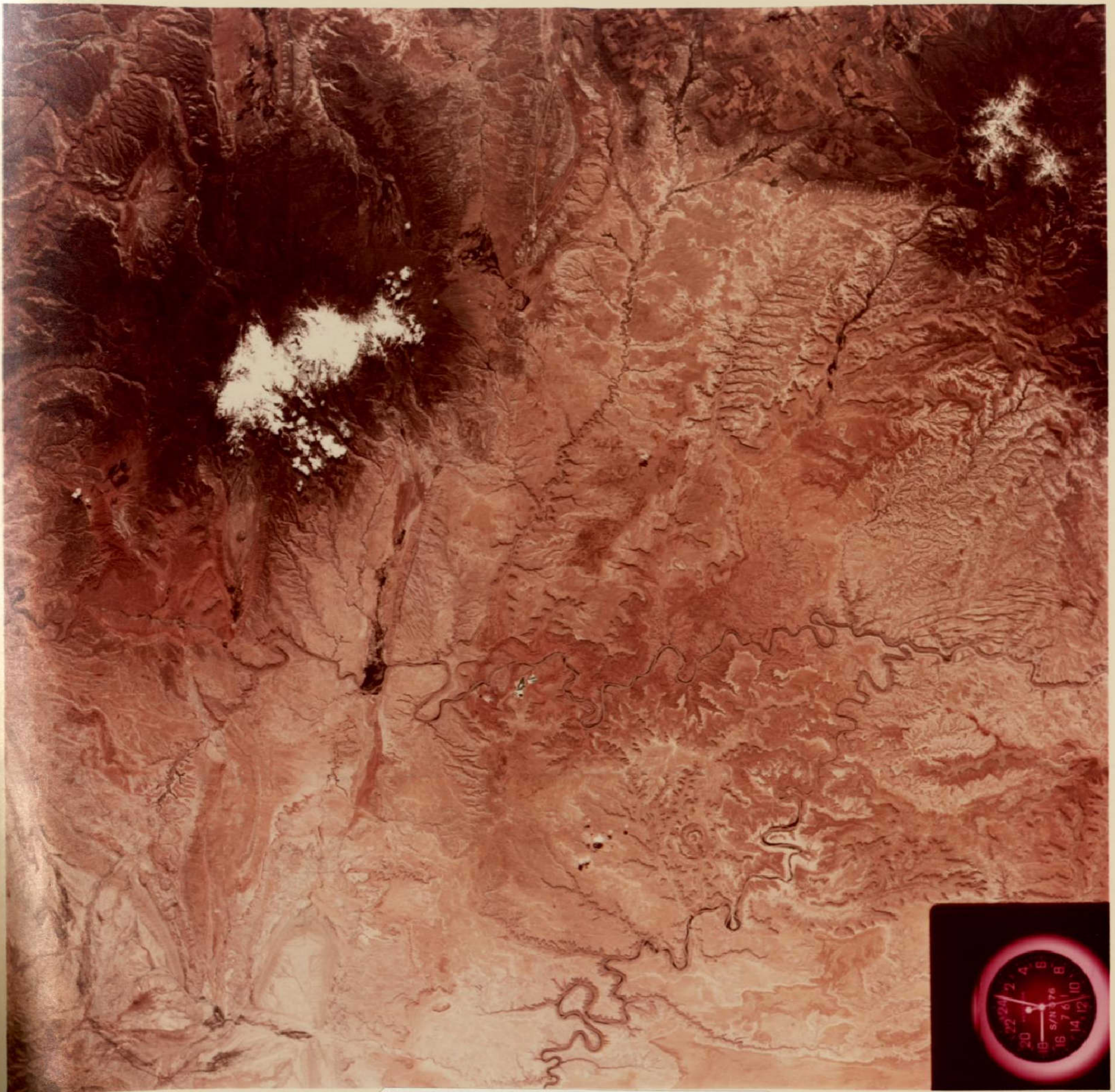

Remote Sensing Report 75-6

Plate 9

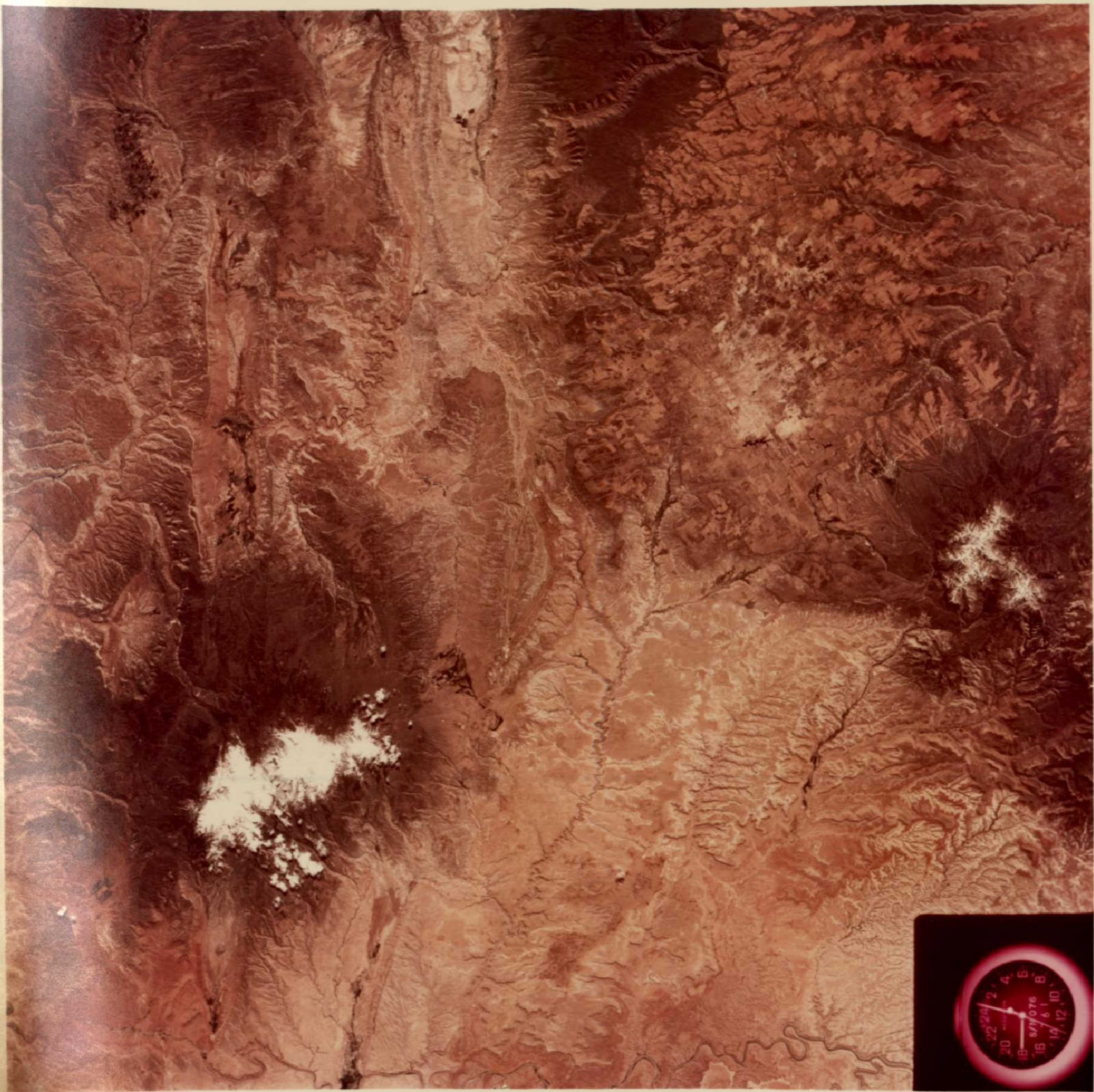

Remote Sensing Report 75-6

Plate 10